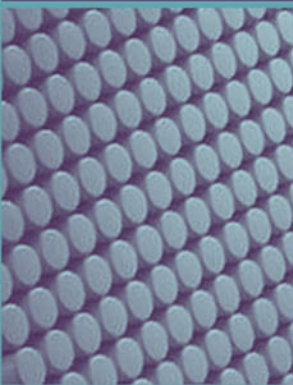


RADAR SYSTEM PERFORMANCE MODELING

second edition



CD-ROM
INCLUDED

G. RICHARD CURRY

Radar System Performance Modeling

Second Edition

DISCLAIMER OF WARRANTY

The technical descriptions, procedures, and computer programs in this book have been developed with the greatest of care and they have been useful to the author in a broad range of applications; however, they are provided as is, without warranty of any kind. Artech House, Inc. and the author and editors of the book titled *Radar System Performance Modeling, Second Edition* make no warranties, expressed or implied, that the equations, programs, and procedures in this book or its associated software are free of error, or are consistent with any particular standard of merchantability, or will meet your requirements for any particular application. They should not be relied upon for solving a problem whose incorrect solution could result in injury to a person or loss of property. Any use of the programs or procedures in such a manner is at the user's own risk. The editors, author, and publisher disclaim all liability for direct, incidental, or consequent damages resulting from use of the programs or procedures in this book or the associated software.

For a listing of recent titles in the *Artech House Radar Library*,
turn to the back of this book.

Radar System Performance Modeling

Second Edition

G. Richard Curry



**ARTECH
HOUSE**

BOSTON | LONDON
www.artechhouse.com

Library of Congress Cataloging-in-Publication Data

A catalog record of this book is available from the U.S. Library of Congress

British Library Cataloguing in Publication Data

A catalog record of this book is available from the British Library

Cover design by Igor Valdman

**© 2005 ARTECH HOUSE, INC.
685 Canton Street
Norwood, MA 02062**

All rights reserved. Printed and bound in the United States of America. No part of this book may be reproduced or utilized in any form or by any means, electronic or mechanical, including photocopying, recording, or by any information storage and retrieval system, without permission in writing from the publisher.

All terms mentioned in this book that are known to be trademarks or service marks have been appropriately capitalized. Artech House cannot attest to the accuracy of this information. Use of a term in this book should not be regarded as affecting the validity of any trademark or service mark.

International Standard Book Number: 1-58053-816-9

10 9 8 7 6 5 4 3 2 1

*To my wife, Nancy, our children,
Sheryl, Ann, Robert, and Tom,
and our grandchildren,
Ryan, T. J., Tyler, Rachel, Trent, Theo, and Andre*

Contents

Preface	<i>xiii</i>
CHAPTER 1	
Introduction	1
1.1 This Book and How to Use It	1
1.2 Concept of Radar Operation	3
1.3 Radar Applications and Functions	4
1.4 Functional Models	5
1.5 Custom Radar Functions	6
1.6 Problems	9
References	9
Selected Bibliography	9
CHAPTER 2	
Radar Configurations	11
2.1 Radar Basing	11
2.2 Frequency Bands	13
2.3 Antenna Types	15
2.4 Waveform Types	16
2.5 Signal Processing Techniques	17
2.6 Monostatic and Bistatic Radar	19
2.7 Problems	19
References	20
Selected Bibliography	20
CHAPTER 3	
Radar Analysis Parameters	21
3.1 Transmitter	21
3.2 Antennas	23
3.3 Phased-Array Antennas	30
3.4 Receiver and Signal Processor	35
3.5 Target Radar Cross Section	37
3.6 Problems	41
References	42
Selected Bibliography	43

CHAPTER 4

Radar Waveforms	45
4.1 Waveform Characteristics	46
4.2 CW Pulses	49
4.3 Linear FM Pulses	51
4.4 Phase-Coded Waveforms	54
4.5 Pulse-Burst Waveforms	56
4.6 Multiple-Time-Around Returns	59
4.7 Radial-Velocity Ambiguities	60
4.8 Problems	60
References	62
Selected Bibliography	62

CHAPTER 5

The Radar Equation	63
5.1 Radar Range Equation	63
5.2 Parameter Definition in the Radar Equation	67
5.3 Reference Range	70
5.4 Pulse Integration	71
5.5 Minimum Range Constraint	76
5.6 Problems	79
5.7 VBA Software Functions for the Radar Equation	80
5.7.1 Function SNR_dB	80
5.7.2 Function Range_km	81
5.7.3 Function Integrated_SNR_dB	83
5.7.4 Function SP_SNR_dB	83
References	85
Selected Bibliography	86

CHAPTER 6

Radar Detection	87
6.1 The Detection Process	87
6.2 False Alarms	89
6.3 Detection Using a Single Pulse or Coherent Dwell	92
6.4 Detection Using Noncoherent Integration	95
6.5 Cumulative Detection	98
6.6 Problems	101
6.7 VBA Software Functions for Radar Detection	102
6.7.1 Function Pfa_Factor	102
6.7.2 Function FRate_per_s	103
6.7.3 Function ProbDet_Factor	103
6.7.4 Function SNR_SP_dB	105
References	106
Selected Bibliography	106

CHAPTER 7

Radar Search Modes	109
--------------------	-----

7.1	The Search Equation	109
7.2	Rotating Search Radar	111
7.3	Volume Search with Phased-Array Radar	116
7.4	Cued Search	123
7.5	Horizon Search with Phased-Array Radar	128
7.6	Horizon Search with Dish Radar	130
7.7	Problems	133
7.8	VBA Software Functions for Radar Search Modes	135
7.8.1	Function SearchR_Rot1_km	135
7.8.2	Function SearchR_Rot2_km	137
7.8.3	Function SearchR_Vol1_km	139
7.8.4	Function SearchR_Vol2_km	142
7.8.5	Function SearchR_Cue1_km	145
7.8.6	Function SearchR_Cue2_km	147
7.8.7	Function SearchR_Hor1_km	151
7.8.8	Function SearchR_Hor2_km	154
7.8.9	Function Sr_BowTie1_km	157
7.8.10	Function Sr_BowTie2_km	159
	References	161
	Selected Bibliography	163

CHAPTER 8

	Radar Measurement and Tracking	165
8.1	Range Measurement Accuracy	167
8.2	Angular Measurement Accuracy	169
8.3	Velocity Measurement Accuracy	172
8.4	Measurement of Target Features	174
8.5	Multiradar Measurements	178
8.6	Measurement Smoothing and Tracking	180
8.7	Radar Tracking Techniques	182
8.8	Problems	183
8.9	VBA Software Functions for Radar Measurement and Tracking	185
8.9.1	Function RangeError_m	185
8.9.2	Function AngleError_mR	186
8.9.3	Function DopVelError_mps	188
8.9.4	Function RadVelError_mps	189
8.9.5	Function CrossVelError_mps	190
8.9.6	Function PredictError_km	191
	References	193
	Selected Bibliography	193

CHAPTER 9

	Environment and Mitigation Techniques	195
9.1	Terrain and Sea-Surface Effects	195
9.2	Precipitation Effects	201
9.3	Troposphere Effects	205
9.4	Ionosphere Effects	209

9.5	Problems	213
9.6	VBA Software Functions for Environment and	
9.6	Mitigation Techniques	215
9.6.1	Function SCR_Surf_dB	215
9.6.2	Function RainLocAtten_dBpkm	215
9.6.3	RainPathAtten_dB	216
9.6.4	Function SCR_Rain_dB	218
9.6.5	Function TropoAtten_dB	219
9.6.6	Function TropoEl_Err_mR	220
9.6.7	Function TropoR_Err_m	221
9.6.8	Function IonoEl_Err_mR	222
9.6.9	Function IonoR_Err_m	222
	References	224
	Selected Bibliography	224

CHAPTER 10

	Radar Countermeasures and Counter-Countermeasures	227
10.1	Radar Countermeasure Summary	228
10.2	Mainlobe Jamming	231
10.3	Sidelobe Jamming	237
10.4	Volume Chaff	241
10.5	Decoy Discrimination	245
10.6	Problems	248
10.7	VBA Software Functions for Radar Countermeasures and	
10.7	Counter-Countermeasures	249
10.7.1	Function DiscProb_Factor	249
10.7.2	Function ML_SJNR_dB	250
10.7.3	Function ML_BTRange_km	251
10.7.4	Function SL_SJNR_dB	254
10.7.5	Function SL_BTRange_km	256
10.7.6	Function SCR_Chaff_dB	259
	References	262
	Selected Bibliography	262

CHAPTER 11

	Airborne and Space-Based Radar Issues	263
11.1	Radar Configurations	264
11.2	Clutter Characteristics	266
11.3	Pulse-Doppler Processing	269
11.4	Displaced Phase Center Arrays (DPCA)	271
11.5	Space-Time Adaptive Processing (STAP)	273
11.6	Synthetic-Aperture Radar (SAR)	274
11.7	Problems	279
11.8	VBA Software Functions for Airborne and SBR	280
11.8.1	Function Graz_Ang_deg	280
11.8.2	Function Dep_Ang_deg	281
11.8.3	Function MB_Clutter_V_mps	282

11.8.4 Function SAR_XR_Res_m	283
References	285
Selected Bibliography	285
CHAPTER 12	
Radar Performance Modeling Techniques and Examples	287
12.1 Methodology	287
12.2 False-Alarm Probability Optimization	289
12.3 Cumulative Detection over Long Periods	292
12.4 Cued Search Using a Dish Radar	295
12.5 Composite Measurement Errors	300
12.6 Detection in Jamming, Chaff, and Noise	304
12.7 Problems	308
References	309
Selected Bibliography	310
Appendix A List of Symbols	311
Appendix B Glossary	319
Appendix C Custom Radar Software Functions	323
Reference	328
Appendix D Unit Conversion	329
Reference	331
Appendix E Problem Solutions	333
Appendix F Self Test	363
About the Author	381
Index	385

Preface

While my career in radar has included radar hardware design, testing, and operation, for the past 38 years, I have been performing design trades and performance analysis of radars as parts of surveillance, weapons, and air traffic control systems. In many cases, these radars had not yet been fully designed, so their detailed characteristics had not yet been defined. In other cases, where the radar was built and operational, the details of its design and operation were so complex that the time needed to analyze and model them was prohibitive. To analyze the performance of these radars at a system level, I found it useful to rely on basic radar principles to model their performance, using top-level parameters to characterize the radar design.

Because of the complex interactions in systems between radar, other sensors, targets, environment, and other system elements, computer simulations are often used to support system analysis. While I am not an expert programmer, I found myself increasingly involved in defining radar models for use in system simulations, and evaluating the simulation outputs to determine how the radar was performing. Some of these simulations used simplistic radar models such as the cookie-cutter model, where the radar is assumed to detect all targets within a defined radius. Others used detailed representations of radar hardware designs and descriptions of multiple operating modes. However, most system simulations required relatively simple radar models, but ones that represent the major radar characteristics and operating modes, interact with other system elements, and are responsive to target characteristics and flight paths. These radar models often were provided by combinations of the top-level models described above.

Over the years, I have developed and collected a number of radar models, having various levels of fidelity, that have been useful in system-level radar analysis and simulation. I am frequently asked by system analysts or simulation programmers to comment on radar models in a simulation, or to recommend an appropriate radar model for some radar function. This book is an effort to document the radar models and analysis tools that have proven useful, in the hope that it will provide answers to such needs in the future. Key models are implemented in VBA custom radar functions, which can be used for radar analysis in Excel workbooks, and also provide a guide for implementing the models in simulations.

After the first edition of this book was published, I developed a course, using the book as a text, which has been given both as a series of lectures, and in written form as a self-study course. The material from this course has been incorporated in this second edition. It includes additional explanations and examples of the radar principles, problems and a self-test with solutions, and suggestions for further reading.

Radar engineers will notice that some aspects of radar theory and design have been simplified, and that the models may not be appropriate for all types of radar implementation. I have tried to indicate where simplifying assumptions were made, and the application limits of each model. These models can be modified or augmented to incorporate features needed in a specific analysis, or to simulate a novel radar configuration. The approach I have taken provides a guide for such activities.

I am grateful to the many people who have shared their radar knowledge and insights with me over my career. I would especially like to acknowledge the numerous helpful discussions with Jack Ballantine, my colleague at both Science Applications International Corporation and General Research Corporation. These interactions have sharpened my understanding of many radar issues and increased the rigor with which I have addressed them. I would also like to thank John Dyer of Sparta, Inc., for his many probing questions, from which I suspect I learned more than I taught him. It was John Illgen of Illgen Simulation Technologies, Inc., whose SimCentral Web venture suggested to me the idea for this book. Lavon Jordan of Frontier Technology, Inc., suggested that I give a radar course based on the book. Finally, I would like to thank Dave Barton for his support over the years, and for his constructive and helpful review of this book.

Introduction

This chapter enables the reader to:

- Know the content and organization of this book, and how to use it to analyze and model radar system performance;
- Understand the concept of radar operation, the functions performed by radar, and how radar may be used in various applications;
- Understand the characteristics of functional radar models and how they are used to analyze overall radar performance.

Radars are increasingly being used as integral parts of complex systems. Examples include air-traffic control systems, ballistic-missile defense systems, air-defense systems, and targeting systems for land attack. Analysis of radar in such systems requires representing the radar operation and performance in the context of the overall system and the external environment. The radar performance must be evaluated in performing system tasks, and the impact of radar operation on system performance must be quantified.

Analysis of such systems may use a variety of tools, ranging from simple off-line calculations of radar performance to complex computer simulations of overall system operation. Models of radar operation and performance are needed for these system-level analyses. The radar representations in these models must be responsive to the key radar characteristics, system interfaces, and performance measures.

However, they should be simple enough to allow their use in large-scale system simulations, and to represent radar whose detailed design is not fully known. Radar simulations used for detailed radar design and analysis are generally too complex for such system-level analysis.

1.1 This Book and How to Use It

This book addresses the needs of system analysts for radar models and analysis tools. It describes the basic principles of radar operation, how radar is configured and used in military and civilian systems, and how to analyze and model radar at the system level. The book presents and explains equations, computational methods, and data, and provides insight on how to use the models in system analysis. The book may serve both as a text for learning radar system performance analysis and modeling, and as a reference for engineers and modelers working in the field.

System-level radar modeling requirements are different from radar design models requirements. The latter involve details of the radar hardware and trace the signals through the various elements of the radar. They focus on how to make the radar work. System models, on the other hand, focus on overall radar performance, and often rely on basic principles. Thus, they may be used for conceptual radar that has not been fully designed or built, or for parametric analyses of radar designs. They usually assume the radar has been, or will be, designed to work properly. These models represent the key features of radar without excessive detail.

The radar models described in this book may be used by system analysts to evaluate systems that include radar, and by modelers and programmers involved in simulating the performance of radar in systems. Several of the key models are programmed into custom radar functions, so that the models may be readily used for radar analysis in Excel workbooks. These may also provide a guide for modelers and simulation programmers.

This book is intended for engineers who are evaluating radar system issues, systems analysts who are involved with systems that include radar, and programmers who are simulating the performance of radar. It is aimed at engineers, scientists, and mathematicians who are not radar experts. Only a general engineering and mathematical background is assumed; no specialized radar engineering or advanced mathematics is required. In developing and describing the models, the book gives the reader a basic understanding of radar principles.

This chapter provides a brief an overview of radar operation and applications, followed by a discussion of functional radar models and their software representations. Chapters 2, 3, and 4 discuss radar configurations, radar parameters and radar waveform characteristics. These provide a general radar understanding for the systems analyst, to serve as background for radar analysis and model development. These chapters may be skipped by those already familiar with basic radar principles, or may be used as reference material.

The radar models are developed and presented in Chapters 5 through 11. In these chapters, the reader may go directly to modeling topics of interest. References are made to discussions and results in other chapters, where they are helpful to understanding the material. The final section in each of these chapters describes the Excel custom radar functions that are based on the chapter topics. Analysis examples using the radar models together to solve practical radar problems, both analytically and in Excel workbooks, are given in Chapter 12.

Most of the models in this book may be found in, or derived from, material in standard radar texts [1–3]. The book collects the radar material needed by system modelers, presents it in a concise format, and provides guidance for using it in systems analysis. Selected bibliographies are provided at the end of each chapter that give sources of additional background and information on the topics addressed in the chapter. They are intended to enrich the reader's knowledge of radar and provide information that goes beyond the scope of this book. A list of symbols used in the book, along with their definitions, is given in Appendix A. Appendix B contains a glossary of key terms and acronyms used in the book. A list of the custom radar functions with directions for their installation and use is provided in Appendix C. Appendix D gives procedures for converting the standard metric units used in the models in this book to and from various measurement units (see Section 1.4).

Practice problems are provided for each chapter, to assist in reviewing the lesson material, and to ensure an understanding of it. These problems may be solved using the methods, equations, and data in this book. Solutions to these problems appear in Appendix E.

A self-test that covers the material presented in this book is provided in Appendix F. This test may be used to evaluate comprehension of the material in the book. Answers to the test questions are provided at the end of the appendix.

1.2 Concept of Radar Operation

Radar stands for RAdio Detection And Ranging. The basic radar concept is that radio frequency (RF) energy is generated by the transmitter, radiated by the transmitting antenna, reflected by the target, collected by the receiving antenna, and detected in the radar receiver. This is illustrated in Figure 1.1. In practice, many radars use the same antenna for both transmitting and receiving.

Since the electromagnetic energy travels with the speed of light (designated c), the range from the radar to the target, R , may be determined by measuring the time interval, t , between the transmitted signal and the received signal:

$$R = \frac{ct}{2} \quad (1.1)$$

The electromagnetic propagation velocity in the atmosphere is nearly the same as that in a vacuum, and the approximation $c = 3 \times 10^8$ m/s is sufficiently accurate for most analyses.

The direction of the target relative to the radar may be determined by using an antenna with a directional pattern, and observing the direction from which the peak of this pattern is pointing when the received signal is maximized.

The target radial velocity, V_R , is the component of target velocity in the direction of the radar. This may be found from the range changes for successive radar measurements, or from the Doppler-frequency shift of the return signal. The frequency of the electromagnetic signal that is reflected from a target that is moving either toward or away from the radar is changed. The target velocity component in the direction of the radar is proportional to this Doppler-frequency shift, f_D , of the received signal:

$$V_R = \frac{f_D c}{2f} \quad (1.2)$$

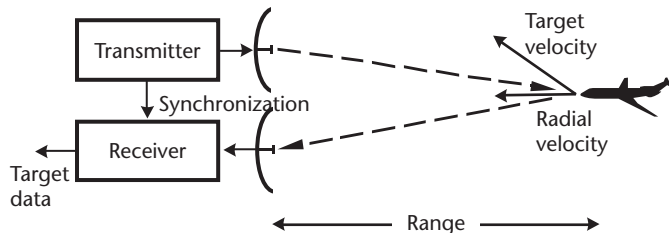


Figure 1.1 Concept of radar operation.

where f is the radar RF frequency [1, pp. 68–70].

The target size is roughly indicated by its radar cross section (RCS), which is a measure of the fraction of the incident RF signal that is returned in the direction of the radar, as discussed in Section 3.5. The RCS may be determined from measurement of the received signal strength, using other radar parameters in the calculation (see Chapter 5 and Section 8.4).

1.3 Radar Applications and Functions

Radar has been used, or proposed for use, in a wide range of applications, both in military and civilian systems. Table 1.1 lists some of these applications, divided into major categories.

The principal radar functions include:

- Search;
- Target detection;
- Target position measurement and tracking;
- Measurement of target characteristics.

Search, also referred to as surveillance, involves the examination of a volume of space for possible targets of interest. This is normally done by periodically directing radar energy in a pattern of beams that cover the search volume. Common radar search modes include:

- Volume search, where a large three-dimensional volume is searched.
- Barrier search, where a two-dimensional region is searched for targets that penetrate the barrier region (more precisely, the third dimension is relatively small). Horizon search is a type of barrier search.

Table 1.1 Radar Applications

<i>Category</i>	<i>Applications</i>
Air traffic control	En route surveillance
	Terminal area surveillance
	Precision approach control
	Ground traffic control
Other civilian	Weather detection
	Search and rescue
	Ground mapping
	Crop measurement
	Satellite surveillance and tracking
	Intrusion detection
Military	Traffic control (speed measurement)
	Ocean surveillance
	Air defense
	Missile defense
	Personnel detection
	Intelligence data collection
	Target detection, identification, and location
	Weapon guidance and control

- Cued search, where a target location is approximately known, and a small volume around the estimated position (the cue), is searched.
- Push-broom search, where a moving radar (e.g., on an aircraft), searches the volume as it moves along its path. This is similar to barrier search, but the barrier moves with the radar platform.

Modeling of radar search modes is addressed in Chapter 7.

Radar detection is the determination that a target is present in the search volume. This is usually accomplished by setting a received-signal threshold that excludes most noise and other interfering signals. Signals that exceed this threshold are the detected targets. Since radar background noise and many target signals fluctuate, detection is a statistical process. It is usually characterized by a probability of detection, P_D , and a probability of false alarm (false detection), P_{FA} [1, pp. 23–25]. Modeling of radar detection is discussed in Chapter 6.

The radar measures target position in range and angular coordinates, as discussed in Section 1.2. Radar tracking is the determination of the path of a moving target from a series of position measurements. In its simplest form, this is simply associating successive measurements with a target and connecting them. Better tracking performance is obtained by using a tracking filter, which smoothes the position measurements, and estimates the target trajectory parameters. When targets can maneuver, the degree of smoothing employed in the tracking filter is a compromise between improving the track accuracy and following the target maneuvers. Models for radar measurement and tracking are discussed in Chapter 8.

A radar may measure other target features in order to better characterize or identify the target, as discussed in Section 8.4. These measures may include RCS (discussed in Sections 1.2 and 3.5); fluctuations of RCS with time, target size, target shape and configuration (using imaging radar – discussed in Section 2.5); and target motion characteristics shown by the Doppler-frequency spectrum of the received signal.

1.4 Functional Models

The radar models presented in this book are termed functional models. This implies that they are generally not intended to simulate details of radar hardware design, electromagnetic propagation, and statistical methods. Rather, the models represent the effects of these characteristics on the overall performance of the radar. In order to apply to a wide range of radar situations, these models are often based on physical principles, rather than details of specific radar designs.

In order to maintain reasonable fidelity while using such simplifications, the models use the key parameters that impact specific results. For example, the radar antenna, (discussed in Section 3.2), requires a number of parameters for complete characterization. However, only the transmit gain, the receive aperture area, and the antenna losses impact the radar sensitivity as measured by the signal-to-noise ratio (S/N). These parameters are used in the models for S/N in Chapter 5. On the other hand, the antenna beamwidth is the key antenna parameter for calculating the radar angular measurement accuracy in Section 8.2, and the antenna sidelobe level

is the critical antenna parameter for radar performance in sidelobe jamming environments, as discussed in Section 10.3.

Radar employs a wide variety of configurations and basing, as discussed in Chapter 2. It is not always practical to develop simple models that apply to all these variations. When the full range of radars cannot be represented in a model, this book focuses on ground-based pulsed monostatic radar. These have wide applicability in air traffic control and military systems, and the resulting models may often be used for other radar types as well.

This approach leads to relatively simple models with broad applicability. Where the applicability is limited to certain configurations or parameter ranges, it is indicated in the discussion, and alternative approaches may be suggested for other cases. A number of issues specific to airborne and space-based radar are addressed in Chapter 11, and models for analyzing the performance of these radars are given.

The analysis and models in this book utilize the standard metric system (SI), also known as mks (meter, kilogram, second), units. This allows for standardization and simplification in the equations and data. When other units are used in the analysis, they may be converted by using the appropriate conversion factors. A number of common conversion factors are given in Appendix D. For dimensionless quantities, the equations use power ratios, rather than decibels (dB). Conversions from power ratios to decibels, and the reverse, utilize:

$$dB = 10 \log(\text{power ratio}) \quad (1.3)$$

$$\text{Power ratio} = 10^{(dB/10)} \quad (1.4)$$

These equations may also be used to convert quantities having dimensions that are expressed in decibels relative to a measurement unit. For example, RCS is often expressed in decibels relative to a square meter (dBsm).

1.5 Custom Radar Functions

A disk containing custom radar software functions, programmed in Microsoft Visual Basic for Applications (VBA), is included with this book. These functions implement 43 key radar system models that are described in this book. They are incorporated into an Excel Add-In file, (having the extension xla). By copying this file to a computer hard drive, the radar functions may be accessed and used in Excel worksheets just as the built-in Excel functions are used. The procedure for copying the file and activating the Add-In is given in Appendix C.

The disk also contains two Excel files that contain example exercises of the custom radar functions and the worksheet analyses of the example problems in Chapter 12. Use of these is also discussed in Appendix C.

Using the custom radar functions in Excel is illustrated here for Function RangeError_m, that calculates the radar range measurement error. The equation, derived in Section 8.1 and 8.6, is:

$$\sigma_R = \left[\frac{\Delta R^2}{2n S/N} + \frac{\sigma_{RF}^2}{n} + \sigma_{RB}^2 \right]^{1/2} \tag{1.5}$$

where:

- σ_R = radar range measurement error (standard deviation)
- ΔR = radar range resolution (see Section 4.1)
- S/N = single-pulse signal-to-noise ratio
- σ_{RF} = fixed radar range error
- σ_{RB} = radar range bias error
- n = number of pulsed used in the measurement

The custom radar function is described in Section 8.9.1. It may be used in an Excel worksheet by selecting Insert, selecting Function (or selecting the f_x icon from the toolbar), selecting User Defined, and choosing the desired function, RangeError_m. Click OK, and the Function Arguments dialog box shown in Figure 1.2 will appear. Key in the desired argument values for RangeRes_m, SNR_dB, RangeFixEr_m, RangeBiasEr_m, and N_Smooth_Integer. The formula result will appear at the bottom of the dialog box. Click OK, and the formula result for RangeError_m will appear in the worksheet cell. Alternatively, type =RangeError_m (values for ΔR , S/N, σ_{RF} , σ_{RB} , and n) in a worksheet cell. Press enter, and the formula result will appear in the cell. As with any Excel function, another cell or an equation may be used for the value of an argument.

Figure 1.2 shows the Function Arguments dialog box as it appears in recent versions of Excel. In earlier versions of Excel, the appearance of the Function Arguments dialog box is slightly different, as shown in Figure 1.3, but the functionality is the same.

The VBA code for the radar functions may be examined and copied by first removing the protection from the .xla file, and then opening the appropriate software module in the Visual Basic Editor. The procedure for doing this is given in Appendix C. The code for this simple function is shown in Figure 1.4. As indicated in the code (and by the non-bold type in the Function Arguments dialog box), the

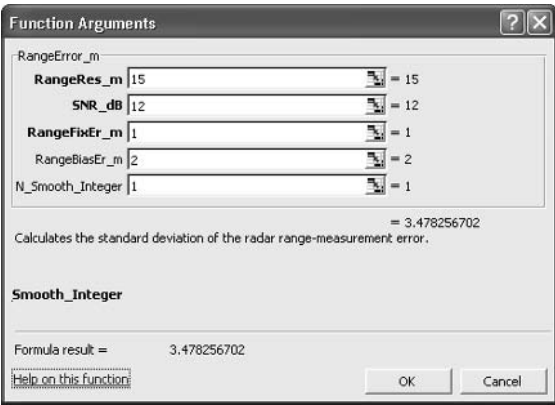


Figure 1.2 Excel Function Arguments dialog box for radar Function RangeError_m (Excel 2002).

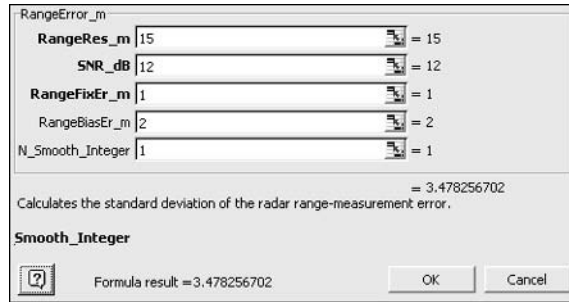


Figure 1.3 Excel Function Arguments dialog box for radar Function RangeError_m (Excel 97).

last two arguments for this function are optional, and need not be entered. If left blank, the default values given in the code (0 and 1, respectively for this example), will be used.

Note that many of the custom radar functions use common engineering units that do not adhere to the metric system discussed in Section 1.4. For example, range is usually given in kilometers rather than meters, and S/N is usually given in decibels rather than as a power ratio. When other units are used in the analysis, they may be converted to the units specified in the functions by applying the appropriate factors. A number of these conversion factors are tabulated in Appendix D. Similarly, power ratios may be converted to decibels (and decibels may be converted to power ratios) using (1.3) and (1.4).

```
Function RangeError_m(RangeRes_m As Single, _
    SNR_dB As Single, RangeFixEr_m As Single, _
    Optional RangeBiasEr_m, _
    Optional N_Smooth_Integer) As Single

    'Calculates the standard deviation of the
    'radar range-measurement error, in m.

    'RangeRes_m = Radar range resolution, in m.
    'SNR_dB = Measurement signal-to-noise
    'ratio, in dB.
    'RangeFixEr_m = Composite of fixed errors
    'in range, in m.
    'RangeBiasEr_m (optional) = Composite of bias
    'errors in range, in m. If blank, zero
    'will be used.
    'N_Smooth_Integer (optional) = Number of
    'range measurements smoothed, integer.
    'If blank, 1 will be used.

    If IsMissing(RangeBiasEr_m) Then _
        RangeBiasEr_m = 0
    If IsMissing(N_Smooth_Integer) Then _
        N_Smooth_Integer = 1

    If N_Smooth_Integer < 1 Then Exit Function

    RangeError_m = (RangeRes_m ^ 2 / (2 * _
        N_Smooth_Integer * 10 ^ (SNR_dB / 10)) _
        + RangeFixEr_m ^ 2 / N_Smooth_Integer _
        + RangeBiasEr_m ^ 2) ^ 0.5

End Function
```

Figure 1.4 VBA code for radar Function RangeError_m.

Descriptions of the custom radar functions appear in the last section of each relevant chapter. A summary table of all the functions is given Appendix C.

1.6 Problems

The following problems are provided to assist in reviewing this chapter, and to ensure a basic understanding of the material. Solutions to these problems are given in Appendix E, Section E.1.

1. What is the time delay between transmission and reception of a radar signal when the target is at a range of 200 km from the radar?
2. What is the radial velocity of a target producing a Doppler shift of +20 Hz (frequency increase in the returned signal), if the transmitted radar frequency is 425 MHz?
3. What is the power ratio corresponding to a decibel level of 22 dB?
4. What is the decibel value corresponding to a power ratio of 75?
5. What range in kilometers is indicated by a radar pulse return that occurs 3.5 ms after the pulse transmission?
6. For a target having a velocity of 700 m/s moving toward the radar at an angle of 30° from the radar line-of-sight (LOS), and a radar frequency of 5.5 GHz:
 - a. What is the radial velocity?
 - b. What is the Doppler-frequency shift?
 - c. What is the frequency of the received signal?
7. Convert 15 dB to a power ratio.
8. Convert 0.03 m^2 to decibels relative to a square meter (dBsm).

References

- [1] Skolnik, M. I., *Introduction to Radar Systems*, 2nd ed., New York: McGraw-Hill, 1980.
- [2] Barton, D. K., *Modern Radar System Analysis*, Norwood, MA: Artech House, 1988.
- [3] Skolnik, M. I., (ed.), *Radar Handbook*, 2nd ed., New York, McGraw-Hill: 1989.

Selected Bibliography

A good history of the development of radar and its use in World War II is given in a paperback book by Buder. A detailed description of the radar research and development done during that war at the Massachusetts Institute of Technology Radiation Laboratory appears in a 28-volume compilation edited by Ridenour, and available on CD-ROM. Much of this early work is still relevant.

A good general description of radar principles, design, and operation is provided by Skolnik in his original 1962 book, that was updated in 1980. Books by Barton in 1964 and 1988 provide analysis of radar performance issues. Skolnik's *Radar Handbook*, first published in 1970, and updated in 1989, provides a wealth

of detail on many radar topics. These are useful references for the radar analyst. Walkenbach describes the development of VBA modules and their use in Excel.

Barton, D. K., *Radar System Analysis*, Englewood Cliffs, NJ: Prentice Hall, 1964.

Barton, D. K., *Modern Radar System Analysis*, Norwood, MA: Artech House, 1988.

Budri, R., *The Invention That Changed the World*, New York: Touchstone, 1996.

M.I.T. *Radiation Laboratory Series, 28 Volumes on 2 CDROMs*, Norwood, MA: Artech House, 1999.

Ridenour, L. N., (ed.), *Massachusetts Institute of Technology Radiation Laboratory Series, Vols. 1 Through 28*, New York: McGraw-Hill, 1951.

Skolnik, M. I., *Introduction to Radar Systems*, New York: McGraw-Hill, 1962.

Skolnik, M. I., *Introduction to Radar Systems*, 2nd ed., New York: McGraw-Hill, 1980.

Skolnik, M. I., (ed.), *Radar Handbook*, New York, McGraw-Hill: 1970.

Skolnik, M. I., (ed.), *Radar Handbook*, 2nd ed., New York: McGraw Hill: 1989.

Walkenbach, J., *Excel 97 Programming for Windows for Dummies*, Foster City, CA: IDG Books Worldwide, 1997.

Radar Configurations

This chapter enables the reader to:

- Compare radar configurations in terms of radar basing, frequency, and antenna type.
- Understand the types and capabilities of radar waveforms and signal-processing techniques.
- Know the differences between monostatic and bistatic radars.

Radar has been proposed and built for a wide variety of applications, as discussed in Section 1.3. This has led to many diverse radar configurations. These may be categorized by characteristics including their basing, operating frequency, antenna type, waveforms employed, and signal-processing techniques. These features are discussed in this chapter. While the models in this book focus on ground-based pulsed monostatic radars, many of the models are also applicable to the other configurations discussed here.

2.1 Radar Basing

Where a radar is based determines to a large degree the spatial coverage of the radar, and what kinds of targets it may observe. The major categories of radar basing are terrestrial, airborne, and space-based. Terrestrial radar includes those based on land or towers, and shipboard radars. They are widely used for surface, air, and space surveillance.

The coverage of terrestrial radar against low-altitude targets is limited by the radar line-of-sight (LOS) in terrain, and by Earth curvature. Within the atmosphere, refraction bends the radar LOS downward (see Section 9.3). This is illustrated in Figure 2.1(a), which shows the radar LOS to a target that is tangent to the smooth-Earth surface. The atmospheric refraction may be accounted for by using an effective Earth radius $4/3$ times the actual radius of 6,371 km, which equals 8,485 km. The atmospheric propagation path is then represented by a straight line, as shown in Figure 2.1(b) [1, pp. 447–450].

The range from the radar to the tangent point, R_R , is given by:

$$R_R = (h_R^2 + 2r_E h_R)^{1/2} \quad (2.1)$$

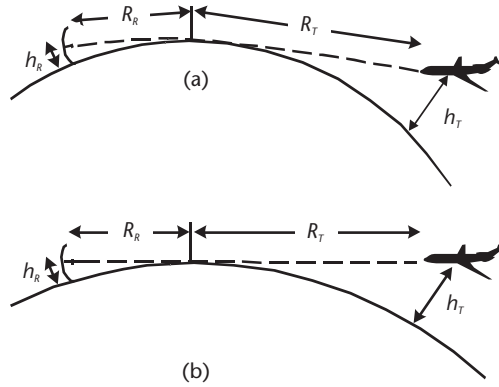


Figure 2.1 Illustration of radar coverage limitation due to Earth horizon blockage. (a) Real Earth. (b) $4/3$ Earth.

where h_R is the height of the radar antenna, and r_E is the effective $(4/3)$ Earth radius. The radar height is plotted as a function of the resulting horizon range in Figure 2.2. This approximation is accurate for altitudes below about 4 km, but is often used for aircraft targets up to 10 km altitude, as discussed in Section 9.3. The range from the horizon to the target, R_T , is similarly given by:

$$R_T = (h_T^2 + 2r_E h_T)^{1/2} \quad (2.2)$$

where h_T is the target altitude. Figure 2.2 also shows the target altitude as a function of the horizon range to the target. The first term on the right in (2.1) and (2.2) is usually negligible, compared with the second term.

The maximum total radar range, R , to the target is the sum of these ranges:

$$R = R_R + R_T \quad (2.3)$$

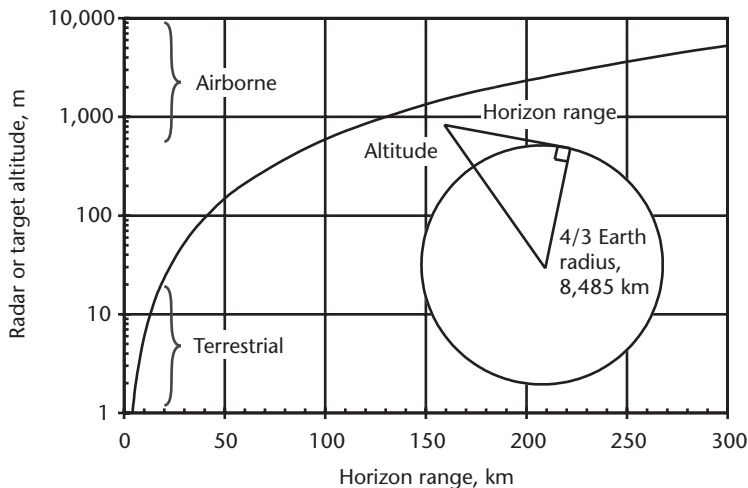


Figure 2.2 Radar or target altitude as a function of horizon range.

Note that other factors, such as rough terrain and multipath propagation (see Section 9.1), may reduce the radar range achievable on low-altitude targets below the values calculated here.

Airborne radar includes surveillance radar such as AWACS and JSTARS, that are installed on relatively large aircraft, and the smaller target acquisition, tracking, and fire-control radar on fighter aircraft [2, pp. 9–20; 3, p. 87]. Airborne radar can provide longer-range coverage on low-altitude targets than terrestrial radar, because of their higher altitudes. This is shown in Figure 2.2.

Other potential advantages of airborne radar is its capabilities to rapidly deploy to areas of interest, and to operate in areas where terrestrial radar cannot readily be sited (e.g., polar regions). Aircraft are limited, however, in the size and weight of their radar payloads, and the time they can remain on station.

Space-based radar (SBR) is installed on satellites that orbit the Earth. SBR may provide coverage of wide Earth areas, due to its high altitude. This comes at the expense of long ranges for targets near the Earth. Satellites are also limited in the size, weight, and prime power available for their radar payloads.

Satellites may provide LOS access to any area on the earth. However, their orbital characteristics do not allow an area to be continually viewed by a satellite, except for geosynchronous satellites that remain fixed at an altitude of 35,871 km above an equatorial point. Low-altitude satellites (altitudes less than about 800 km), have orbital periods of about 90 minutes, and may view a point on the Earth for 15 to 20 minutes [4, pp. 3–5]. Thus, a constellation of several SBRs is needed to provide frequent target observations or continuous coverage (see Section 11.1). SBRs, such as SEASAT and SIR-C, have been used for Earth observation and mapping [4, pp. 10–38]. Continuous coverage is usually not required for these applications.

2.2 Frequency Bands

Radar has been built and operated at a wide range of frequencies. The designations for the frequency bands commonly used by radar are given in Table 2.1. Within these broad bands, certain specific bands have been assigned for radar operation by the International Telecommunication Union (ITU). These assigned bands for Region 2, which includes North and South America, are given in Table 2.1.

Common radar center frequencies in the various bands include: UHF, 425 MHz; L-band, 1.3 GHz; S band, 3.3 GHz; C band, 5.5 GHz; and X-band, 9.5 GHz. Radar generally operates in a relatively narrow band of frequencies, typically 5 to 15% of the center frequency, due both to component limitations and to the band assignments. For example, an X-band radar might operate at frequencies from 9 to 10 GHz, a band of 10.5% of the center frequency of 9.5 GHz.

Key characteristics of the radar frequency bands and their radar applications are summarized in Table 2.2. Frequencies in the HF band reflect off the ionosphere, and are used for over-the-horizon (OTH) radar.

Radar in the VHF and UHF bands requires relatively large antennas to achieve narrow beams, and its propagation through the ionosphere may be distorted (see Section 9.4). The UHF and L bands are often used for search radar. Radar in the X, K_u , and K bands may provide narrow beams and good measurement precision with

Table 2.1 Radar Frequency Bands

<i>Radar Band</i>	<i>Frequency Range</i>	<i>Bands Assigned by ITU</i>
HF	3–30 MHz	
VHF	30–300 MHz	138–144 MHz 216–225 MHz
UHF	300–1,000 MHz	420–450 MHz 890–942 MHz
L band	1–2 GHz	1.215–1.4 GHz
S band	2–4 GHz	2.3–2.5 GHz 2.7–3.7 GHz
C band	4–8 GHz	5.250–5.925 GHz
X band	8–12 GHz	8.50–10.68 GHz
K _u band	12–18 GHz	13.4–14 GHz 15.7–17.7 GHz
K band	18–27 GHz	24.05–24.25 GHz
K _a band	27–40 GHz	33.4–36 GHz
V band	40–75 GHz	59–64 GHz
W band	75–110 GHz	76–81 GHz 92–100 GHz
Millimeter waves	110–300 GHz	126–142 GHz 144–149 GHz 231–235 GHz 238–248 GHz

Source: IEEE Standard for Letter Designations for Radar-Frequency Bands, New York: The Institute of Electrical and Electronic Engineers, Inc., January 8, 2003.

Table 2.2 Radar Band Characteristics and Applications

<i>Frequency Band</i>	<i>Characteristics</i>	<i>Applications</i>
HF	Reflects off ionosphere	OTH radar
VHF, UHF	Very large antennas Ionosphere distorts propagation	Search radar
UHF, L	Large antennas	Search radar
S, C	Moderate size antennas Moderate measurement precision	Multifunction radar
X, K _U , K	Small antennas Precision measurement	Tracking radar Airborne radar
K _U , K, K _A	Very small antennas Good measurement precision Atmospheric and rain loss	Short-range radar Precision-guidance radar
V, W, and millimeter	Severe atmospheric and rain loss	Space-to-space radar

relatively small antennas. They are often used for tracking radar. Multifunction radar that perform both search and tracking often use the S and C bands, that offers a compromise between the characteristics favorable for search and tracking. Atmospheric and rain attenuation limit the range of radar in K_u, K, and K_a bands (see Sections 9.2 and 9.3). Frequencies above K_a band are rarely used in the atmosphere due

to severe absorption. These bands, including V and W band, are often referred to as having millimeter wavelengths.

2.3 Antenna Types

The type and characteristics of the radar antenna strongly influence its performance and capabilities. Most early microwave radar employs reflector antennas that are configured to provide the required radar coverage. The RF energy is directed from a feed horn onto a reflector to form the radar beam. Two types of reflector antennas are illustrated in Figure 2.3.

The dish antenna shown in Figure 2.3(a) employs a circular reflector with a parabolic shape. This shape generates a narrow symmetrical beam, often called a pencil beam. The reflector is steered in two angular coordinates to point the beam toward the target. Dish antennas are well suited to tracking or making observations of individual targets. Due to their narrow beams and beam agility that is limited by mechanical scanning, they are usually not effective in broad area surveillance.

The parabolic reflector antenna illustrated in Figure 2.3(b) generally has a rectangular or oval outline. Its shape usually follows a parabolic contour in the horizontal plane, producing a narrow, focused beam in azimuth. The reflector shaping and feed-horn illumination in the vertical plane are designed to provide a wider beam in elevation, producing a fan-shaped beam pattern. Such radar usually rotates to scan the beam in the azimuth coordinate. The elevation antenna pattern is tailored to provide the desired altitude coverage. The result is volume search around the radar with a periodic revisit at an interval determined by the antenna rotation

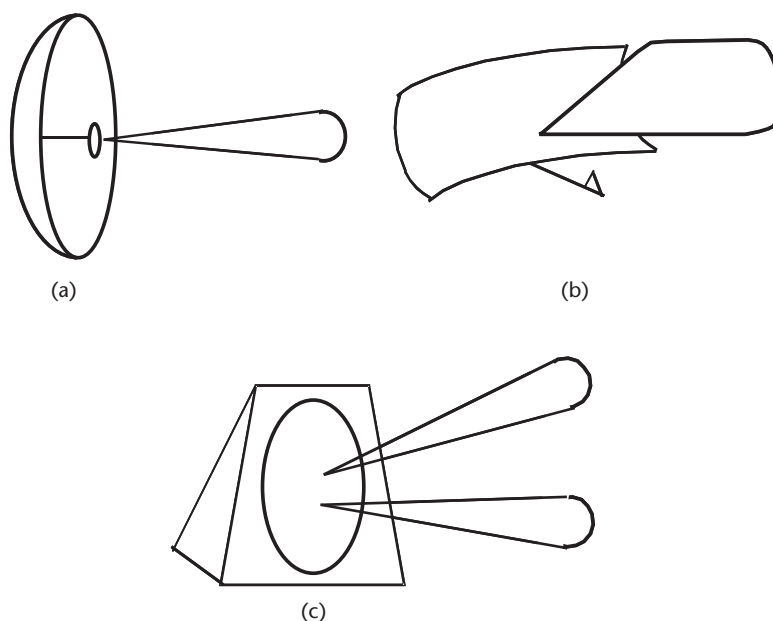


Figure 2.3 Basic antenna types and their beam shapes. (a) Dish reflector with pencil beam. (b) Parabolic reflector with fan beam. (c) Phased array with multiple pencil beams.

period. Since this period is typically from 5 to 20 seconds, radars with these antennas are limited in their ability to track maneuvering targets and to make highrate target observations.

Phased-array antennas employ newer technology, often at a higher cost than for reflector antennas. However, they provide greater flexibility for multifunction applications. An example of a phased-array radar is shown in Figure 2.3(c). These radars usually employ planar faces containing an array of radiating elements [5, pp. 17.7–17.22]. The phase of the RF radiation from each element may be electronically controlled to form a beam pointing in any desired direction within about 60° of the array broadside direction. This allows rapid, electronic beam steering. Planar arrays often generate pencil beams, although the beam cross section may be elliptical if the array is not circular or square. Linear phased-array antennas, which generate fan beams, are occasionally used.

Ground-based phased-array antennas are often built with fixed orientation. Because the coverage of a planar array is limited to a cone having a half-angle of about 60° , three or more array faces are needed to provide hemispheric coverage. Space-based, airborne, and some terrestrial phased-array antennas may be mechanically oriented to provide coverage in the desired direction.

By rapidly repositioning their beams, phased-array antennas may support both wide-area surveillance and high-data-rate target observation and tracking of multiple targets. Most phased-array antennas are computer-controlled, and many have multiple waveforms, operating, and signal-processing modes. They are capable of multimode operation that interleaves the various search, tracking, and measurement functions, and may rapidly respond to the tactical situation and user needs. See Section 3.3 for a discussion of phased-array antenna characteristics.

Of course there are many hybrid antennas that combine the features of reflectors and phased arrays. Often these may be configured to provide specific coverage requirements at a cost lower than that of full-phased arrays. Some of the more common are:

- Phased arrays that are mechanically steered to position their electronic-scan field-of-view (FOV), in the desired direction.
- Dish antennas having feed horns similar to small-phased arrays. This allows limited electronic scanning of the beam (usually limited to a few beamwidths).
- Rotating parabolic antennas or phased-array antennas that generate multiple, stacked beams in elevation. This allows measurement of target elevation angle, so that target altitude may be calculated (see Section 7.2).

2.4 Waveform Types

The waveforms that a radar transmits and receives determine its capabilities for target detection, and particularly for measurements and observations. Most long-range radars employ pulsed waveforms. The radar transmits a pulse and then goes silent, listening for the return of the reflected pulse. This prevents interference between the radar transmitter and receiver, which do not operate at the same time, and allows a single antenna to be used for both transmit and receive.

Another feature of pulsed radar is the capability for measuring target range, by measuring the time between transmission and reception of the pulse (see Section 1.2). For pulses having constant frequency, often called continuous wave (CW) pulses, the precision of range measurement varies inversely with the pulse duration (see Sections 4.2 and 8.1). However, very short pulses may be hard to generate, and the need for high pulse energy, along with transmitter design considerations, often leads to a desire for longer pulses (see Section 3.1).

This conflict may be resolved by using pulse compression. With this technology, the frequency is varied during the pulse in a way that allows the receiver to reduce the duration and to increase the amplitude of the received pulse [6, pp. 3-2–3-3]. A common pulse-compression technique, called chirp, employs linear frequency change during the pulse. Another pulse-compression technique employs a series or burst of pulses. Pulse compression techniques are discussed further in Chapter 4.

Some radars employ continuous RF radiation. These are called CW radar [7, pp. 14.1–14.7], (not to be confused with CW pulses, discussed earlier). CW radar is usually limited in its transmitted power by interference between the transmitter and receiver, which must operate simultaneously. This limits their sensitivity and range. CW waveforms are commonly used in police speed-measurement radar and intrusion-detection radar.

CW radar is well suited to measuring target Doppler shift, from which radial velocity may be calculated (see Sections 1.2 and 8.3). Target range may be measured by changing the transmitter frequency linearly with time, called frequency-modulated continuous-wave (FMCW). The target range is then calculated from the difference between the transmitted and received frequencies.

2.5 Signal Processing Techniques

Signal processing is used in the radar receiver to extract information from the returned radar signal. Target detection, tracking, and measurement were discussed in Section 1.2. These are discussed in more detail, and performance models are presented, in Chapters 6 and 8. Signal processing to mitigate the effects of electronic countermeasures, including radar jamming are discussed in Chapter 10.

Additional signal processing techniques often employed include moving-target indication (MTI), pulse-Doppler, and synthetic-aperture radar (SAR) processing. These are briefly discussed below. Further analysis of these techniques and their applications in airborne and space-based radar is given in Chapter 11.

MTI is often used by terrestrial radar to separate moving targets of interest (e.g., aircraft) from background returns (e.g., from terrain and the ocean), called radar clutter. This is done using the Doppler-frequency shift of the received signals. The clutter has only small radial velocity components due to the motion of vegetation or waves, while moving targets are likely to have larger radial velocities. The MTI filters out the received signal frequencies that have low Doppler-frequency shift and correspond to the clutter. This is done by processing the phases of two or more successive pulses in a canceller [1, pp. 101–117].

Limitations of MTI processing result from the stability of the radar components and the velocity spread of the clutter. Targets traveling tangentially to the radar will

have little or no radial-velocity component, and will be cancelled along with the clutter. MTI processors may be simply characterized by the minimum detectable target velocity (MDV), and the clutter cancellation ratio (see Sections 9.1 and 9.2).

In pulse-Doppler radar [8], a coherent burst of pulses is transmitted. Coherency implies that the phases of the individual pulses are derived from a continuous stable signal, that is also used in processing the received signals. The returned signals are processed using a Fourier-transform-type algorithm to divide the received signal into a series of spectral bands. Those bands that correspond to the Doppler shift of clutter may be rejected, and those that correspond to potential targets may be examined for detections. The pulse-Doppler band in which a target is detected also gives a measure of its Doppler-frequency shift, and hence its radial velocity.

Pulse-Doppler processing is often used in airborne and space-based radar (see Section 11.3). With these moving platforms, the radar returns from terrestrial clutter may have a large Doppler frequency spread, due to the spread of angles at which the clutter is viewed, both in the main radar beam and through the antenna sidelobes (see Section 11.2). Thus, cancellation of the clutter by MTI techniques is often not effective. Pulse-Doppler processing, however, allows rejection of bands having large clutter components, detection of targets in bands clear of clutter returns, and setting of detection thresholds over the clutter signal return in bands, where target returns may exceed clutter returns. Pulse-Doppler processing may be simply characterized by the velocity resolution corresponding to the processed Doppler frequency bands, and the suppression of clutter not in a band.

Synthetic-aperture radar (SAR) processing [9] is used by moving radar (e.g., those on aircraft or satellite platforms), to produce high-resolution terrain maps and images of targets (see Section 11.6). Radar may achieve good range resolution by using short pulses or employing pulse compression. For example, a signal bandwidth of 100 MHz may provide a range resolution of 1.5m. However, with conventional (real-aperture) processing, the radar beamwidth is rarely small enough to provide cross-range target resolution useful for ground mapping. For example, with a beamwidth of 10 mR (0.57°), cross-range resolution at a range of 50 km is 500m.

With SAR, radar data taken while the radar travels a significant distance is processed to produce the effect of an aperture dimension equal to the distance traveled. For example, with an aircraft velocity of 250 m/s and a SAR processing time of 2 seconds, the synthetic aperture is 500m long. With an X-band wavelength of 0.03m, the cross-range resolution at 50 km range is 1.5m. An SAR radar processor may be simply characterized by the resolution it provides, 1.5m in the above example.

SAR processing is based on Fourier transforms, but corrections are made for factors such as changes in target range and platform path perturbations during the processing time. In a strip-mapping mode, a SAR collects and processes data at a fixed angle relative to the platform as it moves along its path. This technique, often referred to as side-looking radar, generates a continuous strip map. In a spotlight SAR, the radar beam is scanned relative to the platform to keep the desired target region in coverage. This allows increased processing time, and hence greater angular resolution for the region imaged.

Some modern airborne multifunction radars may employ both conventional radar modes using MTI and pulse Doppler to detect moving targets, and SAR modes to image terrain, as discussed in Chapter 11.

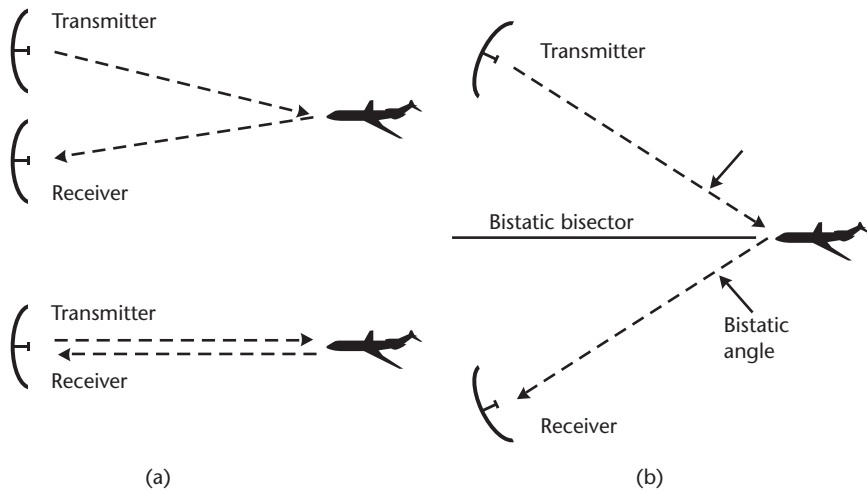


Figure 2.4 Illustrations of (a) monostatic and (b) bistatic radar geometry.

2.6 Monostatic and Bistatic Radar

Most radar has its transmitting and receiving antennas in essentially the same location, as illustrated in Figure 2.4(a). This is referred to as monostatic radar. Radars often use the same antennas for transmitting and receiving, and so is monostatic by definition. Other radars have their transmitting and receiving antennas close together, compared with the target range. These generally have the same characteristics as monostatic radar, and are included in that class. Advantages of monostatic radar are the common use of radar hardware at a single site, illumination of the same region of space by the transmit and receive antennas, and simplified radar coordination.

With bistatic radar, the transmitting and receiving antennas are separated, as shown in Figure 2.4(b). This may be done to avoid interference between the transmitted and received signals; to allow multiple receivers to operate with a single transmitter; to permit light, nonradiating receivers to operate with the heavy transmitters located elsewhere; to take advantage of the large bistatic RCS characteristics of targets (see Section 3.5); or to exploit bistatic geometry. An example of the latter is in intrusion-detection radar, where the region protected lies between the transmitting and receiving antennas. With bistatic radar, it is usually necessary to coordinate operation of the transmitting and receiving sites, to provide multiple receive beams to cover the transmitted beam region, and to take the bistatic geometry into account in the signal processing.

2.7 Problems

The following problems are provided to assist in reviewing this chapter and to ensure a basic understanding of the material. Solutions to these problems are given in Appendix E, Section E.2.

1. What is the range to the radar horizon from a radar having a height of 20m above a smooth earth?

2. What is the range if the height in the above example is increased to 2,000m?
3. Are signal losses from the atmosphere and rain more severe at higher or lower radar frequencies?
4. What type of reflector antenna is well suited for tracking a single target?
5. What is the maximum range that a radar 25m above a smooth earth can observe a target having an altitude of 5 km?
6. At what radar frequencies can the signal be distorted by the ionosphere?
7. What type of radar antenna allows rapid electronic scanning of the radar beam?

References

- [1] Skolnik, M. I., *Introduction to Radar Systems, 2nd Ed.*, New York: McGraw-Hill, 1980.
- [2] Morchin, W. C., *Airborne Early Warning Radar*, Norwood, MA: Artech House, 1990.
- [3] Brookner, E., "Trends in Radar Systems and Technology," In *Aspects of Modern Radar*, E. Brookner, (ed.), Norwood, MA: Artech House, 1988.
- [4] Cantafio, L. J., "Space-Based Radar Systems," Chapter 1 in *Space-Based Radar Handbook*, L. J. Cantafio, (ed.), Norwood, MA, Artech House: 1989.
- [5] Chesron, T. C., and Frank, J., "Phased Array Antennas," Chapter 7 in *Radar Handbook, 2nd Ed.*, M. I. Skolnik, (ed.), New York: McGraw-Hill, 1990.
- [6] Deley, G. D., "Waveform Design." In *Radar Handbook*, M. I. Skolnik, (ed.), New York: McGraw-Hill, 1970.
- [7] Saunders, W. K., "CW and FM Radar," Chapter 14 in *Radar Handbook, 2nd Ed.*, M. I. Skolnik (ed.), New York: McGraw-Hill, 1990.
- [8] Morris, G. V., *Airborne Pulsed Doppler Radar*, Norwood, MA: Artech House, 1988.
- [9] Hovanessian, S. A., *Introduction to Synthetic Array and Imaging Radars*, Dedham, MA: Artech House, 1980.

Selected Bibliography

A general discussion of radar configurations is given by Skolnik in his original 1962 book, which was updated in 1980. Skolnik's *Radar Handbook*, first published in 1970, and updated in 1989, provides more detail on airborne and ground-based radar, antennas, waveform and signal-processing techniques, and bistatic radar.

Further information on airborne radar, including pulse-Doppler operating modes, can be found in Morchin, Morris, and Brookner. SBR is addressed in Cantafio. Design and operation of SAR is treated in Hovanessian.

Brookner, E., *Aspects of Modern Radar*, Norwood, MA: Artech House, 1988.

Cantafio, L. J., ed., *Space-Based Radar Handbook*, Norwood, MA: Artech House, 1989.

Hovanessian, S. A., *Introduction to Synthetic Array and Imaging Radars*, Dedham, MA: Artech House, 1980.

Morchin, W. C., *Airborne Early Warning Radar*, Norwood, MA: Artech House, 1990.

Morris, G. V., *Airborne Pulsed Doppler Radar*, Norwood, MA: Artech House, 1988.

Skolnik, M. I., *Introduction to Radar Systems*, New York: McGraw-Hill, 1962.

Skolnik, M. I., *Introduction to Radar Systems*, 2nd ed., New York: McGraw-Hill, 1980.

Skolnik, M. I., (ed.), *Radar Handbook*, New York: McGraw-Hill, 1970.

Skolnik, M. I., (ed.), *Radar Handbook*, 2nd ed., New York: McGraw-Hill: 1989.

Radar Analysis Parameters

This chapter enables the reader to:

- Understand and use the parameters for characterizing radar transmitters, antennas, receivers and signal processors;
- Compare the characteristics of phased-array antenna configurations including full-field-of-view (FFOV) arrays, limited-field-of-view (LFOV) arrays, and thinned arrays;
- Characterize target RCS in terms of magnitude, fluctuation sources, and Swerling statistical fluctuation models.

Analysis and modeling of radar at the system level utilizes parameters of the radar components and operating modes, and of the environment in which the radar operates. Parameters of the major radar components and of radar targets are described in this chapter. Parameters of measurement error sources and the environment are described in Chapters 8 and 9 respectively. Further details on the parameters and their use in models is given with the model development in Chapters 5 through 11. A list of symbols used for the parameters is provided in Appendix A.

3.1 Transmitter

A key characteristic of radar transmitters is the RF power generated. This is usually characterized by the peak and average RF power output:

P_p = transmitter peak RF power

P_A = transmitter average RF power

The RF pulse duration that a transmitter is capable of generating is also important. The peak power may be maintained for some period, usually determined by the heating of small components of the transmitter tube or solid-state device used to generate the power. This period is usually described by a maximum pulse duration:

τ_M = maximum transmitter pulse duration

The resulting maximum pulse energy is then:

$$E_M = P_p \tau_M \quad (3.1)$$

where:

E_M = maximum transmitter pulse energy

The average transmitted power is usually limited by the prime power available to the radar, the heat removal from the larger transmitter components, and the capability for scheduling radar transmissions. The ratio of average to peak power is called the transmitter duty cycle:

$$DC = \frac{P_A}{P_p} \quad (3.2)$$

where:

DC = transmitter duty cycle

Tubes used in pulsed-radar transmitters (e.g., klystrons, traveling-wave tubes-TWTs), have the capability for high peak powers, but often the small thermal mass of tube elements, particularly the anode, limits the maximum pulse energy. Their duty cycle usually ranges from about 1% to 10%.

Solid-state devices are usually limited in their power capabilities by heating in the semiconductor junctions. Since the thermal mass of these junctions is very small, the peak and average power of solid-state devices are often nearly the same. Thus, they may operate at high duty cycles, and the duty cycle of solid-state radar is often limited by the ability to schedule transmitting and receiving times to 25% to 35%.

The efficiency of a radar transmitter is defined as the ratio of the average RF power produced to the prime power supplied to the transmitter:

$$\eta_T = \frac{P_A}{P_{PT}} \quad (3.3)$$

where:

η_T = transmitter efficiency

P_{PT} = prime power supplied to the transmitter

This parameter characterizes the efficiency of the transmitter in converting prime power into RF power. Values of transmitter efficiency range from about 15% to 35%.

The transmitter power levels are usually specified at the transmitter output. Tube transmitters often use a single tube to generate the RF power for a radar, but in other cases the outputs of two or more tubes are combined to produce the power needed. Solid-state transmitters for large radar combine the outputs from several solid-state devices. When the power is combined in the transmitter, the resulting transmitter output power is usually specified. This output power is normally less than the sum of the powers generated by the individual devices, due to losses in the combining network. The combining losses are usually included in the transmitter efficiency. In phased-array radar (and some other hybrid designs), individual transmitters may directly drive antenna radiating elements. In these cases, the transmitter power is usually specified as the sum of the powers generated by the individual transmitters (see Section 5.2).

The RF power radiated by the antenna is usually less than that generated by the transmitter, due to losses in the microwave circuits between the transmitter and the antenna, and losses in the antenna:

L_{MT} = transmit microwave losses between the transmitter and the antenna

L_{AT} = transmit antenna losses (includes ohmic losses only; (see Section 3.2)

The overall efficiency of the radar is the ratio of the RF power radiated from the antenna to the prime power supplied to the entire radar. This is less than the transmitter efficiency due to power used by other radar components, overhead (such as cooling), and RF losses following the transmitter:

$$\eta_R = \frac{P_A}{P_{PR} L_{MT} L_{AT}} \quad (3.4)$$

where:

η_R = overall radar efficiency

P_{PR} = prime power supplied to the radar

Overall radar efficiency values are typically 5% to 15%. Note that the portion of the prime power that is not radiated as RF power creates heat in the radar. Cooling mechanisms must be provided for removing this heat.

Most modern radar uses coherent transmitters. This means that the phases of the transmitted waveforms are derived from a stable reference signal that is also used by the receiver. This allows the received signals to be processed coherently to measure Doppler-frequency shift (see Section 1.2), to cancel returns from stationary clutter (see Sections 2.5, 9.1 and 9.2), and to perform coherent pulse integration (see Section 5.4). The phase stability of the transmitter determines the degree to which these functions may be performed, and the time interval that may be used. Modern transmitters usually may be designed to provide the stability needed for the functions to be performed. Some older radars were limited in the coherent processing that could be employed, or were not coherent at all [1, pp. 4.25–4.31]

3.2 Antennas

The antenna characteristics of principal interest relate to the far-field radiation pattern produced by the antenna. The most important characteristics are beamwidth, gain, and sidelobe levels. These are illustrated in Figure 3.1, which shows the antenna radiation pattern for a rectangular aperture having uniform illumination in amplitude and phase.

The antenna pattern is usually defined in the far field of the antenna. This is a range at which the rays from the antenna are essentially parallel (also called the Fraunhofer region). The range at which the far field begins is usually given by:

$$R_F = \frac{2w^2}{\lambda} \quad (3.5)$$

where:

R_F = far-field range

w = the antenna dimension in the plane in which the pattern is measured

λ = radar wavelength, given by:

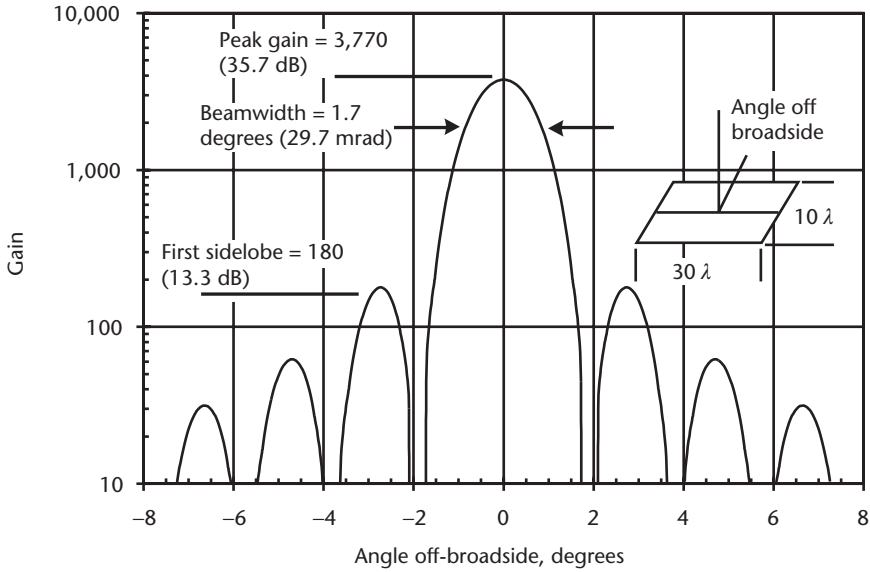


Figure 3.1 Far-field antenna pattern for an aperture with uniform illumination.

$$\lambda = \frac{c}{f} \quad (3.6)$$

where:

c = electromagnetic propagation velocity (approximately 3×10^8 m/s)

f = radar frequency

At this range, the antenna gain (see below), is 99% of that at an infinite range [2, p. 229].

The beamwidth is usually defined at a level of half the power of the beam peak, referred to as the 3-dB beamwidth:

θ = antenna half-power (3-dB) beamwidth

Note that the first pattern null is separated from the beam peak by an angle approximately equal to the beamwidth.

The antenna beamwidth is related to the antenna size, w , and radar wavelength by:

$$\theta = \frac{k_A \lambda}{w} \quad (3.7)$$

where:

k_A = antenna beamwidth coefficient

The antenna beamwidth coefficient, k_A , is usually near unity, and depends on the antenna illumination pattern, as discussed below.

The antenna beamwidth is usually specified in two orthogonal planes, often referred to as the x and y planes, where the y plane is vertical:

θ_y = beamwidth in y plane (vertical)

θ_x = beamwidth in x plane (normal to the y plane)

For antennas with a horizontal (or near-horizontal), beam direction, these correspond (or approximately correspond), to elevation-angle and azimuth coordinates, and these terms are often used to characterize radar beamwidths:

θ_E = beamwidth in the elevation plane

θ_A = beamwidth in the azimuth plane

The beamwidths are calculated using the antenna dimensions in the corresponding planes. For square or circular antennas, the two orthogonal beamwidths are equal; for rectangular or oval shapes, they are unequal. Note that for rotating surveillance radar, the antenna contour and illumination are often designed to produce a fan-shaped beam whose elevation beamwidth may be larger than would be calculated from the vertical antenna dimension (see Sections 2.3 and 7.2).

The antenna mainbeam gain is defined as the maximum radiation intensity divided by the radiation intensity from a lossless isotropic source:

G = antenna mainbeam gain

The gain differs from the antenna directivity, which is defined as the maximum radiation intensity divided by the average radiation intensity, by allowing antenna losses to be included in the gain term.

The effective aperture area determines the received power collected by the antenna:

A = effective antenna aperture area

The effective aperture area is related to the gain by:

$$A = \frac{G\lambda^2}{4\pi} \quad (3.8)$$

Conversely:

$$G = \frac{4\pi A}{\lambda^2} \quad (3.9)$$

The gain is a function of the physical antenna size, the radar wavelength, and antenna losses:

$$G = \frac{4\pi A_A}{\lambda^2 L_A L_E} \quad (3.10)$$

where:

A_A = antenna area

L_A = antenna ohmic losses

L_E = antenna losses due to aperture efficiency

The total antenna losses include ohmic losses in the antenna, L_A , and losses in aperture efficiency due to aperture weighting and spillover, L_E , (discussed below).

These losses may be included in the specified gain and aperture-area values, or they may be specified separately in the antenna loss terms that are applied to these values. The effective aperture area is given by:

$$A = \frac{A_A}{L_A L_E} \quad (3.11)$$

The antenna gain may be estimated from the beamwidths it produces by [3, p. 334]:

$$G \approx \frac{10.75}{\theta_x \theta_y L_A} \quad (3.12)$$

This expression is a good approximation for reflector antennas and filled phased-array apertures (see discussion of filled and thinned phased arrays in Section 3.3).

Many radars use the same antenna to transmit and receive. These radars use microwave switching devices to switch the antenna between the transmitter and receiver. When the gains or aperture areas differ between transmit and receive, gain and aperture area may be specified for each:

G_T = transmit antenna gain

G_R = receive antenna gain

A_T = transmit antenna effective aperture area

A_R = receive antenna effective aperture area

Similarly, if antenna losses are different for transmit and receive, they are designated:

L_{AT} = transmit antenna ohmic losses

L_{AR} = receive antenna ohmic losses

L_{ET} = transmit antenna losses due to aperture efficiency

L_{ER} = receive antenna losses due to aperture efficiency

Antenna sidelobe levels are defined relative to the beam peak:

SL = antenna sidelobe level, relative to the mainbeam gain

Antenna gain and sidelobe levels are often specified in decibels. Gain is expressed in decibels relative to isotropic (dBi), which is the gain of a lossless source radiating uniformly over 4π steradians. Sidelobe levels are usually expressed in decibels relative to the gain (negative values). Sometimes sidelobe levels are expressed in decibels relative to isotropic, which may be found from:

$$SL(dBi) = G(dB) + SL(dB) \quad (3.13)$$

The antenna pattern shown in Figure 3.1 is for a rectangular antenna having uniform amplitude and phase illumination. This means that the RF current density and signal phase are constant across the antenna face. The level of the first sidelobe in the principal angular coordinates (those parallel to the edges of the rectangle), for such antennas is -13.3 dB relative to the beam peak. For circular antennas with uni-

form illumination, the first sidelobe is -17.6 dB relative to the mainbeam [2, pp. 230–233]. The sidelobe levels decrease with distance from the mainbeam.

Lower close-in sidelobe levels are often desired to allow viewing of closely-spaced targets of different sizes or to reject interfering clutter or jamming signals. Close-in sidelobes, those within a few beamwidths of the mainbeam, may be reduced by varying the RF current density, called aperture illumination, across the antenna face, providing lower current density near the edge of the antenna than at the center. This is called tapering or weighting the antenna illumination. In general, the power density pattern in the far field of the antenna is given by a Fourier-transform function of the aperture illumination function [2, pp. 229].

$$G(\psi) = \left[\int a(x) \exp\left(-j2\pi \frac{x}{\lambda} \sin(\psi)\right) dx \right]^2 \quad (3.14)$$

where:

ψ = angle from the antenna mainbeam axis

$a(x)$ = the antenna current density as a function of distance from the antenna center

The current density $a(x)$ is a complex quantity, and a positive phase in $a(x)$ implies a phase retarded, as by a phase shifter. The relationship in (3.14) also applies to the angular dependence of the effective aperture area.

By carefully controlling the illumination weighting, the close-in sidelobes may be reduced to -40 dB or lower. This improvement in close-in sidelobes comes at the cost of reduced antenna efficiency, reduced the gain, and increased beamwidth. For example, a \cos^3 illumination weighting produces a maximum sidelobe level of -39 dB, but the antenna efficiency is reduced from 1.0 (for uniform illumination) to 0.57. This corresponds to an aperture efficiency loss, $L_E = 2.43$ dB. The antenna beamwidth coefficient, k_A , increases from 0.89 to 1.66, which increases the beamwidth by 87% from that of an antenna with uniform illumination.

When aperture weighting is applied in both antenna dimensions, the aperture efficiency and efficiency loss are the product of the factors for the two weighting functions used. The aperture efficiency loss in decibels is then the sum of the aperture efficiency losses, in decibels, for the two weighting functions used.

Details of the antenna patterns resulting from a number of aperture illumination weighting functions are given in [4, pp. 251–333]. The first sidelobe levels, beamwidth coefficients, and aperture efficiencies of several common antenna illumination weighting functions are given in Table 3.1. With the cosine weighting functions, the sidelobes decrease with angle from the mainbeam, while with the Taylor weighting functions, the close-in sidelobes remain about constant at the levels given.

Sidelobes may also be produced in reflector antennas by energy spillover from the feedhorn illuminating the reflector, and by reflections off structural elements. These reduce the aperture efficiency and increase the aperture-efficiency losses.

When separate antennas are used to transmit and receive, they may employ different illumination tapers. The transmit antenna in such cases often uses uniform illumination in order to maximize its radiation efficiency. The needed taper is applied to the receive antenna. Phased-array antennas are often designed to use dif-

Table 3.1 Antenna Characteristics for Common Aperture Illumination Weighting Functions

<i>Aperture Illumination Weighting</i>	<i>Aperture Efficiency</i>	<i>Aperture Efficiency Loss (dB)</i>	<i>Antenna Beamwidth Coefficient (k_A)</i>	<i>Level of First Sidelobe (dB)</i>
Uniform rectangular	1.0	0	0.89	-13.3
Uniform circular	1.0	0	1.02	-17.6
Cos	0.80	0.96	1.19	-23.0
Cos ²	0.66	1.80	1.44	-31.5
Cos ³	0.57	2.43	1.66	-39.0
Cos ⁴	0.51	2.93	1.85	-47.0
Taylor 20 dB	0.95	0.22	0.98	-20.9
Taylor 30 dB	0.85	0.71	1.12	-30.9
Taylor 40 dB	0.76	1.17	1.25	-40.9

ferent illumination functions for transmit and receive. Reflector antennas that use feedhorns and perform both transmit and receive functions usually are configured to use the same illumination pattern for both functions. In these cases, the taper is a compromise between efficiency and sidelobe control.

For most aperture illumination functions, the sidelobes decrease significantly for angles well away from the mainbeam. In practice, these far-out sidelobe levels are determined by the precision of the antenna shape and the illumination pattern [4, pp. 7.37–7.49]

Older radars, and some current rotating surveillance radars, determine the angular position of a target by observing the receive signal amplitude for successive pulses as the beam is scanned past the target. This technique is subject to measurement errors if other factors, such as target RCS changes (see Section 3.5), cause pulse-to-pulse fluctuations of the signal amplitude. Monopulse antennas are configured to avoid this problem by measuring target angular position with a single pulse.

Monopulse radar employs antenna feeds, producing a pattern that is the difference of two beams that are offset in angle slightly to either side of the main radar beam. The difference-pattern signal is processed in a separate receiver channel, and compared with the signal from the mainbeam channel, often called the sum channel, to determine the angle of the target from the center of the sum beam. This allows the angle of the target to be accurately measured from the return of a single pulse (see Section 8.2). An example of an antenna difference pattern, normalized by dividing by the sum-pattern maximum, is shown in Figure 3.2.

The angular measurement sensitivity produced by the difference pattern is determined by the slope of the difference pattern near the beam center, as illustrated in Figure 3.2:

$$k_M = \text{monopulse pattern difference slope}$$

The value of k_M is typically about 1.6, measured by the ratio of sum and difference channel voltages divided by the normalized angle off beam center [5, pp. 400–409]. Difference patterns for a variety of monopulse-antenna weighting functions are given in [3, pp. 251–333].

Monopulse measurement is most accurate when the target is on the beam axis and the monopulse difference signal is zero. Off-axis angular measurements use the

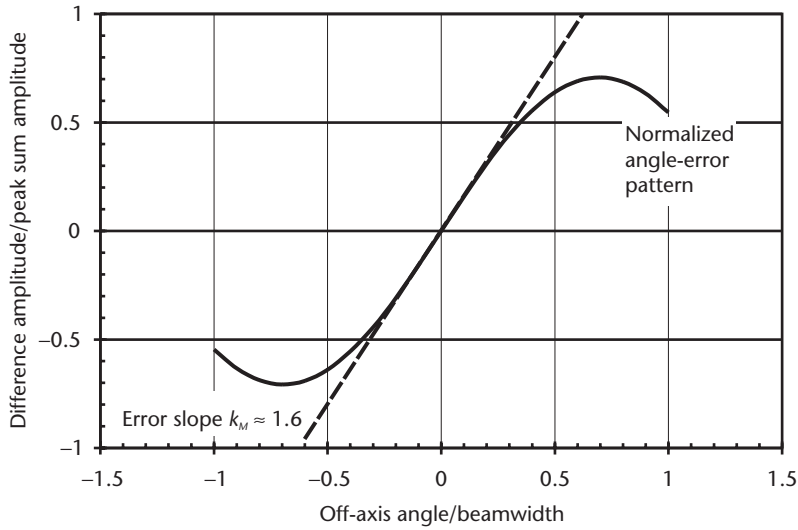


Figure 3.2 Normalized antenna difference pattern for a monopulse radar.

calibrated value of the error slope to relate the normalized difference signal amplitude to the off-axis angle, as shown in Figure 3.2.

To measure target position in two angular coordinates requires the use of two difference patterns. In reflector antennas, these are often produced by a four-horn monopulse feed, although other feed configurations are used. Three receiver channels are needed to process the sum and two difference signals (see Section 3.4).

The polarization of the transmitted RF signal is defined as the direction of its electric field vector. Horizontal and vertical linear polarizations are often used. Horizontal polarization is frequently preferred for surface-based search radar because it produces less clutter return and extends the range by forward scattering from surface. Vertical polarization is preferred for tracking radar and other radar that measure elevation angle because it reduces forward scatter and the resulting multipath errors in the measurement of elevation angle (see Section 9.1).

Circular polarizations (right-circular and left-circular) are sometimes employed. These may be used to cancel clutter returns from rain and minimize the effects of transmission through the ionosphere (see Sections 9.2 and 9.4), [2, pp. 504–506]. Transmitting and receiving antennas are sometimes switched from one polarization to another. Receiving antennas may be configured to simultaneously receive two orthogonal polarizations, using two receiver channels to process the signals.

Another loss associated with the antenna is the beamshape loss:

$$L_{BS} = \text{antenna beamshape loss}$$

This loss results when the peak gain is used to characterize the antenna, and the target is not at the peak of the beam. The beamshape loss is often used in performance calculations of radar search modes, where the target may be located anywhere in the beam (see Chapter 7). When tracking, the target is usually assumed to be near the beam center, and the beamshape loss is neglected.

Additional antenna parameters are associated with the errors and biases in measuring angular coordinates. These are defined and discussed in Chapter 8.

3.3 Phased-Array Antennas

Phased-array antennas offer the advantage that the beam may be electronically scanned almost instantly. This allows search, tracking and other radar functions to be interlaced, and many targets to be observed near-simultaneously. Radar that employ phased arrays often have a large repertoire of waveforms, and operate under computer control.

Phased-array antennas may employ a variety of configurations. The most common is an antenna made of a planar array of uniformly-spaced identical radiating elements. The gain of such phased-array antennas is the sum of the gains of the individual elements, and the aperture area is the sum of the aperture areas of the individual elements.

For an array of identical radiating elements, corresponding to a uniformly-illuminated array, the array-antenna gain and aperture area are given by:

$$G = n_E G_E \quad (3.15)$$

$$A = n_E A_E \quad (3.16)$$

where:

n_E = number of radiating elements in a phased-array antenna face

G_E = gain of phased-array element in the array

A_E = effective aperture area of a phased-array element in the array

Note that G_E and A_E are the effective values of element gain and aperture area when the element is integrated into the array, which may be different than the parameters of an isolated element.

Phased-array radars may employ separate arrays for transmit and receive. Then, the parameters in (3.15) and (3.16) are defined separately for the transmit and receive arrays. Phased-array radars that use the same array for both transmit and receive are often configured with separate transmit and receive tapers, as discussed in Section 3.2. In many phased arrays, receiving amplifiers are connected to each antenna element, and the receive array taper is applied following these amplifiers. The illumination pattern of phased arrays often may be precisely controlled to produce very low close-in sidelobes.

Planar phased-array antenna gain, effective aperture area, and beamwidth are usually defined for beams generated in a direction normal to the array face. This is called the broadside or on-axis direction. When the beam of a phased array is scanned off the broadside direction, the beam is broadened and the array gain and effective aperture area are reduced, relative to the values on broadside.

The gain and effective aperture area are reduced by beam scanning due to two factors:

- The reduced projected array area in the beam direction. This reduction is given by:

$$G_{\varphi} = G \cos \varphi \quad (3.17)$$

$$A_{\varphi} = A \cos \varphi \quad (3.18)$$

where:

φ = scan angle off array broadside

G_{φ} = array gain at scan angle φ

A_{φ} = array effective aperture area at scan angle φ

- A further reduction of gain and effective aperture area of the individual phased-array elements at off-broadside angles. This reduction depends on the element design, and is often smaller than the other factor.

The combined impact of these two factors is characterized by an off-broadside scan loss. This is usually specified as a two-way loss, that is the product of the transmit and receive scan losses:

L_s = two-way off-broadside scan loss

$$L_s = \left(\frac{A}{A_{\varphi}} \right)^2 = \left(\frac{G}{G_{\varphi}} \right)^2 \quad (3.19)$$

The beamwidth produced by a phased-array antenna increases with the scan angle off broadside. This is a consequence of the reduced projected aperture area in the beam direction:

$$\theta_{\varphi} = \frac{\theta_B}{\cos \varphi} \quad (3.20)$$

where:

θ_B = phased-array beamwidth on broadside

θ_{φ} = phased-array beamwidth at scan angle φ

The effects of phased-array gain reduction and beam broadening for scan angles off broadside are illustrated in Figure 3.3.

The maximum off-broadside scan angles of phased arrays are usually limited to about 60 degrees by the acceptable scan loss and by the capability of the radiating elements in the array. A phased array having this capability is often called a full-field-of-view (FFOV)-phased array. As pointed out in Section 2.3, a radar needs three or more such phased-array faces to provide hemispheric coverage.

FFOV phased arrays typically employ dipoles or simple feed horns as radiating elements. The elements are spaced by 0.6λ or less in order to avoid creating spurious grating lobes in the antenna pattern when scanning to large angles. Arrays of these elements typically have a two-way scan loss that is given by [4, pp. 7.10–7.17]

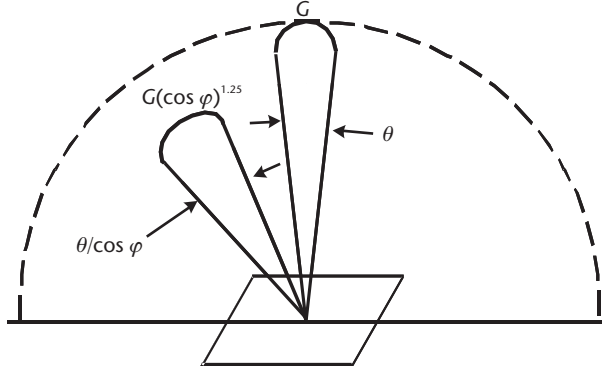


Figure 3.3 Illustration of phased-array gain reduction and beam broadening with off-broadside scan.

$$L_s \approx \cos^{-2.5} \varphi \quad (\text{for FFOV arrays}) \quad (3.21)$$

Note that the total off-broadside scan angle φ can be found from the scan angles in two orthogonal planes, such as the x and y planes, by:

$$\cos \varphi = \cos \varphi_x \cos \varphi_y \quad (3.22)$$

where:

φ_x = off-broadside scan angle in the x plane

φ_y = off-broadside scan angle in the y plane

Thus, the scan loss is the product of the losses calculated for the scan angles in the two orthogonal planes:

$$L_s = L_{sx} L_{sy} \quad (\text{for FFOV arrays}) \quad (3.23)$$

where:

L_{sx} = scan loss for off-broadside scan in the x plane

L_{sy} = scan loss for off-broadside scan in the y plane

When the x -plane and y -plane scan losses are given in decibels, the total scan loss in decibels is the sum of these values.

Similarly, the beam broadening may be calculated for scan angles in two orthogonal planes:

$$\theta_{\varphi_x} = \frac{\theta_B}{\cos \varphi_x} \quad (3.24)$$

$$\theta_{\varphi_y} = \frac{\theta_B}{\cos \varphi_y} \quad (3.25)$$

where:

θ_{φ_x} = phased-array beamwidth in the x plane at scan angle φ_x

θ_{φ_y} = phased-array beamwidth in the y plane at scan angle φ_y

θ_{B_x} = phased-array beamwidth in the x plane on broadside

θ_{B_y} = phased-array beamwidth in the y plane on broadside

Some phased arrays do not have radiating elements completely covering the array face. These are referred to as thinned-phased arrays. Their gain and aperture area may be considerably less than would be expected from the array size, but they are correctly calculated by (3.15) and (3.16), when the elements are identical. Note that (3.12) may not be used to calculate gain of thinned arrays.

Thinned-array beamwidths are found using (3.7). A thinned array may produce the same beamwidth as a filled array, but using far fewer elements, often resulting in cost saving. Thinning that is greater at the edges of the array than at the center of the array produces the effect of aperture illumination weighting. The far-out sidelobe levels of thinned arrays are increased to approximately $1/(1 - F)$, where F is the fraction of active elements in the array. Thus, ultralow sidelobes are not provided by thinned arrays.

Phased arrays configured for electronic scan angles significantly less than 60 degrees are termed limited-field-of-view (LFOV) phased arrays. These phased arrays may use a smaller number of radiating elements than required for FFOV arrays, providing that the radiating elements have a degree of directivity to suppress spurious grating lobes that lie outside the angular region of the scan. Such phased arrays may provide the same beamwidth gain and aperture area as FFOV arrays of the same size.

The phased-array elements must be spaced closely enough that only a single mainbeam is generated for any beam position in the FFOV. The acceptable element spacing is [6, p. 9-6]:

$$d \leq \frac{0.5\lambda}{\sin \varphi_M} \quad (3.26)$$

where:

d = element spacing in the array

φ_M = maximum off-broadside scan angle

Somewhat greater element spacing may be used if the grating lobes need not be completely suppressed.

If the elements in an LFOV phased-array antenna are designed to provide uniform illumination over the element, the resulting scan loss is approximately given by:

$$L_S = \left[\frac{\sin\left(\frac{\pi d}{\lambda} \sin \varphi\right)}{\frac{\pi d}{\lambda} \sin \varphi} \right]^{-4} \quad (\text{for LFOV arrays}) \quad (3.27)$$

This may be approximated in the range of interest by a simpler expression, which is similar in form to that used for FFOV arrays:

$$L_s \approx \cos^{-8} \left(\frac{121 d \phi}{\lambda} \right) \quad (\text{for LFOV arrays, valid for } L_s \leq 15 \text{ dB}) \quad (3.28)$$

A comparison of the properties of filled FFOV arrays, thinned FFOV arrays and LFOV arrays, all having beamwidths of 4 degrees, is shown in Table 3.2. The filled and thinned FFOV arrays both have element spacing of 0.6λ , and provide ± 60 degrees scan coverage. The thinned array has 10 percent of the number of elements as the filled array, and the resulting gain is 10 dB less. The LFOV array also has 10 percent of the number of elements as the filled FFOV array. However, these elements are more widely spaced and have higher element gain, resulting in array gain equal to that of the filled FFOV array. The scan coverage of the LFOV is only ± 15 degrees.

The orientation of a ground-based phased-array antenna is defined by the broadside elevation and azimuth angles:

ϕ_{BE} = array broadside elevation angle

ϕ_{BA} = array broadside azimuth angle

When the y scan direction is defined in the vertical plane, the beam elevation and azimuth angles are given by:

$$\phi_E = (\phi_{BE} + \varphi_y) \cos \varphi_x \quad (3.29)$$

$$\phi_A = \phi_{BA} + \varphi_s \cos \phi_{BE} \quad (3.30)$$

where:

ϕ_E = beam elevation angle

ϕ_A = beam azimuth angle

Ground-based phased arrays often have broadside elevations of 15 to 20 degrees, and the error in neglecting the cosine term in (3.30) for these radars is small.

In phased-array antennas where the elements are fed in parallel with equal line-lengths, the bandwidth of signals that the array may transmit and receive without significant frequency dispersion loss is limited to [4, pp. 7.49–7.58]:

$$B_A \approx \frac{c}{w \sin \varphi} \quad (3.31)$$

where:

B_A = phased-array bandwidth

Table 3.2 Phased-Array Antenna Comparison

<i>Parameter</i>	<i>Filled FFOV</i>	<i>Thinned FFOV</i>	<i>LFOV</i>
Element spacing	0.6λ	0.6λ	1.9λ
Element gain	5 dB	5 dB	15 dB
Number of elements	1,000	100	100
Array gain	35 dB	25 dB	35 dB
Beamwidth	4 degrees	4 degrees	4 degrees
Maximum scan angle	± 60 degrees	± 60 degrees	± 15 degrees
Sidelobe level (isotropic)	-35 dB	-25 dB	-35 dB

This limitation results from the differential time delay for the signal reaching various points on the array. It may be mitigated by using time-delay steering of the elements, or of groups of elements. Conversely, this effect may be exaggerated by adding fixed time delays between the elements, which allows steering of the beam by changing the frequency of narrowband signals.

3.4 Receiver and Signal Processor

The receiver parameter that most affects radar performance is the system noise temperature:

T_s = radar system noise temperature

This parameter directly affects the background noise power that competes with the received signals, and affects target detection and measurement of target properties:

$$P_N = k T_s B_R \quad (3.32)$$

where:

P_N = power of background noise in the radar receiver

k = Boltzmann's constant ($1.38 \cdot 10^{-23}$ J/K)

B_R = receiver bandwidth

The following factors contribute to the system noise temperature:

- The background environmental temperature viewed by the antenna. For ground-based radar, this is a combination of ground temperature (usually taken as 290K), and sky temperature (10 to 100K, depending on the elevation angle, for frequencies between 1 and 10 GHz) [2, pp. 461–464]. This temperature contribution is reduced by the receive antenna and receive microwave losses.
- Noise generated by the receive antenna ohmic losses and the receive microwave losses themselves. These elements are usually assumed to be at 290K, and their noise contribution is approximately given by $290(L_{AR} L_{MR} - 1)$

where:

L_{MR} = receive microwave losses

L_{AR} = receive antenna ohmic losses

(This calculation neglects the reduction in the noise from antenna ohmic loss caused by the microwave loss.)

- Receiver noise. This noise is usually dominated by the noise from the first stage of the receiver, since this is amplified and is likely to exceed the noise levels in later stages of the receiver. The receiver noise temperature may be specified, or a receiver noise figure, F_R (sometimes called the noise factor), may be specified:

T_R = receiver noise temperature

F_R = receiver noise figure

These are related by:

$$T_R = 290(F_R - 1) \quad (3.33)$$

Note that the receiver noise temperature, T_R , is only one component of, and usually lower than, the system noise temperature T_s .

To minimize the radar system noise temperature, radars often use low-sidelobe antennas to limit the contribution of ground temperature, low-loss antennas and microwave circuits to minimize their noise contributions, and low-noise receivers. The lossy components of the antenna and microwave circuits are sometimes cooled to further reduce their noise contribution. In the past, low-noise receivers required cooling components (e.g., to liquid nitrogen temperature), but current technology may provide good low-noise performance at room temperature.

The system noise temperature, T_s , is usually specified at or near the output of the receive antenna (see Section 5.2). Losses in the antenna, L_{AR} , and the microwave circuits, L_{MR} , prior to where T_s is specified, reduce both the signal and the noise power from sources outside the radar, as well as adding noise to the signal as discussed above.

A receiver and signal processor that constitute a matched filter for the received signal waveform is used as the reference case in S/N calculations (see Chapter 5). The S/N is maximized with such a matched filter. When the receiver and signal processor depart from this ideal, a signal-processing loss is produced:

L_{sp} = radar signal-processing losses

Factors that may contribute to L_{sp} include:

- Departure of the analog or digital filter from the ideal;
- Mismatch between signal and receiver bandwidth;
- Quantization error;
- Changes or distortion of the received signal due to target or RF propagation conditions (e.g., Doppler-frequency shift);
- Straddling loss, the failure of a range or Doppler bin to fully encompass the target when dividing the signal into range and Doppler bins.

The detection or demodulation loss occurs when signals with low S/N are detected and then noncoherently integrated:

L_d = detection (or demodulation) loss

This is also a signal-processing loss, but is usually specified separately (see Section 5.4).

Radar receivers often employ multiple receiver channels to process signals from the antenna. These may include:

- A sum channel;
- Monopulse difference channels for azimuth and elevation;
- Channels to handle multiple simultaneous polarizations;
- Auxiliary channels for sidelobe blanking or cancellation (see Section 10.3).

Additional receiver parameters are associated with the errors and biases in measuring range and Doppler-frequency shift. These are defined and discussed in Chapter 8.

3.5 Target Radar Cross Section

The radar cross section (RCS) is the ratio of the power density scattered by the target in the direction of the radar receiver, to the power density incident on the target [7, pp. 11.2–11.4]. It is measured in area units, usually square meters, and often is specified logarithmically in decibels relative to a square meter (dBsm):

$$\sigma = \text{target RCS}$$

While the RCS is generally related to the size of the target, its value may be affected by other factors. For example, flat plates and cylinders may produce large specular RCS returns at angles near the normal to their surfaces. Objects formed from the intersection of three perpendicular planes, called corner reflectors, produce very large RCS values when viewed by monostatic radar (see Section 10.1). On the other hand, stealth techniques, including target shaping and the use of radar absorbing and non-metallic materials, may significantly reduce the RCS of targets.

The RCS of complex objects may vary with the target aspect that is viewed by a radar having a wavelength significantly smaller than the object dimensions. This is a consequence of signals from individual scatterers on the target adding in- or out-of-phase as the aspect changes. The viewing aspect may change as the target rotates, or as the radar LOS changes as the target moves relative to the radar (or as the radar moves relative to the target). The change in the viewing aspect angle that may produce an uncorrelated value of RCS for a complex target is given approximately by [3, p. 172]:

$$\alpha = \frac{\lambda}{2a} \quad (3.34)$$

where:

α = change in aspect angle to the target

a = target dimension

This is illustrated in Figure 3.4(a), which shows the rotation angle needed to change the relative path lengths for typical scatterers, separated in cross range by $a/2$, by an amount equal to $\lambda/4$. This results in a change in the two-way range of $\lambda/2$, causing the relative signal phase to change by 180 degrees. This will cause the scatterers that previously added in-phase, to add out-of-phase.

For example, a target (such as an aircraft), having a 10m dimension, viewed by an L-band radar ($\lambda = 0.23\text{m}$), will produce a decorrelated RCS return after rotating about 0.7 degrees. If the target is rotating at one revolution per minute (six degrees per second), this will occur after about 0.11 seconds.

The RCS of complex targets larger than the signal wavelength also may vary with the radar frequency with which they are viewed. This is a consequence of signals from individual scatterers on the target adding in- or out-of-phase as the signal

wavelength changes. The change in radar frequency required to produce an uncorrelated RCS value is approximately [3, p. 172]:

$$\Delta f = \frac{c}{2a} \quad (3.35)$$

where:

Δf = change in frequency

This frequency change results in changing by one-fourth the number of wavelengths between typical scatterers that are separated in range by $a/2$, as illustrated in Figure 3.4(b). This results in a relative signal phase change of 180 degrees. For example, for a target having a 10m dimension, $\Delta f = 15$ MHz.

Note that the target dimension in the cross range coordinate determines the decorrelation with LOS changes, while the target dimension in the range coordinate determines the decorrelation with frequency changes, as shown in Figure 3.4.

Targets having dimensions smaller than about λ/π do not exhibit this aspect angle or frequency dependent fluctuations of RCS. These targets are said to be in the Rayleigh region, and their RCS varies as λ^{-4} [2, pp. 33–52].

Target RCS may also depend on the polarization of the transmitted and received signal.

The preceding discussion illustrates that the signal returned from a target, often attributed to target RCS, depends on the radar viewing angle, radar frequency and signal polarization, as well as the target configuration. Target RCS may be measured or calculated for each viewing aspect, frequency, and polarization of interest [8]. However, this may be tedious and produce a lot of data. Targets are more conveniently characterized by an average RCS value in a frequency band and range of viewing aspects, and their signal fluctuations in that band and range modeled statistically.

The Swerling target models are frequently used for this purpose. While these models are broadly useful, other statistical models have been developed for special applications. Two probability density functions are used by the Swerling models. For Swerling models 1 and 2:

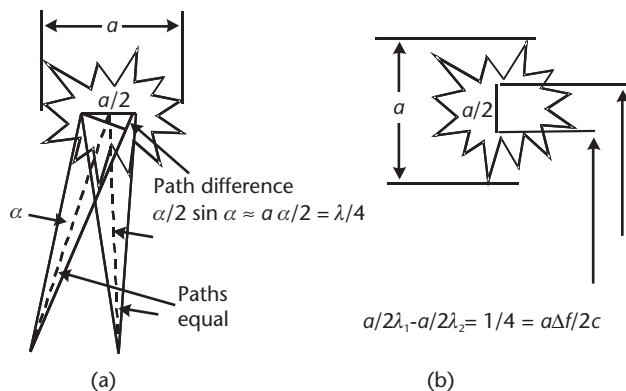


Figure 3.4 How target rotation and signal frequency change may decorrelate the target RCS. (a) LOS rotation. (b) Frequency change.

$$p(\sigma) = \frac{1}{\sigma_{av}} \exp\left(-\frac{\sigma}{\sigma_{av}}\right) \quad (3.36)$$

where:

σ_{av} = average RCS value

The target RCS, which is proportional to the return signal power, has the exponential probability density function. This probability density function is used to characterize targets having many scatterers of comparable magnitude. The target-signal voltage fluctuations have Rayleigh probability density functions, and these targets are often referred to as Rayleigh targets.

For Swerling models 3 and 4:

$$p(\sigma) = \frac{4\sigma}{\sigma_{av}^2} \exp\left(-\frac{2\sigma}{\sigma_{av}}\right) \quad (3.37)$$

This probability density function represents a Rayleigh target observed with dual diversity. It is sometimes used to represent targets having one dominant scatterer and many smaller scatterers.

Two classes of RCS decorrelation are used in the Swerling models:

- Scan-to-scan decorrelation. The target signal is assumed to be constant for pulses in a radar scan or other series of closely-spaced pulses, and to be uncorrelated from scan-to-scan. This is often the case for rotating search radar that use the same frequency for successive pulses. For example, a radar with a 5-second rotation period and a 1-degree azimuth beamwidth would view a target for about 0.014 seconds. In the example for target aspect change given above, the target decorrelation time was 0.11 seconds. If the radar frequency remained constant, the target RCS would likely remain nearly constant during the radar viewing period. On the next observation, 5 seconds later, the RCS would likely be uncorrelated with the previous observation.
- Pulse-to-pulse decorrelation. The target signal is assumed to be independent for each observation. This could be the case for rapidly-fluctuating targets, or for radar such as phased-arrays that views targets at a low observation rate. In the above example, the decorrelation time is 0.11 seconds. If the radar observation interval is 1.0 second, the RCS values for successive observations would likely be decorrelated. If the radar frequency in the example were increased to X-band, the decorrelation time would be reduced to 0.015 seconds, and the returns would likely be decorrelated for observation rates as high as 50 Hz. Pulse-to-pulse decorrelation may be produced when viewing stable targets at high data rates by using pulse-to-pulse variation of the radar frequency. In the above example for frequency variation of RCS, the RCS was found to decorrelate with frequency changes of 15 MHz. If successive radar pulses are changed by at least 15 MHz, the RCS will be decorrelated from pulse-to-pulse, no matter how short the interval between observations.

The relationship of the four Swerling models to these probability distributions and decorrelation times is shown in Table 3.3. The Swerling 1 and 2 models use the first probability distribution given above, with Swerling 1 assuming dwell-to-dwell decorrelation, and Swerling 2 assuming pulse-to-pulse decorrelation. The Swerling 3 and 4 models use the second probability distribution, with Swerling 3 assuming dwell-to-dwell decorrelation, and Swerling 4 assuming pulse-to-pulse decorrelation. A nonfluctuating target signal is sometimes referred to as Swerling 5.

Another example showing the effect of LOS, rotation and frequency change on target RCS is given in Table 3.4. For the 2-m target dimension and X-band radar frequency given, a change in the observation LOS of about 0.5 degrees will produce RCS decorrelation. If the target is rotating at 5 degrees per second, this will take 100 ms. If the target aspect remains fixed, a frequency change of 75 MHz will produce RCS decorrelation.

This example is extended to show the use of the Swerling models for a rotating surveillance radar in Table 3.5. With the parameters from Table 3.4, the target returns will be correlated during a sweep past the target (30 ms), but will be decorrelated on successive sweeps (10 seconds). Thus a Swerling 1 or 3 target model is appropriate. These models were developed for just this situation. If the six pulses that illuminate the target on a sweep are transmitted at frequencies separated by 75 MHz, these target returns will be decorrelated, and a Swerling 2 or 4 model is appropriate.

The preceding discussion of RCS assumed observation by monostatic radar (i.e., those having their transmitting and receiving antennas close together, relative to the target range). The RCS for bistatic radar is generally similar to that for monostatic radar. For small bistatic angles, the bistatic RCS is approximately equal to the monostatic RCS that would be viewed at the bisector of the bistatic angle, illustrated in Figure 2.4(b), reduced by $\cos(\beta/2)$, [9, pp. 25.14–25.18], where:

Table 3.3 Swerling Target-Signal Fluctuation Models

<i>Probability Density Function</i>	<i>Dwell-to-Dwell Decorrelation</i>	<i>Pulse-to-Pulse Decorrelation</i>
$p(\sigma) = \frac{1}{\sigma_{av}} \exp\left(-\frac{\sigma}{\sigma_{av}}\right)$	Swerling 1	Swerling 2
$p(\sigma) = \frac{4\sigma}{\sigma_{av}^2} \exp\left(-\frac{2\sigma}{\sigma_{av}}\right)$	Swerling 3	Swerling 4

Table 3.4 Example of Requirements for RCS Decorrelation from LOS Rotation and Frequency Change

<i>Parameter</i>	<i>Value</i>
Target dimension (<i>a</i>)	2m
Radar frequency	9.5 GHz (X-band)
Wavelength (λ)	0.0316m
LOS rotation required	8 mrad (≈ 0.5 degrees)
Target rotation rate	5 degrees/s
Decorrelation time	100 ms
Frequency change required	75 MHz

Table 3.5 Example of a Rotating Surveillance Radar

<i>Parameter</i>	<i>Value</i>
PRF	200 Hz
Time between pulses	5 ms
Antenna rotation period	10 s
Antenna beamwidth	1 degree
Time on target	30 ms

β = bistatic angle, the angle between the transmitting and receiving LOS measured at the target.

For large bistatic angles approaching 180 degrees, there is a forward-scatter enhancement that may produce a bistatic RCS much larger than that for a monostatic radar.

3.6 Problems

The following problems are provided to assist in reviewing this chapter and to ensure a basic understanding of the material. Solutions to these problems are given in Appendix E, Section E.3.

1. What pulse duration is needed to produce 20 kJ of pulse energy with a 2 MW transmitter? If the transmitter duty cycle is 10%, at what rate may these pulses be produced?
2. If the transmitter tube generates 20 kW of peak power, has a duty cycle of 0.2, and internal losses of 0.7 dB, what is the transmitter average power? If 15 kW of prime power are supplied to the transmitter, what is the transmitter efficiency? If the RF ohmic losses following the transmitter total 1.6 dB, and 28 kW of prime power are required by the radar for the previously-stated tube RF power output, what is the overall radar efficiency?
3. What effective aperture area is needed to provide antenna gain of 40 dB at a frequency of 1.3 GHz (L band)? What area is needed at a frequency of 9.5 GHz (X band)?
4. For a rectangular aperture, if an effective aperture area of 10 m² is required, and 40-dB Taylor weighting is used in both the azimuth and elevation dimensions, and the antenna ohmic losses are 0.8 dB, what physical antenna area is needed? If the physical aperture is 3m high (elevation dimension), and the frequency is 3.3 GHz (S band), what are the beamwidths?
5. If an FFOV array has 10,000 elements spaced by 0.59 λ , what is the broadside gain, neglecting antenna losses? If the array is square, and employs uniform illumination, what is the broadside beamwidth? If the beam is scanned off-broadside in elevation by 30 degrees, what is the gain and elevation beamwidth?

6. Find the system noise temperature when the receiver bandwidth is 1 MHz and the noise power in the radar receiver is 10^{-14} W.
7. A target has dimensions of 10m, is made up of many scatterers of comparable magnitude and is rotating at two rpm. It is observed at a fixed frequency by an X-band radar (9.5 GHz) with a PRF of 100 Hz. What Swerling model should be used to characterize the RCS fluctuations?
8. What is the signal energy in a 5-ms pulse with peak power of 10 kW? How many such pulses would be needed for a total waveform energy of 1,000J?
9. What is the radar duty cycle with peak power of 1 MW and average power of 150 kW? What average power is needed to increase the duty cycle to 25%?
10. For a 10×10 m antenna at 3.3 GHz (S band), with no ohmic losses:
 - a. What is the antenna gain and effective aperture area, assuming uniform illumination?
 - b. What is the antenna gain and effective aperture area, assuming 30-dB Taylor illumination taper in one dimension?
11. Find the level of the first receive sidelobe for the above cases (Problem 10), relative to the mainbeam, and relative to isotropic gain.
12. For an FFOV array with azimuth beamwidth of 1 degree and elevation beamwidth of 2 degrees:
 - a. Estimate the broadside gain, neglecting ohmic loss.
 - b. For scan angles in azimuth of 20 degrees and in elevation of 40 degrees, what are the azimuth and elevation beamwidths? What is the scan loss? What is the resulting gain?
13. For a 5×5 m FFOV array at 9.5 GHz (X band), find the required number of elements, assuming 0.6λ spacing. For a LFOV with the same size and frequency, find the maximum element spacing that will allow a scan angle of ± 20 degrees. Find the required number of elements.
14. What is the receiver noise power when the system noise temperature is 500K and the receive bandwidth is 10 MHz?
15. If the receiver noise figure is 3.5 dB, what is the receiver noise temperature?
16. For a target with dimensions of 2m and rotating at 10 degrees per second, and a C-band (5.5 GHz) radar:
 - a. What is the maximum PRF that will provide decorrelated RCS observations?
 - b. For much higher PRF, what frequency change is needed to decorrelate the RCS between observations?

References

- [1] Weil, T. A., "Transmitters," Chapter 4 in *Radar Handbook*, 2nd ed., M. I. Skolnik, (ed.), New York: McGraw-Hill, 1990.
- [2] Skolnik, M. I., *Introduction to Radar Systems*, 2nd ed., New York: McGraw-Hill, 1980.
- [3] Barton, D. K., and H. R. Ward, *Handbook of Radar Measurement*, Dedham, MA: Artech House, 1984.

- [4] Cheston, T. C., and J. Frank, "Phased Array Antennas," Chapter 7 in *Radar Handbook*, 2nd Ed., M. I. Skolnik, (ed.), New York: McGraw-Hill: 1990.
- [5] Barton, D. K., *Modern Radar System Analysis*, Norwood, MA: Artech House, 1991.
- [6] Mailloux, R. J., "Limited Scan Arrays—Part 1," In *Practical Phased Array Antenna Systems*, E. Brookner, (ed.), Norwood, MA: Artech House, 1991.
- [7] Kell, R. E., and R. A. Ross, "Radar Cross Section," Chapter 11 in *Radar Handbook*, 2nd Ed., M. I. Skolnik, (ed.), New York: McGraw-Hill, 1990.
- [8] Ruck, G. T., et al., *Radar Cross Section Handbook, Volumes 1 and 2*, New York: Plenum Press, 1970.
- [9] Willis, N. J., "Bistatic Radar," Chapter 25 in *Radar Handbook*, 2nd ed., M. I. Skolnik, (ed.), New York: McGraw-Hill, 1990.

Selected Bibliography

The design and operation of radar transmitters is treated by Weil in Skolnik's radar handbooks. Barton and Ward provide antenna patterns and parameters for a wide range of aperture weighting functions in their Appendix A. Both sum and difference (monopulse) patterns are included. Phased-array antennas are treated by Cheston and Frank in Skolnik's radar handbooks, and in a collection of papers edited by Brookner. Radar cross section is addressed by Kell and Ross in Skolnik's radar handbooks, and treated in detail by Ruck, et al. Bistatic radar and RCS are addressed by Caspers and by Willis in Skolnik's 1970 and 1999 radar handbooks, respectively.

Barton, D. K., and H. R. Ward, *Handbook of Radar Measurement*, Dedham, MA: Artech House, 1984.

Brookner, E., (ed.), In *Practical Phased Array Antenna Systems*, Norwood, MA: Artech House, 1991.

Caspers, J. W., "Bistatic and Multistatic Radar," Chapter 36 in *Radar Handbook*, M. I. Skolnik, (ed.), New York: McGraw-Hill, 1970.

Cheston, T. C., and J. Frank, "Array Antennas," Chapter 11 in *Radar Handbook*, M. I. Skolnik, (ed.), New York: McGraw-Hill, 1970.

Cheston, T. C., and J. Frank, "Phased Array Antennas," Chapter 7 in *Radar Handbook*, 2nd ed., M. I. Skolnik, (ed.), New York: McGraw-Hill, 1990.

Kell, R. E., and R. A. Ross, "Radar Cross Section of Targets," Chapter 27 in *Radar Handbook*, M. I. Skolnik, (ed.), New York: McGraw-Hill, 1970.

Kell, R. E. and R. A. Ross, "Radar Cross Section," Chapter 11 in *Radar Handbook*, 2nd ed., M. I. Skolnik, (ed.), New York: McGraw-Hill, 1990.

Ruck, G. T., (ed.), *Radar Cross Section Handbook, Volumes 1 and 2*, New York: Plenum Press, 1970.

Skolnik, M. I., (ed.), *Radar Handbook*, New York: McGraw-Hill, 1970.

Skolnik, M. I., (ed.), *Radar Handbook*, 2nd ed., New York: McGraw-Hill, 1990.

Weil, T. A., "Transmitters," Chapter 7 in *Radar Handbook*, M. I. Skolnik, (ed.), New York: McGraw-Hill, 1970.

Weil, T. A., "Transmitters," Chapter 4 in *Radar Handbook*, 2nd ed., M. I. Skolnik, (ed.), New York: McGraw-Hill, 1990.

Willis, N. J., "Bistatic Radar," Chapter 25 in *Radar Handbook*, 2nd ed., M. I. Skolnik, (ed.), New York: McGraw-Hill, 1990.

Radar Waveforms

This chapter enables the reader to:

- Characterize radar waveforms, using their principal waveform characteristics, including waveform energy, resolution, and rejection of unwanted targets;
- Understand the features of the radar ambiguity function, and how it is used to describe radar waveform characteristics and limitations;
- Quantify the performance provided by waveforms in the major radar waveform classes: CW pulses, linear FM pulses, phase-coded waveforms, and pulse-burst waveforms, and configure radar waveforms in these classes that provide the desired performance features;
- Know the sources and effects of multiple-time-around radar returns and radial-velocity ambiguities, and understand techniques for recognizing and eliminating these returns.

Understanding the characteristics of radar waveforms is important to analyzing and modeling radar performance. The information that a radar may provide on targets is to a large extent determined by the waveforms it employs. The following sections describe the principal characteristics of radar waveforms and how they impact radar observations and performance. Four major classes of radar waveforms, CW pulses, chirp pulses, phase-coded waveforms, and pulse bursts, are discussed in Sections 4.2 to 4.5. The range ambiguities produced by periodic transmission of pulsed waveforms are discussed in Sections 4.6 and 4.7, respectively.

Many simple surveillance radars use a single waveform that is optimized for search. Similarly, tracking radars may use a single waveform optimized for the tracking function performed. Other radars, especially phased arrays, often have a repertoire of many waveform types and durations that may be used to perform the various radar functions as required.

The waveforms described in this chapter are widely used, and a radar may employ either variants of these or combinations of waveform classes. Many additional waveform types have been devised and are used in radar, and this is not intended to be a comprehensive treatment of the subject. Further details on radar waveform design may be found in [1].

4.1 Waveform Characteristics

The major characteristics of radar waveforms are:

- Energy in the waveform;
- Resolution provided in range and radial velocity;
- Rejection of unwanted target responses.

The S/N produced by a radar is directly proportional to the waveform energy, as discussed in Section 5.1. The target detectability and measurement accuracy in turn depend on the S/N, as discussed in Chapters 6 and 8. High waveform energy may also help mitigate the effect of radar jamming, as discussed in Chapter 10.

The radar waveform energy, E_w , is given by the integral of the instantaneous transmitted power over the waveform duration:

$$E_w = \int P(t)dt \quad (4.1)$$

where:

E_w = waveform energy

P = instantaneous transmitted power

In most radars, the transmitter is operated at its peak power. The waveform energy is then determined by the peak transmitter power, P_p , and the waveform duration, τ . The waveform energy is then given by:

$$E_w = P_p \tau \quad (4.2)$$

In the case of multipulse waveforms, where the waveform consists of several subpulses, the waveform energy is the sum of the individual pulse energies:

$$E_w = \sum_n P_p \tau_n \quad (4.3)$$

where:

τ_n = Duration of subpulse n

Long waveforms may be desired to provide high waveform energy when transmitter peak power is limited. However, pulse duration must be consistent with the transmitter capability. The rate at which the waveform is transmitted must also be consistent with the transmitter average power and duty-cycle limitations (see Section 3.1). Waveform duration also impacts minimum range at which targets may be observed, as discussed in Section 5.5, and the target resolution provided, discussed below.

The resolution provided by the waveform determines the radar's ability to separate closely-spaced targets so they may be individually detected, observed, counted, tracked, and their characteristics measured. Targets need only be resolved in one coordinate. They may be resolved in an angular coordinate by the antenna beam-width, in which case the waveform resolution is not critical. However, in many situations the cross range target spacing is less than the cross range resolution of the

radar (range times the beamwidth), and resolution in angle is not possible. In such cases, the targets may be resolved in range or radial velocity by using a suitable radar waveform.

Targets may be separated in range, radial velocity, or a combination of the two [2, pp. 115–118]. Targets are resolved in range when the responses they produce in the radar receiver are sufficiently separated in time. Targets are resolved in radial velocity when the spectra they produce in the receiver are sufficiently separated in frequency. Radar measurement accuracies in range and radial velocity depend on the range and radial-velocity resolution, as discussed in Chapter 8.

The resolution of a waveform in the time and frequency domains are related to the resolutions in range and radial velocity by:

$$\Delta R = c\tau_R / 2 \quad (4.4)$$

$$\Delta V = \lambda f_R / 2 \quad (4.5)$$

where:

ΔR = range resolution

τ_R = time resolution

ΔV = radial-velocity resolution

f_R = frequency resolution.

Equation 4.5 assumes that the frequency resolution is much smaller than the radar frequency, so that λ may be taken as constant over the resolution band.

Radar resolution in time is illustrated in Figure 4.1, which shows the matched-filter receiver response versus time for a rectangular CW pulse for several target conditions. For a single point target, the receiver output signal is triangular, with a total duration 2τ , as shown in Figure 4.1(a) (see Section 4.2).

The response for two in-phase target returns separated by the pulse duration, τ , is shown in Figure 4.1(b). When the RCS of the two targets is equal (the plot on the left), it is evident that there are two targets, although it may be difficult to accurately measure the range of each target. The plot to the right shows the response when the targets have a four-to-one ratio of RCS. It is difficult to see the response to the smaller target, and its position likely could not be measured. When the target returns are separated by twice the pulse duration, as shown in Figure 4.1(c), they are clearly resolved in both cases. This is true regardless of signal phase.

Finally, the waveform determines the capability of the radar to reject or suppress unwanted targets that could interfere with the detection and observation of targets of interest. Such interfering targets may be much larger than the target of interest (e.g., a large building next to a small vehicle), or they may be distributed in range and radial velocity (e.g., clutter from terrain or rain).

Waveforms to cope with such situations should exhibit low responses to targets in these range and radial velocity regions. Figure 4.1 shows how targets that are not adequately resolved in range from the target of interest may interfere. Waveforms also have sidelobe responses, analogous to antenna sidelobes. Large targets in these range and/or radial-velocity regions may interfere with the target of interest. Finally, waveforms that employ repetitive pulses (see Section 4.5 and 4.6), may produce ambiguities

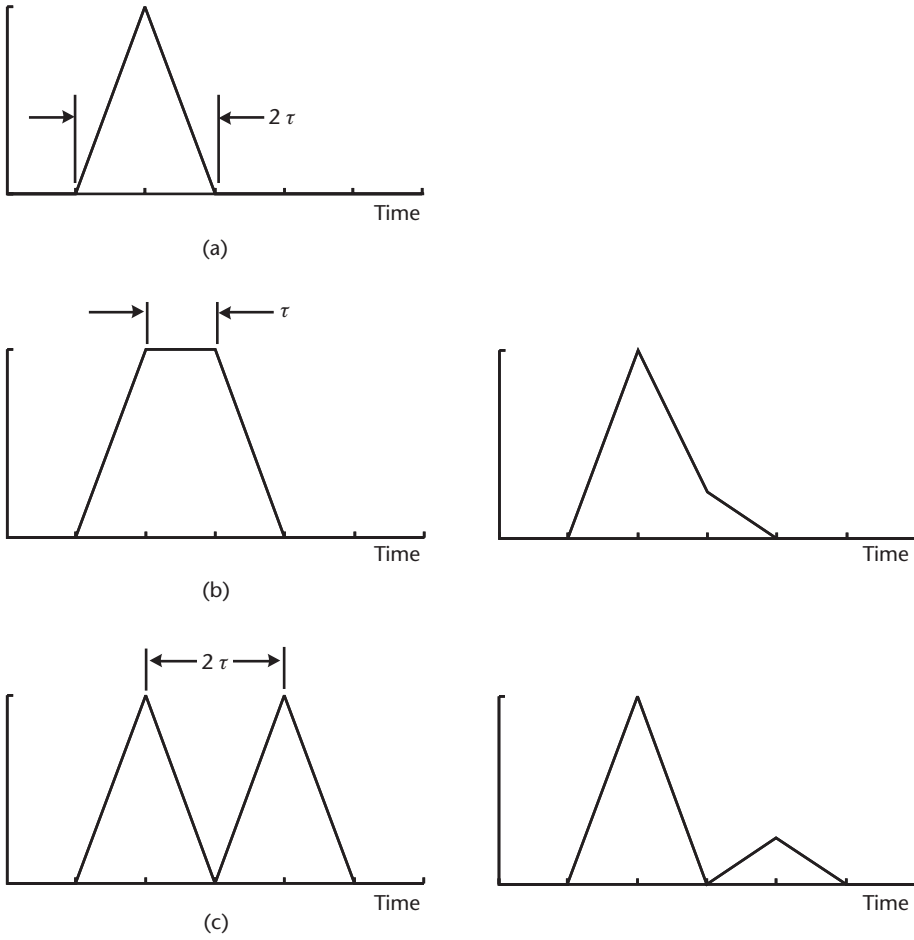


Figure 4.1 Temporal response of a matched-filter receiver to target returns, using a CW pulse. (a) Single target. (b) Two in-phase targets separated by the pulse duration. (c) Two in-phase targets separated by twice the pulse duration.

ties. Waveform ambiguities may cause returns from targets at different ranges or radial velocities that may be difficult to distinguish from the target of interest.

The capabilities of a waveform to resolve targets and suppress the unwanted target responses are described by the waveform ambiguity function, first discussed in [2, pp. 118–120]. The radar waveform ambiguity function is a valuable tool both for analyzing radar waveform designs, and for visualizing their performance. The properties of the ambiguity function also determine basic limitations in waveform design.

The ambiguity function is defined as the squared magnitude of the complex envelope of the output of the radar receiver, as a function of time and frequency. When the receiver is matched to the received waveform, the receiver output is the autocorrelation function with itself, shifted in frequency [3, pp. 411–412]:

$$\chi(t_M, f_M) = \int_{-\infty}^{\infty} u(t) u^*(t - t_M) e^{-2\pi f_M t} dt \quad (4.6)$$

where:

χ = output of the receiver matched filter

t_M = time relative to time to which receiver filter is matched

f_M = Doppler frequency relative to frequency to which receiver filter is matched

$u(t)$ = complex waveform modulation versus time

The asterisk connotes the complex conjugate. The ambiguity function is then given by $|\chi(t_M, f_M)|^2$.

A similar but more general ambiguity function applies for receiver filters that are not matched to the waveform. This could occur from imperfections in the filter, as a result of Doppler-frequency shift in the received signal, or due to deliberate weighting of the filter time or frequency response to suppress signal sidelobe responses.

The ambiguity function has its maximum value at the origin, which represents the time and frequency to which the receiver filter is matched. Along the t_M axis, the ambiguity function is proportional to the squared autocorrelation function of the waveform; along the f_M axis, it is proportional to the squared spectrum of the square of the waveform.

An important property of the ambiguity function is that the total volume under its surface is a constant that depends only on the waveform energy. The constraint that the volume under the ambiguity function surface remains constant shows that waveform ambiguity may not be eliminated by waveform design, but only moved around in the time-frequency plane. Thus waveform design may be thought of as locating the ambiguity volume where it is least troublesome for the target complex of interest. This illustrates the fundamental limitations in designing waveforms that simultaneously have small range and radial-velocity resolutions, low sidelobe responses, and no ambiguities. Examples of waveform ambiguity functions for four common classes of waveforms are given in Sections 4.2 through 4.5.

4.2 CW Pulses

The CW pulse is probably the simplest pulsed-radar waveform. Most early radars, and many simple radars today, employ CW pulses. These are easy to generate in the transmitter, and to process in the receiver. Short pulses may be used to provide the needed range resolution. However, when long pulses are needed to produce sufficient waveform energy, the range resolution suffers.

The CW pulse consists of a constant-frequency, constant-amplitude pulse of duration τ , as illustrated in Figure 4.2(a). The pulse envelope is then a rectangle, as shown in Figure 4.2(b). The time and frequency outputs of a matched-filter receiver are shown in Figure 4.2(c, d). The time resolution, τ_R of a CW pulse is often taken to be equal to the pulse duration, τ , since equal-size target returns separated by this time may just be resolved, as shown in Figure 4.1. This results in a range resolution $\Delta R = c\tau/2$. The Doppler-frequency resolution, f_R , is often taken to be equal to $1/\tau$, which is also approximately equal to the signal bandwidth, B , for CW pulses, since equal-sized target returns separated by this frequency may just be resolved. This results in a radial-velocity resolution $\Delta V = \lambda/2\tau$. Sidelobes extend in Doppler frequency indefinitely beyond the central response, while none extend in time beyond the central response.

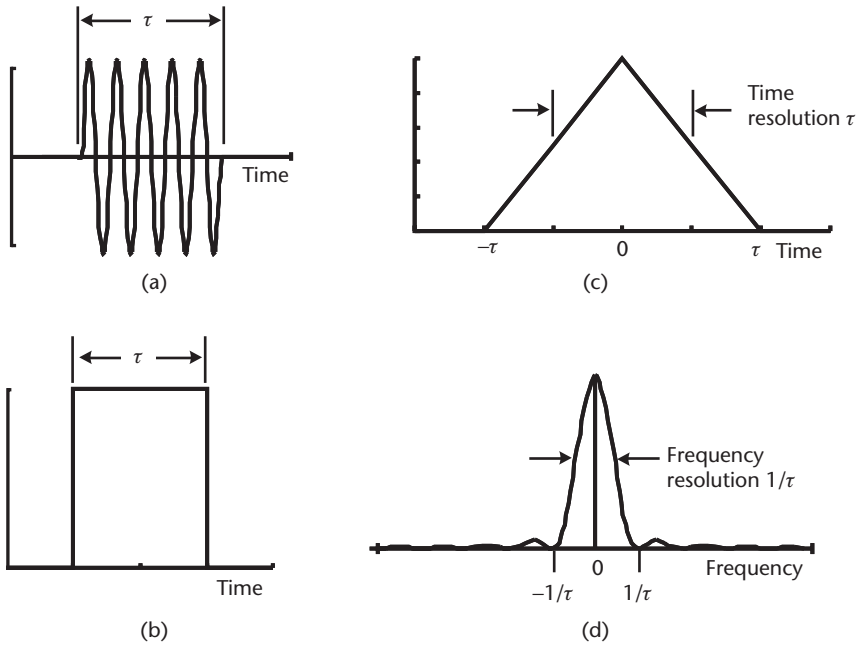


Figure 4.2 Characteristics of the CW pulse. (a) Waveform. (b) Envelope. (c) Time response. (d) Frequency response.

The ambiguity function for the CW pulse is shown in Figure 4.3. The region where the ambiguity function is large is shown in black, while the lower sidelobe response regions are shaded. The sidelobe responses extend indefinitely in Doppler frequency within a time region, $\pm \tau$, from the central response. The time and Doppler-frequency resolutions as defined above are shown, along with the corresponding range and radial-velocity resolutions [3, pp. 414–416]. The product of the former is often called the waveform time-bandwidth product, τB , which is equal to unity for CW pulses.

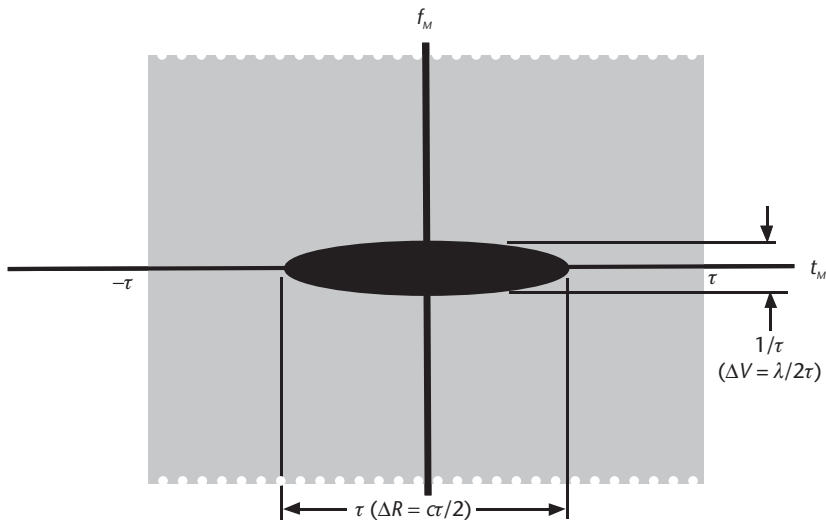


Figure 4.3 Ambiguity function for the CW pulse.

A major limitation of the CW pulse is the difficulty in obtaining both good range and good radial-velocity resolution. This is illustrated by the example CW waveforms in Table 4.1. The waveforms in columns 2 and 3 provide a range resolution of 150 m, which requires a 1- μ s pulse. The resulting radial-velocity resolution at L band (1 GHz), is 150 km/s, and at X band (10 GHz), is 15 km/s. On the other hand, if a radial-velocity resolution of 15 m/s is required, as shown in columns 4 and 5, the pulse duration must be at least 10 ms at L-band, giving a range resolution of 1,500 km. At X band, the pulse duration must be 1 ms, giving a range resolution of 150 km.

When long CW pulses are used to provide good radial-velocity resolution, the spectral width of the signal and the matched filter will be small. Then, if the radial velocity of the target is not well-known, the target returns may fall outside the matched filter, and the target signal may not be received. In such cases, it may be necessary to employ several receiver filters, matched to different frequencies, to ensure reception of the target signal. For example, an L-band radar (1.3 GHz) using a 1 ms pulse has a radial-velocity resolution of about 115 m/s. If the possible range of target velocities is ± 230 m/s, four matched filters must be used to ensure receiving the target-signal return.

The short pulses needed to provide acceptable range resolution with CW waveforms may make it difficult to provide the required pulse energy. This is especially a problem for solid-state transmitters that often operate at low peak power and high duty cycle. This is a major motivation for pulse-compression techniques, discussed in the following three sections.

4.3 Linear FM Pulses

Linear FM pulses are a widely used pulse-compression technique. Linear FM pulses are often called chirp pulses, from the sound of audio signals with this characteristic.

A linear FM pulse has a constant amplitude for a duration τ , with a frequency that varies linearly with time during the pulse. The frequency modulation increases the signal bandwidth, B , beyond that of CW pulse of the same duration. This is illustrated in Figure 4.4, which shows the waveform envelope, the frequency as a function of time, and a representation of the RF signal.

Older radars usually employ analog devices such as dispersive delay lines to generate chirp pulses in the transmitter and to process them in the receiver [4, pp. 10.6–10.15] Digital signal processing is usually used in newer radars for these functions.

The ambiguity function for a chirp waveform is shown in Figure 4.5. The Doppler-frequency resolution for zero relative time is $1/\tau$, the same as for a CW pulse of the same duration. The time resolution for zero relative frequency is now

Table 4.1 CW Pulse Examples

Pulse duration	1 μ s	1 μ s	10 ms	1 ms
Range resolution	150 m	150 m	1,500 km	150 km
Frequency	1 GHz	10 GHz	1 GHz	10 GHz
Velocity resolution	150 km/s	15 km/s	15 m/s	15 m/s

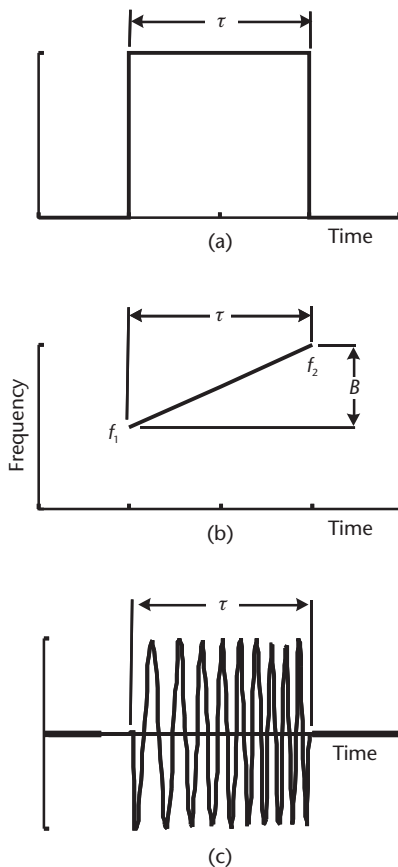


Figure 4.4 Characteristics of linear FM (chirp) waveforms. (a) Envelope. (b) Frequency. (c) Waveform.

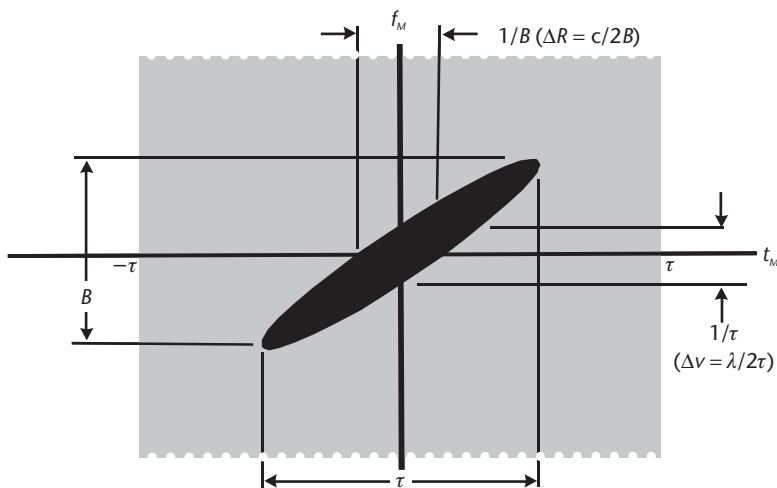


Figure 4.5 Ambiguity function for linear FM (chirp) waveform.

equal to $1/B$ for a chirp pulse, where B may be much larger than $1/\tau$, the value for a CW pulse. This provides range resolution $\Delta R = c/2B$.

For example, an X-band pulse having a duration of 1 ms provides a radial-velocity resolution of 15 m/s, as discussed in the preceding section. If the linear FM signal bandwidth is 1 MHz, the range resolution is 150m, a decrease by a factor of 1,000 from that of a CW pulse with the same duration.

Compared with a CW pulse, the size of the range-resolution cell is reduced by the time-bandwidth product τB . Thus the pulse compression ratio, PC, is given by:

$$PC = \tau B \quad (4.7)$$

This is generally true for pulse-compression waveforms. In the above example, $\tau B = 1,000$, providing a corresponding reduction in the size of the range-resolution cell, compared with a CW pulse, which has a value of $\tau B = 1$.

Linear FM waveforms may be designed and implemented with very large time-bandwidth products -10^6 or greater. They may have both good range resolution and good radial-velocity resolution. The range resolution is determined by the waveform bandwidth, while the radial-velocity resolution depends on both the waveform duration and the signal frequency.

This is illustrated by the waveform examples in Table 4.2. Columns 2 and 3 show waveforms having signal bandwidths of 1 MHz, providing range resolution of 150m, the same as that of the first two waveforms in Table 4.1. However, the pulse duration of these waveforms is 100 μ s, providing velocity resolution of 1.5 km/s at L band (1 GHz), and 150 m/s at X band (10 GHz), decreases of a factor of 100 from the CW pulses in Table 4.1. The time-bandwidth for these waveforms is 100.

Columns 4 and 5 in Table 4.2 show waveforms having signal bandwidths of 100 MHz, providing 1.5 m/s range resolution, and pulse durations of 10 ms, providing velocity resolutions of 15 m/s and 1.5 m/s at L and X band, respectively. The time-bandwidth of these waveforms is 10^6 .

Another feature of the ambiguity function in Figure 4.5 is the coupling between time and frequency for targets away from the origin. The relationship between time offset, t_M , and Doppler-frequency offset, f_M , is given by:

$$t_M = \frac{\tau}{B} f_M \quad (4.8)$$

Thus, a target having a radial velocity that is offset by an amount V_{RO} from the velocity to which the receiver filter is matched, will produce a range offset, R_O , from the true range equal to:

Table 4.2 Linear FM Pulse Examples

<i>Bandwidth</i>	1 MHz	1 MHz	100 MHz	100 MHz
<i>Range resolution</i>	150m	150m	1.5m	1.5m
<i>Pulse duration</i>	100 μ s	100 μ s	10 ms	10 ms
<i>Frequency</i>	1 GHz	10 GHz	1 GHz	10 GHz
<i>Velocity resolution</i>	1.5 km/s	150 m/s	15 m/s	1.5 m/s
<i>Time-bandwidth product</i>	100	100	1,000,000	1,000,000

$$R_O = \frac{\tau f}{B} V_{RO} \quad (4.9)$$

The effect of this range-Doppler coupling on range measurement may be compensated for, if the target radial velocity is known (e.g., from the radar track of the target). Another technique sometimes used is to transmit two chirp signals, one having up, and the other down, frequency variation with time. The range offsets for these two pulses will be in opposite directions so that averaging the resulting two range measurements will give the correct range.

Range-Doppler coupling also may result in targets not being resolved when the responses for targets offset in both range and radial velocity from the desired target lie on the ridge of the ambiguity function. When the relative ranges and radial velocities of targets near the target of interest are known, the direction and rate of the frequency modulation may be chosen to minimize such interference.

The ambiguity functions of both CW pulses and linear FM pulses are sometimes said to have knife-edge shapes [1, pp. 3-16–3-21]. For CW pulses, the knife edge is oriented along the time or frequency axis, depending on the pulse duration and scales used. For chirp pulses, the knife edge is oriented at an angle from the axes, producing the range-Doppler coupling discussed above. In both cases, the sidelobe responses extend indefinitely in frequency, but are constrained to a region $\pm \tau$ along the time axis. These sidelobes may be reduced by weighting the time or frequency response in the receiver, resulting in a mismatched filter.

The linear-FM or chirp waveform allows the use of relatively long pulses having high energy content, while still providing good range resolution. These waveforms are tolerant to Doppler-frequency mismatches in the receiver filter, but produce a range offset proportional to the mismatch.

4.4 Phase-Coded Waveforms

Phase-coded waveforms may provide good range and radial-velocity resolution without the ambiguity region characteristic of the knife-edge ambiguity functions discussed in Section 4.3. However, this ambiguity volume is distributed into the sidelobe region, resulting in higher waveform sidelobe levels than for CW or linear-FM waveforms.

Phase-coded waveforms employ a series of subpulses, each transmitted with a particular relative phase. These are processed in the receiver matched filter to produce a compressed pulse having a time resolution equal to the subpulse duration, τ_s , and a frequency resolution equal to $1/\tau$, where τ is the total waveform duration. Thus, with n_s contiguous subpulses, the waveform duration $\tau = \tau_s n_s$, and the pulse-compression ratio, $PC = n_s$.

A common form of phased-coded waveform, called a binary phase-coded or phase-reversal waveform, employs subpulses having either 0- or 180-degree relative phase. This is illustrated in Figure 4.6(a) for a waveform with five subpulses. The resulting autocorrelation function magnitude (the matched-filter output), is shown in Figure 4.6(b). The central response results from summing in phase the responses

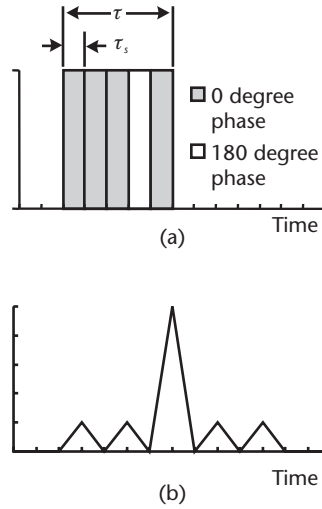


Figure 4.6 Characteristics of a phase-reversal coded waveform. (a) Waveform. (b) Autocorrelation function magnitude.

of the five subpulses, while the sidelobe responses correspond to at most a single subpulse return and has a peak level one-fifth that of the main response.

The waveform illustrated in Figure 4.6 employs a phase sequence corresponding to a Barker code, which has the characteristic of time sidelobes never being larger than $1/n_s$. Barker codes are only known for values of n_s up to 13. For larger values of n_s , sequences may be found that produce sidelobes exceeding $1/n_s$ only occasionally [3, pp. 428–430].

The ambiguity function for a phase-coded waveform is shown in Figure 4.7. The waveform bandwidth, determined by the subpulse duration, is equal to $1/\tau_s$, giving a time resolution equal to τ_s , or equivalently τ/n_s . The Doppler-frequency resolution, determined by the total waveform duration, is equal to $1/\tau$.

The time-bandwidth product, and equivalently the pulse compression ratio, of these phase-coded waveforms is equal to the number of subpulses, $\tau B = n_s$. These waveforms rarely have pulse-compression ratios greater than a few hundred, much smaller than is feasible for linear FM pulses. The range resolution is determined by

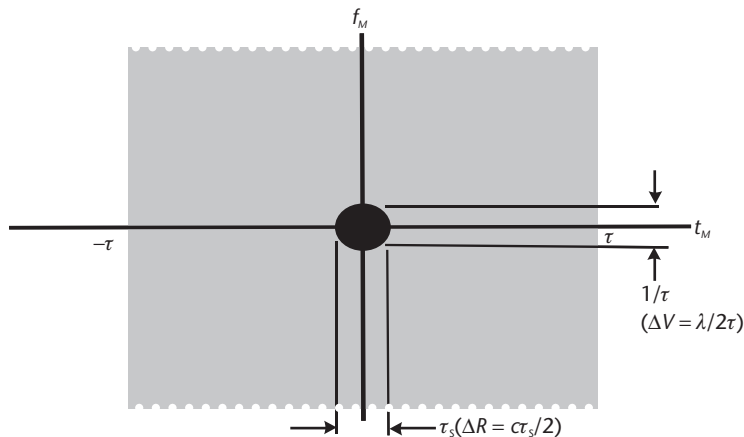


Figure 4.7 Ambiguity function for a phase-coded waveform.

Table 4.3 Phase-Coded Waveform Examples

<i>Subpulse duration</i>	1 μ s	1 μ s	1 μ s	1 μ s
<i>Range resolution</i>	150m	150m	150m	150m
<i>Number of subpulses</i>	10	10	100	100
<i>Waveform duration</i>	10 μ s	10 μ s	100 μ s	100 μ s
<i>Frequency</i>	1 GHz	10 GHz	1 GHz	10 GHz
<i>Velocity resolution</i>	15 km/s	1.5 km/s	1.5 km/s	150 m/s
<i>Time-bandwidth product</i>	10	10	100	100

the subpulse duration, while the radial-velocity resolution is determined by the total waveform duration (as well as the frequency).

Examples of phase-coded waveforms are shown in Table 4.3. In columns 2 and 3, the subpulse duration is 1 μ s and 10 subpulses are used. The resulting range resolution is 150m, and the velocity resolution is 15 km/s at L band (1 GHz), and 1.5 km/s at X band (10 GHz). In the last two columns, the number of subpulses is increased to 100, improving the velocity resolution to 1.5 km/s and 150 m/s at L and X bands, respectively.

The ambiguity function for phase-coded waveforms is sometimes said to resemble a thumbtack, since it does not have any major ambiguities [1, pp. 3-26–3-30]. The sidelobes extend indefinitely in frequency and over $\pm \tau$ in time, like the other waveforms discussed above. Since the volume under the ambiguity function is fixed and the main response of phase-coded waveforms is smaller than that of CW or linear FM pulses of similar duration, the sidelobe levels of the phase-coded waveforms must be higher than those of the CW or chirp waveforms.

Like the linear FM waveform, the phase-coded waveforms may have relatively long duration with high energy content while providing good range resolution. Further, they do not suffer from range-Doppler coupling.

Because of the narrow spectral width of the main response, when long waveforms are used and the target radial velocity is not known, the matched filter may exclude Doppler-shifted signal returns, as is the case with CW pulses. In such cases, multiple receive filters, matched to different frequencies, are needed to cover the range of possible target radial velocities and ensure receiving the target returns, as discussed in Section 4.2.

4.5 Pulse-Burst Waveforms

Pulse-burst waveforms consist of a train of pulses, separated in time, and processed coherently in the receiver matched filter. They may provide very large time-bandwidth products, but they produce periodic ambiguities in both range and radial velocity.

A common pulse-burst waveform consists of n_s identical pulses having duration τ_s , and spaced in time by τ_p . The total waveform duration, $\tau = (n_s - 1)\tau_p$. (For $n_s \gg 1$, $\tau \approx n_s \tau_p$). Such a waveform is illustrated in Figure 4.8. Since radar transmission is not continuous during the pulse burst, (4.2) is not valid for these waveforms, but (4.3) may be used.

The ambiguity function for a uniformly-spaced pulse-burst waveform is shown in Figure 4.9. The time resolution of the central response is determined by the sub-

subpulse provides range resolution of 150m. If 30 subpulses are used with a spacing of $100\ \mu\text{s}$, the waveform duration $\tau = 2.9\ \text{ms}$, and the radial-velocity resolution at X band is approximately 5 m/s. The time-bandwidth product of this waveform is 2,900.

The spacing of the ambiguities may be controlled to some degree by selecting the interpulse period, τ_p . However, it may be necessary to compromise between range and radial-velocity spacing, and the radial-velocity spacing of the ambiguities also depends on the radar frequency. In the above example, the ambiguities are spaced by 15 km in range, and by 150 m/s in radial velocity. When this waveform is used to observe a cluster of targets having dimensions that do not exceed the ambiguity spacing, their relative positions and radial velocities are correctly observed. Targets having separations greater than the ambiguity spacing will produce ambiguous returns that may be difficult to sort out.

Further examples of pulse-burst waveforms are shown in Table 4.4. The first two waveforms employ a relatively small number of CW subpulses. The resulting range resolutions, radial-velocity resolutions, and time-bandwidth products are moderate. The last two example waveforms employ 1,000 linear FM subpulses with 100MHz bandwidth. These have $100\ \mu\text{s}$ subpulse spacing, for a total waveform duration of 100 ms. (For this case, τ is assumed to equal $n_s \tau_p$.) They provide correspondingly better range and radial-velocity resolutions, and time-bandwidth products of 10^7 . The range ambiguity spacing is greater for the last two waveforms than for the first two waveforms, but the reverse is true for the radial-velocity ambiguity spacing.

Variations in the design of pulse-burst waveforms include:

- Use of pulse compression, such as linear FM (chirp), in the subpulses. This increases the subpulse bandwidth and improves the range resolution of the waveform.
- Time weighting, usually applied to the received waveform, to reduce the radial-velocity sidelobe levels.
- Use of staggered or unequal interpulse periods. This eliminates the major ambiguities, but substitutes sidelobe responses over extended intervals.

Table 4.4 Pulse-Burst Waveform Examples

<i>Subpulse duration</i>	1 μs	1 μs	1 μs	1 μs
<i>Subpulse bandwidth</i>	1 MHz	1 MHz	100 MHz	100 MHz
<i>Range resolution</i>	150m	150m	1.5m	1.5m
<i>Number of subpulses</i>	10	10	1,000	1,000
<i>Subpulse separation</i>	10 μs	10 μs	100 μs	100 μs
<i>Waveform duration</i>	90 μs	90 μs	100 ms	100 ms
<i>Frequency</i>	1 GHz	10 GHz	1 GHz	10 GHz
<i>Velocity resolution</i>	1.67 km/s	167 m/s	1.5 m/s	0.15 m/s
<i>Time-bandwidth product</i>	190	190	10,000,000	10,000,000
<i>Range ambiguity spacing</i>	1.5 km	1.5 km	15 km	15 km
<i>Velocity ambiguity spacing</i>	15 km/s	1.5 km/s	1.5 km/s	150 m/s

The duration of a pulse-burst waveform is often less than the target range delay, to allow a group of targets to be observed without ambiguity. A train of coherently integrated pulses, as discussed in Section 5.4, is a form of pulse-burst waveform that has an interpulse period often exceeding the target range delay.

4.6 Multiple-Time-Around Returns

Radar waveforms are often transmitted at periodic intervals that may be described by a pulse-repetition interval (PRI), which is the reciprocal of the pulse-repetition frequency (PRF). A signal return from a target as having a range greater than $c(\text{PRI})/2$, will reach the receiver after the next pulse has been transmitted. It will likely be interpreted as a target return from the latter pulse, and as having a range much shorter than the actual range. This type of range ambiguity is often called a second-time-around return. Even longer-range targets may produce third and higher multiple-time-around returns. This situation is illustrated in Figure 4.10(a). For example, with a PRF of 1,000 Hz, the PRI is 1 ms, corresponding to a range of 150 km. This is called the unambiguous range. The return from a target at a range of 200 km would appear to have a range of 50 km (200 km minus the unambiguous range of 150 km). A target at a range of 400 km would appear as a third-time-around return to have a range of 100 km (400 km minus twice the unambiguous range, 300 km).

Multiple-time-around returns may occur when targets are detected at unexpectedly long ranges. This may be the result of anomalous propagation around the Earth's curvature caused by ducting, discussed in Section 9.3. For example, a ship-board radar at a height above the ocean of 20m has a radar horizon of about 18 km (see Section 2.1). Target ships having heights of 50m or less would have maximum horizon ranges of 29 km. Thus, a radar might use a PRF of 3,000 Hz, which provides unambiguous ranges out to 50 km. If anomalous propagation, or a target hav-

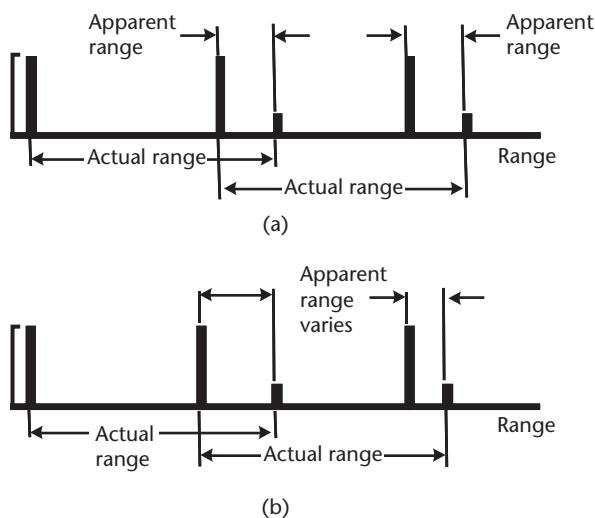


Figure 4.10 Illustration of second-time around return, and effect of PRF jitter. (a) Fixed PRF. (b) Variable PRF.

ing a height greater than 50m were present at a range greater than 50 km, it could produce a multiple-time-around return.

The potential problem with multiple-time-around returns occurs when they are not anticipated and the target range is misinterpreted. One technique to mitigate multiple-time-around returns is to change the interpulse interval from pulse-to-pulse. This is often called jittering the PRF. The result, illustrated by Figure 4.10(b), is that the apparent range of the multiple-time-around return changes from pulse-to-pulse. When the range is measured from the correct transmitted pulse, it remains fixed.

Another method for eliminating multiple-time-around returns is to change the transmitted signal frequency from pulse-to-pulse. The received signal may then be correctly associated with the transmitted pulse by observing its frequency. This method may not be used when coherent processing is used on successive pulse returns, as for MTI or pulse-Doppler processing, or for coherent pulse integration. Other considerations associated with MTI processing are discussed in Chapter 9.

4.7 Radial-Velocity Ambiguities

Radar operating at fixed PRF also produces ambiguities in radial velocity. These are separated by λ (PRF)/2, as may be seen by analogy with the pulse-burst waveform ambiguity function illustrated in Figure 4.9. For example, an X-band radar ($\lambda = 0.0316\text{m}$), operating at a PRF of 200 Hz will produce radial-velocity ambiguities separated by 3.16 m/s. This may be a concern when the radar clutter has a radial-velocity spread greater than the radial-velocity ambiguity, which is often the case for airborne and space-based radar (see Section 11.2). In such cases, the clutter at the ambiguous radial velocities is added to the zero-velocity clutter, which may significantly increase its magnitude.

The radial-velocity ambiguity of target returns may be resolved from prior knowledge of possible target radial velocities, or by calculating the target radial velocity from successive range measurements. These ambiguities may also be resolved by varying the radar PRF in a technique analogous to that described in Section 4.6 for range ambiguities. Finally, a PRF high enough to eliminate the radial-velocity ambiguities may be used. This technique, often used in airborne radar, requires very high values of PRF [e.g., 20 kHz (see Section 11.3)]. This usually leads to highly ambiguous range, which is resolved by techniques such as those discussed earlier.

4.8 Problems

The following problems are provided to assist in reviewing this chapter and to ensure a basic understanding of the material. Solutions to these problems are given in Appendix E, Section E.4.

1. What are the three major characteristics of radar waveforms?
2. What range resolution is provided by a waveform having a bandwidth of 10 MHz? What is the duration of a CW pulse with this range resolution?

3. What are the frequency resolution and the radial-velocity resolution of a waveform having a frequency of 3.3 GHz (S band) and a duration of 50 ms? If this is a CW pulse, what is the range resolution?
4. For a linear FM waveform having a pulse compression ratio of 1,000 and the duration and frequency from Problem 3, what are the range and radial-velocity resolutions?
5. For the linear FM waveform described in Problem 4, and assuming the waveform frequency increases with time, what is the range offset produced by a target with a radial velocity of 300 m/s?
6. An L-band (1.3 GHz) phase-coded waveform employs 500 subpulses, each a CW pulse with a duration of $1\ \mu\text{s}$. What are the waveform duration, the range resolution, the radial-velocity resolution and the approximate peak sidelobe level?
7. For a pulse-burst waveform with subpulse spacing of $100\ \mu\text{s}$, what is the spacing of range ambiguities? If the subpulses are chirp waveforms having duration $1\ \mu\text{s}$ and bandwidth 100 MHz, what is the range resolution? If the waveform consists of 200 subpulses at X band (9.5 GHz), what is the spacing of the ambiguities in radial velocity, and what is the radial-velocity resolution?
8. What is the unambiguous range for a PRF of 200 Hz? If a target has an apparent range of 300 km, what is the actual range if the target is a second-time-around return? What is the range if it is a third-time-around return?
9. What time resolution is needed to provide 10m range resolution? What waveform bandwidth is required?
10. For X band (9.5 GHz), and L band (1.3 GHz), what Doppler frequency resolution is required to provide 100 m/s radial-velocity resolution? What waveform durations are required?
11. What determines the total volume under the ambiguity-function surface?
12. What pulse compression ratios are required to provide the waveform parameters in Problems 9 and 10, assuming single-pulse waveforms?
13. For a chirp waveform having a bandwidth of 100 MHz and a pulse-compression ratio of 10^4 , what are the pulse duration and the corresponding range resolution? For a C band frequency (5.5 GHz), what is the velocity resolution? What is the extent of the sidelobes in range and velocity?
14. For the waveform in Problem 13, what is the range offset for a target closing with a radial velocity of 1 km/s, assuming up-chirp? What is the offset for down-chirp?
15. For a phase-coded waveform, what CW subpulse duration is needed for 15m range resolution? At X band (9.5 GHz), what waveform duration is needed for a velocity resolution of 1 km/s? What is the resulting number of subpulses and the approximate peak range sidelobe level?
16. If a pulse-burst waveform is to provide an ambiguity-free space ± 10 km in range and an ambiguity-free space ± 1 km/s in radial velocity, what is the required subpulse spacing? What is the maximum frequency that may be

used? At this frequency, what are the waveform duration and number of subpulses needed to provide 10 m/s velocity resolution?

17. What is the maximum unambiguous range for a PRF of 500 Hz? What will be the apparent range of a target having an actual range of 700 km?

References

- [1] Deley, G. D., "Waveform Design," Chapter 3 in *Radar Handbook*, M. I. Skolnik, (ed.), New York: McGraw-Hill, 1970.
- [2] Woodward, P. M., *Probability and Information Theory, With Applications to Radar*, New York: McGraw-Hill, 1957.
- [3] Skolnik, M. I., *Introduction to Radar Systems*, 2nd ed., New York: McGraw-Hill, 1980.
- [4] Farnett, E. C., and G. H. Stevens, "Pulse-Compression Radar," Chapter 10 in *Radar Handbook, 2nd Ed.*, M. I. Skolnik, (ed.), New York: McGraw-Hill, 1990.

Selected Bibliography

The radar ambiguity function is developed by Woodward in his small book, which also provides a good background in Fourier analysis of waveform characteristics. A good summary of waveform design theory is given by Deley, in Skolnik's 1970 handbook. (This material is not included in the second edition of the handbook.) The implementation and performance of pulse compression in radar is addressed in Farnett, Howard, and Stevens, and by Farnett and Stevens in Skolnik's 1970 and 1990 handbooks respectively. Radar waveforms for airborne radars are treated in Morchin, and by Morris, and waveforms for space-based radars are discussed in Cantafio.

- Cantafio, L. J., (ed.), *Space-Based Radar Handbook*, Norwood, MA: Artech House, 1989.
- Deley, G. D., "Waveform Design," Chapter 3 in *Radar Handbook*, M. I. Skolnik, (ed.), New York: McGraw-Hill, 1970.
- Farnett, E. C., and G. H. Stevens, "Pulse-Compression Radar," Chapter 10 in *Radar Handbook, 2nd Ed.*, M. I. Skolnik, (ed.), New York: McGraw-Hill, 1990.
- Farnett, E. C., T. B. Howard, and G. H. Stevens, "Pulse-Compression Radar," Chapter 20 in *Radar Handbook*, M. I. Skolnik, (ed.), New York: McGraw-Hill, 1970.
- Morchin, W. C., *Airborne Early Warning Radar*, Norwood, MA: Artech House, 1990.
- Morris, G. V., *Airborne Pulsed Doppler Radar*, Norwood, MA: Artech House, 1988.
- Skolnik, M. I., (ed.), *Radar Handbook*, New York: McGraw-Hill, 1970.
- Skolnik, M. I., (ed.), *Radar Handbook*, 2nd ed., New York: McGraw-Hill, 1990.
- Woodward, P. M., *Probability and Information Theory with Applications to Radar*, New York: McGraw-Hill, 1957.

The Radar Equation

This chapter enables the reader to:

- Use the radar equation to calculate the S/N, and other key radar parameters;
- Understand how radar parameters are defined and correctly used in the radar equation;
- Use radar reference range in radar performance calculations for convenience or when detailed radar parameters are unavailable;
- Model coherent and noncoherent pulse integration in radar calculations, and understand their capabilities and limitations;
- Understand the limitations imposed by the minimum-range constraint, evaluate its impact on radar performance, and learn how it may be mitigated.

The S/N that a radar provides is a key measure of its performance. It determines the radar capabilities for detecting targets, for measuring target characteristics, and for tracking targets, as discussed in Chapters 6 and 8. The radar range equation relates S/N to the key radar and target parameters, including target range. It is widely used in modeling and analyzing radar performance.

The S/N is defined as the ratio of signal power to noise power at the output of the radar receiver. For radar receivers that employ a matched filter, this is equal to the ratio of the signal energy at the input to the receiver to the noise power per unit bandwidth [1, pp. 17–18]. Radar normally employs filters matched to the received radar signal, or at close approximations to them, because these filters maximize the S/N of the received signal. A matched filter has a frequency response that is the complex conjugate of the received signal, and therefore has the same signal bandwidth as the received signal (see Section 4.1).

5.1 Radar Range Equation

The basic form of the radar range equation gives the ratio of signal power from the target S, to the background noise power at the radar receiver N, which includes both noise received from the external environment and noise added in the radar [2, pp. 18–19].

$$\frac{S}{N} = \frac{P_p \tau G_T \sigma A_R}{(4\pi)^2 R^4 k T_s L} \quad (5.1)$$

where:

S/N = radar signal-to-noise ratio (power ratio)

P_p = radar transmitted peak RF power (W)

τ = radar pulse duration (sec)

G_T = radar transmit antenna gain (power ratio)

σ = target radar cross section (RCS, in m^2)

A_R = radar receive antenna effective aperture area (m^2)

R = range from the radar to the target (m)

k = Boltzmann's constant (1.38×10^{-23} J/K)

T_s = radar system noise temperature (K)

L = radar system losses (power ratio)

This equation may be thought of as the waveform energy, $P_p\tau$, amplified by the transmit antenna gain, G_T , diminished by the space spreading term, $1/(4\pi R^2)$, producing the power density at the target. Multiplying by σ gives the energy density scattered by the target in the direction of the radar. This energy density is reduced by the space spreading factor, $1/(4\pi R^2)$, and the receive antenna aperture area, A_R , gives the portion of the signal energy intercepted by the radar antenna. This, reduced by the system losses, L , represents the signal term. The noise energy is given by kT_s . The value of k given above assumes all other parameters are in the standard metric system, also known as the mks system, as indicated (see Section 1.4 and Appendix D).

The power ratios S/N , G_T , and L are often specified in decibels. When this is the case, they should be converted to power ratios for use in the radar range equation:

$$\text{Power ratio} = 10^{(\text{dB}/10)} \quad (5.2)$$

Target RCS is commonly expressed in dBsm, which should similarly be converted to square meters:

$$\text{RCS } (m^2) = 10^{(\text{dBsm}/10)} \quad (5.3)$$

The receive antenna aperture area A_R , may be calculated from the receive gain G_R by:

$$A_R = \frac{G_R \lambda^2}{4\pi} \quad (5.4)$$

where:

G_R = receive antenna gain (power ratio)

λ = radar wavelength (m)

When the same antenna is used for transmit and receive, the receive gain G_R , may equal the transmit gain G_T . However, when more severe illumination taper is used for receive than for transmit to reduce the receive sidelobes, G_R may be slightly less than G_T . This is often the case for phased-array antennas (see Sections 3.2 and 3.3).

The radar system noise temperature, T_s , includes both external and internal radar noises. External noise comes from the temperature of objects that the antenna main beam and sidelobes observe, principally the sky and the Earth. The noise is attenuated by the receive antenna and microwave losses to the point where T_s is defined. The principal source of internal radar noise is the first stage of the radar receiver. Other sources are later stages of the receiver and the receive antenna and microwave elements. These are adjusted by the gains and losses to the point where T_s is defined (see Section 3.4).

The losses that should be included in the system loss factor, L , include:

- Transmit microwave loss, L_{MT} , measured from the point where the transmit power is defined, to the antenna;
- Two-way off-broadside scan loss, L_s , for phased arrays;
- Two-way propagation losses, L_p , from the atmosphere, ionosphere, and rain (see Chapter 9);
- Receive microwave loss, L_{MR} , measured from the antenna to the point where the system noise temperature is defined;
- Signal processing losses, L_{sp} (e.g., quantization error, filter mismatch).

Note that the transmit antenna ohmic losses, L_{AT} , and the aperture efficiency losses, L_{ET} , are included in the transmit gain, G_T , as defined in Section 3.2. Similarly, the receive antenna ohmic losses, L_{AR} , and aperture efficiency losses, L_{ER} , are included in the effective receive aperture area, A_R . Thus, these losses are not included in the radar system losses, L (see Section 5.2).

The beamshape loss, L_{BS} , is usually associated with the search mode, and is normally added when the search is configured (see Chapter 7). The system loss, L , is the product of the individual losses when each is expressed as a power ratio. The system loss in decibels is the sum of the individual losses given in decibels. Note that losses here are defined as factors larger than unity or positive values in decibels.

For example, consider a radar having a peak power of 20 kW (20,000 W), a pulse duration of 1 ms (0.001 s), a transmit and receive gain of 35 dB (power ratio = 3,162), system noise temperature of 500K, transmit and receive microwave losses of 1.5 dB each (power ratio = 1.41), and signal processing losses of 1.0 dB (power ratio = 1.26). For an S-band radar frequency of 3.3 GHz, the wavelength is 0.09091m, and the receive aperture area from (5.4) is 2.079 m². The radar observes a target having a RCS of 10 dBsm (10 m²), at a range of 200 km (200,000 m). The target is at the center of the radar beam, so there is no beamshape loss. The radar employs a reflector antenna, so there is no scan loss. The propagation losses are estimated at 3.3 dB (power ratio = 2.14), from Chapter 9. This example is summarized in Table 5.1. The input radar parameters are given in the second column in the commonly used engineering units specified. They are converted to mks (SI) values in the fourth column. The radar wavelength and receive aperture area are calculated in column 3. The assumed loss values total 7.3 dB, and this value is shown in the third column of the table, and converted to a power ratio (5.37) in the fourth column. Applying (5.1) to the values in column 4 gives the S/N power ratio as 53.39. It is converted to 17.3 dB in column 3.

Table 5.1 Radar Equation Example

<i>Parameter</i>	<i>Input Value</i>	<i>Calculated</i>	
		<i>Value</i>	<i>mks Value</i>
P_P	20 kW		20,000W
τ	1 ms		0.001s
G_T	35 dB		3,162
σ	10 dBsm		10 m ²
G_R	35 dB		3,162
f	3.3 GHz		3,300,000,000 Hz
λ		0.0909m	
A_R		2.079 m ²	2.079 m ²
R	200 km		200,000 m
T_S	500K		500K
L		7.3 dB	5.370
S/N		17.3 dB	53.39
<i>Bandwidth formulation</i>			
B	1 MHz		1,000,000 Hz
PC	1,000		1,000
<i>Loss</i>			
L_{MT}	1.5		
L_{MR}	1.5		
L_P	3.3		
L_{SP}	1.0		
Total, L	7.3		

The radar equation is sometimes given using the signal bandwidth, B , rather than the pulse duration τ :

$$\frac{S}{N} = \frac{P_P G_T \sigma A_R PC}{(4\pi)^2 R^4 B k T_S L} \quad (5.5)$$

where:

B = radar signal bandwidth (Hz)

PC = radar signal pulse compression ratio (power ratio)

This equation is valid when the radar employs a matched filter for the pulse compression [1, pp. 220–224, 2, pp. 29–33]. The pulse compression ratio (see Chapter 4), is approximately equal to τB , so this form of the radar equation is equivalent to (5.1). Since τ is replaced by PC/B , it is essential to include the pulse-compression ratio, PC , when using this formulation.

Extending the previous example, if the radar employs a pulse compression waveform having a bandwidth of 1 MHz (1,000,000 Hz), the pulse compression ratio is 1,000. These values are shown in the last two lines of Table 5.1. Assuming the receiver employs a filter matched to the pulse-compression waveform, (5.5) may be used, and gives the same result as previously.

The radar range equation may be used to calculate the radar system performance in terms of the S/N achieved. Values of S/N in of the order of 10 to 100 (10 to 20 dB), are useful for detection and tracking. Alternatively, the equation

may be rearranged to calculate the range at which a given value of S/N may be obtained, or to calculate the pulse duration required to achieve a given S/N at a given range:

$$R = \left[\frac{P_p \tau G_T \sigma A_R}{(4\pi)^2 (S/N) k T_s L} \right]^{1/4} \quad (5.6)$$

$$\tau = \frac{(4\pi)^2 (S/N) R^4 k T_s L}{P_p G_T \sigma A_R} \quad (5.7)$$

For the radar in the previous example, the range at which $S/N = 15$ dB may be calculated from (5.6) as 290 km (290,000m). The pulse duration required to provide $S/N = 15$ dB at a range of 300 km may be calculated from (5.7) as 1.64 ms (0.00164s).

5.2 Parameter Definition in the Radar Equation

It is important that the radar parameters be consistently defined. Failure to consistently define the transmitter power, system noise temperature, antenna gain and aperture area, and the microwave losses may lead to errors in calculating performance using the radar equation. Figure 5.1 shows the signal path from the transmitter through the antenna to the target, and back to the receiver and signal processor. The transmitted power is conventionally defined at the output of the transmitter. Its value may be less than the power output of the transmitter RF power source (tube or solid-state devices), due to losses in the transmitter circuits leading to the transmitter output (see Section 3.1). In some cases, the transmitted power may be defined and measured at some point between the transmitter and the antenna. In either case, the microwave losses, L_{MT} , following the point where the transmitted power is defined are included in the radar system loss L .

Similarly, the system noise temperature, T_s , is conventionally defined at the output of the receive antenna. However, in some cases the system noise temperature may be defined at some point between the antenna and the receiver, or at the receiver input. The microwave losses, L_{MR} , between the antenna and that point are included in L .

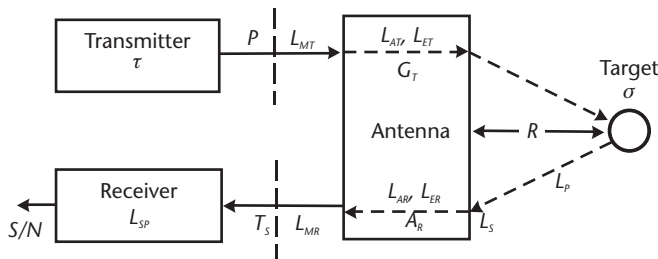


Figure 5.1 Radar and target elements showing consistent definitions of radar parameters used in the radar range equation.

The transmit antenna is characterized by the transmit gain, G_T , which includes the effect of the transmit antenna ohmic loss, L_{AT} , and the transmit aperture-efficiency loss, L_{ET} ; they should not be included again in the system losses (see Section 3.2). However, when the transmit antenna gain that corresponds to the physical aperture area is used (i.e., the antenna directivity), the transmit ohmic and aperture-efficiency losses should be included in the system losses. Similarly, the receive aperture area may be characterized by the physical aperture area, A_A , in which case the receive antenna ohmic loss, L_{AR} , and the receive aperture-efficiency loss, L_{ER} , should be included in the system losses. If the receive effective aperture area, A_R , is used, then the receive ohmic and aperture-efficiency losses are already included, and they should not be included again in the system losses.

The two-way propagation losses to the target, L_p , and (for phased arrays), the two-way off-axis scan losses, L_s , should be included in L . Losses due to suboptimal signal processing, L_{sp} , are also included in L . The definition of radar parameters in a phased-array radar employing transmit-receive modules (see Sections 2.3 and 3.3) is shown in Figure 5.2. The transmitted power is the sum of the RF power from all the modules, measured at the output of the module, or at some point between the module and the antenna element associated with that module. When the module powers are equal, which is usually the case, the transmitted power for an array of n_M identical modules is then n_M times the transmitted power from a single module, P_M :

$$P = n_M P_M \quad (5.8)$$

The transmit microwave loss, L_{MT} , affects the power from each module identically, and thus is included in the system loss, L .

In modular phased-arrays, each module often feeds a separate radiating element in the array antenna, as shown in Figure 5.2. In some designs, a module may feed more than one element, or a radiating element may be fed by more than one module.

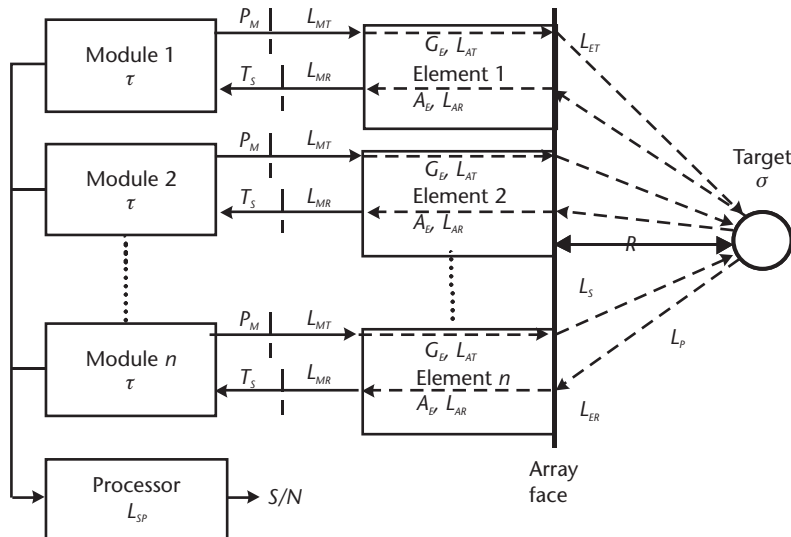


Figure 5.2 Modular phased-array radar and target elements showing consistent definitions of radar parameters used in the radar range equation.

In any case, the phased-array antenna gain is the sum of the gains of the n_E individual radiating elements, G_E , and the effective receive aperture area is the sum of the effective aperture areas, A_E , of the individual elements. When the elements are identical, which is usually the case:

$$G_T = n_E G_E \quad (5.9)$$

$$A_R = n_E A_E \quad (5.10)$$

The effective element gain, G_E , and the effective element aperture area, A_E , should include the antenna ohmic loss factors, L_{AT} and L_{AR} , respectively. If they are not so included, they should be included in the system loss, L . Note that the properties of radiating elements in the array may differ from the properties of these same elements measured individually outside the array. It is the gain and effective area of the elements when located in the array that are used for G_E and A_E .

The noise temperature is measured at the input to each module, or between the receive antenna and the module. For identical modules, this is the same for all modules, and the radar receiver noise temperature, T_s , is equal to the noise temperature for the modules. The receive microwave loss to the point where the noise temperature is measured, L_{MR} , is included in the system loss, L .

In the rare cases where values of the noise temperature and antenna and microwave ohmic losses for the modules are not identical, average parameter values may be calculated and used.

Receive aperture weighting is often used in phased arrays to reduce the receive antenna sidelobes (see Section 3.3). This usually involves reducing the signal gain in modules located around the array periphery. The effect is to reduce the effective aperture area. The receive aperture area (or equivalently the receive gain), should be specified accordingly. If it is not, the receive aperture efficiency loss, L_{ER} , is added to L . If transmit aperture weighting is used, its effect should be included in the transmit gain. If it is not, the transmit aperture efficiency, L_{ET} , loss is added to L .

For example, consider the phased-array radar described in Table 5.2. It employs 1,000 transmit-receive modules, each connected to its own antenna element. If the module power $P_M = 10\text{W}$, the total radar power $P_p = 10\text{ kW}$ (10,000W). If the element gain $G_E = 5\text{ dB}$ (power ratio = 3.16), and the element receive area $A_E = 0.000251\text{ m}^2$ (corresponding to X-band wavelength of 0.0316m), the total antenna gain $G_T = 35\text{ dB}$ (power ratio = 3,160), and the aperture area $A_R = 0.251\text{ m}^2$. The antenna microwave losses, L_{AT} and L_{AR} , are

Table 5.2 Phased-Array Antenna Example

<i>Input Parameters</i>		<i>Calculated Values</i>	
n_M	1,000		
P_M	10W	P_p	10 kW
n_E	1,000		
G_E	5 dB	G_T	35 dB
f	9.5 GHz	λ	0.0316m
		A_E	0.000251 m ²
		A_R	0.251 m ²

included in G_E and A_E , respectively, and so are included in the calculated values of G_T and A_R .

If Taylor 30 dB weighting is used in the receive aperture in this example, the aperture efficiency loss, L_{ER} , = 0.71 dB (see Table 3.1). The resulting effective aperture area may be reduced by this factor to give an effective aperture area of 0.231 m². The system noise temperature, T_s , and the microwave loss parameters, L_{MT} and L_{MR} , are equal to those common to the modules and elements.

5.3 Reference Range

The radar range equation relates the target range and S/N to the key radar and target parameters. When these parameters are not available, and a radar reference range is provided, the reference range may be used to analyze and model radar performance.

The radar reference range, R_{ref} , is given for specified values of pulse duration, τ_{ref} , target RCS, σ_{ref} , and S/N, $(S/N)_{ref}$. The reference range is usually specified assuming the target is broadside to the radar antenna (for phased arrays), so there is no scan loss; at the center of the beam, so there is no beam-shape loss; and without propagation losses. The radar range, for other combinations of pulse duration, τ , σ , and S/N, may be calculated by scaling from the reference range. Losses from off-broadside scan, L_S , beamshape, L_{BS} , and propagation, L_P , for the specific scenario may also be included in the calculation:

$$R = R_{ref} \left[\frac{\tau}{\tau_{ref}} \frac{\sigma}{\sigma_{ref}} \frac{(S/N)_{ref}}{(S/N)} \frac{1}{L_S L_{BS} L_P} \right]^{1/4} \quad (5.11)$$

Any consistent set of parameters may be used in the ratios. Note that S/N and the losses must be power ratios and σ must be in units of area. If they are given in decibels or decibels relative to a square meter, they must be converted to power ratios or areas, as discussed earlier.

For example, consider a radar having a reference range R_{ref} = 500 km, for a pulse duration τ_{ref} = 1 ms, S/N_{ref} = 15 dB, and target RCS_{ref} = -10 dBsm (0.1 m²). There are no scan, beamshape, or propagation losses, consistent with the definition of reference range. These reference parameters are shown in the second column of Table 5.3.

Table 5.3 Examples of Radar Reference Range Calculations

<i>Parameter</i>	<i>Reference Value</i>	<i>Range Calculation</i>	<i>S/N Calculation</i>	<i>τ Calculation</i>
R	500 km	360 km	250 km	400 km
τ	1 ms	1 ms	0.5 ms	0.216 ms
S/N	15 dB	20 dB	20.5 dB	18 dB
σ	-10 dBsm	-5 dBsm	-10 dBsm	0 dBsm
$L_S L_{BS} L_P$	0 dB	5.7 dB	3.5 dB	4.2 dB

Equation 5.11 may be used to find the radar range for $S/N = 20$ dB on a -5 dBsm (0.316 m^2) target, using the same waveform. Assume $L_S = 2.5$ dB, $L_{BS} = 0$ dB, and $L_P = 3.2$ dB. The total additional losses in (5.11) are 5.7 dB (power ratio = 3.72). The resulting range is 360 km, as shown in the third column of Table 5.3.

Similar equations may be used to calculate S/N , pulse duration, or RCS for given values of the other parameters. For example:

$$\frac{S}{N} = \left(\frac{S}{N} \right)_{ref} \left(\frac{R_{ref}}{R} \right)^4 \frac{\tau}{\tau_{ref}} \frac{\sigma}{\sigma_{ref}} \frac{1}{L_S L_{BS} L_P} \quad (5.12)$$

The fourth column in Table 5.3 shows the calculation of S/N for a range of 250 km, a pulse duration of 0.5 ms, and an RCS value of -10 dBsm, assuming the additional losses are 3.5 dB. The resulting $S/N = 20.5$ dB. The final column in Table 5.3 shows the calculation of the pulse duration needed to provide S/N of 18 dB on a 0 dBsm target at a range of 400 km, with additional losses of 4.2 dB. The value of $\tau = 0.216$ ms.

To be most useful, the reference range should be defined on broadside of phased-array antennas, at the center of the radar beam, and with no propagation losses, as discussed above. However, when the radar range is specified for other conditions, the desired reference range may be found by adjusting the range to compensate for removing the scan loss, L_S , beamshape loss, L_{BS} , and propagation loss, L_P , as indicated in (5.11). Appropriate adjustments may also be made for any differences between the radar system losses assumed for the reference case, and those in the scenario being addressed. Additional losses specific to radar search modes may also be added in calculations using reference range (see Chapter 7).

The radar reference range may be calculated directly from the radar and target parameters, when they are available:

$$R_{ref} = \left[\frac{P_p \tau_{ref} G_T \sigma_{ref} A_R}{(4\pi)^2 (S/N)_{ref} k T_S L_F} \right]^{1/4} \quad (5.13)$$

where L_F = fixed radar system loss (excluding off-broadside scan, beamshape, and propagation losses).

Calculating and using such a reference range may simplify radar modeling and analysis procedures. For example, reference range is a useful tool for calculating radar performance when parameters are varied, for example in worksheet calculations. Thus, it is sometimes useful to calculate and use the reference range even when a complete set of radar parameters is available.

5.4 Pulse Integration

Radar sensitivity may be increased by adding the return signals from several transmitted radar pulses. Such pulse integration may be coherent or noncoherent.

Coherent integration (also called predetection integration) occurs when these signal returns are added prior to the envelope detection process in the radar receiver.

The signals are then sinusoidal RF or intermediate frequency (IF) waves. If n signal returns are added in-phase, the resulting signal amplitude (voltage) is n times the amplitude of a single return, and the power of the integrated signal is n^2 times the power of a single signal, S .

The noise is also added, but since the noise returns associated with the n signal returns are not correlated, they add in a root-mean-square (rms) fashion. The integrated noise power, N , is n times the noise power associated with a single return. The resulting coherently integrated signal-to-noise ratio $(S/N)_{CI}$, is n times the S/N for a single return pulse:

$$(S/N)_{CI} = n S/N \quad (5.14)$$

The coherent integration gain, defined as the ratio of integrated S/N to single-pulse S/N , is then equal to the number of pulses integrated, n . In practice, additional signal processing losses in the integration process, L_{SPI} , may reduce the integrated S/N from this theoretical value.

Losses in coherent integration that reduce the effective gain may occur when the signal processing is not optimum, or when the signal returns do not maintain the expected phase relationship. The latter may occur when:

- The transmitted signal is not sufficiently stable from pulse to pulse (this is usually not the limiting factor in modern radar).
- The target return is not stable (e.g., a tumbling target with rapid amplitude and phase fluctuations).
- The propagation path is not stable (e.g., fluctuations of lower-frequency radar signals caused by the ionosphere, see Section 9.4).
- Target range changes result in changes in the phase of the signal returns, preventing them from adding in-phase.

The last factor above may be compensated for in the signal processing if the range changes are precisely known. This may be the case when a target is in track and its radial velocity is well known. An alternative, used in pulse-Doppler processing, is to perform coherent processing for all possible radial velocities, and select the output with the largest integrated return (see Sections 2.5 and 11.3) [3, pp. 17.1–17.9]. These techniques are limited by changes in the radial velocity caused by target radial acceleration or changes of the viewing LOS. Specifically, if a constant target radial velocity is assumed, the coherent integration time is limited by the radial component of target acceleration to:

$$t_{CI} \leq \left(\frac{\lambda}{2a_R} \right)^{1/2} \quad (5.15)$$

where:

t_{CI} = coherent integration time

a_R = target radial acceleration

The result of the collective factors given above is to limit the time over which coherent integration may effectively be performed, and hence the coherent integration gain that may be obtained. Coherent integration times of a few tenths of a second may typically be obtained for stable, nonmaneuvering targets. For example, the constraint in (5.15) would limit coherent integration for an X-band radar ($\lambda = 0.0316\text{m}$), to 0.4 seconds for a target having a radial acceleration of $0.1g$.

For fixed targets, or where changes in radial velocity and radial acceleration may be compensated for (e.g., orbital objects), integration times of a few seconds may be feasible. Coherent integration may also be limited by the portion of the radar power (or number of pulses) that may be devoted to a target.

Noncoherent integration (also called postdetection or incoherent integration) occurs when signal returns are added after the demodulation, or envelope detection process in the radar receiver. The detection loss for returns having low S/N limits the efficiency of noncoherent integration. The effect of this loss is different from the impact of noncoherent integration on target detection probability, where noncoherent integration may improve target detectability in some circumstances (see Chapter 6). When considering the impact of S/N on radar measurement accuracy (see Chapter 8), the detection loss, L_D , for a signal return having a single-pulse S/N is given by [4, pp. 82–84]:

$$L_D = \frac{1 + \frac{S}{N}}{\frac{S}{N}} \quad (\text{Radar measurement}) \quad (5.16)$$

For n pulses noncoherently integrated, the noncoherently integrated signal-to-noise ratio $(S/N)_{NI}$ is given by:

$$\left(\frac{S}{N}\right)_{NI} = n \left(\frac{S}{N}\right) \frac{\frac{S}{N}}{1 + \frac{S}{N}} \quad (\text{Radar measurement}) \quad (5.17)$$

For example, with a single-pulse S/N = 3 dB (power ratio = 2.0), the detection loss $L_D = 1.5$ (1.76 dB). Noncoherently integrating 10 such pulses would give $(S/N)_{NI} = 13.33$ (11.25 dB). With coherent integration for these parameters, $(S/N)_{CI} = 20$ (13.0 dB). To achieve $(S/N)_{NI} = 32$ (15.5 dB), would require noncoherent integration of 24 pulses, while coherent integration would require only 16 pulses.

The single-pulse S/N needed to provide a desired $(S/N)_{NI}$ is given by:

$$\frac{S}{N} = \frac{\left(\frac{S}{N}\right)_{NI}}{2n} + \left(\frac{\left(\frac{S}{N}\right)_{NI}^2}{4n^2} + \frac{\left(\frac{S}{N}\right)_{NI}}{n} \right)^{\frac{1}{2}} \quad (\text{Radar measurement}) \quad (5.18)$$

For example, to provide a value of $(S/N)_{NI} = 15$ dB by noncoherently integrating 10 pulses would require a single-pulse S/N = 5.98 dB. With coherent integration, the single-pulse S/N needed would be 5 dB.

When considering the impact of S/N on radar detection, the detection loss, L_D , is given approximately by [1, pp. 63–66]:

$$L_D \approx \frac{2.3 + \frac{S}{N}}{\frac{S}{N}} \quad (\text{Radar detection}) \quad (5.19)$$

The integrated S/N is then given by:

$$\left(\frac{S}{N}\right)_{NI} \approx n \left(\frac{S}{N}\right) \frac{\frac{S}{N}}{2.3 + \frac{S}{N}} \quad (\text{Radar detection}) \quad (5.20)$$

The single-pulse S/N may then be found from:

$$\frac{S}{N} = \frac{\left(\frac{S}{N}\right)_{NI}}{2n} + \left(\frac{\left(\frac{S}{N}\right)_{NI}^2}{4n^2} + \frac{2.3 \left(\frac{S}{N}\right)_{NI}}{n} \right)^{\frac{1}{2}} \quad (\text{Radar detection}) \quad (5.21)$$

The resulting detection loss, L_D , when radar detection is considered, is larger than the loss discussed earlier for radar measurement. The procedures for calculating radar detection parameters, given in Chapter 6, take these losses into account.

The noncoherent integration gain is always smaller than n (the coherent integration gain), as a result of the detection loss. The detection loss is small for single-pulse S/N values useful for detection and tracking ($S/N = 10$ to 100 , or 10 to 20 dB). This loss is often neglected in such cases. However, when many pulses are integrated noncoherently to achieve these useful $(S/N)_{NI}$ values, the S/N of the individual pulses is small, and the loss may be significant. For this reason, noncoherent integration of large numbers of pulses (e.g., hundreds) is inefficient and is often avoided.

This is illustrated by Figure 5.3, which shows the integrated S/N for radar measurement, as a function of number of pulses integrated, both coherently and noncoherently, for several values of single-pulse S/N . (The coherently integrated S/N is also reduced by the detection loss to make results comparable to those for noncoherent integration, which are also subject to detection loss.) The plot shows that for single-pulse S/N values of 10 dB and greater, noncoherent and coherent integration provide comparable results. For lower values of single-pulse S/N , the losses for noncoherent integration are significant.

For example, with single-pulse $S/N = -10$ dB, coherently integrating about 300 pulses produces an integrated $S/N = 15$ dB. It would take about $3,500$ pulses, more than 10 times as many pulses, noncoherently integrated, to produce this same integrated S/N . The noncoherent integration losses for radar detection are larger than those shown in Figure 5.3, but these losses are still small for S/N of 10 dB or greater.

Noncoherent integration is generally easier to implement than coherent integration, and for small numbers of pulses integrated, the additional integration losses are

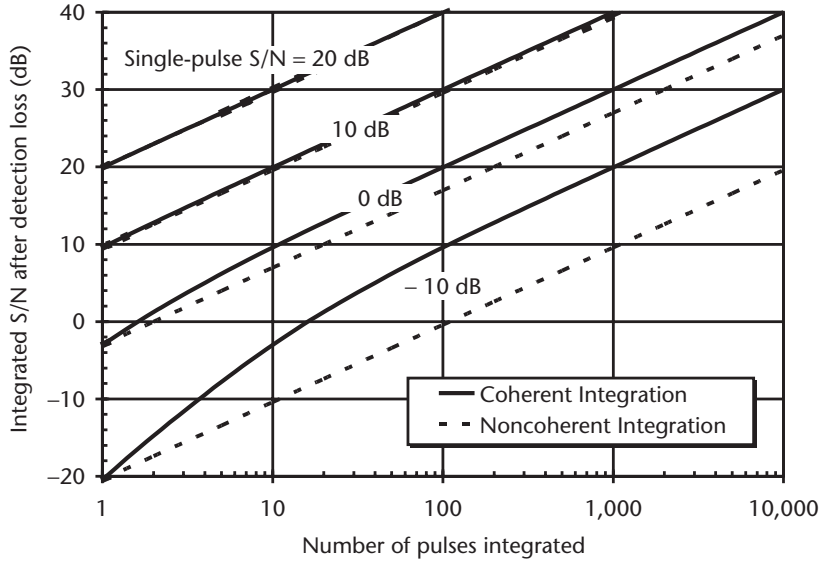


Figure 5.3 Integrated S/N for radar measurements as a function of number of pulses coherently and noncoherently integrated for various single-pulse S/N values.

small. Since the phase of the signal returns is not used in noncoherent integration, the limitations discussed above for coherent integration due to phase uncertainty are not relevant. A stable transmitter, target and propagation path, and precise knowledge of target range changes are not required.

However, the target range change, δR , during noncoherent integration must be small compared with the range equivalent of the compressed pulse duration τ_c :

$$\delta R \ll c\tau_c/2 \quad (5.22)$$

or equivalently:

$$\delta R \ll c/2B \quad (5.23)$$

If this condition is not met, the pulses will be skewed in time so that their envelopes do not all add, a situation called range walk, resulting in an integration loss. (Range walk is also associated with SAR, see Section 2.5.) Knowledge of target radial velocity may be used to compensate for range walk. This is similar to the velocity compensation used for coherent integration, but the accuracy required is far less, especially when τ_c is large. When range walk is not a consideration, or when it is adequately compensated for, noncoherent integration times of up to several seconds may be achieved.

When pulse integration is used by a radar, the radar range equation, (5.1), may be used to calculate the single-pulse S/N. The integrated S/N, $(S/N)_{CI}$ or $(S/N)_{NI}$, may then be calculated using (5.14), (5.17), or (5.20), and then used to evaluate radar tracking or detection performance. In the case of coherent integration, $(S/N)_{CI}$ may be calculated directly from (5.1) by substituting $n\tau$ for τ :

$$\left(\frac{S}{N}\right)_{CI} = \frac{P_p n \pi G_T \sigma A_R}{(4\pi)^2 R^4 k T_s L} \quad (5.24)$$

To calculate radar range when pulse integration is used, first find the single-pulse S/N that will produce the desired integrated S/N , using (5.18) or (5.21) for noncoherent integration, and for coherent integration:

$$S/N = \frac{(S/N)_{CI}}{n} \quad (5.25)$$

Then calculate R from (5.6).

Examples of pulse integration for radar measurement are given in Table 5.4. The second column shows that coherent integration of 16 pulses, each having $S/N = 3$ dB, gives an integrated S/N of about 15 dB. With noncoherent integration of the same pulses, the detection loss is about 1.76 dB, and the integrated S/N is about 13.3 dB, as shown in the third column. The 15 dB integrated S/N value may be achieved with noncoherent integration either by increasing the single-pulse S/N to 4.35 dB (fourth column), or increasing the number of pulses integrated to 24 (fifth column).

Either coherent or noncoherent integration may increase the signal-processing losses, L_{SP} , in the radar. This increase may be included in the total radar system losses, L , or the integrated S/N , $(S/N)_{CI}$ or $(S/N)_{NI}$, may be reduced by the amount of the additional integration processing loss, L_{SP} .

While coherent integration would appear to offer better performance than noncoherent integration, it requires a high degree of phase stability in the transmitter, the target return, and the propagation path; and precise knowledge of the target radial velocity. When these conditions are not met, noncoherent integration must be used. Even if the conditions for coherent integration are met, when only a few pulses need be integrated to provide usable S/N , as in the examples in Table 5.4, noncoherent integration is often used because of its simpler implementation and lower signal-processing losses. Detection of fluctuating targets may actually be enhanced by integrating a small number of pulses noncoherently, as discussed in Chapter 6.

5.5 Minimum Range Constraint

The practical requirement that a monostatic radar not begin to receive signals until the end of the transmitted pulse limits the minimum radar range, R_M , to:

Table 5.4 Pulse Integration Examples

<i>Parameter</i>	<i>Coherent</i>		<i>Noncoherent Integration</i>	
	<i>Integration</i>			
Single-pulse S/N	3 dB	3 dB	4.35 dB	3 dB
Number of pulses, n	16	16	16	24
Integrated S/N	15.04 dB	13.28 dB	15.03 dB	15.04 dB
Detection loss, L_D	—	1.76 dB	1.36 dB	1.76 dB

$$R_M = \frac{c\tau}{2} \quad (5.26)$$

In airborne pulse-Doppler radar, this overlap of transmitted and received pulses is often taken into account by an eclipsing loss [3, pp. 17.33–17.40]. In ground-based radar, the overlap is usually avoided by using suitable pulse durations, as discussed below. This limitation may be significant in solid-state radar that often has long pulse duration. For example, a radar using a 1-ms pulse has a minimum range of 150 km.

If the radar range, R , calculated from (5.6), for a given value of S/N is less than R_M , the target may not be fully observed at that S/N with that pulse duration, and (5.6) may not be used. When this is the case, the target may be observed by reducing the pulse duration to $\tau = 2R/c$, which reduces the S/N to:

$$\frac{S}{N} = \frac{2P_P G_T \sigma A_R}{(4\pi)^2 R^3 c k T_s L} \quad (R < R_M) \quad (5.27)$$

The S/N obtained is the smaller of that given by (5.1) or (5.27).

If the prior value of S/N is to be maintained, the pulse duration and range capability must be reduced even further. Then, the maximum range at which the target may be observed is:

$$R = \left[\frac{2P_P G_T \sigma A_R}{(4\pi)^2 (S/N) c k T_s L} \right]^{1/3} \quad (R < R_M) \quad (5.28)$$

The resulting pulse duration $\tau = 2R/c$.

The maximum range at which a target may be observed may also be calculated using the radar reference range:

$$R = R_{ref}^{4/3} \left[\frac{2\sigma(S/N)_{ref}}{c\tau_{ref} \sigma_{ref} (S/N) L_s L_{BS} L_p} \right]^{1/3} \quad (R < R_M) \quad (5.29)$$

When the minimum range constraint does not apply, the radar range, R , is calculated from (5.6), using the desired value for τ . The maximum feasible radar range is the smaller of that given by (5.6) or by (5.28).

The assumption is made in (5.27–5.29) that the radar pulse duration may be adjusted to the exact value that maximizes S/N or range. Actual radars usually have a finite number of pulse durations. Often these decrease from the maximum

Table 5.5 Minimum-Range Example

	15 dBsm	0 dBsm	0 dBsm	0 dBsm
σ	15 dBsm	0 dBsm	0 dBsm	0 dBsm
τ	10 ms	10 ms	4.64 ms	2.5 ms
S/N	15 dB	15 dB	15 dB	15 dB
R	2,001 km	844 km	696 km	597 km
R_M	1,500 km	1,500 km	696 km	375 km

pulse duration by factors of two. For example, a set of pulse durations might be 10, 5, 2.5, 1.25 and 0.625 ms. When the minimum-range constraint prevents using the 10 ms pulse ($R < 1,500$ km), a shorter pulse that does not violate the minimum-range constraint is used. The resulting S/N and range will usually be less than the values given by (5.27–5.29) when a suboptimum waveform duration is used.

For example, consider a radar having the pulse durations discussed above, and the following parameters: $P_p = 500$ kW, $G_T = 31$ dB, $A_R = 10$ m², $T_s = 453$ K, and $L = 6$ dB. The range for S/N of 15 dB, using a 10 ms pulse on a target having an RCS of 15 dBsm, is 2,001 km, from (5.6). This range exceeds the minimum range for the 10 ms pulse of 1,500 km, so the 10 ms pulse may be used. This case is summarized in the second column of Table 5.5.

If the target RCS is reduced to 0 dBsm, as shown in the third column of Table 5.5, the range from (5.6) is 844 km, which is smaller than the minimum range for the 10 ms pulse. Using the optimum pulse duration, the maximum range for this RCS value is found from (5.28) to be 696 km, and the resulting pulse duration is 4.64 ms, as shown in the fourth column. The next smaller radar waveform available is 2.5 ms, and the radar range using that waveform is 597 km, from (5.6), as shown in the last column.

The impact of the minimum-range constraint on radar range is illustrated in Figure 5.4, which shows radar range for the above parameters, as a function of target RCS. For values of RCS that provide ranges where the maximum pulse duration may be used, the range varies as the fourth root of RCS, as indicated by (5.6). For smaller values of RCS, and when the pulse duration is adjusted to provide maximum range, range varies as the cube root of RCS, as indicated by (5.28). When a finite set of pulse durations is used, the range decreases in steps for RCS values below those where the optimum pulse duration may be used, and the range varies with the fourth root of RCS in the regions where each pulse duration is used.

Note that pulse integration of several short pulses may be used to increase the S/N or radar range when use of a single long pulse is precluded by the minimum-

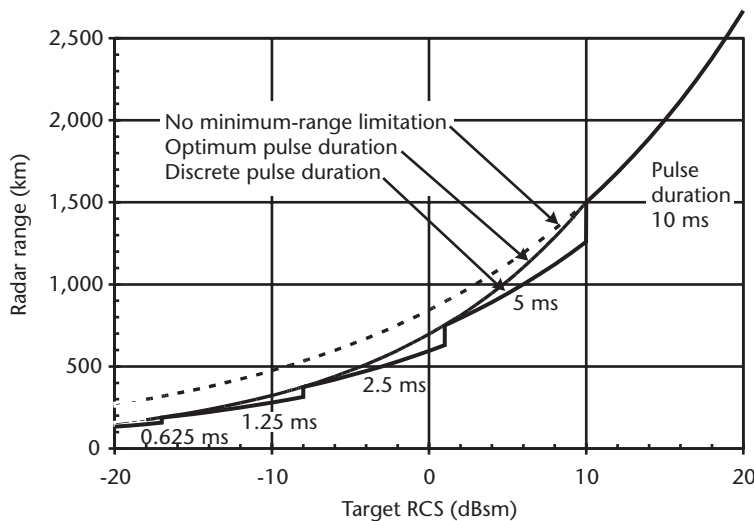


Figure 5.4 Radar range as a function of target RCS, showing the impact of radar minimum-range constraint.

range constraint. In the above example, as few as two pulses could be integrated to provide the 844-km range for the 0 dBsm target. These would have 5-ms duration, and a minimum range of 750 km. The detection loss for noncoherent integration would be small in this case.

In a more general example, ten 1-ms pulses could be coherently integrated to provide the same sensitivity as a single 10-ms pulse, and these shorter pulses would allow a minimum range of 150 km, while the longer pulse constrains the minimum range to 1,500 km. If noncoherent integration were used in this case, the resulting integration loss would either reduce the radar sensitivity, or require that about 13 pulses be noncoherently integrated.

5.6 Problems

The following problems are provided to assist in reviewing this chapter and to ensure a basic understanding of the material. For maximum benefit, the problems should first be solved without using the VBA custom radar functions. Solutions to these problems are given in Appendix E, Section E.5.

1. Find the S/N for a 5-dBsm target at a range of 175 km with a radar having the following parameters: $P_p = 5$ kW, $G_T = G_R = 35$ dB, $f = 3.3$ GHz (S band), $PC = 10^5$, $B = 100$ MHz, $T_s = 450$ K, and $L = 4$ dB. What is the pulse duration? Is the minimum-range constraint violated?
2. What loss components are included in the transmit microwave loss, L_{MT} , and the receive microwave loss, L_{MR} ?
3. A phased-array antenna consists of 2,000 elements, each with an element gain, G_E , of 5.5 dB, and transmit ohmic loss, L_{AT} , and receive ohmic loss, L_{AR} , of 0.2 dB each. If uniform aperture illumination is used for transmit and the transmit antenna losses are not included in the transmit gain, G_T , what is that transmit gain? If the radar operates at 5.5 GHz (C band), employs 20-dB Taylor aperture weighting on receive, and the receive antenna losses are not included in the effective receive aperture area, A_R , what is the receive aperture area?
4. A radar is said to provide S/N = 15 dB on a 1 m² target at a range of 1,000 km, an elevation angle of 5 degrees, and an off-broadside scan angle of 30 degrees using a 5-ms pulse. If the radar is an FFOV phased array, and the two-way propagation loss at 5 degrees elevation angle is 0.8 dB (discussed in Chapter 9), what is the reference range for the pulse duration, S/N and RCS values given? What pulse duration is needed to provide a S/N of 12 dB on a -10 dBsm target at a range of 500 km, assuming no propagation or scan losses? Does this pulse duration violate the minimum-range constraint?
5. If the single-pulse S/N = 7.5 dB and 10 pulses are integrated, what is the integrated S/N? If 100 pulses are to be integrated to provide this integrated S/N, what is the single-pulse S/N? Solve the above for coherent integration, noncoherent integration for measurement, and noncoherent integration for detection, assuming no additional signal-processing losses.

6. For the radar in Problem 4 and the calculated reference range, what is the pulse duration needed to provide 15 dB S/N on a -10 -dBsm target at 750 km range? Does this violate the minimum-range constraint? If so, what is the maximum range at which this target may be observed at this S/N, and what is the resulting pulse duration?
7. Find the S/N for the following radar and target parameters: $P_p = 20$ kW, $\tau = 1$ ms, $G_T = 30$ dB, $RCS = 1$ m², $A_R = 10$ m², $R = 200$ km, $T_s = 500$ K, $L = 6$ dB. Is the minimum-range constraint violated?
8. For the radar parameters in Problem 7, with a signal bandwidth of 10 MHz and a pulse compression ratio of 1,000, what is the range for S/N = 18 dB? How many pulses must be integrated to provide $R = 200$ km, using coherent integration, noncoherent integration for measurement, noncoherent integration for detection? Assume no integration loss.
9. For an X-band (9.5 GHz) phased array with 10,000 elements and effective element gain of 5 dB, what is the effective element aperture area? What is the array gain and aperture area on broadside? If the module noise temperature is 450 K, the element transmit and receive microwave losses are 0.1 dB each, what is the array noise temperature, and two-way microwave losses?
10. What type of signal integration requires aligning the phases of the received pulses, and hence precise knowledge of the target radial velocity? What type of integration requires aligning only the pulse envelopes, but suffers from detection loss?
11. An FFOV array radar has a reference range of 500 km with S/N = 15 dB, $RCS = 1$ m², and pulse duration of 1 ms. Find the range for S/N = 12 dB, $RCS = 0.1$ m², and pulse duration 1 ms, with off-broadside scan of 20 degrees in azimuth and 30 degrees in elevation, and two-way propagation losses of 2.5 dB (assume no beamshape loss). What is the range when ten 1-ms pulses are integrated to obtain an integrated S/N = 12 dB, using coherent integration, noncoherent integration for measurement, and noncoherent integration for detection, with 0.5 dB integration loss in each case?
12. For the radar in Problem 7, neglecting scan and propagation losses, what is the range for a -10 dBsm target and S/N = 15 dB? Does this violate the minimum-range constraint? If so, what is the maximum range at which the target may be observed by reducing the pulse duration, and what is that pulse duration? If the radar has binary decreasing pulse durations (0.5 ms, 0.25 ms, etc.), what is the longest pulse duration that may be used, and what is the resulting range?

5.7 VBA Software Functions for the Radar Equation

5.7.1 Function SNR_dB

Purpose Calculates the S/N for specified radar and target parameters.

Reference Equations (5.1) and (5.27).

Features Allows user selection to: (1) ignore the minimum-range constraint, (2) optimize pulse duration to maximize S/N while avoiding the minimum-range constraint, and (3) select from specified pulse durations to maximize S/N while avoiding the minimum-range constraint.

Input Parameters (with units specified)

Pp_kW = radar peak transmitted power (kW).

Gt_dB = radar transmit antenna gain (dB).

RCS_dBsm = target radar cross section (dBsm).

Ar_m2 = radar receive antenna aperture area (m²).

R_km = range from radar to target (km).

Ts_K = radar system noise temperature (K).

L_db = total radar system losses (dB).

Select_123 = select 1 to ignore the minimum-range constraint, 2 to use the optimum pulse duration within the minimum-range constraint, or 3 to use a specified pulse duration to maximize S/N within the minimum-range constraint (integer). Other values give no output.

Tau1_ms = primary (longest) radar pulse duration (ms). This parameter is used in Option 1 and is the maximum pulse duration for Options 2 and 3.

Tau2_ms, Tau3_ms, Tau4_ms, Tau5_ms, Tau6_ms (optional) = alternate shorter pulse durations used in Option 3, in descending order (ms). These may be left blank for Options 1 and 2, or when fewer than six pulse durations are available.

Function Output Radar S/N in decibels. This is the single-pulse S/N when a single pulse is used, or the integrated S/N when multiple pulses are integrated. In Option 3, when none of the specified pulse durations will avoid the minimum-range constraint, no result is generated, indicated by an output of -1.

The Excel Function Arguments parameter box for Function SNR_dB is shown in Figure 5.5, with sample parameters and solution.

5.7.2 Function Range_km

Purpose Calculates the radar range capability for specified radar and target parameters.

Reference Equations (5.6) and (5.28).

Features Allows user selection to: (1) ignore the minimum-range constraint, (2) optimize pulse duration to maximize range while avoiding the minimum-range constraint, and (3) select from specified pulse durations to maximize range while avoiding the minimum-range constraint. This function may be used to calculate the radar reference range by using the reference values of RCS, S/N, and pulse duration, and the fixed radar system losses [see (5.13)].

Input Parameters (with units specified)

Pp_kW = radar peak transmitted power (kW).

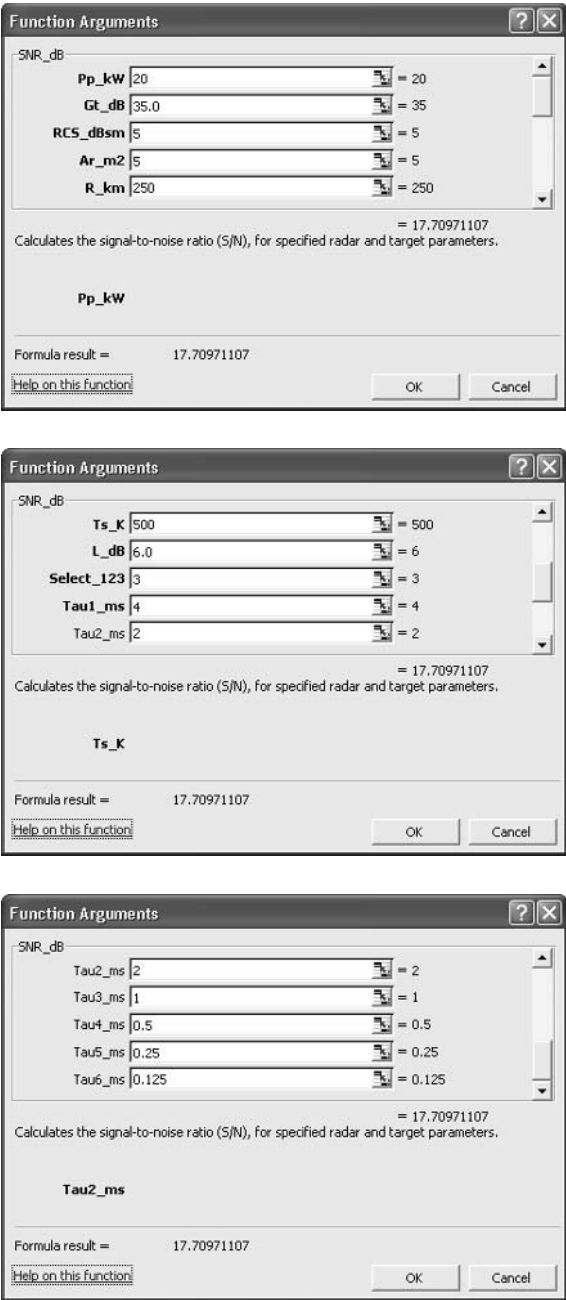


Figure 5.5 Excel parameter box for Function SNR_db.

- Gt_dB = radar transmit antenna gain (dB).
- RCS_dBsm = target radar cross section (dBsm).
- Ar_m2 = radar receive antenna aperture area (m²).
- S/N_dB = radar signal-to-noise ratio (dB). May use single-pulse or integrated value of S/N as appropriate.
- Ts_K = radar system noise temperature (K).

L_{db} = total radar system losses (dB).

Select_123 = select 1 to ignore the minimum-range constraint, 2 to maximize range within the minimum-range constraint, or 3 to use a specified pulse duration to maximize range within the minimum-range constraint (integer).

Other values give no output.

Tau1_ms = primary (longest) radar pulse duration (ms). This parameter is used in Option 1 above, and is the maximum pulse duration for Options 2 and 3.

Tau2_ms, Tau3_ms, Tau4_ms, Tau5_ms, Tau6_ms (optional) = alternate shorter pulse durations used in Option 3, in descending order (ms). These may be left blank for Options 1 and 2, or when fewer than six pulse durations are available.

Function Output Range from radar to target in kilometers. In Option 3, when none of the specified pulse durations will avoid the minimum-range constraint, no result is generated, indicated by an output of -1.

The Excel Function Arguments parameter box for Function Range_km is shown in Figure 5.6, with sample parameters and solution.

5.7.3 Function Integrated_SNR_dB

Purpose Calculates the integrated $(S/N)_{CI}$ or $(S/N)_{NI}$, when pulse integration is used.

Reference Equations (5.14), (5.17), and (5.20).

Features Allows user to select either: (1) coherent integration, (2) noncoherent integration for radar measurement, or (3) noncoherent integration for radar detection. Additional signal processing loss for integration may be included.

Input Parameters (with units specified)

SP_SNR_dB = single-pulse S/N (dB).

N_Pulses_Int = number of pulses integrated (integer).

Sel_1C2Nm3Nd = select 1 for coherent integration, 2 for noncoherent integration for radar measurement, or 3 for noncoherent integration for radar detection (integer). Other values will give no output.

Int_Loss_dB (optional) = additional signal processing loss associated with pulse integration (dB). If left blank, the function will assume no added loss.

Function Output Integrated $(S/N)_{CI}$ or $(S/N)_{NI}$ in decibels.

The Excel Function Arguments parameter box for Function Integrated_SNR_dB is shown in Figure 5.7, with sample parameters and solution.

5.7.4 Function SP_SNR_dB

Purpose Calculates the single-pulse S/N required to produce a specified integrated $(S/N)_{CI}$ or $(S/N)_{NI}$, when pulse integration is used.

Reference Equations (5.18), (5.21), and (5.25).

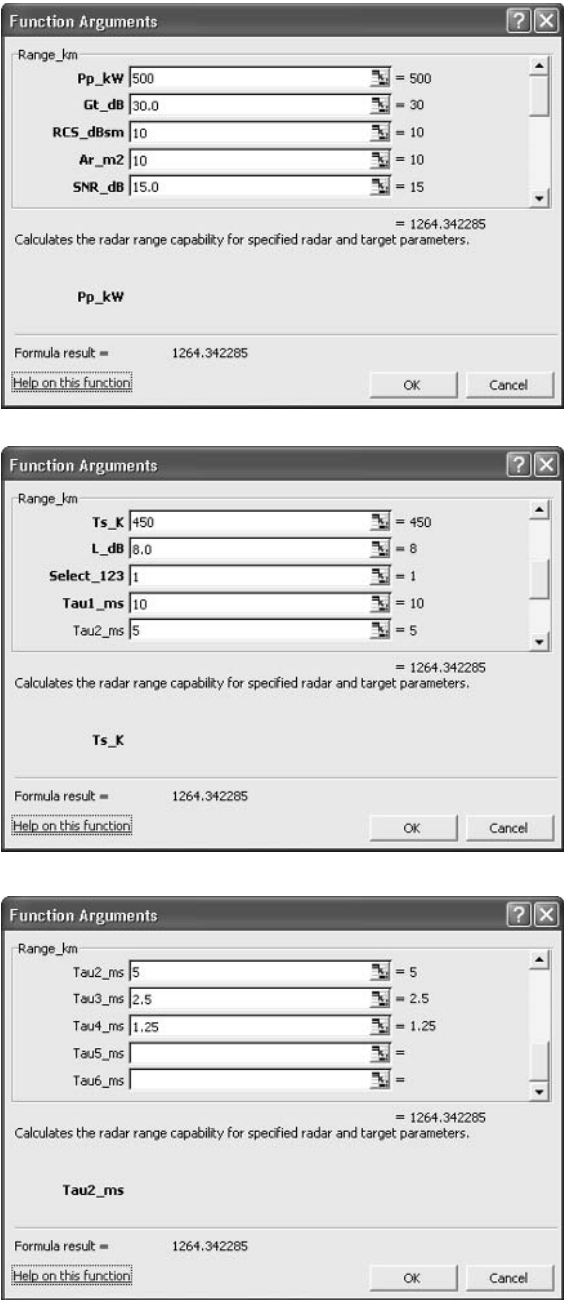


Figure 5.6 Excel parameter box for Function Range_km.

Features Allows user to select either: (1) coherent integration, (2) noncoherent integration for radar measurement, or (3) noncoherent integration for radar detection. Additional signal processing loss for integration may be included.

Input Parameters (with units specified)

Int_SNR_dB = integrated S/N (dB).

N_Pulses_Int = number of pulses integrated (integer).

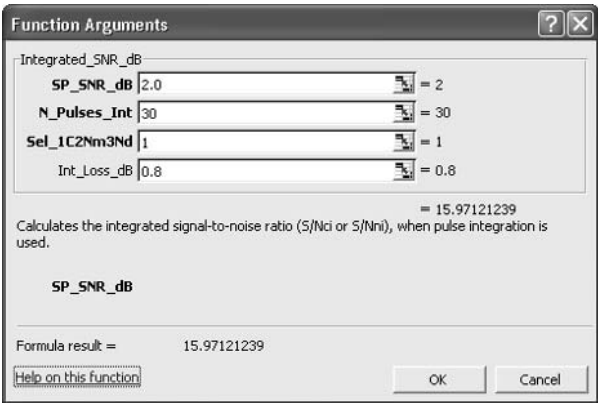


Figure 5.7 Excel parameter box for Function Integrated_SNR_dB.

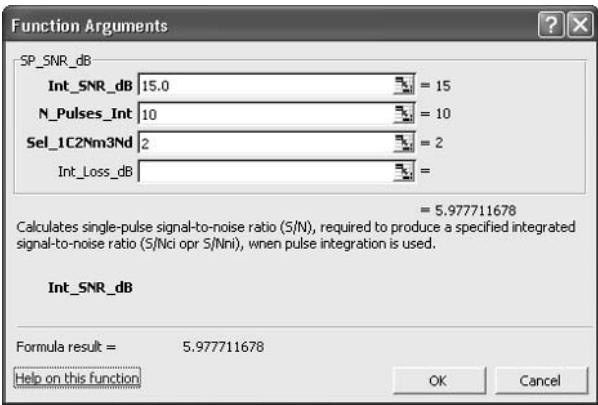


Figure 5.8 Excel parameter box for Function SP_SNR_dB.

Sel_1C2Nm3Nd = select 1 for coherent integration, 2 for noncoherent integration for radar measurement, or 3 for noncoherent integration for radar detection (integer). Other values will give no output.

Int_Loss_dB (optional) = additional signal processing loss associated with pulse integration (dB). If left blank, the function will assume no added loss.

Function Output Single-pulse S/N in decibels.

The Excel Function Arguments parameter box for Function SP_SNR_dB is shown in Figure 5.8, with sample parameters and solution.

References

- [1] Barton, D. K., *Modern Radar System Analysis*, Norwood, MA: Artech House, 1991.
- [2] Skolnik, M. I., *Introduction to Radar Systems, 2nd Ed.*, New York: McGraw-Hill, 1980.
- [3] Long, W. H., D. H. Mooney, and W. A. Skillman, "Pulse-Doppler Radar," Chapter 17 in *Radar Handbook, 2nd Ed.*, M. I. Skolnik, (ed.), New York: McGraw-Hill, 1990.
- [4] Barton, D. K., and H. R. Ward, *Handbook of Radar Measurement*, Dedham, MA: Artech House, 1984.

Selected Bibliography

The radar equation is widely discussed in most general radar references, including Skolnik and Barton. The detection (or demodulation) loss for radar measurements is treated in Section 3.7 of Barton and Ward, and for radar detection in Chapter 2 of Barton (1988).

Barton, D. K., *Radar System Analysis*, Englewood Cliffs, NJ: Prentice Hall, 1964.

Barton, D. K., *Modern Radar System Analysis*, Norwood, MA: Artech House, 1988.

Barton, D. K., and H. R. Ward, *Handbook of Radar Measurement*, Dedham, MA: Artech House, 1984.

Skolnik, M. I., *Introduction to Radar Systems*, New York: McGraw-Hill, 1962.

Skolnik, M. I., *Introduction to Radar Systems*, 2nd ed., New York: McGraw-Hill, 1980.

Skolnik, M. I., (ed.), *Radar Handbook*, New York: McGraw-Hill, 1970.

Skolnik, M. I., (ed.), *Radar Handbook*, 2nd ed., New York: McGraw-Hill, 1990.

Radar Detection

This chapter enables the reader to:

- Understand the process of setting the detection threshold and detecting varying target signals in a noise background;
- Calculate the false-alarm rate and average time between false alarms from the false-alarm probability and other radar parameters;
- Find the probability of detection for targets with Swerling-type fluctuations, as a function of the false-alarm probability and S/N;
- Evaluate the impact of coherent and noncoherent pulse integration and cumulative detection on the probability of detection;
- Enhance detection probability of fluctuating targets by using noncoherent integration and cumulative detection.

Radar detection is the process of examining the radar signal return and determining that a target is present. Since both the target signal returns and the radar noise background result from random processes, detection is a statistical process.

The detection process is described in Section 6.1, followed by a discussion of false alarms in Section 6.2. The principal detection modes are: detection with a single pulse or coherently integrated pulses, detection using noncoherently integrated pulses, and cumulative detection. These are described in Sections 6.3, 6.4, and 6.5 respectively.

6.1 The Detection Process

In the radar detection process, the received signal amplitude is compared with a threshold level. The threshold is usually set to exclude most noise signals. When the signal exceeds the threshold, a target detection is declared. Because both the target and background noise signals have random amplitude variations, the noise signal will occasionally exceed the threshold, producing what is called a false alarm. Similarly, a target signal may fail to exceed the threshold, and thus not be detected. This is illustrated in Figure 6.1.

The resulting radar detection performance is usually characterized by the probability that a target is detected, called the probability of detection, P_D , and the probability that a detection will be declared when no target is present, called the probability of false alarm, P_{FA} . These depend on the threshold setting, the S/N, the statistical characteristics of the target and noise signals, and the detection processing

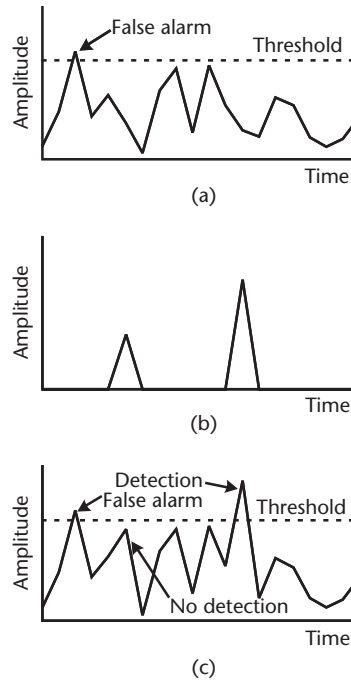


Figure 6.1 Illustration of the detection process and the effect of the detection threshold. (a) Noise. (b) Target signals. (c) Signal plus noise.

mode. When the other factors remain fixed, decreasing the threshold amplitude will increase P_D , at the expense of also increasing P_{FA} , and vice versa.

In early radars, detection was performed subjectively by an operator observing a cathode-ray tube (CRT) display. In most modern radars, detection is performed in the signal processor, using either analog or digital techniques. The techniques described in this chapter are those employed by such signal processors. Experiments have shown that the performance of alert, well-trained operators with good displays is close to the optimum achieved by the signal processors [1, pp. 6–9].

Calculations of detection and false-alarm probabilities usually assume that the background noise is characterized by a uniform spectral density and Gaussian probability density function. Such noise is called white Gaussian noise. Most noise sources that contribute to radar system noise have these characteristics. Wideband noise jamming signals (see Chapter 10) may also approximate white Gaussian noise. Other interfering signals, such as clutter and some jamming signals, may have different characteristics, and the use of this model may produce inaccurate results when these background signals predominate.

Detection analysis often uses the Swerling models for target-signal fluctuation due to RCS, although other target models exist. The Swerling models are discussed in Section 3.5, and summarized in Table 3.3. These models are members of the Chi-square family with specific values of the signal fluctuation parameter K . Their principal characteristics are given in Table 6.1. Note that even with a nonfluctuating target, designated here as Swerling 5, the radar signal-plus-noise return will have fluctuating properties.

Other statistical target models have been developed for special classes of targets, for example stealth targets, and are discussed in the references given in the selected

Table 6.1 Characteristics of Swerling Target-Signal Models.

<i>Model</i>	<i>Target Configuration</i>	<i>Decorrelation</i>	<i>Chi-Square Parameter, K</i>
Swerling 1	Many comparable scatterers	Dwell-to-dwell	1
Swerling 2	Many comparable scatterers	Pulse-to-pulse	n
Swerling 3	Dominant scatterer	Dwell-to-dwell	2
Swerling 4	Dominant scatterer	Pulse-to-pulse	$2n$
Swerling 5	Single scatterer	Nonfluctuating	Infinity

bibliography. Similarly, while white Gaussian is a good model for noise from thermal sources, and is used in this analysis, backgrounds from other sources may have different amplitude statistics. Thus, while the detection results given below are widely used for radar analysis, special target and background statistics may require further analysis.

6.2 False Alarms

The radar receiver threshold is set to provide the desired (or acceptable) false-alarm probability. Assuming a white Gaussian noise background, the IF signal voltage at the output of the matched filter has a Rayleigh probability density and the noise power, Y , has an exponential probability density [2, pp. 58–60]:

$$p(Y) = e^{-Y} \quad (6.1)$$

where Y is the power of the IF signal, normalized to the noise level.

When a single observation is used for detection, as discussed in Section 6.3, the resulting probability of false alarm is given by:

$$P_{FA} = \int_{Y_T}^{\infty} e^{-Y} dY = e^{-Y_T} \quad (\text{single observation}) \quad (6.2)$$

where Y_T is the normalized threshold power level. The threshold level for a desired P_{FA} may be found from:

$$Y_T = \ln(1/P_{FA}) \quad (\text{single observation}) \quad (6.3)$$

where \ln represents the natural logarithm.

When several observations are used in the detection process, as discussed in Section 6.4, the false-alarm probability is given by:

$$P_{FA} = \frac{1}{(n-1)!} \int_{Y_T}^{\infty} Y^{n-1} e^{-Y} dY \quad (6.4)$$

where n is the number of observations used [3, pp. 347–384]. This integral corresponds to a version of the incomplete gamma function, and may be found in tabulated form, or calculated using recursive methods [4].

The receiver will produce independent samples of noise at time intervals equal to $1/B_N$, where B_N is the noise bandwidth [2. pp. 58–60]. For a matched filter, B_N is approximately equal to the signal bandwidth, B , and to the reciprocal of the compressed pulse duration, τ_c . When the receiver operates continuously, the false alarm rate, r_{FA} , is given by:

$$r_{FA} = P_{FA} B = P_{FA} / \tau_c \quad (\text{continuous operation}) \quad (6.5)$$

The average time between false alarms, t_{FA} , is the reciprocal of the false-alarm rate:

$$t_{FA} = 1/r_{FA} = 1/(P_{FA} B) = \tau_c / P_{FA} \quad (\text{continuous operation}) \quad (6.6)$$

For example, for a signal bandwidth $B = 1$ MHz, and a probability of false alarm $P_{FA} = 10^{-6}$, the false-alarm rate $r_{FA} = 1$ per second. The average time between false alarms t_{FA} is 1 second.

In many radar search modes, the receive observation period is matched to the expected ranges of targets. The receiver then does not operate continuously, as assumed above, and the number of false-alarm opportunities is smaller. For a receive range window, R_w , that is observed at the PRF, the average false alarm rate is:

$$r_{FA} = \frac{2R_w}{c} PRF P_{FA} B = \frac{2R_w}{c\tau_c} PRF P_{FA} \quad (\text{range window}) \quad (6.7)$$

and the average time between false alarms is:

$$t_{FA} = \frac{c}{2R_w PRF P_{FA} B} = \frac{c\tau_c}{2R_w PRF P_{FA}} \quad (\text{range window}) \quad (6.8)$$

For example, with the parameters of the previous example, a range window $R_w = 150$ km, and a PRF = 500 Hz, the average false alarm rate is reduced to 0.5 per second, and the average false-alarm time is increased to 2 seconds.

When the radar is performing a cued search (discussed in Section 7.4), or tracking a target, only a few $1/B$ range intervals may need to be examined, and the range window may be small. A higher value of P_{FA} or a larger signal bandwidth may then be used with little penalty.

Illustrations of false-alarm calculations are given in Table 6.2. The example in the second column shows that, for continuous receiver operation with a moderate signal bandwidth of 1 MHz, $P_{FA} = 10^{-6}$ produces a false-alarm rate of one per second. If the search mode requires the radar receiver to operate only half of the time (column 3), then this rate is reduced to 0.5 per second. If the signal bandwidth is increased to 100 MHz, as shown in column 4, the false-alarm rate increases correspondingly to 100 per second. This rate may well be unacceptably large, and may be reduced in two ways:

- Reduce the range window, as shown in column 5.
- Reduce the value of P_{FA} , as shown in column 6.

Table 6.2 False-Alarm Examples

P_{FA}	10^{-6}	10^{-6}	10^{-6}	10^{-6}	10^{-8}
B	1 MHz	1 MHz	100 MHz	100 MHz	100 MHz
R_w	Continuous	150 km	Continuous	1.5 km	Continuous
PRF		500 Hz		500 Hz	
r_{FA}	1 per second	0.5 per second	100 per second	0.5 per second	1 per second
t_{FA}	1 sec	2 sec	0.01 sec	2 sec	1 sec

When multiple receiver filters are used, each provides the opportunity for false alarms. Such multiple receiver filters are often used with CW pulses or phase-reversal waveforms when the matched-filter signal bandwidth of the waveform is narrower than the target radial-velocity uncertainty (see Sections 4.2 and 4.4), or when multiple filters are used for coherent integration when the radial velocity is not precisely known (see Section 5.4). In these cases, the false alarm rate is equal to that for a single receiver matched filter, multiplied by the number of matched filters used.

A radar search mode may employ several pulse trains having different waveforms and receive observation windows to cover the desired search volume (see Chapter 7). Then the overall false-alarm rate is the sum of the false-alarm rates for the individual pulse trains:

$$r_{FA} = \sum_i \frac{2R_{wi}}{c} PRF_i P_{FAi} B_i \quad (6.9)$$

where R_{wi} , PRF_i , P_{FAi} , and B_i are the parameters of the individual search pulse trains. The average time between false alarms is then:

$$t_{FA} = 1/r_{FA} \quad (6.10)$$

Setting the false-alarm rate in a radar design is a trade-off between the radar energy required to reduce the false-alarm rate, and the radar resources and other activities needed to cope with the false alarms that occur. The latter may include radar energy to attempt confirmation and track initiation on the false targets, signal-processing resources, and operator attention. In practice, P_{FA} is often set to give an acceptable false-alarm level, and the required P_D is then obtained by providing the needed value of S/N. False-alarm probabilities are typically in the range from 10^{-2} to 10^{-10} . An example of determining the false-alarm probability that minimizes radar power usage is given in Section 12.2.

As discussed above, the detection threshold is set relative to the receiver system noise level, N , to produce the desired P_{FA} . This might be done after calculating or measuring the noise level, and then not changed. In practice, however, the system noise level may change, producing change in P_{FA} . Such changes may be due to changing atmospheric conditions or component temperatures, drift in the receiver circuits, or to a varying noise background from jamming or other interference. In the cases of external clutter and jamming signals, the changes in the noise level and the resulting P_{FA} may be dramatic.

Many radars employ receiver techniques to compensate for such system-noise level changes called constant-false-alarm rate (CFAR) processing. The CFAR cir-

cuits automatically adjust the detection threshold to maintain the desired P_{FA} . In some radars, the false-alarm rate is monitored, and feedback is employed to adjust the threshold. In other radars, the system noise level is measured directly, and the threshold set accordingly. When the threshold level is increased to compensate for increased background noise level, the P_D will be reduced. In addition, the automatic adjustment of the threshold in CFAR circuits is accompanied by a loss, caused by the error in estimating the interference level. This requires the threshold to be set somewhat higher than actually required [2, p. 90]. This CFAR loss, often about 1 or 2 dB, should be included in the signal-processing loss, L_{SP} (see Section 3.4).

6.3 Detection Using a Single Pulse or Coherent Dwell

When the detection threshold has been set relative to the receiver noise level, N , the detection probability, P_D , is determined by the S/N and the target-signal statistics. Note from Table 6.1 that for a single target observation, the target statistics for Swerling 1 and 2 are the same, and those for Swerling 3 and 4 are the same.

Detection using a single pulse and detection using a series of pulses coherently integrated are treated together here, because in both cases the signal is a single sample of the target amplitude distribution. A burst of coherently integrated pulses generates a single target observation, and produces the same target statistics as a single pulse [5]. This is because coherent integration requires a stable target-signal return, that is, a signal that is correlated from pulse-to-pulse during the integration period, as discussed in Section 5.4. The coherent dwell simply has a S/N which is n times the single-pulse S/N (reduced by the signal processing loss, L_{SPI} , as appropriate), where n is the number of pulses coherently integrated. This implies a Swerling 1, 3, or 5 target model. If the signal has significant pulse-to-pulse decorrelation, then it is better represented by a Swerling 2 or 4 model, and noncoherent integration must be used. Detection using noncoherent pulse integration is discussed in Section 6.4.

Coherent integration requires knowledge (or a good estimate) of the target radial velocity, or use of multiple receive filters covering the range of possible target radial velocities. Most modern radar use fast-Fourier-transform (FFT), or similar processing, to implement a filter bank covering the required radial velocities. When multiple filters are used, each may produce false alarms with the specified P_{FA} , so that the overall false-alarm rate is proportional to the number of filters, as described in Section 6.2.

When coherent integration is used, the integrated S/N , $(S/N)_{CI}$, should be used to determine the detection probability. Taking into account the integration loss, L_{SPI} , this is given by:

$$S/N_{ci} = n S/N / L_{SPI} \quad (6.11)$$

where n is the number of pulses coherently integrated, and S/N is the single-pulse S/N .

The detection probability using n observations in Gaussian noise that is independent from observation to observation is given by:

$$P_D = \int_{V_T}^{\infty} \left(\frac{V}{X} \right)^{(n-1)/2} e^{V-X} I_{n-1}(2\sqrt{VX}) dV \quad (6.12)$$

where:

V = sum of the signal-plus-noise, (S + N), values for the n observations

X = sum of the S/N values for the n observations

V_T = threshold power level

I_{n-1} = modified Bessel function of the order $n - 1$

For the case of a single observation, $n = 1$, and the P_D is given by:

$$P_D = \int_{V_T}^{\infty} e^{V-X} I_0(2\sqrt{VX}) dV \quad (\text{single observation}) \quad (6.13)$$

The computation of P_D from (6.12) and (6.13) is sufficiently complicated, so that tables, plots, or computer programs are usually used to find P_D . These integrals were evaluated numerically and the resulting values of P_D versus S/N, with P_{FA} as a parameter for the various target models, are plotted [3, pp. 349–358, 380–389 and 395–403]. (In this reference, the peak S/N, \mathfrak{R}_p , is twice the value of S/N defined here, so that 3 dB should be subtracted from the abscissa in the plots. The false alarm number, n' , used in the reference is equal to $0.693/P_{FA}$.) Various techniques for calculating P_D using approximations and recursive methods have been developed (4–6). The recursive method described in [4] is used in the custom radar function described in Section 6.7.3.

The S/N or $(S/N)_{Cl}$ required in a single pulse or coherent dwell to provide various values of P_D for a fixed value of P_{FA} of 10^{-6} is plotted in Figure 6.2. Curves are given for Swerling 1 or 2, Swerling 3 or 4, and Swerling 5 (nonfluctuating) target signals. The plot shows that the S/N required for detection increases with increasing

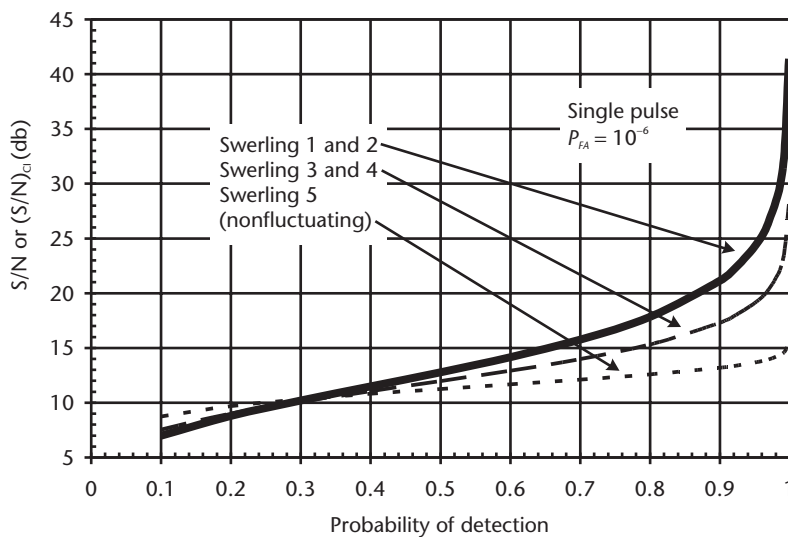


Figure 6.2 S/N for a single pulse or coherent dwell versus probability of detection for the Swerling target-cases

target-signal fluctuation for values of P_D greater than about 0.4. This is because the fluctuating target-plus-noise signal must exceed the threshold almost all the time to achieve a high detection probability in these cases. For example, for $P_D = 0.99$, the signal-plus-noise must remain above the threshold for 99% of the samples. With $P_{FA} = 10^{-6}$, this requires $S/N = 31.4$ dB for the highly fluctuating Swerling 1 and 2 targets, $S/N = 22.9$ dB for the moderately fluctuating Swerling 3 and 4 targets, and only 14.5 dB for the nonfluctuating Swerling 5 target. The opposite effect occurs for values of S/N below about 0.4, since the fluctuations increase the probability of exceeding the threshold in this region.

The sensitivity of the S/N required to the P_{FA} is illustrated in Figure 6.3. This figure shows the S/N or $(S/N)_{CI}$ required in a single pulse or coherent dwell to provide various values of P_D with P_{FA} as a parameter. The S/N required for detection increases moderately as P_{FA} decreases. For example, decreasing P_{FA} by two orders of magnitude, from 10^{-6} to 10^{-8} , for $P_D = 0.9$ requires increasing the S/N by only about 1.2 dB, or 32%. This is typical of the impact of P_{FA} requirements on S/N .

Examples showing the S/N required for detection are shown in Table 6.3. The second column shows that a rather high value of $S/N = 31.4$ dB is needed to provide a high single-pulse $P_D = 0.99$ for the highly fluctuating Swerling 1 or 2 target (these are the same, since only a single pulse is used). If the target is stable over the 10-pulse coherent-dwell interval (Swerling 1), the single-pulse $S/N = 21.4$ dB is one-tenth that of the integrated S/N , as shown in column 3 (neglecting integration loss). Column 4 shows the impact of reducing the P_{FA} by two orders of magnitude. The 1.3 dB increase in S/N required is typical, as shown in Figure 6.3. Columns 5 and 6 show the S/N required for Swerling 3 or 4 targets and Swerling 5 (nonfluctuating) targets respectively. Since the Swerling 3 or 4 target is not as highly fluctuating as the Swerling 1 or 2 target in column 2, a lower $S/N = 22.9$ dB will still assure that only one percent of the samples are below the detection threshold. An even lower $S/N = 14.5$ dB is needed for the nonfluctuating target.

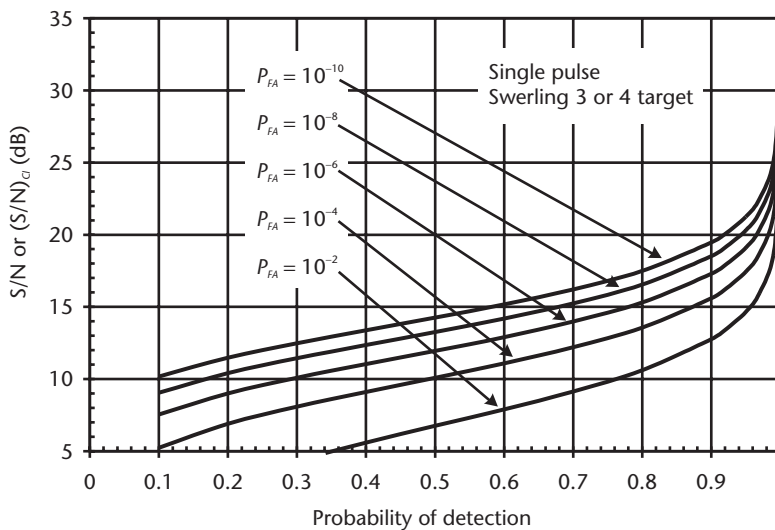


Figure 6.3 S/N for a single pulse or coherent dwell versus probability of detection for various values of false-alarm probability.

Table 6.3 Single-Pulse and Coherent Integration Detection Examples

P_D	0.99	0.99	0.99	0.99	0.99
P_{FA}	10^{-6}	10^{-6}	10^{-8}	10^{-6}	10^{-6}
n (coherent)	1	10	1	1	1
Swerling model	1 or 2	1	1 or 2	3 or 4	5
Pulse S/N	31.4 dB	21.4 dB	32.7 dB	22.9 dB	14.5 dB

6.4 Detection Using Noncoherent Integration

Noncoherent integration is frequently used in radar for target detection. Noncoherent integration is easier to implement than coherent integration, especially for searching when the target velocity is not known, because it avoids the limitations associated with coherent integration (e.g., precise knowledge of target radial velocity, phase stability), and because it may provide better performance against fluctuating targets, as discussed below. Noncoherent integration, sometimes called postdetection or incoherent integration, does require compensating for target range changes that are greater than the compressed-pulse duration to avoid range walk, as discussed in Section 5.4.

When noncoherent integration is used, the false-alarm probability is determined by the threshold setting and the number of pulses integrated, n , according to (6.4). The detection probability is then given by (6.12). As discussed in the preceding section, this may be evaluated numerically, read from plots, or calculated [3, pp. 349–538, 380–389 and 395–403, 4–6].

The single-pulse signal-to-noise ratio required to provide a P_D of 0.9 with a P_{FA} of 10^{-6} is plotted as a function of the number of pulses noncoherently integrated in Figure 6.4, for the five Swerling target-signal cases. Because of the detection loss (discussed in Section 5.4), more signal energy is needed to detect nonfluctuating tar-

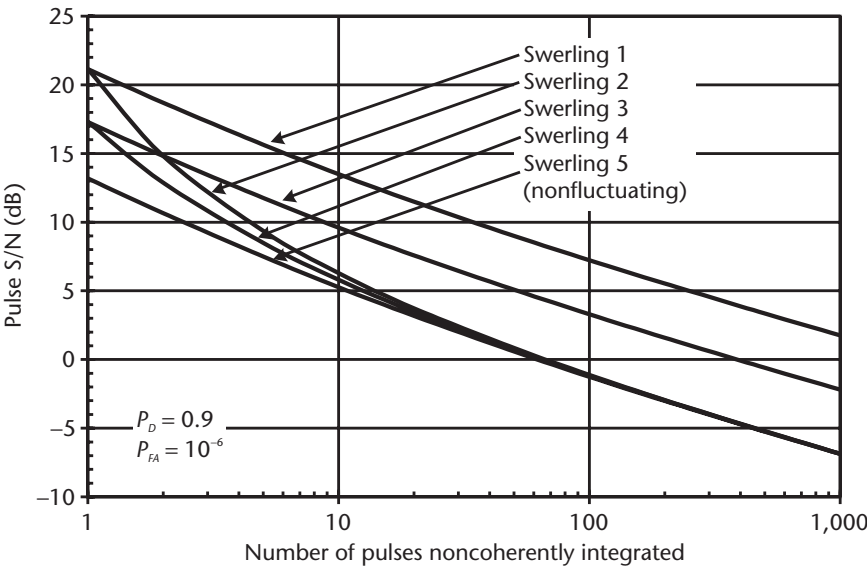


Figure 6.4 Pulse S/N required for detection versus number of pulses noncoherently integrated for the Swerling target cases.

gets using noncoherent integration than using a single pulse or coherent integration. This may be seen in Figure 6.4 for Swerling 1, 3, and 5 targets, where the required pulse S/N decreases more slowly than $1/n$, where n is the number of pulses noncoherently integrated. For these Swerling cases, the target returns are correlated for the pulses noncoherently integrated. The S/N decreasing more slowly than $1/n$ is a consequence of the increased threshold needed for pulse integration, and the detection loss with noncoherent integration. The result is that more signal energy is required for detection using noncoherent integration for these cases than for using a single pulse or coherent integration.

For example, for a Swerling 1 target and the detection parameters in the figure, a single pulse requires a S/N of about 21.2 dB. If 10 pulses are coherently integrated (without additional processing losses), each requires a S/N of about 11.2 dB (21.2 dB -10 dB). Figure 6.4 shows that, with noncoherent integration of 10 pulses, a S/N of about 13.5 dB is required. Thus, in this case noncoherent integration requires about 2.3 dB more signal energy than a single pulse or coherent integration.

With fluctuating targets, however, the pulse S/N required decreases more rapidly than $1/n$ for small values of n , as shown in Figure 6.4, for Swerling 2 and 4 targets. For these targets, the signal returns are uncorrelated from pulse-to-pulse. It is therefore unlikely that successive returns will have amplitudes near the minimum value, and a lower value of S/N will still ensure detection. With a fluctuating target, the S/N of a single pulse must be increased until there is a low probability $(1 - P_D)$ that an observation is below the threshold. For high values of P_D , this produces a range of n where noncoherent integration requires less signal energy than a single pulse or coherently integrated pulses. This effect is more pronounced for the highly fluctuating Swerling 2 target than for the moderately fluctuating Swerling 4 target.

This effect is illustrated by Figure 6.5, which shows the pulse S/N multiplied by the number of pulses noncoherently integrated as a function of the number of pulses integrated for Swerling 2 and 4 targets and three detection probabilities, with P_{FA}

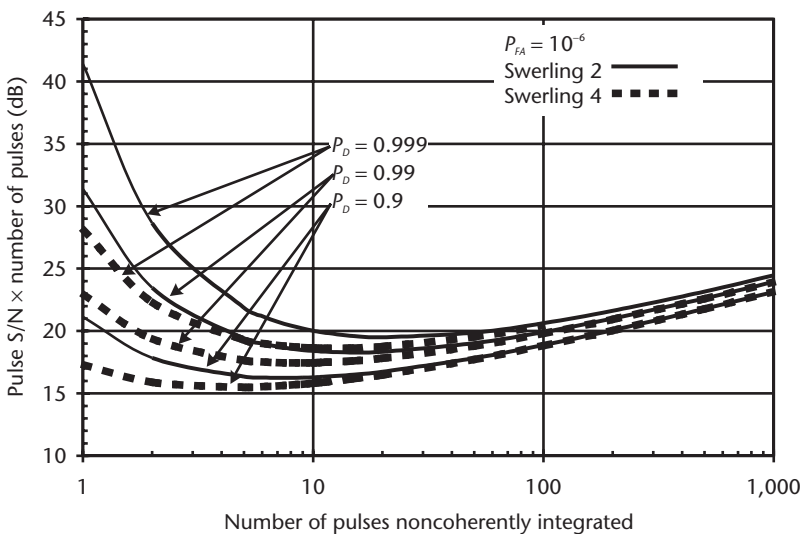


Figure 6.5 Pulse S/N multiplied by number of pulses noncoherently integrated versus number of pulses for the Swerling fluctuating-target cases.

held constant at 10^{-6} . The ordinate in this figure is proportional to the total energy transmitted in the pulse train that is noncoherently integrated. Detection using single pulse or a coherent pulse train having the same total energy would require a S/N equal to the ordinate value for $n = 1$ in Figure 6.5. The decrease in the curves from this value for larger values of n shows the reductions in waveform energy that noncoherent integration provides for fluctuating targets. This reduction is greater for high values of P_D , and for the more highly fluctuating Swerling 2 targets.

The curves exhibit broad minima at numbers of pulses that depend on P_D and target fluctuation. For the cases shown, the minima occur for 5 to 20 pulses noncoherently integrated. These represent the minimum energy required for detecting these targets. The optimum number of pulses is greater for higher values of P_D , and for the more highly fluctuating Swerling 2 target.

Noncoherent integration may be used with both fluctuating and nonfluctuating targets, but it is more efficient with fluctuating targets, as discussed above. Pulse-to-pulse frequency diversity may be used to produce Swerling 2 or 4 pulse-to-pulse target-signal decorrelation for multiscatterer targets that would otherwise have Swerling 1 or 2 characteristics (see Section 3.5). This technique may be used to improve the detection capability for these targets.

Note that several series of coherent dwells may be integrated noncoherently. In this case, the $(S/N)_{CI}$ is used in place of the pulse S/N in calculating the resulting P_D . This technique may be useful when: it is necessary to use a large number of pulses, coherent integration time is limited by target coherence, and the advantages of noncoherently integrating a small number of observations is desired. For example, if the maximum radar pulse energy may produce $S/N = 0$ dB, about 60 pulses would have to be noncoherently integrated to provide $P_D = 0.9$ and $P_{FA} = 10^{-6}$ on a Swerling 4 target. If groups of 10 pulses could be coherently integrated, producing $(S/N)_{CI} = 10$ dB, the detection criteria may be met using four such groups. This technique uses only 40 pulses, compared with 60 needed for noncoherent integration of all pulses.

Examples of detection using noncoherent integration are shown in Table 6.4. The second column is identical to the second column in Table 6.3, and is used as a baseline with a relative energy of unity (100%). When 10 pulses are noncoherently integrated (column 3 of Table 6.4), the single-pulse S/N is 8.4 dB, and the total relative energy is only 5% of that needed for a single pulse. When 1,000 pulses are noncoherently integrated (column 4), the relative energy increases to 18%. If the target is stable (Swerling 1), then groups of 100 pulses may be coherently integrated. Frequency agility may be used between groups of 100 pulses to produce Swerling 2 fluctuation of the groups. The 10 groups may then be noncoherently integrated, bringing the relative energy back to 5%, as shown in column 5.

Table 6.4 Noncoherent Integration Detection Examples

P_D	0.99	0.99	0.99	0.99
P_{FA}	10^{-6}	10^{-6}	10^{-6}	10^{-6}
n	1	10	1,000	$100 \times 10^*$
Swerling model	2	2	2	1/2
Pulse S/N	31.4	8.4	-6.1	-11.6
Relative energy	100%	5%	18%	5%

* 10 groups of 100 coherently integrated pulses

6.5 Cumulative Detection

Cumulative detection is another technique for using multiple pulses for target detection. It involves transmitting and receiving a series of pulses. If at least one of the signal returns exceeds the detection threshold, a detection is declared [3, p. 476]. Cumulative detection is sometimes called binary detection because only *detected* or *not detected* is recorded for each pulse.

This process is often easier to implement than noncoherent integration, and it does not require compensation for target range walk. It offers flexibility in pulse scheduling, since the pulses used on a target need not be contiguous or confined to a short time span. For fluctuating target signals (Swerling 2 and 4), and small values of n , it may produce performance close to that of noncoherent integration.

Cumulative detection is not effective for nonfluctuating targets, since returns from these targets are highly correlated. If such a target is detected by one pulse, it likely will be detected by all the pulses, and vice versa. Along with the threshold increase needed to maintain the false-alarm probability (see below), this results in little reduction in the single-pulse S/N required for cumulative detection.

When n pulses are used for cumulative detection, there is a detection opportunity and false-alarm opportunities for each pulse return. The overall P_{FA} must be reduced by the factor n to obtain the false-alarm probability for a single observation, P_{FAO} :

$$P_{FAO} = P_{FA} / n \quad (6.14)$$

The threshold is set using (6.3), and substituting P_{FAO} for P_{FA} .

For targets with pulse-to-pulse fluctuations, the detection probability for a single observation, P_{DO} , is related to the overall detection probability, P_D , by:

$$P_{DO} = 1 - (1 - P_D)^{1/n} \quad (\text{fluctuating targets}) \quad (6.15)$$

and inversely:

$$P_D = 1 - (1 - P_{DO})^n \quad (\text{fluctuating targets}) \quad (6.16)$$

The value of P_{DO} is calculated from (6.13), using techniques described earlier.

The pulse S/N for individual observations is plotted as a function of the number of pulses used for cumulative detection, n , in Figure 6.6 for Swerling 2 and 4 targets. The required pulse S/N decreases for increasing numbers of pulses. Comparison with Figure 6.4 shows that the decrease with cumulative detection is not as great as with noncoherent integration for these fluctuating targets, especially for large numbers of pulses.

For example, with five pulses and a Swerling 4 target, the required pulse S/N for $P_D = 0.9$ and $P_{FA} = 10^{-6}$ is 8.5 dB with noncoherent integration, and 11.3 dB with cumulative detection. While cumulative detection requires 2.8 dB greater pulse S/N in this case, its use may be justified by processing simplicity and reduced processing losses. For much larger values of n , the difference is more pronounced, and cumulative detection is usually not attractive.

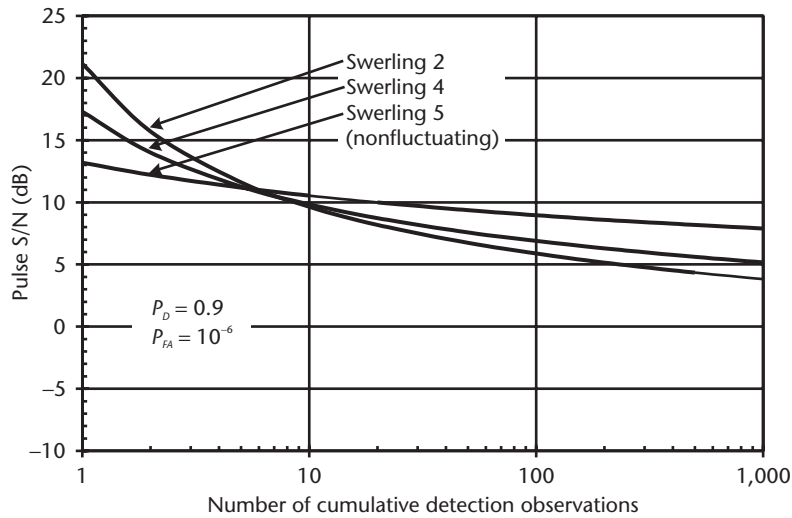


Figure 6.6 Pulse S/N required for detection versus number of pulses used in cumulative detection for the fluctuating Swerling target cases.

The pulse S/N for Swerling 5 nonfluctuating targets is also shown in Figure 6.6 for comparison. For these targets, the pulse S/N decreases only slightly with increasing n , and cumulative detection is not attractive, as discussed earlier.

The total cumulative-detection energy used is proportional to the product of the pulse S/N and the number of pulses used. This is plotted as a function of number of pulses in Figure 6.7 for Swerling 2 and 4 targets and three values of P_D with P_{FA} held constant at 10^{-6} . As in the case of noncoherent integration shown in Figure 6.5, the total energy needed is reduced by cumulative detection when using small numbers of pulses. This effect is more pronounced for the highly fluctuating Swerling 2 target and for higher values of P_D .

The results differ from the results for noncoherent integration, however, in that: the optimum number of pulses for cumulative detection is smaller than for nonco-

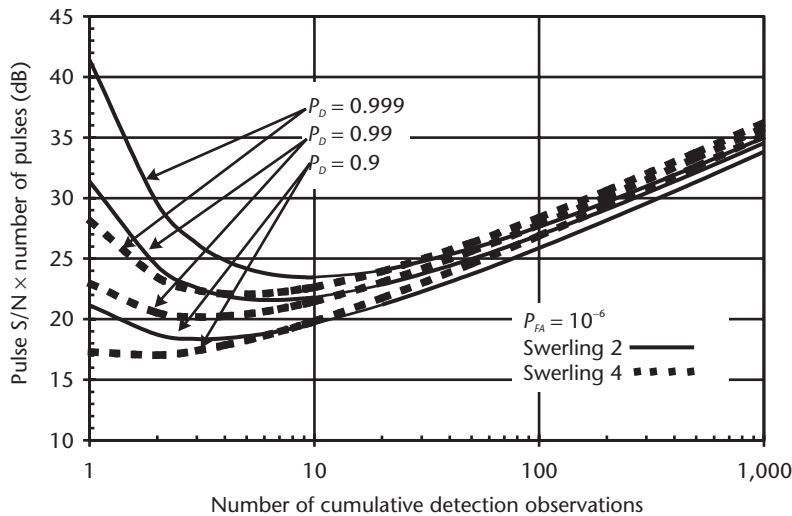


Figure 6.7 Pulse S/N multiplied by the number of pulses used in cumulative detection versus number of pulses for the fluctuating Swerling target cases.

herent integration, the resulting total signal energy is greater for cumulative detection, and the total energy goes up more rapidly for large numbers of pulses used in cumulative detection. For example, for $P_D = 0.99$, $P_{FA} = 10^{-6}$, and Swerling 4 target signals, the minimum value of n S/N with noncoherent integration is 17.4 dB, and occurs using eight pulses. With cumulative detection, the minimum value of n S/N is 20.2 dB, and occurs using three pulses.

These results suggest that cumulative detection using small numbers of pulses may be used in place of noncoherent integration to detect fluctuating targets in situations where its simplicity outweighs its slightly reduced effectiveness.

Coherent dwells may be used to make observations for cumulative detection, as discussed in Section 6.4. Since cumulative detection is most efficient with small numbers of observations, use of coherent integration in this mode, where practical, may increase its effectiveness. Extending the example given in Section 6.4, no reasonable number of pulses having S/N = 0 dB could provide $P_D = 0.9$ and $P_{FA} = 10^{-6}$ on a Swerling 4 target, using cumulative detection. If groups of 10 pulses were coherently integrated to produce $(S/N)_{CI} = 10$ dB, 9 such groups, or 90 pulses would provide the detection requirement. If 20 pulses could be coherently integrated to provide $(S/N)_{CI} = 13$ dB, only 3 such groups, or 60 pulses would be needed.

Cumulative detection as discussed here is a special case of a broader detection technique called m -out-of- m detection or binary integration [2, pp. 33–34]. In the general case, n pulses are transmitted, and detection requires m threshold crossings. Cumulative detection as discussed above is then one-out-of- n detection.

Another similar technique is called sequential detection. In this mode, a single pulse or dwell is used, with the threshold set to allow a relatively high false-alarm rate. When a threshold crossing occurs, a second pulse or dwell is transmitted to see if the threshold crossing was a target detection or a false alarm. In elaborations of this technique, several sequential pulses or dwells having different threshold levels may be used.

Cumulative detection as discussed in this section employs relatively closely spaced pulses or dwells that occur while the target is at nearly the same range. The technique may also be used in a search mode that employs widely spaced pulses or dwells to detect the target as the range decreases. This is discussed further in Chapter 7. An example of cumulative detection over a long period where the target range changes with time is given in Section 12.3.

Examples of cumulative detection are shown in Table 6.5. Column 2 is the baseline case from Tables 6.3 and 6.4. The effect of cumulative detection using 10 pulses is shown in column 3. The total energy required is 11% of that for a single pulse (compared with 5% for noncoherent integration in Table 6.4). Cumulative detec-

Table 6.5 Cumulative Detection Examples

P_D	0.99	0.99	0.99	0.99
P_{FA}	10^{-6}	10^{-6}	10^{-6}	10^{-6}
n	1	10	1,000	$100 \times 10^*$
Swerling model	2	2	2	1 / 2
Pulse S/N	31.4	11.8	4.6	-8.2
Relative energy	100%	11%	209%	11%
* 10 groups of 100 coherently integrated pulses				

tion with 1,000 pulses (column 4) is seen to require over twice the total signal energy of a single pulse (compared with 18% for noncoherent integration in Table 6.4). Coherently integrating groups of 100 nonfluctuating pulses and then using frequency diversity between groups to allow effective cumulative detection is shown in column 5 to bring the relative energy back to 11%.

6.6 Problems

The following problems are provided to assist in reviewing this chapter and to ensure a basic understanding of the material. For maximum benefit, the problems should first be solved without using the VBA custom radar functions. Solutions to these problems are given in Appendix E, Section E.6.

1. What is the threshold level relative to the system noise level that gives $P_{FA} = 10^{-6}$ for detection using a single pulse or coherent integration?
2. What are the false-alarm rate and average time between false alarms for a radar having a signal bandwidth of 2 MHz and a P_{FA} of 10^{-8} , assuming continuous receiver operation? If a range window of 10 km is observed at a PRF of 500, what P_{FA} will produce the same false-alarm rate?
3. What single-pulse S/N is needed to provide $P_D = 0.9$ and $P_{FA} = 10^{-6}$ for Swerling 1, 2, 3, 4, and 5 targets? If 20 pulses are coherently integrated, what is the single-pulse S/N needed to give the above results for Swerling 1, 3, and 5 targets?
4. How many pulses having S/N = 10 dB must be noncoherently integrated to give $P_D = 0.9$ and $P_{FA} = 10^{-6}$ for Swerling 1, 2, 3, 4, and 5 targets? How many such pulses must be used in cumulative detection to give the same detection performance for Swerling 2, 4, and 5 targets?
5. For a Swerling 1 target, what is the single-pulse S/N needed when 10 pulses are coherently integrated to provide $P_D = 0.99$ and $P_{FA} = 10^{-6}$? If frequency diversity is used to produce Swerling 2 fluctuations and noncoherent integration is used, what is the single-pulse S/N needed? How much more or less energy is needed for noncoherent integration than for coherent integration? Repeat the above analysis for 1,000 pulses.
6. Answer the same questions as in Problem 5, but for cumulative detection.
7. A Swerling 3 target is observed with 100 pulses. If $P_D = 0.9$ and $P_{FA} = 10^{-6}$ is required, what is the single-pulse S/N if coherent integration is used? What is the single-pulse S/N if frequency diversity is used to produce Swerling 4 fluctuations, and noncoherent integration is used? What is the single-pulse S/N if groups of 10 Swerling 3 pulses are coherently integrated, frequency diversity is used to produce Swerling 4 fluctuations between these groups, and the groups are noncoherently integrated?
8. What is the P_{FA} required to produce an average false-alarm rate of 1 per second, for a radar operating continuously with a signal bandwidth of 10 MHz? For this threshold setting, what is the average false-alarm rate with a PRF of 200 Hz and an observation range window of 250 km?

9. What is the detection probability for $S/N = 15$ dB and $P_{FA} = 10^{-6}$ for Swerling 1, 2, 3, 4, and 5 targets?
10. What single-pulse S/N is needed for a Swerling 3 target to get $P_D = 0.95$ when 100 pulses are coherently integrated, and $P_{FA} = 10^{-4}$? For $P_{FA} = 10^{-8}$?
11. What is the single-pulse S/N for 1, 10, and 100 pulses noncoherently integrated to provide $P_D = 0.9$ and $P_{FA} = 10^{-6}$, for Swerling 2 and 4 targets? What is the loss, relative to coherent integration of Swerling 1 and 3 targets, in each case?
12. Answer the same questions as in Problem 11, but for cumulative detection.
13. For $P_D = 0.99$, $P_{FA} = 10^{-6}$, and a Swerling 4 target, what is the single-pulse S/N needed when 10 pulses are noncoherently integrated? Answer the same question when the pulses are used for cumulative detection.
14. With a single-pulse $S/N = 0$ dB, groups of 10 pulses are coherently integrated. For a Swerling 3 target, how many such groups must be noncoherently integrated to give $P_D = 0.9$ and $P_{FA} = 10^{-6}$? If the coherently integrated groups are decorrelated using frequency diversity, what is the number of groups needed? If cumulative detection is used on the decorrelated groups, what is the number of groups needed?

6.7 VBA Software Functions for Radar Detection

6.7.1 Function Pfa_Factor

Purpose Calculates the probability of false alarm (P_{FA}), required to provide a specified false-alarm rate (r_{FA}), in a defined search mode.

Reference Equations (6.7) and (6.8).

Features Allows the receive range window to be specified. If it is not, the receiver is assumed to be operating continuously.

Input Parameters (with units specified)

FArate_per_s = false-alarm rate, r_{FA} , required (s^{-1}). The reciprocal of the average time between false alarms, t_{FA} , (in seconds), may be used.

Bandwidth_MHz = receiver filter bandwidth, B , (MHz). The reciprocal of the compressed pulse duration, τ_C , (in microseconds), may be used.

PRF_Hz = pulse repetition frequency (Hz). The reciprocal of the PRI (in seconds) may be used.

R_Window_km (optional) = duration of the receive range window (km). If this parameter is left blank, the default value of $c/(2 \text{ PRF_Hz})$ will be used. If a value greater than the default value is input, the function will not produce a result, indicated by an output of -1 .

Function Output The false-alarm probability, P_{FA} , for the false-alarm rate and search mode specified.

The Excel Function Arguments parameter box for Function Pfa_Factor is shown in Figure 6.8, with sample parameters and solution

6.7.2 Function FArate_per_s

Purpose Calculates the false-alarm rate (r_{FA}), for a given probability of false alarm (P_{FA}), in a defined search mode.

Reference Equations (6.7) and (6.8).

Features Allows the receive range window to be specified. If it is not, the receiver is assumed to be operating continuously. The false-alarm rates calculated for multiple pulse trains may be added to obtain the overall false-alarm rate [see (6.9)].

Input Parameters (with units specified)

- Pfa_Factor = false-alarm probability, P_{FA} , specified.
- Bandwidth_MHz = receiver filter bandwidth, B , (MHz). The reciprocal of the compressed pulse duration, τ_c , (in microseconds), may be used.
- PRF_Hz = pulse repetition frequency (Hz). The reciprocal of the PRI (in seconds) may be used.
- R_Window_km (optional) = duration of the receive range window (km). If this parameter is left blank, the default value of $c/(2 \text{ PRF_Hz})$ will be used. If a value greater than the default value is input, the function will not produce a result, indicated by an output of -1.

Function Output The false-alarm rate, r_{FA} , (in s^{-1}) for the false-alarm probability, P_{FA} , for the search mode specified. When several pulse trains are used, the total false-alarm rate is the sum of the individual false-alarm rates calculated by this function [see (6.9)]. The average time between false alarms, t_{FA} , is the reciprocal of the false-alarm rate.

The Excel Function Arguments parameter box for Function FArate_per_s is shown in Figure 6.9, with sample parameters and solution

6.7.3 Function ProbDet_Factor

Purpose Calculates the probability of detection (P_D), for specified signal, target, and detection parameters.

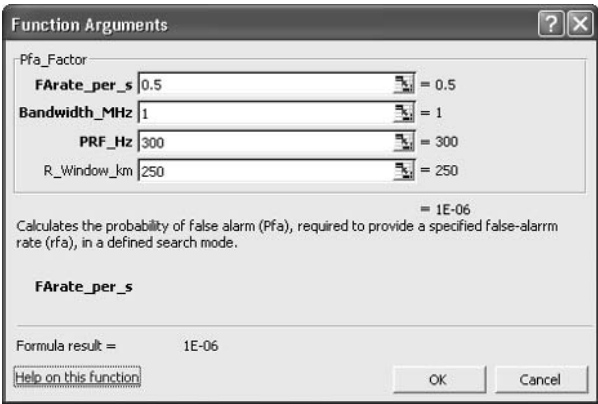


Figure 6.8 Excel parameter box for Function Pfa_factor.

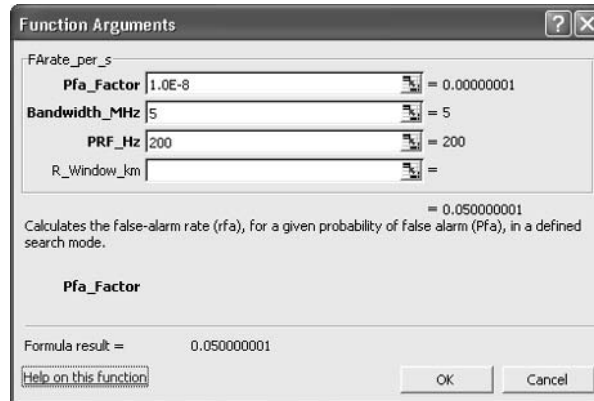


Figure 6.9 Excel parameter box for Function FArate_per_s.

Reference Equations (6.11), (6.12), and (6.13).

Features For multiple pulses, allows user selection of: (1) noncoherent integration for all Swerling target types, (2) coherent integration for non-fluctuating target types (Swerling 1, 3, and 5 targets), or (3) cumulative detection for pulse-to-pulse fluctuating target types (Swerling 2 and 4 targets); and nonfluctuating targets (Swerling 5). Coherent dwells may be used in place of pulses for Options 1 and 3.

Input Parameters (with units specified)

SNR_SP_dB = single-pulse S/N, (dB). When a series of coherent dwells is used, the coherently integrated S/N, $(S/N)_{CI}$, should be used for this parameter.

Pfa_Factor = probability of false alarm, P_{FA} , from 10^{-1} to 10^{-10} . Values outside this range produce no result, indicated by an output of -3 .

NPulses_Integ = number of pulses or coherent dwells, n , used for detection from 1 to 1,000 (integer). Values outside this range produce no result, indicated by an output of -4 .

SWcase_12345 = Swerling target-signal statistics case (integer). Use 1 for Swerling type 1 targets, 2 for Swerling type 2 targets, 3 for Swerling type 3 targets, 4 for Swerling type 4 targets, and 5 for nonfluctuating targets.

Sel_1Nc2Ci3Cd = select 1 for noncoherent integration, 2 for coherent integration, or 3 for cumulative detection (integer). If 2 is selected, no result will be generated for Swerling 2 and 4 targets, indicated by an output of -1 . If 3 is selected, no result will be generated for Swerling 1 and 3 targets, indicated by an output of -2 .

Function Output Probability of detection, P_D , for specified parameters. This function uses the recursive calculation method described in [4]. The maximum value of P_D is 0.999, except for Swerling 1 targets, where it is 0.99. The accuracy in P_D is about 0.0003, except for Swerling 1 targets, where it is about 0.001.

The Excel Function Arguments parameter box for Function Prob_Det_Factor is shown in Figure 6.10, with sample parameters and solution.

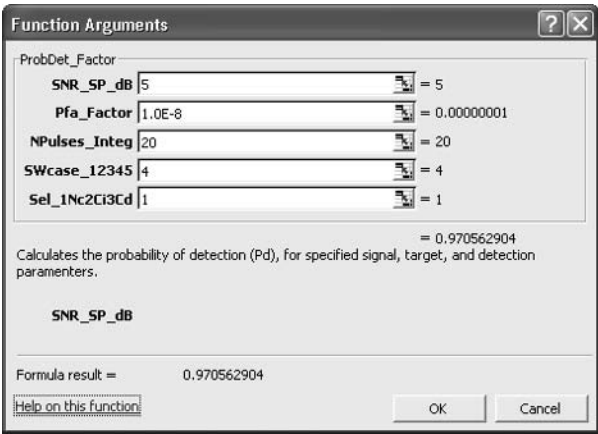


Figure 6.10 Excel parameter box for Function Prob_Det_Function.

6.7.4 Function SNR_SP_dB

Purpose Calculates the single-pulse S/N, or coherent dwell $(S/N)_{CI}$, required to provide the detection parameters for specified target and processing parameters.

Reference Equations (6.11), (6.12), and (6.13).

Features For multiple pulses, allows user selection of: (1) noncoherent integration for all Swerling target types, (2) coherent integration for nonfluctuating target types (Swerling 1, 3, and 5 targets), or (3) cumulative detection for pulse-to-pulse fluctuating target types (Swerling 2 and 4 targets); and nonfluctuating targets (Swerling 5). Coherent dwells may be used in place of pulses for Options 1 and 3.

Input Parameters (with units specified)

- Prob_Det_Factor = required probability of detection, P_D , from 0.3 to 0.999, except for Swerling 1 targets, where it is from 0.3 to 0.99. Values outside this range produced no result, indicated by an output of -5 .
- Pfa_Factor = probability of false alarm, P_{FA} , from 10^{-1} to 10^{-10} . Values outside this range produce no result, indicated by an output of -3 .
- NPulses_Integ = number of pulses or coherent dwells, n , used for detection from 1 to 1,000 (integer). Values outside this range produce no result, indicated by an output of -4 .
- SWcase_12345 = Swerling target-signal statistics (integer). Use 1 for Swerling type 1 targets, 2 for Swerling type 2 targets, 3 for Swerling type 3 targets, 4 for Swerling type 4 targets, and 5 for nonfluctuating targets.
- Sel_1Nc2Ci3Cd = select 1 for noncoherent integration, 2 for coherent integration, or 3 for cumulative detection (integer). If 2 is selected, no result will be generated for Swerling 2 and 4 targets, indicated by an output of -1 . If 3 is selected, no result will be generated for Swerling 1 and 3 targets, indicated by an output of -2 .

Function Output The single-pulse S/N for the specified parameters (dB). When coherent dwells are used, the output is the coherently integrated S/N, $(S/N)_{CI}$, for the

coherent dwell. This function uses the recursive calculation method described in [4]. The accuracy in S/N is about 0.01 dB.

The Excel Function Arguments parameter box for Function SNR_SP_dB is shown in Figure 6.11, with sample parameters and solution.

References

- [1] Barton, D. K., *Radar System Analysis*, Englewood Cliffs, NJ: Prentice Hall, 1964.
- [2] Barton, D. K., *Modern Radar System Analysis*, Norwood, MA: Artech House, 1988.
- [3] DiFranco, J. V., and W. L. Rubin, *Radar Detection*, Englewood Cliffs, NJ: Prentice Hall, 1969.
- [4] Mitchell, R. L, and J. F. Walker, "Recursive Methods for Computing Detection Probabilities," *IEEE Trans. of Aerospace and Electronic Systems*, Vol. AES-7, No. 4, July 1971, pp. 671–676.
- [5] Shnidman, D. A., "Radar Detection Probabilities and Their Calculation," *IEEE Trans. of Aerospace and Electronic Systems*, Vol. 31, No. 3, July 1995, pp. 928–950.
- [6] Helstrom, C. W., "Approximate Evaluation of Detection Probabilities in Radar and Optical Communications," *IEEE Trans. of Aerospace and Electronic Systems*, Vol. AES-14, No. 4, July 1978, pp. 630–640.

Selected Bibliography

The book by DiFranco and Rubin gives a detailed discussion of radar detection, derives the key equations for calculating detection probabilities, and also treats cumulative and sequential detection. This book provides plots of detection probability as a function of S/N with false-alarm probability as a parameter, for the five Swerling target classes and various numbers of pulses integrated. These plots use the two-sided S/N, \mathfrak{R}_p , and the false-alarm number, n' . As discussed in Section 6.3, it is necessary to subtract 3 dB from the \mathfrak{R}_p values, in these plots to get S/N, and use $P_{FA} = 0.693/n$.

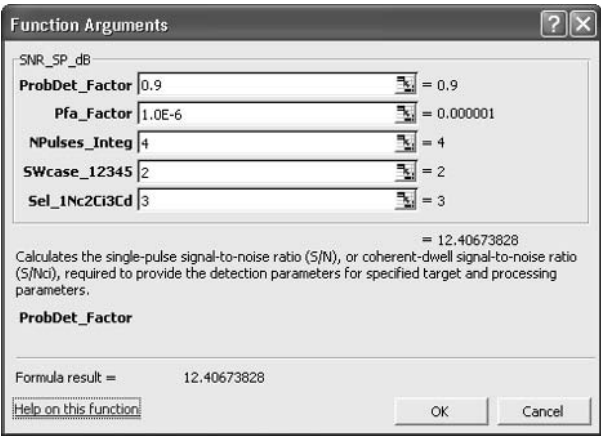


Figure 6.11 Excel parameter box for Function SNR_SP_dB.

Chapter 2 of Barton discusses detection theory and gives empirical techniques and plots for finding detection probability. Barton also gives a number of references related to calculation of detection probability.

Papers by Mitchell and Walker, Snidman, and Helstrom describe computational techniques for evaluating probability of detection. The truncated series approach in Mitchell is used in the custom radar function ProbDet_Factor described Section 6.7.3. Shnidman offers to provide Fortran code implementing his technique to readers who request it.

Barton, D. K., *Modern Radar System Analysis*, Norwood, MA: Artech House, 1988.

DiFranco, J. V., and W. L. Rubin, *Radar Detection*, Englewood Cliffs, NJ: Prentice Hall, 1969.

Helstrom, C. W., "Approximate Evaluation of Detection Probabilities in Radar and Optical Communications," *IEEE Trans. of Aerospace and Electronic Systems*, Vol. AES-14, No. 4, July 1978, pp. 630–640.

Mitchell, R. L., and J. F. Walker, "Recursive Methods for Computing Detection Probabilities," *IEEE Trans. of Aerospace and Electronic Systems*, Vol. AES-7, No. 4, July 1971, pp. 671–676.

Shnidman, D. A., "Radar Detection Probabilities and Their Calculation," *IEEE Trans. of Aerospace and Electronic Systems*, Vol. 31, No. 3, July 1995, pp. 928–950.

Radar Search Modes

This chapter enables the reader to:

- Understand the radar search equation and the key parameters that affect radar performance in search, including the power-aperture product;
- Evaluate the search performance of rotating search radar, and dish radar in horizon search modes;
- Configure and evaluate volume search modes using phased-array radar;
- Configure and evaluate cued search modes using dish radar and phased-array radar;
- Configure and evaluate horizon search modes using dish radar and phased-array radar.

Radar search, also called radar surveillance, is the process of examining a volume of space with the objective of detecting targets in that volume. The search objectives usually include the search volume, the characteristics of the targets to be detected, and the detection requirements. The detection requirements are often defined by the probability of detection, P_D , and the probability of false alarm, P_{FA} , or the false alarm rate r_{FA} . The required P_{FA} may be calculated from r_{FA} using the techniques given in Section 6.2.

Common radar search modes include:

- Volume search, where a relatively large volume of space is searched. Volume search using rotating search radars is described in Section 7.2, and using phased-array radars in Section 7.3.
- Cued search, where a search is preformed in a relatively small volume to acquire a target whose position is approximately known. Cued search using phased arrays and dish radars is described in Section 7.4.
- Horizon search, where the radar searches for targets coming over the radar horizon. Horizon search by phased-array radars is described in Section 7.5, and by dish radars in Section 7.6.

7.1 The Search Equation

The radar detection range in a search mode, R_D , is given by general form of the radar search equation [1, p. 255]:

$$R_D = \left[\frac{P_A A_R t_s \sigma}{4\pi \psi_s (S/N) k T_s L} \right]^{1/4} \quad (7.1)$$

where:

t_s = search time;

ψ_s = search solid angle;

σ = target RCS;

S/N = signal-to-noise ratio;

k = Boltzmann's constant (1.38×10^{-23});

T_s = radar system noise temperature (see Section 3.4);

L = radar losses, (including search losses described below, as well as the fixed radar losses described in Chapters 3 and 5).

Equation (7.1) shows that the detection range, R_D , is proportional to the fourth root of the product of the radar average power, P_A , and the receive aperture area, A_R . This is often called the power-aperture product. When only a portion of the radar power is used in a search mode, P_A in (7.1) refers to that portion of the total radar average power used for search.

The absence of the transmit antenna gain from this relationship results from the dependence of gain on beamwidth, as discussed in Section 3.2 (3.12). While higher gain increases the radar sensitivity, it also narrows the beam so that more beam positions must be searched and less energy may be allocated to each beam position.

The losses, L , in the search equation include search losses, in addition to the radar system losses discussed previously. These include: (1) losses due to the non-ideal distribution of radar energy in the search volume; (2) the beamshape loss, L_{BS} ; and (3) the loss resulting from beam overlap that is characterized by the beam-packing factor, f_p . The search losses also include pulse integration losses and any additional signal-processing losses from the search mode. Propagation losses are also included here.

Equation (7.1) shows that the radar detection range in search, R_D , is proportional to $(P_A A_R)^{1/4}$, when the search time, t_s , is fixed. R_D also increases with the fourth root of search time. While increasing the search time increases the detection range, using too long a search time may decrease the assured acquisition range for targets that are approaching the radar. This is because the search scan might not observe a target until the end of the search time interval (see Section 7.3). In these situations, the search time that maximizes the assured acquisition range, t_{SM} , is equal to [2, 3]:

$$t_{SM} = R_D / (4 V_R) \quad (7.2)$$

where V_R is the target radial velocity.

Substituting this into (7.1) gives:

$$R_D = \left[\frac{P_A A_R \sigma}{16\pi V_R \psi_s (S/N) k T_s L} \right]^{1/3} \quad (7.3)$$

When this optimum search time is used, the detection range is seen to vary with $(P_A A_R)^{1/3}$.

In practice, search times considerably shorter than calculated by (7.2) are often used. This results from: realistic antenna mechanical-scan times (see Section 7.2); limitations in pulse integration; desire for rapid assured acquisition of targets (see Section 7.4), or for rapid detection of targets coming into radar angular coverage; and requirements to detect targets while they remain in the radar search coverage (see Sections 7.5 and 7.6).

When shorter search times than the optimum given by (7.2) are used, the detection range is reduced from that given by (7.3) by the fourth root of the ratio of the search time to the optimum search time. In such cases, the detection range may be found directly from (7.1). The assured acquisition range is reduced by a smaller factor than the detection range, due to the smaller target range change during the shorter search time.

For example, if the detection range from (7.3) is 300 km, the assured acquisition range is $R_D - V_R t_{sm} = 300 - 300/4 = 225$ km. If a search time equal to one-tenth the optimum is used, the detection range is reduced by 44% to 169 km. However, the assured acquisition range is $R_D - 0.1 V_R t_{SM} = 169 - 0.1 (300/4) = 162$ km, a reduction of 28% from the value obtained using the optimum search time.

The radars search equations given above may provide an estimate of the radar search range and are useful for comparing radar capabilities. The search performance of radars is often compared using their power-aperture products. When the system noise temperature, T_s , and losses, L , differ significantly among radars being compared, these terms may be included in the comparison. The radars are then compared by their $P_A A_R / (T_s L)$ values.

The radar search performance in specific modes is more accurately calculated as described in the following sections. These describe simplified representations of commonly used search modes. They are useful for estimating and comparing radar performance, but are not intended to be precise representations of actual radar performance. The design of detailed radar search modes, such as the beam-by-beam search designs used by many phased-array radars, is a complex process and is beyond the scope of this book.

7.2 Rotating Search Radar

Rotating search radars often employ a narrow azimuth beam and a broad elevation beam, called a fan-shaped beam. The fan-shaped beam may be formed by a parabolic reflector, as discussed in Section 2.3, or generated by a planar-array antenna, and may be shaped in elevation angle to provide the desired elevation coverage. The antenna is rotated continuously in azimuth, usually at a fixed rate. The radar searches the volume covered by the fan beam in elevation, and 360 degrees in azimuth.

The radar antenna rotation rate, the azimuth beamwidth, and the PRF are usually chosen so that several pulses illuminate a target as the radar beam scans by. The number of pulses, n_p , that illuminate the target between the 3-dB points of the azimuth beam is given by:

$$n_p = \frac{\theta_A t_R \text{PRF}}{2\pi} \quad (7.4)$$

where:

θ_A = azimuth beamwidth (in radians);

t_R = antenna rotation period ($t_R = 2\pi/\omega_R$, where ω_R is the antenna angular rotation rate in radians/s);

PRF = radar pulse repetition frequency.

For example, for an azimuth beamwidth of 2° (0.035 radians), a rotation period of 10 sec ($\omega_R = 36^\circ/\text{s}$ or 0.628 radians/s), and a PRF of 200 Hz, approximately 11 pulses would illuminate the target between the 3-dB points of the azimuth beam. This is illustrated by Figure 7.1, which shows the pulse returns from a nonfluctuating target for the parameters in this example.

The pulse returns produced as the beam sweeps past the target, illustrated by Figure 7.1, are usually combined to detect the target and measure its angular position. For older radars, the target returns were often displayed on plan position indicator (PPI). The detection performance of operators using such displays is similar to that of noncoherent integration. Modern radar usually uses processors to perform the noncoherent or coherent integration of the n_p pulses that illuminate the target as the beam sweeps past. Coherent integration is often used in modern radar, implemented by a bank of digital filters that cover the expected range of radial velocities, as discussed in Section 6.3. Cumulative detection is rarely used, except for small values of n_p and rapidly fluctuating targets, where the integration loss is not too large.

Target azimuth is often measured by estimating the center of the sequence of returns, such as shown in Figure 7.1. While target fluctuations may increase the measurement error in such cases, relative to the value predicted for a steady target in thermal noise, the increase is often small when several pulses are used (see Chapter 8).

If the radar frequency is fixed, then the target RCS will often not fluctuate from pulse-to-pulse while the scan illuminates the target, and Swerling 1 or 3 models may be used (these models were developed for just this situation). If the target return is

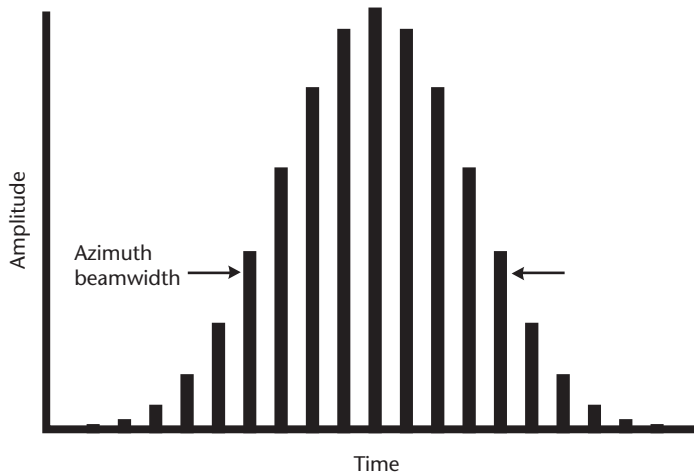


Figure 7.1 Pulse returns from a nonfluctuating target produced by the azimuth scan of a rotating surveillance radar.

fluctuating rapidly or pulse-to-pulse frequency changes are used to decorrelate the target returns (as discussed in Section 3.5), then Swerling 2 or 4 models may be used. Swerling 5 may be used for nonfluctuating targets. The single-pulse S/N required to provide the desired probability of detection, P_D , and probability of false alarm, P_{FA} , are determined as discussed in Chapter 6.

When calculating the single-pulse S/N that is provided by a radar in this search mode, three additional loss factors must be included with the fixed radar losses, L_F , described in Section 5.3:

- Propagation losses, L_p . These depend on the radar frequency, target elevation angle, and range, as discussed in Chapter 9.
- Beamshape loss, L_{BS} . This loss accounts for the radar signal returns that are less than those at the peak of the radar beam, as shown in Figure 7.1. A value of 1.6 dB (power ratio = 1.45) is used to account for the azimuth beam shape when the target is at the peak of the fan-shaped elevation beam [4, pp. 463–464].
- Scanning loss for rotating search radar, L_{RS} . This loss is due to the motion of the beam between transmission and reception. (This loss is distinct from the off-broadside scan loss used with phased-array antennas.) The scanning loss is negligible when six or more pulses illuminate the target during the scan and the PRF is unambiguous. For other cases, it may be found from Figure 7.2 [4, pp. 463–464], using the maximum expected target range to be conservative.

For example, when 11 pulses illuminate a Swerling 1 target, a P_D of 0.9 and a P_{FA} of 10^{-6} are required, and noncoherent integration is used, the required single-pulse S/N = 13.2 dB (power ratio = 20.9). Assume a radar with a reference range (see Section 5.3) of 100 km for a S/N = 15 dB (power ratio = 31.6), a target RCS = 1 m², and the pulse duration used. The additional search losses are: L_p = 1.2 dB (assumed),

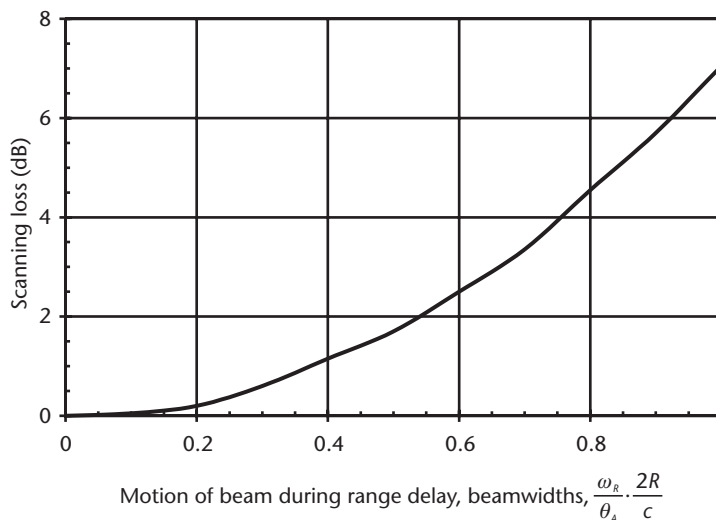


Figure 7.2 Scanning loss for rotating search radar as function of beam motion in beamwidths during the range delay.

$L_{BS} = 1.6$ dB, and $L_{RS} = 0$ dB, for a total of 2.8 dB (power ratio = 1.91). The detection range, R_D , for a 0.3 m^2 target is then calculated from (5.11) in Chapter 5:

$$R_D = 100 \left[\frac{0.3}{1} \frac{316}{209} \frac{1}{191} \right]^{1/4} = 69.8 \text{ km} \quad (7.5)$$

If radar parameters are given rather than the reference range, (5.6) may be used to calculate R_D .

With coherent integration, the required single-pulse $S/N = 10.7$ dB, and the detection range is 80.6 km. If pulse-to-pulse frequency diversity is used to convert the target to Swerling 2 and noncoherent integration is used, the required single-pulse $S/N = 5.9$ dB, and the detection range increases to 106.3 km. If cumulative-detection processing is used with the Swerling 2 target, the required single-pulse $S/N = 9.4$ dB, and the detection range is 86.9 km.

A target having a radial velocity, V_R , relative to the radar, may reach the detection range, R_D , any time during the rotation period of the radar antenna. Thus the range at which the target is acquired with the required P_D may be less than R_D . The range at which acquisition of a closing target is assured, R_A , is given by:

$$R_A = R_D - V_R t_R \quad (V_R \geq 0) \quad (7.6)$$

where the target radial velocity, V_R , is positive for closing targets. The average target acquisition range, R_p , may be needed for some system analysis applications. For targets entering the search coverage randomly, it is given by:

$$R_p = R_D - 0.5 V_R t_R \quad (V_R \geq 0) \quad (7.7)$$

For many rotating search radar cases, the search times are much shorter than calculated by (7.2). When $V_R t_R \ll R_D$, R_D may be used for the target acquisition range.

In the preceding example, with noncoherent integration and a Swerling 1 target, the detection range is 69.8 km. With the specified radial velocity of 300 m/s and the rotation period of 10 sec, the target travels 3 km during the search scan. The assured acquisition range, $R_A = 66.8$ km, and the average acquisition range $R_p = 68.3$ km. The results of the preceding examples are summarized in Table 7.1

The cumulative-detection mode in the above example uses cumulative detection over a single scan of the radar. Cumulative detection is more often used for multiple scans or observations that provide detection opportunities. In the above example, search scans occur at 10 sec intervals. If cumulative detection were used for six such scans (total time 60 sec), and scan-to-scan decorrelation occurred (Swerling 1), the detection probability for each scan, P_{DO} , could be reduced to [see (6.15)]:

$$P_{DO} = 1 - (1 - 0.9)^{1/6} = 0.32 \quad (7.8)$$

The single-pulse S/N could be reduced from the values given above, or the detection range would be increased. In realistic cases, the target range does not remain fixed, so that P_D varies from scan to scan. In addition, targets detected with low

Table 7.1 Rotating Search Radar Example

<i>Swerling Case</i>	<i>Processing Type</i>	<i>Single-Pulse S/N (dB)</i>	<i>Detection Range (km)</i>	<i>Assured Acquisition Range (km)</i>	<i>Average Acquisition Range (km)</i>
1	Noncoherent integration	13.2	69.8	66.8	68.3
1	Coherent integration	10.7	80.6	77.6	79.1
2	Noncoherent integration	5.9	106.3	103.3	104.8
2	Cumulative detection	9.4	86.9	83.9	85.4

probability may not be maintained in track. An example including these considerations is given in Section 12.3.

Many rotating search radars are designed to detect aircraft having maximum altitudes that are much less than the desired detection range. To avoid wasting radar energy at high elevation angles, where long range is not required, these radars often employ elevation beams having gain that varies with elevation angle. The resulting coverage is illustrated in Figure 7.3(a). Coverage is provided to the maximum range from near the horizon to an elevation angle of θ_1 , and the coverage is maintained at a fixed altitude from θ_1 to a maximum elevation angle of θ_2 .

The radar elevation coverage shown in Figure 7.3(a) is provided by an elevation gain pattern that varies with elevation angle, θ , as the cosecant-squared of the elevation angle for elevation angles between θ_1 and θ_2 [5, pp. 26–27]:

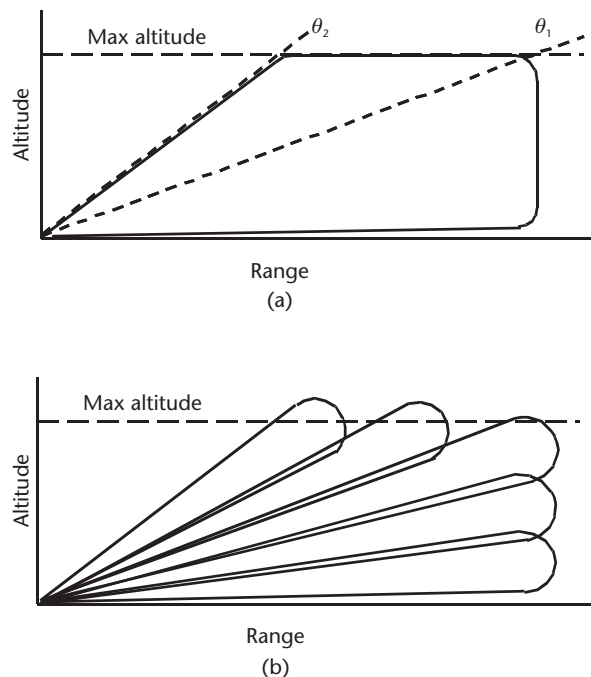


Figure 7.3 Elevation coverage of a search radar providing coverage of targets up to a maximum altitude. (a) Cosecant-squared beam. (b) Multiple beams.

$$G(\theta) = \frac{G(\theta_1) \csc^2 \theta}{\csc^2 \theta_1} \quad (\theta_1 < \theta < \theta_2) \quad (7.9)$$

This gain variation applies to both G_T and A_R .

Providing the coverage at elevation angles greater than θ_1 results in a modest reduction in the gain at elevation angles less than θ_1 :

$$G_H = \frac{G}{2 - \theta_1 \cot \theta_2} \quad (\theta_1 < \theta_2) \quad (7.10)$$

where G_H is the maximum gain with the cosecant-square pattern, and G is the gain without coverage above θ_1 . For typical parameters, the gain reduction is 2 dB, and the maximum gain reduction is 3 dB for $\theta_2 = 90^\circ$.

Some rotating search radars employ multiple stacked elevation beams, illustrated in Figure 7.3(b), rather than a single fan-shaped beam. This allows measurement of target elevation angle, using a technique similar to monopulse measurement (see Section 3.2). The elevation coverage may be tailored to provide coverage to a maximum target altitude, as shown in the figure. The beam positions may be illuminated simultaneously using a fan beam for transmit and multiple receive beams, or individual transmit-receive beams may be used. In the latter case, the beams scan rapidly over the elevation sector during each azimuth dwell.

The above analysis procedure may be used to calculate detection and acquisition ranges for these cases, if reference range or the values of G_T , A_R , L_{BS} , and number of pulses illuminating the target, n_p , for the appropriate elevation angle are used. If the parameters corresponding to a beam peak are used and the target is not assured to be at the peak of the beam, an elevation beamshape loss of 1.6 dB should be included in the calculation, in addition to the 1.6-dB azimuth beamshape loss, for a total beamshape loss of 3.2 dB.

7.3 Volume Search with Phased-Array Radar

Phased-array radar generally employs narrow pencil beams that may be rapidly positioned within the radar field-of-view (FOV) by electronic steering, as discussed in Sections 2.3 and 3.3. Volume search is performed by transmitting and receiving in a sequence of beam positions that cover the angular coordinates of the search volume. Electronic scan limits the search coverage of a single FFOV phased array to about $\pm 60^\circ$ in each of two angular coordinates. The angular coverage of LFOV phased array is less than this, as discussed in Section 3.3.

The search beams are usually arranged on a rectangular or triangular grid, as illustrated in Figure 7.4 for circular beams. The figure shows some overlap of the beams, which reduces the depth of the nulls between beams. The spacing of the beams in the grid is a tradeoff between the number of beams required to fill the search volume, and the beamshape loss due to reduced antenna gain in areas between the beam centers. The beam spacing that minimizes the radar power needed for search depends on the search grid used, and on the number of pulses transmitted and their processing in the receiver. However, the power required remains near the

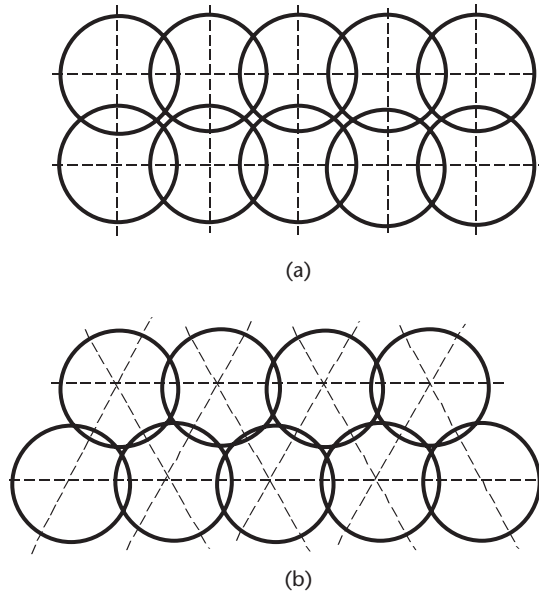


Figure 7.4 Grids of circular beams used for phased-array radar search. (a) Rectangular beam grid. (b) Triangular beam grid.

minimum for beam spacing from 0.5 to 1.5 beamwidths [6, pp. 45–55]. When detections from adjacent beams are considered, even closer beam spacing may be efficient [7]. Typical beam spacing results in beamshape loss over two angular coordinated of 2.5 dB [5, p. 30].

The total number of beams, n_B , needed to fill the search solid angle, ψ_S , is given by:

$$n_B = f_P \psi_S / \psi_B \quad (7.11)$$

where:

ψ_B = solid angle of radar beam within 3-dB contour;

f_P = beam-packing factor.

The beam-packing factor accounts for the two-dimensional overlap in beam coverage in the grid. A typical value of f_P that is consistent with 2.5-dB beamshape loss is 1.2 (J. H. Ballantine, personal communication). (The 2.5-dB beamshape loss here is smaller than the 3.2-dB beamshape loss used above for radar that scan in two dimensions, since the beams here are arranged in a grid, and a beam-packing factor is used.)

Since the beamwidth and scan loss for phased arrays depend on the off-broadside scan angle, these will vary with beam position in the search pattern. If the beam coverage grid uses the array-broadside beamwidths, the beam solid angle is given by:

$$\psi_B = \frac{\pi}{4} \theta_{Bx} \theta_{By} \quad (7.12)$$

where:

- θ_{Bx} = phased-array beamwidth in the x plane on broadside;
- θ_{By} = phased-array beamwidth in the y plane on broadside.

When the beam is scanned off-broadside, the beamwidth increases, as discussed in Section 3.3. The beam solid angle is then given by:

$$\psi_B = \frac{\pi}{4} \frac{\theta_{Bx}}{\cos \varphi_x} \frac{\theta_{By}}{\cos \varphi_y} \quad (7.13)$$

where:

- φ_x = off-broadside scan angle in the x plane;
- φ_y = off-broadside scan angle in the y plane.

If the search angular coverage (or a portion of that coverage) is approximated by rectangular coverage in the orthogonal coordinates of the array face, the average beam solid angle, ψ_{BA} , for that search coverage is given by:

$$\psi_{BA} = \frac{\pi}{4} \frac{\theta_{Bx}}{\varphi_{x2} - \varphi_{x1}} \int_{\varphi_{x1}}^{\varphi_{x2}} (\cos \varphi_x)^{-1} d\varphi_x \frac{\theta_{By}}{\varphi_{y2} - \varphi_{y1}} \int_{\varphi_{y1}}^{\varphi_{y2}} (\cos \varphi_y)^{-1} d\varphi_y \quad (7.14)$$

where φ_{x1} , φ_{y1} , φ_{x2} , and φ_{y2} are the coverage coordinates in the x and y directions. The integral in (7.14) is plotted in Figure 7.5 as a function of the integration limits to aid in evaluating the equation. The integral from zero to some upper limit may be read directly from the curve. When the desired lower limit is not zero, the integral from zero to the lower limit may be subtracted from the integral from zero to the upper limit.

The ratio of the average beam solid angle to the broadside beam solid angle may be given by a beam broadening factor, f_B :

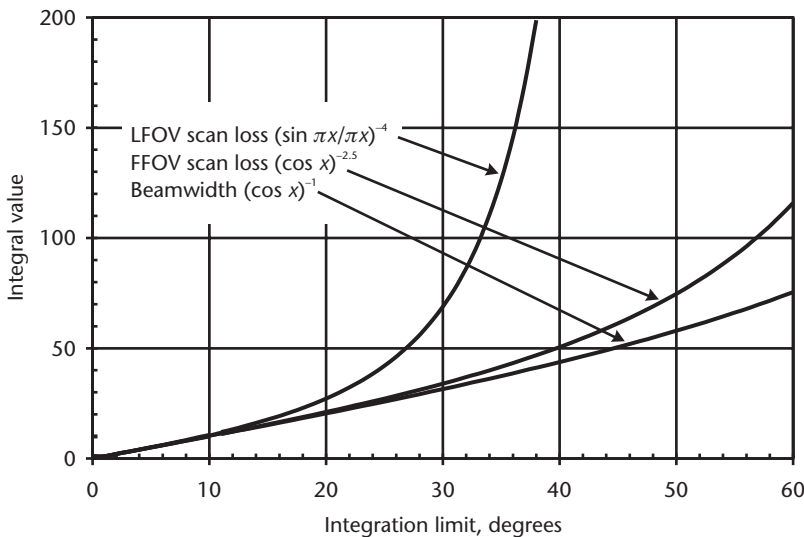


Figure 7.5 Integrals of normalized scan loss and beamwidth from a lower limit of zero, as functions of the upper integration limit.

$$f_B = \psi_{BA} / \psi_B \quad (7.15)$$

For example, for an x -plane (azimuth) beamwidth of 1 degree, and search in the x plane from $+45^\circ$ to -45° , the first term in (7.14) will be $(1/90) \times (50.5 + 50.5) = 1.12^\circ$. For a y -plane (elevation) beamwidth of 2° , and search in the y plane from -15° to $+25^\circ$, the second term may be similarly evaluated as 2.05° . The average beam solid angle is then 1.80 square degrees or 0.000548 steradians. The broadside beam solid angle is 1.57 square degrees or 0.000478 steradians. The beam-broadening factor, f_B , is 1.15. This coverage corresponds approximately to that of an array face having a boresight elevation angle of 20° searching from 5° to 45° in elevation and $\pm 45^\circ$ in azimuth. The number of beams required to cover the search volume is $1.2 \times 90 \times 40 / 1.80 = 2,400$. If beam broadening is not considered, 2,750 beams would be required to cover the search area.

The scan loss from off-broadside phased-array scan is a function of the scan angle, as described in Section 3.3. To maintain the radar performance for off-broadside search, the energy transmitted in off-broadside radar beams must be increased to compensate for this loss. Note that the beam-broadening partially offsets the needed increase in radar energy per unit of solid angle searched off-broadside. The search mode may use fixed radar beam spacing in order to reduce the required increase in radar energy in off-broadside beams.

The average scan loss over the search volume, L_{SA} , is given for a rectangular search volume and FFOV arrays is approximately given by:

$$L_{SA} = \frac{1}{\varphi_{x2} - \varphi_{x1}} \int_{\varphi_{x1}}^{\varphi_{x2}} (\cos \varphi_x)^{-2.5} d\varphi_x \frac{1}{\varphi_{y2} - \varphi_{y1}} \int_{\varphi_{y1}}^{\varphi_{y2}} (\cos \varphi_y)^{-2.5} d\varphi_y \quad (7.16)$$

$$(\theta_{Rx} < (\varphi_{x2} - \varphi_{x1}), \theta_{Ry} < (\varphi_{y2} - \varphi_{y1})) \quad (\text{FFOV})$$

This integral is plotted in Figure 7.5 to aid in evaluating these equations. For the example given above, for a FFOV array, the average scan loss is $(61.3 + 61.3)/90 \times (15.4 + 27.2)/40 = 1.45$ or 1.62 dB.

For LFOV arrays, L_{SA} , a rectangular search volume is approximately given by a similar expression using the scan loss terms in (3.27) or (3.28). The upper curve in Figure 7.5 gives the integral of the scan loss for LFOV arrays, given in (3.27). To use this curve, enter the value of $d \sin \varphi / \lambda$, converted from radians to degrees (i.e., multiply by 57.3).

The search sectors assumed in these average calculations have rectangular angular dimensions in phased-array coordinates, defined by x and y angular coordinates (see Section 3.3). For small values of array broadside elevation angle, these approximate rectangular angular scan volumes in azimuth and elevation angle. In other cases, the search volume may be approximated by one or several volumes, each having rectangular x and y coordinates.

The approximate search detection range, R_D , may be found from (7.1) or (7.3) by including beamshape loss, L_{BS} , average scan loss, L_{SA} , and propagation losses, L_P , in the loss factor and adjusting the search solid angle, ψ_s , to include the beam-packing factor, f_p , and the beam-broadening factor, f_B . The resulting equation assumes that a single pulse is transmitted in each beam position, or equivalently that

coherent integration is used for all pulses transmitted in a beam position. This is not practical in many cases, due to limitations in pulse duration, minimum-range constraints (see Section 5.5), and the difficulty of performing coherent integration in a search mode (see Sections 5.4 and 6.3).

When noncoherent integration or cumulative detection is used to combine multiple pulses transmitted in a beam position, the S/N term in (7.1) or (7.3) is replaced by $n_p S/N$, where n_p is the number of pulses used in a beam position, and S/N is the single-pulse S/N required to provide the detection parameters. The resulting range may be greater or less than for a single pulse, depending on the target fluctuation characteristics, the detection parameters, and the number of pulses used (see Sections 6.4 and 6.5).

Using (7.3), which assumes the optimum search time, t_{SM} , given in (7.2), and including multipulse search and the beam-packing and beam-broadening factors, gives:

$$R_D = \left[\frac{P_A A_R \sigma f_B}{16\pi V_R \psi_s n_p (S/N) k T_s L f_p} \right]^{1/3} \quad (\text{volume search}) \quad (7.17)$$

The detection range also may be calculated from the radar reference range (see Section 5.3), using:

$$R_D = \left[\frac{R_{ref}^4 D C \sigma (S/N)_{ref}}{4V_R n_p n_B \tau_{ref} \sigma_{ref} (S/N) L_s L_{BS} L_p} \right]^{1/3} \quad (\text{volume search}) \quad (7.18)$$

When less than the entire radar power is used for search, the value of P_A in (7.17) and DC in (7.18) is that part of the radar resources used in the search mode.

Note that radar duty cycle is required in (7.18) to quantify the radar pulse-rate capability when reference range is used. The duty cycle is also used to calculate the pulse duration, which is given by:

$$t = \frac{DC t_s}{n_p n_B} = \frac{DC R_D}{4V_R n_p n_B} \quad (\text{volume search}) \quad (7.19)$$

The number of pulses used per beam position, n_p , must be large enough so that the resulting pulse duration is short enough to avoid the minimum-range constraint. When noncoherent integration or cumulative detection are used, it is also desirable to use a value of n_p that minimizes the total energy in a beam position, as shown in Figures 6.5 and 6.7, and discussed in Sections 6.4 and 6.5.

When the search is performed by sequentially illuminating beam positions, the assured acquisition range, R_A , is given by the range of a worst-case target that is illuminated at the end of the search scan, and:

$$R_A = \frac{3}{4} R_D \quad (\text{volume search}) \quad (7.20)$$

Similarly, the average acquisition range, R_p , for a target at a random angular location in the search coverage is given by:

$$R_p = \frac{7}{8} R_D = \frac{7}{6} R_A \quad (7.21)$$

Like the detection range, R_D , these ranges are proportional to the cube root of the radar power-aperture product.

The use of multiple pulses in a beam position is illustrated by an example using the beam coverage parameters given in the previous example and the following radar and detection parameters:

$$P_A = 5 \text{ kW};$$

$$DC = 0.1;$$

$$A_R = 17 \text{ m}^2 \text{ (consistent with the beamwidths given earlier, for an S-band radar);}$$

$$\sigma = 0.1 \text{ m}^2;$$

$$V_R = 500 \text{ m/s};$$

$$\psi_s = 90^\circ \times 40^\circ = 1.10 \text{ steradians};$$

$$T_s = 500\text{K};$$

$$L = 7.42 \text{ dB (3-dB fixed loss, 2.5-dB beamshape loss, 1.62-dB average scan loss, and 0.3-dB propagation loss);}$$

$$f_B = 1.15;$$

$$f_P = 1.2;$$

$$P_D = 0.9;$$

$$P_{FA} = 10^{-6};$$

Swerling 2 signal fluctuations.

Table 7.2 gives the single-pulse S/N versus number of pulses transmitted in a beam position for noncoherent integration and cumulative detection. Coherent

Table 7.2 Volume Search Example for Various Numbers of Pulses per Beam Position Using Noncoherent Integration or Cumulative Detection

<i>Pulses per Beam</i>									
<i>Position</i>	<i>Noncoherent Integration</i>					<i>Cumulative Detection</i>			
	<i>S/N (dB)</i>	<i>Assured Acquisition Range (km)</i>	<i>Pulse Duration (ms)</i>	<i>Minimum Range (km)</i>		<i>S/N (dB)</i>	<i>Assured Acquisition Range (km)</i>	<i>Pulse Duration (ms)</i>	<i>Minimum Range (km)</i>
1	21.1	294	8.17	1,225		21.1	294	8.17	1,225
2	14.8	379	5.26	789		15.7	353	4.91	736
3	12.1	407	3.77	565		13.6	363	3.36	504
4	10.5	418	2.90	435		12.4	361	2.51	376
5	9.4	422	2.35	352		11.6	357	1.98	297
6	8.5	426	1.97	296		11.0	351	1.63	244
7	7.8	427	1.69	254		10.6	344	1.37	205
8	7.2	427	1.48	223		10.2	339	1.18	177
9	6.7	427	1.32	198		9.9	334	1.03	155
10	6.3	425	1.18	177		9.6	330	0.917	137

integration is not used due to the rapid target fluctuation. The corresponding assured acquisition ranges, calculated from (7.17) and (7.20), are given in the table. The pulse durations are calculated from (7.19), assuming that 2,400 beam positions are searched, and using the radar duty cycle of 0.1. The resulting minimum ranges are also shown (see Section 5.5).

Table 7.2 shows that for a single pulse per beam position, the assured acquisition range would be 294 km. However, the pulse duration would be 8.17 ms, producing a minimum range much larger than the acquisition range, so a single pulse is not viable. Use of a single pulse might also be precluded if the radar transmitter, could not generate a pulse as long as 8.17 ms. Further, for a fluctuating target signal, using several pulses per beam position provides a larger acquisition range. The optimum is seen to be about eight pulses for noncoherent integration, and three pulses for cumulative detection.

For this example, the minimum number of pulses that will avoid minimum-range eclipsing is five for both processing modes. The best assured acquisition range with noncoherent integration is 427 km, provided by using the optimum number of about eight pulses per beam position. The best assured acquisition range with cumulative detection is 357 km, provided by using the minimum number of pulses to avoid minimum-range eclipsing (five).

These values assume that the required pulse durations, 1.48 and 1.98 ms respectively, are available. If the desired pulse duration is not available in the radar, the next shorter available pulse duration would be used, with the corresponding adjustment in the number of pulses per beam position and range. Note that this example uses the average beam size and scan loss over the search volume. An actual radar search design might adjust the number of pulses and pulse duration in each beam position, or in groups of beam positions, to provide a near-constant detection range over the search volume.

In a realistic search situation, it may be desirable to have the minimum range substantially less than the calculated assured acquisition range, to allow for uncertainties in the radar sensitivity and target RCS. If the minimum range in the above problem is required to be less than half of the assured acquisition range, then nine pulses per beam position should be used for both noncoherent integration and cumulative detection. The resulting assured acquisition range is unchanged (within the calculation precision) for noncoherent integration, and is reduced from 357 km to 334 km for cumulative detection.

While the assured acquisition range with noncoherent integration is greater than with cumulative detection, the latter might be used because it may be more easily implemented. Pulses in a beam position need not be transmitted contiguously with cumulative detection, as they usually are with noncoherent integration. This would allow the search volume to be scanned several times during the search time using cumulative detection (five or nine in the above example). This could allow gaps or nulls in a scan coverage to be covered by subsequent scans, produce decorrelation of Swerling 1 and 3 targets without frequency diversity, and provide earlier detection of some targets. In cases where a large number of pulses per beam position must be used, groups of pulses may be noncoherently integrated and then combined using cumulative detection.

Actual search patterns may employ nonrectangular angular coverage. The spacing between beams may be held constant, or may be varied in steps. Different pulse durations and numbers of pulses may be used in various parts of the angular coverage to maintain the radar sensitivity. Thus, the analyses presented here should be considered only as approximations to these actual volume search patterns that serve to illustrate the important radar search performance factors, and to provide estimates of volume search performance.

7.4 Cued Search

In some system applications, the approximate position of a target is known from data external to the radar. The radar may then perform a cued search over the uncertainty volume to acquire the target. When the target-position cue comes from measurements by another sensor, the target is often said to be handed over from that sensor to the radar.

The required search volume may be characterized by an uncertainty radius, r_s . This could be the $3\text{-}\sigma$ error in the target position cue, or the $3\text{-}\sigma$ value of the largest semi-axis of an ellipsoidal handover volume. When the uncertainty volume is not spherical, an equivalent search radius may be defined. This may correspond to the largest uncertainty dimension projected in the direction of the radar, or, if the orientation of the uncertainty volume is known, to a circle having the same area as the projection of the uncertainty volume. Since the range uncertainty for the target is usually small, the number of range cells that are searched may also be small. This allows the use of a relatively large probability of false alarm, P_{FA} , as discussed in Section 6.2.

A fixed time, t_s , is usually specified for acquiring a target when using cued search. It is possible to maximize the assured acquisition range for cued search by selecting the search time in a manner similar to that described in Section 7.3 for volume search. This is done by substituting $R_D/(4V_R)$ for t_s in the equations given below. However, this implies using a significant portion of the radar average power and time to acquire each target, and is not often done.

For a target closing with a radial velocity, V_R , the assured acquisition range, R_A , is given by:

$$R_A = R_D - V_R t_s \quad (\text{cued search}) \quad (7.22)$$

where R_D is the target detection range for the required detection parameters. If the radial distance traveled by the target during the search time is small relative to the range, the search solid angle may be approximated by:

$$\psi_s = \frac{\pi r_s^2}{R_D^2} \quad (V_R t_s \ll R_D) \quad (7.23)$$

When the angular sector required for cued search lies within a single radar beam, as shown in Figure 7.6(a), either a dish radar or a phased-array radar may be used to perform the search. The detection range, R_D , may then be calculated from:

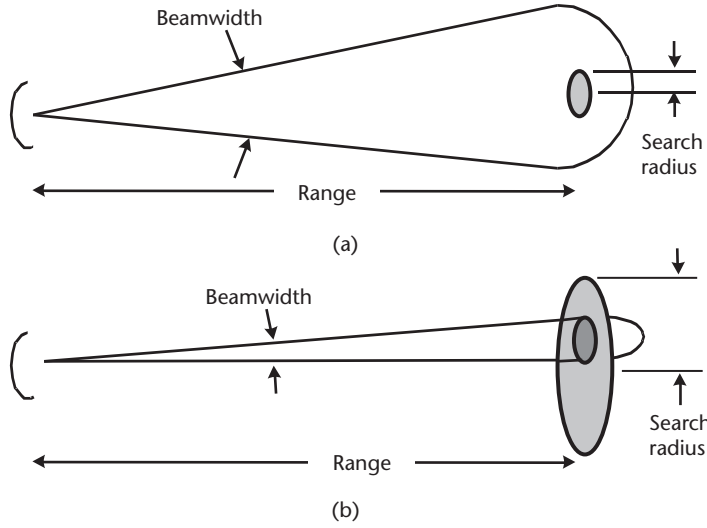


Figure 7.6 Illustration of geometry for cued-search cases. (a) Search radius smaller than beam. (b) search radius larger than beam.

$$R_D = \left[\frac{P_A t_s G_T \sigma A_R}{(4\pi)^2 n_p (S/N) k T_s L} \right]^{1/4} \quad (\text{single-beam cued search}) \quad (7.24)$$

where n_p is the number of pulses transmitted during the search time t_s . Using the reference range:

$$R_D = \left[\frac{R_{ref}^4 D C t_s \sigma (S/N)_{ref}}{\tau_{ref} \sigma_{ref} n_p (S/N) L_s L_{BS} L_P} \right]^{1/4} \quad (\text{single-beam cued search}) \quad (7.25)$$

In both cases, the scan loss, beamshape loss, and propagation loss are included in the calculation. For phased-array radar, the off-broadside scan loss, L_s , may be calculated from (3.21), (3.27), or (3.28). Dish-type radar that illuminate the target during the cued-search interval have no scan loss. For both radar types, the beamshape loss, L_{BS} , is a function of the portion of the beam over which the cued search is required. For circular beams and cued-search areas, the beamshape loss is approximately given by:

$$L_{BS} \approx \left[\cos \left(\frac{2.2 r_s}{R_D \theta} \right) \right]^{-1.3} \quad (2 r_s \leq R_D \theta) \quad (7.26)$$

When the beam or cued-search area is not circular, using the smaller beam angle and larger angular dimension of the search area in (7.26) will give a conservative value for L_{BS} . Since the detection range depends on the value of L_{BS} , it is necessary to iterate the calculation until R_D and L_{BS} agree with sufficient accuracy.

For example, consider an X-band phased-array radar with the following parameters:

$$P_A = 10 \text{ kW};$$

$DC = 0.2$;
 $G_T = 50$ dB;
 $A_R = 7$ m²;
 $T_s = 400$ K;
 $L_F = 3$ dB;
 $\theta = 0.7^\circ$ (12 mR) on broadside;
 $\tau = 10$ ms maximum.

The cued-search parameters are:

$r_s = 5$ km;
 $t_s = 5$ sec;
 $P_D = 0.99$;
 $P_{FA} = 10^{-4}$;
 $\sigma = 0.1$ m²
 Swerling 4 signal fluctuation;
 Off-broadside scan: 10° elevation, 40° azimuth.

Using the maximum pulse duration, the number of pulses n_p is found to be 100. The corresponding single-pulse S/N required for noncoherent integration is -1.0 dB. Assuming $L_p = 0.3$ dB, calculating the scan loss, $L_s = 3.1$ dB, and assuming no beamshape loss, $L = 6.4$ dB. The detection range from (7.24) is 1,842 km. Using a beamwidth of 14 mR to account for the off-broadside beam broadening, the beamshape loss from (7.26) is 0.5 dB. Recalculating the detection range gives 1,786 km. This range change does not significantly affect the beamshape loss, so no further iteration is needed. The target radial travel during the search time is 10 km, giving $R_A = 1,776$ km, which is larger than the minimum range, R_M , of 1,500 km. The results of this single-beam example are summarized in columns 2 and 3 of Table 7.3.

When the cued-search radius is large enough so that several radar beams are required for angular coverage, the search solid angle, ψ_s , is approximately given by [see Figure 7.6(b)]:

Table 7.3 Cued Search Examples

<i>Parameter</i>	<i>Single Beam</i>		
	<i>Single Beam</i>	<i>Recalculation</i>	<i>Multibeam</i>
r_s	5 km	5 km	50 km
n_p	100	100	7
Pulse S/N	-1.0 dB	-1.0 dB	7.9 dB
L_s	3.1 dB	3.1 dB	3.1 dB
L_{BS}	0 dB	0.5 dB	2.5 dB
L	6.4 dB	6.9 dB	8.9 dB
R_D	1,842 km	1,786 km	457 km
f_B	N/A	N/A	1.3
n_B	N/A	N/A	307
τ	10 ms	10 ms	0.47 ms
R_A	1,832 km	1,776 km	447 km
R_M	1,500 km	1,500 km	70.5 km

$$\psi_s = \pi r_s^2 / R_A^2 \quad (r_s \ll R_A) \quad (7.27)$$

For phased-array radar, the detection range is then given by:

$$R_D = \left[\frac{P_A A_R t_s \sigma f_B}{4\pi^2 r_s^2 n_p (S/N) k T_s L f_p} \right]^{1/2} \quad (\text{multi-beam cued search}) \quad (7.28)$$

where f_B is the beam-broadening factor; n_p is the number of pulses used in each beam position; S/N is the single-pulse S/N required for detection; the loss term, L , includes scan loss, beamshape loss, and propagation loss; and f_p is the beam-packing factor. When the search is performed by sequentially illuminating the beam positions, the assured acquisition range, R_A , is given by (7.22), and the average acquisition range, R_p , is given by:

$$R_p = R_D - \frac{V_R t_s}{2} \quad (\text{multi-beam cued search}) \quad (7.29)$$

The cued-search detection range also may be calculated from the radar reference range (see Section 5.3), using:

$$R_D = \left[\frac{R_{ref}^4 D C t_s \sigma (S/N)_{ref}}{\tau_{ref} \sigma_{ref} n_B n_p (S/N) L_s L_{BS} L_p} \right]^{1/4} \quad (\text{multi-beam cued search}) \quad (7.30)$$

where the number of beam positions searched, n_B , is given by:

$$n_B = \frac{\pi f_p r_s^2}{R_D^2 \psi_{BA}} \quad (\text{multi-beam cued search}) \quad (7.31)$$

The beam-broadening factor, f_B , and the off-broadside scan loss, L_s , may be calculated using (7.14) to 7.16). However, in many cases the variation over the scan volume is small, and (7.13), (3.21), (3.27), and (3.28) may be used with sufficient accuracy. A two-coordinate beamshape loss, L_{BS} , of 2.5 dB and a beam-packing factor, f_p , of 1.2 are appropriate.

For example, if the search radius in the above example is changed to 50 km, multibeam search is required. The beam-broadening factor is 1.3. With the 2.5-dB beamshape loss, the total losses are 8.9 dB. Using seven pulses per beam position to minimize $n_p S/N$ for noncoherent integration, the required single-pulse $S/N = 7.9$ dB. The detection range from (7.28) is 457 km, and the assured acquisition range is 447 km. At this range, 307 beam positions must be searched, and the resulting pulse duration is 0.47 ms. The minimum range is well below the acquisition range. These results are shown in column 4 of Table 7.3.

When the number of beam positions is small, the number of beam positions and the beamshape loss depend on details of the beam shape and search volume. For multibeam search, the combination of the beamshape loss and packing factor equal 3.3 dB. The single-beam beamshape loss reaches 3.3 dB for $r_s/R_D = 0.45\theta$. Thus, it is

convenient, and usually sufficiently accurate for system analysis, to use the single-beam calculation for $r_s \leq 0.45 R_D \theta$, and multibeam calculation for larger values of r_s .

Dish-type radar is not usually suitable for volume search, as described in Section 7.3, due to mechanical limitations in rapidly positioning the beam. However, they may be used for cued search of one or a few beam positions. Their use in single-beam search is similar to that of phased arrays, as discussed above. In multibeam search, the radar beam is mechanically scanned to cover the search volume. Various scan patterns have been used, including circular or elliptical scan, spiral scan, and raster scan.

The search time of dish radar is often determined by the time it takes the radar to mechanically scan the beam over the search pattern. This is limited by the maximum angular velocity and acceleration of the antenna in azimuth and elevation:

- ω_{EM} = maximum antenna angular velocity in elevation direction;
- ω_{AM} = maximum antenna angular velocity in azimuth direction;
- a_{EM} = maximum antenna angular acceleration in elevation direction;
- a_{AM} = maximum antenna angular acceleration in azimuth direction.

For example, a dish radar scanning a circular pattern with angular radius, φ_s , in a time, t_s , will have an azimuth position, φ_A , relative to the center of the scan of:

$$\varphi_A = \varphi_s \sin(2\pi t/t_s) \quad (7.32)$$

The azimuth angular velocity, ω_A , and acceleration, a_A , are given by:

$$\omega_A = (2\pi \varphi_s/t_s) \cos(2\pi t/t_s) \quad (7.33)$$

$$a_A = -(4\pi^2 \varphi_s/t_s^2) \sin(2\pi t/t_s) \quad (7.34)$$

For a given value of φ_s , the minimum feasible scan time is constrained by the maximum azimuth angular velocity and acceleration:

$$t_s \geq 2\pi \varphi_s / \omega_{AM} \quad (7.35)$$

$$t_s \geq 2\pi (\varphi_s / a_{AM})^{1/2} \quad (7.36)$$

The elevation scan is similarly constrained. For example, values of $\varphi_s = 2^\circ$, $\omega_{AM} = \omega_{EM} = 5^\circ/\text{s}$, and $a_{AM} = a_{EM} = 2^\circ/\text{s}^2$, the scan time is limited by antenna angular acceleration to 6.3 sec or longer.

The target detection range may be calculated using the technique described in Section 7.2. For the circular scan described above with the minimum scan time of 6.3 sec, the angular velocity is $2^\circ/\text{s}$. With a 1° beam and a PRF of 100, 50 pulses could be integrated noncoherently. The scanning loss, L_{RS} , is negligible, and a value of 2.5 dB should be used for the beamshape loss, L_{BS} , to account for targets anywhere in the beam swath.

A spiral scan may be modeled by a series of circular scans. An example of such a dish-radar cued-search mode is given in Section 12.4.

7.5 Horizon Search with Phased-Array Radar

Horizon search is a type of barrier search where the objective is to detect targets soon after they rise above the radar horizon. It is frequently used for detecting mortar rounds, artillery shells, and ballistic missiles, and it may also be used for detecting aircraft and satellites at long ranges.

The concept of horizon search is illustrated in Figure 7.7. An elevation-angle sector is searched often enough to ensure an opportunity for detecting a target as it traverses the sector. The minimum search time depends on the target range, the vertical component of its velocity (actually, the velocity component tangential to the radar LOS and normal to the search fence), and the width of the elevation sector searched.

When the radar searches an elevation-angle sector of width ϕ_H and a specified azimuth sector ϕ_A , and targets pass through this sector with a maximum vertical velocity component, V_V (which is measured normal to the radar LOS), the scan time, t_s , that assures that targets are observed as they pass thorough the elevation sector is given by:

$$t_s = R_H \phi_H / V_V \quad (\text{horizon search}) \quad (7.37)$$

where R_H is the range to the target. The total search solid angle is given by:

$$\psi_s = \phi_H \phi_A \quad (\text{horizon search}) \quad (7.38)$$

The search is normally performed at a low elevation angle, ϕ_E , in order to provide early detection opportunities. However, the minimum elevation angle may be constrained by propagation anomalies and losses, as described in Chapter 9.

The radar detection range in horizon search is given by:

$$R_D = \left[\frac{P_A A_R R_H \sigma f_B}{4\pi \phi_A V_V n_p (S/N) k T_s L f_p} \right]^{1/4} \quad (\text{horizon search}) \quad (7.39)$$

The loss term includes average scan loss, calculated using the method of (7.14); beamshape loss of 2.5 dB; and propagation loss. The beam-broadening factor is calculated from (7.14) and (7.15), and the beam-packing factor is 1.2.

When the target is at the detection range ($R_H = R_D$), the detection range is a maximum, and varies with the cube root of the radar power-aperture product. It is independent of the elevation search sector, θ_H , because searching a larger elevation

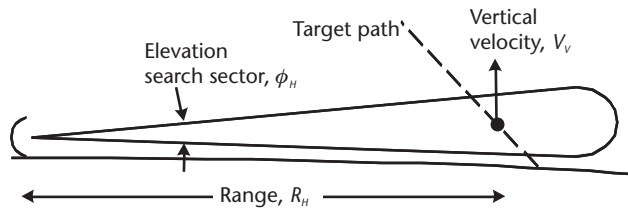


Figure 7.7 Search geometry and parameters for horizon search.

sector allows proportionately more time for search, as shown by (7.37). The elevation search sector is usually kept as small as possible, in order to provide early target detection. Often the horizon scan consists of a single row of adjacent beams.

The detection range may also be calculated from the radar reference range using:

$$R_D = \left[\frac{R_{ref}^4 \phi_H R_H DC \sigma (S/N)_{ref}}{\tau_{ref} \sigma_{ref} V_V n_B n_P (S/N) L_S L_{BS} L_P} \right]^{1/3} \quad (\text{horizon search}) \quad (7.40)$$

where:

$$n_B = f_P \phi_H \phi_A / \psi_{BA} \quad (\text{horizon search}) \quad (7.41)$$

For example, consider the radar parameters given in Section 7.4, and the following horizon-search requirements:

$$V_V = 1 \text{ km/s};$$

Target at maximum range;

$$\phi_A = 90^\circ (\pm 45^\circ \text{ from array broadside});$$

$$P_D = 0.99;$$

$$P_{FA} = 10^{-6}$$

$$\sigma = 1 \text{ m}^2$$

Swerling 2 signal fluctuations.

If the scan elevation angle is 5° and the array boresight elevation angle is 20° , the average beam-broadening factor is 1.16, and the average scan loss is 1.7 dB. Using 2.5 dB beamshape loss, and assuming 0.4 dB for propagation loss, the total losses are 7.6 dB. For seven pulses noncoherently integrated per beam position, the required single-pulse $S/N = 10.3$ dB. For the case where R_H is assumed equal to R_D , the detection range from (7.39) is 1,117 km. The number of beams from (7.39), using a beam-packing factor of 1.2, is 187. If a single row of beams is used in the scan, the scan time from (7.37) is 13.9 sec, and the pulse duration is found to be 2.22 ms. The minimum range, R_M , is far less than the acquisition range. These results are shown in column 2 of Table 7.4.

When the target may appear at a range R_H that is shorter than R_D in the mode described above, the horizon-search time must be reduced or the elevation search sector increased. This also reduces R_D from its maximum value. In the previous example, if the minimum target range, $R_H = 500$ km, the search time would be reduced to 6.2 sec, and R_D is reduced to 914 km, as shown in column 3 of Table 7.3. When the target has a significant radial velocity, V_R , the assured and average acquisition ranges may be calculated using (7.6) and (7.7), respectively.

Other, more efficient, methods may be used to provide horizon-search coverage of targets that are at less than the maximum detection range. One technique employs additional, shorter-range search fences above the first fence. Another approach is to use cumulative detection, so that the search sector is scanned several

Table 7.4 Phased-Array Horizon Search Example

<i>Parameter</i>	$R_H = R_D$	$R_H \geq 500 \text{ km}$
f_B	1.16	1.16
L_F	3.0 dB	3.0 dB
L_S	1.7 dB	1.7 dB
L_{BS}	2.5 dB	2.5 dB
L_P	0.4 dB	0.4 dB
L	7.6 dB	7.6 dB
n_P	7	7
Pulse S/N	10.3 dB	10.3 dB
R_D	1,117 km	914 km
f_P	1.2	1.2
n_B	178	178
t_S	13.9 sec	6.20 sec
τ	2.22 ms	0.995 ms
R_M	333 km	149 km

times during the overall scan time. This allows for more frequent detection opportunities for shorter-range targets.

7.6 Horizon Search with Dish Radar

Two techniques for using dish radar in horizon search are described in this section. The first simply uses the dish radar like a rotating search radar described in Section 7.2, but of course with an elevation coverage much smaller than for most rotating search radars. The beam elevation remains fixed at an angle near the radar horizon, providing elevation coverage, ϕ_E , approximately equal to the elevation beamwidth, θ_E . The antenna is rotated at a constant azimuth rate, ω_A , providing 360° azimuth coverage with a rotation period, t_R , given by:

$$t_R = 2\pi/\omega_A \quad (7.42)$$

The number of pulses illuminating the target between the 3-dB points of the azimuth beam is then given by (7.4). The detection range, R_D , is calculated as described in Section 7.2, using a value of 2.5 dB for the scan loss in two angular coordinates. When fewer than six pulses illuminate the target, a scanning loss should also be included (see Section 7.2).

To assure observation of the target during this horizon search, the target vertical velocity, V_V , is constrained by:

$$V_V \leq R_H \theta_E / t_R = R_H \theta_E \omega_A / 2\pi \quad (7.43)$$

where:

R_H = target range ($R_H \leq R_D$);

θ_E = Radar elevation beamwidth.

For example, a dish radar having a beamwidth of 1 degree and a maximum azimuth scan rate of 10°/s, searching for targets at a range of 1,000 km, would be

assured of observing targets having vertical velocity less than 485 m/s. With the rotation period of 36 sec and a PRF of 100 Hz, the number of pulses on target is 10 [from (7.4)]. These results are shown in the second column of Table 7.5.

When the condition in (7.43) is not met, or when less than 360° azimuth coverage is needed, the bow-tie scan pattern may be used. This horizon-search mode may provide longer detection ranges and shorter revisit times for search sectors that are limited in azimuth. The bow-tie scan configuration is the most efficient use of a mechanically scanned pencil-beam antenna in barrier search of angular sectors [8].

The bow-tie scan is illustrated in Figure 7.8. It provides two crossing constant-angular-velocity linear scans that cover an azimuth sector ϕ_A . The beam revisits the ends of the linear scans once each scan period, t_s , and revisits the middle of the linear scans twice each scan period. Thus, the target may move two beamwidths in elevation during the scan time. The scan time that provides assured observation for a vertical velocity, V_V , and a minimum target range, R_H , is given by:

$$t_s = 2\theta_E R_H / V_V \quad (\text{Bow-tie scan}) \quad (7.44)$$

where θ_E is the elevation beamwidth of the radar.

The end portions of the scan, shown by dashed lines in Figure 7.8, are for reversing the angular velocity of the antenna, and are not used for target detection. The azimuth coverage, ϕ_A , increases with linear scan rate, ω_A , until the time needed to reverse the scan direction becomes so large that the linear scan time is significantly reduced.

Table 7.5 Examples of Horizon Search With Dish Radar

Parameter	360° Search	Bow-tie Search		
θ_E and θ_A	1 degree	1 degree	1 degree	1 degree
R_H	1,000 km	1,000 km	1,000 km	1,000 km
V_V	485 m/s (maximum)	1 km/s	1 km/s	1 km/s
a_{MA}	N/A	$5^\circ/\text{s}^2$	$5^\circ/\text{s}^2$	$5^\circ/\text{s}^2$
ϕ_A	360°	191°	134°	100°
ω_A	$10^\circ/\text{s}$ (maximum value)	$21.8^\circ/\text{s}$ (exceeds maximum value)	$10^\circ/\text{s}$ (maximum value)	6.8
PRF	100 Hz	N/A	100 Hz	100 Hz
n_p	10	N/A	10	15

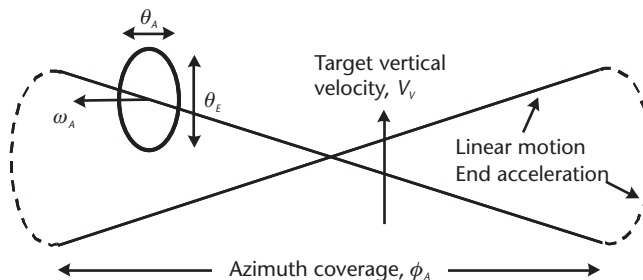


Figure 7.8 Geometry of bow-tie horizon search scan.

When the maximum azimuth angular acceleration, a_{AM} , is used to reverse the antenna scan direction, the azimuth scan coverage, ϕ_A , is given by:

$$\phi_A = \frac{\omega_A \theta_E R_H}{V_V} - \frac{2\omega_A^2}{a_{AM}} \quad (\text{Bow-tie scan}) \quad (7.45)$$

The maximum value of ϕ_A then is:

$$\phi_A(\text{max}) = \frac{\theta_E^2 R_H^2 a_{AM}}{8V_V} \quad (\text{Bow-tie scan}) \quad (7.46)$$

This value of ω_A is obtained with an azimuth scan rate of:

$$\omega_A(\text{max } \phi_A) = \frac{\theta_E R_H a_{AM}}{4V_V} \quad (\text{Bow-tie scan}) \quad (7.47)$$

If the radar maximum azimuth scan rate, ω_{AM} , is less than the value given in (7.47), the maximum azimuth coverage is less than given by (7.46). Similar limitations are placed on the elevation scan, but the azimuth scan limitations usually dominate the bow-tie scan performance.

The minimum azimuth scan rate that provides an azimuth coverage, ϕ_A , is given by:

$$\omega_A = \frac{\theta_E R_H a_{AM}}{4V_V} - \left[\frac{\theta_E^2 R_H^2 a_{AM}^2}{16V_V^2} - \frac{\phi_A a_{AM}}{2} \right]^{1/2} \quad (\text{Bow-tie scan}) \quad (7.48)$$

The radar detection range may be calculated using this angular velocity, by the method described in Section 7.2 and at the beginning of this section. The number of pulses between the 3-dB points of the azimuth beam is given by:

$$n_p = \theta_A \text{PRF} / \omega_A \quad (\text{Bow-tie scan}) \quad (7.49)$$

A 2.5-dB beamshape loss should be used, consistent with search in two angular coordinates, and where appropriate, a scanning loss, L_{RS} , should be included (see Section 7.2).

For example, consider the previous dish radar having a beamwidth of 1 degree and maximum azimuth angular velocity of $10^\circ/\text{s}$. Assume a maximum azimuth angular acceleration of $5^\circ/\text{s}^2$. For a target range, $R_H = 1,000$ km and vertical velocity, $V_V = 1$ km/s, the maximum azimuth coverage from (7.46) would be 191° , as shown in column 3 of Table 7.5. The corresponding angular scan rate from (7.47) would be $21.8^\circ/\text{s}$, which exceeds the $10^\circ/\text{s}$ capability of the radar.

Using the maximum angular scan rate in (7.45) gives the maximum azimuth coverage for this radar of 134° , as shown in column 4 of Table 7.5. Since this coverage uses the maximum azimuth scan rate of $10^\circ/\text{s}$, with a PRF of 100 Hz, the number of pulses on target is 10, the same as for the 360° scan shown in column 2 of the table.

For a required azimuth coverage of 100° (less than the maximum), the required angular velocity from (7.48) is $6.8^\circ/\text{s}$, as shown in column 5 of Table 7.5. With a PRF of 100, about 15 pulses illuminate the target during the linear scan.

The detection range for these cases may be calculated from (5.1) or (5.11), using the single-pulse S/N needed to provide the detection parameters with the number of pulses on the target. For example, to provide $P_D = 0.99$ and $P_{FA} = 10^{-6}$ with Swerling 4 signal fluctuations and 15 pulses noncoherently integrated, the single-pulse S/N = 5.8 dB. To meet the minimum target range requirement, the radar must provide this S/N on the target RCS at $R_H = 1,000$ km. If the detection range, $R_D > R_H$, targets between these ranges will be acquired with at least the required probability. A beamshape loss of 2.5 dB should be used, and a scanning loss from Figure 7.2 included if less than six pulses illuminate the target. If the target has a significant radial velocity, the assured and average acquisition ranges may be calculated using (7.6) and (7.7).

7.7 Problems

The following problems are provided to assist in reviewing this chapter and to ensure a basic understanding of the material. For maximum benefit, the problems should first be solved without using the VBA custom radar functions. Solutions to these problems are given in Appendix E, Section E.7.

1. What are the two primary radar parameters on which the search performance depends?
2. A radar has an average transmit power of 100 kW, an effective receive aperture area of 20 m^2 , a system noise temperature of 450K, and system losses of 4 dB. Assume 50% of the radar power is used to search a volume 90° in azimuth and 45° in elevation using the optimum search time, and that the additional search losses total 6.5 dB. At what detection range can the radar achieve a S/N of 15 dB on a -15 dBsm target with a radial velocity of 2 km/s? What is the search time? What are the assured acquisition range and the average acquisition range?
3. A rotating search radar has an azimuth beamwidth of 2° and an angular rotation rate of $20^\circ/\text{s}$. What is the rotation period? What PRF is needed to have 15 pulses illuminate the target on each scan? Using noncoherent integration and this PRF, what is the single-pulse S/N needed to provide $P_D = 0.9$ and $P_{FA} = 10^{-6}$ on a Swerling 1 target? If frequency diversity is used to convert the target return to Swerling 2, what is the required single-pulse S/N? If the radar average power is 20 kW, the transmit gain is 25 dB, the receive aperture area is 13 m^2 (an L-band radar), the fixed radar losses are 5.0 dB, the system noise temperature is 550K, and the propagation losses are negligible, what is the detection range for a 5 m^2 target for the above two cases?
4. If the radar in Problem 2 is an FFOV phased array with the search sector $\pm 45^\circ$ in azimuth and from -10 to $+35^\circ$ in elevation, what are the average beam broadening factor and scan loss? If 100% of the power is used for volume search, 10 pulses are used in each beam position for search, and the

- single-pulse $S/N = 8.0$ dB, what is the detection range on the target in Problem 2? What is the optimum search time? If the broadside beamwidth is 1.3° (S-band radar), how many beam positions are searched? If the radar duty cycle is 20%, what is the pulse duration? Does this satisfy the minimum-range constraint?
5. A C-band dish radar has an average power of 25 kW, transmit gain of 40 dB, receive aperture area of 2.5 m^2 , system noise temperature of 500K, and losses of 4.5 dB. The radar is used to perform a single-beam cued search for a -20 dBsm Swerling 4 target. The search radius is 5 km, the search time is 10 sec with a PRF of 100 Hz, the desired detection probability is 0.99, with a P_{FA} of 10^{-6} , and noncoherent integration is used. Find the detection range. What is the radar beamwidth? Is the single-beam criteria met?
 6. An FFOV phased-array radar is used to perform horizon search using a single row of beams at an elevation angle 15° below its broadside elevation angle, and covering an azimuth $\pm 40^\circ$ from broadside azimuth. Find the average beam-broadening factor and scan loss. The average power used for search is 40 kW, the receive aperture area is 10 m^2 , the system noise temperature is 400K, and the fixed losses are 5 dB. If the target RCS is 1 m^2 with Swerling 2 fluctuations, the vertical velocity is 1.5 km/s, and the propagation loss is 1.5 dB, find the maximum range at which the target may be detected with $P_D = 0.9$ and $P_{FA} = 10^{-6}$, assuming cumulative detection using five pulses per beam position. What is the search time? If the azimuth and elevation boresight beamwidths are 32 mrad (S-band frequency), find the number of beams searched, the total number of search pulses used, and the number of search pulses per second. If the radar duty cycle is 5%, is the minimum range constraint violated?
 7. What type of search discussed in this chapter is a special case of barrier search?
 8. Consider an FFOV array radar with $P_A = 10$ kW, $A_R = 9 \text{ m}^2$, $T_s = 500\text{K}$, and fixed losses = 5 dB, having a broadside elevation angle of 15° . The radar performs a volume search from 5 to 35° in elevation, and $\pm 30^\circ$ in azimuth. Target RCS = 1 m^2 , and the search time is 50 sec. Find the search solid angle and the average off-broadside scan loss. Assume $L_p = 2$ dB. Calculate the detection range for $P_D = 0.9$, $P_{FA} = 10^{-6}$ and a Swerling 4 target, assuming that a single pulse or coherent dwell is used in each beam position. For what target radial velocity is this search time optimum?
 9. For the same parameters as in Problem 8, find the beam-broadening factor. Assume noncoherent integration of 10 pulses per beam position, and calculate the detection range for the optimum search time for a target radial velocity of 2 km/s. If the azimuth and elevation beamwidths on broadside are 1.25° , how many beam positions are in the search volume? If the duty cycle is 20%, what are the pulse duration and minimum range? What are the assured and average acquisition ranges?
 10. A rotating search radar has an azimuth beamwidth of 1.5° , a rotation period of 12 sec, and a PRF of 250 Hz. How many pulses illuminate the target? What is the scanning loss? For a Swerling 3 target, what is the single-pulse

S/N needed to provide $P_D = 0.9$ and $P_{FA} = 10^{-6}$, assuming coherent integration, and assuming noncoherent integration? If the radar reference range is 100 km for S/N = 15 dB, for the pulse duration used in search and for the target RCS, what are the detection ranges for the two integration modes? Ignore propagation loss.

11. Consider an array radar having azimuth and elevation beamwidths of 10 mrad, a duty cycle of 20%, and a reference range of 1,000 km for S/N = 15 dB, RCS = 1 m², and a 10-ms pulse. Find the cued search detection range for a -10 dBsm Swerling 3 target with a search radius of 25 km and a search time of 10 sec, $P_D = 0.9$, and $P_{FA} = 10^{-6}$. Assume coherent integration of 10 pulses per beam position, and ignore propagation, off-broadside losses, and beam-broadening. How many beam positions are searched? What is the pulse duration and minimum range?
12. A dish radar has a 2° beamwidth, a maximum azimuth angular velocity of 8°/s, and maximum azimuth angular acceleration of 2°/s². In a bow-tie search for a target with a minimum range of 500 km and vertical velocity of 1.5 km/s, what is the maximum azimuth coverage capability? For an azimuth coverage of 25°, what are the azimuth angular velocity and the number of pulses on the target, with a PRF of 100 Hz? What single-pulse S/N is required to give $P_D = 0.9$, and $P_{FA} = 10^{-6}$ on a Swerling 1 target, using noncoherent integration?

7.8 VBA Software Functions for Radar Search Modes

Two versions of each software function are provided: one uses the radar parameters to calculate radar sensitivity, and the other uses the radar reference range.

7.8.1 Function SearchR_Rot1_km

Purpose Calculates target acquisition ranges for rotating search radar for specified detection parameters, using radar parameters.

Reference Equations (7.4), (7.6), (7.7), and (5.6).

Features May be used for search by fan-beam, stacked-beam, and rotating-dish radar. Calculates number of pulses illuminating the target, and scanning loss for either the input maximum target range or the maximum ambiguous range. Detection parameters, and either noncoherent integration, coherent integration, or cumulative detection may be specified. Output may be selected for detection range, R_D , average target acquisition range, R_p , or assured acquisition range, R_A . No result is produced when less than one pulse illuminates the target, when the returned pulse falls out of the azimuth beam, or when the minimum-range constraint is not satisfied.

Input Parameters (with units specified) Pd_Factor = required probability of detection from 0.3 to 0.999 (0.3 to 0.99 for Swerling 1 targets) (factor).

Pfa_Factor = required probability of false alarm from 10^{-1} to 10^{-10} (factor).

RCS_dBsm = target average RCS (dBsm).

SWcase_12345 = Swerling target-signal statistics case (integer). Use 1 for Swerling type 1 targets, 2 for Swerling type 2 targets, 3 for Swerling type 3 targets, 4 for Swerling type 4 targets and 5 for nonfluctuating targets.

Sel_1Nc2Ci3Cd = select 1 for noncoherent integration, 2 for coherent integration, or 3 for cumulative detection of signal returns in the beam (integer). If 2 is selected, no result will be generated for Swerling 2 and 4 targets, indicated by an output of -1. If 3 is selected, no result will be generated for Swerling 1 and 3 targets, indicated by an output of -2.

Az_Beam_deg = azimuth beamwidth of radar (degrees).

T_Revisit_s = antenna rotation period or target revisit time (seconds).

PRF_Hz = radar pulse repetition frequency (Hz). For stacked beams, use the PRF in the beam nearest the target elevation.

P_Av_kW = average transmitted power (kW). Use the portion of radar average power that is used in this search mode. For stacked beams, use the average power for the beam nearest the target elevation.

DC_Factor = radar duty cycle (factor). The duty cycle may be calculated from the pulse duration, τ , by: $DC = \tau \text{ PRF}$. Use the portion of the duty cycle that is used in this search mode. For stacked beams, use the portion of the duty cycle for the beam nearest the target elevation.

Gain_T_dB = transmit antenna gain (dB). For cosecant-squared beams, use the gain for the target elevation. For stacked beams, use the gain of the beam nearest the target elevation.

Area_R_m2 = receive antenna effective aperture area (m^2). For cosecant-squared beams, use the effective aperture area for the target elevation. For stacked beams, use the aperture area for the beam nearest the target elevation.

Noise_T_K = system noise temperature (K).

Fixed_L_dB = fixed radar losses (dB).

Prop_L_dB = average propagation losses (dB).

BeamS_L_dB = beamshape loss (dB). For fan-beam search, use 1.6 dB. For multibeam search or rotating dish horizon search, use 2.5 dB.

Sel_1Rd2Rp3Ra (optional) = select 1 for radar detection range, 2 for average acquisition range, or 3 for assured acquisition range (integer). If this input is left blank, the assured acquisition range will be calculated.

V_Rad_kmps (optional) = target radial velocity (km/s). This is used to calculate average and assured acquisition ranges. If left blank, a value of zero will be used.

R_Max_km (optional) = maximum target range for purposes of calculating the beam scanning loss (km). If left blank, maximum unambiguous range will be used. No result is generated if returned pulse is out of the azimuth beam, indicated by an output of -3.

Function Output Target acquisition range for the option selected (detection range, average acquisition range, or assured acquisition range), (km). No result is generated if less than one pulse illuminates the target, indicated by an output of -4,

or if the minimum-range constraint is not met (see Section 5.5), indicated by an output of -5.

The Excel Function Arguments parameter box for Function SearchR_Rot1_km is shown in Figure 7.9, with sample parameters and solution.

7.8.2 Function SearchR_Rot2_km

Purpose Calculates target acquisition ranges for rotating search radar for specified detection parameters, using radar reference range.

Reference Equations (7.4), (7.6), (7.7), and (5.11).

Features May be used for search by fan-beam, stacked-beam, and rotating-dish radar. Calculates number of pulses illuminating the target and scanning loss for either the input maximum target range or the maximum ambiguous range. Detection parameters and either noncoherent integration, coherent integration, or cumulative detection may be specified. Output may be selected for detection range, R_D , average target acquisition range, R_P , or assured acquisition range, R_A . No result is produced when less than one pulse illuminates the target, when the returned pulse falls out of the azimuth beam, or when the minimum-range constraint is not satisfied.

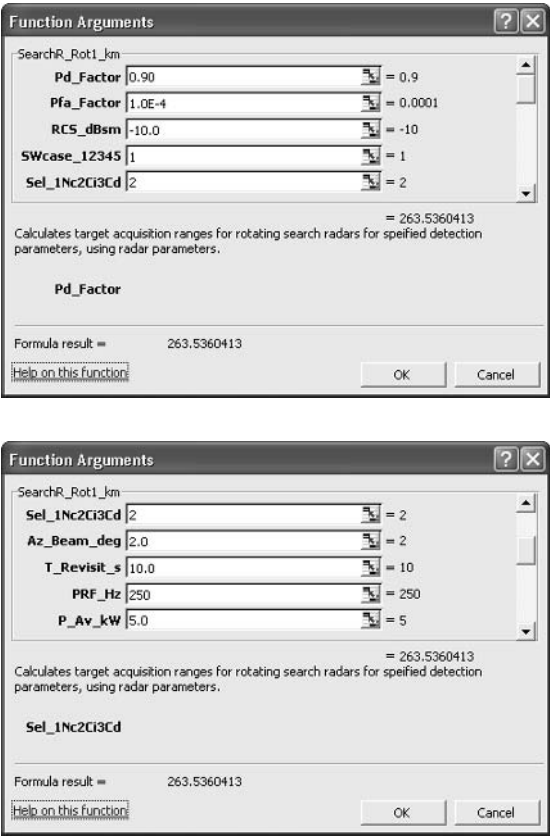


Figure 7.9 Excel parameter box for Function SearchR_Rot1_km.

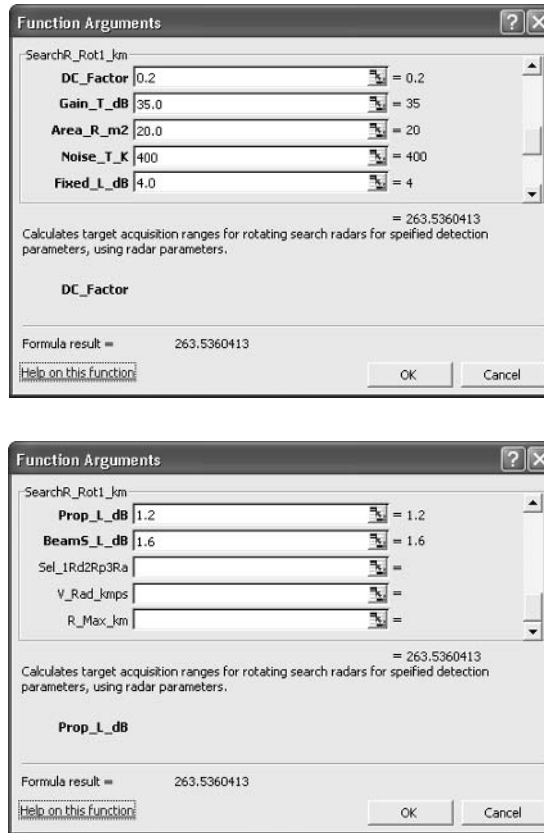


Figure 7.9 (continued).

Input Parameters (with units specified)

Pd_Factor = required probability of detection from 0.3 to 0.999 (0.3 to 0.99 for Swerling 1 targets) (factor).

Pfa_Factor = required probability of false alarm from 10^{-1} to 10^{-10} (factor).

RCS_dBsm = target average RCS (dBsm).

SWcase_12345 = Swerling target-signal statistics case (integer). Use 1 for Swerling type 1 targets, 2 for Swerling type 2 targets, 3 for Swerling type 3 targets, 4 for Swerling type 4 targets, and 5 for nonfluctuating targets.

Sel_1Nc2Ci3Cd = select 1 for noncoherent integration, 2 for coherent integration, or 3 for cumulative detection of signal returns in the beam (integer). If 2 is selected, no result will be generated for Swerling 2 and 4 targets, indicated by an output of -1. If 3 is selected, no result will be generated for Swerling 1 and 3 targets, indicated by an output of -2.

Az_Beam_deg = azimuth beamwidth of radar (degrees).

T_Revisit_s = antenna rotation period or target revisit time (seconds).

PRF_Hz = radar pulse repetition frequency (Hz). For stacked beams, use the PRF for the beam nearest the target in elevation.

DC_Factor = radar duty cycle (factor). The duty cycle may be calculated from the pulse duration, τ , by: $DC = \tau \text{ PRF}$. Use the portion of the duty cycle that

is used in this search mode. For stacked beams, use the portion of the duty cycle for the beam nearest the target elevation.

R_Ref_km = radar reference range (km). For cosecant-squared or multiple-beam antennas, the reference range should be adjusted for the gain reduction at the higher elevation angles. For stacked beams, use the reference range for the beam nearest the target elevation.

SNR_Ref_dB = reference S/N (dB).

Tau_Ref_ms = reference pulse duration (ms).

RCS_Ref_dBsm = reference RCS (dBsm).

Prop_L_dB = average propagation losses (dB).

BeamS_L_dB = beamshape loss (dB). For fan-beam search, use 1.6 dB. For multibeam search or rotating dish horizon search, use 2.5 dB.

Sel_1Rd2Rp3Ra (optional) = select 1 for radar detection range, 2 for average acquisition range, or 3 for assured acquisition range (integer). If this input is left blank, the assured acquisition range will be calculated.

V_Rad_kmps (optional) = target radial velocity (km/s). This is used to calculate average and assured acquisition ranges. If left blank, a value of zero will be used.

R_Max_km (optional) = maximum target range for purposes of calculating the beam-scanning loss. If left blank, maximum unambiguous range will be used. No result is generated if returned pulse is out of the azimuth beam, indicated by an output of -3.

Function Output Target acquisition range for the option selected (detection range, average acquisition range, or assured acquisition range), (km). No result is generated if less than one pulse illuminates the target, indicated by an output of -4, or if the minimum-range constraint is not met (see Section 5.5), indicated by an output of -5.

The Excel Function Arguments parameter box for Function SearchR_Rot2_km is shown in Figure 7.10, with sample parameters and solution.

7.8.3 Function SearchR_Vol1_km

Purpose Calculates target acquisition ranges for phased-array radar in volume search for specified detection parameters, using radar parameters.

Reference Equations (7.11) to (7.17), and (7.19) to (7.21).

Features Uses the search time that maximizes the assured acquisition range. Calculates the beam-broadening factor and scan loss for FFOV phased-array radar and the angular coverage parameters input. (For LFOV phased-array radar, the additional scan loss may be calculated and input with the propagation loss.) Uses nominal beamshape loss of 2.5 dB and beam-packing factor of 1.2. Detection parameters and either noncoherent integration, coherent integration, or cumulative detection may be specified. The number of pulses per beam position is input. If this results in a pulse duration that violates the minimum-range constraint, no result is produced (see Section 7.3). The number of pulses may be varied to find the optimum

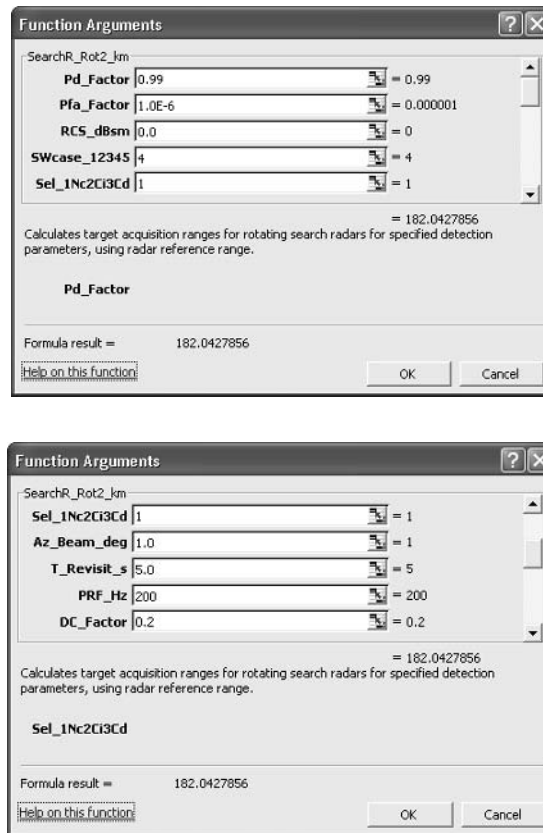


Figure 7.10 Excel parameter box for Function SearchR_Rot2_km.

acceptable value. Output may be selected for detection range, R_D , average target acquisition range, R_P , or assured acquisition range, R_A .

Input Parameters (with units specified)

Pd_Factor = required probability of detection from 0.3 to 0.999 (0.3 to 0.99 for Swerling 1 targets) (factor).

Pfa_Factor = required probability of false alarm from 10^{-1} to 10^{-10} (factor).

RCS_dBsm = target average RCS (dBsm).

SWcase_12345 = Swerling target-signal statistics case (integer). Use 1 for Swerling type 1 targets, 2 for Swerling type 2 targets, 3 for Swerling type 3 targets, 4 for Swerling type 4 targets and 5 for nonfluctuating targets.

Sel_1Nc2Ci3Cd = select 1 for noncoherent integration, 2 for coherent integration, or 3 for cumulative detection of signal returns in the beam (integer). If 2 is selected, no result will be generated for Swerling 2 and 4 targets, indicated by an output of -1 . If 3 is selected, no result will be generated for Swerling 1 and 3 targets, indicated by an output of -2 .

V_Rad_kmps = target radial velocity (km/s).

Az_Min_deg = minimum search angle in the x plane relative to array broadside, maximum magnitude 60° . This and the following five parameters

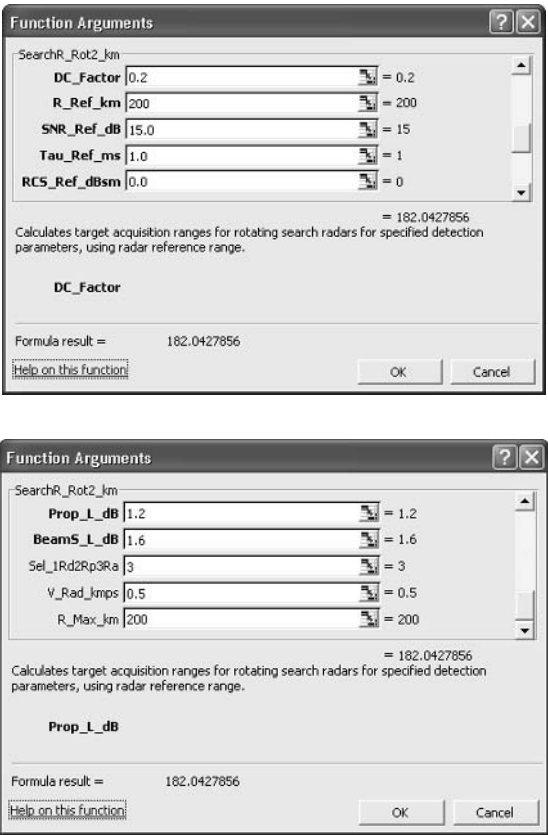


Figure 7.10 (continued).

are measured in orthogonal angular coordinates relative to the array broadside direction. These may approximate azimuth and elevation in many cases, and this terminology is used for convenience here. The search parameters are used to calculate the search solid angle, the beam broadening factor, and the off-axis scan loss.

`Az_Max_deg` = maximum search angle in the x plane relative to array broadside, maximum magnitude 60° .

`El_Min_deg` = minimum search angle in the y plane relative to array broadside, maximum magnitude 60° .

`El_Max_deg` = maximum search angle in the y plane relative to array broadside, maximum magnitude 60° .

`Az_Beam_deg` = beamwidth of radar in the x plane (degrees).

`El_Beam_deg` = beamwidth of radar in the y plane (degrees).

`Npulses_Integer` = number of pulses per beam position from 1 to 1,000 (integer). This value may be varied to find the optimum number.

`P_Av_kW` = average transmitted power (kW). Use the portion of the total radar power used in this search mode.

`DC_Factor` = radar duty cycle (factor). Use the portion of the duty cycle that is used in this search mode.

Area_R_m2 = receive antenna effective aperture area (m²).

Noise_T_K = system noise temperature (K).

Fixed_L_dB = fixed radar losses (dB).

Prop_L_dB = average propagation losses (dB).

Sel_1Rd2Rp3Ra (optional) = select 1 for radar detection range, 2 for average acquisition range, or 3 for assured acquisition range. If this input is left blank, the assured acquisition range will be calculated.

Function Output Target acquisition range for the option selected (detection range, average acquisition range, or assured acquisition range), (km). No result is generated if the minimum-range constraint is not met (see Section 5.5), indicated by an output of -3.

The Excel Function Arguments parameter box for Function SearchR_Vol1_km is shown in Figure 7.11, with sample parameters and solution.

7.8.4 Function SearchR_Vol2_km

Purpose Calculates target acquisition ranges for phased-array radar in volume search for specified detection parameters, using radar reference range.

Function Arguments

SearchR_Vol1_km

Pd_Factor 0.9 = 0.9

Pfa_Factor 1.0E-6 = 0.000001

RCS_dBsm -10.0 = -10

SWcase_12345 2 = 2

Sel_1Nc2C3Cd 1 = 1

= 423.4312134

Calculates target acquisition ranges for phased-array radars in volume search for specified detection parameters, using radar parameters.

Pd_Factor

Formula result = 423.4312134

[Help on this function](#)

OK Cancel

Function Arguments

SearchR_Vol1_km

V_Rad_kmps 0.5 = 0.5

Az_Min_deg -45 = -45

Az_Max_deg 45 = 45

El_Min_deg -15 = -15

El_Max_deg 25 = 25

= 423.4312134

Calculates target acquisition ranges for phased-array radars in volume search for specified detection parameters, using radar parameters.

V_Rad_kmps

Formula result = 423.4312134

[Help on this function](#)

OK Cancel

Figure 7.11 Excel parameter box for Function SearchR_Vol1_km.

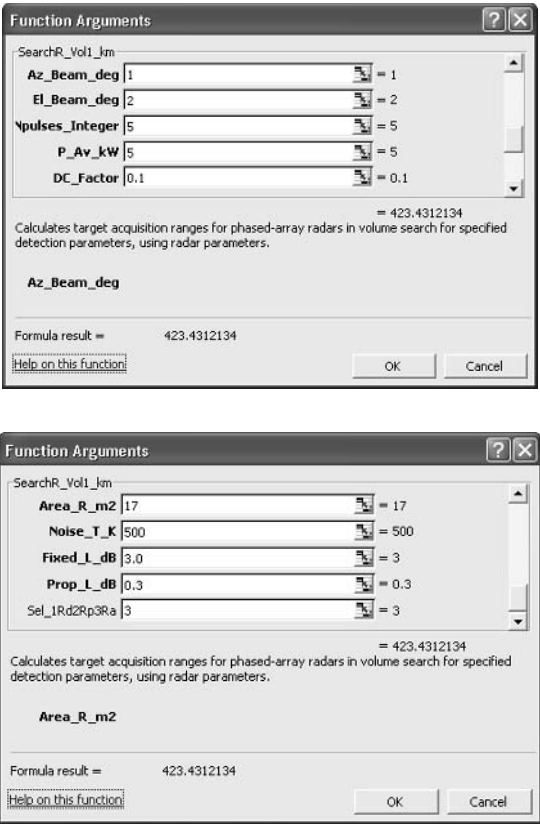


Figure 7.11 (continued).

Reference Equations (7.11) to (7.16), and (7.18) to (7.21).

Features Uses the search time that maximizes the assured acquisition range. Calculates the beam-broadening factor and scan loss for FFOV phased-array radar and the angular coverage parameters input. (For LFOV phased-array radar, the additional scan loss may be calculated and input with the propagation loss.) Uses nominal beamshape loss of 2.5 dB and beam-packing factor of 1.2. Detection parameters and either noncoherent integration, coherent integration, or cumulative detection may be specified. The number of pulses per beam position is input. If this results in a pulse duration that violates the minimum-range constraint, no result is produced (see Section 7.3). The number of pulses may be varied to find the optimum acceptable value. Output may be selected for detection range, R_d , average target acquisition range, R_p , or assured acquisition range, R_A .

Input Parameters (with units specified)

- P_d_Factor = required probability of detection from 0.3 to 0.999 (0.3 to 0.99 for Swerling 1 targets) (factor).
- P_{fa_Factor} = required probability of false alarm from 10^{-1} to 10^{-10} (factor).
- RCS_dBsm = target average RCS (dBsm).

SWcase_12345 = Swerling target-signal statistics case (integer). Use 1 for Swerling type 1 targets, 2 for Swerling type 2 targets, 3 for Swerling type 3 targets, 4 for Swerling type 4 targets, and 5 for nonfluctuating targets.

Sel_1Nc2Ci3Cd = select 1 for noncoherent integration, 2 for coherent integration, or 3 for cumulative detection of signal returns in the beam (integer). If 2 is selected, no result will be generated for Swerling 2 and 4 targets, indicated by an output of -1. If 3 is selected, no result will be generated for Swerling 1 and 3 targets, indicated by an output of -2.

V_Rad_kmps = target radial velocity (km/s).

Az_Min_deg = minimum search angle in the x plane relative to array broadside, maximum magnitude 60° . This and the following five parameters are measured in orthogonal angular coordinates relative to the array broadside direction. These may approximate azimuth and elevation in many cases, and this terminology is used for convenience here. The search parameters are used to calculate the search-solid angle, the beam-broadening factor, and the off-axis scan loss.

Az_Max_deg = maximum search angle in the x plane relative to array broadside, maximum magnitude 60° .

El_min_deg = minimum search angle in the y plane relative to array broadside, maximum magnitude 60° .

El_Max_deg = maximum search angle in the y plane relative to array broadside, maximum magnitude 60° .

Az_Beam_deg = beamwidth of radar in the x plane (degrees).

El_Beam_deg = beamwidth of radar in the y plane (degrees)

Npulses_Integer = number of pulses per beam position from 1 to 1,000 (integer). This value may be varied to find the optimum number.

R_Ref_km = radar reference range (km).

SNR_Ref_dB = reference S/N (dB).

Tau_Ref_ms = reference pulse duration (ms).

RCS_Ref_dBsm = reference RCS (dBsm).

DC_Factor = radar duty cycle (factor). Use the portion of the total radar duty cycle used in this search mode.

Prop_L_dB = average propagation losses (dB).

Sel_1Rd2Rp3Ra = select 1 for radar detection range, 2 for average acquisition range, or 3 for assured acquisition range. If this input is left blank, the assured acquisition range will be calculated.

Function Output Target acquisition range for the option selected (detection range, average acquisition range, or assured acquisition range) (km). No result is generated if the minimum-range constraint is not met (see Section 5.5), indicated by an output of -3.

The Excel Function Arguments parameter box for Function SearchR_Vol2_km is shown in Figure 7.12, with sample parameters and solution.

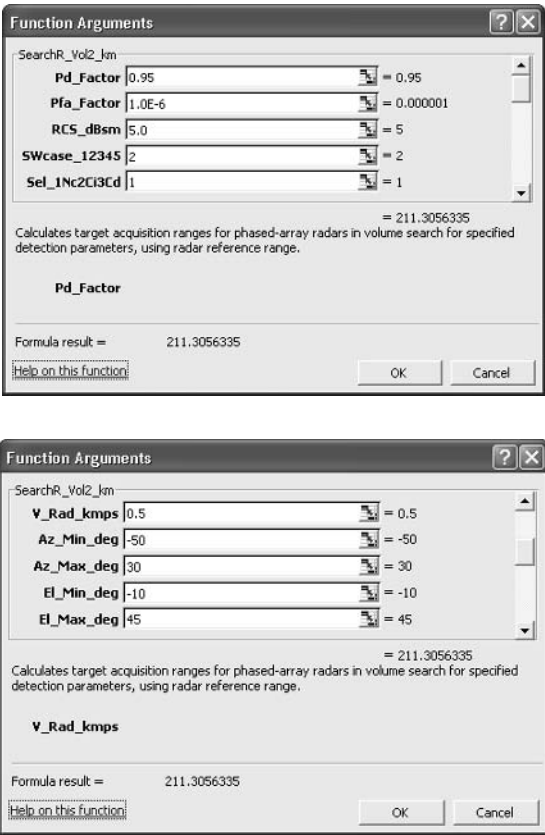


Figure 7.12 Excel parameter box for Function SearchR_Vol2_km.

7.8.5 Function SearchR_Cue1_km

Purpose Calculates target acquisition ranges for phased-array and dish radar in cued search for specified detection parameters, using radar parameters.

Reference Equations (7.22) to (7.24), and (7.26) to (7.29).

Features Evaluates both single-beam and multibeam cued search for phased-array radar, and single-beam search for dish radar. Calculates the beam-broadening factor and scan loss for FFOV phased-array radar. (For LFOV phased-array radar, the additional scan loss may be calculated and input with the propagation loss.) Uses a beam-packing factor of 1.2 and beamshape loss of 2.5 dB for multi-beam search, and calculates the beamshape loss for single-beam search from Equation 7.26. Calculates transmit gain for single-beam search from antenna beamwidths using Equation 3.12. (This is valid for dish radar and filled arrays; for thinned arrays and losses not included elsewhere, add the loss factors to the propagation loss input.) Detection parameters and either noncoherent integration, coherent integration, or cumulative detection may be specified. The number of pulses per beam position is input. If this results in a pulse duration that violates the minimum-range constraint, no result is produced. The number of pulses may be varied to find the optimum acceptable value. Output may be selected for detection range, R_D , average target acquisition range, R_p , or assured acquisition range, R_A .

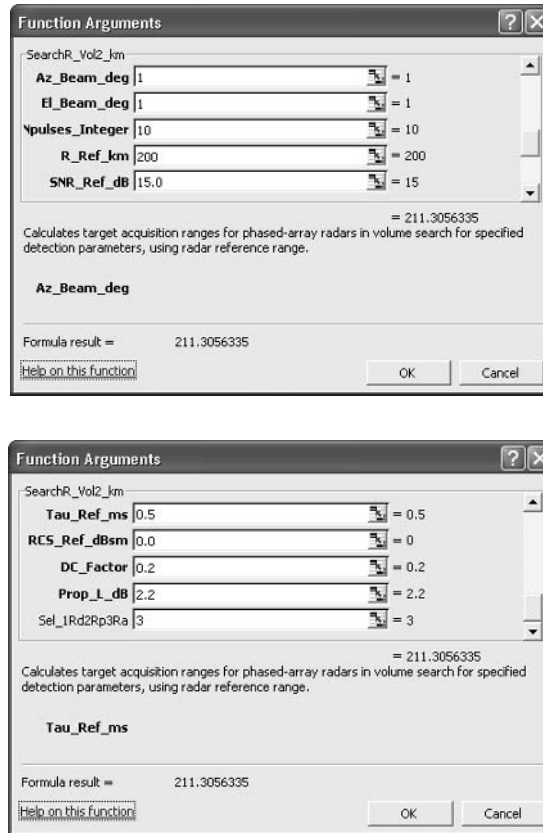


Figure 7.12 (continued).

Input Parameters (with units specified)

Pd_Factor = required probability of detection from 0.3 to 0.999 (0.3 to 0.99 for Swerling 1 targets) (factor).

Pfa_Factor = required probability of false alarm from 10^{-1} to 10^{-10} (factor).

RCS_dBsm = target average RCS (dBsm).

SWcase_12345 = Swerling target-signal statistics case (integer). Use 1 for Swerling type 1 targets, 2 for Swerling type 2 targets, 3 for Swerling type 3 targets, 4 for Swerling 4 targets, and 5 for nonfluctuating targets.

Sel_1Nc2Ci3Cd = select 1 for noncoherent integration, 2 for coherent integration, or 3 for cumulative detection of signal returns in the beam (integer). If 2 is selected, no result will be generated for Swerling 2 and 4 targets, indicated by an output of -1. If 3 is selected, no result will be generated for Swerling 1 and 3 targets, indicated by an output of -2.

Search_Rad_km = cued-search radius, or equivalent search radius (km).

Search_t_sec = cued search time.

Az_deg = search angle, relative to array broadside in the x plane (degrees).

This and the following three parameters are measured in orthogonal angular coordinates relative to the array broadside direction. These may approximate azimuth and elevation in many cases, and this terminology is used for

convenience here. The search parameters are used to calculate the beam broadening factor and the off-axis scan loss. When Az_deg and El_deg are both zero, a dish radar is assumed.

El_deg = search angle, relative to array broadside in the y plane (degrees).

When Az_deg and El_deg are both zero, a dish radar is assumed.

Az_Beam_deg = beamwidth of radar in the x plane (degrees).

El_Beam_deg = beamwidth of radar in the y plane (degrees)

Npulses_Integer = number of pulses per beam position from 1 to 1,000 (integer). This value may be varied to find the optimum number.

P_Av_kW = average transmitted power (kW). Use the portion of the total radar power that is used in this search mode.

DC_Factor = radar duty cycle (factor). Use the portion of the total radar duty cycle used in this search mode.

Area_R_m2 = receive antenna effective aperture area (m^2).

Noise_T_K = system noise temperature (K).

Fixed_L_dB = fixed radar losses (dB).

Prop_L_dB = average propagation losses (dB).

Sel_1Rd2Rp3Ra (optional) = select 1 for radar detection range, 2 for average acquisition range, or 3 for assured acquisition range. If this input is left blank, the assured acquisition range will be calculated.

V_Rad_kmps (optional) = target radial velocity (km/s). This is used to calculate average and assured acquisition ranges. If left blank, a value of zero will be used.

Function Output Target acquisition range for the option selected (detection range, average acquisition range, assumed to be midway between detection and assured acquisition ranges, or assured acquisition range) (km). For dish radar (indicated by inputs of Az_deg and El_deg of zero), when single-beam search may not provide the required search coverage, no result is generated, indicated by an output of -3 . No result is generated if the minimum-range constraint is not met (see Section 5.5), indicated by an output of -4 .

The Excel Function Arguments parameter box for Function SearchR_Cue1_km is shown in Figure 7.13, with sample parameters and solution.

7.8.6 Function SearchR_Cue2_km

Purpose Calculates target acquisition ranges for phased-array and dish radar in cued search for specified detection parameters, using radar reference range.

Reference Equations (7.22), (7.23), (7.25) to (7.27), and (7.29) to (7.31).

Features Evaluates both single-beam and multibeam cued search for phased-array radar, and single-beam search for dish radar. Calculates the beam-broadening factor and scan loss for FFOV phased-array radar. (For LFOV phased-array radar, the additional scan loss may be calculated and input with the propagation loss.) Uses a beam-packing factor of 1.2 and beamshape loss of 2.5 dB for multibeam search, and calculates the beamshape loss for single-beam search from (7.26). Detection parameters and either noncoherent integration,

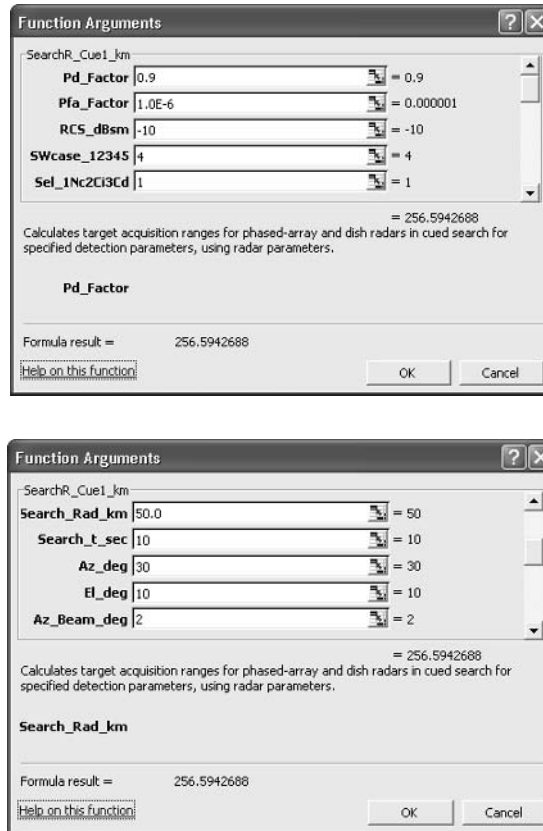


Figure 7.13 Excel parameter box for Function SearchR_Cue1_km.

coherent integration, or cumulative detection may be specified. The number of pulses per beam position is input. If this results in a pulse duration that violates the minimum-range constraint, no result is produced. The number of pulses may be varied to find the optimum acceptable value. Output may be selected for detection range, R_D , average target acquisition range, R_p , or assured acquisition range, R_A .

Input Parameters (with units specified)

Pd_Factor = required probability of detection from 0.3 to 0.999 (0.3 to 0.99 for Swerling 1 targets) (factor).

Pfa_Factor = required probability of false alarm from 10^{-1} to 10^{-10} (factor).

RCS_dBsm = target average RCS (dBsm).

SWcase_12345 = Swerling target-signal statistics case (integer). Use 1 for Swerling type 1 targets, 2 for Swerling type 2 targets, 3 for Swerling type 3 targets, 4 for Swerling type 4 targets and 5 for nonfluctuating targets.

Sel_1Nc2Ci3Cd = select 1 for noncoherent integration, 2 for coherent integration, or 3 for cumulative detection of signal returns in the beam (integer). If 2 is selected, no result will be generated for Swerling 2 and 4 targets, indicated by an output of -1 . If 3 is selected, no result will be generated for Swerling 1 and 3 targets, indicated by an output of -2 .

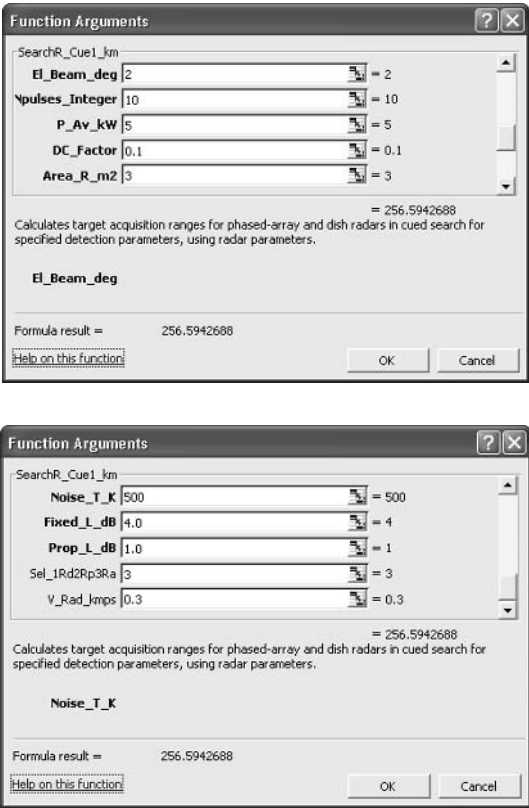


Figure 7.13 (continued).

- Search_Rad_km = cued search radius, or equivalent search radius (km).
- Search_t_sec = cued search time (s).
- Az_deg = search angle, relative to array broadside in the x plane (degrees). This and the following three parameters are measured in orthogonal angular coordinates relative to the array broadside direction. These may approximate azimuth and elevation in many cases, and this terminology is used for convenience here. The search parameters are used to calculate the beam-broadening factor and the off-axis scan loss. When Az_deg and El_deg are both zero, a dish radar is assumed.
- El_deg = search angle, relative to array broadside in the y plane(degrees). When Az_deg and El_deg are both zero, a dish radar is assumed.
- Az_Beam_deg = beamwidth of radar in the x plane (degrees).
- El_Beam_deg = beamwidth of radar in the y plane (degrees)
- Npulses_Integer = number of pulses per beam position from 1 to 1,000 (integer). This value may be varied to find the optimum number.
- R_Ref_km = radar reference range (km).
- SNR_Ref_dB = reference S/N (dB).
- Tau_Ref_ms = reference pulse duration (ms).
- RCS_Ref_dBsm = reference RCS (dBsm).

DC_Factor = radar duty cycle (factor). Use that portion of the total duty cycle that is used in this search mode.

Prop_L_dB = average propagation losses (dB).

Sel_1Rd2Rp3Ra (optional) = select 1 for radar detection range, 2 for average acquisition range, or 3 for assured acquisition range. If this input is left blank, the assured acquisition range will be calculated.

V_Rad_kmps (optional) = target radial velocity (km/s). This is used to calculate average and assured acquisition ranges. If left blank, a value of zero will be used.

Function Output Target acquisition range for the option selected (detection range, average acquisition range, assumed to be midway between detection and assured acquisition ranges, or assured acquisition range) (km). For dish radar (indicated by inputs of Az_deg and El_deg of zero), when single-beam search may not provide the required search coverage, no result is generated, indicated by an output of -3. No result is generated if the minimum-range constraint is not met (see Section 5.5), indicated by an output of -4.

The Excel Function Arguments parameter box for Function SearchR_Cue2_km is shown in Figure 7.14, with sample parameters and solution.

Function Arguments

SearchR_Cue2_km

Pd_Factor	0.9	= 0.9
Pfa_Factor	1.0E-4	= 0.0001
RCS_dBsm	-5.0	= -5
SWcase_12345	3	= 3
Sel_1Nc2Ci3Cd	2	= 2

= 563.7362061

Calculates target acquisition ranges for phased-array and dish radars in cued search for specified detection parameters, using radar reference range.

Pd_Factor

Formula result = 563.7362061

[Help on this function](#)

OK Cancel

Function Arguments

SearchR_Cue2_km

Search_Rad_km	2.5	= 2.5
Search_t_sec	2	= 2
Az_deg	0	= 0
El_deg	0	= 0
Az_Beam_deg	1	= 1

= 563.7362061

Calculates target acquisition ranges for phased-array and dish radars in cued search for specified detection parameters, using radar reference range.

Search_Rad_km

Formula result = 563.7362061

[Help on this function](#)

OK Cancel

Figure 7.14 Excel parameter box for Function SearchR_Cue2_km.

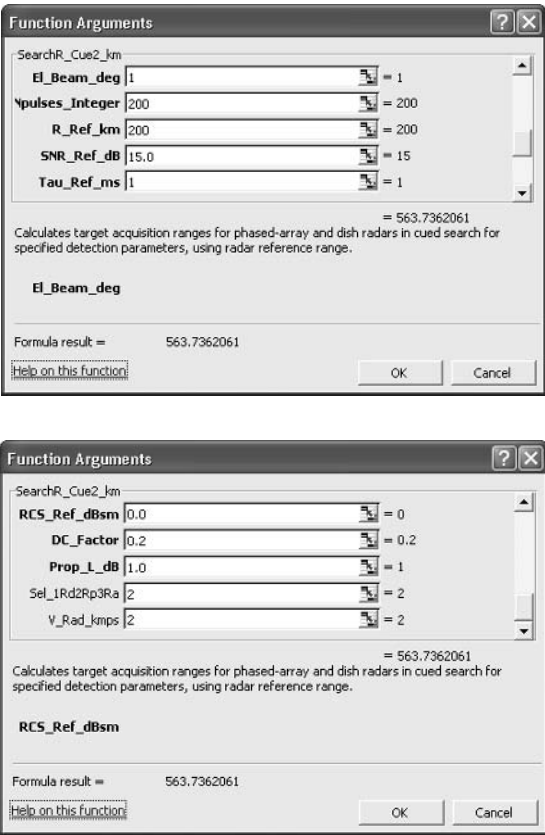


Figure 7.14 (continued).

7.8.7 Function SearchR_Hor1_km

Purpose Calculates target acquisition ranges for phased-array radar in horizon search for specified detection parameters, using radar parameters.

Reference Equations (7.37) to (7.39).

Features Uses the search time that maximizes the assured acquisition range, allowing for a specified minimum target range. Calculates the beam broadening factor and scan loss for the angular parameters input. Uses nominal beamshape loss of 2.5 dB and beam-packing factor of 1.2. Detection parameters and either noncoherent integration, coherent integration, or cumulative detection may be specified. The number of pulses per beam position is input. If this results in a pulse duration that violates the minimum-range constraint, no result is produced. The number of pulses may be varied to find the optimum acceptable value. Output may be selected for detection range, R_D , average target acquisition range, R_p , or assured acquisition range, R_A . Assumes a single row of beams in elevation.

Input Parameters (with units specified)

Pd_Factor = required probability of detection from 0.3 to 0.999 (0.3 to 0.99 for Swerling 1 targets) (factor).

Pfa_Factor = required probability of false alarm from 10^{-1} to 10^{-10} (factor).

RCS_dBsm = target average RCS (dBsm).

SWcase_12345 = Swerling target-signal statistics case (integer). Use 1 for Swerling type 1 targets, 2 for Swerling type 2 targets, 3 for Swerling type 3 targets, 4 for Swerling type 4 targets and 5 for nonfluctuating targets.

Sel_1Nc2Ci3Cd = select 1 for noncoherent integration, 2 for coherent integration, or 3 for cumulative detection of signal returns in the beam (integer). If 2 is selected, no result will be generated for Swerling 2 and 4 targets, indicated by an output of -1. If 3 is selected, no result will be generated for Swerling 1 and 3 targets, indicated by an output of -2.

V_Vert_kmps = target velocity component normal to the radar LOS (km/s).

Az_Min_deg = minimum search angle in the x plane relative to array broadside, maximum magnitude 60° . This and the following three parameters are measured in orthogonal angular coordinates relative to the array broadside direction. These may approximate azimuth and elevation in many cases, and this terminology is used for convenience here. The search parameters are used to calculate the search azimuth coverage, the beam-broadening factor, and the off-axis scan loss.

Az_Max_deg = maximum search angle in the y plane relative to array broadside, maximum magnitude 60° .

El_deg = search elevation relative to array broadside (degrees).

Az_Beam_deg = beamwidth of radar in the x plane (degrees).

El_Beam_deg = beamwidth of radar in the y plane (degrees)

Npulses_Integer = number of pulses per beam position from 1 to 1,000 (integer). This value may be varied to find the optimum number.

P_Av_kW = average transmitted power (kW). Use that portion of the total radar power used in this search mode.

DC_Factor = radar duty cycle (factor). Use that portion of the total duty cycle that is used in this search mode.

Area_R_m2 = receive antenna effective (m^2)

Noise_T_K = system noise temperature (K).

Fixed_L_dB = fixed radar losses (dB).

Prop_L_dB = average propagation losses (dB).

V_Rad_kmps (optional) = target radial velocity (km/s). This is used to calculate average and assured acquisition ranges. If left blank, a value of zero will be used.

Sel_1Rd2Rp3Ra (optional) = select 1 for radar detection range, 2 for average acquisition range, or 3 for assured acquisition range. If this input is left blank, the assured acquisition range will be calculated.

Rh_Min_km (optional) = minimum target range (km). If left blank, a target at the maximum detection range is assumed.

Function Output Target acquisition range for the option selected (detection range, average acquisition range, or assured acquisition range) (km). If the radar is not

capable of providing assured detection for the specified azimuth coverage and the specified minimum target range, no result will be generated, indicated by an output of -3. No result is generated if the minimum-range constraint is not met (see Section 5.5), indicated by an output of -4.

The Excel Function Arguments parameter box for Function SearchR_Hor1_km is shown in Figure 7.15, with sample parameters and solution.

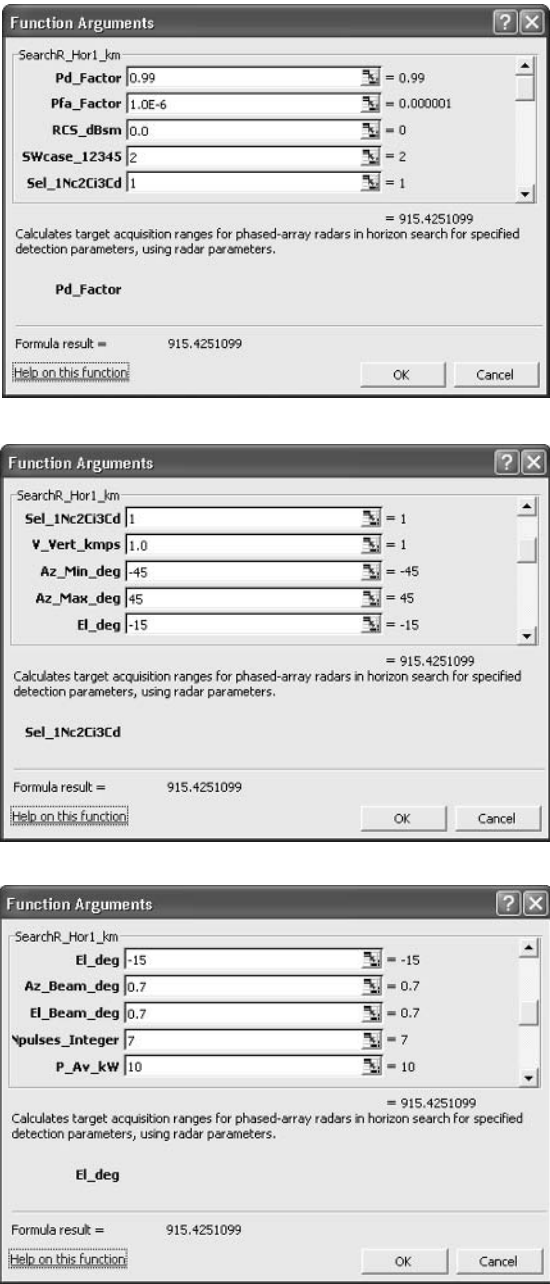


Figure 7.15 Excel parameter box for Function SearchR_Hor1_km.

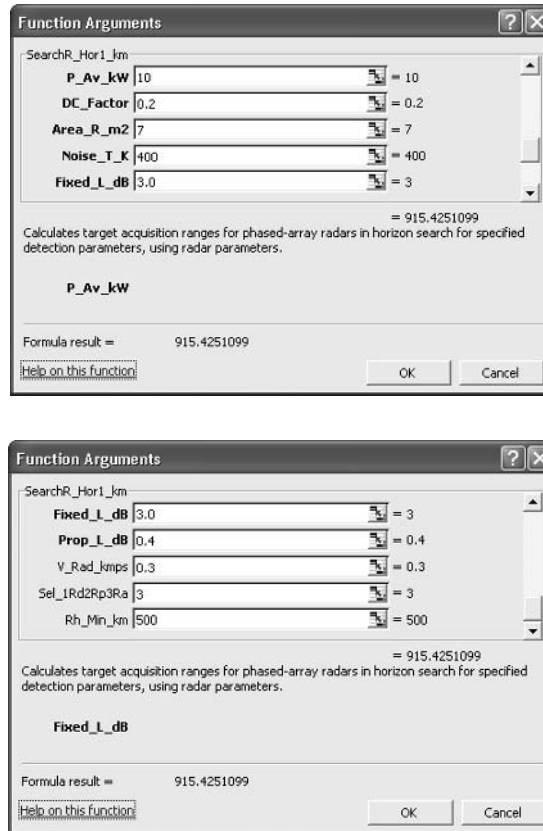


Figure 7.15 Continued.

7.8.8 Function SearchR_Hor2_km

Purpose Calculates target acquisition ranges for phased-array radar in horizon search for specified detection parameters, using radar reference range.

Reference Equations (7.37), (7.38), (7.40), and (7.41).

Features Uses the search time that maximizes the assured acquisition range, allowing for a specified minimum target range. Calculates the beam-broadening factor and scan loss for the angular parameters input. Uses nominal beamshape loss of 2.5 dB and beam-packing factor of 1.2. Detection parameters and either noncoherent integration, coherent integration, or cumulative detection may be specified. The number of pulses per beam position is input. If this results in a pulse duration that violates the minimum-range constraint, no result is produced. The number of pulses may be varied to find the optimum acceptable value. Output may be selected for detection range, R_D , average target acquisition range, R_p , or assured acquisition range, R_A . Assumes a single row of beams in elevation.

Input Parameters (with units specified)

Pd_Factor = required probability of detection from 0.3 to 0.999 (0.3 to 0.99 for Swerling 1 targets) (factor).

Pfa_Factor = required probability of false alarm from 10^{-1} to 10^{-10} (factor).

RCS_dBsm = target average RCS (dBsm).

SWcase_12345 = Swerling target-signal statistics case (integer). Use 1 for Swerling type 1 targets, 2 for Swerling type 2 targets, 3 for Swerling type 3 targets, 4 for Swerling type 4 targets, and 5 for nonfluctuating targets.

Sel_1Nc2Ci3Cd = select 1 for noncoherent integration, 2 for coherent integration, or 3 for cumulative detection of signal returns in the beam (integer). If 2 is selected, no result will be generated for Swerling 2 and 4 targets, indicated by an output of -1. If 3 is selected, no result will be generated for Swerling 1 and 3 targets, indicated by an output of -2.

V_Vert_kmps = target velocity component normal to the radar LOS (km/s).

Az_Min_deg = minimum search angle in the x plane relative to array broadside, maximum magnitude 60° . This and the following three parameters are measured in orthogonal angular coordinates relative to the array broadside direction. These may approximate azimuth and elevation in many cases, and this terminology is used for convenience here. The search parameters are used to calculate the search azimuth coverage, the beam-broadening factor, and the off-axis scan loss.

Az_Max_deg = maximum search angle in the y plane relative to array broadside, maximum magnitude 60° .

El_deg = search elevation relative to array broadside (degrees).

Az_Beam_deg = beamwidth of radar in the x plane (degrees).

El_Beam_deg = beamwidth of radar in the y plane (degrees).

Npulses_Integer = number of pulses per beam position from 1 to 1,000 (integer). This value may be varied to find the optimum number.

R_Ref_km = radar reference range (km).

SNR_Ref_dB = reference S/N (dB).

Tau_Ref_ms = reference pulse duration (ms).

RCS_Ref_dBsm = reference RCS (dBsm).

DC_Factor = radar duty cycle (factor). Use that portion of the radar duty cycle used in this search mode.

Prop_L_dB = average propagation losses (dB).

V_Rad_kmps (optional) = target radial velocity (km/s). This is used to calculate average and assured acquisition ranges. If left blank, a value of zero will be used.

Sel_1Rd2Rp3Ra (optional) = select 1 for radar detection range, 2 for average acquisition range, or 3 for assured acquisition range. If this input is left blank, the assured acquisition range will be calculated.

Rh_Min_km (optional) = minimum target range (km). If left blank, a target at the maximum detection range is assumed.

Function Output Target acquisition range for the option selected (detection range, average acquisition range, or assured acquisition range) (km). If the radar is not capable of providing assured detection for the specified azimuth coverage and the specified minimum target range, no result will be generated, indicated by an output

of -3. No result is generated if the minimum-range constraint is not met (see Section 5.5), indicated by an output of -4.

The Excel Function Arguments parameter box for Function SearchR_Hor2_km is shown in Figure 7.16, with sample parameters and solution.

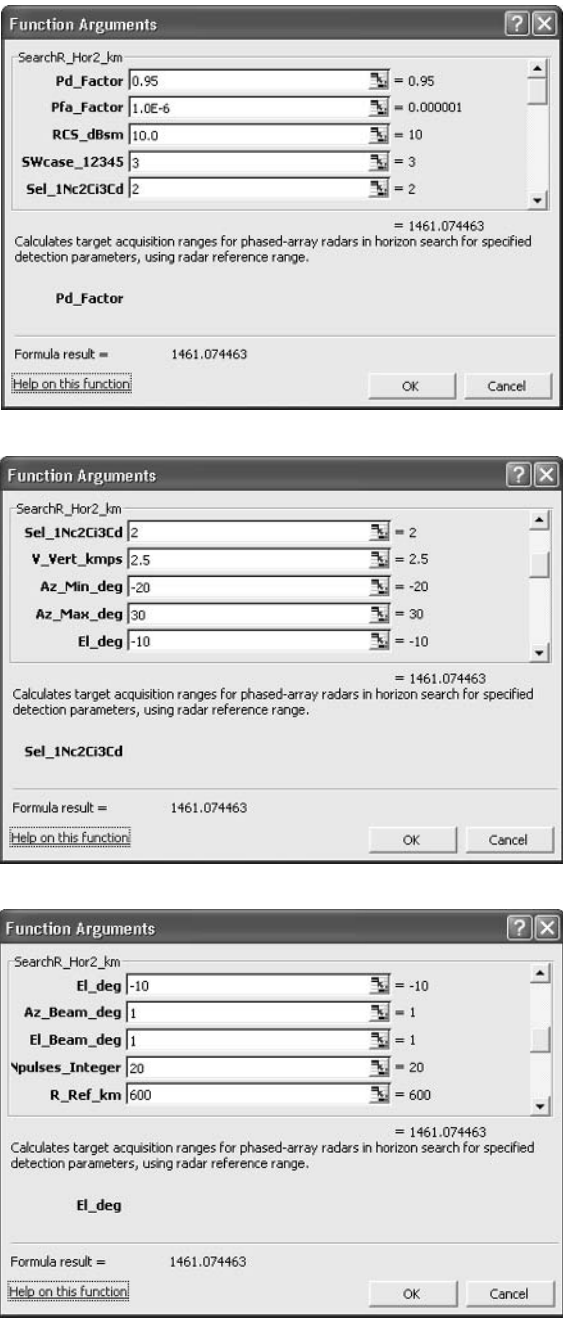


Figure 7.16 Excel parameter box for Function SearchR_Hor2_km.

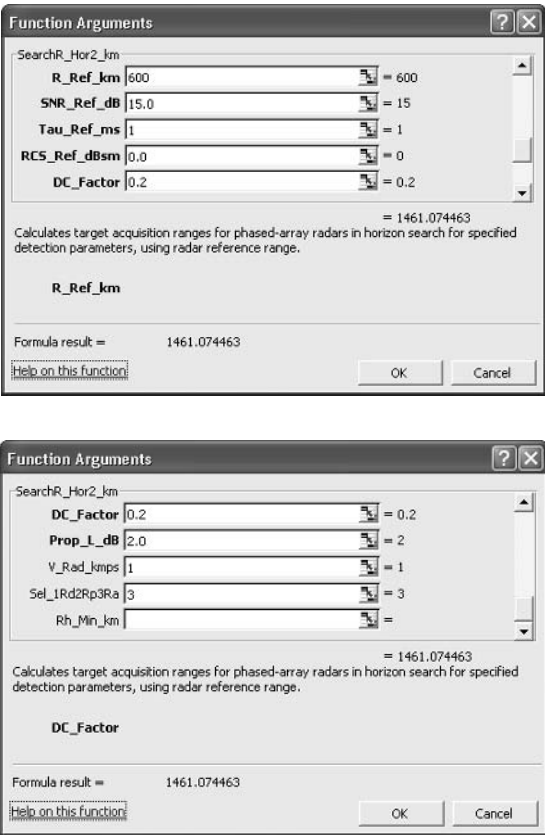


Figure 7.16 (continued).

7.8.9 Function `Sr_BowTie1_km`

Purpose Calculates target acquisition ranges for mechanically scanned dish radar in bow-tie horizon search for specified detection parameters, using radar parameters.

Reference Equations (7.42) to (7.49), (5.1).

Features Calculates minimum azimuth scan rate to provide the required azimuth search coverage, using the mechanical-scan parameters. Uses a beamshape loss of 2.5 dB. Calculates the number of pulses illuminating the target and the scanning loss. Detection parameters and either noncoherent integration, coherent integration, or cumulative detection may be specified. No result is generated if the specified azimuth coverage cannot be provided by the radar. Output may be selected for detection range, R_D , average target acquisition range, R_p , or assured acquisition range, R_A .

Input Parameters (with units specified)

- Pd_Factor = required probability of detection from 0.3 to 0.999 (0.3 to 0.99 for Swerling 1 targets) (factor).
- Pfa_Factor = required probability of false alarm from 10^{-1} to 10^{-10} (factor).

RCS_dBsm = target average RCS (dBsm).

SWcase_12345 = Swerling target-signal statistics case (integer). Use 1 for Swerling type 1 targets, 2 for Swerling type 2 targets, 3 for Swerling type 3 targets, 4 for Swerling type 4 targets, and 5 for nonfluctuating targets.

Sel_1Nc2Ci3Cd = select 1 for noncoherent integration, 2 for coherent integration, or 3 for cumulative detection of signal returns in the beam (integer). If 2 is selected, no result will be generated for Swerling 2 and 4 targets, indicated by an output of -1. If 3 is selected, no result will be generated for Swerling 1 and 3 targets, indicated by an output of -2.

V_Vert_kmps = target velocity component normal to the radar LOS (km/s).

Rh_Min_km = minimum target range (km).

Az_Cov_deg = search coverage requirement in azimuth (degrees).

Az_Vmax_dps = maximum azimuth angular velocity (degrees/s). The function assumes that the elevation rate and acceleration are not limiting in the scan.

Az_Amax_dps2 = maximum azimuth angular acceleration (degrees/s²).

Az_Beam_deg = azimuth beamwidth of radar (degrees).

El_Beam_deg = elevation beamwidth of radar (degrees)

P_Av_kW = average transmitted power (kW).

PRF_Hz = radar PRF (Hz). No result is generated if less than one pulse illuminates the target, indicated by an output of -4

DC_Factor = radar duty cycle (factor). Duty cycle may be calculated from the pulse duration, τ , by: $DC = \tau \text{ PRF}$.

Area_R_m2 = receive antenna effective aperture area (m²).

Noise_T_K = system noise temperature (K).

Fixed_L_dB = fixed radar losses (dB).

Prop_L_dB = average propagation losses (dB).

V_Rad_kmps (optional) = target radial velocity (km/s). This is used to calculate average and assured acquisition ranges. If left blank, a value of zero will be used.

Sel_1Rd2Rp3Ra (optional) = select 1 for radar detection range, 2 for average acquisition range, or 3 for assured acquisition range. If this input is left blank, the assured acquisition range will be calculated.

R_Max_km (optional) = maximum target range for calculating the beam-scanning loss (km). If left blank, maximum unambiguous range will be used. No result is generated if the returned pulses are out of the azimuth beam, indicated by an output of -5.

Function Output Target acquisition range for the option selected (detection range, average acquisition range, or assured acquisition range) (km). If the radar is not capable of providing the specified azimuth coverage, no result will be generated, indicated by an output of -3. The acquisition range output may be less than the specified minimum range. No result is generated if the minimum-range constraint is not met (see Section 5.5), indicated by an output of -6.

The Excel Function Arguments parameter box for Function Sr_BowTie1_km is shown in Figure 7.17, with sample parameters and solution.

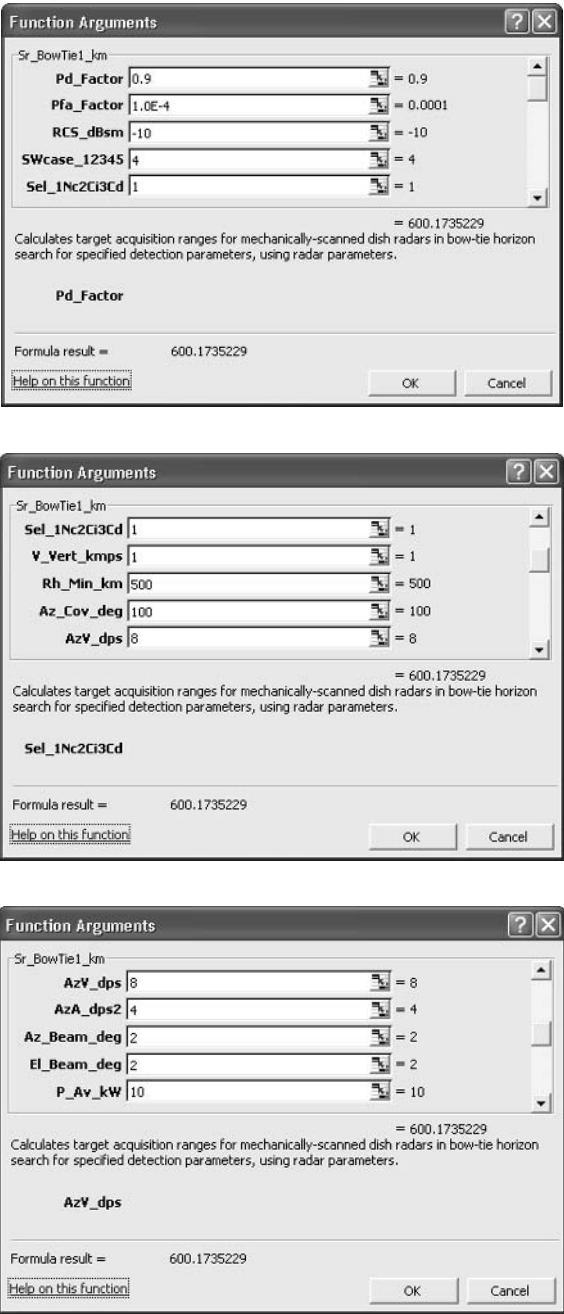


Figure 7.17 Excel parameter box for Function Sr_BowTie1_km.

7.8.10 Function Sr_BowTie2_km

Purpose Calculates target acquisition ranges for mechanically scanned dish radar in bow-tie horizon search for specified detection parameters, using radar reference range.

Reference Equations (7.42) to (7.49), (5.11).

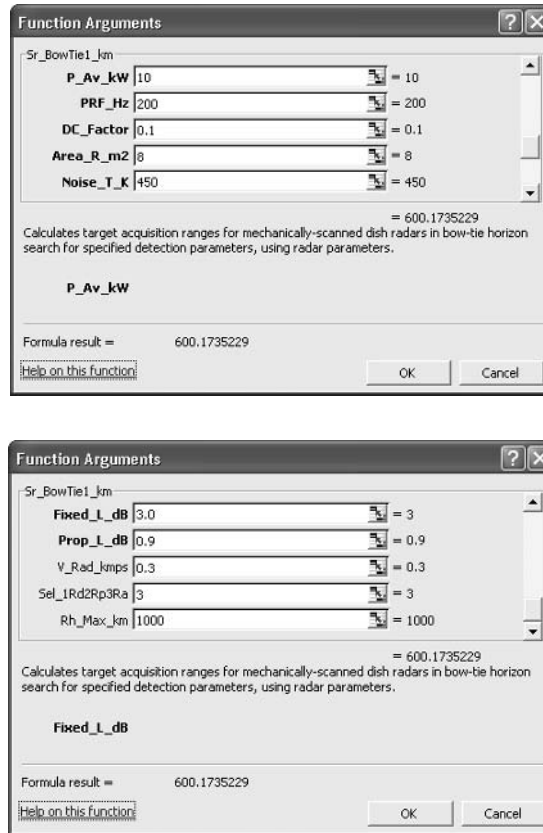


Figure 7.17 (continued).

Features Calculates minimum azimuth scan rate to provide the required azimuth search coverage, using the mechanical-scan parameters. Uses a beamshape loss of 2.5 dB. Calculates the number of pulses illuminating the target and the scanning loss. Detection parameters and either noncoherent integration, coherent integration, or cumulative detection may be specified. No result is generated if the specified azimuth coverage cannot be provided by the radar. Output may be selected for detection range, R_D , average target acquisition range, R_p , or assured acquisition range, R_A .

Input Parameters (with units specified)

Pd_Factor = required probability of detection from 0.3 to 0.999 (0.3 to 0.99 for Swerling 1 targets) (factor).

Pfa_Factor = required probability of false alarm from 10^{-1} to 10^{-10} (factor).

RCS_dBsm = target average RCS (dBsm).

SWcase_12345 = Swerling target-signal statistics case (integer). Use 1 for Swerling type 1 targets, 2 for Swerling type 2 targets, 3 for Swerling type 3 targets, 4 for Swerling type 4 targets, and 5 for nonfluctuating targets.

Sel_1Nc2Ci3Cd = select 1 for noncoherent integration, 2 for coherent integration, or 3 for cumulative detection of signal returns in the beam (integer). If 2 is selected, no result will be generated for Swerling 2 and 4

targets, indicated by an output of -1 . If 3 is selected, no result will be generated for Swerling 1 and 3 targets, indicated by an output of -2 .

V_Vert_kmps = target velocity component normal to the radar LOS (km/s).

Rh_Min_km = minimum target range (km).

Az_Cov_deg = search coverage requirement in azimuth (degrees).

Az_Vmax_dps = maximum azimuth angular velocity (degrees/s). The function assumes that the elevation rate and acceleration are not limiting in the scan.

Az_Amax_dps2 = maximum azimuth angular acceleration (degrees/s²).

Az_Beam_deg = azimuth beamwidth of radar (degrees).

El_Beam_deg = elevation beamwidth of radar (degrees)

R_Ref_km = radar reference range (km).

SNR_Ref_dB = reference S/N (dB).

Tau_Ref_ms = reference pulse duration (ms).

RCS_Ref_dBsm = reference RCS (dBsm).

PRF_Hz = radar pulse repetition frequency (Hz). No result is generated if less than one pulse illuminates the target, indicated by an output of -4

DC_Factor = radar duty cycle (factor). Duty cycle may be calculated from the pulse duration, τ , by: $DC = \tau \text{ PRF}$.

Prop_L_dB = average propagation losses (dB).

V_Rad_kmps (optional) = target radial velocity (km/s). This is used to calculate average and assured acquisition ranges. If left blank, a value of zero will be used.

Sel_1Rd2Rp3Ra (optional) = select 1 for radar detection range, 2 for average acquisition range, or 3 for assured acquisition range. If this input is left blank, the assured acquisition range will be calculated.

R_Max_km (optional) = maximum target range for calculating the beam-scanning loss (km). If left blank, maximum unambiguous range will be used. No result is generated if the returned pulses are out of the azimuth beam, indicated by an output of -5 .

Function Output Target acquisition range for the option selected (detection range, average acquisition range, or assured acquisition range) (km). If the radar is not capable of providing the specified azimuth coverage, no result will be generated, indicated by an output of -3 . The acquisition range output may be less than the specified minimum range. No result is generated in the minimum-range constraint is not met (see Section 5.5), indicated by an output of -6 .

The Excel Function Arguments parameter box for Function Sr_BowTie2_km is shown in Figure 7.18, with sample parameters and solution.

References

- [1] Barton, D. K., "Radar System Performance Charts," *IEEE Trans. on Military Electronics*, Vol. MIL-9, Nos. 3 and 4, July–October 1965.

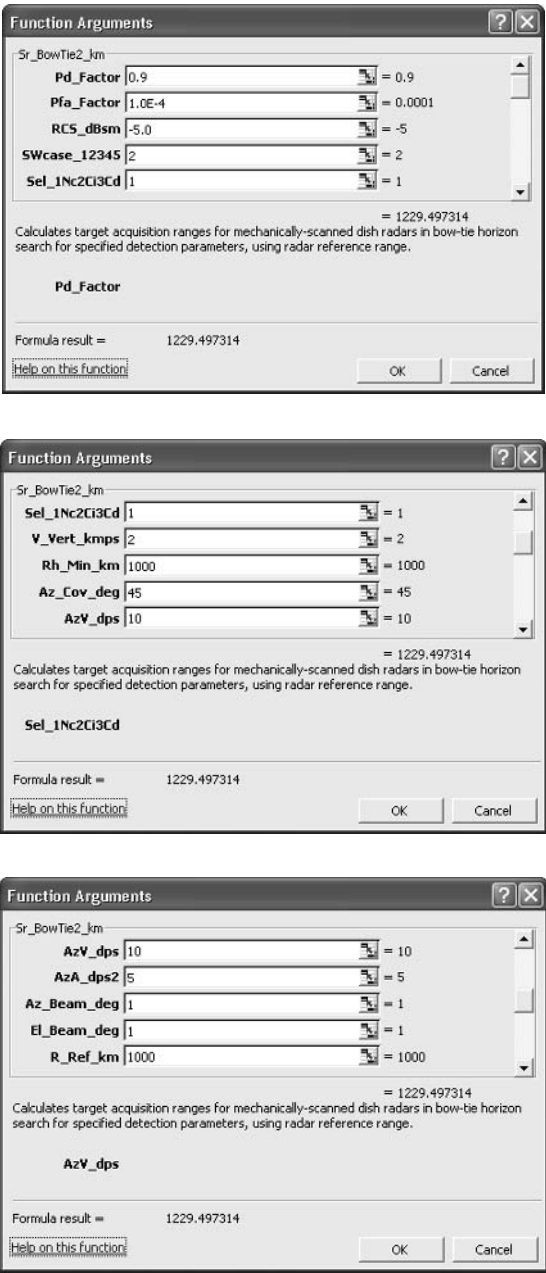


Figure 7.18 Excel parameter box for Function Sr_BowTie2_km.

[2] Mallett, J. D., and L. E. Brennan, “Cumulative Probability of Detection for Targets Approaching a Uniformly Scanning Search Radar,” *Proc. of the IEEE*, Vol. 81, No. 4, April 1963, pp. 595–601.

[3] Mallett, J. D., and L. E. Brennan, “Correction to Cumulative Probability of Detection for Targets Approaching a Uniformly Scanning Search Radar,” *Proc. of the IEEE*, Vol. 82, No. 6, April 1964, pp. 708–709.

[4] DiFranco, J. V., and W. L. Rubin, *Radar Detection*, Englewood Cliffs, NJ: Prentice Hall, Inc., 1988.

[5] Barton, D. K., *Modern Radar System Analysis*, Norwood, MA: Artech House, 1991.

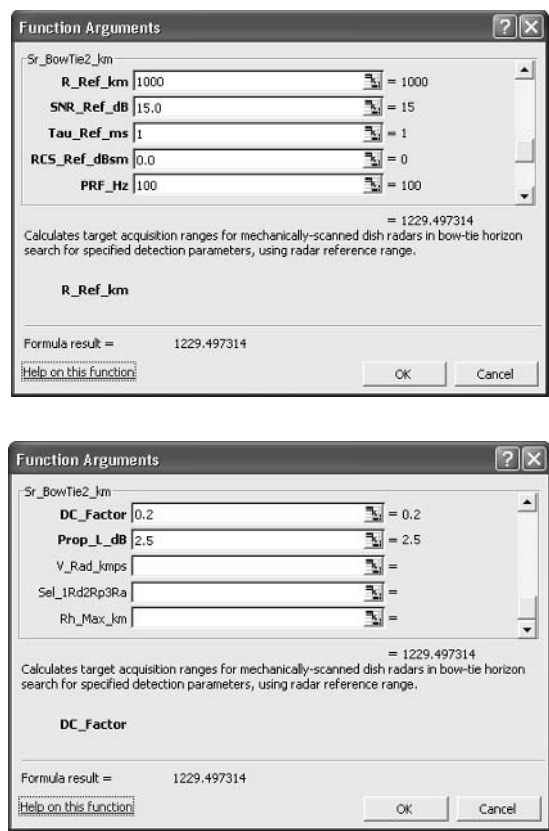


Figure 7.18 (continued).

[6] Billetter, D. R., *Multifunction Array Radar*, Norwood, MA: Artech House, 1989.

[7] Fielding, J. E., “Beam Overlap Impact on Phased-Array Target Detection,” *IEEE Trans. on Aerospace and Electronic Systems*, Vol. 29, No. 2, April 1993, pp. 404–411.

[8] Matthiesen, D. J., “Bow Tie Search Theory and Design,” *IEE International Radar Conference, Edinburgh, Scotland, Record*, 1997, pp. 775–782.

Selected Bibliography

The radar search equation was first described by Barton (1965), and it is addressed in his books. Rotating search radar are treated in Skolnik. Search using phased-array radar is analyzed in Billetter, and in papers in the compendium by Brookner. The concept of choosing the search time to maximize the assured acquisition range was first addressed by Mallett and Brennan. A paper by Matthiesen analyzes the bow-tie search pattern for dish radar.

Barton, D. K., “Radar System Performance Charts,” *IEEE Trans. on Military Electronics*, Vol. MIL-9, Nos. 3 and 4, July–October 1965.

Barton, D. K., *Radar System Analysis*, Englewood Cliffs, NJ: Prentice Hall, 1964.

Barton, D. K., *Modern Radar System Analysis*, Norwood, MA: Artech House, 1988.

Billetter, D. R., *Multifunction Array Radar*, Norwood, MA: Artech House, 1989.

Brookner, E., (ed.), in *Practical Phased Array Antenna Systems*, Norwood, MA: Artech House, 1991.

Mallett, J. D., and L. E. Brennan, "Cumulative Probability of Detection for Targets Approaching a Uniformly Scanning Search Radar," *Proc. of the IEEE*, Vol. 81, No. 4, April 1963, pp. 595–601.

Mallett, J. D., and L. E. Brennan, "Correction to Cumulative Probability of Detection for Targets Approaching a Uniformly Scanning Search Radar," *Proc. of the IEEE*, Vol. 82, No. 6, April 1964, pp. 708–709.

Matthiesen, D. J., "Bow-Tie Search Theory and Design," *IEE International Radar Conference, Edinburgh, Scotland, Record*, 1997, pp. 775–782.

Skolnik, M. I., *Introduction to Radar Systems*, New York: McGraw-Hill, 1962.

Skolnik, M. I., *Introduction to Radar Systems*, 2nd ed., New York: McGraw-Hill, 1980.

Radar Measurement and Tracking

This chapter enables the reader to:

- Understand the radar measurement error sources and factors affecting the accuracy of radar measurements;
- Quantify the accuracy of radar measurements of target range, angle, and velocity;
- Know how target features are measured by radar, and quantify the accuracy of measuring common features;
- Understand the enhancement in measurement accuracy and other features provided by multiradar measurements and single-radar multilateration;
- Understand measurement-smoothing and target-tracking concepts, and common tracking implementation techniques.

While radar search and target detection are essential to radar use, most applications also require measurement of target characteristics. These may include target position and velocity, as described in Sections 8.1 through 8.3, and indicators of target size, shape and rotation, as described in Section 8.4. The use of multiple radar to improve measurement accuracy is discussed in Section 8.5. Combining radar measurements into target tracks, issues associated with radar tracking, and tracking methods are discussed in Sections 8.6 and 8.7.

Radar can provide measurement of target position in range and in two angular coordinates, relative to the radar location. The angular coordinates are usually defined as elevation angle relative to the local horizontal, and azimuth, which may be measured relative to true north, or for phased arrays, relative to array broadside azimuth. This measurement geometry is illustrated in Figure 8.1. Radars employing coherent processing may also directly measure the target radial velocity.

To measure target characteristics, the target must be resolved by the radar. This requires that the target be separated from other targets by the radar resolution in at least one of the measurement coordinates [1, pp. 3–6]. Radar resolution in angle is usually defined by the beamwidth in two orthogonal angular coordinates, usually azimuth and elevation (see Section 3.2). The required target separation, D , in an angular coordinate, often called cross-range separation, is given by:

$$D = R\theta \quad (8.1)$$

where θ is the radar beamwidth in the angular coordinate, and R is the target range.

Radar range resolution, R_r , is given by:

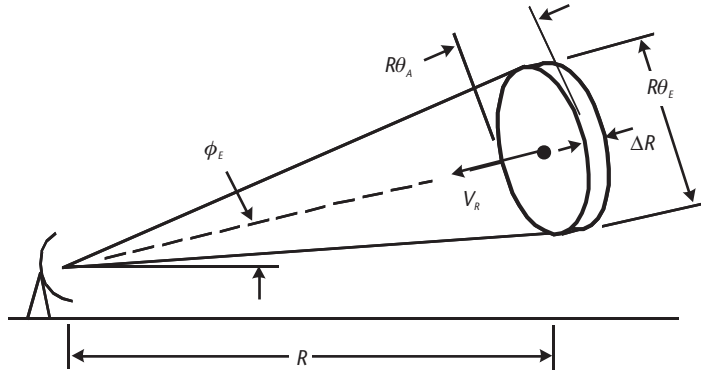


Figure 8.1 Geometry for radar measurement and target resolution.

$$\Delta R = \frac{c \tau_R}{2} = \frac{c}{2B} \quad (8.2)$$

where τ_R is the radar resolution in time, which is approximately equal to the reciprocal of the signal bandwidth, B (see Chapter 4). The geometry of the radar resolution cell is shown in Figure 8.1.

Targets that occupy the same range and angle resolution cell may be resolved in radial velocity by radars that employ coherent processing. The velocity resolution, ΔV , is given by:

$$\Delta V = \frac{\lambda f_R}{2} = \frac{\lambda}{2\tau} \quad (8.3)$$

where f_R is the Doppler-frequency resolution of the radar waveform, which is approximately equal to the reciprocal of the total waveform duration, τ (see Chapter 4).

Note that resolution is required in only one dimension to allow the measurement of target characteristics.

The accuracy with which a radar may measure a target characteristic is determined by several error sources:

- A S/N-dependent random measurement error. These errors vary with $(S/N)^{-1/2}$.
- A random measurement error having fixed standard deviation, due to noise sources in the latter stages of the radar receiver. These errors are usually small, and correspond to S/N-dependent errors produced at large S/N values. Thus, they set a limit on how far random errors may be reduced by increasing S/N.
- A bias error associated with the radar calibration and measurement process. These errors may vary randomly with drift in radar calibration, only with correlation times that are long compared with the usual radar observation period.
- Errors due to radar propagation conditions, or uncertainties in correcting for the propagation conditions, as discussed in Chapter 9. Components of these errors may vary randomly from observation to observation like the radar random measurement errors, or remain fixed for extended periods like the radar bias errors.

- Errors from interference sources such as radar clutter (see Sections 9.1 and 9.2), and radar jamming signals (see Sections 10.2 and 10.3).
- Errors due to target scintillation and glint (see Section 9.4).

The first three error sources above, S/N-dependent, fixed random, and bias, are discussed in this chapter. The errors from propagation, clutter, jamming, scintillation, and glint may be evaluated using techniques described elsewhere in this book and in the references. These errors may be combined with the S/N-dependent, fixed random, and bias errors to produce three major error components. This is illustrated by an example in Section 12.5.

The radar accuracy is characterized in the analyses in this section by the standard deviation of a Gaussian distribution, designated by σ , which reasonably models measurement-error distributions for many cases of interest [1, p. 201]. For many applications, it is appropriate to use multiples of σ to characterize the outer bound of the error distribution. The probability that a one-dimensional measurement will occur between several specified error bounds for this distribution is given in Table 8.1. For example, half the measurements will occur between $\pm 0.675 \sigma$. Only 1 in 370 measurements will occur outside a $\pm 3\text{-}\sigma$ bound.

8.1 Range Measurement Accuracy

A pulsed radar determines radar range, R , by measuring the time interval, t , between the transmitted and received signal:

$$R = ct/2 \quad (8.4)$$

In early radars, the receive time was measured by observing the pulse return on a display, such as an A scope. Some later radars use automatic range measurement, using two contiguous range gates, called early and late gates. When the energy in the two gates is equal, the crossover time between the gates is at the center of the received pulse. Many modern radars sample the received signal and determine the target range by fitting the sample data to a replica of the pulse, such as shown in Figure 4.1(a).

The range-measurement accuracy is characterized by the rms measurement error, σ_R , given by the root-sum-square (rss) of the three error components.

$$\sigma_R = (\sigma_{RN}^2 + \sigma_{RF}^2 + \sigma_{RB}^2)^{1/2} \quad (8.5)$$

Table 8.1 Error Bounds and Their Occurrence Probabilities for a Gaussian Distribution.

<i>Error Bound</i>	<i>Probability of Measurement Occurring Within the Error Bound</i>
0.675 σ	0.5
1 σ	0.683
2 σ	0.955
3 σ	0.997
4 σ	0.9994

where:

σ_{RN} = S/N -dependent random range measurement error;

σ_{RF} = range fixed random error, the rss of the radar fixed random range error and the random range error from propagation;

σ_{RB} = range bias error, the rss of the radar range bias error and the range bias error from propagation.

The S/N-dependent error usually dominates the radar range error. It is random, with a standard deviation given by:

$$\sigma_{RN} = \frac{\Delta R}{\sqrt{2(S/N)}} = \frac{c}{2B\sqrt{2(S/N)}} \quad (8.6)$$

For single-pulse measurements, the value of S/N in (8.6) is the single-pulse S/N (assuming S/N is large enough that the detection loss may be neglected; see Section 5.4).

When multiple pulses are used, the integrated S/N should be used in (8.6) [1, pp. 35–44 and 82–86]. This is given by (5.14) for coherent integration, and by (5.17) for noncoherent integration. With phased-array radar and dish-tracking radar, the target is usually assumed to be near the center of the beam, as discussed above. When it is not, an appropriate beamshape loss, L_{BS} , should be used in calculating S/N (see Chapter 7). With rotating search radar, measurements are made as the beam sweeps past the target, and a beamshape loss, L_{BS} (usually 1.6 dB), should be included in calculating S/N (see Section 7.1). If pulse integration produces a signal-processing loss, L_{SP} , the integrated S/N should be reduced by this loss (see Section 5.4).

The fixed random range error may limit the range measurement accuracy for large values of S/N. Internal radar noise typically produces an equivalent S/N of 25 to 35 dB, which results in random fixed errors of 1/25th to 1/80th of the range resolution. Random range errors due to propagation are usually small, except when multipath conditions exist (see Chapter 9).

The magnitude of radar range bias errors usually depends on the care taken to reduce them. Since bias errors are constant for a series of measurements, or for multiple targets in the same general area, they do not affect radar tracking or the relative locations of targets. Thus, little effort is made to reduce range bias errors in many radars, and they may have values of tens of meters. When absolute target position is important, careful calibration may reduce radar range bias errors to the level of fixed range random errors. Range bias errors from propagation conditions are usually small, and are discussed in Chapter 9.

For example, a radar having a waveform bandwidth, $B = 1$ MHz has a range resolution, $\Delta R = 150$ m. If the S/N (either single-pulse or integrated) is 15 dB, $\sigma_{RN} = 18.9$ m. If the fixed error, σ_{RF} , is 0.02 times the resolution (3 m), and the bias error, $\sigma_{RB} = 10$ m, the overall range-measurement accuracy, $\sigma_R = 21.6$ m. The relative error between observations or targets is calculated without the bias error: $\sigma_R = 19.1$ m.

Additional examples of range measurement error calculations are shown in Table 8.2. The second column shows the range error from using a single pulse at the S/N shown. The total error is the rss of the three components shown in the column. The corresponding relative error is shown in column 3. In this case, the bias error is

Table 8.2 Range Measurement Examples

<i>Parameter</i>	<i>Single Pulse</i>	<i>Single Pulse (Relative)</i>	<i>Coherent Integration</i>	<i>Noncoherent Integration</i>
ΔR	15m	15m	15m	15m
Pulse S/N	8 dB	8 dB	8 dB	8 dB
n	1	1	10	10
Integrated S/N	N/A	N/A	18 dB	17.4 dB
σ_{RN}	4.22m	4.22m	1.34m	1.44m
σ_{RF}	0.5m	0.5m	0.5m	0.5m
σ_{RB}	1.0m	N/A	1.0m	1.0m
σ_R	4.37m	4.25m	1.75m	1.82m

not included in the rss combination, leading to a lower error value. Columns 4 and 5 show the impact of pulse integration. Ten pulses are coherently integrated in column 4, and noncoherently integrated in column 5, giving the integrated S/N values shown. The S/N-dependent errors are calculated using these integrated S/N values, and the total error values calculated using these smaller S/N-dependent error values.

8.2 Angular Measurement Accuracy

Radar angular measurements are commonly made using monopulse receive antennas that produce simultaneous receive beams slightly offset in angle to either side of the transmit beam. The difference pattern formed by these beams may be used to measure target angular position with a single signal transmission, as described in Section 3.2.

Other angle-measurement techniques involve transmission and reception of multiple signals at different angles around the target. With rotating search radar, target angular position may be measured by finding the center of a series of pulse returns as the antenna sweeps past the target, as shown in Figure 7.1. Early tracking radar either used a similar technique, or transmitted in several beam positions around the target and found the angular position where the signal return was maximum. For nonfluctuating targets, these techniques may produce an angular measurement accuracy comparable to that of monopulse radar [1, pp. 33–35].

The measurement accuracy in each angular coordinate is characterized by the rms measurement error, σ_A , given by the rss of the three error components.

$$\sigma_A = (\sigma_{AN}^2 + \sigma_{AF}^2 + \sigma_{AB}^2)^{1/2} \quad (8.7)$$

where:

σ_{AN} = S/N -dependent random angular measurement error;

σ_{AF} = angular fixed random error, the rss of the radar fixed random angle error and the random angle error from propagation;

σ_{AB} = angle bias error, the rss of the radar angle bias error and the angle bias error from propagation.

The S/N-dependent error usually dominates the radar angle errors. It is random, with a standard deviation given for monopulse radar by:

$$\sigma_{AN} = \frac{\theta}{k_M \sqrt{2(S/N)}} \quad (8.8)$$

where θ is the radar beamwidth in the angular coordinate of the measurement, and k_M is the monopulse pattern difference slope (see Section 3.2). The value of k_M is typically 1.6 [1, pp. 24–32]. For single-pulse measurements, the single-pulse S/N is used in (8.8), while for multipulse measurements, the integrated S/N is used, as discussed in Section 8.1 for range-measurement accuracy. As in the previous discussion, signal-processing losses from integration and beamshape losses should be used, when appropriate, in calculating S/N.

Radar clutter and jamming may affect the radar sum and difference channels differently than Gaussian noise sources. In such cases, treating their impacts as contributions to S/N using (8.8) is not valid, and more complex analysis is needed for accurate results [1, pp. 135–142, 158–158, 215–229].

Equation (8.8) with a value of $k_M = 1.6$ also gives the approximate angular error for nonmonopulse radar that employ multipulse measurements of nonfluctuating targets [1, pp. 33–44]. Corrections for fluctuating targets employing multipulse measurements of nonmonopulse radar are discussed in [1, pp. 171–182].

As with range measurement, the fixed angular random errors may limit the angular measurement accuracy for large values of S/N. Typical internal radar noise levels discussed above would produce angular errors 1/40th to 1/125th of the beamwidth. This is sometimes referred to as a maximum beam-splitting ratio of 40 to 125. Random angular errors due to propagation are usually small (see Chapter 9).

The magnitude of radar angular bias errors depends on the care taken to reduce them. Since bias errors are constant for a series of measurements, or for multiple targets in the same general area, they do not affect radar tracking or the relative locations of targets. With careful calibration, radar angular bias errors from radar calibration may be reduced to the level of fixed angular errors. Angular bias errors from propagation may be significant if not corrected, especially elevation-angle errors at low elevation angles, as discussed in Chapter 9. The radar alignment errors may be reduced by tracking targets with known locations, or by tracking satellites over a portion of their trajectories. Tropospheric propagation errors may be reduced by correcting for known or estimated conditions, as discussed in Section 9.3.

For example, for an azimuth radar beamwidth of 1 degree and S/N = 12 dB, $\sigma_{AN} = 0.11$ degrees, or 1.9 mrad. If $\sigma_{AF} = 0.2$ mrad, and $\sigma_{AB} = 0.5$ mrad, then the overall azimuth measurement error is $\sigma_A = 2.0$ mrad.

Another angular error source, not analyzed here, is target glint. Glint is the effect of target scatterers separated in the cross-range direction producing fluctuations of the apparent angle-of-arrival of the signal return. These may exceed the angular extent of the target, and may be a major source of angular error at short ranges (e.g., with target-seeking radar) [1, pp. 164–171].

With phased-array radar, the parameters that determine angular measurement errors may vary with the beam scan angle off-broadside. The array beamwidth, θ_d , in an angular coordinate at a scan angle off-broadside of φ in that coordinate is given by:

$$\theta_{\varphi} = \theta_B / \cos \varphi \quad (8.9)$$

where θ_B is the broadside beamwidth in the angular coordinate (see Section 3.3).

The fixed and bias angular errors, σ_{AF} and σ_{AB} , may have components that are both independent of scan angle, and scan-dependent components that are defined in sine space [2, pp. 2–19]. The latter produce angular measurement errors that are approximately proportional to $1/\cos \varphi$. Errors that are independent of scan angle may include atmospheric errors and bias errors from unknown array orientation. Scan-dependent errors may result from errors in element spacing and relative phasing. The value of the error at a particular scan angle is the rss of the nonvarying and the varying error components.

In the previous example, if the azimuth scan angle off-broadside is 30 degrees, the azimuth beamwidth increases to 1.15 degrees and $\sigma_{AN} = 2.2$ mrad. If an additional scan-dependent fixed random error component is $0.0001 \sin \varphi$ (often called 0.1 msine), $\sigma_{AF} = (0.20^2 + 0.11^2)^{1/2} = 0.23$ mrad. Similarly, with an additional scan-dependent azimuth bias error of 0.3 msine, $\sigma_{AB} = 0.61$ mrad. The overall azimuth measurement error, $\sigma_A = 2.3$ mrad.

These angle-measurement error examples are summarized in Table 8.3. The measurement and error parameters are given in the first column. The errors for a dish radar are calculated in column 2, where the beam is not broadened by off-broadside scan, and the scan-dependent errors do not apply. The S/N-dependent error is 1.9 mrad, and the overall error is found by rss in combination with the fixed random and bias error values. Column 3 shows the results for a phased array. The beamwidth at 30° scan angle is 1.15°, and the S/N dependent error increases to 2.2 mrad (assuming the S/N remains at 12 dB). The fixed random and bias errors are found by rss combining the nonscan-dependent and scan-dependent components, and the resulting overall error is calculated as the rss of these terms.

Depending on the accuracy required, the angular measurement error components may be calculated at each scan angle of interest, or average values may be used.

The measurement error normal to the radar LOS, called the cross-range error, is found by multiplying the angular measurement error (in radians), by the target

Table 8.3 Examples of Angle-Measurement Errors

<i>Parameter</i>	<i>Dish Radar</i>	<i>Array Radar</i>
θ	1°	1° (broadside)
φ	N/A	30°
θ_{φ}	N/A	1.15°
S/N	12 dB	12 dB
σ_{AN}	1.9 mrad	2.2 mrad
Fixed	0.2 mrad	0.2 mrad
Scan-dependent fixed	N/A	0.1 msine
σ_{AF}	0.2 mrad	0.23 mrad
Bias	0.5 mrad	0.5 mrad
Scan-dependent bias	N/A	0.3 msine
σ_{AB}	0.5 mrad	0.61 mrad
σ_A	2.0 mrad	2.3 mrad

range. The error in measuring the cross-range target position in an angular coordinate direction, σ_D , is given by:

$$\sigma_D = R\sigma_A \quad (8.10)$$

The resulting target uncertainty volume has standard deviations in the cross-range dimensions of $R_{\sigma A1}$ and $R_{\sigma A2}$, where the numbers refer to the orthogonal angular coordinates, and a standard deviation in the range dimension σ_R . For most radars, the cross-range errors that result from angular-measurement errors at useful ranges far exceed the range-measurement errors. The resulting target uncertainty volume is a relatively flat, circular, or elliptical disk that is normal to the radar LOS, as illustrated in Figure 8.1.

8.3 Velocity Measurement Accuracy

Target radial velocity may be measured in two ways:

- From the Doppler-frequency shift of the received signal;
- From multiple range measurements.

Measurements using Doppler-frequency shift almost always give significantly better accuracy than noncoherent processing of range measurements.

A coherent radar may measure the target radial velocity, V_R , from the Doppler-frequency shift of the received signal:

$$V_R = \lambda f_D / 2 \quad (8.11)$$

where f_D is the Doppler-frequency shift and λ is the radar signal wavelength.

The radial-velocity measurement accuracy from measuring Doppler-frequency shift is characterized by the rms measurement error, σ_V , given by the rss of the three error components.

$$\sigma_V = (\sigma_{VN}^2 + \sigma_{VF}^2 + \sigma_{VB}^2)^{1/2} \quad (8.12)$$

where:

- σ_{VN} = S/N -dependent random radial-velocity measurement error;
- σ_{VF} = radial-velocity fixed random error, the rss of the radar fixed random radial-velocity error, and the random radial-velocity error from propagation;
- σ_{VB} = radial-velocity bias error, the rss of the radar radial-velocity bias error, and the radial-velocity bias error from propagation.

The S/N-dependent error usually dominates the radar radial-velocity error. It is random, with a standard deviation given by [1, pp. 101–103]:

$$\sigma_{VN} = \frac{\lambda}{2\tau\sqrt{2(S/N)}} = \frac{\Delta V}{\sqrt{2(S/N)}} \quad (8.13)$$

where τ is the duration of the radar waveform that is coherently processed, and ΔV is the radial-velocity resolution given by (8.3). As with the measurements in the previous two sections, the single-pulse or integrated S/N may be used, and appropriate integration processing and beamshape losses should be applied.

The fixed random radial-velocity error may limit the measurement accuracy for very large values of S/N. Random radial-velocity errors due to propagation are usually small. The magnitude of radar radial-velocity bias errors depends on the care taken to reduce them. With careful calibration, they may be reduced to the level of random radial-velocity errors. Bias errors from propagation conditions are usually small, as discussed in Chapter 9.

The target radial velocity also may be found from the difference of two range measurements, divided by the time between the measurements:

$$V_R = \frac{R_1 - R_2}{t_1 - t_2} \quad (8.14)$$

where R_1 and R_2 are the ranges and t_1 and t_2 are the respective measurement times. The resulting radial-velocity accuracy is given by [1, p. 356]:

$$\sigma_V = \frac{\sqrt{2} \sigma_R}{(t_1 - t_2)} \quad (\text{two pulse}) \quad (8.15)$$

The bias error, σ_{RB} , should not be included in σ_R for this calculation, since it will be constant for the two measurements.

For n periodic measurements over a time period, t_N , this result may be extended to [1, p. 357]:

$$\sigma_V = \frac{\sqrt{12} \sigma_R}{\sqrt{n} t_N} \quad (\text{pulse train, } n \geq 6) \quad (8.16)$$

The PRF for these parameters is equal to n/t_N . This result is for a pulse train having many pulses. For $n < 6$, (8.15) calculates a smaller error than does (8.16), and should be used.

For comparable processing times, the measurement of Doppler frequency provides much greater accuracy in V_R than the noncoherent modes described above. For example, at S band ($\lambda = 0.09\text{m}$), with a pulse duration $\tau = 1\text{ ms}$ and $S/N = 15\text{ dB}$, $\sigma_{VN} = 5.7\text{ m/s}$ using Doppler processing. Assuming a range resolution of 15m ($B = 10\text{ MHz}$), and $S/N = 15\text{ dB}$, $\sigma_{RN} = 1.9\text{m}$. Two pulses separated by 1 ms will give $\sigma_{VN} = 2,680\text{ m/s}$, far greater than the error with Doppler processing. The two pulses would have to be separated by 471 ms to provide accuracy comparable to that using Doppler processing. Using these pulses at a PRF of $1,000\text{ Hz}$, 110 pulses over a period of 110 ms would be needed to provide the same radial-velocity accuracy as Doppler processing.

These examples are summarized in Table 8.4. The coherent Doppler measurement parameters are given in the second column of the table. The velocity resolution is 45 m/s , and the S/N dependent random Doppler-velocity measurement error in the column is shown to be 5.7 m/s . When multiple range measurements are used, the S/N-dependent random range error in column 3 is shown to be 1.9m . For two pulses

Table 8.4 Radial-Velocity Measurement Examples

<i>Parameter</i>	<i>Doppler Velocity</i>	<i>2-Pulse Range</i>	<i>Multipulse Range</i>
λ	0.09m	N/A	N/A
τ	1 ms	N/A	N/A
ΔV	45 m/s	N/A	N/A
S/N	15 dB	15 dB	15 dB
ΔR	N/A	15m	15m
σ_{RN}	N/A	1.9m	1.9m
Pulse Separation	N/A	1 ms	N/A
Number of Pulses	N/A	2	110
PRF	N/A	N/A	1,000 Hz
$t_1 - t_2$ or t_N	N/A	1 ms	110 ms
σ_{VN}	5.7 m/s	2,680 m/s	5.7 m/s

separated by 1 ms, the resulting radial velocity error is 2,680 m/s, as shown in column 3. Column 4 shows the result when 110 pulses are used over a period of 110 ms. The measurement error is then 5.7 m/s, which is equal to the error with a single pulse when using Doppler measurement.

The preceding has addressed radial-velocity measurement. Angular or cross-range velocity measurements may be made using the noncoherent measurement techniques described above and in (8.14) to 8.16). The resulting cross-range velocity accuracy, σ_c , is given by:

$$\sigma_c = \frac{\sqrt{2}R\sigma_A}{(t_2 - t_1)} \quad (\text{two pulse}) \quad (8.17)$$

$$\sigma_c = \frac{\sqrt{12}R\sigma_A}{\sqrt{n}t_N} \quad (\text{pulse train, } n \geq 6) \quad (8.18)$$

The values of φ_A should be calculated without the angular bias, φ_{AB}

As with position measurement, the angular or cross-range velocity errors usually far exceed the radial-velocity error. This is especially true when coherent processing is used to measure radial velocity from target Doppler shift.

8.4 Measurement of Target Features

Radar can measure a number of target features. Such measurements may allow the class of target or perhaps even the type of target to be identified. The following paragraphs describe several common radar measurements:

- Target RCS, measured from the amplitude of the return signal;
- Target radial length, measured from the time duration of the returned signal;
- Target rotational velocity, measured by the Doppler-frequency spread of the returned signal.

Additional information on the target may be inferred from the variation of these measurements with time. The interpretation of radar measurements of target characteristics is a complex process that will not be addressed here. This is not intended as a comprehensive list of potential measurements of target features, which would be beyond the scope of this book.

The target RCS may be determined by measuring the returned S/N and calculating the RCS from the radar equation (see Section 5.1). The RCS measurement accuracy is characterized by the rms measurement error, σ_s , given by the rss of the three error components.

$$\sigma_s = (\sigma_{SN}^2 + \sigma_{SF}^2 + \sigma_{SB}^2)^{1/2} \quad (8.19)$$

where:

σ_{SN} = S/N-dependent random RCS measurement error;

σ_{SF} = RCS fixed random error, the rss of the radar fixed random RCS error, and the random RCS error from propagation;

σ_{SB} = RCS bias error, the rss of the radar RCS bias error, and the RCS bias error from propagation.

The S/N-dependent RCS error is proportional to the error in measuring the received power. It is random, with a standard deviation approximately given by [3, pp. 4-1–4-8]:

$$\sigma_{SN} \approx \frac{\sqrt{2} \sigma}{\sqrt{(S/N)}} \quad (8.20)$$

where σ in the numerator refers to the target RCS. As with the measurement errors discussed in the previous sections, either the single-pulse or integrated S/N may be used in (8.20). Any losses for beamshape and integration processing will affect both the S/N value and the calculation of RCS.

For example, with S/N = 20 dB, the standard deviation of the S/N dependent error is $\pm 14\%$. If the RCS value is 10 m², the standard deviation is ± 1.4 m².

The random fixed errors and random propagation errors will usually be small, as discussed earlier. Bias errors in RCS measurement result when the radar parameters used to calculate the RCS are not accurately known. These may be significant unless care is taken to calibrate the radar. Such bias errors also may be reduced by calibrating the radar using a target of known RCS value. If the radar parameters (e.g., transmitter peak power) drift with time, frequent calibration may be necessary, and some RCS bias may be produced. RCS bias errors may also be produced by atmospheric and rain attenuation (discussed in Chapter 9). These errors may be reduced by estimating the attenuation, but the accuracy of doing this may be questionable, especially with rain. Note that RCS-measurement bias errors caused by uncorrected signal-path attenuation or changes in radar parameters are factors multiplying RCS.

Target RCS may depend on the transmitted and received signal polarizations. Most radars that transmit linear polarization receive the same-sense linear polarization, and those that transmit circular polarization receive the opposite-sense circu-

lar polarization. These are often referred to as the principal receive polarizations. Some radar also have the capability to receive the orthogonal polarization, either using two receivers, or on successive pulses with a single receiver. A few radars also have the capability for transmitting two orthogonal polarizations on successive pulses. The RCS measurements made by these radars may provide additional information on target characteristics [4, pp. 13–21].

Target length in the radial dimension may be measured by radar having range resolution, ΔR , that is less than the target radial dimension, a . This is illustrated in Figure 8.2 for a target having two scatterers that are resolved in range [Figure 8.2(a)], and for a target having several scatterers that are not resolved [Figure 8.2(b)]. In the first case, the range of each scatterer may be measured and the target radial length is determined by their range separation:

$$a = R_2 - R_1 \quad (8.21)$$

where the subscripts correspond to the two measurements.

The accuracy of each range measurement is given by (8.5), and the accuracy of the radial length measurement, σ_L , is given by:

$$\sigma_L = (\sigma_{R1}^2 + \sigma_{R2}^2)^{1/2} \quad (8.22)$$

where the accuracies of the two measurements may be different due to differences in the S/N for the two scatterers. Since the bias errors, σ_{RB} , will be the same for both measurements, they should not be used in calculating the range measurement errors.

When the individual target scatterers cannot be resolved, as shown in Figure 8.2(b), the accuracy of the radial length measurement cannot be evaluated with precision. However, it may be approximated, using an average value of the S/N for cal-

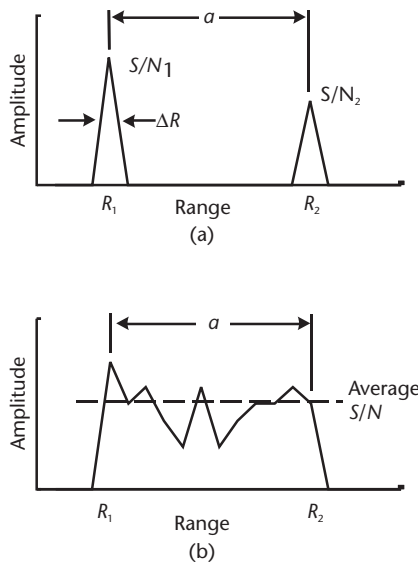


Figure 8.2 Target signal returns as a function of range for a radar waveform having range resolution less than the target radial dimension. (a) Resolved scatterers. (b) Unresolved scatterers.

culating the range measurement error, σ_R . The resulting length-measurement accuracy may be estimated by:

$$\sigma_L \approx \sqrt{2} \sigma_R \quad (8.23)$$

The spread in Doppler-frequency shift in the signal return from a target is determined by the relative radial velocities of the target scatterers. This is illustrated in Figure 8.3(a) for a disk or cylinder with diameter a , having scatterers at its periphery, and rotating with an angular velocity ω_T . If the angle between the radar LOS and the target rotational axis is γ , ΔV_R is given by:

$$\Delta V_R = a \omega_T \sin \gamma \quad (8.24)$$

The resulting spread in the target Doppler-frequency shift, Δf_D , is illustrated in Figure 8.3(b), and is given by:

$$\Delta f_D = \frac{2a\omega_T f}{c} \sin \gamma \quad (8.25)$$

For example, for a cylindrical target having a diameter of 2m, rotating at one rpm ($\omega = 2\pi/60$), and with the rotation axis 30 degrees from the radar LOS, $\Delta V_R = 0.105$ m/s. At C band (5.5 GHz), the resulting Doppler-frequency spread, $\Delta f_D = 3.8$ Hz.

To measure the spread in Doppler-frequency shift, Δf_D , the waveform frequency resolution, f_R , must be smaller than Δf_D , or equivalently, the waveform velocity resolution, ΔV , must be smaller than the target radial velocity spread, ΔV_R . In addition, if the radar waveform has velocity ambiguities, they must be separated by an amount greater than ΔV_R (see Section 4.5 and Figure 4.9). The accuracy of measurement of the Doppler-frequency spread, σ_{f_D} , is determined similarly to that of the target length. When the scatterers are not resolved, it is given by:

$$\sigma_F \approx \sqrt{2} \sigma_V \quad (8.26)$$

A more complex measurement, called range-Doppler imaging, involves generating a two-dimensional plot of signal return versus radial range and radial Doppler

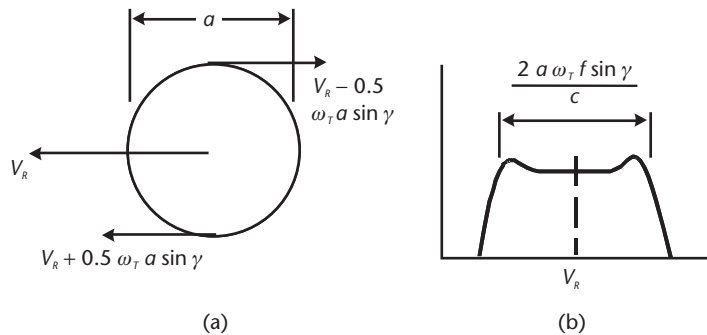


Figure 8.3 Target rotational geometry and the resulting Doppler-frequency spectrum. (a) Rotational geometry. (b) Spectrum.

velocity for a rotating target. In each resolvable range cell, a spectrum similar to that shown in Figure 8.3(b) is generated. The position of scatterers in this spectrum corresponds to their locations on the target. The target scatterers on this plot may be interpreted as a target image in the range and cross-range dimensions. Range-Doppler imaging may be used to determine the configuration of rotating objects. It may also be used on stationary objects when the LOS rotation is produced by a moving radar.

8.5 Multiradar Measurements

The use of two or more radars to measure target characteristics may offer a number of advantages. These include:

- Improved position and velocity accuracy by using multiple-range and radial-velocity measurements to reduce cross-range measurement errors;
- Target feature measurements from multiple viewing angles and at multiple frequencies;
- Increased opportunity for providing favorable location, measurement geometry, and radar frequency for making radar measurements.

The accuracy improvements provided by the first item above is addressed in this section. The last two factors depend on details of the system application.

In most pulsed radars, the range accuracy is significantly better than the cross-range accuracy (the angular accuracy multiplied by the target range). Similarly, the radial-velocity accuracy is significantly better than the cross-range velocity accuracy. When two or more radars observe the target, their range measurements may be combined to greatly improve the overall position and velocity measurement accuracy. This technique is sometimes called multilateration.

This is illustrated in Figure 8.4, which shows two radars observing a target with LOS that are separated by an angle α . The two radars have range measurement errors of σ_{R1} and σ_{R2} . The cross-range errors are large, so the target position uncertainty for each radar is shown by parallel lines. The position measurement error in

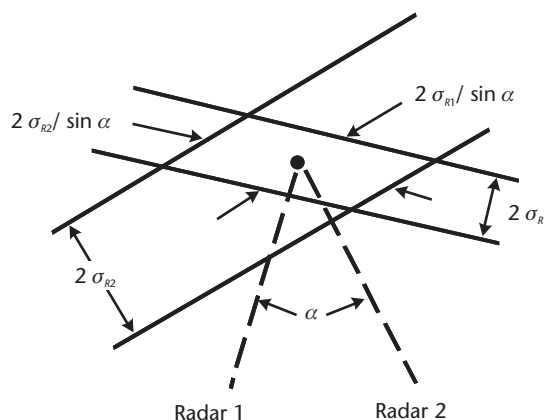


Figure 8.4 Geometry for target position determination using range measurements by two radar.

the plane defined by the radars and the target is shown in the figure. The maximum position measurement error in this plane, σ_{PD} , is approximately given by:

$$\sigma_{PD} \approx \frac{\sigma_R}{\sin \alpha} \quad (8.27)$$

where σ_R is the larger of the two range measurement errors.

For the most favorable geometry, $\alpha = 90^\circ$, and $\sigma_{PD} = \sigma_R$. When α is less than 90° , the measurement error increases. This is sometimes referred to as geometric dilution of precision (GDOP). When α approaches zero, there is no longer any benefit to using two radars. Then the error from (8.27) becomes very large, and the cross-range accuracy is determined by the radar angular measurement error.

A similar result is obtained for measuring target velocity in the plane defined by the radars and the target. The maximum target velocity error in the plane, σ_{VD} , is approximately given by:

$$\sigma_{VD} \approx \frac{\sigma_V}{\sin \alpha} \quad (8.28)$$

where σ_V is larger of the two radial velocity measurement errors.

For example, if two radars observe a target with aspect angles that differ by 45° and have range-measurement accuracies of 1.5m and 3.0m, the resulting maximum position error in the plane of the radars and target is approximately 4.2m. If the two radial velocity-measurement accuracies are 5 m/s and 2 m/s, the resulting radial velocity measurement error is approximately 7.1 m/s.

The measurement-error reduction discussed above occurs in the plane defined by the target and the radars. Adding radars in that plane may further reduce the measurement errors in that plane, but will not affect the out-of-plane cross-range errors. This is often approximately the situation for several ground-based radars observing surface or low-altitude airborne targets. Reducing the out-of-plane errors using this technique requires adding one or more radar well out of the plane defined by the other radars and the target. The accuracy provided by these may be analyzed by defining other planes containing two or more radars and the target.

The preceding analyses assume that the radar measurements are made simultaneously, or that the target is stationery. This requirement may be relaxed when radar measurements are smoothed or processed in a tracking filter, as described in the following section.

Under some circumstances, a single radar may be used to provide the advantages of multilateration. For example, a radar flying past a fixed ground target may provide multilateration measurements. Similarly, a fixed radar may provide multilateration measurements on a target flying past the radar. In this latter case, the characteristics of the target path must be known (or estimated) to correctly combine the radar measurements. This technique may be used on targets assumed to fly straight paths, and on missiles and satellites on ballistic trajectories.

Use of multiple radars for target measurement assumes that the measurements on a target by the multiple radars may be correctly associated with that target. This is usually possible when a single target is in the beam of each radar. When multiple targets are in the radar beam, incorrect measurement associations may occur, and

ghost targets may be generated. This is analogous to the ghosting problem for passive tracking, discussed in Chapter 10.

8.6 Measurement Smoothing and Tracking

Radar measurement data may be smoothed to increase the measurement accuracy, estimate target trajectory parameters, and predict future target position. The combining of two or more measurements to determine radial and cross-range velocity is discussed in Section 8.3, and the resulting measurement accuracies are given in (8.15) through (8.18).

The random components of radar position measurements may be reduced by averaging measurements. For example, when n range measurements are combined, the resulting smoothed range error, σ_{RS} , is given by:

$$\sigma_{RS} = \left(\frac{\sigma_{RN}^2 + \sigma_{RF}^2}{n} + \sigma_{RB}^2 \right)^{1/2} \quad (8.29)$$

The S/N-dependent random error and the random fixed range error are reduced by $n^{1/2}$. The bias error is not reduced by smoothing. It should not be included in the calculation when relative range measurements are considered, as discussed in Section 8.1. Note that measurement errors from radar clutter may not be independent from measurement-to-measurement, and thus may not be reduced by $n^{1/2}$ [1, pp. 136–142].

For the example given in Section 8.1, if 20 range measurements are averaged, the S/N-dependent random range error is reduced from 18.9m to 4.2m, and the fixed random range error is reduced from 3m to 0.7m. The resulting range-measurement accuracy from (8.29) is 10.9m, compared to 21.6m with no smoothing. The smoothed measurement error is seen to be dominated by the 10m bias error, which is not reduced by smoothing. If this bias term is not included, the measurement error with smoothing is 4.3m.

The smoothed angular measurement error, σ_{AS} , is similarly given by:

$$\sigma_{AS} = \left(\frac{\sigma_{AN}^2 + \sigma_{AF}^2}{n} + \sigma_{AB}^2 \right)^{1/2} \quad (8.30)$$

Future target position may be predicted, based on measurements of position and velocity. For a prediction time, t_p , the accuracy of the predicted range position, σ_{PR} , and cross-range position, σ_{PC} , are given by:

$$\sigma_{PR} = \left[\sigma_R^2 + (\sigma_V t_p)^2 \right]^{1/2} \quad (\text{non-maneuvering}) \quad (8.31)$$

$$\sigma_{PC} = \left[(R\sigma_A)^2 + (\sigma_C t_p)^2 \right]^{1/2} \quad (\text{non-maneuvering}) \quad (8.32)$$

Equations (8.31) and (8.32) assume that the target velocity remains constant during the prediction time, and that the observation geometry does not change significantly during this time. They are therefore valid only for relatively short prediction periods. For longer time periods, the LOS to the target may rotate, so that a cross-range prediction error component appears in the range direction.

For long prediction times, the predicted error due to velocity measurement [the second term in (8.31) and (8.32)] usually dominates the prediction accuracy, and the errors due to angular measurement errors are usually much greater than the range measurement errors. The largest semi-axis of the predicted target position error ellipsoid, σ_p , is then given approximately by:

$$\sigma_p \approx \sigma_c t_p = \frac{\sqrt{12} R \sigma_A t_p}{\sqrt{n} t_N} \quad (\text{non-maneuvering}) \quad (8.33)$$

where σ_c and σ_A are the larger of the two cross-range and angular measurement errors, respectively. When the target velocity remains constant, (8.33) may be used for long prediction times. It may also be used for predicting the position errors of orbital targets, whose flight paths follow Keplerian laws, but with less accuracy, due to the effect of orbital mechanics on the shape and orientation of the error ellipsoid.

For the angle-measurement example given in Section 8.2, the azimuth error (excluding bias error) is 2 mrad. Assuming that this error is larger than the elevation error, if the angular velocity is measured by 30 pulses at a 10-Hz rate over a period of 3 sec at a target range of 100 km, the predicted target position error for a prediction time of 50 sec is 2.11 km.

The preceding discussion has dealt with nonmaneuvering targets. These include aircraft with straight, level, and constant-velocity flight paths, and exoatmospheric objects in Keplerian orbits. The measurements on such targets may be smoothed over long periods of time to reduce the random error components, as indicated by (8.29) and (8.30), and their positions may be predicted well into the future, as indicated by (8.33). Many other targets may have random maneuvers or other accelerations. The measurement-smoothing times and prediction times for these targets are limited by their acceleration characteristics [5, p. 459].

Tracking filters are usually used for smoothing the measurements and predicting the future positions of maneuvering targets. Simple tracking filters use fixed smoothing coefficients. The α - β filter uses an α parameter for smoothing target position, and a β parameter for smoothing target velocity. The values of these parameters are a compromise between providing good smoothing to reduce random measurement errors, and providing rapid response to target maneuvers. Target acceleration may produce a dynamic-lag error in such filters that may dominate the total error in some cases. Some such filters add a third parameter, γ , for smoothing target acceleration [6, pp. 184–186].

In Kalman filters, the radar measurements are matched to a model of the measurement errors and target dynamics. If these are accurately modeled, the Kalman filter will minimize the mean-square measurement error. Kalman filters are somewhat more complex to implement than fixed-parameter filters, but they are widely used in modern radar because of their capabilities for dealing with missing data, variable

measurement noise, and variable target dynamics [7, pp. 19–44]. Radars such as dish-tracking radars continuously observe a target and provide measurements at a high data rate. Other radars may be limited in the measurement rate they provide on a target. For example, rotating search radars operate in a track-while-scan (TWS) mode discussed below, and generate a measurement in each rotational period. Such low measurement rates may limit the accuracy provided by the tracking filter on maneuvering targets [5, pp. 445–446].

Multifunction phased-array radars may limit the measurement rate in order to track multiple targets or perform other radar functions. However, the tracking rate must be high enough to provide the required tracking accuracy for maneuvering targets, and to assure that the radar does not lose track of the target between observations. Phased-array radars usually illuminate the predicted target position with a beam. For successful tracking, the target should appear within that beam most of the time.

The error in predicting the target position is approximately given by the rss of the cross-range target prediction error, given in (8.32), and by the error due to target maneuver. For a maximum target acceleration of a_T , the error in predicting target position due to maneuver, σ_M , is given by:

$$\sigma_M = \frac{a_T t_p^2}{2} \quad (8.34)$$

To assure that the predicted target position is within the radar beam for most observations the $3\text{-}\sigma$ value of the total prediction error should be less than half the beamwidth times the radar range:

$$\left[(\sigma_C t_p)^2 + \left(\frac{a_T t_p^2}{2} \right)^2 \right]^{1/2} \leq \frac{R\theta}{6} \quad (8.35)$$

When multiple targets are in track by a radar, it is important that new measurements be associated with the correct target track. This is often done using a nearest-neighbor assignment of new measurements. However, for closely spaced targets, a technique that incorporates all target observations in the neighborhood of the predicted target position is sometimes used [7, pp. 9–10]. Association of target measurements may be improved by increasing the measurement rate above that which is needed to maintain track on a single target.

8.7 Radar Tracking Techniques

Many techniques are used to implement tracking in radar systems. In early rotating surveillance radars (see Section 7.2), the target positions on successive scans were marked on a PPI display, and the positions connected. Later, digital processing provided automatic measurement of target position and calculation of target course and speed. Such techniques are called track-while-scan (TWS).

Dish-tracking radars usually employ a measurement technique to determine the target offset from the beam center. These include:

- Sequential lobing, where successive beams are transmitted and received slightly offset in angle from the main beam;
- Conical scan, where the antenna scans a small cone around the target position;
- Monopulse measurement, where target angular position is measured with a single pulse by using difference antenna patterns (see Section 3.2).

A servo is used to direct and maintain the antenna pointing in the direction of the target. The angular tracking filter parameters are incorporated into the servo control loop.

Phased-array radars often track many targets simultaneously, and have great flexibility in determining when tracking measurements are made. These radars usually use monopulse angular measurements. The tracking filter is implemented in a digital computer, which also controls the radar measurement process. Many such radars use recursive Kalman filters for tracking, but others collect the radar data and employ batch processing.

When multiple radars in a system are observing a target, the tracking filter may use measurement data from more than one radar. This may provide the advantages of multilateration, described in Section 8.5, as well as more frequent track updates and the possibility of more favorable measurement geometry. Such multiradar tracking may employ fusion of individual radar tracks, or it may combine all collected measurement data into a single track. Critical issues in implementing such techniques include accurate knowledge of relative position and orientation of all radars, radar calibration (especially reduction of bias errors), and correct association of targets between radar.

8.8 Problems

The following problems are provided to assist in reviewing this chapter and to ensure a basic understanding of the material. For maximum benefit, the problems should first be solved without using the VBA custom radar functions. Solutions to these problems are given in Appendix E, Section E.8.

1. In how many dimensions must a target be resolved from other targets in order to make measurements on it?
2. A radar has a range resolution of 15m (bandwidth = 10 MHz), a fixed random range error of 1m, and a range bias error of 5m. If the $S/N = 18$ dB, what are the standard deviations of the relative and of the absolute range errors? What are the $3\text{-}\sigma$ values of these errors? What is the $3\text{-}\sigma$ absolute range-measurement error if 50 pulses are smoothed to make the measurement?

3. A phased-array radar has a beamwidth on broadside of 2.5 degrees, a fixed random angle error of 2 mrad, a fixed scan-dependent random angle error of 1 msine, an angle bias error of 3 mrad, and a scan-dependent angle bias error of 1.5 msine. If the $S/N = 12$ dB, what is the $1\text{-}\sigma$ angular measurement error on broadside? What is the error at a 30-degree scan angle? What is the cross-range measurement error at a range of 150 km for these cases?
4. An X-band radar (9.5 GHz), has a pulse duration of 1 ms and a pulse-compression ratio of 1,000. If the $S/N = 15$ dB, what is the error in measuring radial velocity using Doppler-frequency shift? What is the accuracy of measuring radial velocity noncoherently using two such pulses separated by 20 ms? Neglect fixed random and bias errors.
5. A radar observes a target having $RCS = 10 \text{ m}^2$ with $S/N = 18$ dB. If the fixed random measurement error is 5% of the RCS, what is the RCS measurement error, neglecting bias? If rain attenuation of 2 dB is not accounted for in the radar calibration, what is the resulting RCS measurement bias error? What is the overall measurement error?
6. A radar has range resolution of 15m and beamwidth of 1.5 degrees. It makes 20 periodic measurements on the target at a range of 200 km over a total period of 10 sec, with $S/N = 12$ dB for each measurement. What are the measurement errors for range, angle, radial velocity (noncoherent measurements), and cross-range velocity? What are the predicted position errors in range and cross-range, if the prediction time is 50 sec? Neglect fixed random and bias errors.
7. For a one-dimensional Gaussian error distribution, what error bound will include all but 4.5% of the observations?
8. A dish radar observes a target with $S/N = 12$ dB. The signal bandwidth is 10 MHz, the fixed range error is 2m, and the range bias error is 10m. The beamwidth is 2 degrees, the fixed angle error is 1 mrad, and the angle bias error is 1.5 mrad. The waveform duration is 10 ms, the frequency is 9.5 GHz (X band), the fixed radial-velocity error is 0.2 m/s, and the radial velocity bias error is 0.1 m/s.
 - a. Find the $3\text{-}\sigma$ errors in absolute and relative range, angle and radial-velocity (from Doppler-frequency measurement).
 - b. Find the $3\text{-}\sigma$ absolute and relative cross-range measurement errors at 500 km range.
 - c. Find the $3\text{-}\sigma$ absolute and relative range and angle measurement errors when 10 measurements are averaged.
 - d. Find the $3\text{-}\sigma$ radial and cross-range velocity errors when 10 pulses are used at a PRF of 5 Hz, at a target range of 500 km. Assume radial velocity is obtained from range measurements.
9. Find the $1\text{-}\sigma$ angular-measurement error for a phased array when the beam is scanned at an angle of 45 degrees in the angular measurement coordinate. The broadside beamwidth is 1 degree, $S/N = 15$ dB, the fixed errors are 0.2 mrad and 0.3 msine (scan-dependent), and the bias errors are 0.1 mrad and 0.2 msine (scan-dependent).

10. What is the $1\text{-}\sigma$ radial length measurement error for a radar having 0.5m range resolution, $S/N = 20$ dB, and fixed range error of 0.1m? What is the impact of decreasing S/N to 12 dB?
11. Consider two identical radars viewing a target with LOS separated by 45 degrees. The S/N for the two radars are 20 dB and 12 dB. Both radars have range resolution 20m, fixed range error 1m, range bias error 1.5m, velocity resolution 10 m/s, fixed velocity error 0.5 m/s, and velocity bias error 0.7 m/s. Find the approximate maximum $3\text{-}\sigma$ position and velocity errors.
12. A radar has azimuth and elevation beamwidths of 1 and 3 degrees, respectively. It observes a nonmaneuvering target at a range of 500 km for 10 sec at a PRF of 5 Hz, and $S/N = 12$ dB. What is the $3\text{-}\sigma$ value of the largest error semi-axis, predicted 150 sec after the observation period? Neglect fixed and bias errors.

8.9 VBA Software Functions for Radar Measurement and Tracking

8.9.1 Function RangeError_m

Purpose Calculates the standard deviation of the radar range-measurement error.

Reference Equations (8.5), (8.6), and (8.29).

Features Combines calculated S/N -dependent random range error with fixed random range error and range bias error. Range bias error may be omitted to calculate the relative range error. Smoothing of random error components over multiple measurements may be modeled.

Input Parameters (with units specified)

RangeRes_m = radar range resolution (m). A value of $1/B$ may be used, where B is the radar signal bandwidth.

SNR_dB = measurement S/N (dB). This may be the single-pulse S/N or integrated S/N as appropriate. The value input should take into account any beamshape loss or additional signal-processing loss for pulse integration. For single-pulse S/N values less than about 12 dB, the detection loss (5.16) should also be included.

RangeFixEr_m = composite fixed random range error (m). This parameter is the rss of the radar fixed random range error and any random range errors due to propagation and other sources.

RangeBiasEr_m (optional) = composite range bias error (m). This parameter is the rss of the radar range bias error and any range bias errors due to propagation and other sources. If left blank, a zero value will be assumed for this parameter.

N_Smooth_Integer (optional) = number of range measurements that are smoothed in the calculated range accuracy (integer). If left blank, a single-pulse, or single integrated pulse-group measurement will be assumed. No output is generated for values less than 1.

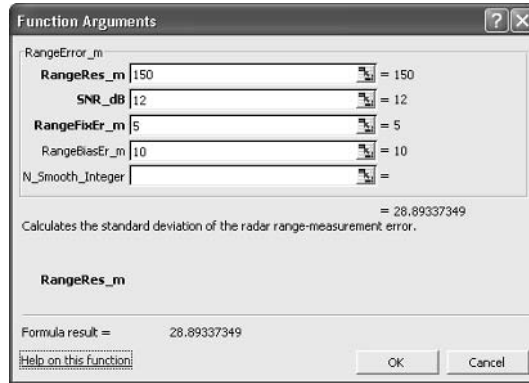


Figure 8.5 Excel parameter box for Function RangeError_m.

Function Output The standard deviation of the range-measurement error for the parameters specified (m).

The Excel Function Arguments parameter box for Function RangeError_m is shown in Figure 8.5, with sample parameters and a solution.

8.9.2 Function AngleError_mR

Purpose Calculates the standard deviation of the radar angular-measurement error.

Reference Equations (8.7), (8.8), (8.9), and (8.30).

Features Combines calculated S/N-dependent random angle error with fixed random angle error and angle bias error. A monopulse measurement with a difference slope $k_M = 1.6$ is assumed. Angle bias error may be omitted to calculate the relative angle error. Allows modeling of phased-array beam broadening and scan angle dependent fixed random and bias angle errors. Smoothing of random error components over multiple measurements may be modeled.

Input Parameters (with units specified)

Beamwidth_mR = radar antenna beamwidth on array broadside in the angular measurement coordinate (mrad).

SNR_dB = measurement S/N (dB). This may be the single-pulse S/N or integrated S/N as appropriate. The value input should take into account any beamshape loss or additional signal-processing loss for pulse integration. For single-pulse S/N values less than about 12 dB, the detection loss (5.16) should also be included.

AngleFixEr_mR = composite fixed random angle error in the measurement coordinate (mrad). This parameter is the rss of the radar fixed random angle error and any random angle errors due to propagation and other sources.

ScanAngle_deg (optional) = scan angle for phased arrays in the measurement coordinate (degrees). If this parameter is omitted, a value of zero will be assumed.

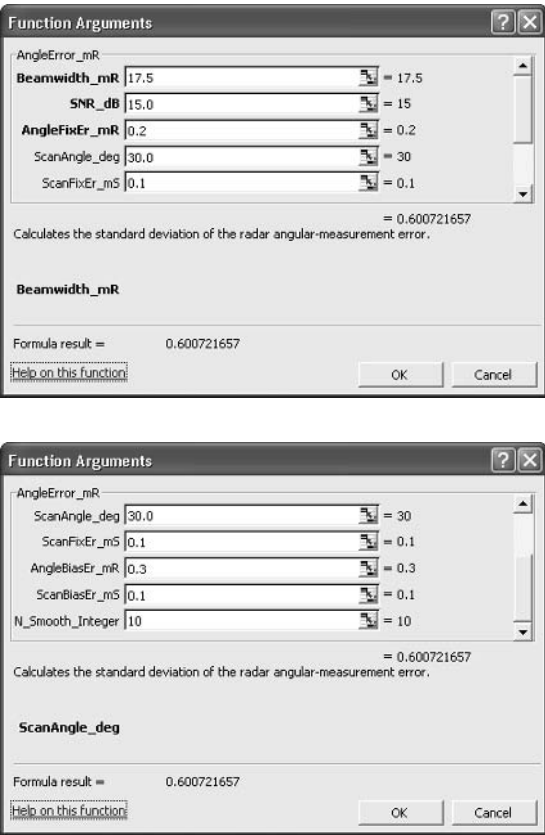


Figure 8.6 Excel parameter box for Function AngleError_mR.

ScanFixEr_mS (optional) = scan-angle dependent radar random angle error in the measurement coordinate for phased-arrays (msine). If this parameter is omitted, a value of zero will be assumed.

AngleBiasEr_mR (optional) = composite angle bias error in the measurement coordinate (mrad). This parameter is the rss of the radar angle bias error in the measurement coordinate and any angle bias errors due to propagation and other sources. If left blank, a zero value will be assumed for this parameter.

ScanBiasEr_mS (optional) = scan-angle dependent radar angle bias error in the measurement coordinate for phased arrays (msine) If left blank, a zero value will be assumed for this parameter.

N_Smooth_Integer (optional) = number of angle measurements that are smoothed in the calculated angle accuracy (integer). If left blank, a single-pulse, or integrated pulse-group measurement will be assumed. No output is generated for values less than 1.

Function Output The standard deviation of the angular-measurement error for the parameters specified (mrad). The Excel Function Arguments parameter box for Function AngleError_mR is shown in Figure 8.6, with sample parameters and a solution.

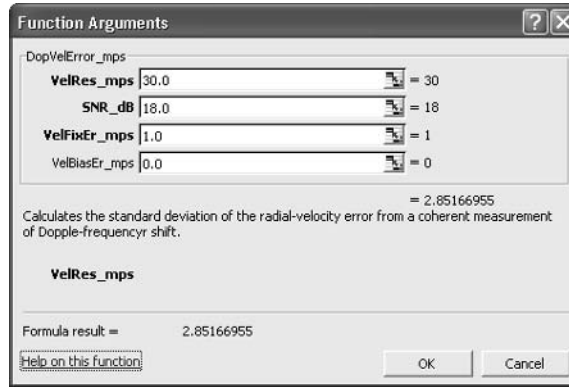


Figure 8.7 Excel parameter box for Function AngleError_mR.

8.9.3 Function DopVelError_mps

Purpose Calculates the standard deviation of the radar radial-velocity measurement error from a coherent measurement of Doppler-frequency shift.

Reference Equations (8.12) and (8.13).

Features Combines calculated S/N-dependent random radial-velocity error with fixed random radial-velocity error and radial-velocity bias error. Radial-velocity bias error may be omitted to calculate the relative radial-velocity error.

Input Parameters (with units specified)

VelRes_mps = radar radial-velocity resolution (m/s). A value of $\lambda/2\tau$ may be used, where λ is the radar signal wavelength, and τ is the duration of the coherently processed waveform.

SNR_dB = measurement S/N (dB). This may be the single-pulse S/N or integrated S/N as appropriate. The value input should take into account any beamshape loss or additional signal-processing loss for pulse integration. For single-pulse S/N values less than about 12 dB, the detection loss (5.16) should also be included.

VelFixEr_mps = composite fixed random radial-velocity error (m/s). This parameter is the rss of the radar fixed random radial-velocity error and any random radial-velocity errors due to propagation and other sources.

VelBiasEr_mps (optional) = composite radial-velocity bias error (m/s). This parameter is the rss of the radar radial-velocity bias error and any radial-velocity bias errors due to propagation and other sources. If left blank, a zero value will be assumed for this parameter.

Function Output The standard deviation of the radial-velocity measurement error from coherent measurement of Doppler-frequency shift for the parameters specified (m/s).

The Excel Function Arguments parameter box for Function DopVelError_mps is shown in Figure 8.7, with sample parameters and a solution.

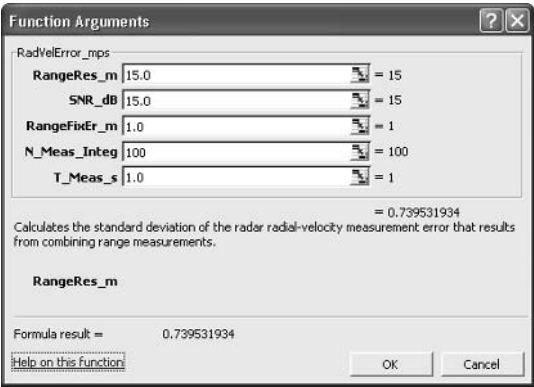


Figure 8.8 Excel parameter box for Function RadVelError_mps.

8.9.4 Function RadVelError_mps

Purpose Calculates the standard deviation of the radar radial-velocity measurement error that results from combining range measurements.

Reference Equations (8.15) and (8.16).

Features Calculates the range measurement error from radar range error-parameter inputs. Calculates the radial-velocity error from either the difference of two range measurements, or from processing a train of six or more range measurements.

Input Parameters (with units specified)

RangeRes_m = radar range resolution (m). A value of $1/B$ may be used, where B is the radar signal bandwidth.

SNR_db = range measurement S/N (dB). This may be the single-pulse S/N or integrated S/N as appropriate. The value input should take into account any beamshape loss or additional signal-processing loss for pulse integration. For single-pulse S/N values less than about 12 dB, the detection loss (5.16) should also be included.

RangeFixEr_m = composite fixed random range-measurement error (m). This parameter is the rss of the radar fixed random range error and any random range errors due to propagation and other sources.

N_Meas_Integer = number of range measurements used in the radial-velocity measurement (integer). If 2 to 5 is input, (8.15) is used. If 6 or greater is input (8.16) is used. No result is produced for input values less than 2, indicated by an output of -1.

T_Meas_s = duration of measurements (sec). For two measurements, this is the time separation of the measurements. For a pulse train, this is the duration of the pulse train used.

Function Output The standard deviation of radial-velocity measurement error from combining range measurements for the parameters specified (m/s).

The Excel Function Arguments parameter box for Function RadVelError_mps is shown in Figure 8.8, with sample parameters and a solution.

8.9.5 Function CrossVelError_mps

Purpose Calculates the standard deviation of the radar cross-range velocity measurement error that results from combining angle measurements.

Reference Equations (8.17) and (8.18).

Features Calculates the angular measurement error from radar angle error-parameter inputs. Calculates the cross-range velocity error from either the difference of two angle measurements, or from processing a train of angle measurements, using the specified target range. A value of $k_M = 1.6$ is assumed. Allows modeling of phased-array beam broadening and scan-dependent errors.

Input Parameters (with units specified)

Beamwidth_mR = radar antenna beamwidth on the array broadside in the cross-range measurement coordinate (mrad).

SNR_dB = angle measurement S/N (dB). This may be the single-pulse S/N or integrated S/N as appropriate. The value input should take into account any beamshape loss or additional signal-processing loss for pulse integration. For single-pulse S/N values less than about 12 dB, the detection loss (5.16) should also be included.

AngleFixEr_mR = composite fixed random angle error in the measurement coordinate (mrad). This parameter is the rss of the radar fixed random angle error and any random angle errors due to propagation and other sources.

TgtRange_km = range of target (km).

N_Meas_Integer = number of angle measurements used in the cross-range velocity measurement (integer). If 2 to 5 is input, (8.17) is used. If 6 or greater is input, (8.18) is used. No result is produced for input values less than 2, indicated by an output of -1.

T_Meas_s = duration of measurements (sec). For 2 measurements, this is the time separation of the measurements. For a pulse train, this is the duration of the pulse train used.

ScanAngle_deg (optional) = scan angle in the measurement coordinate for phased arrays (degrees). If this parameter is omitted, a value of zero will be assumed.

ScanFixEr_mS (optional) = scan-angle dependent radar random angle error in the measurement coordinate for phased-arrays (msine). If this parameter is omitted, a value of zero will be assumed.

Function Output The standard deviation of cross-range velocity measurement error from combining angle measurements for the parameters specified (m/s).

The Excel Function Arguments parameter box for Function CrossVelError_mps is shown in Figure 8.9, with sample parameters and a solution.

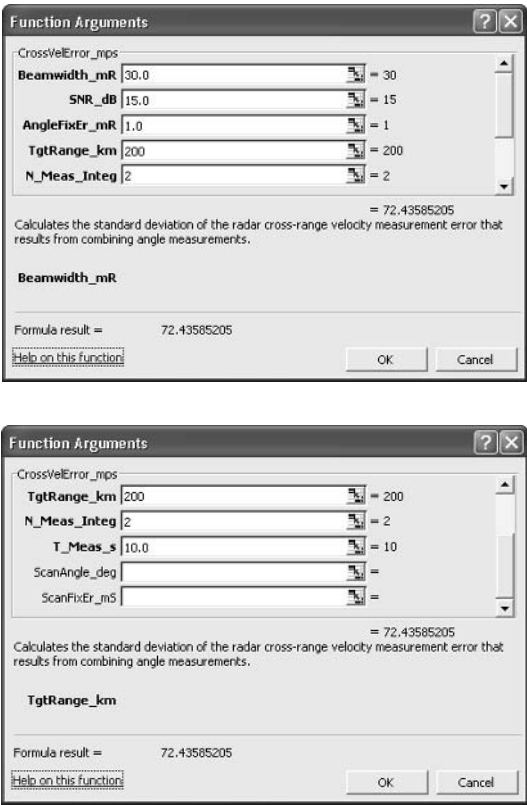


Figure 8.9 Excel parameter box for Function CrossVelError_mps.

8.9.6 Function PredictError_km

Purpose Calculates the approximate standard deviation of the error in predicted position from radar measurements for nonmaneuvering targets.

Reference Equation (8.7) to (8.9), (8.30), and (8.33).

Features Calculates the angular measurement error from radar angle-error parameter inputs. Calculates the cross-range velocity error from processing a train of angle measurements and the specified target range. Calculates predicted position error from the cross-range velocity error and the given prediction time. The cross-range coordinate having the larger measurement error (beamwidth) should be used to produce the largest predicted-position error semi-axis. A value of $k_M = 1.6$ is assumed. Allows modeling of phased-array beam broadening and scan-dependent errors.

Input Parameters (with units specified)

- Beamwidth_mR = radar antenna beamwidth on array broadside in the cross-range measurement coordinate (mrad).
- SNR_dB = angle measurement S/N (dB). This may be the single-pulse S/N or integrated S/N as appropriate. The value input should take into account any beamshape loss or additional signal-processing loss for pulse integration. For

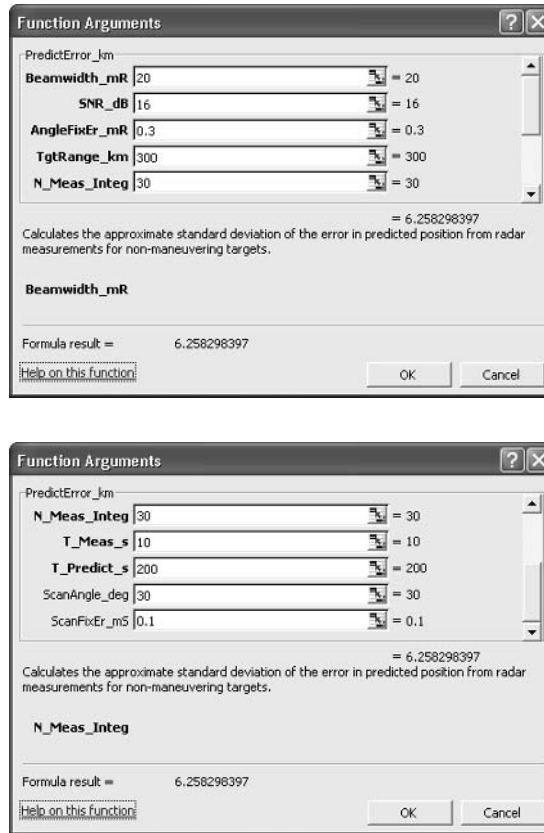


Figure 8.10 Excel parameter box for Function PredictError_km.

single-pulse S/N values less than about 12 dB, the detection loss (5.16) should also be included.

AngleFixEr_mR = composite fixed random angle error in the measurement coordinate (mrad). This parameter is the rss of the radar fixed random angle error and any random angle errors due to propagation and other sources.

TgtRange_km = range of target (km).

N_Meas_Integer = number of range measurements in the pulse train used for the cross-range velocity measurement (integer). No result is produced for an input of less than 2, indicated by an output of -1.

T_Meas_s = duration of the pulse train used for cross-range velocity measurement (sec).

T_Predict_s = time after cross-range velocity measurement that prediction error is calculated for (sec).

ScanAngle_deg (optional) = Scan angle in the measurement coordinate for phased arrays (degrees). If this parameter is omitted, a value of zero will be assumed.

ScanFixEr_mS (optional) = Scan-angle dependent radar random angle error in the measurement coordinate for phased-arrays (msine). If this parameter is omitted, a value of zero will be assumed.

Function Output The standard deviation predicted position error in the coordinate of the cross-range velocity measurement (km).

The Excel Function Arguments parameter box for Function PredictError_km is shown in Figure 8.10, with sample parameters and a solution.

References

- [1] Barton, D. K., and H. R. Ward, *Handbook of Radar Measurements*, Dedham, MA: Artech House, 1984.
- [2] Brookner, E., “Antenna Array Fundamentals,” Chapter 2 in *Practical Phased-Array Antenna Systems*, Norwood, MA: Artech House, 1991.
- [3] Swerling, P., “Radar Measurement Accuracy,” Chapter 4 in *Radar Handbook*, M. I. Skolnik, (ed.), New York: McGraw-Hill, 1970.
- [4] Ruck, G. T., et al., *Radar Cross Section Handbook, Volume 1*, New York: Plenum Press, 1970.
- [5] Barton, D. K., *Modern Radar System Analysis*, Norwood, MA: Artech House, 1988.
- [6] Skolnik, M. I., *Introduction to Radar Systems*, 2nd ed., New York: McGraw-Hill, 1980.
- [7] Blackman, S. S., *Multiple-Target Tracking with Radar Applications*, Dedham, MA: Artech House, 1986.

Selected Bibliography

Radar measurement techniques, error sources, and measurement accuracy are treated in some detail in Barton and Ward. Radar measurement and tracking are also treated in Barton and in Skolnik. Angular measurement errors in phased arrays are addressed in Chapter 2 of Brookner. The design and implementation of tracking radar is described by Dunn, Howard and Pendleton, and by Howard in Skolnik. Design and analysis of tracking filters and associated systems is treated by Blackman, and extensions to multiple targets and multiple sensors are addressed by Bar-Shalom and Blair.

- Bar-Shalom, Y., and D. Blair, *Multitarget/Multisensor Tracking: Applications and Advances—Volume III*, Norwood, MA: Artech House, 2000.
- Barton, D. K., *Radar System Analysis*, Englewood Cliffs, NJ: Prentice Hall, 1964.
- Barton, D. K., *Modern Radar System Analysis*, Norwood, MA: Artech House, 1988.
- Barton, D. K., and H. R. Ward, *Handbook of Radar Measurement*, Dedham, MA: Artech House, 1984.
- Blackman, S., and R. Popoli, *Design and Analysis of Modern Tracking Systems*, Norwood, MA: Artech House, 1999.
- Brookner, E., (ed.), in *Practical Phased Array Antenna Systems*, Norwood, MA: Artech House, 1991.
- Dunn, J. H., D. D. Howard, and K. B. Pendleton, “Tracking Radar,” Chapter 21 in *Radar Handbook*, M. I. Skolnik, (ed.), New York: McGraw-Hill, 1970.
- Howard, D. D., “Tracking Radar,” Chapter 18 in *Radar Handbook*, 2nd ed., M. I. Skolnik, (ed.), New York: McGraw-Hill, 1990.
- Skolnik, M. I., *Introduction to Radar Systems*, New York: McGraw-Hill, 1962.
- Skolnik, M. I., *Introduction to Radar Systems*, 2nd ed., New York: McGraw-Hill, 1980.
- Skolnik, M. I., (ed.), *Radar Handbook*, New York, McGraw-Hill: 1970.
- Skolnik, M. I., (ed.), *Radar Handbook*, 2nd ed., New York: McGraw-Hill, 1990.

Environment and Mitigation Techniques

This chapter enables the reader to:

- Know the characteristics of radar clutter from terrain, sea surface, and rain, how to quantify the signal-to-clutter ratio (S/C), and how to mitigate the effects of clutter;
- Understand the causes of radar multipath, and its impact on radar range and measurement accuracy;
- Quantify the radar losses caused by tropospheric attenuation, lens loss, rain attenuation, and ionospheric attenuation;
- Quantify the range and elevation-angle measurement errors caused by tropospheric and ionospheric refraction, and how well they may be corrected;
- Understand the characteristics of the ionosphere, and their effects in rotating radar signal polarization and limiting signal bandwidth.

The radar environment includes terrain and sea surfaces, the atmosphere (including precipitation), and the ionosphere. These may degrade radar observations and performance by producing clutter and other spurious returns, signal attenuation, and bending of the radar-signal path. Radar techniques that may avoid or minimize the impact of many of these effects are available.

This chapter addresses these environmental effects and potential mitigation techniques:

- Terrain and sea surfaces, which may produce target masking, radar clutter, and multipath interference;
- Precipitation, principally rain, which may produce signal attenuation and clutter returns;
- The troposphere, which may produce refraction that bends the radar signal path, signal attenuation, and a lens loss;
- The ionosphere, which may produce refraction that bends the radar signal path, signal fluctuation and attenuation, waveform dispersion, and rotation of signal polarization.

9.1 Terrain and Sea-Surface Effects

The Earth's surface may affect radar operation in three ways:

- The Earth may block the LOS to the target, making radar observations impossible.
- Radar energy may be scattered from the Earth's surface back to the radar receive antenna. When this energy interferes with the target signal, it is called surface, terrain, or sea clutter.
- Radar energy may be forward-scattered from the Earth's surface and reach the target by this indirect path. This is called multipath propagation.

Terrain may block the radar LOS to low-altitude targets, preventing their observation. While ground-based radar is usually sited to minimize terrain blockage, the effects still may be significant. Terrain blockage is less serious for airborne or space-based radar, but rough terrain may still cause blockage. For smooth terrain and sea surfaces, the LOS is limited by the radar horizon, discussed in Sections 2.1 and 9.3.

Radar signals returned from terrain and the sea surface may interfere with target signals, degrading radar detection and measurement. Such returns are termed radar clutter. The primary clutter return that interferes with the target signal is that signal from the same resolution cell as the target. This is illustrated in Figure 9.1, which shows the surface dimension of the clutter that is in the same range-resolution cell as the target, and that in the same elevation beam as the target. The cross-range dimension of the clutter in the same resolution cell as the target is determined by the azimuth beamwidth, θ_A , and the target range, R , and is equal to $R\sigma_A$.

When the extent of the clutter in the range dimension is determined primarily by the range resolution, as shown in Figure 9.1, the clutter area, A_s , that contributes to the clutter in the target resolution cell is given by:

$$A_s = \frac{R\theta_A \Delta R}{\cos \gamma} \quad \left(\frac{R\theta_E}{\Delta R} \geq \tan \gamma \right) \quad (9.1)$$

where ΔR is the radar range resolution and γ , called the grazing angle, is the angle between the terrain surface and the radar LOS. At higher grazing angles, the eleva-

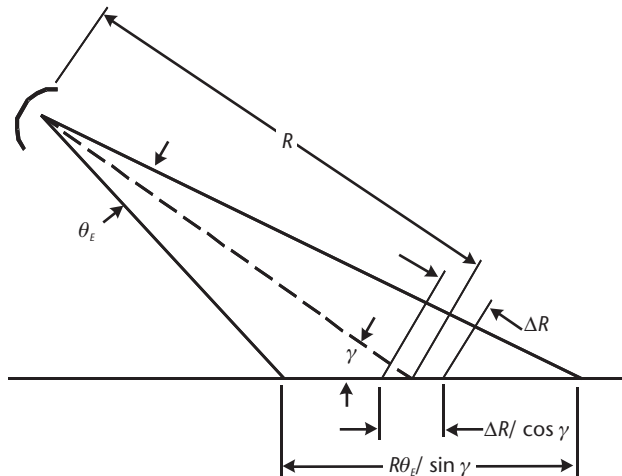


Figure 9.1 Geometry for the range extent of radar clutter in the target resolution cell.

tion beamwidth, θ_E , may determine the range dimension of the clutter area. Then it is given by:

$$A_s = \frac{R^2 \theta_A \theta_E}{\sin \gamma} \quad \left(\frac{R \theta_E}{\Delta R} \leq \tan \gamma \right) \quad (9.2)$$

where the factor $\pi/4$ is included in the beamshape loss, as discussed later. For most ground-based pulsed-radar cases, and many airborne and space-based radar cases, the clutter range dimension is determined by the radar range resolution, and (9.1) should be used.

The preceding discussion addresses mainbeam clutter for radar having no range ambiguities. For radar that employs high levels of range ambiguity (see Sections 4.5 and 4.6), the clutter contributions from ambiguous range cells must be considered, and clutter from radar sidelobes may be significant. This is often the case for airborne pulse-Doppler radar (see Sections 2.5 and 11.3).

The clutter reflectivity is characterized by an RCS per unit area, designated by σ^0 . The parameter σ^0 is dimensionless ($\text{m}^2 \text{ RCS}/\text{m}^2 \text{ surface area}$), usually less than unity, and is often specified in negative values of decibels. The clutter RCS, σ_c , is given by:

$$\sigma_c = \frac{\sigma^0 A_s}{L_{BS}} \quad (9.3)$$

where L_{BS} is the beamshape loss for the radar viewing the clutter. When the clutter range extent is limited by range resolution (9.1), $L_{BS} \approx 1.6 \text{ dB}$; when it is limited by elevation beamwidth (9.2), $L_{BS} \approx 3.2 \text{ dB}$.

The value of σ^0 depends on the radar frequency and polarization, the grazing angle, and the terrain type or sea state. It generally increases with frequency, grazing angle, and terrain or sea roughness. Some typical values for σ^0 are given in Table 9.1. Detailed data from clutter measurement programs is given in [1, pp. 62–80] and other sources.

The variation of σ^0 with grazing angle, γ , may be modeled by:

$$\sigma^0 = a \sin \gamma \quad (9.4)$$

where a is a parameter that describes the scattering effectiveness of the surface [3, p. 124]. This model agrees well with measured data for grazing angles above a few degrees to about 60° . At lower grazing angles, destructive interference from multi-

Table 9.1 Typical Values for Clutter Reflectivity (σ^0)

<i>Frequency Band</i>	<i>Land Clutter (Mountainous Regions)</i>	<i>Sea Clutter (Sea State 4 – Rough)</i>
L (1.3 GHz)	–29	–51.5
S (3.0 GHz)	–25	–47.5
C (5.4 GHz)	–22	–44.5
X (9.4 GHz)	–20	–42.5

Source: [2, p. 15.12].

path returns result in values of σ^0 lower than given by (9.4), while at the higher grazing angles, specular returns produce values of σ^0 greater than given by (9.4) [4, pp. 139–140]. For land clutter, a is usually between -20 dB and -5 dB and almost independent of frequency. For sea clutter, a is proportional to frequency and increases with sea state [3, pp. 125–129].

The clutter signal is often the coherent sum of returns from many small scatterers in the clutter area, A_s . This leads to a Rayleigh distribution of clutter signal voltage, the same as for radar noise [5, p. 137]. However, in many cases the amplitude distribution differs from Rayleigh, including those where one or a few large discrete scatterers are in the clutter area, (e.g., from structures), or when very-small range and angle resolution is used, and only a few scatterers are in the clutter area.

The clutter return signal is also characterized by a Doppler-frequency spread due to the radial velocity of the scatterers in the resolution cell. This is determined by the terrain type and wind speed. For ground-based radar, the clutter produces a narrow spectrum, usually centered on zero velocity. For terrain, the rms clutter velocity spread varies from near-zero for rocky terrain to about 0.33 m/s for wooded terrain in high wind [5, p. 139]. The velocity spread of sea clutter, σ_v , is given approximately by:

$$\sigma_v \approx 0.125 V_w \quad (9.5)$$

where V_w is the wind velocity. Rotating antennas add a component to the velocity spread, σ_{VR} , which is equal to the radial velocity of the antenna edge [6, p. 214]:

$$\sigma_{VR} = \frac{\omega_A w}{2} \quad (9.6)$$

where ω_A is the antenna azimuth radial velocity, and w is the horizontal antenna dimension. For airborne radar, the clutter spectrum depends on the aircraft speed and terrain viewing angle, and may result in a relatively large spectral spread, as discussed in Section 11.2.

Targets that have radial-velocity magnitude greater than a few meters per second may be separated from the clutter spectrum in Doppler frequency. The clutter returns may then be suppressed by Doppler-frequency processing, without significantly affecting the target returns. The two techniques commonly used for clutter rejection are:

- *Moving target indication (MTI)*. In this technique, often used in ground-based radar, two or more pulse returns are processed to create a null region around zero Doppler-frequency shift to reject the clutter spectrum.
- *Pulse-Doppler processing*. In this technique, a train of pulses is coherently processed using a Fourier-transform-type algorithm to divide the received signal into a series of narrow spectral bands. The target is then separated both from the zero-velocity mainbeam clutter, and from most of the sidelobe clutter that may occur at other velocities for moving radar. This technique is often used in airborne radar [7], as well as some ground-based radars (see Section 11.3).

The clutter reduction performance may be characterized by a cancellation ratio (CR), which is the factor by which the clutter signal is reduced relative to the target signal; and by the minimum detectable velocity (MDV), which is a measure of the width of the rejected signal spectrum. CR is taken here to be a factor greater than unity, which may be expressed as a positive value in decibels. The CR depends on details of the canceller design, the number of pulses processed, the spectral spread of the clutter signal, the stability of the transmitter, and the dynamic range of the receiver. Typical values for CR are in the range of 20 to 40 dB [2, pp. 15.11–15.23].

The radar performance in surface clutter may be described by a signal-to-clutter ratio (S/C), which is given by:

$$S/C = \frac{\sigma CR}{\sigma_c} = \frac{\sigma CRL_{BS}}{\sigma^0 A_s} \quad (\text{surface}) \quad (9.7)$$

where A_s is given by (9.1) or (9.2). Note that S/C does not depend on the radar sensitivity, since this affects the returns from both σ and σ_c equally. Radar parameters that affect S/C are the range resolution and beamwidth, as well as the clutter cancellation ratio.

Combining the clutter-signal power with noise power into an interference power, $N + C$, must consider both the amplitude statistics and the temporal correlation of the clutter signal. If the clutter signal (or its residue after MTI cancellation or pulse-Doppler processing), is Gaussian and random from pulse to pulse, the clutter signal return may be combined with the radar system noise, and $S/(N + C)$ may be used for detection and measurement accuracy in place of S/N :

$$\frac{S}{N + C} = \frac{1}{\frac{1}{(S/N)} + \frac{1}{(S/C)}} \quad (9.8)$$

Equation (9.8) must be used with care, since many clutter sources have non-Gaussian statistics, the clutter returns may not be independent from pulse-to-pulse, and the clutter signal may affect the monopulse difference channels differently than the sum channel (see Section 8.2).

For example, for a radar having azimuth and elevation beamwidths of 1 degree and a range resolution of 150m, the quantity $R\theta_E/\Delta R = 11.6$ at a range of 100 km. The range extent of the clutter area is determined by the range resolution, and (9.1) may be used for grazing angles up to 85° . For a grazing angle of 5° , the clutter area is 262,800 m². With a value of $\sigma^0 = -25$ dB and $L_{BS} = 1.6$ dB, the clutter RCS is 574.9 m². For a target with 10 dBsm RCS, with no clutter cancellation, $S/C = -17.6$ dB. If 30 dB of clutter cancellation is provided, $S/C = 12.4$ dB. If $S/N = 18$ dB, in the latter case $S/(N + C) = 11.3$ dB.

Terrain blockage, discussed earlier, may eliminate terrain clutter in regions behind the blocking feature. Targets in these regions that are not blocked by the terrain (e.g., aircraft at altitude) may be observed with no clutter interference. Clutter fences are sometimes built around radar intended to view high-altitude targets. These fences block clutter returns, as well as returns from low-altitude targets.

When the radar beam illuminates terrain or sea surface as well as the target, reflected radar energy may reach the target, creating a second, slightly longer signal path. The geometry of this multipath propagation is illustrated in Figure 9.2. For a flat-Earth approximation and small grazing angles, the difference in the direct and reflected path ranges, δR , is approximately given by:

$$\delta R \approx \frac{2h_T h_R}{R} \quad (9.9)$$

In many cases, the direct and reflected signal may not be resolved in range or elevation angle by the radar. For example, for a radar height of 10m, and a target at an altitude of 500m and a range of 100 km, $\delta R = 0.1\text{m}$.

When the signals from the direct and reflected signal paths are not resolved in range, they are combined in the receiver, creating interference due to the different path lengths. With a perfectly reflecting surface, the ratio of signal power returned to the radar with multipath to that in free space, η_M , is given by [7]:

$$\eta_M = 16 \sin^4 \left(\frac{2\pi h_T h_R}{\lambda R} \right) \quad (9.10)$$

When the grazing angle is near zero, the path lengths are essentially equal. The signal reflected from the terrain is reversed in phase by the scattering process, so that if the reflection coefficient is unity and the antenna gain is the same for both paths, the direct and reflected signals cancel, and no signal is returned to the radar. For a grazing angle where the direct and reflected path lengths differ by $\lambda/2$, the two signals add in phase, producing a power density at the target four times that of the direct signal alone. The signal reflected from the target also reaches the radar by both the direct and reflected paths. These signals also add in phase, producing a returned signal power 16 times that if only the direct path were used. This effect doubles the radar range from that given by only the direct path. The result is a series of lobes that are separated in elevation angle by $\Delta\phi_E$, which is given by:

$$\Delta\phi_E = \frac{\lambda}{2h_R} \quad (9.11)$$

The minimum elevation angle, ϕ_{EM} , at which the radar range is equal to the normal free-space range, is given by:

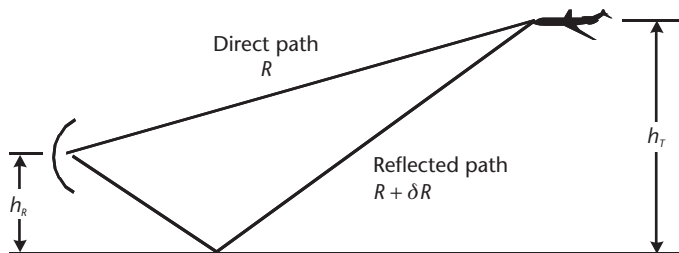


Figure 9.2 Geometry for multipath propagation.

$$\phi_{EM} = \frac{\lambda}{12h_R} \quad (9.12)$$

For an L-band radar ($\lambda = 0.23\text{m}$), with an antenna height of 20m, $\phi_{EM} = 0.2^\circ$.

When the surface is perfectly reflecting, as is the case of the sea at low elevation angles, the radar range at the peak of the lobes is twice the normal range, and the nulls between lobes give zero range, as discussed above. At higher elevation angles or with terrain that is not perfectly reflecting, the peaks and nulls are less pronounced. This simplified analysis assumes a flat Earth. Similar results are obtained with a round Earth, but the peaks and nulls are less pronounced [8, pp. 422–447].

Operators of early shipboard rotating search radars estimated the target altitude from the ranges where the target entered nulls. Modern radar often avoids lobing by using stacked beams or a scanning beam in elevation to avoid illuminating the target and Earth simultaneously, at least for target elevation angles greater than the elevation beamwidth.

Multipath returns also produce measurement errors, especially in elevation angle. For a smooth reflecting surface, producing secular reflection, the elevation-angle error due to multipath is about 0.5 times the elevation beamwidth, θ_E , for elevation angles less than about $0.8\theta_E$. For rough surfaces, producing diffuse scattering, the elevation-angle errors are smaller, typically $0.1\theta_E$, for elevation angles less than the elevation beamwidth [5, pp. 142–150].

Multipath from a smooth level surface causes no error in target azimuth. Rough surfaces may cause azimuth errors of the order of 0.1 to $0.2\theta_A$ for elevation angles less than θ_E . Small errors in range and target Doppler shift are also produced by multipath when the target elevation is less than θ_E [5, pp. 151–158].

Multipath errors exhibit random fluctuations as the target moves. However, the fluctuation rate is usually slow, compared with normal radar observation times [5, pp. 145–152]. Thus, these errors will not usually be reduced by smoothing, but are uncorrelated between targets. They should be conservatively treated as fixed random bias errors in evaluating radar measurement performance (see Chapter 8). However, when such measurements are used to derive target velocity, the rate of change of the multipath error may exceed the target rate being measured.

Measurement errors and signal reductions from multipath are best prevented by not illuminating the Earth surface with the radar beam. To avoid these effects, the radar beam center should be kept above the radar horizon by an amount equal to the elevation beamwidth, θ_E .

9.2 Precipitation Effects

Precipitation, primarily rain, may affect radar performance in two ways:

- Attenuation of the radar signal passing through the rain;
- Clutter from rain in the same resolution cell as the target.

Both effects are more severe at higher radar frequencies, and may often be neglected at frequencies below 1 GHz.

Rain produces significantly greater attenuation and clutter than snow and hail, due to the higher absorption of water in the liquid state than in solid states [9, pp. 618–621; 10, pp. 685–688]. This section therefore addresses primarily attenuation and clutter from rain. Extensions to other precipitation forms may be found in the Selected Bibliography.

Attenuation of the radar signal due to rainfall is exponential with path length, and may be expressed in decibels per kilometer of path. This parameter, a_R , increases with both the radar frequency and the rainfall rate. Representative two-way values for rain attenuation are given in Table 9.2 for light (1 mm/hr), moderate (4 mm/hr), and heavy (16 mm/hr) rainfall rates, and for frequencies from 1 to 30 GHz. The rain loss may usually be neglected at frequencies below 1 GHz. The total two-way loss from rain attenuation in decibels is given by:

$$L_{PR} = a_R d_R \quad (9.13)$$

where d_R is the signal path length (in kilometers) in the rain.

This suggests that a long path in heavy rain at high frequency could produce very large attenuation. However, rainfall is not uniform over extended regions, and high rainfall rates are usually confined to relatively small areas. A model that accounts for variation of rain density over the propagation path was developed by Crane [11]. It is summarized below, and is used in the rain-path attenuation VBA custom radar function described in Section 9.6.3.

Statistics for point rainfall rate were collected and tabulated for the eight rain-rate climate regions described in Table 9.3. Region D was further divided into three subregions in the United States (D1, D2, and D3). The data is summarized in Figure 9.3, which shows the point rainfall rate values, measured in one-minute intervals, as functions of the fraction of the year that the rate is exceeded. For example, in region D2 (east-central United States), the rainfall rate that is exceeded 1% of the year is 3.0 mm/hr.

An empirical model was developed that relates path attenuation to path length and point rainfall rate. At high-point–rainfall rates, the heavy rain falls close to the point, and lesser rates occur over long paths. Conversely, for low-point–rainfall rates, higher rates are more likely to occur over longer paths.

The path length in the rain includes only that portion of the path below the 0° isotherm. Above this altitude, the water is assumed to be in solid form, and not to

Table 9.2 Two-Way Radar Signal Attenuation in Rain (dB/km)

<i>Frequency (GHz)</i>	<i>Rainfall Rate (mm/hr)</i>		
	<i>1</i>	<i>4</i>	<i>16</i>
1	0.0003	0.001	0.004
3	0.0009	0.004	0.019
5	0.0028	0.015	0.086
10	0.025	0.13	0.66
16	0.083	0.38	1.72
22	0.17	0.77	3.53
30	0.34	1.51	6.70

Calculated using the methodology in [11].

Table 9.3 Rain Climate Regions

<i>Region</i>	<i>Location</i>	<i>Characteristics</i>	<i>Designation</i>
Polar		Tundra (dry)	A
Polar		Taiga (moderate)	B
Temperate		Maritime	C
Temperate		Continental	D (D1, D2, and D3)
Subtropical		Wet	E
Subtropical		Arid	F
Tropical		Moderate	G
Tropical		Wet	H

Source: [11].

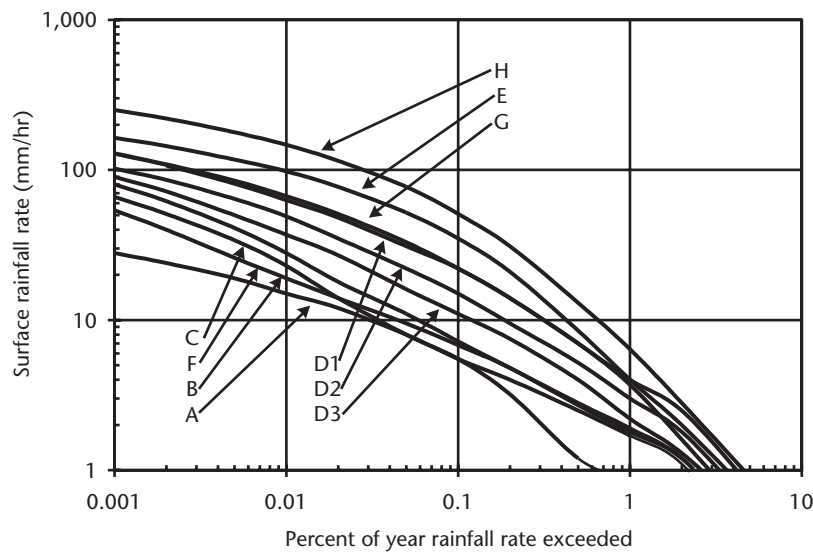


Figure 9.3 Point rainfall rates for the climate regions indicated for one-minute intervals, as a function of the fraction of the year the rate is exceeded. (After: [11].)

contribute significantly to the attenuation. The zero degrees C isotherm altitude is given as a function of latitude and the probability that the altitude is exceeded. For a 1% probability of occurrence, the altitude is about 4.5 km for latitudes below about 30°, and decreases to zero altitude for a latitude of 70°. Using the 1% probability of occurrence represents an average situation, considering that liquid water may exist at somewhat lower temperatures than zero (i.e., at somewhat higher altitude than the zero-degree isotherm). A probability of 0.001% is said to represent a worst-case situation (highest altitude).

For example, for climate region D2, the rainfall rate that is exceeded 1% of the year was found from Figure 9.3 to be 3 mm/hr. At a radar frequency of 9.5 GHz (X-band), the two-way attenuation parameter for this rate is 0.077 dB/km. For a propagation path length of 200 km, (9.13) gives the rain attenuation as 15.4 dB. However, attenuation from precipitation is only significant when it is in the liquid state. At 40° latitude, the zero-degree isotherm altitude for 1% probability is found from Crane to be 2.5 km. For a ground-based radar and an elevation angle of 10°, the slant path length in the rain is 14.3 km. Using the Crane model, the resulting

attenuation is found to be 2.1 dB, significantly less than the 15.4 dB found using (9.13). These results are summarized in column 2 of Table 9.4

The difference is even more pronounced for higher-point rainfall rates. Column 3 of Table 9.4 shows the comparison for a 0.01% exceedance, where the point rainfall rate is 49 mm/hr. The attenuation calculated by (9.13) is 430 dB, while that calculated by the Crane model is only 19.1 dB.

Since the propagation loss from rain (as well as that from the troposphere, as discussed in Section 9.3) is a complex function of range, it is often not possible to calculate radar range in closed form. In these cases, an iterative approach is used.

The loss from rain may be considered an RCS-measurement bias error, σ_{SB} (see Section 8.4). This bias error may be reduced if the rain loss is estimated and included in the calculation of RCS.

Rain may also scatter energy back to the radar, creating clutter that may compete with targets in the same resolution cell. The principal scattering volume is defined by the radar beam area and the range resolution, and is given by:

$$V_S = R^2 \theta_A \theta_E \Delta R \quad (9.14)$$

where the factor $\pi/4$ is included in the beamshape loss, as discussed later. As with the terrain clutter discussed in Section 9.1, radar having range ambiguities may need to consider rain clutter in ambiguous ranges and in antenna sidelobes.

Rain clutter reflectivity is characterized by a volume reflectivity, η_V , which has the dimension of square meter of RCS per cubic meter of rain volume, or m^{-1} . This volume reflectivity is a function of the rainfall rate, r in millimeters per hour, and the radar wavelength, λ , and is given by [5, p.138]:

$$\eta_V = \frac{6 \times 10^{-14} r^{1.6}}{\lambda^4} \quad (9.15)$$

The clutter RCS, σ_C , is then given by:

$$\sigma_C = \frac{\eta_V V_S}{L_{BS}} \quad (9.16)$$

Table 9.4 Rain Attenuation Examples

<i>Region</i>	<i>D2</i>	<i>D2</i>
Rain exceedance	1%	0.01%
Point rate	3 mm/hr	49 mm/hr
Frequency	9.5 GHz	9.5 GHz
a_R	0.077 dB/km	2.15 dB/km
d_R	200 km	200 km
L_{PR} (9.12)	15.4 dB	430 dB
Latitude	40°	40°
Isotherm probability	1%	1%
Isotherm altitude	2.5 km	2.5 km
Elevation angle	10°	10°
Rain path	14.3 km	14.3 km
L_{PR} (Crane model)	2.1 dB	19.1 dB

where L_{BS} is the two-dimensional beamshape loss, approximately 3.2 dB.

For example, at C band (5.5 GHz), with a rainfall rate of 16 mm/hr, $\eta_V = 5.7 \times 10^{-7} \text{ m}^2/\text{m}^3$. A radar having azimuth and elevation beamwidths of 2° and 15m range resolution will have a scattering volume $V_s = 1.4 \times 10^8 \text{ m}^3$ at a range of 100 km. The clutter in the resolution cell $\sigma_C = 38 \text{ m}^2$.

Rain clutter may be suppressed by MTI or pulse-Doppler processing, as discussed in Section 9.1 for terrain clutter. However, the mean velocity of rain clutter is equal to the wind velocity, which may be several tens of meters per second. Further, the velocity spread of rain clutter is from 2 to 4 m/s [2, p. 139], an order of magnitude greater than for terrain clutter. This requires a relatively wide MTI velocity-rejection notch that follows the clutter mean velocity. The result is greater processing complexity and possibly less effective cancellation.

Rainfall is characterized by spherical drops. When a radar radiates a circularly polarized signal, the signal returned from the raindrops is circularly polarized in the opposite sense. For example, if right circular polarization is radiated, the rain clutter is left circularly polarized. Normally, radar that employs circular polarization receives the opposite sense to that transmitted, in order to maximize the signal returned from smooth targets that also reverse the polarization. However, complex targets, such as aircraft, may return nearly equal signal energy in each of the two circular polarizations. Thus, by receiving the same sense circular polarization that is transmitted, the radar may reject the rain clutter at the expense of a small reduction the target signal strength, typically 2 to 4 dB.

The degree of rain-clutter cancellation depends on the shape of the raindrops, and on the precision with which the circular polarizations are transmitted and received. Rain-clutter cancellation of 40 dB may be achieved in ideal conditions, but in heavy, nonspherical rain, it is often limited to a range from 5 to 15 dB [8, p. 505].

The S/C in rain clutter is given by:

$$S/C = \frac{\sigma_C R}{\sigma_C L_x} = \frac{\sigma_C R L_{BS}}{\eta_V V_s L_x} \quad (\text{volume}) \quad (9.17)$$

where the CR combines the MTI or pulse-Doppler cancellation and the cancellation from same-sense circular polarization, and L_x is the target polarization loss from same-sense circular polarization. Since rain clutter comes from many small scatterers, it has Gaussian statistics, and (9.8) may be used.

In the previous example, if the target RCS is 1 m^2 with no clutter cancellation, $S/C = -15.8 \text{ dB}$. If cancellation from same-sense circular polarization is used, and 30 dB of cancellation is achieved with a same-sense circular polarization loss of 3 dB, $S/C = 11.2 \text{ dB}$. If an additional 10 dB were obtained from pulse-Doppler processing, the S/C is increased to 21.2 dB.

9.3 Troposphere Effects

The troposphere is the portion of the atmosphere below the stratosphere, which extends about 30 km in altitude from the Earth's surface. It affects radar performance in three ways:

- Radar signal attenuation;
- Lens loss;
- Refractive bending of the radar signal path.

Tropospheric attenuation is caused by the molecular absorption by oxygen and water vapor [12, pp. 646–655]. The two-way loss in decibels per kilometer for each of these components, and the total loss, are given for various radar frequencies in Table 9.5, assuming sea level, 20°C, and 1% water vapor. The total loss is relatively constant in the 1 to 10 GHz range. Water resonance produces a loss peak at 22.3 GHz, and oxygen absorption produces a resonant loss peak at 60 GHz (not shown in the table). These frequencies are usually avoided in terrestrial radar.

For short paths near sea level, the two-way loss in decibels per kilometer, a_T , may be used to calculate tropospheric loss, L_{PT} :

$$L_{PT} = a_T d_T \quad (9.18)$$

where d_T is the signal path length in kilometers. At higher altitudes, the tropospheric loss is reduced due to the lower density of the atmospheric gasses.

The two-way attenuation for signal paths from sea level to beyond the troposphere is shown in Figure 9.4 as a function of radar frequency, with beam elevation angle as a parameter. The loss decreases rapidly for frequencies lower than 1 GHz. About half the loss occurs below 3 km altitude [6, p. 469], and little attenuation occurs above 10 km altitude. Plots of tropospheric attenuation as a function of range and frequency for various elevation angles are given in [13, pp. 210–216; and 14, pp. 2-48–2-51], and are incorporated into the tropospheric attenuation VBA custom radar function described in Section 9.6.5.

As with the rain attenuation discussed in Section 9.2, tropospheric loss may be considered an RCS-measurement bias error, σ_{SB} (see Section 8.4). This bias error may be reduced if the tropospheric loss is estimated and included in the calculation of RCS.

Another troposphere-related loss factor is called lens loss. This loss, significant only at low elevation angles, is caused by the difference in the tropospheric refraction at the top and bottom of the beam (see discussion later in this section). The refractive difference spreads the beam, reducing the effective gain, which is charac-

Table 9.5 Two-Way Tropospheric Attenuation for Various Frequencies, at Sea Level, 20C, and 1% Water Vapor

Frequency (GHz)	Attenuation (dB/km)		
	Oxygen	Water vapor	Total
1	0.012	Negligible	0.012
3	0.014	0.0004	0.014
5	0.015	0.001	0.016
10	0.016	0.006	0.022
16	0.017	0.028	0.045
22	0.020	0.320	0.340
30	0.028	0.100	0.128

Source: [12, p. 663].

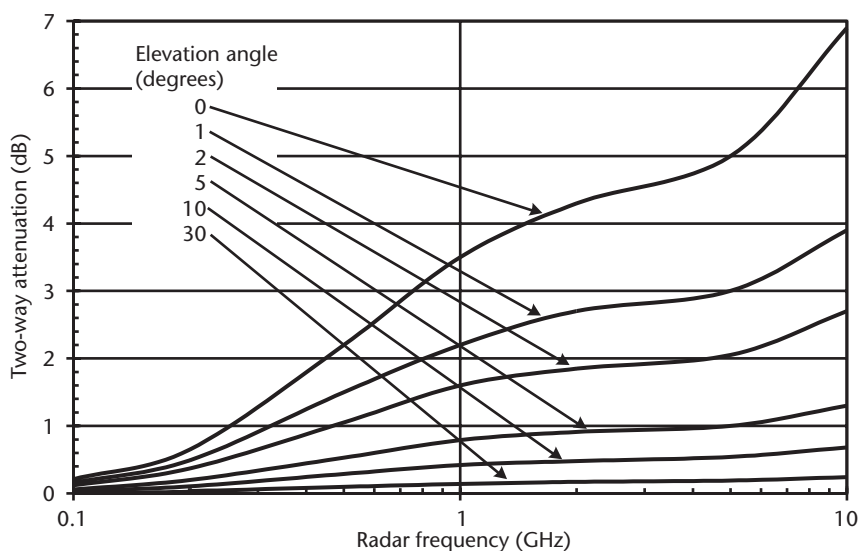


Figure 9.4 Two-way tropospheric loss for signal paths from sea level to above the troposphere. (After: [14].)

Table 9.6 Two-Way Lens Loss at Sea Level (dB)

Elevation Angle (Degrees)	Slant Range (km)				
	200	500	1,000	2,000	5,000
0	0.37	1.30	2.15	2.55	2.78
0.5	0.33	1.02	1.58	1.85	1.97
1	0.30	0.78	1.18	1.38	1.45
2	0.24	0.54	0.70	0.80	0.82
4	0.14	0.26	0.31	0.34	0.35
8	0.08	0.09	0.10	0.11	0.12

Source: [1, p. 323].

terized as a loss. Lens loss is a function of elevation angle and range. Representative two-way values of lens loss at sea level are given in Table 9.6.

The total loss due to the atmosphere is the product of the tropospheric attenuation loss and the lens loss, given by the sum of these losses in decibels. This total loss is found by the tropospheric loss VBA custom radar function, described in Section 9.6.5.

Refraction or bending of the radar signal path is caused by the variation of the propagation velocity with altitude. The index of refraction, n , is defined as the ratio of the free-space propagation velocity to the local propagation velocity. It varies with atmospheric pressure, water vapor content, and temperature. These normally decrease with increasing altitude, producing a refractive index that decreases with increasing altitude. This causes the signal path to bend downward [8, pp. 447–450].

The refractivity, N , is related to the index of refraction by:

$$N = (n - 1) \times 10^6 \quad (9.19)$$

The surface refractivity, N_s , is typically between 300 and 350, with a standard value of 313, and the refractivity decreases approximately exponentially with increasing altitude [13, p. 304].

Refraction within the atmosphere is often accounted for by using an effective Earth radius $4/3$ times the actual Earth radius, and representing the propagation paths as straight lines. This is discussed in Section 2.1 and illustrated in Figure 2.1. This model neglects the variation of surface refractivity, and assumes a linear, rather than exponential, decrease in refractivity with increasing altitude, but the error is small for altitudes below about 4 km [14, p. 304].

Signal paths are more accurately determined by ray tracing. The errors in measuring radar elevation angle and range due to tropospheric refraction have been calculated for a standard atmosphere. Values of these errors are given in Table 9.7, for signal paths from a surface-based radar to a target outside the troposphere (i.e., having an altitude greater than 30 km). At zero elevation angle, the error in elevation angle is 13 mrad, and the range error is 105 m. The errors decrease with increasing elevation angle, and may often be neglected for elevation angles greater than 5° .

The errors are proportional to surface refractivity, so they may vary from the values in Table 9.7 by about $\pm 10\%$. These errors are independent of frequency, for frequencies below 20 GHz. Plots of elevation-angle and range errors due to tropospheric refraction as functions of range for various elevation angles are given in [5, pp. 366–371], and are incorporated into the tropospheric error VBA custom radar functions described in Sections 9.6.6 and 9.6.7.

These measurement errors should be treated as bias errors when determining measurement accuracy, since they may not be reduced by smoothing (see Chapter 8). They may be significantly reduced, however, by correcting the radar measurements for the estimated values of the errors. The errors may be corrected to approximately 10% to 15% of their value by assuming the standard atmosphere. If the surface refractivity is measured at the radar, the accuracy of the corrections is about 5%. Greater accuracy in estimating refraction errors requires the meas-

Table 9.7 Measurement Errors Due to Tropospheric Refraction for a Surface-Based Radar Viewing Targets Above the Troposphere in a Standard Atmosphere

<i>Elevation</i>		
<i>Angle (mrad) Radar Measurement Error</i>		
	<i>Elevation</i>	
	<i>Angle (mrad) Range (m)</i>	
0	13.0	105
4	13.0	93
8	10.5	85
15	8.5	70
30	6.5	52
65	4.0	30
100	2.9	22
200	1.5	11
400	0.7	5
900	0.3	3

Source: [5, pp. 368–369].

urement of the refractivity profiles along the signal path, which is rarely done [14, pp. 306–307].

For example, at 4 mrad elevation angle, the elevation-angle error for a target outside the troposphere is 13 mrad, and the range error is 93m. If these errors are corrected assuming the standard atmosphere, the residual bias errors will be about 10% of these values, or 1.3 mrad in elevation angle and 9.3m in range.

Under some anomalous atmospheric conditions, the refractivity above the surface decreases much more rapidly than in the standard atmosphere discussed above. This may cause a condition called ducting, where the signal from a ground-based radar is propagated around the Earth's curvature. This may provide detection of surface and low-altitude targets at ranges greater than normal. It may also lead to unexpected multiple-time-around returns (see Section 4.6). Such conditions occur most often over the ocean in warm climates [6, pp. 450–456].

9.4 Ionosphere Effects

The ionosphere may affect the performance of radar in several ways:

- Radar signal attenuation and scintillation;
- Rotation of radar signal polarization;
- Dispersion of frequencies in the radar waveform;
- Refractive bending of the radar signal path.

The effects of the ionosphere on radar signal propagation vary inversely with various powers of frequency, and are rarely significant at frequencies above about 1 GHz.

The ionosphere consists of several layers or regions of ionized electrons. The regions that affect radar propagation extend in altitude from about 55 km to 1,000 km, with the peak electron density at about 400 km altitude. Thus, the ionosphere may affect observations by terrestrial radar of targets in space, and observations by space-based radar of terrestrial targets.

The impact of the ionosphere on radar propagation depends on the integrated electron density along the radar signal path. Thus, these effects depend on the elevation angle and target range. The electron density in the ionosphere responds to solar radiation, and so is significantly higher in the daytime than at night. The electron density also varies with latitude, and increases in response to sunspot activity. Therefore, the impact of the ionosphere on radar-signal propagation may vary slowly with time and with location, and the values given in this section should be considered as representative [13, pp. 177–178; 15, pp. 151–152].

The ionosphere produces signal attenuation that may be significant at frequencies below about 300 MHz. The attenuation in decibels is inversely proportional to the square of radar frequency, and depends on the angle of the signal path through the ionosphere, and the integrated electron density [16, pp. 373–377].

Representative values of two-way ionospheric attenuation are given in Table 9.8 for ground-based radar at two frequencies in the VHF band. The target is assumed to be at 500-km altitude, where most of the attenuation has occurred, and

Table 9.8 Two-Way Ionospheric Attenuation Values for a Surface Radar Viewing a Target at 500-km Altitude

<i>Elevation Angle (Degrees)</i>	<i>Daytime Attenuation (dB)</i>	
	<i>100 MHz</i>	<i>300 MHz</i>
0	2.6	0.3
5	2.2	0.2
10	1.8	0.1
20	1.2	< 0.1
45	0.6	< 0.1
90	0.4	< 0.1

Source: [16, pp. 373–377].

values for normal daytime ionospheric conditions are given. Corresponding two-way attenuation values for nighttime conditions are all less than 0.1 dB.

The nonuniform electron density in the ionosphere produces random variations in the amplitude and phase of signals passing through the ionosphere. These signal variations are called signal scintillation. This scintillation is most severe at latitudes between $\pm 20^\circ$, and in polar regions. In these regions, heavy scintillation often occurs in the VHF and UHF bands, and occasionally at L band. Less severe scintillation may occur in the microwave frequency bands, depending on ionospheric conditions [17, pp. 83–90].

While the average signal power returned is unaffected by scintillation, the fluctuations may affect individual radar measurements, especially measurement of target RCS (see Section 8.4). In addition, the signal fluctuations, superimposed on the fluctuations due to target characteristics, may affect detection performance. Since the fluctuations decorrelate with changes in frequency, detection techniques such as noncoherent integration of pulses transmitted at different frequencies may mitigate any degradation in detection performance [17, pp. 97–117].

The ionosphere rotates the polarization of linearly polarized signals. The magnitude of this rotation is inversely proportional to the square of signal frequency, and is a function of the integrated electron density along the signal path and the direction of propagation relative to the magnetic field.

Values of polarization rotation for two-way transmission through the ionosphere are given in Table 9.9 for several frequencies, and for both daytime and nighttime ionospheric conditions. The values are for signal paths that are not near

Table 9.9 Rotation of Linear Signal Polarization for Two-Way Transmission Through the Ionosphere

<i>Frequency (MHz)</i>	<i>Linear Polarization Rotation (Degrees)</i>			
	<i>Daytime Ionosphere</i>		<i>Nighttime Ionosphere</i>	
	<i>0° Elevation</i>	<i>90° Elevation</i>	<i>0° Elevation</i>	<i>90° Elevation</i>
100	17,400	5,400	4,800	1,400
300	1,800	560	510	15
1,000	174	54	48	14
3,000	18	6	5	2

Source: [16, pp. 363].

normal to the magnetic field lines, the condition that is most common and that gives the larger rotation values [16, pp. 360–364].

At radar frequencies below about 1 GHz, the ionosphere may rotate the linear polarization of a signal, so that it may not match the linear polarization of the receive antenna. The response of the receive antenna to the signal may then reduce the received signal, or in severe polarization-rotation cases, produce signal fluctuations. These effects may be eliminated if the receive antenna is able to receive two orthogonal linear polarizations. More often, radar with frequencies below 1 GHz that view targets through the ionosphere use circular polarization, which is not affected by the ionospheric rotation of linear polarization.

Signals that pass through the ionosphere are subject to dispersion, due to the variation of the ionosphere's refractive index with frequencies in the waveform. The magnitude of this effect depends on the radar frequency and the integrated electron density along the path. The effect of this dispersion is to limit the signal bandwidth, and therefore the range resolution, that may effectively be used (see Chapter 4), [16, pp. 364–371].

The approximate maximum signal bandwidths that may be supported by the daytime ionosphere for an elevation angle of 90° are given for several frequencies in Table 9.10. The bandwidth supported varies as $f^{1.5}$. At lower elevation angles, the signal bandwidth supported by the ionosphere will be less than the values in Table 9.10, reaching about one-third of the values given in Table 9.10 at zero-elevation angle. At nighttime, considerably larger bandwidths may be supported. Processing of the received signal to compensate for the estimated dispersion may allow larger signal bandwidth than indicated here to be used.

The refractive index in the ionosphere is less than unity. The refractivity is therefore negative, and its magnitude is proportional to the electron density and inversely proportional to the square of signal frequency. This causes the path of radar signals from terrestrial radar to be refracted downward in the lower portion of the ionosphere, and then be refracted upward in the upper portion of the ionosphere. The signal path leaving the ionosphere is approximately parallel to that entering the ionosphere, but offset below it [13, pp. 192–197].

The elevation-angle and range errors from ionospheric refraction for a ground-based radar are shown as a function of altitude in Figures 9.5 and 9.6, respectively. The plots are for a radar frequency of 200 MHz, with daytime ionospheric conditions. The elevation-angle error increases with altitude, reaches a peak at about 500-km altitude, and then decreases after the direction of refraction reverses. The

Table 9.10 Approximate Maximum Signal Bandwidth Supported by the Daytime Ionosphere for Vertical Signal Paths

<i>Radar Frequency (GHz)</i>	<i>Maximum Signal Bandwidth (MHz)</i>
0.1	0.5
0.3	2.6
1	16
3	82
10	500

Source: [16, pp. 368–369].

range errors increase monotonically in the ionosphere, and reach their maximum values at about 500-km altitude.

The elevation-angle and range errors due to the ionosphere decrease with increasing radar elevation angle, due to the decreasing total electron density in the signal path. The errors vary inversely with the square of radar frequency. For nighttime conditions, the errors are about one-third the values shown in Figures 9.5 and 9.6, and during periods of heavy ionospheric disturbances, they may be about three times the values shown.

These measurement errors due to the ionosphere should be treated as bias errors in evaluating the accuracy of radar measurements (see Chapter 8). The variable nature of ionospheric conditions makes it difficult to accurately estimate the measurement errors, and in some cases the errors may be considerably larger than those calculated for standard conditions. It is therefore usually not possible to correct radar measurements for errors due to ionospheric propagation by using estimated error values.

For example, at a radar frequency of 200 MHz, 20° elevation angle, and a target altitude of 1,000 km, the standard daytime elevation-angle error is 0.9 mrad, and the range error is 600m. With standard nighttime ionospheric conditions, the errors would be reduced to about 0.3 mrad and 200m, respectively. With severe ionospheric disturbances, the errors could increase to 2.7 mrad and 1.8 km, respectively.

One approach to improving the estimate is to make measurements on a target at two frequencies, and calculate the errors that would produce these observations. In cases where better measurement accuracy is needed, it may be possible to “calibrate” the ionosphere by tracking satellites or other objects on known trajectories. When information on the ionospheric conditions is not available, it is reasonable to use the calculated errors for standard daytime conditions as bias errors. Values for these may be found from the VBA custom radar functions in Section 9.6.8 and 9.6.9.

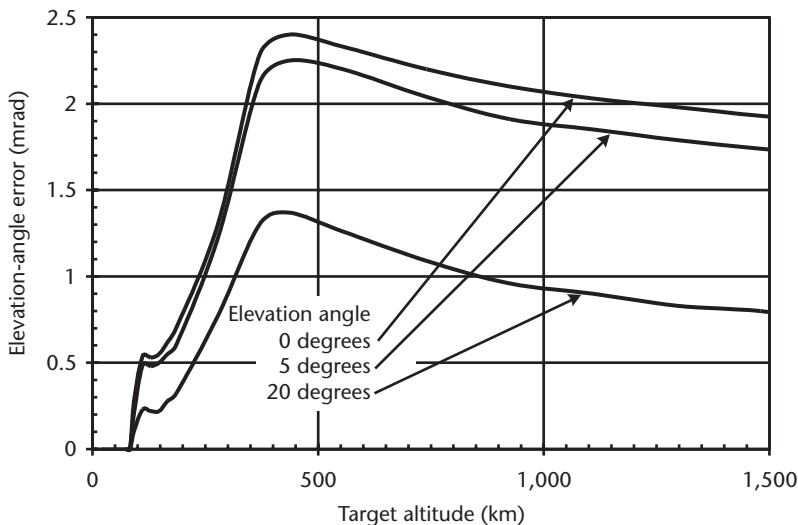


Figure 9.5 Elevation-angle errors due to the daytime ionospheric refraction for a 200-MHz ground-based radar. (After: [16, p. 334].)

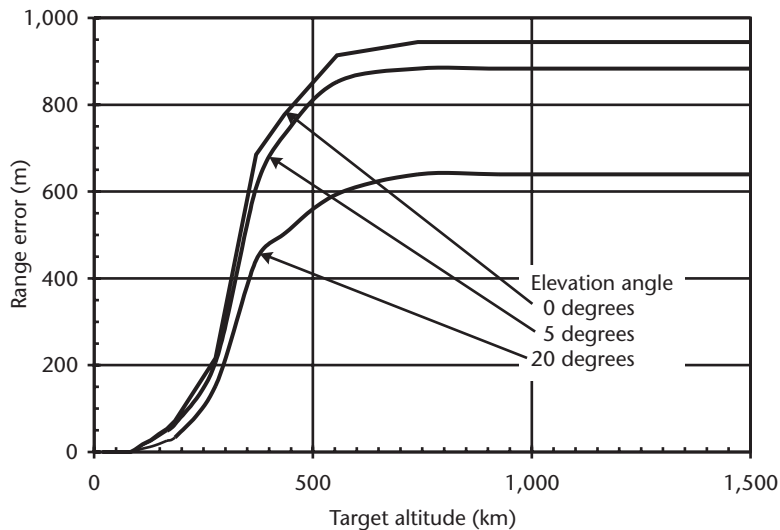


Figure 9.6 Range errors due to the daytime ionospheric refraction for a 200-MHz ground-based radar. (After: [16, p. 343].)

For frequencies in the HF band (3–30 MHz), the refraction in the lower portion of the ionosphere is so severe that the signal paths may be redirected to the Earth. This produces long-range terrestrial propagation of radio signals in these bands, and provides the basis for OTH radar [6, pp. 529–536].

9.5 Problems

The following problems are provided to assist in reviewing this chapter and to ensure a basic understanding of the material. For maximum benefit, the problems should first be solved without using the VBA custom radar functions. Solutions to these problems are given in Appendix E, Section E.9.

1. For a radar having range resolution of 150m and a pencil beam antenna with beamwidth 2° , what is the clutter area at a range of 50 km and a grazing angle of 15° , assuming it is limited by range resolution, and assuming it is limited by the elevation beamwidth? Which of these results should be used? If the clutter reflectivity, σ^0 , is -30 dB, what is the clutter RCS? If the target RCS is 10 m^2 , and 20 dB of MTI clutter cancellation is used, what is the S/C?
2. An S-band radar (3.3 GHz), with its antenna sited 20m above a perfectly reflecting sea surface, observes a target at low elevation angle. If the antenna gain is the same for the target and the multipath return, what is the minimum elevation angle at which the radar return is the same as it would be in free space? What is the elevation-angle separation of the lobes that are generated? Assume a flat Earth.
3. For what radar frequencies are precipitation effects more pronounced? With what frequencies may they usually be ignored?

4. For a tropical, wet climate, what is the rainfall rate that is exceeded only one hour per year? How many hours per year is a rainfall rate of 16 mm/hr exceeded? For a C band radar (5 GHz), what is the attenuation per kilometer for this latter rainfall rate?
5. What is the rain clutter volume reflectivity for a rainfall rate of 10 mm/hr and a radar frequency of 9.5 GHz (X-band)? For this case, what is the clutter RCS at a range of 50 km for a radar having azimuth and elevation beamwidths of 1 degree and 3°, respectively, and a signal bandwidth of 10 MHz?
6. A ground-based X-band radar (9.5 GHz) observes a target at an elevation angle of 5° and range of 1,000 km. What is the two-way tropospheric loss? What is the lens loss? What is the total two-way loss from the atmosphere? What are the elevation-angle and range measurement errors due to tropospheric propagation?
7. What is the daytime and the nighttime two-way ionospheric attenuation for a radar at a frequency of 100 MHz viewing a target at an altitude of 500 km with an elevation angle of 20°? What are the elevation-angle and range errors from the ionosphere for these conditions and the normal daytime and nighttime ionosphere?
8. What is the ground clutter area for a radar range of 100 km, azimuth and elevation beamwidths of 1 degree, range resolution of 15m, and grazing angle of 5°? What grazing angle would make the elevation beamwidth determine the clutter area? For the 5° grazing angle, what is the clutter RCS if $\sigma^0 = -25$ dB? If the target RCS is 1 m², what is the S/C? What clutter CR is needed to give S/C = 15 dB?
9. What is the two-way rain attenuation for a 20-km path in 4-mm/hr rain at 10 GHz? What percent of the year is this rainfall rate exceeded in region D2?
10. What is the rain clutter volume for range of 200 km, azimuth and elevation beamwidths of 1.5°, and range resolution of 150m? What is the rain clutter reflectivity at 3.3 GHz and 4 mm/hr rainfall? What is the resulting rain clutter RCS? For a target RCS of -5 dBsm, 30 dB of clutter cancellation, and 3 dB of target cancellation loss, what is the S/C?
11. What is the two-way tropospheric loss for a 1-GHz radar at 2° elevation angle and target altitude of 100 km? What is the lens loss? What is the total loss from the atmosphere? What are the elevation and range measurement errors, both uncorrected and corrected to 10%?
12. What radar frequencies are most affected by the ionosphere? At what frequencies may ionospheric effects usually be ignored?
13. What is the two-way daytime ionospheric loss for a target at 500 km altitude, elevation angle of 5°, and a radar frequency of 300 MHz? Is rotation of linear polarization a concern for this case? What is the maximum signal bandwidth without special processing? What are the normal daytime elevation and range measurement errors? How might these vary at nighttime, and for disturbed ionospheric conditions?

9.6 VBA Software Functions for Environment and Mitigation Techniques

9.6.1 Function SCR_Surf_dB

Purpose Calculates the S/C for surface (terrain and sea) clutter.

Reference Equations (9.1) to (9.3), and (9.6).

Features Determines whether range resolution or elevation beamwidth determines the range extent of the clutter return, and calculates clutter area accordingly. Uses 1.6-dB beamshape loss for range-resolution limited clutter, and 3.2 dB for elevation-beamwidth limited clutter. Allows input of clutter CR.

Input Parameters (with units specified)

Range_km = target range (km).

Az_Beam_mR = radar azimuth beamwidth (mrad).

El_Beam_mR = radar elevation beamwidth (mrad).

Range_Res_m = radar range resolution (m).

Gr_Angle_deg = grazing angle, (angle between the terrain surface and the radar LOS), from 0 to 90°.

Tgt_RCS_dBsm = target RCS (dBsm).

Sig_Zero_dB = clutter RCS per unit area observed, σ^0 , normally a factor less than unity, represented by a negative decibel value (dB).

Clutter_Cancel_dB (optional) = clutter cancellation factor provided by MTI or pulse-Doppler processing, normally a factor greater than unity, represented by a positive decibel value (dB). If no value is input, no cancellation is assumed.

Function Output The S/C for the parameters specified (dB).

The Excel Function Arguments parameter box for Function SCR_Surf_dB is shown in Figure 9.7, with sample parameters and a solution.

9.6.2 Function RainLocAtten_dBpkm

Purpose Calculates the two-way attenuation per kilometer due to rainfall in a local region.

Reference Equations (9.13).

Features Uses methodology and parameters from Crane [11] to calculate two-way attenuation in decibels per kilometer as a function of radar frequency and rainfall rate.

Input Parameters (with units specified)

Freq_GHz = radar frequency from 1 to 100 (GHz). Frequencies outside this range will produce no result, indicated by an output of -1.

RainR_mmphh = local rainfall rate (mm/hr).

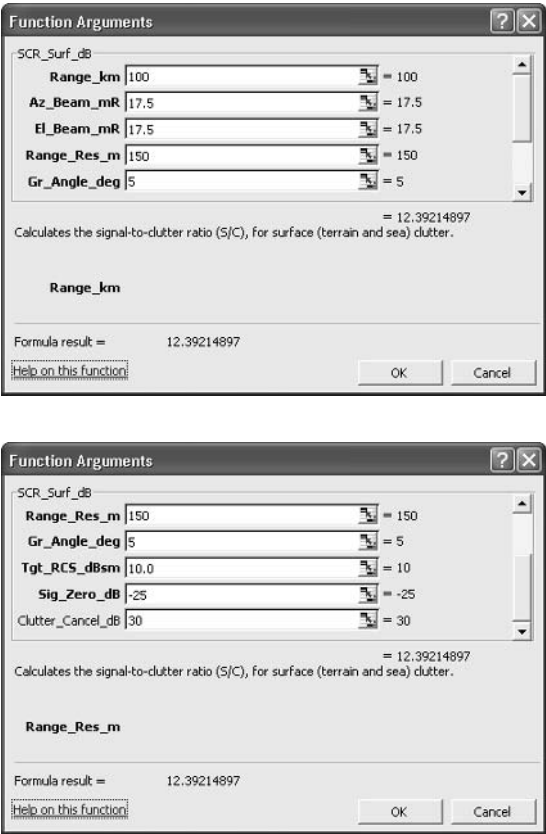


Figure 9.7 Excel parameter box for Function SCR_Surf_dB.

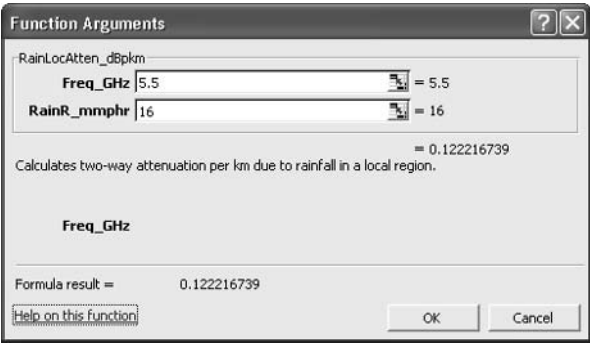


Figure 9.8 Excel parameter box for Function RainLocAtten_dBpkm.

Function Output Local two-way attenuation due to rain (dB/km).

The Excel Function Arguments parameter box for Function RainLocAtten_dBpkm is shown in Figure 9.8, with sample parameters and a solution.

9.6.3 RainPathAtten_dB

Purpose Calculates the probable two-way attenuation from rainfall over a specified radar signal path.

Reference Equations None.

Features Uses the methodology and data in Crane [11] to calculate the two-way attenuation due to rainfall over a specified propagation path, that is exceeded a specified fraction of the time over the year. Takes into account radar frequency, the rainfall region (see Table 9.3), signal-path geometry, and altitude of the 0° isotherm as a function of latitude and probability of occurrence. May be used for radar at high altitude observing near-surface targets by substituting target location for radar location.

Input Parameters (with units specified) Region_number = rain climate region from Table 9.3 (number):

Input 1 for Region A
 Input 2 for Region B
 Input 3 for Region C
 Input 4.1 for Region D1
 Input 4.2 for Region D2
 Input 4.3 for Region D3
 Input 5 for Region E
 Input 6 for Region F
 Input 7 for Region G
 Input 8 for Region H

Any other input will produce no result, indicated by an output of -1.

Exceed_percent = fraction of the year that the rainfall rate used in the function is to be exceeded, from 0.001 to 2 percent (percent). Values outside this range will produce no result, indicated by an output of -2.

Radar_Alt_km = altitude of radar above sea level (km).

Radar_El_deg = radar elevation angle (degrees).

Freq_GHz = radar frequency, from 1 to 100 (GHz). Frequencies outside this range will produce no result, indicated by an output of -3.

Radar_Lat_deg = latitude of the radar location from 0 and 70° positive or negative (degrees). Values outside this range will produce no result, indicated by an output of -4. For latitude larger than 70°, input 70°.

Iso_percent = probability of occurrence of the zero-degree isotherm altitude used in the calculation, from 0.001 to 1 percent (percent). Values outside this range will produce no result, indicated by an output of -5.

Range_km (optional) = radar range to target in propagation path (km). If blank, target is assumed to be above the zero-degree isotherm.

Function Output Calculated two-way attenuation from rain for the specified path, parameters, and percent of the year it will be exceeded (dB).

The Excel Function Arguments parameter box for Function RainPathAtten_dB is shown in Figure 9.9, with sample parameters and a solution.

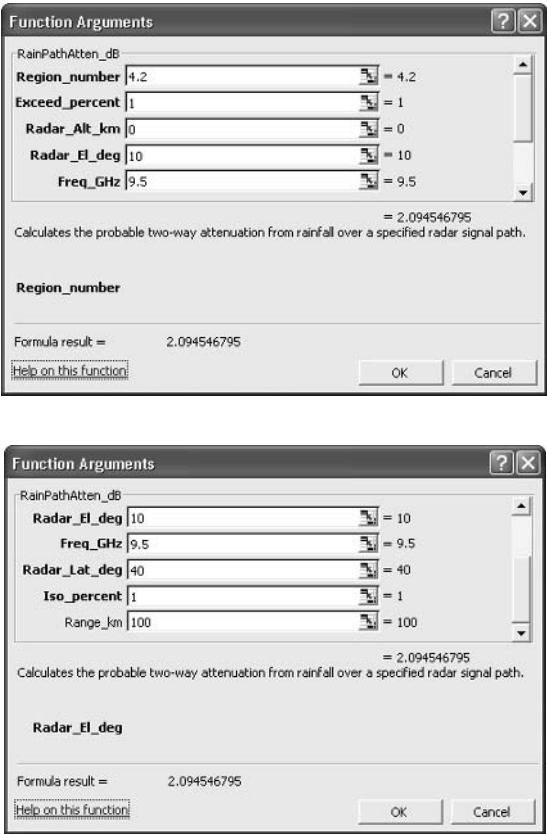


Figure 9.9 Excel parameter box for Function RainPathAtten_dB.

9.6.4 Function SCR_Rain_dB

Purpose Calculates the S/C for volume rain clutter.

Reference Equations (9.14) to (9.17).

Features Uses 3.2-dB beamshape loss. Allows input of clutter CR and target polarization loss, L_x .

Input Parameters (with units specified)

- Range_km = target range (km).
- Az_Beam_mR = radar azimuth beamwidth (mrad).
- El_Beam_mR = radar elevation beamwidth (mrad).
- Range_Res_m = radar range resolution (m).
- RainR_mmphr = rainfall rate (mm/hr).
- Freq_GHz = radar frequency (GHz).
- Tgt_RCS_dBsm = target RCS (dBsm).
- Clutter_Cancel_dB (optional) = combined clutter cancellation factor provided by MTI or pulse-Doppler processing, and receiving same-sense circular

polarization, normally a factor greater than unity, represented by a positive decibel value (dB). If no value is input, no cancellation is assumed.

Tgt_Pol_L_dB (optional) = target polarization loss from using same-sense receive circular polarization (dB). If left blank, no loss will be assumed.

Function Output The S/C for the parameters specified (dB).

The Excel Function Arguments parameter box for Function SCR_Rain_dB is shown in Figure 9.10, with sample parameters and a solution.

9.6.5 Function TropoAtten_dB

Purpose Calculates the two-way loss due to tropospheric attenuation and lens loss for a radar at sea level and a specified signal path.

Reference Equations None.

Features May be used for sea-based and most ground-based radars, except those deployed at high altitudes, and for airborne and space-based radar viewing surface targets. Assumes standard atmospheric conditions. Considers target locations both within and outside the troposphere. Tropospheric attenuation is based on data in

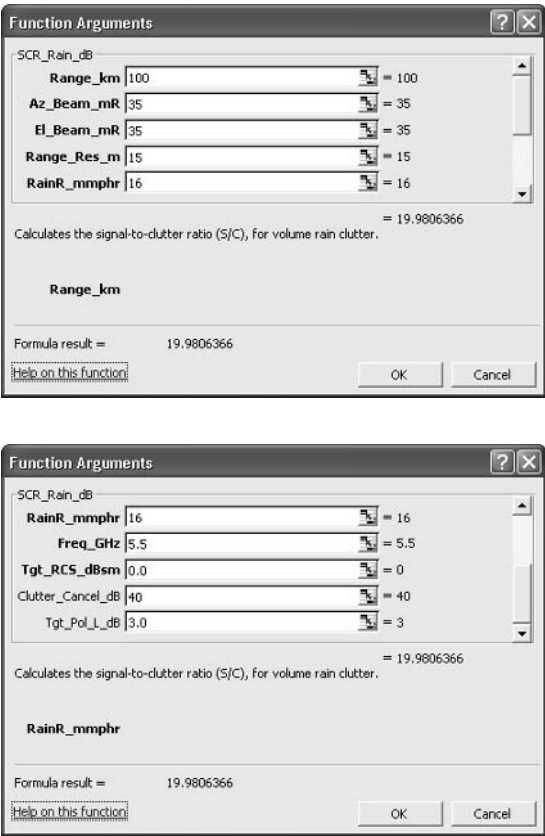


Figure 9.10 Excel parameter box for Function SCR_Rain_dB.

Blake [13, pp. 210—216; 14, pp. 2-48–2-51], and lens loss is based on data in [1, p. 323], with interpolation used to estimate losses for the specific parameters input.

Input Parameters (with units specified)

Freq_GHz = radar frequency from 0.1 to 10 (GHz). Frequencies outside this range will produce no result, indicated by an output of -1 .

Range_km = target range from 0 to 60,000 (km). Ranges outside this range will produce no result, indicated by an output of -2 .

El_Angle_deg = radar elevation angle from 0 to 90 (degrees). Elevation angles outside this range will produce no result, indicated by an output or -3 .

Function Output Two-way tropospheric attenuation for standard atmospheric conditions for the radar frequency and signal path defined by the input data (dB).

The Excel Function Arguments parameter box for Function TropoAtten_dB is shown in Figure 9.11, with sample parameters and a solution.

9.6.6 Function TropoEl_Err_mR

Purpose Calculates the elevation-angle measurement error due to tropospheric refraction for a radar at sea level and a specified signal path.

Reference Equations None.

Features May be used for sea-based and most ground-based radars, except those deployed at high altitudes, and for grazing angle for airborne and space-based radar viewing surface targets. Allows an error-correction factor to be input. Considers target locations both within and outside the troposphere. Assumes standard atmospheric conditions. Based on data in Barton and Ward [5, p. 369], with interpolation used to estimate the error for the specific parameters input.

Input Parameters (with units specified)

Range_km = target range, from 10 to 60,000 (km). Values outside this range will produce no result, indicated by an output of -1 .

El_Angle_deg = radar elevation angle from 0.23 to 51.5 (degrees). Values outside this range will produce no result, indicated by an output of -2 .

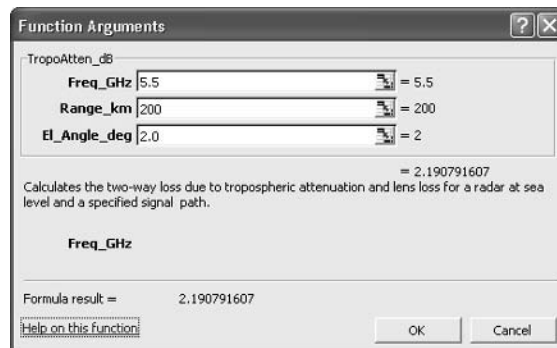


Figure 9.11 Excel parameter box for Function TropoAtten_dB.

Err_Correct_percent (optional) = correction factor to which measurement error may be reduced (percent). If left blank, no correction will be assumed.

Function Output Elevation-angle error due to the tropospheric refraction for standard atmospheric conditions for the signal path defined by the input data, with the specified correction factor applied (mrad).

The Excel Function Arguments parameter box for Function TropoEl_Err_mR is shown in Figure 9.12, with sample parameters and a solution.

9.6.7 Function TropoR_Err_m

Purpose Calculates the range measurement error due to tropospheric refraction for a radar at sea level and a specified signal path.

Reference Equations None.

Features May be used for sea-based and most ground-based radars, except those deployed at high altitudes, and for airborne and space-based radar viewing surface targets. Allows an error-correction factor to be input. Considers target locations both within and outside the troposphere. Assumes standard atmospheric conditions. Based on data in Barton and Ward [5, p. 368], with interpolation used to estimate the error for the specific parameters input.

Input Parameters (with units specified)

- Range_km = target range, from 10 to 60,000 (km). Values outside this range will produce no result, indicated by an output of -1.
- El_Angle_deg = radar elevation angle from 0 to 51.5 (degrees). Values outside this range will produce no result, indicated by an output of -2.
- Err_Correct_percent (optional) = correction factor to which measurement error may be reduced (percent). If left blank, no correction will be assumed.

Function Output Range error due to the tropospheric refraction for standard atmospheric conditions for the signal path defined by the input data, with the specified correction factor applied (m).

The Excel Function Arguments parameter box for Function TropoR_Err_mR is shown in Figure 9.13, with sample parameters and a solution.

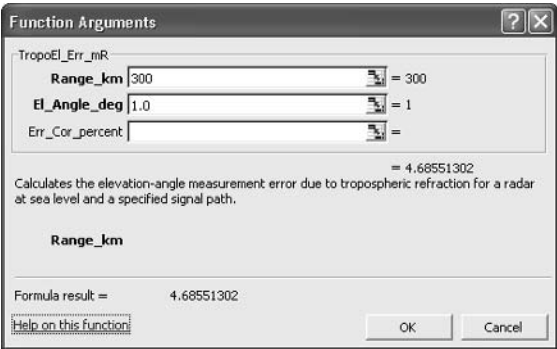


Figure 9.12 Excel parameter box for Function TropoEl_Err_mR

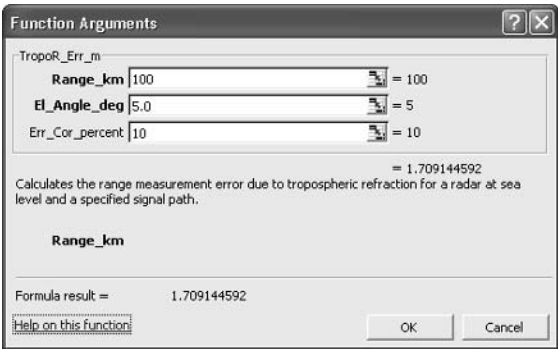


Figure 9.13 Excel parameter box for Function TropoR_Err_mR.

9.6.8 Function IonoEl_Err_mR

Purpose Calculates the elevation-angle measurement error due to standard daytime ionospheric refraction for a radar at sea level and a specified signal path.

Reference Equations None.

Features May be used for most surface-based and airborne radar with acceptable accuracy, and for grazing angle for space-based radar viewing terrestrial targets. Considers target locations both within and outside the ionosphere. Assumes standard daytime ionospheric conditions. Based on data in Millman [16, pp. 334–335], with scaling for frequency, interpolation in elevation angle, and extension in altitude. Results for target altitudes greater than 1,850 km and elevation angles greater than 20° are based on extrapolation of the data and may not be accurate.

Input Parameters (with units specified)

- Range_km = target range from 10 to 60,000 (km). Values outside this range will produce no result, indicated by an output of –1.
- El_Angle_deg = radar elevation angle from 0 to 90 (degrees). Values outside this range will produce no result, indicated by an output of –2.
- Freq_GHz = radar frequency from 0.1 to 1 (GHz). Values outside this range will produce no result, indicated by an output of –3.

Function Output Elevation-angle error due to the ionosphere for standard daytime ionospheric conditions for the frequency and signal path defined by the input data (mrad).

The Excel Function Arguments parameter box for Function IonoEl_Err_mR is shown in Figure 9.14, with sample parameters and a solution.

9.6.9 Function IonoR_Err_m

Purpose Calculates the range measurement error due to standard daytime ionospheric refraction for a radar at sea level and a specified signal path.

Reference Equations None.

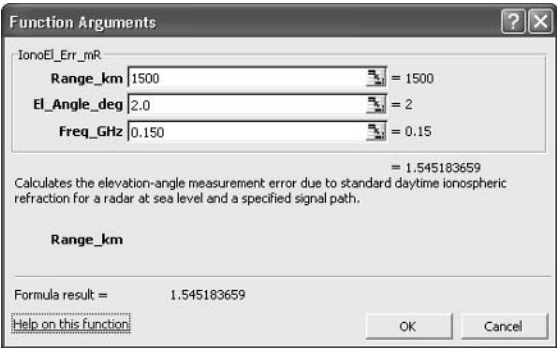


Figure 9.14 Excel parameter box for Function IonoEl_Err_mR

Features May be used for most surface-based and airborne radars with acceptable accuracy, and for space-based radar viewing terrestrial targets. Considers target locations both within and outside the ionosphere. Assumes standard daytime ionospheric conditions. Based on data in Millman [16, p. 343], with scaling for frequency and interpolation in elevation angle. Results for target altitudes greater than 1,850 km and elevation angles greater than 20° are based on extrapolation of the data and may not be accurate.

Input Parameters (with units specified)

- Range_km = target range from 10 to 60,000 (km). Values outside this range will produce no result, indicated by an output of -1.
- El_Angle_deg = radar elevation angle from 0 to 90 (degrees). Values outside this range will produce no result, indicated by an output of -2.
- Freq_GHz = radar frequency from 0.1 to 1 (GHz). Values outside this range will produce no result, indicated by an output of -3.

Function Output Range error due to the ionosphere for standard daytime ionospheric conditions for the frequency and signal path defined by the input data (m).

The Excel Function Arguments parameter box for Function TropoR_Err_mR is shown in Figure 9.15, with sample parameters and a solution.

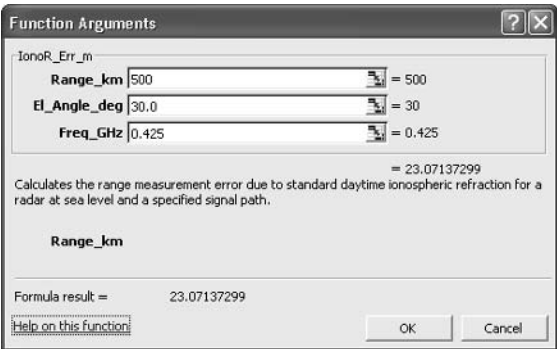


Figure 9.15 Excel parameter box for Function TropoR_Err_mR

References

- [1] Morchin, W., *Radar Engineer's Sourcebook*, Norwood, MA: Artech House, 1993.
- [2] Shrader, W. W., and V. Gregers-Hansen, "MTI Radar," Chapter 15 in *Radar Handbook*, 2nd Ed., M. I. Skolnik, (ed.), New York: McGraw-Hill, 1990.
- [3] Barton, D. K., *Modern Radar System Analysis*, Norwood, MA: Artech House, 1988.
- [4] Morchin, W. C., *Airborne Early Warning Radar*, Norwood, MA: Artech House, 1990.
- [5] Barton, D. K., and H. R. Ward, *Handbook of Radar Measurements*, Dedham, MA: Artech House, 1984.
- [6] Barton, D. K., *Radar System Analysis*, Englewood Cliffs, NJ: Prentice Hall, 1964, p. 214.
- [7] Morris, G. V., *Airborne Pulsed Doppler Radar*, Norwood, MA: Artech House, 1988.
- [8] Skolnik, M. I., *Introduction to Radar Systems*, 2nd ed., New York: McGraw-Hill, 1980.
- [9] Goldstein, H., "The Intensity of Meteorological Echoes," in *Propagation of Short Radio Waves*, D. E. Kerr, (ed.), New York: McGraw-Hill, 1951, pp. 607–621.
- [10] Goldstein, H., "Attenuation by Condensed Water," in *Propagation of Short Radio Waves*, D. E. Kerr, (ed.), New York: McGraw-Hill, 1951, pp. 671–692.
- [11] Crane, R. K., "Prediction of Attenuation by Rain," *IEEE Trans. on Communications*, Vol. COM-28, No. 9, September 1980, pp. 1717–1733.
- [12] Van Vleck, J. H., "Theory of Absorption by Uncondensed Gasses," in *Propagation of Short Radio Waves*, D. E. Kerr, (ed.), New York: McGraw-Hill, 1951, pp. 646–664.
- [13] Blake, L. V., *Radar Range-Performance Analysis*, Dedham, MA: Artech House, 1986.
- [14] Blake, L. V., "Prediction of Radar Range," Chapter 2 in *Radar Handbook*, 2nd ed., M. I. Skolnik, (ed.), New York: McGraw-Hill, 1970.
- [15] Bougish, A. J., Jr., *Radar and the Atmosphere*, Norwood, MA: Artech House, 1989.
- [16] Millman, G. H., "Atmospheric Effects on Radio Wave Propagation," Chapter 1 in *Modern Radar*, R. S. Berkowitz, (ed.), New York: John Wiley & Sons, 1965.
- [17] Knepp, D. L., and J. T. Reinking, "Ionospheric Environment and Effects on Space-Based Radar Detection," Chapter 3 in *Space-Based Radar Handbook*, L. J. Cantafio, (ed.), Norwood, MA: Artech House, 1989.

Selected Bibliography

Radar clutter, its characteristics, and its effects on radar observations, and the impact of multipath on radar measurement, are treated in Chapter 5 of Barton and Ward. Further data on radar clutter is found in Morchin Chapter 3, and in Long, Ulaby and Dobson, and in Billingsley. MTI radar is discussed by Shrader, and Shrader and Gregers-Hansen in Skolnik. Airborne MTI and pulse-Doppler radar are discussed by Staudaher in Skolnik. Airborne pulse-Doppler radar is also treated by Morris.

Theory and measurements of meteorological scattering and attenuation are found in Goldstein, in Volume 13 of the MIT Radiation Laboratory series. The model for rain attenuation is given a paper by Crane. More detail and more complex models are given in a book by Crane, which includes a disk with VBA functions of the models.

Theory and measurements of tropospheric attenuation are found in Van Vleck, in Volume 13 of the MIT Radiation Laboratory series. The effects of radar multipath, tropospheric effects and ionospheric effects on radar detection and measurement are addressed by Blake. The more recent tropospheric loss data given by Blake

(1986 and 1989), give losses that are slightly larger than given earlier in Blake (1970), as a result of improved calculation techniques. This later data is used in Section 9.3 and in the VBA custom radar function TropoAtten_dB, described in Section 9.6.5. Lens loss is quantified in Chapter 15 of Morchin. Ionospheric characteristics and their impact on radar performance are treated by Bougish, and by Knepp and Reinking.

Barton, D. K., and H. R. Ward, *Handbook of Radar Measurement*, Dedham, MA: Artech House, 1984.

Billingsley, J. B., *Low-Angle Radar Land Clutter*, Christchurch, New Zealand: SciTech/William Andrews, 2001.

Blake, L. V., "Prediction of Radar Range," Chapter 2 in *Radar Handbook*, M. I. Skolnik, (ed.), New York: McGraw-Hill, 1970.

Blake, L. V., "Prediction of Radar Range," Chapter 2 in *Radar Handbook, 2nd Ed.*, M. I. Skolnik, (ed.), New York: McGraw-Hill, 1990.

Blake, L. V., *Radar Range-Performance Analysis*, Dedham, MA: Artech House, 1986.

Bougish, A. J., Jr., *Radar and the Atmosphere*, Norwood, MA: Artech House, 1989.

Crane, R. K., "Prediction of Attenuation by Rain," *IEEE Trans. on Communications*, Vol. COM-28, No. 9, September 1980, pp. 1717–1733.

Crane, R. K., *Electromagnetic Wave Propagation Through Rain*, New York: John Wiley & Sons, 1996.

Goldstein, H., "The Intensity of Meteorological Echoes," In *Propagation of Short Radio Waves*, D. E. Kerr, (ed.), New York: McGraw-Hill, 1951, pp. 607–621.

Goldstein, H., "Attenuation by Condensed Water," In *Propagation of Short Radio Waves*, D. E. Kerr, (ed.), New York: McGraw-Hill, 1951, pp. 671–692.

Knepp, D. L., and J. T. Reinking, "Ionospheric Environment and Effects on Space-Based Radar Detection," Chapter 3 in *Space-Based Radar Handbook*, L. J. Cantafio, (ed.), Norwood, MA: Artech House, 1989.

Long, M. W., *Radar Reflectivity of Land and Sea, Third Edition*, Norwood, MA: Artech House, 2001.

Morchin, W., *Radar Engineer's Sourcebook*, Norwood, MA: Artech House, 1993.

Morchin, W. C., *Airborne Early Warning Radar*, Norwood, MA: Artech House, 1990.

Morris, G. V., *Airborne Pulsed Doppler Radar*, Norwood, MA: Artech House, 1988.

Ridenour, L. N., (ed.), *Massachusetts Institute of Technology Radiation Laboratory Series, Vols. 1 through 28*, New York: McGraw Hill, 1951. *M.I.T. Radiation Laboratory Series, 28 Volumes on 2 CD ROMs*, Norwood, MA: Artech House, 1999.

Shrader, W. W. "MTI Radar," Chapter 17 in *Radar Handbook*, M. I. Skolnik, (ed.), New York: McGraw-Hill, 1970.

Shrader, W. W., and V. Gregors-Hansen, "MTI Radar," Chapter 15 in *Radar Handbook, 2nd Ed.*, M. I. Skolnik, (ed.), New York: McGraw-Hill, 1990.

Skolnik, M. I., (ed.), *Radar Handbook*, New York: McGraw-Hill, 1970.

Skolnik, M. I., (ed.), *Radar Handbook*, 2nd ed., New York: McGraw-Hill, 1990.

Staudaher, F. M., "Airborne MTI," Chapter 18 *Radar Handbook*, M. I. Skolnik, (ed.), New York: McGraw-Hill, 1970.

Staudaher, F. M., "Airborne MTI," Chapter 16 *Radar Handbook*, 2nd ed., M. I. Skolnik, (ed.), New York: McGraw-Hill, 1990.

Ulaby, F. T., and M. C. Dobson, *Handbook of Radar Scattering Statistics for Terrain*, Norwood, MA: Artech House, 1989.

Van Vleck, J. H., "Theory of Absorption by Uncondensed Gasses," In *Propagation of Short Radio Waves*, D. E. Kerr, (ed.), New York: McGraw-Hill, 1951, pp. 646–664.

Radar Countermeasures and Counter-Countermeasures

This chapter enables the reader to:

- Understand the concepts of employing countermeasures to degrade radar performance, and the use of counter-countermeasures by radar designers and operators to reduce or eliminate the resulting performance degradation;
- Quantify the impacts of mainlobe and sidelobe jamming on radar performance, and evaluate capabilities of radar characteristics and operating modes to mitigate these impacts;
- Quantify the impact of volume chaff on radar performance, and evaluate the capabilities of radar characteristics and operating modes to mitigate these impacts;
- Understand the concept of employing decoys that match radar targets, and quantify the ability to discriminate between intended targets and such decoys using radar measurements.

Military radar may be subjected to deliberate interference by an enemy. Such an interfering tactic is called a radar countermeasure (CM). When it employs electromagnetic radiation such as jamming, it is called an electronic countermeasure (ECM). A technique employed in the radar to mitigate these interfering tactics is called a counter-countermeasure (CCM), or electronic counter-countermeasure (ECCM).

Radar countermeasures may attempt to:

- Mask targets of interest to the radar by using, for example, electronic jamming signals or radar volume chaff;
- Overload or confuse the radar operator or signal processor by generating large numbers of false targets, either electronically or with physical objects;
- Deceive the radar operator or signal processor by using false electronic targets or physical objects, often called decoys, that resemble the targets of interest.

Most military radars employ CCMs to eliminate or reduce the impact of the CMs. Radar CCMs may employ:

- Radar design features that improve performance in countermeasure environments. Examples are low antenna sidelobes and high-resolution waveforms.

- Radar operating modes and procedures that respond to the countermeasures employed. Examples are use of high-energy waveforms and pulse integration, and precise tracking and radar signature measurements.
- Special CM circuits, techniques, and actions, such as sidelobe blankers, sidelobe cancellers, added transmitter power for burnthrough, and passive tracking.

The CM designer attempts to exploit weaknesses in the radar design, while the radar designer attempts to anticipate potential CMs and provide CCMs that reduce their effectiveness. While it may not be possible to eliminate entirely the effects of CMs, their impact usually may be reduced. Alternatively, CCMs may significantly increase the cost of CMs needed to degrade radar performance, so that the tactic may no longer be attractive to an enemy.

Even when radar is not subjected to intentional CMs, it may have to cope with various forms of electromagnetic interference and complex target configurations. Therefore, even nonmilitary radar may employ some CCM-like techniques to reduce the impact of these interfering or confusing signals.

Common CMs and the CCMs that may reduce their impact are briefly discussed in Section 10.1. The three principal masking CM techniques, mainlobe noise jamming, sidelobe noise jamming, and volume radar chaff, and their CCMs, are amenable to system-level analysis, and are described in Sections 10.2, 10.3, and 10.4, respectively. Discrimination of radar decoys using radar measurements is addressed in Section 10.5. VBA custom radar functions for evaluating the impact of these techniques are described in Section 10.7.

Confusion and deception CMs often exploit the detailed characteristics of radar waveforms, operating modes, and signal processing. The CCMs in turn modify or enhance radar characteristics to reduce the radar vulnerability. Analysis of these detailed CM and CCM characteristics is provided in [1–3], and is beyond the scope of this book.

10.1 Radar Countermeasure Summary

Common radar CMs are listed in Table 10.1 for three CM classes: masking, confusion, and deception. Potential CCMs are given for each CM. These are discussed below.

Radar jammers emit electromagnetic radiation toward the radar antenna. To be effective, the jamming signal must occupy the same spectral band as the radar signal being received. Then the jamming signal may mask the target returns, or produce false target-like signals in the radar receiver. The jammer may be located on or near the target, in which case the jamming signal enters the radar antenna through the main beam of a radar observing the target. If the jammer is not located near the target, its signal must enter the radar antenna through the sidelobe region of such a radar. In this case, considerably more jammer power is needed to overcome the sidelobe rejection.

When details of the radar signal are not known to the jammer, masking jammers are most effective when they employ white Gaussian noise that covers the band of

Table 10.1 Common Radar CMs and CCMs

<i>CM Class</i>	<i>CM</i>	<i>CCM</i>
Masking	Mainlobe jammer	Frequency agility
		Burnthrough
		Passive tracking
	Sidelobe jammer	Low sidelobes
		Frequency agility
		Burnthrough
Confusion	Pulsed jammer	Sidelobe cancellation
		Range resolution
		Velocity resolution
	Traffic decoys	Sidelobe blanking
		Frequency agility
		Tracking
	Debris	Range resolution
		Bulk filtering
		Tracking
Deception	Repeater jammer	Bulk filtering
		Tracking
		Frequency agility
	Track-breaking jammer	PRF agility
		Signal processing
		Signal processing
	Spot chaff	Tracking
		Radar measurements
	Decoy	Tracking
		Radar measurements
		Tracking

the radar receiver [4, p. 560]. This jamming signal adds to the radar background noise, and may degrade target detection and measurement. A spot jammer has a relatively narrow spectral band, and may be effective if the jammer band matches the radar signal band. If the radar signal band is not known to the jammer, or if the radar employs frequency agility (pulse-to-pulse frequency changes), the spot jammer loses its effectiveness. The jammer must then employ a wide frequency band that encompasses the expected radar frequency variations. Such a jammer, called a barrage-noise jammer, requires more power than a spot jammer, since only some of its power lies in the radar receiver signal band.

The preceding discussion shows that frequency agility, and for sidelobe jammers (SLJs), low sidelobes, may be effective CCMs. The effective sidelobe level may be further reduced by sidelobe cancellation, described in Section 10.3. Increasing the radar signal energy that competes with the jamming signal may improve performance. This is called radar burnthrough, and may employ higher-energy waveforms, pulse integration, and increased transmitter power and transmit gain. Mainlobe jammers (MLJs) and their associated targets may be located by measuring the angle of arrival of the jamming signal at the radar, called passive tracking. These CCM techniques are described further in Section 10.2.

Pulsed jammers may be used to create false targets that are intended to confuse the radar operator. When the jammer is in the radar sidelobes, these targets may be rejected by sidelobe-blanking, as discussed in Section 10.3. Signals from pulsed jammers may also be reduced or rejected by using frequency agility. Because the jammer

can only tune to each new radar frequency after receiving the pulse, the jamming signals will have a delay greater than that of a target at the same range as the jammer, and may be rejected on that basis. Those false targets that reach the radar receiver will likely not produce credible trajectories in the tracker, but it is desirable to reduce the number of such targets to limit the number of possible targets that must be tracked.

Swept spot jammers may also create false targets as the jamming frequency sweeps through the signal band of the radar. Swept jammers having very rapid sweep rates produce an effect in the radar receiver similar to broadband noise, and may mask targets over a broad frequency band [5, p. 140].

Repeater jammers create false targets by transmitting a replica of the radar signal synchronized with the reception of radar pulses at the jammer. When the radar uses frequency agility and/or variation in the PRF, the jammer must sense the transmitted signal and retransmit the replica at a later time. This causes the false targets to appear at a greater range than the jammer, which is usually located with the target. Such false targets often may be identified and rejected by radar signal processing or tracking, as discussed above.

More sophisticated repeater jammers are designed to break the radar track on the target by gradually moving the false target away from the real target in range, velocity and/or angle [1, pp. 143–165]. If the false target is larger than the real target, the tracker may follow the false target. Radar CCMs to this technique involve sophisticated signal processing and tracking to avoid the deception.

Chaff consists of a cloud of many small reflecting targets. These often are metallic dipoles, which are wires cut to one-half the wavelength of the radar, to produce a relatively large signal return. The collective signal return from a chaff cloud may be large, and may mask a target within the same radar resolution cell as the chaff. To be useful in masking a target, the chaff cloud must have a relatively large range dimension. The amount of chaff that masks the target may be reduced by using a waveform having a small range resolution cell (large signal bandwidth). Chaff is also likely to have a velocity spread from dispensing velocity, tumbling motion, and the effect of wind. Thus pulse-burst waveforms having small velocity resolution cells (see Section 4.5) may also reduce the amount of chaff competing with the target. Atmospheric drag may reduce the chaff velocity to that of the air mass in which it is embedded, usually well below that of an aircraft target. Then the target may be resolved from all the chaff in radial velocity.

Small clusters of chaff may be used to create false targets. These may be identified and rejected based on their slowdown in the atmosphere, or on the radar measurements discussed in Section 10.5 for decoys.

Traffic decoys and debris (e.g., pieces of junk from spent rockets) may be used against ballistic-missile defense and other military radar to create large numbers of false radar targets. Placing all these objects in track and performing discrimination measurements on them may overwhelm the radar resources.

For example, corner reflectors having a small physical size compared with a real target may create comparable RCS with monostatic radar. These objects, also called retroreflectors, consist of three planes oriented at right angles, so that incident radar energy is reflected back to the radar. The resulting monostatic RCS is given approximately by [6, pp. 588–596]:

$$\sigma \approx \frac{4\pi A_E^2}{\lambda^2} \quad (10.1)$$

where A_E is the corner-reflector area projected in the direction of the radar. At X band, a corner reflector having dimensions of about 0.2m may produce a monostatic RCS of 20 m².

Often such targets may be rejected by simple measurement thresholds. This is referred to as bulk filtering. For example, in ballistic-missile attacks, many debris objects may have smaller RCS than the target, and may be rejected using an RCS threshold. Another case is when the debris or traffic decoys have different radial velocities than the target, and may be rejected using a Doppler-frequency threshold. To perform these measurements, the objects must be resolved, so small range resolution cells may be needed. Objects that may not be rejected by bulk filtering must be placed in track, and sufficient traffic-handling capacity is needed.

A decoy is an object made to appear like a real target to the radar. It may have similar RCS and even shape, and may follow a credible trajectory or flight path. Since the decoy is generally much lighter and cheaper than a real target, it will likely not exactly match the characteristics of the real target. The discrimination process for distinguishing real targets from decoys employs radar measurements. For example, a radar might measure object RCS, fluctuations in RCS, length, and Doppler-frequency spread (see Section 8.4). The capability to use radar measurements for discriminating decoys is quantified in Section 10.5.

10.2 Mainlobe Jamming

Mainlobe jamming signals enter the radar through the main beam of the radar antenna that is directed at the target. A mainlobe jammer (MLJ), located on the target, is called a self-screening jammer (SSJ). The receive-antenna gain and the range are the same for both the target and the jammer. A jammer located on a vehicle that remains near the target is called an escort jammer (ESJ). The antenna gain and range in this case may differ somewhat from those of the target, but often may be assumed to be the same.

A jammer may be characterized by the bandwidth of the jammer signal, B_j , and by the jammer effective radiated power (ERP). The jammer ERP is the product of the jamming transmitter power, P_j , and the jammer antenna gain in the direction of the radar, G_j , reduced by the losses in the jammer, L_j :

$$ERP = \frac{P_j G_j}{L_j} \quad (10.2)$$

While the ERP of a jammer is generally specified at the peak of the jammer antenna gain, a jammer may produce different effective values of ERP for different radars being jammed due to differences in the jammer antenna gain in the directions of the radars. ERP is often specified in decibels relative to a watt, or dBW.

The radar is affected only by the jamming power reaching the radar that has the same polarization as the radar antenna. If the radar employs a single polarization

that is known to the jammer, the jammer may radiate all its power on that polarization. If the jammer polarization does not match the receive antenna polarization, the jamming power affecting the radar is reduced by a polarization loss, L_{POL} .

If the jammer does not know the radar polarization, the radar uses dual polarizations; or if the jammer cannot control the orientation of the transmitted polarization, the jammer may transmit independent jamming signals on two orthogonal polarizations. This assures that half the total jamming power is effective against the radar. This case may be modeled using a 3-dB polarization loss, or the ERP per polarization may be used in the analysis without polarization loss.

For example, a MLJ might have a transmitter power of 50W, transmit losses of 0.5 dB, and antenna gain of 5 dB. The resulting ERP = 141W (21.5 dBW). This antenna could be a simple feed horn or a dipole over a ground plane. The beamwidth of about 60° could easily be oriented in the general direction of the radar. If two such jammers were employed radiating independent jamming signals on orthogonal polarizations, the resulting total ERP would be 282W, and the ERP per polarization would be 141W.

The effect of a jammer on radar performance may be characterized by the signal-to-jammer ratio (S/J), where J is the jamming power at the output of the radar receiver filter (which is approximately matched to the radar waveform). When the jammer employs white Gaussian noise, S/J is given by:

$$\frac{S}{J} = \frac{P_p \tau G_T \sigma B_J L_{POL}}{4\pi R^2 L_T ERP} \quad (B_J \geq B_R) \quad (10.3)$$

where:

L_T = radar transmit losses, which include the transmit microwave losses, L_{MT} , and the one-way propagation losses, $L_p^{1/2}$.

The transmit antenna ohmic losses, L_{AT} , and the transmit antenna losses from aperture efficiency, L_{ET} , are assumed to be included in G_T . If they are not, they should be included in L_T . When dual polarization is used and the ERP per polarization is specified, there is no polarization loss ($L_{POL} = 1$).

The radar receiver bandwidth, B_R , is equal to the signal bandwidth, B , for receivers that employ matched filters (see Section 5.1). S/J may be expressed using the signal bandwidth, B , rather than the pulse duration, :

$$\frac{S}{J} = \frac{P_p G_T \sigma PC B_J L_{POL}}{4\pi R^2 B L_T ERP} \quad (B_J \geq B_R) \quad (10.4)$$

where $PC = \tau B$ is the matched-filter pulse compression ratio (see Chapter 4 and Section 5.1).

Equations (10.3) and (10.4) assume that the jammer is at the same range as the target, and the radar gain is the same for both the jammer and the target. This is the case for SSJs, by definition, and is usually nearly the case for ESJs. Where the range or gain for an ESJ is significantly different for the target and the jammer, (10.11) and (10.12) for sidelobe jamming, given in Section 10.3, may be used.

The jammer effectiveness depends on the fraction of its power that lies in the radar bandwidth. The jammer is most effective when $B_j = B$, often called spot noise jamming. There is no advantage to the jammer in reducing its jamming bandwidth below the receiver bandwidth, and in fact that could allow the receiver to filter out the jamming signal.

When the jammer does not know the exact frequencies of the radar signal, it must increase its bandwidth, B_j , to cover the uncertainty in signal frequency. This may occur when the jammer lacks the capability to measure the signal frequency of an individual pulse. Another situation where the jammer is forced to jam a wide band is when the radar uses frequency agility. The radar signals then occupy a wide spectral band. Even if a jammer measures the frequency of an individual signal, it often cannot jam that frequency in time to mask the target. If the jammer does not jam uniformly over the radar spectrum, the radar may sense frequencies with less jamming power, and exploit these. In these cases, the jammer may be forced to jam the full operating band of the radar, which may be 10% to 15% of the radar frequency. This is called barrage noise jamming.

Barrage noise jamming may be the most effective jamming tactic when the radar employs effective ECCM against pulsed and deceptive jamming, and frequency agility to avoid spot jamming. It is therefore a common ECM threat, and the performance of military radar against this threat is frequently analyzed. Higher radar frequency is usually advantageous in countering mainlobe jamming, due to the higher transmit antenna gain and agile signal bandwidth available.

For example, consider a radar with $P_p = 40\text{ kW}$, $G_T = 40\text{ dB}$, and $L_T = 3\text{ dB}$. The radar waveform has a 1 ms duration and a pulse compression ratio of 1,000, so the signal bandwidth $B = 1\text{ MHz}$. These parameters are summarized in the top portion of Table 10.2. If a target at a range of 200 km has an RCS of 5 m^2 and a MLJ with an ERP per polarization of 100W jamming the signal band, the resulting $S/J = 0.0199$ or -17.0 dB , as shown in column 2 of the lower part of the table. If the radar employs frequency agility over a 1 GHz band, and the jammer is forced to jam over that band, S/J increases to a power ratio of 19.9 or 13.0 dB, as shown in column 3.

Table 10.2 Mainlobe Jamming Examples

<i>Radar Parameters</i>		
P_P	40 kW	
G_T	40 dB	
L_T	3 dB	
τ	1 ms	
PC	1,000	
B	1 MHz	
<i>Target Parameters</i>		
R	200 km	200 km
σ	5 m ²	5 m ²
ERP/pol	100W	100W
B_j	1 MHz	1 GHz
S/J	-17.0 dB	13.0 dB

In addition to the radar signal bandwidth or agile frequency band discussed above, the radar parameters that influence performance in mainlobe jamming are the signal energy (the product of transmitter peak power and waveform duration), the transmit antenna gain, and the transmit losses. For a given radar design (P_p , G_T , and L_T), the performance in mainlobe jamming may be improved by increasing the signal energy, through use of longer waveform duration or pulse integration. This is often called radar burnthrough on a jammer. When the waveform duration, τ , is increased, the performance may be calculated from (10.3). When pulse integration is used to increase the signal energy, the single-pulse S/J is calculated using (10.3) or (10.4), and integrated S/J is calculated using (5.14) or (5.17) from Section 5.4, substituting S/J for S/N. Use of multiple-pulse burnthrough for detection may be analyzed using the techniques in Sections 6.3 to 6.5.

In the previous example, if the target RCS is changed to 0.1 m² for the barrage jammer case, S/J = 3.0 dB. The pulse duration may not be increased much within the minimum range constraint (see below). However the S/J may be increased to 15.0 dB by coherently integrating 16 1-ms pulses or noncoherently integrating 24 such pulses.

When the jammer employs Gaussian noise, the received jamming signal combines with the radar noise, and signal-to-jammer-plus-noise ratio, S/(J + N), may be calculated:

$$\frac{S}{J + N} = \frac{\frac{P_p \tau G_T \sigma A_R}{(4\pi)^2 R^4 L_T L_R}}{\frac{ERP A_R}{4\pi R^2 B_J L_{POL} L_R} + k T_s} \quad (10.5)$$

where:

L_R = radar receive losses, which include the receive microwave losses, L_{MR} , the radar signal-processing losses, L_{SP} , and the one-way propagation losses, $L_p^{1/2}$.

The receive antenna losses, L_{AR} , and the receive antenna losses from aperture efficiency, L_{ER} , are assumed to be included in A_R . If they are not, they should be included in L_R . The total radar system loss, $L = L_T + L_R$. Equation (10.5) shows that the jamming signal dominates when the first term in the denominator becomes larger than the second, that is when $ERP > 4\pi R^2 B_J L_{POL} L_R k T_s / A_R$.

For the parameters in the previous example, and with $A_R = 0.8$ m² (X band frequency), $L_R = 3$ dB, and $T_s = 500$ K, S/(J + N) is -17.0 dB when $B_J = 1$ MHz, and 12.6 dB when $B_J = 1$ GHz. Comparison with Table 10.2 shows that, in this example, the radar system noise has negligible effect when added to the spot jamming signal, and only a small effect when added to the barrage jamming signal.

The S/(J + N) may be used in place of S/N in (5.14) and (5.17) to calculate integrated S/(J + N), and in the equations of Chapter 8 to calculate measurement accuracy. It may also be used in place of S/N for radar detection calculations (see Chapter 6).

For radar detection, a threshold is set, based on the noise level, to provide the desired false-alarm probability. When the jamming signal adds to the noise level, the

threshold must be reset, or the false-alarm probability will increase, often dramatically. In most radars, this is accomplished using a CFAR process [1, pp. 225–226] (see Section 6.2). The CFAR processor either measures the total noise level in the receiver and sets the threshold level accordingly, or monitors the false-alarm rate and adjusts the threshold in a feedback loop. The result is that when noise from jamming is significant, the false-alarm rate remains constant, but both radar measurement accuracy and detection are degraded. Use of CFAR usually produces a small loss, which should be included in L_{sp} , as discussed in Section 6.2.

The values of S/J and $S/(J + N)$ increase with decreasing range. The range at which a radar may detect or perform measurements on a target is called the burn-through range. This range for specified value of $S/(J + N)$ is given for a MLJ by:

$$R = \left\{ \left[\left(\frac{ERP A_R}{8\pi B_J L_{POL} L_R k T_s} \right)^2 + \frac{P_p \tau G_T \sigma A_R}{(4\pi)^2 L_T L_R \frac{S}{J+N} k T_s} \right]^{1/2} - \frac{ERP A_R}{8\pi B_J L_{POL} L_R k T_s} \right\}^{1/2} \quad (10.6)$$

When pulse integration is used, the single-pulse $S/(J + N)$, found from (5.18) or (5.22), should be used in (10.6).

When the range is less than the minimum range, $R_M = c\tau/2$, the target may not be observed using that pulse duration, as discussed in Section 5.5. Then the pulse duration must be reduced, and the maximum range at which the target may be observed is given by:

$$R = \left[\frac{b}{2} + \left(\frac{b^2}{4} + \frac{a^3}{27} \right)^{1/2} \right]^{1/3} - \left[-\frac{b}{2} + \left(\frac{b^2}{4} + \frac{a^3}{27} \right)^{1/2} \right]^{1/3} \quad (10.7)$$

where:

$$a = \frac{ERP A_R}{4\pi k T_s B_J L_{POL} L_R} \quad (10.8)$$

$$b = \frac{2P_p G_T \sigma A_R}{(4\pi)^2 c L_T L_R \frac{S}{J+N} k T_s} \quad (10.9)$$

The resulting pulse duration, τ , is equal to $2R/c$. When a radar has a set of pulse durations, a pulse duration smaller than that calculated above must be used, and the resulting range calculated from (10.6).

For example, with the parameters from the previous example, and barrage noise jamming ($B_J = 1$ GHz), the range at which $S/(J + N) = 15$ dB on a 5 m^2 target is found from (10.6) to be 155 km. This range is slightly greater than the minimum range for the 1-ms pulse of 150 km. If the jammer ERP per polarization is increased to 200W, the range calculated by (10.6) for a 5 m^2 target decreases to 111 km, which is less than the minimum range for the 1-ms pulse. The range calculated from (10.7) to

(10.9) is 83 km. The maximum pulse duration is then 0.55 ms. If the next shorter pulse is 0.5 ms, the range for that pulse from (10.6) is 79 km.

Figure 10.1 shows the range for the radar in this example with $S/(J + N) = 15$ dB for a 5 m² target as a function of jammer ERP per polarization for three cases: the minimum range limitation is ignored, the optimum pulse duration is used, and pulses are selected durations that decrease by factors of two.

Note that the optimum pulse duration and the selected pulse durations are calculated for a specific value of target RCS. Smaller targets will not produce the required $S/(J + N)$ with the optimum pulse durations, and larger targets could be detected at longer ranges by using longer pulses. In practice, a radar designer may choose pulse durations that give minimum ranges shorter than the calculated burn-through range, to allow for uncertainties in the radar parameter values and the RCS. This leads to somewhat shorter burnthrough ranges than given above and shown in the Figure 10.1 (see Section 7.3).

When it is not possible for the radar to burn through to detect a target with a MLJ, it may be possible to locate the target by passively measuring the jammer position in angular coordinates. For SSJs, locating the jammer directly locates the target. For ESJs, the target of interest will likely be near the ESJ. The angular measurement accuracy may be determined using (8.7) to (8.10) in Section 8.2, with S/N replaced by the jammer-to-noise ratio (J/N), which is given by:

$$\frac{J}{N} = \frac{ERP A_R}{4\pi R^2 B_J L_{POL} L_R k T_S} \quad (10.10)$$

Since J/N is large for cases of interest here, the error component that depends on this parameter is likely to be small, so that the fixed random and bias angular-

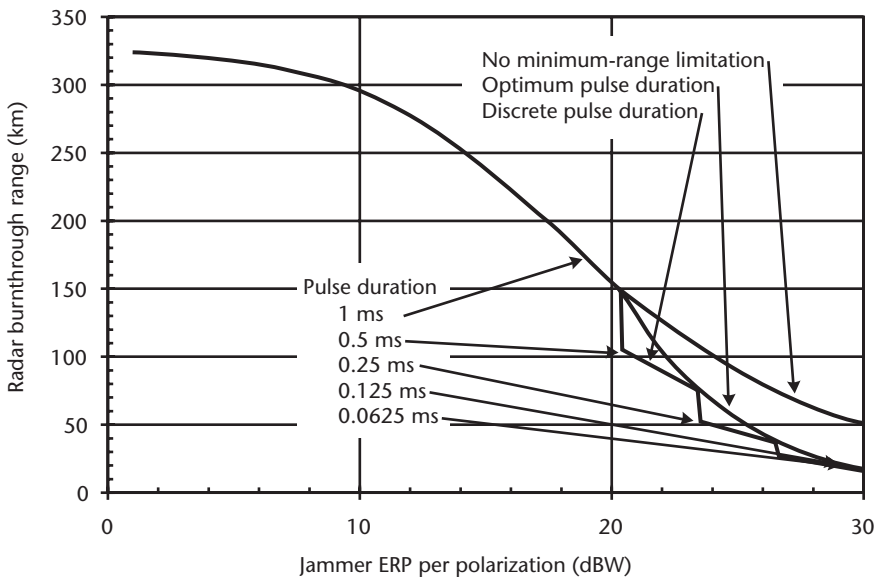


Figure 10.1 Radar range as a function of mainlobe jammer ERP per polarization for parameters in the example.

measurement errors dominate. Further, passive angular measurements do not require radar power, so a large number of such measurements may be smoothed to reduce the random errors (see Section 8.6).

Passive measurements by a single radar do not directly provide radar range. However, range may be estimated from a passive track if assumptions (e.g., constant velocity) are made about the target path. When two or more radars passively measure target angular position, the target may be located using triangulation, similar to the multilateration described in Section 8.5. When this technique is used with multiple jammers, ghosts may be produced when angular measurements by the radar are not correctly associated with the correct target.

10.3 Sidelobe Jamming

Sidelobe jamming signals enter the radar through the sidelobes of the receive antenna. A sidelobe jammer (SLJ) is separated from the target it screens. The jammer frequently remains outside the range of hostile weapons, at ranges greater than the targets it protects [1, pp. 11–13]. Such sidelobe jammers are called stand-off jammers (SOJ).

SLJs generally require significantly higher ERP than MLJs to overcome the effects of radar sidelobes and increased range from the radar. They often employ high-power transmitters, and large antennas that are directed toward the radar to be jammed. For example, a jammer with power of 20 kW, 1-dB loss, and a 30-dB antenna gain has an ERP of 15.9 MW (72.0 dBW). Such a jammer has a relatively narrow beam (5°), which must be directed at the radar. Additional jammers may be needed to jam multiple radars that are separated in angle.

When SLJs employ pulsed signals to create false targets (see Section 10.1), these signals may be rejected by using a sidelobe-blanking technique [2, pp. 100–102]. In this ECCM technique, illustrated in Figure 10.2, the signal from an auxiliary, low-gain broadbeam antenna is compared with the signal from the main antenna. When a jamming pulse enters the radar sidelobes, the signal from the auxiliary antenna is larger than the signal from the main antenna, and the signal from the main antenna is turned off for the duration of the pulse. A signal entering the mainbeam is larger than that signal from the auxiliary antenna, and is not rejected.

This sidelobe blanker (SLB) technique is widely used in both military and civil radar to protect against receiving random pulses from nearby radars that operate in the same frequency band. It may not be used with continuous jammers, since the main antenna signal could then be continuously shut off.

SLJs often use noise jamming, such as discussed above for MLJs. Much of the discussion of MLJs in Section 10.2 also applies to SLJs. SLJs may employ spot noise jamming when the radar signal band is known, or barrage noise jamming to cover the operating band of a radar when the signal band is unknown, or when the radar employs frequency agility. Radar characteristics that influence the performance in sidelobe jamming include the radar peak power, pulse duration, transmitter gain, and the bandwidth the jammer is forced to use.

With SLJs, the receive antenna sidelobe level (SL) also plays an important role in reducing the jamming power that enters the radar receiver. While close-in sidelobes

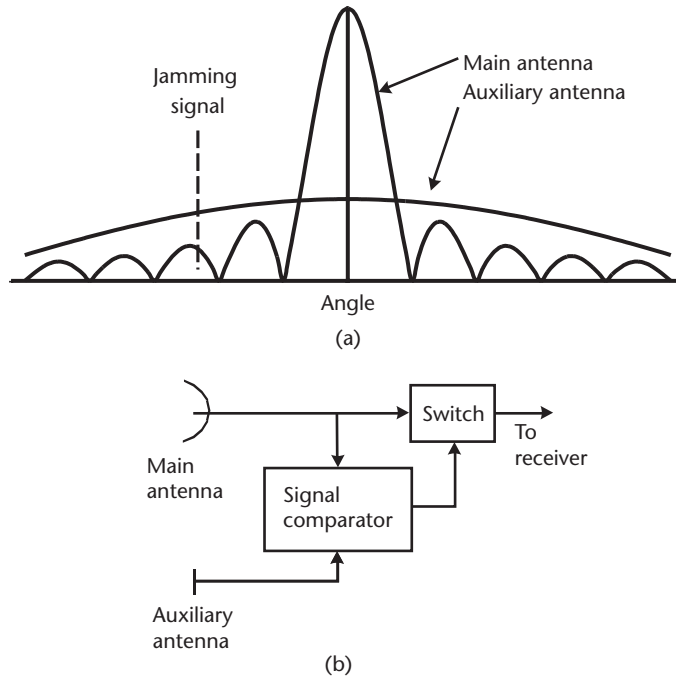


Figure 10.2 Sidelobe blanking antenna patterns and blanking circuit configuration. (a) Antenna patterns. (b) Blanking circuit.

often have levels of -13 to -20 dB relative to the peak gain, far-out sidelobes are commonly 0 to -5 dB relative to isotropic [1, p. 224], and levels of -15 dB relative to isotropic are sometimes achieved in ultralow sidelobe antennas (see Section 3.2). Thus, an antenna having 40-dB gain might have sidelobes as low as -55 dB.

The effective SL may be further reduced by using sidelobe cancellers (SLCs). This ECCM technique is illustrated in Figure 10.3. A low-gain broadbeam auxiliary antenna is used to receive the jamming signal with very little contribution from the target return. This jamming signal is subtracted from the main receiver channel, with the amplitude and phase adjusted to cancel the jamming signal in the main channel. Sidelobe cancellation differs from sidelobe blanking, discussed above, in that the jamming signal in the main channel is reduced while the signal is relatively unaffected [2, p. 102]. SLCs may be used with continuous jammers, while sidelobe blankers may be used only with pulsed jammers.

A SLC in effect modifies the main antenna pattern by reducing the SL in the direction of the jammer. Sidelobe reductions of 20 to 30 dB are typical [1, p. 224], and reductions of 40 dB and greater may be achieved. When multiple jammers are present, multiple auxiliary antennas and cancellation circuits are required. With wideband signals, the position of the sidelobe null created by the SLC may change with frequency, and more than one auxiliary may be needed per jammer [7, pp. 172–182].

The S/J for sidelobe jamming may be found from:

$$\frac{S}{J} = \frac{P_p \tau G_T \sigma R_J^2 B_J L_{POL} SLC}{4\pi R^4 L_T ERP SL} \quad (B_J \geq B_R) \quad (10.11)$$

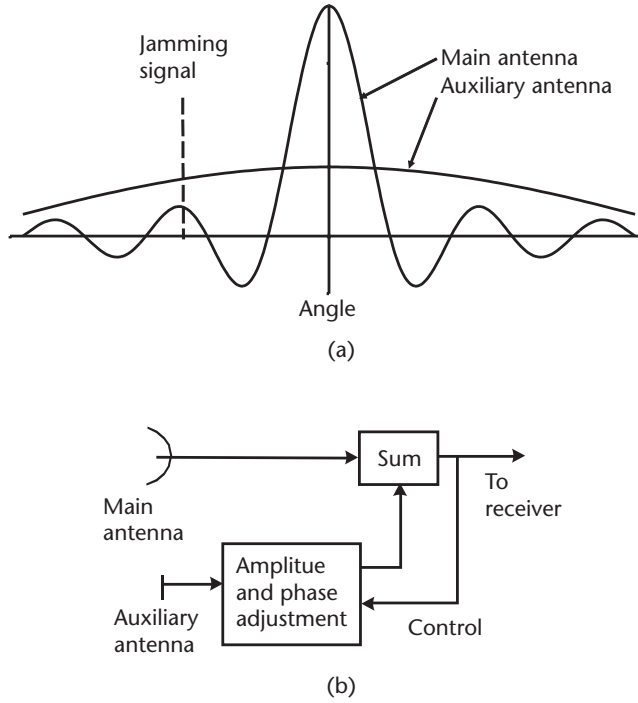


Figure 10.3 Sidelobe cancellation antenna patterns and cancellation circuit configuration. (a) Antenna patterns. (b) Cancellation circuit.

$$\frac{S}{J} = \frac{P_p G_T \sigma P C R_j^2 B_j L_{POL} SLC}{4\pi R^4 B L_T ERP SL} \quad (B_j \geq B_R) \quad (10.12)$$

where:

R_j = range of jammer from the radar.

SL = radar antenna sidelobe level, relative to the main beam (a value less than unity, represented by a negative dB value).

SLC = sidelobe cancellation ratio (a value greater than unity, represented by a positive dB value).

The $S/(J + N)$ for sidelobe jamming is given by:

$$\frac{S}{J + N} = \frac{\frac{P_p \tau G_T \sigma A_R}{(4\pi)^2 R^4 L_T L_R}}{\frac{ERP A_R SL}{4\pi R_j^2 B_j L_{POL} L_R SLC} + k T_s} \quad (10.13)$$

The radar burnthrough range when the minimum-range constraint is not exceeded is given by:

$$R = \left[\frac{\frac{P_p \tau G_T \sigma A_R}{(4\pi)^2 L_T L_R \frac{S}{J+N}}}{\frac{ERP A_R SL}{4\pi L_R R_j^2 B_j L_{POL} SLC} + kT_s} \right]^{1/4} \quad (10.14)$$

When the target range is limited by the minimum-range constraint, the maximum burnthrough range at which the target may be observed is given by:

$$R = \left[\frac{\frac{2P_p G_T \sigma A_R}{(4\pi)^2 c L_T L_R \frac{S}{J+N}}}{\frac{ERP A_R SL}{4\pi R_j^2 B_j L_{POL} L_R SLC} + kT_s} \right]^{1/3} \quad (10.15)$$

For example, consider the radar parameters in the example in Section 10.2, a SL of -40 dB (zero dBI), 3-dB receive losses, and a system noise temperature of 500K. These parameters are shown in the top portion of Table 10.3. An SOJ having an ERP per polarization of 50 MW (77.0 dBW), and a jamming bandwidth of 1 GHz, is at a range of 250 km. For a 0.5-m² target at 200-km range, the S/(J + N) from (10.13) is -12.1 dB, as shown in column 2 in the lower portion of the table. If an SLC with a 30-dB CR is used, the S/(J + N) increases to 12.3 dB, as shown in column 3. The burnthrough range is calculated for S/(J + N) = 15 dB for the case with the SLC, using

Table 10.3 Sidelobe Jamming Examples

<i>Radar Parameters</i>			
P_P	40 kW		
G_T	40 dB		
A_R	0.8 m ²		
T_S	500K		
L_T	3 dB		
L_R	3 dB		
τ	1 ms		
PC	1,000		
B	1 MHz		
SL	−40 dB		
<i>Target Parameters</i>			
R	200 km	200 km	171 km
σ	0.5 m ²	0.5 m ²	0.5 m ²
R_j	250	250	250
ERP/pol	50 MW	50 MW	50 MW
B_j	1 GHz	1 GHz	1 GHz
SLC	0 dB	30 dB	30 dB
S/(J+N)	−12.1 dB	12.3 dB	15 dB

(10.14). The result, as shown in column 4, is 171 km. This range exceeds the minimum range for the 1-ms pulse.

When multiple jammers are present, it is often possible to combine their characteristics into an equivalent set of parameters for use in (10.11) through (10.15):

$$\left[\frac{ERP SL}{R_J B_J L_{POL} SLC} \right]_{EQUIV} = \sum_i \frac{ERP_i SL_i}{R_{Ji} B_{Ji} L_{POLi} SLC_i} \quad (10.16)$$

10.4 Volume Chaff

Radar volume chaff consists of a large number of small reflectors that are deployed around the target of interest. The signals returned from the chaff particles may then mask the signal returned from the target, preventing target detection or measurement of target characteristics. Chaff may be deployed around a target to mask that target, or it may be deployed in a corridor to mask targets passing through the corridor.

Short metallic wires that are resonant at the radar frequency are often used for chaff. These are generally dipoles having length equal to about one-half the radar wavelength. For linear signal polarizations, the RCS of such a dipole at its resonant frequency, averaged over all orientations, σ_D , is given by [8, pp. 297–301]:

$$\sigma_D = 0.15\lambda^2 \quad (\text{linear polarization}) \quad (10.17)$$

The total chaff RCS, σ_T , for a group of n_T dipoles with random orientations, is then:

$$\sigma_T = 0.15n_T\lambda^2 \quad (\text{linear polarization}) \quad (10.18)$$

For circular polarizations:

$$\sigma_D = 0.10\lambda^2 \quad (\text{circular polarization}) \quad (10.19)$$

$$\sigma_T = 0.10n_T\lambda^2 \quad (\text{circular polarization}) \quad (10.20)$$

The total chaff RCS may be related to the total weight of the chaff, W_C , for common types of airborne chaff dipoles by [1, pp. 188–190; 5, pp. 134–135]:

$$\sigma_T \approx 22,000\lambda W_C \quad (10.21)$$

For example, at X band (9.5 GHz), with linear polarization, a dipole has an average RCS, $\sigma_D = 0.00015 \text{ m}^2$. It takes about 6,700,000 such dipoles to produce a total RCS, $\sigma_T = 1,000 \text{ m}^2$. The weight of this chaff, from (10.21), is about 1.4 kg. The mechanism for dispensing this chaff would add weight to the overall chaff system design.

The frequency band over which the chaff dipole RCS remains large is equal to about 10% of the primary resonant frequency (the frequency for which the dipole is

one-half wavelength). Chaff dipoles produce some RCS at other than their primary resonant frequency, but this is relatively small, except at multiples of the primary resonant frequency. Therefore, chaff CMs may use dipoles having several lengths, either to cover the band of a wide-bandwidth radar, or to screen targets from radars at several frequency bands. While dipole chaff is the most common, other types of chaff have been used. For example, rope chaff (long metallic strands) has the advantage of broadband frequency coverage.

The chaff-scattering volume that contributes to its radar return, V_s , is the portion in the radar resolution cell, given by:

$$V_s = D_A D_E \Delta R \quad (10.22)$$

where:

D_A = the smaller of the horizontal dimension of the chaff cloud and the azimuth cross-range resolution $R\theta_A$;

D_E = the smaller of the vertical dimension of the chaff cloud and the elevation cross-range resolution $R\theta_E$;

ΔR = the radar range resolution, assumed to be smaller than the range extent of the chaff.

This is illustrated in Figure 10.4, which shows the elevation profile for a case where the beam is smaller than the chaff cloud [Figure 10.4(a)], and one where the beam is larger than the chaff cloud [Figure 10.4(b)]. The factor of $\pi/4$ is not included in (10.22), but is included in the beamshape loss, discussed below.

The chaff RCS in the chaff resolution volume, σ_C , is given by:

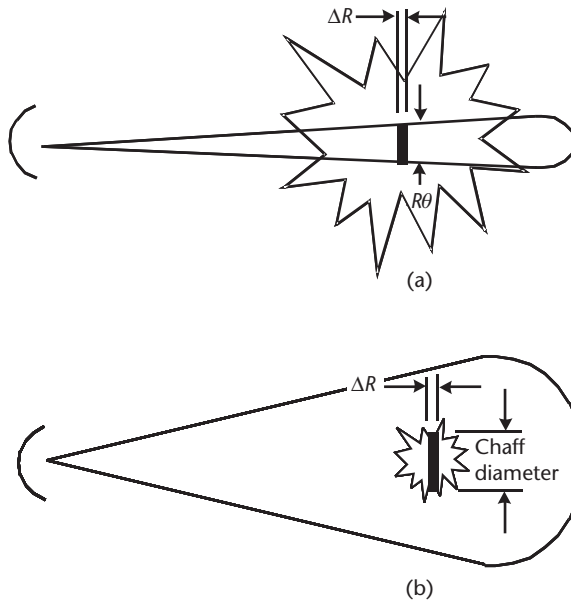


Figure 10.4 Illustrations of chaff volume that contribute to the radar return. (a) Beam smaller than chaff cloud. (b) Beam larger than chaff cloud.

$$\sigma_C = \frac{\sigma_D n_C}{L_{BS}} \quad (10.23)$$

where:

n_C = the number of chaff dipoles in the resolution volume;

L_{BS} = the two-dimensional beamshape loss for the chaff. This may range from $\pi/4$ (1.05 dB) for a circular chaff cloud projection when the beam is much larger than the chaff dimensions, to 3.2 dB when the beam is much smaller than the chaff dimensions.

If the chaff is distributed uniformly over a total volume, V_T , then:

$$\sigma_C = \frac{\sigma_D n_T V_s}{L_{BS} V_T} = \frac{\sigma_T V_s}{L_{BS} V_T} \quad (10.24)$$

For example, consider the 1,000 m² of X-band chaff discussed above, distributed uniformly in a sphere of 5-km diameter. A radar having 2° azimuth and elevation beamwidths, and 150m range resolution observes the chaff from a range of 200 km. The cross-range resolution at 200-km range is about 7 km, so the entire chaff cloud is within the radar beam. The total volume of the chaff, V_T , is 65 km³, and the chaff resolution volume at the center of the cloud, V_s , is 3.8 km³. The beamshape loss for this case is estimated at 1.5 dB, to account for the $\pi/4$ factor and some reduction in antenna gain across the cloud. The chaff RCS in the resolution volume, σ_C , is 41 m². If the range resolution is improved to 15m, the chaff RCS decreases to 4.1 m².

As indicated above, (10.24) is valid when the chaff is uniformly distributed over the cloud. While this is a convenience for calculation and is used in the examples and problems in this book, the chaff density in actual chaff clouds may be highly non-uniform. For example, chaff is often deployed in clumps or from canisters. The dispensed dipoles are given a spread of radial velocities, so that the cloud expands nonuniformly, possibly to overlap with other such clouds. The resulting chaff density may be both nonuniform and time-varying.

In many cases, it is possible to reduce the chaff signal by exploiting the velocity spread of the chaff or the velocity difference between the chaff and target. Chaff deployed in the atmosphere is rapidly slowed to air velocity by atmospheric drag [1, p. 189]. The chaff will then have the mean velocity of the local wind, and a velocity spread from about 2 to 4 m/s, comparable to that of rain (see Section 9.2). Most aircraft targets, and many ground targets, will have radial velocities considerably greater than the chaff, and MTI or pulse-Doppler processing may be used to suppress the chaff return. Chaff cancellation ratios (CR) from 20 to 40 dB may be achieved in such cases.

Note that the use of MTI or pulse-Doppler waveforms is incompatible with pulse-to-pulse frequency agility, described earlier as an effective ECCM against spot noise jamming. An effective ECM technique is to use a combination of chaff and spot noise jamming. This may force the radar to maintain its frequency for three or more successive pulses in order to perform coherent processing to reject the chaff, which allows the jammer to set on and jam the selected radar frequency after the first pulse of the burst has been received.

Chaff deployed with targets outside the atmosphere may remain near the target velocity. However, there is a spread in the radial velocity of such exoatmospheric chaff, due to differences in the deployment velocity, the spinning of individual dipoles, and differences in the angle between the chaff velocity and the radar LOS across the radar beam. Radar waveforms having good Doppler-velocity resolution (see Chapter 4) may be able to reject a significant portion of the chaff that has radial velocity different from that of the target. Pulse-burst waveforms (see Section 4.5) may be suitable in such situations.

The signal-to-chaff ratio, S/C , is given by:

$$\frac{S}{C} = \frac{\sigma_C R}{\sigma_C} = \frac{\sigma_C R L_{BS} V_T}{\sigma_T V_s} = \frac{\sigma_C R L_{BS} V_T}{\sigma_D n_T V_s} \quad (10.25)$$

Examples of calculations of S/C in chaff are shown in Table 10.4. The radar and chaff parameters are given in the top portion of the table. As in the previous example, to provide a total chaff RCS of 1,000 m² for linear radar polarization, 6,700,000 dipoles are required, which would weigh about 1.4 kg. For a spherical chaff cloud having a diameter of 5 km, the total chaff volume is 65 km³. If the chaff is assumed uniform over this volume, the RCS density is 15.4 m² per km³. The lower part of the table shows that at a range of 200 km, the 2° beamwidths produce cross-range resolutions of 7 km, so that the 5-km chaff cloud diameter defines the chaff volume. With a range resolution of 150m (column 2), the resolution cell volume is 3.8 km³. Since the gain variation across the beam may not be neglected for this case, the beamshape loss is estimated at 1.5 dB. The resulting chaff RCS [from (10.24)] is 41 m². For a 1-m² target and no chaff cancellation, $S/C = -16.1$ dB. Column 3 shows the 10-dB improvement for a 15m range resolution, and column 4 shows the further 20-dB improvement, if 20 dB of chaff cancellation may be provided.

Table 10.4 Volume Chaff Examples

f	9.5 GHz		
Polarization	Linear		
σ_D	0.00015 m ²		
σ_C	1,000 m ²		
n_T	6,700,000		
W_C	1.4 kg		
Volume diameter	5 km		
V_T	65 km ³		
θ_A, θ_E	2°		
ΔR	150m	15m	15m
R	200 km	200 km	200 km
$R\theta_A, R\theta_E$	7 km	7 km	7 km
V_s	3.8 km ³	3.8 km ³	3.8 km ³
L_{BS} (estimated)	1.5 dB	1.5 dB	1.5 dB
σ_C	41 m ²	4.1 m ²	4.1 m ²
σ	1 m ²	1 m ²	1 m ²
CR	0 dB	0 dB	20 dB
S/C	-16.1 dB	-6.1 dB	13.9 dB

Radar characteristics that provide good performance with chaff CMs are small range resolution and beamwidths, and good radial-velocity resolution with Doppler-frequency processing. These are more readily obtained at higher radar frequencies. In addition, (10.21) shows that, for a given chaff weight, the chaff RCS varies inversely with frequency.

It is convenient to combine the chaff interference with that from radar noise and the combination of noise and jamming, giving:

$$\frac{S}{C+N} = \frac{1}{\frac{1}{S/C} + \frac{1}{S/N}} \quad (10.26)$$

$$\frac{S}{J+C+N} + \frac{1}{\frac{1}{S/J} + \frac{1}{S/C} + \frac{1}{S/N}} \quad (10.27)$$

These equations are valid when the chaff (and the jamming) have Gaussian statistics, and, when pulse integration is used, pulse-to-pulse decorrelation. This is a reasonable assumption for chaff when the chaff return is made up of many contributors of comparable size. An example of target detection in the presence of jamming, clutter, and noise is given in Section 12.6.

10.5 Decoy Discrimination

Discrimination is the process of distinguishing between targets of interest (e.g., missile warheads) and decoy objects that are made to resemble the targets of interest. A similar process, often called target classification, may be used to distinguish between types of targets in a target class (e.g., types of aircraft).

Radar measurements that may be used for discrimination include:

- Target RCS and RCS fluctuation;
- Target radial length;
- Target spectral characteristics;
- Features of target range-Doppler images;
- Target trajectory or flight path characteristics.

The measurement of these features is described in Chapter 8.

For a measurement to be useful for discrimination, the distribution of measurement values must be different for the targets of interest and for the decoys. When the values of a measurement of a target and decoy property have Gaussian distributions with equal standard deviations, the quality of discrimination that the measurement provides may be represented by a K factor:

$$K = \Delta_x / \sigma_x \quad (10.28)$$

where σ_x is the standard deviation of the distribution of the measurement of parameter x , and Δ_x is the separation of the distribution peaks for the two types of objects, as illustrated in Figure 10.5.

A measurement threshold may be set to provide a required low probability of leakage, P_L . This is the probability that a real target will be rejected as a decoy, and is analogous to $1 - P_D$ in radar detection. The false acceptance probability, P_A , is the probability that a decoy will be declared a real target. It is given by (J. H. Ballantine, personal communication):

$$P_A = 1 - \operatorname{erf}\left[K - \operatorname{erf}^{-1}(1 - P_L)\right] \quad (10.29)$$

where erf is the error function, a tabulated function given by:

$$\operatorname{erf}(x) = \frac{1}{\sqrt{2\pi}} \int_{-\infty}^x e^{-x^2/2} dx \quad (10.30)$$

The probability of leakage may be found from a specified probability of false acceptance by:

$$P_L = 1 - \operatorname{erf}\left[K - \operatorname{erf}^{-1}(1 - P_A)\right] \quad (10.31)$$

These relationships are also given by the nomograph in Figure 10.6 (Roy Nichols, personal communication). To use this nomograph, enter one of the prob-

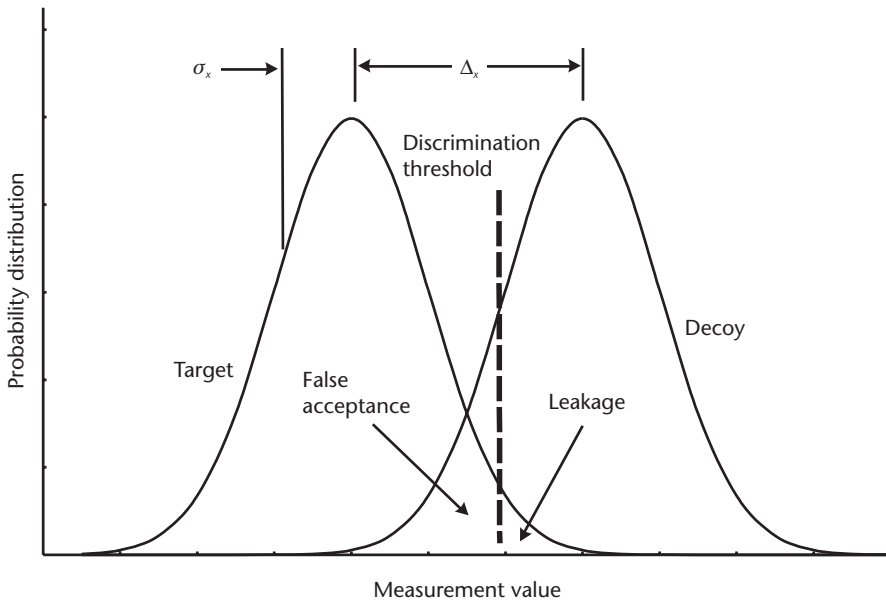


Figure 10.5 The K factor used to describe the discrimination quality provided by a radar measurement.

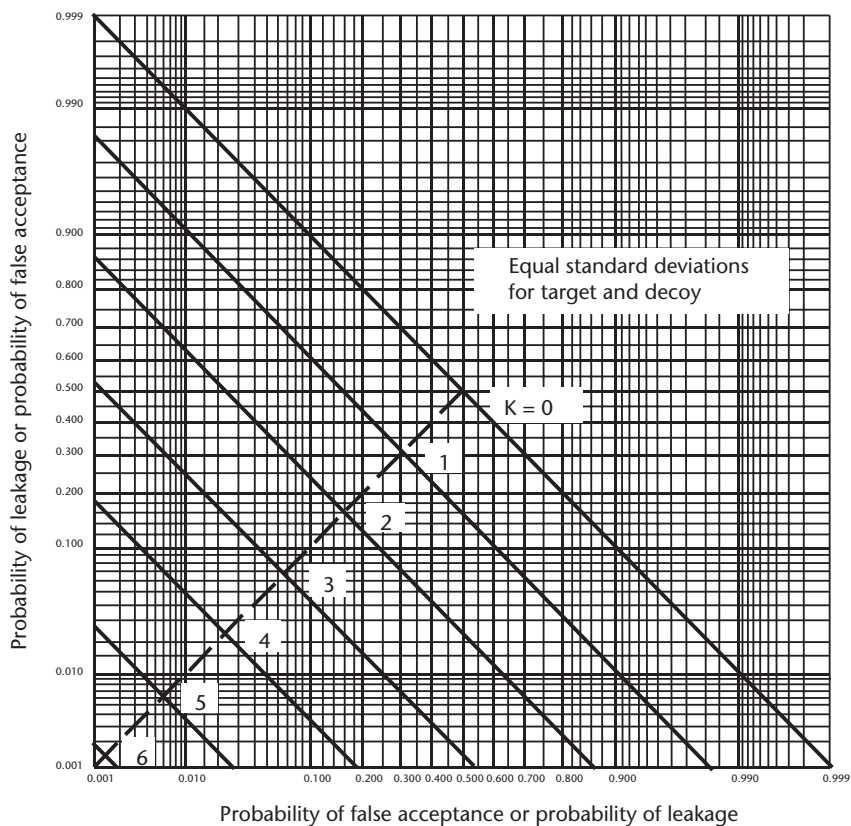


Figure 10.6 Nomograph for discrimination probability.

abilities on the x axis, go vertically to the appropriate K-factor value, and then go horizontally to the y axis to read the other probability.

Examples of discrimination probability for this type of measurement distribution are shown in Table 10.5. In the first example (column 2), the probability of leakage, P_L (the probability that a target of interest is declared to be a decoy), is set to 1% (0.01). With a K factor of 4, the resulting probability of false acceptance, P_A (the probability that a decoy is declared to be a target), is 0.047, or 4.7%. Thus, if there are 20 decoys, it is probable that about one will be declared to be a real target, while 99 percent of the real targets are properly identified.

If the separation of the target and decoy distribution means decreases so that $K = 3$, and the value of P_L is kept the same, the value of P_A increases to 25% (see column 3 in the table). Then about five of the 20 decoys will be declared as real targets. Alternatively, if K is reduced to 3 and P_A remains at 4.7%, the value of P_L increases to 9.3% (see column 4 in the table). If low values of both P_A (1%) and P_L (0.1 %) are desired, a value of $K = 5.4$ is required, as shown in column 5 of the table.

Table 10.5 Examples of Discrimination Probabilities

K	4	3	3	5.4
P_A	4.7%	25%	4.7%	1.0%
P_L	1.0%	1.0%	9.3%	0.1%

While it is convenient to characterize the discrimination capabilities of a radar measurement by the K factor, the distributions of real measurements may not match the model assumed above. In addition, multiple measurements may be combined to enhance the discrimination capability. The algorithms for combining measurements and evaluating the resulting discrimination capabilities are beyond the scope of this book.

Since the flight paths of decoys may not be as carefully controlled as those of real targets, tracking measurements may also be used for discrimination. For example, aircraft targets may maneuver to avoid obstacles or other threats, while decoys may not. Missile targets will likely be aimed at valuable assets, while decoys may not be so aimed.

10.6 Problems

The following problems are provided to assist in reviewing this chapter and to ensure a basic understanding of the material. For maximum benefit, the problems should first be solved without using the VBA custom radar functions. Solutions to these problems are given in Appendix E, Section E.10.

1. In what class of CMs is a barrage noise jammer? In what class is a pulsed jammer?
2. If it is required to limit the discrimination leakage of targets of interest to 1%, and the measurement K factor is 4, what is the probability of false acceptance of decoys? If 80 decoys and one real target are observed, what is the expected number of objects that will be declared to be real targets?
3. A jammer generates 5 kW of RF power, has a loss of 0.5dB, and a gain of 20 dB in the direction of the target. What is its ERP? If independent jamming signals having one-half the total power are used on each of two orthogonal polarizations, what is the polarization loss? What is the ERP per polarization?
4. A radar has a peak transmitted power of 100 kW, transmit gain of 42 dB, and transmit losses of 1.8 dB. Its waveform has a signal bandwidth of 1 MHz and a pulse compression ratio of 10^3 . What is the waveform duration? What is the S/J for a 3 m² target at 350 km range with a MLJ having a total ERP of 60W, divided equally in independent signals on two orthogonal polarizations, and a bandwidth matched to the radar signal? If the radar employs frequency agility over a 300 MHz band, and the jammer band matches that bandwidth, what is the S/J?
5. A radar has a peak transmit power of 10 kW, pulse duration of 1 ms, transmit gain of 30 dB, transmit loss of 1.5 dB, receive aperture area of 2 m², receive loss of 1.2 dB, and system noise temperature of 450K. The radar observes a 10-dBsm target at a range of 250 km, with a SOJ at a range of 350 km radiating 50 dBW per polarization over a band of 0.5 GHz toward the radar. If the radar sidelobes are isotropic and no sidelobe cancellation is used, what is the S/(J + N)? What is the S/(J + N) if 20 dB of sidelobe cancellation is applied? What is the S/N with no jamming?

6. A chaff cloud consists of 20 lbs. of X-band (9.5 GHz) chaff uniformly distributed over a spherical volume 5 km in diameter. What is the chaff total RCS and volume, assuming linear signal polarization? A radar with 2° azimuth and elevation beamwidths and 150m range resolution observes a 1 m² target at a range of 500 km in the center of the chaff cloud. What is the S/C, assuming no chaff cancellation? What is the S/C if the range resolution is 1.5m? What is the S/C with 1.5m range resolution and 20 dB of chaff cancellation?
7. For discrimination with a K factor of 3 and a 2% target leakage probability, what is the probability of incorrectly accepting a decoy as a target? If we wish to correctly reject 98% of the decoys while maintaining 2% leakage, what K factor is required?
8. What is the ERP/polarization for a jammer generating a total of 1 kW of RF power, having a microwave loss of 0.2 dB, and radiating independent jamming signals through two antennas having orthogonal polarizations and gains of 5 dB?
9. With what type of jammers should a sidelobe blanker be used?
10. For a radar with $P_p = 100$ kW, $G_T = 50$ dB, a 10-ms pulse duration, and 2-dB transmit losses, what is the S/J when observing a 1 m² target at a range of 2,000 km, using an MLJ with ERP/polarization of 25 dBW, and a noise bandwidth of 10 GHz? Find the range for $S/(J + N) = 15$ dB if $A_R = 10$ m², $T_s = 500$ K, and $L_R = 2$ dB. Is the minimum-range constraint violated?
11. For the radar and target in Problem 10, and assuming isotropic sidelobes and no sidelobe cancellation, what is the $S/(J + N)$ with an SOJ at range 2,500 km, an ERP/polarization of 10¹⁰W, and a bandwidth of 10 GHz? What sidelobe CR will increase the $S/(J + N)$ to 10 dB?
12. What is the average RCS of a dipole at C band (5.5 GHz) with linear signal polarization? How many such dipoles are needed for a total chaff RCS of 5,000 m²? What is the weight of this chaff package, assuming 100% overhead for the dispensing mechanism (i.e., the dispenser weighs the same as the chaff dipoles)?
13. Consider a uniform chaff cloud having a diameter of 20 km and a total chaff RCS of 10,000 m². A radar having a 1° beamwidth observes a target near the center of the cloud at a range of 200 km. If the radar range resolution is 15m, what is the volume of the chaff observed, and what is the resulting chaff RCS? If the target RCS = 20 dBsm, what is the S/C? What chaff CR is needed to increase the S/C to 15 dB?

10.7 VBA Software Functions for Radar Countermeasures and Counter-Countermeasures

10.7.1 Function DiscProb_Factor

Purpose Calculates the decoy false acceptance probability or the probability of target discrimination leakage, for Gaussian measurement distributions and a given K factor.

Reference Equations (10.28) to (10.31).

Features May be used either to calculate the decoy false acceptance probability or the target discrimination leakage, due to the symmetry of the relationship. Uses the error function in the Excel Analysis ToolPak-VBA (which must be installed).

Input Parameters (with units specified)

Prob_Factor = probability of discrimination leakage or probability of decoy false acceptance (factor). Values greater than 1 or less than 0 produce no output.

K_Factor = discrimination K factor (factor).

Function Output Probability of decoy false-acceptance or probability of discrimination leakage, depending on which factor was input (factor).

The Excel Function Arguments parameter box for Function DiscProb_Factor is shown in Figure 10.7, with sample parameters and solution.

10.7.2 Function ML_SJNR_dB

Purpose Calculates the $S/(J + N)$ for a noise jammer in the radar main beam.

Reference Equations (10.5).

Features Assumes the jammer radiates white Gaussian noise over the specified band. Assumes the range and receive-antenna gain are the same for the jammer and the target. (If they differ significantly, Function SL_SJNR_dB may be used.) Will calculate the S/J (10.3) if the system noise temperature, T_sK , is set to zero. Allows user selection to: (1) ignore the minimum-range constraint, (2) optimize pulse duration to avoid the minimum-range constraint, or (3) select from specified pulse durations to avoid the minimum-range constraint.

Input Parameters (with units specified)

Pp_kW = radar peak transmitted power (kW).

Gt_dB = radar transmit gain (dB).

Ar_m2 = radar receive antenna aperture area, (m^2).

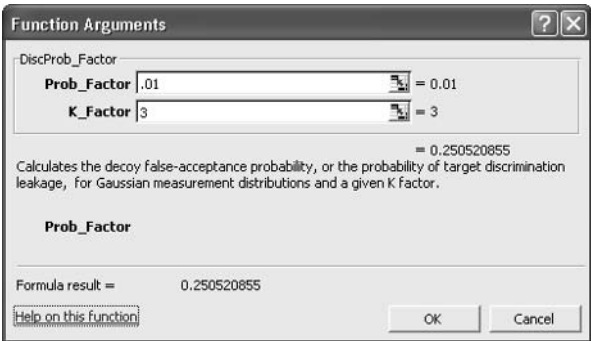


Figure 10.7 Excel parameter box for Function DiscProb_Factor.

Ts_K = radar system noise temperature (K).

Lt_dB = radar transmit losses (dB). Transmit losses include transmit microwave losses and transmit antenna losses that are not included elsewhere, and one-way propagation losses.

Lr_dB = radar receive losses (dB). Receive losses include receive microwave losses and receive antenna losses that are not included elsewhere, radar signal-processing losses, and one-way propagation losses.

RCS_dBsm = target RCS (dBsm).

R_km = range from radar to target and jammer (km).

ERP_dBW = jammer ERP (dBW). When two orthogonal polarizations are jammed, the ERP per polarization may be input.

Bj_GHz = bandwidth of the jammer signal (GHz).

Select_123 = select 1 to ignore the minimum-range constraint, 2 to use the optimum pulse duration within the minimum range constraint, or 3 to use a specified pulse duration within the minimum-range constraint (integer). Other values give no result.

Tau1_ms = primary (longest) radar pulse duration (ms). This pulse duration is used in Option 1, and is the maximum for Options 2 and 3.

Tau2_ms, Tau3_ms, Tau4_ms, Tau5_ms, Tau6_ms (optional) = alternate shorter pulse durations used in Option 3 in descending order (ms). These may be left blank for Option 1 or 2, or when fewer than six pulse durations are available.

Lpol_dB (optional) = loss due to jammer polarization not matching radar receive antenna polarization (dB). When two orthogonal polarizations are jammed and the ERP per polarization is input for ERP_dBW, the polarization loss should be 0 dB. If no value is specified, a value of 0 dB will be used.

Function Output The $S/(J + N)$ for the specified radar and jammer parameters (dB). In Option 3, when none of the specified pulse durations avoid the minimum-range constraint, no result is produced, indicated by an output of -100.

The Excel Function Arguments parameter box for Function ML_SJNR_dB is shown in Figure 10.8, with sample parameters and a solution.

10.7.3 Function ML_BTRange_km

Purpose Calculates the burnthrough range for a target with a noise jammer in the radar main beam.

Reference Equations (10.6) to (10.9).

Features Calculates the radar range for a specified value of $S/(J + N)$. Assumes jammers radiate white Gaussian noise over the specified band. Assumes the range and receive-antenna gain are the same for the jammer and the target. (If they differ significantly, Function SL_BTRange_km may be used.) Allows user selection to: (1) ignore the minimum-range constraint, (2) optimize pulse duration to maximize range while avoiding the minimum-range constraint, or (3) select from specified pulse durations to maximize range while avoiding the minimum-range constraint.

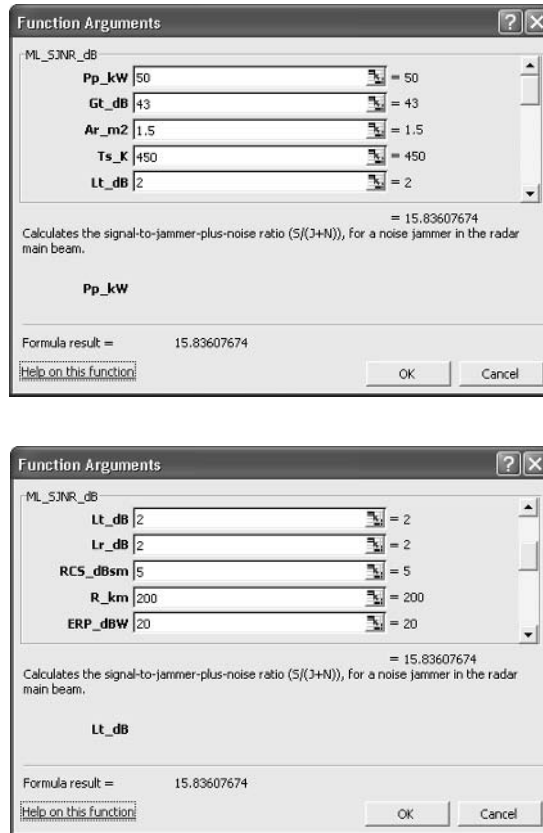


Figure 10.8 Excel parameter box for Function `ML_SJNR_dB`.

Input Parameters (with units specified)

`SJNR_dB` = the $S/(J + N)$, required for burnthrough (dB).

`Pp_kW` = radar peak transmitted power (kW).

`Gt_dB` = radar transmit gain (dB).

`Ar_m2` = radar receive antenna aperture area (m^2).

`Ts_K` = radar system noise temperature (K).

`Lt_dB` = radar transmit losses (dB). Transmit losses include transmit microwave losses and transmit antenna losses that are not included elsewhere, and one-way propagation losses.

`Lr_dB` = radar receive losses (dB). Receive losses include receive microwave losses and receive antenna losses that are not included elsewhere, radar signal-processing losses, and one-way propagation losses.

`RCS_dBsm` = target RCS (dBsm).

`ERP_dBW` = jammer ERP (dBW). When two orthogonal polarizations are jammed, the ERP per polarization may be input.

`Bj_GHz` = bandwidth of the jammer signal (GHz).

`Select_123` = select 1 to ignore the minimum-range constraint, 2 to maximize range within the minimum range constraint, or 3 to use a specified pulse

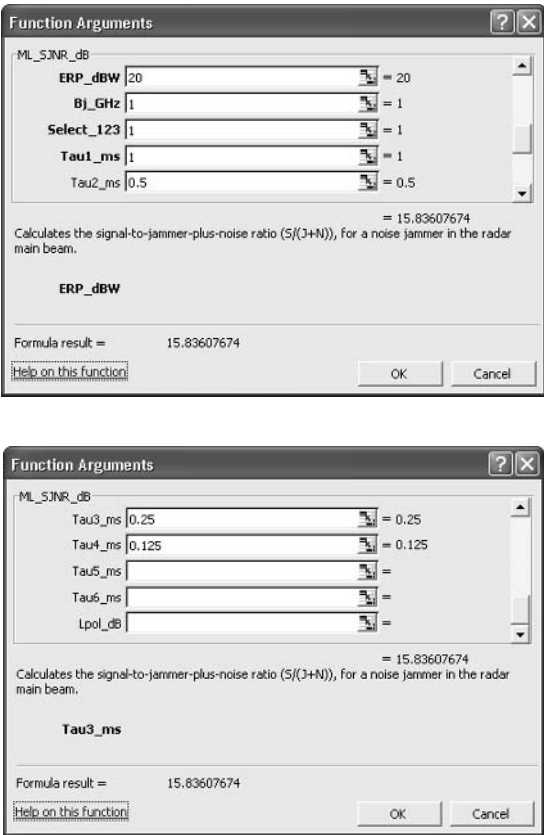


Figure 10.8 (continued).

duration to maximize range within the minimum-range constraint (integer). Other values give no result.

`Tau1_ms` = primary (longest) radar pulse duration (ms). This pulse duration is used in Option 1, and is the maximum for Options 2 and 3.

`Tau2_ms`, `Tau3_ms`, `Tau4_ms`, `Tau5_ms`, `Tau6_ms` (optional) = alternate shorter pulse durations used in Option 3 in descending order (ms). These may be left blank for Option 1 or 2, or when fewer than six pulse durations are available.

`Lpol_db` (optional) = loss due to jammer polarization not matching radar receive antenna polarization (dB). When two orthogonal polarizations are jammed and the ERP per polarization is input for `ERP_dBW`, the polarization loss should be 0 dB. If no value is specified, a value of 0 dB will be used.

Function Output The radar burnthrough range for the parameters and option specified (km). In Option 3, when none of the specified pulse durations will avoid the minimum-range constraint, a range of zero is output.

The Excel Function Arguments parameter box for Function `ML_BTRange_km` is shown in Figure 10.9, with sample parameters and a solution.

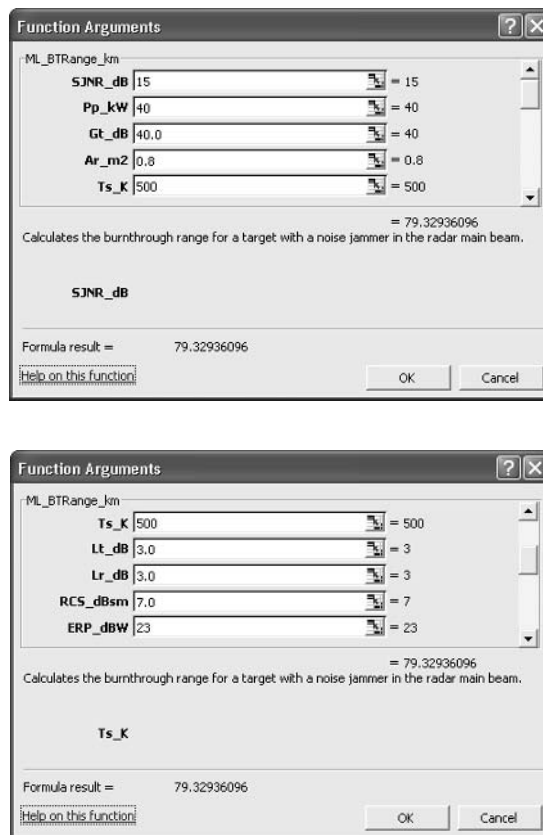


Figure 10.9 Excel parameter box for Function ML_BTRange_km.

10.7.4 Function SL_SJNR_dB

Purpose: Calculates the $S/(J + N)$ for a noise jammer in the radar sidelobes.

Reference Equations (10.13).

Features Assumes the jammer radiates white Gaussian noise over the specified band. Will calculate the S/J (10.11) if the system noise temperature, Ts_K , is set to zero. Allows user selection to: (1) ignore the minimum-range constraint, (2) optimize pulse duration to maximize range while avoiding the minimum-range constraint, or (3) select from specified pulse durations to maximize range while avoiding the minimum-range constraint. Multiple jammers may be modeled by an equivalent jammer using (10.16).

Input Parameters (with units specified)

Pp_kW = radar peak transmitted power (kW).

Gt_dB = radar transmit gain (dB).

Ar_m2 = radar receive antenna aperture area (m^2).

SL = radar sidelobe level, relative to the main-beam peak, at the angle of the jamming signal (dB). This is normally a negative decibel value.

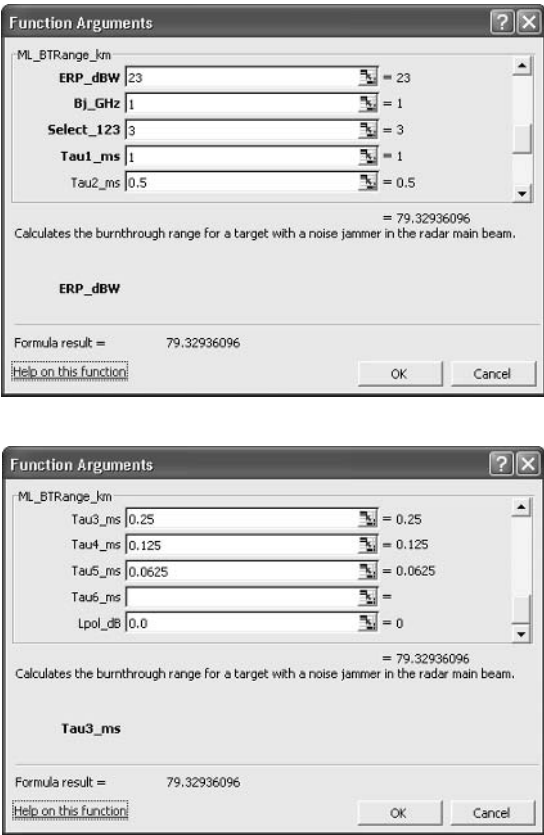


Figure 10.9 Continued.

SLC = sidelobe cancellation factor (dB). This is normally 0 dB (for no cancellation) or a positive decibel value.

Ts_K = radar system noise temperature (K).

Lt_dB = radar transmit losses (dB). Transmit losses include transmit microwave losses and transmit antenna losses that are not included elsewhere, and one-way propagation losses.

Lr_dB = radar receive losses (dB). Receive losses include receive microwave losses and receive antenna losses that are not included elsewhere, radar signal-processing losses, and one-way propagation losses.

RCS_dBsm = target RCS (dBsm).

R_km = range from radar to the target (km).

Rj_km = range from radar to the jammer (km).

ERP_dBW = jammer ERP (dBW). When two orthogonal polarizations are jammed, the ERP per polarization may be input.

Bj_GHz = bandwidth of the jammer signal (GHz).

Select_123 = Select 1 to ignore the minimum-range constraint, 2 to use the optimum pulse duration within the minimum range constraint, or 3 to use a specified pulse duration within the minimum-range constraint (integer). Other values give no result.

Tau1_ms = primary (longest) radar pulse duration (ms). This pulse duration is used in Option 1, and is the maximum for Options 2 and 3.

Tau2_ms, Tau3_ms, Tau4_ms, Tau5_ms, Tau6_ms (optional) = alternate shorter pulse durations used in Option 3 in descending order (ms). These may be left blank for Option 1 or 2, or when fewer than six pulse durations are available.

Lpol_dB (optional) = Loss due to jammer polarization not matching radar receive antenna polarization (dB). When two orthogonal polarizations are jammed and the ERP per polarization is input for ERP_dBW, the polarization loss should be 0 dB. If no value is specified, a value of 0 dB will be used.

Function Output The $S/(J + N)$ for the specified radar and jammer parameters (dB). In Option 3, when none of the specified pulse durations avoid the minimum-range constraint, no result is produced, indicated by an output of -100.

The Excel Function Arguments parameter box for Function SL_SJNR_dB is shown in Figure 10.10, with sample parameters and a solution.

10.7.5 Function SL_BTRange_km

Purpose Calculates the burnthrough range for a target with a noise jammer in the radar sidelobes.

Reference Equations (10.14) and (10.15).

Features Calculates the radar range for a specified value of $S/(J + N)$. Assumes jammers radiate white Gaussian noise over the specified band. Allows user selection to: (1) ignore the minimum-range constraint, (2) optimize pulse duration to maximize range while avoiding the minimum-range constraint, or (3) select from specified pulse durations to maximize range while avoiding the minimum-range constraint. Multiple jammers may be modeled by an equivalent jammer using (10.16).

Input Parameters (with units specified)

SJNR_dB = the $S/(J + N)$ required for burnthrough (dB).

Pp_kW = radar peak transmitted power (kW).

Gt_dB = radar transmit gain (dB).

Ar_m2 = radar receive antenna aperture area (m^2).

SL = radar sidelobe level, relative to the main-beam peak, at the angle of the jamming signal (dB). This is normally a negative decibel value.

SLC = sidelobe cancellation factor (dB). This is normally 0 dB (for no cancellation), or a positive decibel value.

Ts_K = radar system noise temperature (K).

Lt_dB = radar transmit losses (dB). Transmit losses include transmit microwave losses and transmit antenna losses that are not included elsewhere, and one-way propagation losses.

Lr_dB = radar receive losses (dB). Receive losses include receive microwave losses and receive antenna losses that are not included elsewhere, radar signal-processing losses, and one-way propagation losses.

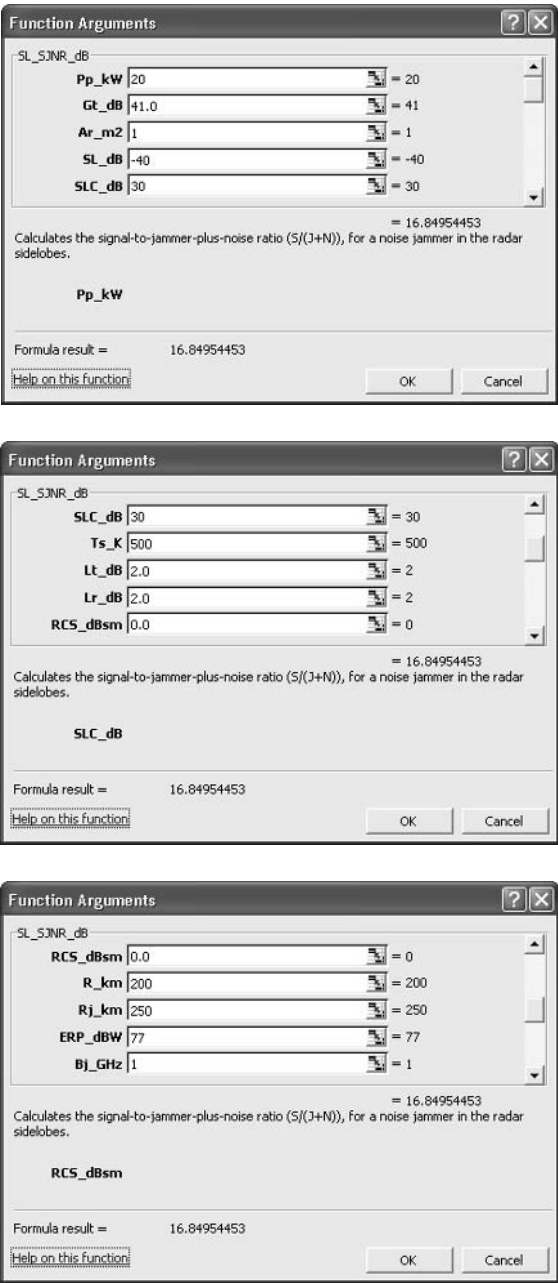


Figure 10.10 Excel parameter box for Function SL_SJNR_dB.

- RCS_dBsm = target RCS (dBsm).
- Rj_km = range from radar to the jammer (km).
- ERP_dBW = jammer ERP (dBW). When two orthogonal polarizations are jammed, the ERP per polarization may be input.
- Bj_GHz = bandwidth of the jammer signal (GHz).
- Select_123 = select 1 to ignore the minimum-range constraint, 2 to maximize range within the minimum range constraint, or 3 to use a specified pulse

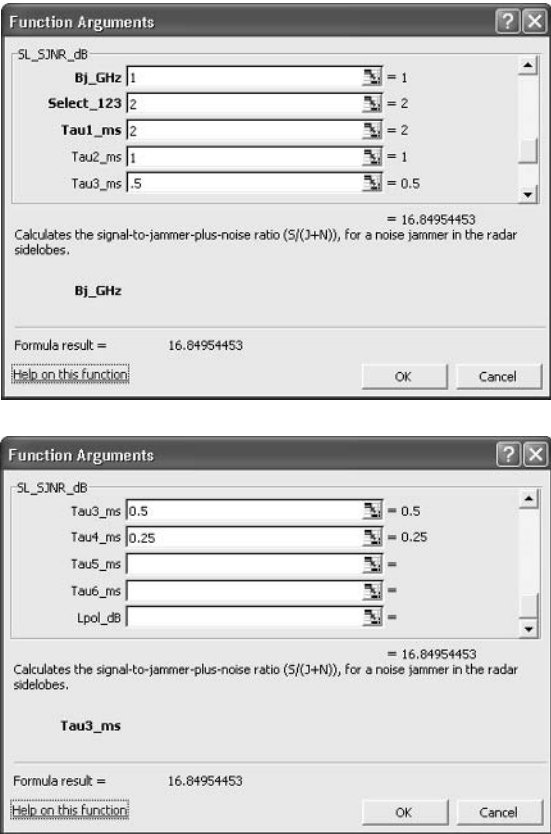


Figure 10.10 (continued).

duration to maximize range within the minimum-range constraint. Other values give no result.

Tau1_ms = primary (longest) radar pulse duration (ms). This pulse duration is used in Option 1, and is the maximum for Options 2 and 3.

Tau2_ms, Tau3_ms, Tau4_ms, Tau5_ms, Tau6_ms (optional) = alternate shorter pulse durations used in Option 3 in descending order (ms). These may be left blank for Option 1 or 2, or when fewer than six pulse durations are available.

Lpol_dB (optional) = Loss due to jammer polarization not matching radar receive antenna polarization (dB). When two orthogonal polarizations are jammed and the ERP per polarization is input for ERP_dBW, the polarization loss should be 0 dB. If no value is specified, a value of 0 dB will be used.

Function Output The radar burnthrough range for the parameters and option specified (km). In Option 3, when none of the specified pulse durations will avoid the minimum-range constraint, a range of zero is output.

The Excel Function Arguments parameter box for Function SL_BTRange_km is shown in Figure 10.11, with sample parameters and a solution.

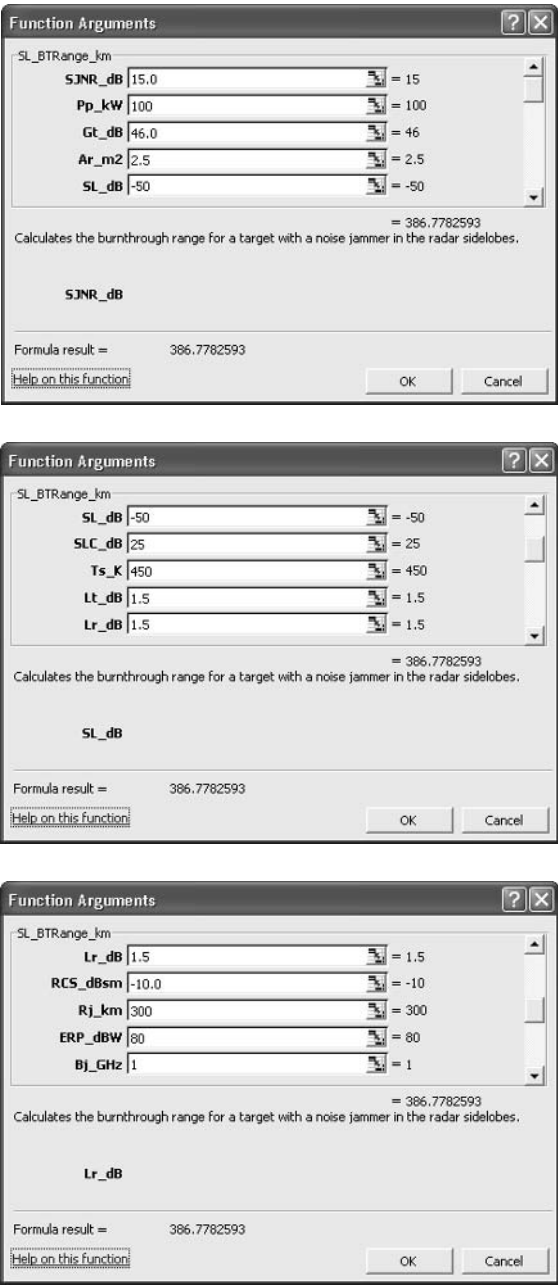


Figure 10.11 Excel parameter box for Function SL_BTRange_km.

10.7.6 Function SCR_Chaff_db

Purpose Calculates the S/C for uniform radar volume chaff.

Reference Equations (10.22) to (10.25).

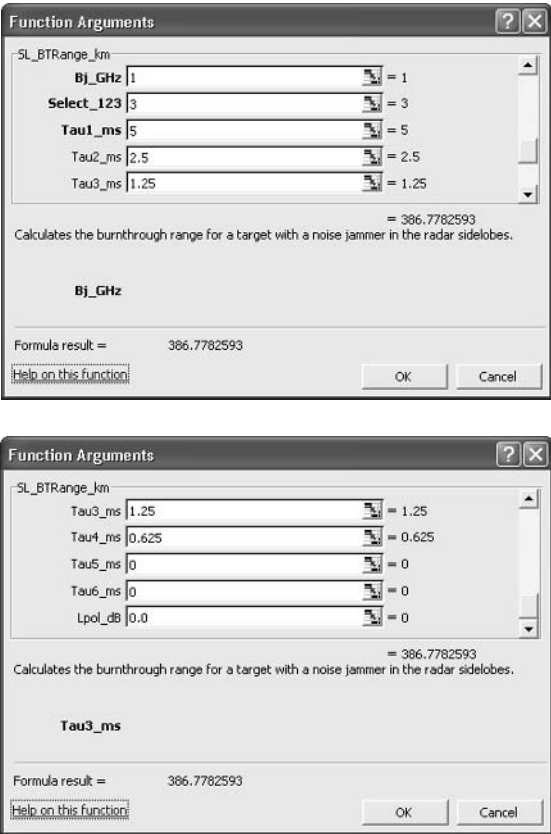


Figure 10.11 (continued).

Features Calculates the contributing chaff volume from the range resolution and the smaller of the chaff cross-range dimensions or the radar angular resolution. Assumes chaff is uniformly distributed over the chaff volume. Allows input of a beamshape loss, or uses a beamshape loss of 3.2 dB when the radar angular resolution is smaller than the chaff dimension in both azimuth and elevation; 2.13 dB when the radar angular resolution is smaller than the chaff dimension in either azimuth or elevation; and a loss of 1.05 dB when both chaff dimensions are smaller than the angular resolution.

Input Parameters (with units specified)

- Range_km = range from radar to target (km).
- Tgt_RCS_dBsm = target RCS (dBsm).
- Az_Beam_mR = radar azimuth beamwidth (mrad).
- El_Beam_mR = radar elevation beamwidth (mrad).
- Range_Res_m = radar range resolution (m).
- C_Cancel_dB = chaff CR (dB). This is normally 0 dB (for no cancellation) or a positive decibel value.
- C_RCS_dBsm = total RCS of the chaff cloud (dBsm).
- C_Vol_km3 = total volume of the chaff cloud (km³).

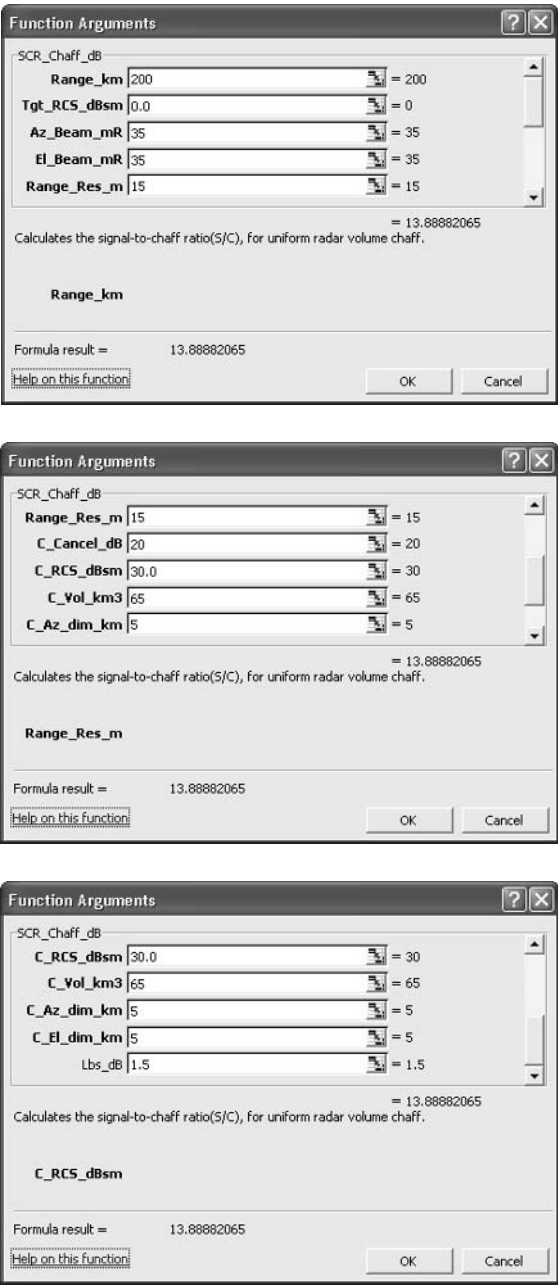


Figure 10.12 Excel parameter box for Function SCR_Chaff_dB.

C_Az_dim_km = chaff cloud dimension in the radar azimuth coordinate (km).

C_El_dim_km = chaff cloud dimension in the radar elevation coordinate (km).

Lbs_dB (optional) = beamshape loss (dB). If no value in input, calculation will use a beamshape loss of 3.2 dB when the radar angular resolution is smaller than the chaff dimension in both azimuth and elevation; 2.13 dB when the

radar angular resolution is smaller than the chaff dimension in either azimuth or elevation; or a loss of 1.05 dB when both chaff dimensions are smaller than the angular resolution.

Function Output The S/C for specified parameters (dB).

The Excel Function Arguments parameter box for Function SCR_Chaff_dB is shown in Figure 10.12, with sample parameters and a solution.

References

- [1] Schleher, D. C., *Introduction to Electronic Warfare*, Dedham, MA: Artech House, 1986.
- [2] Chrzanowski, E. J., *Active Radar Electronic Countermeasures*, Norwood, MA: Artech House, 1990.
- [3] Farina, A., "Electronic Counter-Countermeasures," Chapter 9 in *Radar Handbook*, 2nd Ed., M. I. Skolnik, (ed.), New York: McGraw-Hill, 1990.
- [4] Skolnik, M. I., *Introduction to Radar Systems*, New York: McGraw-Hill, 1962.
- [5] Barton, D. K., *Modern Radar System Analysis*, Norwood, MA: Artech House, 1988.
- [6] Ruck, G. T., "Complex Bodies," Chapter 8 in *Radar Cross Section Handbook*, G. T. Ruck, et al., (eds.), New York: Plenum Press, 1970.
- [7] Mailloux, R. J., *Phased Array Antenna Handbook*, Norwood, MA: Artech House, 1994.
- [8] Barrick, D. E., "Cylinders," Chapter 4 in *Radar Cross Section Handbook*, G. T. Ruck, et al., (eds.), New York: Plenum Press, 1970.

Selected Bibliography

A summary of radar ECM and ECCM techniques is given by Farina, in Skolnik. More detail is given by Schleher, and by Chrzanowski, in their books on electronic warfare. Analysis of target RCS is contained in Ruck, including corner reflectors in Chapter 8, and chaff dipoles in Chapter 4. Chaff characteristics are also treated by Barton. A detailed treatment of sidelobe cancellers is found in Mailloux.

Barton, D. K., *Modern Radar System Analysis*, Norwood, MA: Artech House, 1988.

Chrzanowski, E. J., *Active Radar Electronic Countermeasures*, Norwood, MA: Artech House, 1990.

Farina, A., "Electronic Counter-Countermeasures," Chapter 9 in *Radar Handbook*, 2nd Ed., M. I. Skolnik, (ed.), New York: McGraw-Hill, 1990.

Mailloux, R. J., *Phased Array Antenna Handbook*, Norwood, MA: Artech House, 1994.

Ruck, G. T., (ed.), *Radar Cross Section Handbook*, Volumes 1 and 2, New York: Plenum Press, 1970.

Schleher, D. C., *Introduction to Electronic Warfare*, Dedham, MA: Artech House, 1986.

Skolnik, M. I., (ed.), *Radar Handbook*, 2nd ed., New York: McGraw-Hill, 1990.

Airborne and Space-Based Radar Issues

This chapter enables the reader to:

- Understand the limitations that airborne and space-based platforms impose on radar configurations;
- Know the characteristics of surface clutter as viewed by moving platforms;
- Understand the capabilities and limitations of pulse-Doppler processing, displaced phase center arrays (DPCA), and space-time adaptive processing (STAP), to allow targets to be viewed against a terrestrial-clutter background;
- Quantify the capabilities of synthetic-aperture radar (SAR) to image terrain and targets.

Airborne and space-based radar (SBR) offer the potential to cover large geographic areas that may be unavailable to ground-based radar, and to observe terrestrial and low-altitude targets at long ranges, as discussed in Section 2.1.

However, airborne and space platforms may limit the antenna configurations, prime power, and weight of radar that may be deployed on them. These limitations, and the resulting radar configurations, are discussed in Section 11.1.

Airborne and SBR are often used to view targets against a background of terrestrial clutter. The terrestrial clutter viewed from these platforms has significantly greater range extent than such clutter viewed from ground-based radar. Further, terrain clutter encountered by radars on moving platforms may have a large Doppler-frequency spectral spread, requiring special techniques for detecting targets in such backgrounds. The characteristics of radar clutter observed from moving platforms is described in Section 11.2.

Viewing targets against such clutter backgrounds generally may be categorized as:

- Airborne moving target indication (AMTI);
- Ground moving target indication (GMTI).

Techniques for detecting airborne and moving ground targets in clutter are discussed in Sections 11.3 to 11.5.

Airborne and SBR are also used to image terrain and terrestrial targets. The imaging capabilities of synthetic aperture airborne and SBR are discussed in Section 11.6.

11.1 Radar Configurations

Radar deployed on aircraft must have:

- Antennas consistent with the aerodynamic properties of the aircraft. Antennas that may fit within the aircraft envelope, or require minor modifications to it, may meet this requirement. Major changes to the aerodynamics require special designs, and usually are employed on dedicated aircraft.
- Weight compatible with the aircraft payload. This depends on the aircraft size, as well as the other payload requirements placed on the aircraft.
- Prime-power requirements that may be met by the aircraft generation capability. Prime power is usually generated by the aircraft engines, or by an auxiliary power unit (APU).

Fighter aircraft usually employ nose-mounted antennas having diameters of about 1m. A radome protects the antenna and provides the required aerodynamic shape. Such radar often operates in the X band (e.g., 9.5 GHz), and has pencil beams with beamwidths of about 2° [1, p. 3].

Older radars of this type employed dish antennas that were gimbaled to provide mechanical scan in azimuth and elevation, relative to the aircraft heading. Phased-array antennas are often used in modern fighter radar to allow multimode operation (search, track, and image), and to provide for simultaneously tracking multiple targets. These arrays are often gimbaled to increase the angular coverage available beyond that of the electronic scan.

Radar surveillance missions are often performed by dedicated aircraft. Aircraft such as the Airborne Warning and Control System (AWACS) employ rotating antennas in rotodomes mounted above the aircraft body to provide 360° coverage in azimuth [1, pp. 446–447]. Such antennas provide relatively narrow beams in azimuth, but the small vertical dimensions of the rotodomes result in broad elevation beams. The rotation rates of these antennas are comparable to those of rotating ground-based search radar (see Section 7.2), so that target tracking employs a track-while-scan (TWS) mode.

Other airborne surveillance radars, such as the Joint Surveillance and Target Attack Radar (JSTARS), employ phased-array antennas mounted along the fuselage or in pods conformal with the fuselage. These arrays may have large horizontal dimensions, producing narrow azimuth beams, but their vertical dimensions are limited by the aircraft size, so the elevation beams are relatively broad [2].

These phased-array radars may scan a region, typically $\pm 60^\circ$ in azimuth on one or both sides of the aircraft. They may provide multimode operation and multiple target tracks. Gaps in such coverage may be filled to some degree by other antennas located in the wings and/or tail of the aircraft.

Advanced airborne-radar concepts call for conformal phased-arrays to be mounted at various locations on the aircraft. The signals from these would be combined to provide all-around radar coverage.

Note that virtually all airborne radar concepts have antennas that are limited in height by the aircraft platform, and so have relatively broad elevation beams.

SBR may employ antennas that are compatible in size with their launch vehicles, which limits their dimensions to a few meters. Alternatively, they may use deployable antennas [3]. Dish antennas may employ an unfolding rib and mesh structure, a technology widely employed in communications satellites. The larger of such antennas employ articulating ribs. The mechanical-scan limitations of dish radar usually preclude their use for surveillance, but such antennas have been used for tracking and rendezvousing with spacecraft.

Phased-arrays have been used on radars such as radar satellite for ocean measurement (SEASAT) [4, pp. 14–15], and Spaceborne Imaging Radar–C/X Band Synthetic Aperture Radar (SIR-C) [5], to provide wide-area coverage of the Earth. Such phased-array antennas may be unfolded after deployment from their launch vehicles, providing large antenna areas. They may provide wide-area, multimode coverage without mechanical steering, using electronic scanning.

Most SBRs use a combination of solar cells and storage batteries to provide their prime power. The solar cells charge the batteries when the satellite is in view of the Sun, and the radar uses the battery power during its operation. The size of the solar-cell array and the storage battery depend on the portion of the time the satellite views the Sun and the portion of the time the radar is operating, as well as the radar prime-power requirement. Other potential SBR prime-power sources include chemical energy, radioisotopes, and nuclear reactors [6].

The removal of waste heat from SBR usually employs thermal radiation, since conduction and convection are not available in space.

Minimizing radar weight is a prime consideration for SBR, because of the cost of launching heavy payloads, and the payload limitation of satellite launch vehicles. An SBR is generally launched in a single payload, since assembly in orbit of a radar launched in multiple payloads is not attractive.

The capability of SBR to view terrestrial targets is limited by satellite orbital mechanics [4, pp. 3–10]. Satellites in low-Earth circular orbits (e.g., 1,000-km altitude) have satellite orbital velocities of about 7 km/s, and orbital periods of about 100 minutes. An SBR on such a satellite may view a terrestrial region for about 15 minutes, but will not revisit this region on the next orbit, due to the rotation of the Earth. A constellation of about 30 such SBRs is needed to provide continuous worldwide coverage.

Satellites at higher altitudes have lower velocities and longer orbital periods. They may view a larger region, and for a longer period. A smaller number of such SBRs is needed for continuous worldwide coverage, as shown in Figure 11.1. Satellites in geosynchronous orbits (35,871-km altitude) may continuously view a region approaching half the Earth. However, higher-altitude SBRs have longer radar ranges (see Figure 11.1), requiring larger radar, and the cost for launching a given payload to a higher altitude is higher.

SBR, as well as airborne radar, may be ineffective in viewing targets below them, due to the increased terrain-clutter return and reduced radial velocity of targets moving on horizontal paths. For SBR, this may lead to a gap in coverage for grazing angles greater than about 60°, sometimes called the nadir hole. In such cases, more satellites than indicated in Figure 11.1 are needed for continuous worldwide coverage.

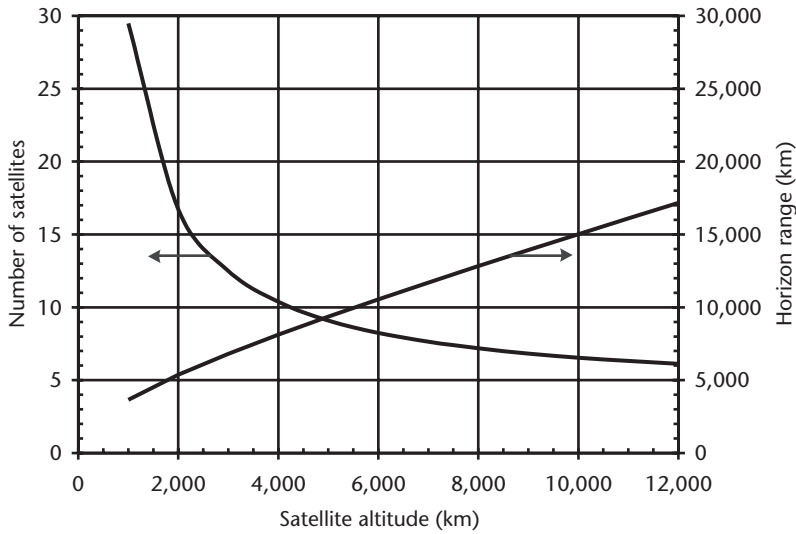


Figure 11.1 Number of satellites required for continuous worldwide coverage and range to the 1° grazing angle radar horizon versus satellite altitude. (After: [7].)

11.2 Clutter Characteristics

Many airborne and SBR observe airborne and surface targets with a terrain or sea-surface backgrounds, and employ AMTI and/or GMTI techniques to suppress the clutter, so that the targets may be detected and tracked [8]. The terrain clutter viewed by radar on airborne and space-based platforms differs from that viewed by ground-based radar in two important ways:

- The radial velocity of the clutter may vary between $\pm V_p$, where V_p is the velocity of the radar platform. For ground-based radar, the platform velocity is zero, and the clutter velocity spread is determined by the internal clutter movement, at most a few meters per second (see Section 9.1).
- The range extent of radar clutter extends to the radar horizon. For airborne platforms, this may extend to 300 km or more, and for space-based platforms to much greater ranges; while for ground-based radar, it is limited to about 20 km (see Section 2.1).

A consequence of the large range and velocity spread of the clutter is that radar waveforms may have range and/or velocity ambiguities that lie in the clutter regions (see Chapter 4). This is further discussed in Section 11.3.

Note that stationary air platforms, such as airships and geosynchronous satellites, may have little or no velocity relative to the Earth, so that the clutter velocity spread they observe may be small. This clutter is similar to that of ground-based radar, although the range extent of the clutter may be large.

The radar viewing geometry for an airborne or space-based radar is shown in Figure 11.2. The radar platform is at an altitude of h_R , and has a velocity in the illustrated plane of V_R . The angle in this plane between the radar LOS and the platform velocity is defined as the depression angle, ϕ_D . The radial velocity of the clutter observed on this LOS, V_C , is given by:

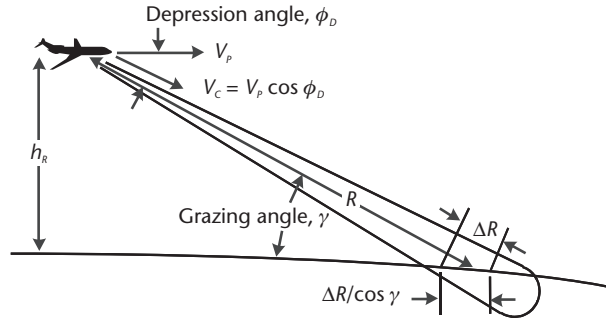


Figure 11.2 Geometry of airborne radar clutter observation in a vertical plane containing the radar velocity and the radar LOS.

$$V_c = V_p \cos \phi_D \quad (\text{plane of platform velocity}) \quad (11.1)$$

The signal path will be refracted downward by atmospheric refraction, and for SBR, by ionospheric refraction. The radar also will be subject to propagation losses and other effects from the atmosphere, rain, and the ionosphere (see Sections 9.2 to 9.4).

The angle between the radar LOS and the terrain is termed the grazing angle, γ . The range dimension of the clutter is normally limited by the radar range resolution, ΔR , and is given by $\Delta R / \cos \gamma$ (see Section 9.1). At low grazing angles, multipath may affect the signal strength and elevation-angle measurement for low-altitude targets (see Section 9.1).

A plan view of the airborne and SBR clutter geometry is shown in Figure 11.3. The component of platform velocity for a radar azimuth scan angle relative to the platform velocity of ϕ_A is $V_p \cos \phi_A$. If this value is substituted for V_R in Figure 11.2, the clutter radial velocity is seen to be:

$$V_c = V_p \cos \phi_A \cos \phi_D \quad (11.2)$$

Thus, the clutter radial velocity observed from the platform varies between $\pm V_p \cos \phi_D$, or, when the depression angle is small, between $\pm V_p$ [9, pp. 17-1–17-5]. For example, if the depression angle at the radar horizon is 10° , and the platform velocity is 300 m/s, the sidelobe clutter velocity spread is ± 295 m/s.

The area of the mainlobe clutter observed by the radar, when the clutter range extent is limited by the radar range resolution, is given by (see Section 9.1):

$$A_s = \frac{R \theta_A \Delta R}{\cos \gamma} \quad (11.3)$$

where:

A_s = the mainlobe clutter area

R = range to the clutter area

θ_A = radar azimuth beamwidth

Since the clutter radial velocity varies with azimuth, there is a spread of clutter velocities across the radar azimuth beamwidth. The first nulls of the azimuth beam occur at approximately $\pm \theta_A$, and the clutter radial velocities at these points are given

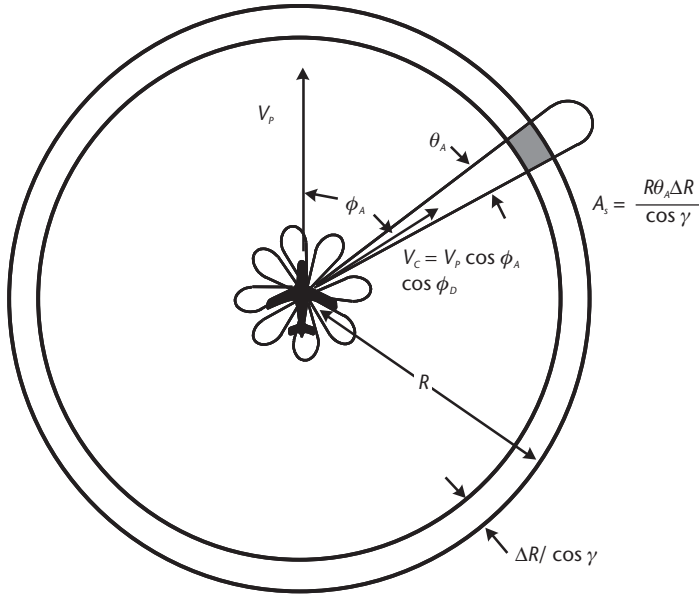


Figure 11.3 Plan view of radar clutter observation from a moving platform.

by $V_p \cos(\phi_A \pm \theta_A) \cos \phi_D$. When θ_A is small, the radial velocity spread between the nulls of the azimuth beam is given by:

$$V_{ML} = 2V_p \theta_A \sin \phi_A \cos \phi_D \quad (11.4)$$

where:

V_{ML} = radial-velocity spread of clutter in the main beam

The mainbeam clutter velocity spread is largest when $\phi_A = 90^\circ$ (i.e., when the beam is normal to the direction of platform travel).

For example, for a platform velocity of 300 m/s, a beamwidth of 1° (17.5 mrad), beam azimuth of 30° , and a mainbeam depression angle of 25° , the mainbeam velocity spread is 4.75 m/s.

Clutter returns also enter the radar through the radar sidelobes, especially when a high-PRF waveform is used and range ambiguities are present. Sidelobe clutter returns from below the radar platform are often prominent because of the high grazing angle and the short range. Such returns are sometimes called the altitude return.

A composite plot of the velocity distribution of terrain clutter as seen by an airborne or SBR is shown in Figure 11.4. As discussed earlier, the sidelobe clutter extends between radial velocities of $\pm V_R$ (neglecting the depression angle). The altitude return creates a peak near zero radial velocity. The mainlobe clutter peak occurs at a radial velocity that depends on the azimuth scan angle, and has a width that depends on the scan angle and the azimuth beamwidth [9, p. 17.2].

The Doppler-frequency shift of the clutter returns are related to the radial velocity, V_C , by:

$$f_c = \frac{2V_C}{\lambda} \quad (11.5)$$

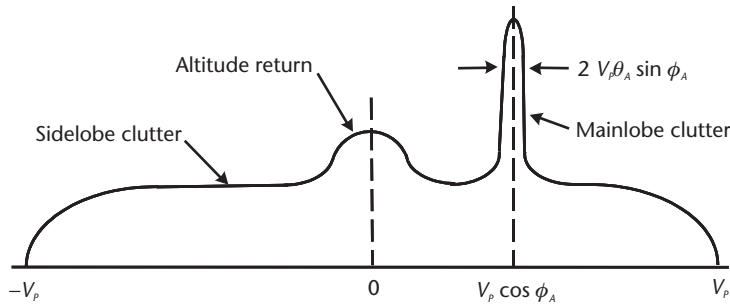


Figure 11.4 Airborne and SBR clutter features versus radial velocity, neglecting depression angle.

where:

f_c = Doppler-frequency of the radar clutter return relative to the transmitted radar signal frequency

λ = radar signal wavelength ($\lambda = c/f$, where f is the radar signal frequency)

For the previous examples, for an X-band radar (9.5 GHz), the sidelobe Doppler-frequency spread is ± 18.7 kHz, and the mainbeam clutter spread is 301 Hz.

While the clutter for all radars on moving platforms will have the features illustrated in Figure 11.4, their relative magnitudes will depend on the geometry of the radar observation, the radar sidelobe levels, and the ambiguities in the radar waveform. Compared with airborne radar, SBR often has higher gain, lower sidelobes, higher altitude-relative-to-target range, and radar waveforms that are shorter than the round-trip signal time and produce fewer range ambiguities. This usually results in sidelobe clutter and altitude return in SBR that are less critical than those in airborne radar.

11.3 Pulse-Doppler Processing

Pulse-Doppler processing, briefly discussed in Section 2.5, is a technique commonly used by airborne and SBR to detect and observe moving targets in the presence of clutter, such as described in the previous section. A train of radar pulses is transmitted, and the returned signals are processed to resolve a series of adjacent narrow spectral bands. Such processing employs a Fourier transform, or similar computational method. This technique, along with good range resolution, reduces or eliminates the clutter in the same range and radial-velocity resolution cell that competes with the target [9].

The waveform parameters used in pulse-Doppler processing, and the performance that may be achieved, depend on the radar, platform, and target characteristics. The waveform parameters are often classified as high, medium, or low PRF [1, pp. 323–326]. These are discussed below.

A high-PRF waveform is unambiguous in radial velocity, but is highly ambiguous in range. These waveforms may be used for targets traveling toward the radar platform with an aspect near the platform velocity vector. Then the radial velocity of the target is greater than the maximum clutter radial velocity. Since the waveform is unambiguous in radial velocity, the target is free of clutter in the velocity domain.

For example, for a radar platform having a velocity, V_p , of 300 m/s, and a target traveling at a velocity of 300 m/s directly toward the radar at an aspect angle, ϕ_A , of 20° , the relative velocity is 582 m/s, greater than the maximum radial clutter velocity of 300 m/s. If an X-band (9.5 GHz) radar on the platform uses a PRF of 60 KHz, the ambiguous velocity is 947 m/s (see Section 4.7), and the target is resolved from the clutter in radial velocity. Such a waveform is highly ambiguous in range, having 2.5 km range-ambiguity spacing.

High-PRF waveforms are effective for targets traveling toward the radar with small aspect angles. They are often used in fighter aircraft radar for engaging other aircraft that are closing with frontal aspect angles.

Medium-PRF waveforms are ambiguous in both range and radial velocity, but with ambiguities that may usually be resolved once the target is put into track. These waveforms are used for targets having radial velocity that is within the sidelobe clutter region and range that is within the sidelobe clutter range extent. In such cases, the target competes with the sidelobe clutter that is in both the same range-resolution cell and velocity-resolution cell as is the target. For search, a detection threshold is set for each range-velocity cell, often based on the clutter levels of adjacent cells. The target is detected and may be tracked if it is sufficiently larger than the clutter return for the range-velocity cell it occupies.

Target detection is usually not possible in range-velocity cells containing main-lobe clutter, due to the significantly larger clutter amplitude in such cells. This limitation may be characterized by a minimum detectable velocity (MDV), which is equal to one-half of the mainlobe clutter velocity spread given by (11.4):

$$MDV = V_p \theta_A \sin \phi_A \cos \phi_D \quad (11.6)$$

For example, an X-band radar that employs a PRF of 5 kHz will have range ambiguities spaced by 30 km, and velocity ambiguities spaced by 79 m/s. If an airborne radar velocity is 300 m/s as above, the radar beamwidth is 2° , the target aspect angle is 45° , and the depression angle is 10° , then the MDV is 7.3 m/s.

SBR in other than geostationary orbits have much higher platform velocities than airborne radar. While they also often have narrower azimuth beams, they usually cannot achieve values of MDV as small as airborne radar may achieve. For example, for satellite platform velocity of 7 km/s, an azimuth beamwidth of 0.5° , an aspect of 45° , and a depression angle of 20° , the MDV is 41 m/s. This would allow detection of most aircraft targets, but would severely limit the capability of such an SBR to detect moving ground targets. The techniques described in Sections 11.4 and 11.5 may offer improved performance in such situations.

Medium-PRF waveforms may be effective against targets observed with a clutter background, and with radial velocities smaller than the platform velocity. They are often used in fighter aircraft radar for engaging other aircraft in side and tail aspect geometries, and for detecting moving surface vehicles, within their MDV limitations.

Medium-PRF waveforms may also be used by SBR for detecting moving targets against an Earth background. Because of the MDV limitation discussed above, this mode is more suitable for AMTI than for GMTI. Techniques described in Sections 11.4 and 11.5 are more effective for ground-target detection.

A low-PRF waveform is unambiguous in range, but is highly ambiguous in radial velocity. These waveforms may be used when the target is not in mainlobe clutter, such as when the target range is greater than the horizon range of the clutter, or when the target altitude allows it to be resolved from the clutter in elevation angle. Since the waveform is unambiguous in range, the target is free of mainbeam clutter in the range domain.

For example, for a radar platform having an altitude of 3 km, the clutter horizon extends to a range of about 226 km, and a target at a range of 250 km would be free of clutter. A radar employing a PRF of 300 Hz is unambiguous in a range out to 500 km, and may view such a target with no clutter background. Such a waveform is highly ambiguous in radial velocity, having 4.7-m/s ambiguity spacing.

Such a waveform could also be used for targets at ranges shorter than 226 km but having high altitude, so that the radar mainbeam does not illuminate the terrain. Sidelobe clutter will compete with the target return in such cases, and the target detectability will depend on the magnitude of the sidelobe clutter and the target RCS.

Low-PRF waveforms are effective against long-range and high-altitude targets. They are often used in airborne surveillance radar and fighter radar for long-range search and tracking.

The three pulse-Doppler modes discussed above are compared in Table 11.1. The waveforms are those discussed above, and are appropriate for the platform and target parameters given there.

Pulse-Doppler processing in early airborne radar employed banks of analog filters. Most modern airborne radar employs digital signal processing. This allows flexibility in adapting the waveform and processing characteristics to the platform and target situation, and facilitates multimode operation [1, pp. 586–589].

11.4 Displaced Phase Center Arrays (DPCA)

The previous section describes how detection of slow-moving targets against a clutter background by medium-PRF pulse-Doppler waveforms is limited by the radial-velocity spread of the mainbeam clutter. The DPCA eliminates the spread of mainbeam clutter radial velocities. This is done by moving the phase center of the antenna in the opposite direction to the platform motion on successive pulses. This is accomplished by using different portions of the transmit and/or receive antenna on the successive pulses [9, pp. 16-8–16-9].

A simple implementation of the DPCA is illustrated in Figure 11.5, which shows a phased array aligned with the platform velocity vector. The first pulse of a pulse pair uses the portion of the phased array indicated, while the remaining elements are

Table 11.1 Examples of Pulse-Doppler Waveforms

<i>Parameter</i>	<i>High PRF</i>	<i>Medium PRF</i>	<i>Low PRF</i>
Frequency	9.5 GHz	9.5 GHz	9.5 GHz
PRF	60 kHz	5 kHz	300 Hz
Range ambiguity spacing	2.5 km	30 km	500 km
Velocity ambiguity spacing	947 m/s	79 m/s	4.7 m/s

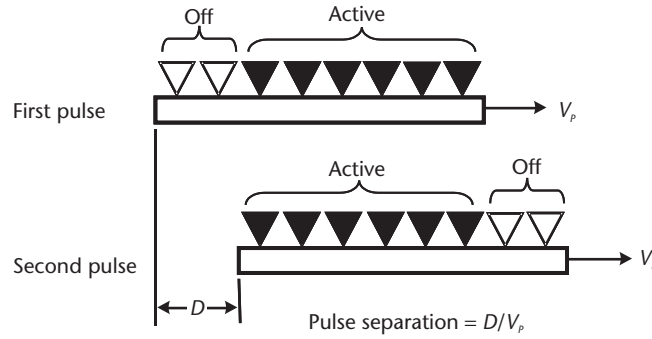


Figure 11.5 Illustration of DPCA operation.

inactive. The second pulse of the pair uses a different portion of the array, as indicated in the figure. The pulse separation (the reciprocal of the radar PRF) is adjusted to match the platform velocity and the separation of the active array segments, so that the active portion of the array is in the same location in space on the two successive pulses.

The result is that the clutter returns from the two pulses are identical. The returns are processed in a two-pulse MTI canceller, which cancels the clutter return, leaving signals from moving targets (see Section 9.1). The requirement for effective cancellation is that the transmit-receive virtual phase center be in the same location for successive pulses. The virtual phase center is midway between the phase centers of the active portion of the array at transmit and the active portion of the array at receive.

Other DPCA configurations provide three or more transmit-receive signal paths with the same virtual phase center. These allow multipulse MTI cancellation that provides improved performance in the presence of velocity spread due to internal clutter motion (see Section 9.1). In some radars, the MTI processor is followed by a pulse-Doppler processor to deal with sidelobe clutter.

DPCA requires the use of different portions of the transmit and/or receive antennas on successive pulses. For this reason, it is usually implemented in phased-array antennas. For airborne radar, DPCA is well-suited for side-looking radar, where the long dimension of the array is aligned with the aircraft fuselage.

The required radar PRF is determined by the platform velocity, V_p , and the antenna phase-center spacing:

$$PRF = V_p / D \quad (11.7)$$

where D is the phase-center spacing. Thus, the PRF must be adjusted for platform velocity.

DPCA may be effective in GMTI by canceling mainbeam clutter and allowing detection of low-velocity targets against clutter background. However, its performance may be limited by several factors:

- Differences in the antenna pattern for the different phase centers;
- Imperfect alignment of the antenna (e.g., due to aircraft flight-path perturbations);

- PRF mismatch due to errors in adjusting for platform velocity;
- Mismatch in transmit-receive channels for successive pulses;
- Clutter internal velocity, which affects all MTI implementations.

The DPCA technique is sometimes called a special case of STAP, discussed in the following section [10, p. 114].

11.5 Space-Time Adaptive Processing (STAP)

In most traditional radars, the angle response is determined by the radar antenna (e.g., by adjusting the phases of the elements in a phased-array antenna). The Doppler-frequency response is determined by processing in the receiver, for example by pulse-Doppler processing. With STAP, the antenna array elements (the space dimension), and the successive pulse returns (the time dimension), are processed jointly to allow greater flexibility in reducing interference such as clutter and jamming [10, pp. 1–6].

STAP may exploit the structure of clutter in airborne and SBR to allow detection of low-velocity targets against clutter backgrounds, such as slowly moving ground vehicles in a GMTI mode. Specifically, it may allow detection of such targets in the mainbeam clutter, and with radial velocities within the MDV of pulse-Doppler radar.

The detailed clutter structure in this case is shown in Figure 11.6. The main part of the figure is a plot of angle over the mainlobe of the radar azimuth beam versus radial velocity over the mainbeam clutter velocity spread. The clutter radial velocity varies with the azimuth relative to the platform velocity, as given in (11.2), producing coupling between angle and radial velocity. It is thus represented by a diagonal

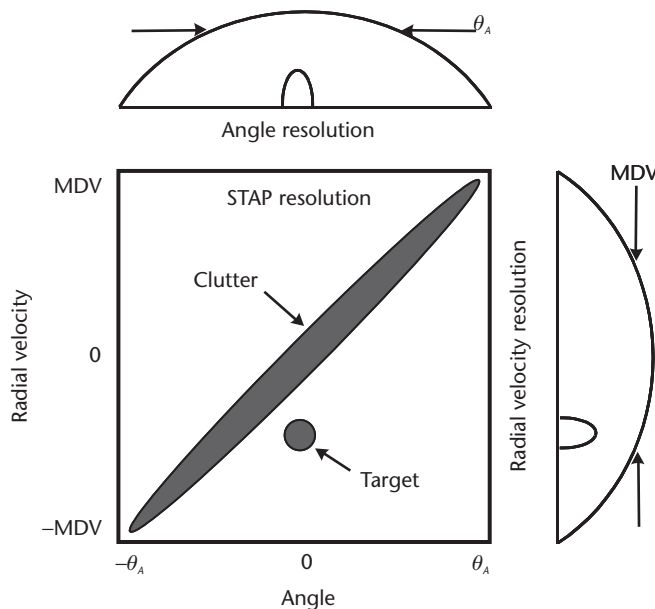


Figure 11.6 Structure of terrain clutter and a target in the radar azimuth beam and radial-velocity resolution.

ridge in Figure 11.6. A target, slightly offset from this clutter ridge, is also shown [10, pp. 51–64].

The plot at the top of Figure 11.6 shows the angular response of the antenna. The clutter fills the beam and screens the target. Similarly, the plot at the right of the figure shows the radial-velocity response of a pulse-Doppler processor. Here, the clutter fills the region $\pm\text{MDV}$, screening the target. Neither form of independent processing will allow detection of the target. With STAP, the angle and radial-velocity data are jointly processed, allowing detection of the target.

STAP involves processing of the M pulses in the pulse train with each of the N elements in the linear array that forms the azimuth beam. Thus, the processing has a dimensionality of NM , which may be orders of magnitude greater than the processing for either array beam formation (N elements), or pulse-Doppler processing (M pulses). For example, with 500 linear array elements and 200 pulses processed, $NM = 10^5$.

STAP processing involves calculation of NM complex weights that, when applied to the signal data, will minimize the interference. The signal data in each range-resolution interval is then processed to yield the desired target signal. Both of these steps involve $NM \times NM$ matrix inversions [10, p. 65–71].

This processing may be computationally intense. However, NM degrees of freedom are rarely needed to cancel the interference, and STAP processing usually employs reduced-rank processing, reducing the computational requirements [10, pp. 114–162]. Much current STAP research is addressing techniques for reducing the computational requirements [11].

Application of STAP cancels jammers as well as clutter. However, the jamming interference occurs at fixed angles independent of Doppler frequency. The sidelobe canceling technique described in Section 10.3, or its equivalent using an N -element matrix, may be used. Thus, STAP is not required just for jamming cancellation, but if it is applied for mainlobe clutter cancellation, it cancels jammers as well.

Factors that may limit the performance of STAP include:

- Clutter that is nonstationary, and clutter that is discrete;
- Clutter internal motion and scintillation;
- Uncorrected antenna motion perturbations;
- Radar transmitter and receiver instabilities.

11.6 Synthetic-Aperture Radar (SAR)

SAR is used to generate two-dimensional images of terrain and associated ground targets. Conventional radar may provide good range resolution by using wideband waveforms (see Chapter 4). However, the cross-range resolution is limited by the radar azimuth beamwidth, θ_A , to $R\theta_A$.

For example, with a 50-MHz signal bandwidth, the range resolution is 3m. With a grazing angle of 20° , the ground resolution in the range dimension is 3.2m (see Section 9.1). An azimuth beamwidth as small as 3 mrad, produced by an 11-m aperture at X-band, provides a cross-range resolution of 300m at a range of 100 km, two orders of magnitude greater than the range resolution (see Section 8.2).

As the name suggests, SAR produces the effect of very large airborne or space-based apertures, creating very narrow effective beams that can give cross-range resolution comparable to the range resolution. In an SAR mode, the moving radar views the target from successive locations of the antenna. The signal returns are combined coherently to give the effect of a large aperture that is equal in length to the space occupied by the antenna during the processing interval.

This is illustrated in Figure 11.7. The real-aperture antenna having a dimension of w_{RA} produces a beamwidth, θ_{RA} , of λ/w_{RA} , as shown in Figure 11.7(a), giving a cross-range resolution of $R\lambda/w_{RA}$. Figure 11.7(b) shows the same real aperture as it moves through several successive positions to create a synthetic aperture having a dimension w_{SA} . The angular resolution, or beamwidth, θ_{SA} , produced by this synthetic aperture is given by [12, pp. 21-4–21-7]:

$$\theta_{SA} = \lambda/(2w_{SA}) \quad (11.8)$$

and the cross-range resolution, ΔCR , is given by [1, p. 616].

$$\Delta CR = R\lambda/(2w_{SA}) \quad (11.9)$$

The factor of two in the denominators of (11.8) and (11.9) is a consequence of radar transmission and reception being done independently at each successive antenna location in the synthetic array, while a real aperture illuminates the target with a single field and receives the composite target return from that illumination [12, p. 159].

For example, if the synthetic-aperture dimension is 500m, the SAR beamwidth at X-band is about 0.032 mrad, and the cross-range resolution at a range of 100 km

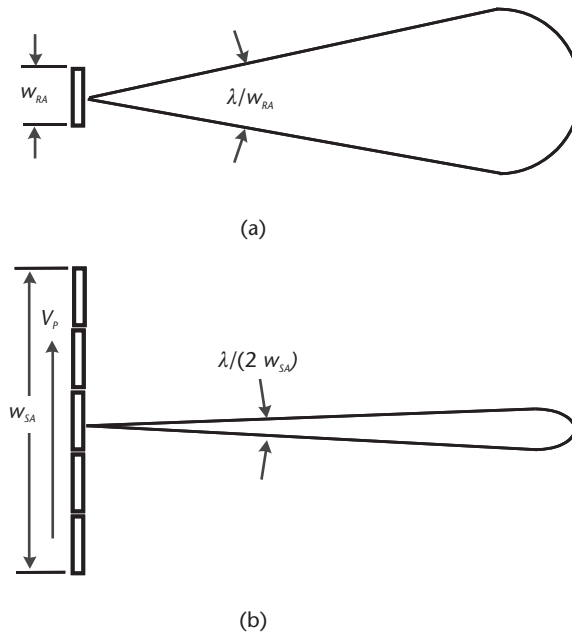


Figure 11.7 Illustration of real-aperture and synthetic-aperture beam formation. (a) Real aperture. (b) Synthetic aperture.

is 3.2m, the same as the range resolution in the previous example. For a platform velocity of 300 m/s, the time to generate this synthetic aperture is 1.67 sec. Such an SAR could generate images of the terrain and targets with resolution of 3.2m in the two orthogonal dimensions.

To avoid grating lobes in the SAR beam pattern, the synthetic aperture must be sampled often enough to produce the effect of a filled array (see Section 3.3). The required radar PRF is given by [13, pp. 21-18–21-21]:

$$PRF \geq \frac{4V_p}{w_{RA}} \quad (11.10)$$

Since SAR relies on platform motion to generate the synthetic aperture, it may not be used by stationary platforms such as airships or synchronous satellites. A similar technique, called inverse SAR (ISAR), is sometimes used to image targets that are moving past a radar, or are rotating [1, pp. 617–618 and 640–651].

SAR processing uses the phase changes during the processing time to determine the angular position of stationary ground objects. Moving targets that have radial velocity have additional linear phase change from pulse to pulse, which makes them appear offset in angle from their true positions. For example, vehicles may appear to be off the roads on which they are actually traveling. When this apparent position change is a problem, special processing techniques may be used to correct for it.

SAR techniques may be classified by the complexity of the processing employed and the resulting radar capabilities. Three such classes of SAR (Doppler beam sharpening, side-looking SAR, and spotlight SAR) are addressed below.

The processing of radar returns in Doppler beam sharpening assumes linear phase progression from successive returns. This is referred to as unfocused Doppler processing. The phase changes, due to the changing target range as the radar passes the target, cause the synthetic-aperture length to be limited to [13, pp. 21-4–21-7]:

$$w_{SA} \leq (R\lambda)^{1/2} \quad (\text{Doppler beam sharpening}) \quad (11.11)$$

and the resulting cross-range resolution is limited to:

$$\Delta CR \leq 0.5(R\lambda)^{1/2} \quad (\text{Doppler beam sharpening}) \quad (11.12)$$

For example, an X-band (9.5 GHz) radar, observing targets at 100-km range, would be limited to a synthetic-aperture length of 56m, and could produce cross-range resolution no less than 28m. For platform velocity of 300 m/s, the maximum processing time is 0.19 sec. These results are summarized in column 2 of the lower part of Table 11.2, which also gives the radar characteristics in the upper part of the table.

Such cross-range resolution is usually not useful for terrain imaging. However, it may be used for resolving, detecting, tracking, and measuring the characteristics of closely-spaced targets. The cross-range resolution is also limited to one-half of the real-aperture size, as discussed below for side-looking radar, but this rarely a limitation for Doppler beam sharpening.

Table 11.2 SAR Examples

<i>Parameter</i>	<i>Value</i>			
Frequency	9.5 GHz			
Antenna length (real aperture)	2m			
Antenna beamwidth (real aperture)	0.905°			
Platform velocity	300 m/s			
PRF	1,000 Hz			
Target range	100 km			
<i>SAR Mode</i>	<i>Doppler Beam Sharpening</i>	<i>Side-Looking SAR</i>	<i>Spotlight SAR</i>	
Synthetic-aperture length	56m (maximum)	1,580m (maximum)	3,160m	
Cross-range resolution	28m (minimum)	1m (minimum)	0.5m	
Processing time	0.19 sec (maximum)	5.27 sec (maximum)	10.53 sec	

In side-looking SAR, the radar antenna is usually oriented to look normal to the platform flight path. The elevation beam is broad enough to cover the ground area of interest, and may be shaped to equalize the sensitivity at the various ranges, as illustrated in Figure 11.8. The SAR processing generates a continuous map of the range swath observed as the platform passes the terrain (see Figure 11.8). This is often called a strip map.

Side-looking SAR usually employs focused processing, which corrects the signal phase for range changes as the radar passes the targets. The synthetic-aperture length is limited by the viewing angles for which the target remains within the real-aperture beamwidth, (θ_{RA} , to ([13, pp. 21-4– to 21-7]):

$$w_{SA} \leq R\theta_{RA} \quad (\text{side-looking SAR}) \tag{11.13}$$

The resulting cross-range resolution is limited to no less than one-half of the real-aperture linear dimension, w_{RA} :

$$\Delta CR \geq w_{RA}/2 \quad (\text{side-looking SAR}) \tag{11.14}$$

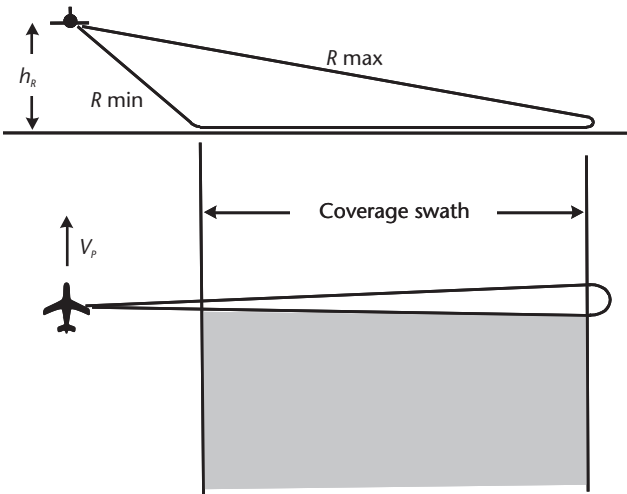


Figure 11.8 Geometry for side-looking SAR.

These performance measures are independent of range, since the time that a ground target remains in the real-aperture beam is proportional to range.

For example, for an X-band radar having a 2m real aperture, the beamwidth is 0.905° (15.8 mrad), as given in the upper portion of Table 11.2. At a range of 100 km, the maximum synthetic-aperture length is about 1,580m, and the minimum cross-range resolution cell is 1m. The maximum processing time is 5.27 sec. These results are summarized in column 3 of the bottom portion of Table 11.2.

In side-looking SAR, the PRF determines the unambiguous range extent of the strip map that may be generated, as well as being constrained by (11.10). For example, with a platform velocity of 300 m/s and a 2m real aperture, the PRF must be at least 600 Hz. With this PRF, the unambiguous range is 250 km, and this is the maximum range extent of the strip map that may be generated.

Side-looking radar is widely used on aircraft and satellites for mapping terrain and sea surface. While most dedicated side-looking radar operates with the beam normal to the platform velocity, other look angles may be used, with some degradation in the resolution.

Spotlight SAR is used when cross-range resolution is required to be better than that provided by side-looking SAR. This may be the case when extremely small resolution is required, for example to identify the type of ground vehicle, or when a large antenna is used to provide the required radar sensitivity. The latter situation often occurs for SBR, where large antennas are required, due to the long ranges [14].

In spotlight SAR, the radar beam remains on the target area long enough to generate the desired synthetic aperture. The processing corrects for range changes as the radar passes the target. It may also correct for motion of target pixels between range and cross-range cells, using techniques that are sometimes called extended coherent processing. This allows large synthetic apertures to be generated, producing small cross-range resolution [15]. To achieve long observation times, either the flight path must curve, or the beam must steer to follow the region being imaged. The latter mode is usually employed, using phased-array radar.

The length of the synthetic aperture in a spotlight mode is given by:

$$w_{SA} = V_p t_p \quad (\text{spotlight SAR}) \quad (11.15)$$

where t_p is the processing time. The cross-range resolution is then [14, p. 503]:

$$\Delta CR = \frac{R\lambda}{2w_{SA}} = \frac{R\lambda}{2V_p t_p} \quad (\text{spotlight SAR}) \quad (11.16)$$

An example is shown in column 4 of the lower portion of Table 11.2. In this example, a cross-range resolution of 0.5m is desired at a range of 100 km. This is one-half of the cross-range resolution that is provided by the side-looking SAR in the previous example shown in column 3. The required synthetic-aperture length is 3,160m, which is produced with a processing time of 10.53 sec, twice the values for the side-looking SAR. Note that the cross-range resolution for spotlight SAR is proportional to range.

Spotlight SAR may be used to generate a high-resolution image of a limited surface region, such as a factory complex or an airfield. In this mode, a pencil-beam antenna pattern may be used. As with strip mapping, spotlight SAR may be done at

look angles other than normal to the flight path, but with degraded resolution. The pencil-beam phased-array radar in fighter aircraft may be used in this mode, given suitable processing.

Spotlight SAR may also be used by phased-array radar to produce images of large areas, or strip maps that have smaller cross-range resolution than indicated by (11.14). This is achieved by revisiting each portion of the terrain area periodically using electronic scan, so that the limitation imposed by the array beamwidth does not apply. Such techniques are used by large airborne surveillance radars, and by SBRs with their large antennas [14, pp. 503–505].

In spotlight SAR, the PRF also determines the unambiguous range extent of the area that can be observed.

SAR signal processing employs Fourier-transform-like algorithms. It must correct for perturbations in the flight path. Early SAR used optical elements to perform the processing, with the resulting images recorded on film [16, pp. 23–17–21–23]. Most modern SAR use digital processors, which gives flexibility to handle a variety of modes and parameters. The complexity of the required processing increases rapidly with decreasing cross-range resolution, both due to the increased data and to the complexity of the algorithms needed [1, pp. 632–636].

When strip maps or images of limited regions are produced at different times, it is often of interest to find changes (e.g., the deployment of new weapons) that have occurred between observations. This is accomplished by a technique called change detection, which maps one image onto another image of the same area, and identifies features that have changed.

SAR may be used to identify objects in the images it produces. Algorithms for doing this are beyond the scope of this book, but typically from 10 to 50 resolved pixels on the target are needed to reliably identify the target [17].

This discussion of SAR has addressed two-dimensional imaging of terrain and surface targets. It is possible to measure the altitude of terrain and targets in SAR images by using interferometry between two SAR antennas having vertical separation.

11.7 Problems

The following problems are provided to assist in reviewing this chapter and to ensure a basic understanding of the material. For maximum benefit, the problems should first be solved without using the VBA custom radar functions. Solutions to these problems are given in Appendix E, Section E.11.

1. What physical factors limit the antennas that may be used for airborne radar?
2. For a radar on an aircraft with a velocity of 350 m/s and having a depression angle when viewing the radar horizon of 10° , what is the velocity spread of the sidelobe clutter? If the radar frequency is 3.3 GHz (S band), what is the spectral spread of the sidelobe clutter? If the mainbeam has an azimuth of 60° relative to the platform velocity, and a depression angle of 25° , what is the mainbeam clutter velocity? What is the corresponding Doppler-

- frequency shift? If the azimuth beamwidth is 1.5° , what is the mainbeam velocity spread? What is the corresponding mainlobe spectral spread?
3. What class of pulse-Doppler waveforms is used to view targets that are traveling toward the front of an aircraft radar platform?
 4. What is the maximum PRF that may be used to view targets that are free of mainlobe clutter at ranges up to 500 km in a low-PRF mode?
 5. For DPCA operation with antenna phase centers separated along the platform velocity vector by 2m, and with a platform velocity of 300 m/s, what is the required radar PRF?
 6. Which airborne and SBR technique may be used to resolve and detect targets that are not resolved in angle or in radial velocity from the mainbeam clutter?
 7. An SBR has a velocity of 7 km/s, a frequency of 5.5 GHz, and an antenna dimension parallel to the velocity vector of 10m. If the radar views a target at a range of 5,000 km, what is the maximum cross-range resolution using Doppler-beam sharpening? What is the maximum cross-range resolution using side-looking SAR? In spotlight SAR, what processing time is needed to provide a cross-range resolution of 2m? What is the minimum PRF that may be used?
 8. Approximately how many SBR satellites are needed to provide continuous worldwide coverage using circular orbits at 5,000 km altitude? What radar range is needed to view targets at the radar horizon (1° grazing angle)?
 9. An airborne X-band (9.5 GHz) radar has a velocity of 325 m/s. A target is flying toward the radar with a velocity of 350 m/s at an angle 15° from the radar platform velocity vector. What is the minimum PRF that will avoid sidelobe clutter when observing the target? Neglect depression angle.
 10. Against what type of targets is DPCA most effective?
 11. If an array radar has 700 elements in the horizontal dimension, and processes a waveform having 150 pulses, what is the dimension of the matrix that must be inverted for STAP, assuming no rank reduction is employed?
 12. What SAR mode is used to generate strip maps? In this mode, what is the cross-range resolution for an antenna with a horizontal dimension of 5m? What signal bandwidth will give equal range resolution? If the platform velocity is 1,000 m/s, what is the minimum PRF? What is the resulting limitation on the range extent of the strip map?

11.8 VBA Software Functions for Airborne and SBR

11.8.1 Function Graz_Ang_deg

Purpose Calculates the Earth-grazing angle for a slant path from an elevated platform to the Earth's surface.

Reference Equations None.

Features Calculates grazing angle for the geometry shown in Figure 11.2. Corrects grazing angle for tropospheric refraction using Function TropoEl_Err_mR.

Input Parameters (with units specified)

Surf_Range_km = range from the elevated platform to the Earth’s surface, from 10 to 60,000 km (values outside this range will produce no result, indicated by an output of -1), (km).

Plat_Alt_km = Altitude of elevated platform (km).

Function Output The grazing angle, measured between the radar LOS and the Earth’s tangent, as corrected for tropospheric refraction (degrees). No result is produced when the input Surf_Range_km is less than Plat_Alt_km, or greater than Plat_Alt_km plus twice the Earth’s radius, indicated by an output of -2. No output is produced when the grazing angle is less than zero, indicated by an output of -3.

The Excel Function Arguments parameter box for Function Graz_Ang_deg is shown in Figure 11.9, with sample parameters and a solution.

11.8.2 Function Dep_Ang_deg

Purpose Calculates the depression angle for a slant path from an elevated platform to the Earth’s surface.

Reference Equations None.

Features Calculates depression angle, measured from the local horizontal at the radar platform, for the geometry shown in Figure 11.2.

Input Parameters (with units specified)

Surf_Range_km = range from the elevated platform to the Earth’s surface, from 10 to 60,000 km (values outside this range will produce no result, indicated by an output of -1), (km).

Plat_Alt_km = Altitude of elevated platform (km).

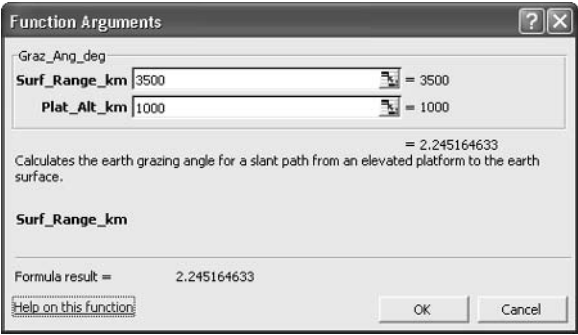


Figure 11.9 Excel parameter box for Function Graz_Ang_deg.

Function Output The depression angle, measured between the local horizontal at the elevated platform and the radar LOS (degrees). No result is produced when the input Surf_Range_km is less than Plat_Alt_km, or greater than Plat_Alt_km plus twice the Earth's radius, indicated by an output of -2. No output is produced when the grazing angle is less than zero, indicated by an output of -3.

The Excel Function Arguments parameter box for Function Dep_Ang_deg is shown in Figure 11.10, with sample parameters and a solution.

11.8.3 Function MB_Clutter_V_mps

Purpose Calculates the surface-clutter radial velocity at the center of the main beam or the radial-velocity spread between the nulls of the main beam, for a moving radar platform.

Reference Equations (11.2) and (11.4).

Features Allows selection to calculate: (1) the clutter radial velocity at the center of the main beam, or (2) the radial velocity spread between the nulls of the main beam. Calculates the radar depression angle, measured from the local horizontal at the radar platform, from the input platform altitude and surface range. The maximum sidelobe-clutter radial velocity may be calculated in mode (1) by setting the scan azimuth to zero and the surface range to produce zero grazing angle (the maximum range that produces an output).

Input Parameters (with units specified)

Sel_1ctr2spd = calculation selection (integer). Select 1 to calculate the radial velocity at the center of the main beam, or 2 to calculate the spread of radial velocity between the mainbeam nulls. Other values give no output.

Plat_Vel_mps = radar platform velocity (m/s).

Az_Scan_deg = radar azimuth scan angle, measured from the platform velocity vector (degrees).

Plat_Alt_km = Altitude of elevated platform (km).

Surf_Range_km = range from the elevated platform to the Earth's surface, from 10 to 60,000 km (values outside this range will produce no result, indicated by an output of -1), (km).

Az_Beam_deg (optional) = Radar azimuth beamwidth (degrees). This parameter is required for calculating the mainbeam velocity spread.

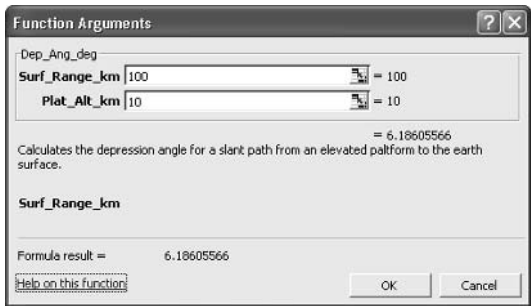


Figure 11.10 Excel parameter box for Function Dep_Ang_deg.

Function Output The clutter radial velocity at the center of the main beam or the radial velocity spread between the nulls of the radar main beam (m/s). No result is produced when the input Surf_Range_km is less than Plat_Alt_km, or greater than Plat_Alt_km plus twice the Earth's radius, indicated by an output of -2. No output is produced when the grazing angle is less than zero, indicated by an output of -3.

The Excel Function Arguments parameter box for Function MB_Clutter_V_mps is shown in Figure 11.11, with sample parameters and a solution.

11.8.4 Function SAR_XR_Res_m

Purpose Calculates the cross-range resolution for SAR in the selected mode.

Reference Equations (11.12), (11.14), and (11.16).

Features Allows SAR-mode selection of: (1) Doppler beam sharpening, (2) side-looking SAR, or (3) spotlight SAR. Calculates the smallest cross-range resolution for the selected mode. Only the parameters needed for the mode selected need be input. When option (1) is selected and the real-aperture width is input, the cross-range resolution is the larger of that from Doppler beam sharpening or side-looking radar.

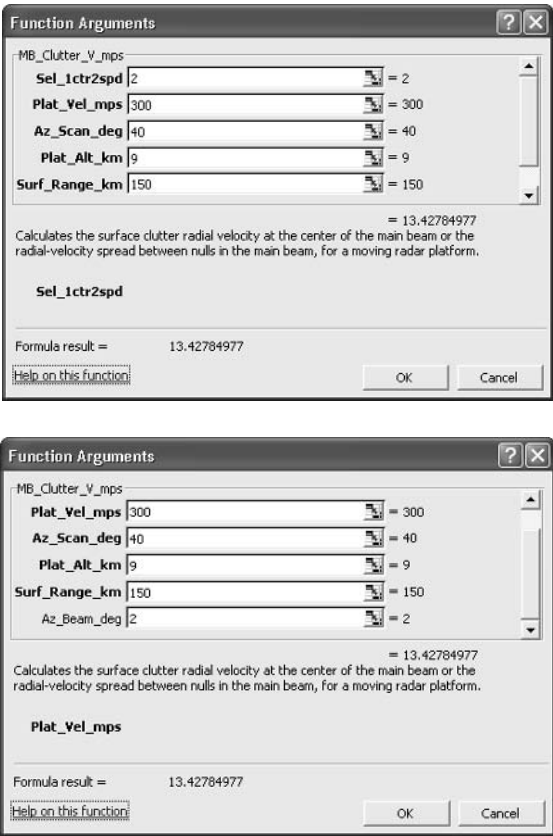


Figure 11.11 Excel parameter box for Function MB_Clutter_V_mps.

Input Parameters (with units specified)

Sel_1db52sl3sp = SAR mode selection (integer). Select 1 for Doppler beam sharpening, 2 for side-looking SAR, or 3 for spotlight SAR. Other values give no output.

Range_km (optional) = radar range for which the cross-range resolution is calculated (km). This parameter is required for calculating Doppler beam sharpening and spotlight SAR resolution.

Freq_GHz (optional) = radar frequency (GHz). This parameter is required for calculating Doppler beam sharpening and spotlight SAR resolution.

Real_Aper_L_m (optional) = length of the radar real aperture in the direction of the platform velocity (m). This parameter is required for calculating side-looking SAR resolution, and may be input to limit the resolution for Doppler beam sharpening to that for side-looking SAR.

Plat_Vel_mps (optional) = velocity of the radar platform (m/s). This parameter is required for calculating spotlight SAR resolution.

Proc_Time_s (optional) = processing time for spotlight SAR (sec). This parameter is required for calculating spotlight SAR resolution.

Function Output The smallest achievable cross-range resolution for the mode selected and parameters input. If the parameters required for the specified mode are not input, no result will be generated, indicated by no output or an output of zero.

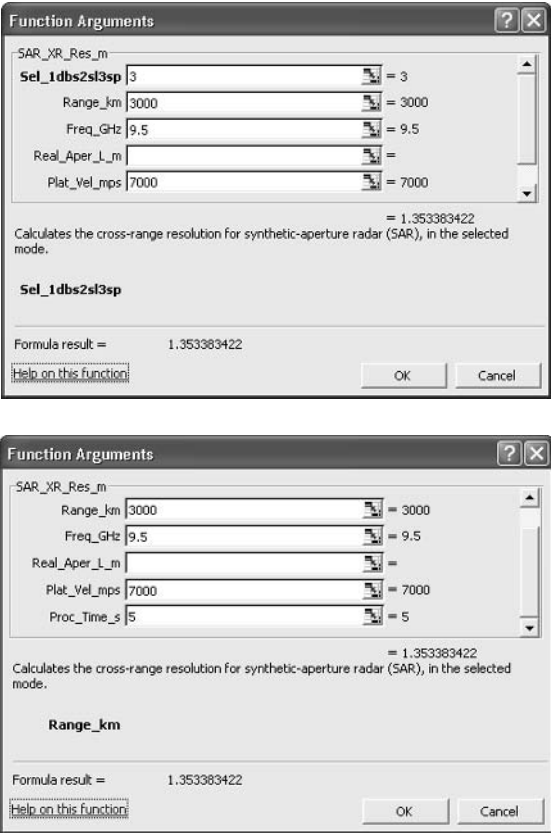


Figure 11.12 Excel parameter box for Function SAR_XR_Res_m.

The Excel Function Arguments parameter box for Function SAR_XR_Res_m is shown in Figure 11.12, with sample parameters and a solution.

References

- [1] Edde, B., *Radar Principles, Technology, Applications*, Upper Saddle River, NJ: Prentice Hall, 1995.
- [2] Brookner, E., *Aspects of Modern Radar*, Norwood, MA: Artech House, 1988.
- [3] Cantafio, L. J., "Space Antenna Technology," Chapter 12 in *Space-Based Radar Handbook*, L. J. Cantafio, (ed.), Norwood, MA: Artech House, 1989.
- [4] Cantafio, L. J., "Space-Based Radar Systems," Chapter 1 in *Space-Based Radar Handbook*, L. J. Cantafio, (ed.), Norwood, MA: Artech House, 1989.
- [5] Stuhr, F., R. Jordan, and M. Werner, "SIR-C/X-SAR," *IEEE AES System Magazine*, Vol. 10, October 1995, pp. 15–24.
- [6] Boretz, J. E., "Prime Power Systems in Space," Chapter 15 in *Space-Based Radar Handbook*, L. J. Cantafio, (ed.), Norwood, MA: Artech House, 1989.
- [7] Curry, G. R., "A Low-Cost Space-Based Radar System Concept," *IEEE AES System Magazine*, Vol. 11, September 1996, pp. 21–29.
- [8] Staudaher, F. M., "Airborne MTI," Chapter 16 in *Radar Handbook*, 2nd ed., M. I. Skolnik, (ed.), New York: McGraw-Hill, 1990.
- [9] Long, W. H., D. H. Mooney, and W. A. Skillman, "Pulse Doppler Radar," Chapter 17 in *Radar Handbook*, 2nd Ed., M. I. Skolnik, (ed.), New York: McGraw-Hill, 1990.
- [10] Guerci, J. R., *Space-Time Adaptive Processing for Radar*, Norwood, MA: Artech House, 2003.
- [11] "Special Collection of Papers on STAP," W. L. Melvin, (ed.), *IEEE Trans. on Aerospace and Electronic Systems*, Vol. 36, No. 2, April 2000.
- [12] Morris, G. V., *Airborne Pulsed Doppler Radar*, Norwood, MA: Artech House, 1988.
- [13] Cutrona, L. J., "Synthetic Aperture Radar," Chapter 21 in *Radar Handbook*, 2nd ed., M. I. Skolnik, (ed.), New York: McGraw-Hill, 1990.
- [14] Mrstik, V., "Agile-Beam Synthetic Aperture Radar Opportunities," *IEEE Trans. on Aerospace and Electronic Systems*, Vol. 34, No. 2, April 1998, pp. 500–507.
- [15] Munson, D. C., J. D. O'Brien, and W. K. Jenkins, "A Tomographic Formulation of Spotlight-Mode Synthetic Aperture Radar," *Proc. IEEE*, Vol. 71, No. 5, August 1983, pp. 917–925.
- [16] Cutrona, L. J., "Synthetic Aperture Radar," Chapter 23 in *Radar Handbook*, M. I. Skolnik, (ed.), New York: McGraw-Hill, 1970.
- [17] Irving, W. W., L. M. Novak, and A. S. Willsky, "A Multiresolution Approach to Discrimination in SAR Imagery," *IEEE Trans. on Aerospace and Electronic Systems*, Vol. 33, No. 4, October 1997, pp. 1157–1168.

Selected Bibliography

Discussion and photos of airborne radar hardware are given by Edde. SBR configurations, orbits and constellations are addressed in Cantafio. Further detail on SBR constellations for continuous worldwide coverage are given in Luders, Beste, and Ballard.

The characteristics of clutter viewed from a moving platform, and techniques for target detection in such backgrounds, including pulse-Doppler processing and

DPCA, are addressed by Staudaher, by Mooney and Skillman, by Long, Mooney and Skillman, in Skolniks handbooks and by Edde. Additional, more detailed material is given in Morchin, Morris, and Brookner. Clutter and clutter-rejection issues specific to SBRs are discussed by Andrews and Gerlach. STAP is addressed by Guerci, and by Melvin.

SAR configurations and techniques are discussed by Cutrona, in Skolniks handbooks, and by Edde. More detailed material is found in Hovanessian, and in Sullivan.

Andrews, G. A., and K. Gerlach, K., "SBR Clutter and Interference," Chapter 11 in *Space-Based Radar Handbook*, L. J. Cantafio, (ed.), Norwood, MA: Artech House, 1989.

Ballard, A. H., "Rosette Constellations of Earth Satellites," *IEEE Trans. on Aerospace and Electronic Systems*, Vol. AES-16, No. 5, September 1980, pp. 656–673.

Beste, D. C., "Design of Satellite Constellations for Optimal Continuous Coverage," *IEEE Trans. on Aerospace and Electronic Systems*, Vol. AES-14, No. 3, May 1978, pp. 466–473.

Brookner, E., *Aspects of Modern Radar*, Norwood, MA: Artech House, 1988.

Cantafio, L. J., (ed.), *Space-Based Radar Handbook*, Norwood, MA: Artech House, 1989.

Cantafio, L. J., "Space-Based Radar Systems and Technology," Chapter 22 in *Radar Handbook, 2nd Ed.*, M. I. Skolnik, (ed.), New York: McGraw-Hill, 1990.

Cutrona, L. J., "Synthetic Aperture Radar," Chapter 23 in *Radar Handbook*, M. I. Skolnik, (ed.), New York: McGraw-Hill, 1970.

Cutrona, L. J., "Synthetic Aperture Radar," Chapter 21 in *Radar Handbook, 2nd Ed.*, M. I. Skolnik, (ed.), New York: McGraw-Hill, 1990.

Edde, B., *Radar Principles, Technology, Applications*, Upper Saddle River, NJ: Prentice Hall, 1995.

Guerci, J. R., *Space-Time Adaptive Processing for Radar*, Norwood, MA: Artech House, 2003.

Hovanessian, S. A., *Introduction to Synthetic Array and Imaging Radar*, Dedham, MA: Artech House, 1980.

Long, W. H., D. H. Mooney, and W. A. Skillman, "Pulse Doppler Radar," Chapter 17 in *Radar Handbook, 2nd Ed.*, M. I. Skolnik, (ed.), New York: McGraw-Hill, 1990.

Luders, R. D., "Satellite Networks for Continuous Zonal Coverage," *ARS Journal*, Vol. 31, February 1961, pp. 179–184.

Melvin, W. L., "A STAP Overview," *IEEE A&E Systems Magazine*, Vol. 19, No. 1, Part 2, January 2004, pp. 19–35.

Mooney, D. H., and W. A. Skillman, "Pulse-Doppler Radar," Chapter 19 in *Radar Handbook*, M. I. Skolnik, (ed.), New York: McGraw-Hill, 1970.

Morchin, W. C., *Airborne Early Warning Radar*, Norwood, MA: Artech House, 1990.

Morris, G. V., *Airborne Pulsed Doppler Radar*, Norwood, MA: Artech House, 1988.

Skolnik, M. I., *Radar Handbook*, New York: McGraw-Hill, 1970.

Skolnik, M. I., *Radar Handbook, 2nd Ed.*, New York: McGraw-Hill, 1990.

"Special Collection of Papers on STAP," W. L. Melvin, (ed.), *IEEE Trans. on Aerospace and Electronic Systems*, Vol. 36, No. 2, April 2000.

Staudaher, F. M., "Airborne MTI," Chapter 18 in *Radar Handbook*, M. I. Skolnik, (ed.), New York: McGraw-Hill, 1970.

Staudaher, F. M., "Airborne MTI," Chapter 16 in *Radar Handbook, 2nd Ed.*, M. I. Skolnik, (ed.), New York: McGraw-Hill, 1990.

Sullivan, R. J., *Microwave Radar: Imaging and Advanced Concepts*, Norwood, MA: Artech House, 2000.

Radar Performance Modeling Techniques and Examples

This chapter enables the reader to:

- Analyze radar system problems and formulate a step-by-step approach to solving them;
- Combine radar models, equations, and data to produce needed answers to radar performance questions;
- Address missing data by using reasonable assumptions or by parametric analysis;
- Produce clear and meaningful descriptions of radar problems addressed and results obtained;
- Understand the approaches and solutions to example problems.

This chapter presents a brief discussion of radar performance analysis and modeling methodology, followed by five example problems and their solutions.

12.1 Methodology

Radar system performance modeling problems are usually stated in terms of the system performance results required. Input data on the radar system and its operating modes, the target complex and countermeasures applied, and environmental conditions may or may not be sufficient to fully define the problem. It is the task of the radar system analyst to:

- Analyze the problem;
- Develop an approach to generating the required results;
- Obtain the necessary data, or make reasonable assumptions;
- Perform the calculations required;
- Present the results in a meaningful fashion.

While there are often many ways to approach and solve a problem, the following steps have proved useful:

- Define the objectives of the analysis. What output data is required? What would be a useful format for presenting the results? It may be useful to generate notional plots or tables of the expected results.
- Review the available problem data. What radar parameters are available? Is a radar reference range defined? What target data is provided? Do radar CMs or environmental effects play a role, and are they adequately defined? Straight-forward radar parameter calculations may be made at this step. For example, wavelength may be calculated from frequency, and aperture area from antenna gain.
- Lay out the analysis steps. One useful approach is to work backward from the desired results. Another approach is to work forward from the data available. In some cases, both approaches may be used. This is often an iterative step, which requires reviewing the available data, the computational tools, and the required results.
- Address missing data. Often missing data may be generated by making reasonable assumptions. For example, beamwidths may be calculated from antenna dimensions, by making assumptions of the aperture weighting functions used (see Section 3.2). In other cases, it may be necessary to estimate parameters. For example, a solid-state radar duty cycle would likely be about 25% (see Section 3.1). In cases where there is no reasonable basis to estimate a parameter, a parametric analysis may be performed. For example, performance might be calculated parametrically with target RCS. In any case, analysis assumptions should be explicitly stated with the analysis results.
- Perform the calculations. This may be done manually, or using a computational aid such as a spreadsheet. At this step, radar models, such as those given in this book, are combined to generate the needed results. For example, atmospheric attenuation (see Section 9.3) and rain attenuation (see Section 9.2), may be calculated and combined into the propagation loss term in the S/N calculation (see Section 5.1). In some cases, the S/N may be combined with S/J and S/C to obtain an overall signal-to-interference ratio (S/I) (see Sections 9.1, 9.2, 10.2, 10.3, and 10.4). This S/I may then be used to calculate target detectability (see Chapter 6), and measurement accuracy (see Chapter 8).
- Present analysis results. The results should include a statement of the problem as interpreted by the analyst, the data used, any assumptions made, and the results of the calculations. Sometimes it is also useful to include descriptions of the methodology and tools used in the analysis. While only a single answer is sometimes required, it is usually helpful to tabulate related results and supporting data. Plots and graphs are also helpful for presenting parametric results.

Analysis of complex radar system problems is a skill that is developed through experience. Often it is necessary to revise the initial approach or adopt a new approach altogether. The above steps are intended only as a guide to this process.

The following five sections present five examples of evaluating radar performance using the models, equations, and data in this book. For each example, the problem, with its key parameters and principal assumptions, is first stated. Then the analysis approach is described, and the solution is developed using the methods

described in this book. Finally, an Excel spreadsheet analysis is described, which uses the VBA custom radar functions included with this book. The example-problem worksheets and the plots of the analysis results are also given in a file (Example Problems 2nd Ed.xls), which is included on the disk with the software functions provided with this book.

12.2 False-Alarm Probability Optimization

Problem Determine the probability of false alarm that will minimize the total radar power used by a phased-array radar for a given probability of detection, when each detection-threshold crossing is followed by up to two confirmation attempts. A lower P_{FA} (higher detection threshold), requires a higher S/N, increasing the search power needed, while a higher P_{FA} (lower threshold), results in attempted confirmation and track initiation of more false alarms, increasing the power used for these functions.

Consider a radar that searches a 250-km range interval 200 times per second. The range resolution is 150m, and the required P_D is 0.95. When the detection threshold is exceeded, a confirmation pulse is transmitted, using the same waveform and detection threshold. A range interval of 450m is examined to confirm the detection. If the presence of a target is not confirmed, a second confirmation pulse is transmitted. If the presence of a target is still not confirmed, the alarm is declared to be false. Different signal frequencies are used for the search and each of the two confirmation pulses, so that the detection probabilities for these are uncorrelated.

Approach The problem statement includes definition of the detection and confirmation modes, but no further data on the radar. Since the same waveform is used for search and confirmation, the total radar power used is proportional to the pulse rate required. The analysis is performed parametrically with false-alarm probability over a range from 10^{-10} to 10^{-1} , with the following steps:

- Calculate the pulse rate required to perform both search and confirmation.
- Find the S/N for the detection parameters and the value of false-alarm probability.
- Multiply these to find the total relative power required.

Solution The probability that a target will be acquired, P_A , is given by:

$$P_A = P_D \left(1 - (1 - P_D)^2 \right) \quad (12.1)$$

For the specified detection probability of 0.95, $P_A = 0.948$. Thus, the confirmation process does not cause many detections to be lost. Note that if the requirement were specified as $P_A = 0.95$, the required value of P_D would be 0.952.

The false-alarm rate for the search mode may be calculated from (6.7), using $B = c/(2\Delta R)$:

$$r_{FA} = 200 \times 250,000 \times P_{FA} / 150 = 333,333 P_{FA} \quad (12.2)$$

The probability of a false confirmation with a single confirmation pulse is given by $(450/150)P_{FA} = 3P_{FA}$. The rate of confirmed false targets is given by $2 \times 3P_{FA} \times 333,333P_{FA} = 2 \times 10^6 P_{FA}^2$. For most cases, the false confirmation rate is very low. For example, with $P_{FA} = 10^{-6}$, the false alarm rate is 0.33 per second, and the rate of false confirmations is 2×10^{-6} per second, or about one every 5.8 days.

In the absence of targets, the number of pulses transmitted per second for this search and confirmation mode is as follows:

Search 200

First confirmation $333,333P_{FA}$

Second confirmation $333,333P_{FA}$

Total $200 + 666,666P_{FA}$

The pulse energy, for fixed target RCS and range, is proportional the S/N required for detection. The total power usage is then proportional to $(200 + 666,666P_{FA})$ S/N. This may be evaluated as a function of P_{FA} for the given value of $P_D = 0.95$, as described in Section 6.3, using data such as Figure 6.3 and [1, pp. 349, 380, and 411].

Spreadsheet Analysis The worksheet showing the problem parameters and the calculations is given in Figure 12.1, and may also be found in file Example Problems 2nd Ed.xls.

The problem parameters are summarized in column B, rows 3 through 8 at the top of the spreadsheet. Parametric values for P_{FA} from 10^{-1} to 10^{-10} are shown in column A, rows 12 through 21. The false-alarm rate is calculated in column B using Function FRate_per_s (see Section 6.7.2). The bandwidth variable for this function is calculated from $c/2 \Delta R$ at the top of the sheet. The total number of pulses per second is calculated in column C, as discussed above.

The S/N required for the specified detection probability of 0.95 is calculated using Function SNR_SP_dB (see Section 6.7.4), with the number of pulses set to one, and the integration option irrelevant. The values of S/N (in decibels) for Swerling 1 and 2 targets are given in column D, for Swerling 3 and 4 targets in column F, and for Swerling 5 (nonfluctuating) targets in column H. Since a single pulse is used for detection, S/N is the same for Swerling 1 and 2, and for 3 and 4 targets.

The relative radar power required is the product of the pulse rate column in C and the calculated S/N, converted from decibels to a power ratio. These relative power values are given in decibels in column E for Swerling 1 and 2 targets, in column G for Swerling 3 and 4 targets, and in column I for Swerling 5 targets.

The analysis results are plotted in Figure 12.2, which shows the relative power in decibels needed for each of the target types as a function of the false-alarm rate. The minimum power usage is obtained with false-alarm probability of about 10^{-4} for the parameters of this problem. The penalty for using $P_{FA} = 10^{-8}$, rather than $P_{FA} = 10^{-4}$, ranges from 1.8 dB for Swerling 1 and 2 targets to 1.1 dB for Swerling 5 targets.

Note that additional power will be needed to confirm actual target detections, and perform other functions. Such power needs are independent of the probability of false alarm, and so do not affect the results given above.

In all the example problems, the parameters are displayed in the worksheet given in Example Problems 2nd Ed.xls, and these values are used in the equations

	A	B	C	D	E	F	G	H	I
1	False-Alarm Probability Optimization (Section 12.2)								
2									
3	Range Res, m	150							
4	Bandwidth, MHz	1							
5	PRF, Hz	200							
6	R Window, km	250							
7	Confirm Pulses	2							
8	Pd	0.95							
9									
10	Swerling	2				4		5	
11	Pfa	FA rate	PPS	S/N dB	PPSxS/N dB	S/N dB	PPSxS/N dB	S/N dB	PPSxS/N dB
12	1.E-01	33333.33	66866.66	16.44	64.69	12.03	60.28	8.14	56.40
13	1.E-02	3333.333	6866.667	19.50	57.86	14.66	53.03	10.15	48.52
14	1.E-03	333.3333	866.6667	21.28	50.66	16.27	45.65	11.40	40.77
15	1.E-04	33.33333	266.6667	22.53	46.79	17.43	41.69	12.32	36.58
16	1.E-05	3.333333	206.6667	23.51	46.66	18.35	41.51	13.05	36.20
17	1.E-06	0.333333	200.6667	24.30	47.33	19.12	42.14	13.67	36.69
18	1.E-07	0.033333	200.0667	24.98	47.99	19.76	42.77	14.19	37.21
19	1.E-08	0.003333	200.0067	25.56	48.57	20.32	43.33	14.66	37.67
20	1.E-09	0.000333	200.0007	26.07	49.08	20.81	43.83	15.07	38.08
21	1.E-10	3.33E-05	200.0001	26.53	49.54	21.25	44.26	15.45	38.46

Figure 12.1 Worksheet for False-Alarm Probability Optimization (from Example Problems 2nd Ed.xls, Sheet "Sec 12.2").

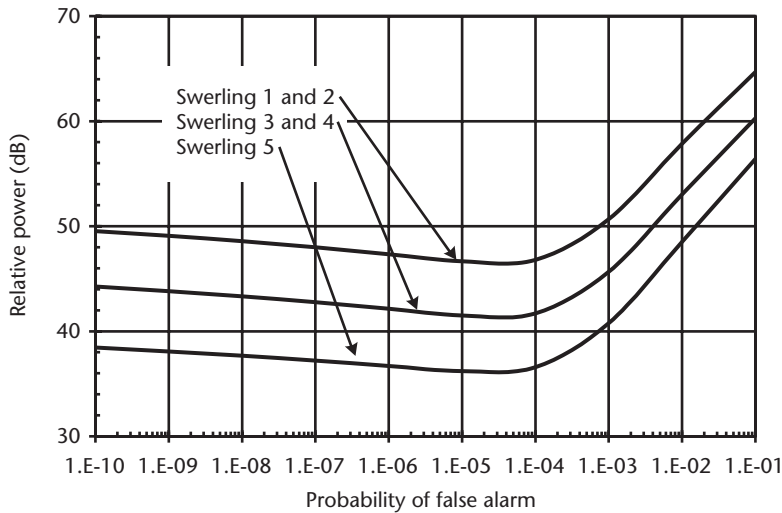


Figure 12.2 Relative power required as a function of false-alarm rate for the parameters of the example problem (from Example Problems 2nd Ed.xls, Sheet "Fig 12.2").

and functions, rather than entering the data directly. This makes the parameters visible to the analyst. It also allows the parameters to be easily changed, with the resulting change in the analysis results displayed in the worksheet and in the plots.

12.3 Cumulative Detection over Long Periods

Problem Determine the range at which a target approaching a rotating surveillance radar has a cumulative detection probability of 0.99. Consider a surveillance radar with a single-pulse reference range of 150 km for $S/N = 10$ dB on the target RCS. The target has Swerling 3 RCS fluctuations, which means that the RCS is constant over a scan, but fluctuates from scan-to-scan. The radar has a PRF of 400 Hz, a 1-degree azimuth beamwidth, and a rotation period of 10 seconds. The target enters the radar coverage at a range of 250 km, and approaches the radar at a constant radial velocity of 300 m/s.

Approach The rotating radar in this problem has a detection opportunity every 10 seconds. The cumulative probability of detection, which is the probability that the target is detected in the current look or one of the previous looks, is calculated. The steps in the analysis are:

- Calculate the radar range at each look from the target geometry data given.
- Calculate the S/N , using this range and the radar reference range data.
- Find the detection probability for each look.
- Calculate the cumulative detection probability from the detection probability for each look and that of the previous looks.

Solution The target travels 3 km during each antenna rotation period, so detection opportunities occur at ranges of 250 km, 247 km, 244 km, and so forth. The single-pulse S/N at the 250-km range, using (5.12), is found to be 1.13 dB. The number of pulses that illuminate the target during each observation dwell is found

from (7.4) as 11. For this analysis, assume that the antenna beam in which the target is observed does not illuminate the Earth's surface (so that multipath may be neglected), and that propagation losses may be neglected. A beamshape loss of 1.6 dB is used. The scanning loss is negligible for this case (see Section 7.2). The resulting average single-pulse $S/N = -0.47$ dB.

Assuming a P_{FA} of 10^{-6} , the detection probability, as described in Section 6.4, and using data such as [1, pp. 414–415], is found to be 0.079. The S/N and detection probability are found for the other target observation dwells, using this methodology. Since the RCS is independent from dwell to dwell (see Section 3.5), the cumulative detection probability, P_{CUM} , is given by:

$$P_{CUM} = 1 - \prod_N (1 - P_{DN}) \quad (12.3)$$

where P_{DN} is the detection probability of dwell N . The product includes the dwells up to the time for which P_{CUM} is evaluated.

Spreadsheet Analysis The worksheet showing the problem parameters and the calculations is given in Figure 12.3, and may also be found in file Example Problems 2nd Ed.xls.

The problem parameters are summarized in column B, rows 3 through 11 of the worksheet. The 1.6-dB scan loss is given in row 8, and the number of pulses illuminating the target in each look is given in row 9.

The times of the radar dwells, at 10-second intervals starting at zero, are shown in column A, starting with row 14. The target range for each dwell is calculated in column B, and the resulting single-pulse S/N is calculated in column C, using (5.12). The detection probability for each dwell is calculated in column D, using Function ProbDet_Factor (see Section 6.7.3). The cumulative probability of detection is calculated in column E, using (12.3).

The cumulative detection probability is plotted as a function of target range in Figure 12.4. The value of P_{CUM} reaches 0.99 at time 170 seconds, when the target range is 199 km.

Figure 12.3 shows that many dwells having detection probabilities of 0.3 or less contribute to the cumulative detection. In a realistic scenario, many of these detections would not lead to target confirmation and track initiation. A more conservative approach is to require detection and confirmation on a subsequent dwell. A simple such target confirmation algorithm requires detection on at least one of the two dwells following the initial detection. The resulting probability of confirmation, P_{CONF} , is given by:

$$P_{CONF} = 1 - (1 - P_{DN+1})(1 - P_{DN+2}) \quad (12.4)$$

where P_{DN+1} and P_{DN+2} are the detection probabilities for the two dwells following the initial detection.

This probability of confirmation is calculated in column F. The probability of detection plus confirmation is the product of P_{CUM} and P_{CONF} , and is calculated in column G. The cumulative probability of detection plus confirmation is calculated using (12.3) in column H, and is also plotted in Figure 12.4. As expected, it is lower

	A	B	C	D	E	F	G	H
1	Cumulative Detection Over Long Periods (Section 12.3)							
2								
3	Revisit, s	10						
4	Start R, km	250						
5	Rad V, km/s	-0.3						
6	Ref R, km	150						
7	Ref S/N,dB	10						
8	Loss, dB	1.6						
9	N pulses	11						
10	Swerling	3						
11	Pfa	1.E-06						
12								
13	<u>Time, s</u>	<u>Range, km</u>	<u>S/N, dB</u>	<u>Pdn</u>	<u>Pcum</u>	<u>Pconf</u>	<u>PdntxPconf</u>	<u>Cum Pdxconf</u>
14	0	250	-0.47	0.079	0.079	0.182	0.014	0.014
15	10	247	-0.26	0.090	0.162	0.205	0.018	0.033
16	20	244	-0.05	0.102	0.247	0.229	0.023	0.055
17	30	241	0.16	0.115	0.333	0.256	0.029	0.083
18	40	238	0.38	0.129	0.420	0.284	0.037	0.117
19	50	235	0.60	0.145	0.504	0.314	0.046	0.157
20	60	232	0.82	0.162	0.584	0.345	0.056	0.204
21	70	229	1.05	0.181	0.659	0.378	0.068	0.258
22	80	226	1.28	0.201	0.728	0.412	0.083	0.320
23	90	223	1.51	0.222	0.788	0.447	0.099	0.387
24	100	220	1.75	0.244	0.840	0.483	0.118	0.459
25	110	217	1.99	0.268	0.883	0.519	0.139	0.535
26	120	214	2.23	0.293	0.917	0.555	0.163	0.610
27	130	211	2.47	0.319	0.944	0.591	0.189	0.684
28	140	208	2.72	0.347	0.963	0.627	0.217	0.753
29	150	205	2.97	0.375	0.977	0.662	0.248	0.814
30	160	202	3.23	0.403	0.986	0.695	0.281	0.866
31	170	199	3.49	0.433	0.992	0.728	0.315	0.908
32	180	196	3.75	0.463	0.996	0.758	0.351	0.940
33	190	193	4.02	0.493	0.998	0.787	0.388	0.964
34	200	190	4.29	0.523	0.999	0.814	0.426	0.979
35	210	187	4.57	0.553	1.000	0.839	0.464	0.989
36	220	184	4.85	0.583	1.000	0.861	0.502	0.994
37	230	181	5.14	0.613	1.000	0.882	0.540	0.997
38	240	178	5.43	0.642	1.000	0.900	0.578	0.999
39	250	175	5.72	0.670	1.000	0.916	0.614	1.000
40	260	172	6.02	0.697	1.000	0.930	0.649	1.000
41	270	169	6.33	0.723	1.000	0.943	0.682	1.000
42	280	166	6.64	0.749	1.000	0.953	0.714	1.000
43	290	163	6.96	0.772	1.000	0.962	0.743	1.000
44	300	160	7.28	0.795	1.000	0.970	0.771	1.000
45	310	157	7.61	0.816	1.000	0.976	0.797	1.000
46	320	154	7.94	0.836	1.000	0.981	0.820	1.000
47	330	151	8.28	0.854	1.000	0.985	0.842	1.000
48	340	148	8.63	0.871	1.000	0.989	0.862	1.000
49	350	145	8.99	0.887	1.000	0.992	0.879	1.000
50	360	142	9.35	0.901	1.000	0.994	0.895	1.000
51	370	139	9.72	0.914	1.000	0.995	0.910	1.000
52	380	136	10.10	0.926	1.000	0.997	0.922	1.000
53	390	133	10.49	0.936	1.000	0.997	0.934	1.000
54	400	130	10.89	0.945	1.000	0.998	0.944	1.000
55	410	127	11.29	0.953	1.000	0.999	0.952	1.000
56	420	124	11.71	0.961	1.000	0.999	0.960	1.000
57	430	121	12.13	0.967	1.000	0.999	0.966	1.000
58	440	118	12.57	0.972	1.000	1.000	0.972	1.000
59	450	115	13.02	0.977	1.000	1.000	0.977	1.000
60	460	112	13.47	0.981	1.000	1.000	0.981	1.000
61	470	109	13.95	0.985	1.000	1.000	0.984	1.000
62	480	106	14.43	0.987	1.000	1.000	0.987	1.000
63	490	103	14.93	0.990	1.000			
64	500	100	15.44	0.992	1.000			

Figure 12.3 Worksheet for Cumulative Detection over Long Periods (from Example Problems 2nd Ed.xls, Sheet “Sec 12.3”).

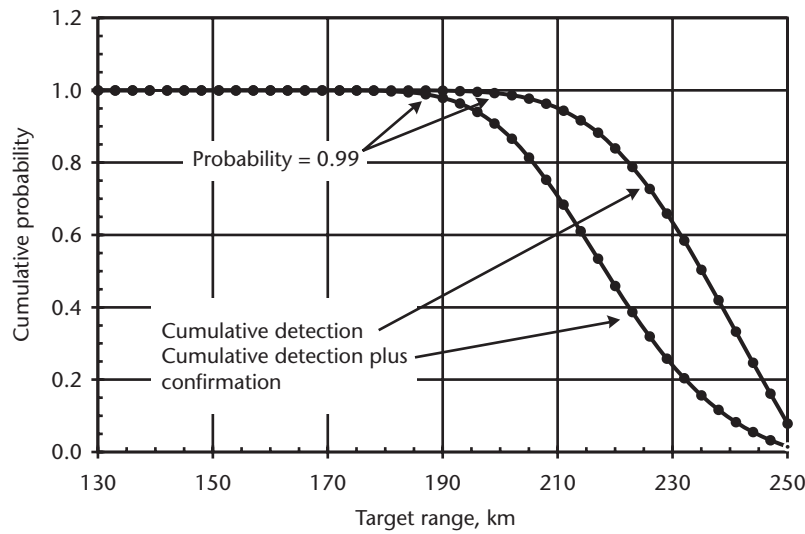


Figure 12.4 Cumulative probability of detection, and detection plus confirmation, as functions of range for the example problem (from Example Problems 2nd Ed.xls, Sheet “Fig 12.4”).

than P_{CUM} . It reaches a value of 0.99 at time 220 seconds, when the target range is 184 km.

The methodology in this example may be used for more complex scenarios. For example, the range may be calculated versus time for other target paths. The target viewing aspect may be calculated and the corresponding RCS value used to calculate the S/N.

12.4 Cued Search Using a Dish Radar

Problem Define a cued-search scan pattern for a dish radar, and determine the target acquisition range that may be obtained. The cued search area is circular with a radius of 15 km, and the search time is 25 seconds. The required probability of detection is 0.9. The detection threshold is to be adjusted so that one false alarm occurs in every 1,000 searches (on the average). The dish radar has a beamwidth of 1 degree, an angular scan velocity of $10^\circ/\text{s}$, and angular acceleration of $5^\circ/\text{s}^2$ in both azimuth and elevation angle. The radar PRF is 100 Hz, the range observation interval is 150 km, and the range resolution is 150m. The single-pulse reference range on the target of interest is 300 km for the radar waveform used, and a reference S/N = 3 dB. The target RCS fluctuations are Swerling 4.

Approach The two key issues in using a dish radar for search are:

- Covering the angular search volume in the required search time.
- The number of pulses that illuminate the target, which determines the detection probability.

The approach taken for this problem is to approximate a spiral angular scan by a series of nonoverlapping circular angular scans, called rings. Since the cued search radius is specified (15 km), the number of rings that may be searched determines the

minimum search range. At longer ranges, fewer rings need to be searched to cover the search area, and slower angular rates may be used, allowing more pulses on the target, and hence greater detection range.

The rings are scanned at a uniform rate, which is appropriate when the target positions are uniformly distributed over the search coverage. If cueing source is such that the target is more likely to be near the center of the search coverage, the search may be optimized by providing more energy (i.e., slower scan) near the center of the coverage.

The steps in the analysis are then:

- Find the minimum search range as a function of the number of search rings used.
- Determine the capability of the radar to mechanically scan the various numbers of rings.
- Find the number of pulses illuminating the target for each number of rings.
- Find the false-alarm probability needed to provide the required false-alarm performance for each case.
- Find the detection probability versus range.

Solution The search scan is modeled by a series of circular scans having angular radii at the beam center of, for example, 0.5, 1.5, and 2.5°. These cover an angular radius to 1, 2, and 3°, respectively. This is intended to approximate a spiral scan, as discussed in Section 7.4. A single ring, with an angular radius of 1°, will cover the 15-km search radius at ranges of 859 km and greater. Two rings, providing an angular radius of 2°, will cover the search radius at ranges of 430 km and greater. Additional rings are needed for shorter ranges.

The minimum time needed to mechanically scan a ring is limited by the radar angular scan velocity and the angular scan acceleration, as given by (7.33) and (7.34). For the single smallest ring, with these parameters, the angular acceleration is the limiting parameter. The minimum scan time for this ring is 1.99 seconds, and the maximum angular velocity is 1.58°/s. When only this ring is used (i.e., at ranges of 859 km or greater), the scan of the ring path length of 3.14° must be completed in the 25-second search time, and a much slower angular velocity of 0.126°/s is used. With the radar PRF of 100 Hz and the 1-degree beamwidth, 796 pulses illuminate the target during the scan.

At ranges less than 859 km where additional rings are needed, the additional ring path lengths must be included when calculating the angular scan velocity. In addition, the maximum scan velocities for the individual rings may not be exceeded. This may increase the scan velocity required for the other rings in some cases. It also results in a maximum number of rings that may be scanned during the 25-second scan time (five rings in this case). Thus, the cued search can not be completed for target ranges less than 172 km.

The single-pulse S/N is calculated by scaling from the reference range [see (5.12)]. A 3.2-dB beamshape loss is used, although this may be optimistic for high values of P_D , as will be discussed later. At 859-km range, $S/N = -18.5$ dB. The false-alarm rate is given by the required probability of a false alarm during the search (0.001), multiplied by the number of beams searched (3.14 for the single ring),

divided by the number of range resolution cells in the range observation interval (1,000). For a single ring, this equals 3.14×10^{-6} . The detection probability is found, assuming noncoherent integration of the number of pulses that illuminate the target, the S/N and P_{FA} , and the Swerling target type, as described in Section 6.4, and using data such as [1, pp. 428–436]. With the values given above for a single ring, the P_D is negligibly small.

Spreadsheet Analysis The worksheet showing the problem parameters and the calculations is given in Figure 12.5, and may also be found in file Example Problems 2nd Ed.xls.

The problem parameters are summarized in column B, rows 3 through 16, of the worksheet. A 3.2-dB beamshape loss is used (row 13), for the two-dimensional scanning (see Section 7.3 and later discussion).

The number of rings is varied parametrically in worksheet rows 19 through 24. Column A gives the number search rings. Column B gives the minimum range for which that number of rings may be used, and column C gives the angular radius of the ring. The minimum scan time for the ring as limited by angular velocity is given in column D, and the minimum scan time as limited by angular acceleration is given in column E (see Section 7.4). The minimum scan time for the ring is the larger of these, given in column F; in this example, always limited by angular acceleration.

The cumulative minimum scan times are given in column G. The cumulative minimum scan time for six rings (27.7 seconds), exceeds the specified search time, so five rings is the maximum that may be used for this scenario, as discussed above. The angular path length (in degrees) around each ring is given in column H, and the cumulative angular path length is given in column I.

The maximum angular velocity for each ring (the ring path divided by the ring time), is given in column J. The candidate average angular velocity, calculated by dividing the cumulative path by the 25-second search time, is given in column K. This average velocity may be used for the 1-, 2-, and 3-ring cases, since the values do not exceed any of the maximum scan velocities in column J.

With four rings, the candidate average velocity in column K is greater than the maximum velocity for ring 1. Then the maximum velocity from column J is used for ring 1. The scan velocity for the other rings is calculated in column L, by subtracting the path length for ring 1 from the cumulative path length, and subtracting the minimum ring time for ring 1 from the search time. The result is 2.05°/s. The average scan velocity for five rings exceeds the maximum for both ring 1 and ring 2. The scan velocity for the other rings is calculated in column M, using the method described above.

The resulting maximum scan velocities are shown in bold type, copied to column N, and used to calculate the number of pulses that illuminate the target for each number of rings from 1 to 5. These values are given in column O. (Since the calculation of maximum scan velocities is specific to the scenario addressed here, it is not possible to change these results by changing the input parameters in the Example Problems 2nd Ed.xls worksheet.)

The radar performance as a function of range is shown in rows 28 through 51. The range is given parametrically in column A, with range values added to show the change with the number of rings required. The number of rings and the number of

	A	B	C	D	E	F	G	H	I	J	K	L	M	N	O
1	Cued Search Using a Dish Radar (Section 12.4)														
2															
3	Srch Rad,km	15													
4	Search t, s	25													
5	False Det	0.001													
6	Beam, deg	1													
7	Beam, R	0.017453													
8	Vel, deg/s	10													
9	Acc deg/s ²	5													
10	PRF, Hz	100													
11	Ref R, km	300													
12	Ref S/N dB	3													
13	Loss, dB	3.2													
14	Swirling	4													
15	R res, m	150													
16	R int, km	150													
17															
18	<u># Rings</u>	<u>Rmin, km</u>	<u>Ring r, deg</u>	<u>t vel lim, s</u>	<u>t acc lim, s</u>	<u>Ring t, s</u>	<u>Cum t, s</u>	<u>Path, deg</u>	<u>Cum Path</u>	<u>Vmax, deg/s</u>	<u>Vel Avg</u>	<u>Vel 1 max</u>	<u>Vel 1&2 max</u>	<u>Vel,deg/s</u>	<u># Pulses</u>
19	1	859	0.5	0.314	1.987	1.987	1.987	3.142	3.142	1.581	0.126			0.126	796
20	2	430	1.5	0.942	3.441	3.441	5.428	9.425	12.566	2.739	0.503			0.503	199
21	3	286	2.5	1.571	4.443	4.443	9.871	15.708	28.274	3.536	1.131			1.131	88
22	4	215	3.5	2.199	5.257	5.257	15.128	21.991	50.265	4.183	2.011	2.048		2.048	49
23	5	172	4.5	2.827	5.961	5.961	21.089	28.274	78.540	4.743	3.142		3.371	3.371	30
24	6	143	5.5	3.456	6.590	6.590	27.679	34.558	113.097	5.244	4.524				
25															
26															
27	<u>Range, km</u>	<u># Rings</u>	<u># Pulses</u>	<u>S/N, dB</u>	<u>Pfa</u>	<u>Pd</u>									
28	900	1	796	-19.28	3.14E-06	0.0000									
29	880	1	796	-18.89	3.14E-06	0.0000									
30	859	1	796	-18.47	3.14E-06	0.0000									
31	858.9	2	199	-18.47	1.26E-05	0.0000									
32	800	2	199	-17.24	1.26E-05	0.0000									
33	700	2	199	-14.92	1.26E-05	0.0001									
34	600	2	199	-12.24	1.26E-05	0.0004									
35	500	2	199	-9.07	1.26E-05	0.0072									
36	450	2	199	-7.24	1.26E-05	0.0526									
37	430	2	199	-6.45	1.26E-05	0.1220									
38	429.9	3	88	-6.45	2.84E-05	0.0268									
39	400	3	88	-5.20	2.84E-05	0.0906									
40	350	3	88	-2.88	2.84E-05	0.5551									
41	323	3	88	-1.48	2.84E-05	0.9026									
42	300	3	88	-0.20	2.84E-05	0.9946									
43	286	3	88	0.63	2.84E-05	0.9990									
44	285.9	4	49	0.64	5.10E-05	0.9698									
45	277	4	49	1.19	5.10E-05	0.9911									
46	240	4	49	3.68	5.10E-05	0.9990									
47	215	4	49	5.59	5.10E-05	0.9990									
48	214.9	5	30	5.60	8.33E-05	0.9990									
49	200	5	30	6.84	8.33E-05	0.9990									
50	185	5	30	8.20	8.33E-05	0.9990									
51	172	5	30	9.46	8.33E-05	0.9990									

Figure 12.5 Worksheet for Cued Search Using a Dish Radar (from Example Problems 2nd Ed.xls, Sheet "Sec 12.4").

pulses on the target (from column O) are given in columns B and C, respectively. The single-pulse S/N is calculated by scaling from the reference range (see Section 5.3), and is given in column D. The false-alarm probability needed to provide the required number of false alarms (one per 1,000 searches) is calculated, and is given in column E. Finally, the detection probability for the single-pulse S/N, the number of pulses illuminating the target, and the false-alarm probability, assuming noncoherent integration, are calculated in column F, using Function ProbDet_Factor (see Section 6.7.3).

The results are plotted in Figure 12.6, which gives the number of rings and the probability of detection as functions of the search range. The number of rings steps with range, as described earlier. The P_D increases with decreasing range for a fixed number of rings, but decreases when the number of rings has to be increased.

The required detection probability of 0.9 is achieved when the target reaches a range of 323 km, using a search scan of three rings. When the range decreases to 286 km, a search scan of four rings is necessary, and the detection probability dips (and then recovers) as the range decreases. The dip is a result of the quantization of the number of rings used in the scan. In an actual spiral scan, such dips would not likely appear. As noted above, cued search can not be performed for ranges less than 172 km, with the parameters of this problem.

As mentioned above, using a beamshape loss of 3.2 dB may give optimistic results for high values of P_D . When many pulses are integrated on a Swerling 4 target, the detection statistics are close to those of a steady target, and the beamshape loss varies significantly with P_D . For example, with the beam spacing of one beamwidth used in this example, if a target at the beam center achieves a P_D of 0.99, there will be a 1.6-dB beamshape loss in the coordinate that is scanned rapidly, and a nearly 4-dB beamshape loss in the coordinate that is scanned slowly (successive rings). This is because targets at the edge of the beam will be reduced by 6 dB, causing a reduction in P_D that is much greater than any possible increase in P_D for targets at the beam center, which may only increase from 0.99 to near 1.0 [2]. When high P_D is required, most search scan patterns use beam spacing of about 0.7 beamwidths to reduce this effect.

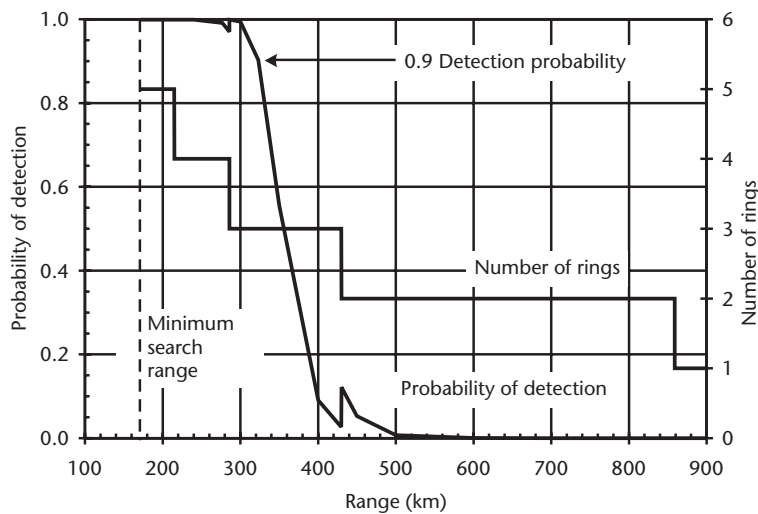


Figure 12.6 Probability of detection and number of search rings for the cued search example problem using a dish radar (from Example Problems 2nd Ed.xls, Sheet “Fig 12.6”).

This analysis approach may also be used with elliptical scan paths to cover an ellipsoidal target of uncertain volume. A raster scan could also be considered to cover a rectangular or irregular scan volume.

12.5 Composite Measurement Errors

Problem Determine the overall measurement errors in range, azimuth, elevation, and radial velocity, for a ground-based phased-array radar observing a target with an altitude of 10 km, at ranges between 200 and 100 km. The radar has the following parameters:

Peak power = 10 kW

Transmit gain = 39.5 dB

Receive effective aperture area = 6 m²

System noise temperature = 500K

System losses = 6 dB

Frequency = 3.3 GHz

Pulse duration 0.5 ms

Range resolution = 15m

Number of pulses noncoherently integrated = 10

Integration loss = 1.0 dB

Azimuth beamwidth = 2°

Elevation beamwidth = 2°

Array azimuth broadside angle = 0°

Array elevation broadside angle = 20°

Radar fixed random and bias errors are as follows:

Range fixed random error = 1m

Range bias error = 2m

Azimuth fixed random scan independent error = 800 μ rad

Azimuth fixed random scan dependent error = 500 μ sine

Azimuth bias scan independent error = 400 μ rad

Azimuth bias scan dependent error = 200 μ sine

Elevation fixed random scan independent error = 800 μ rad

Elevation fixed random scan dependent error = 500 μ sine

Elevation bias scan independent error = 400 μ rad

Elevation bias scan dependent error = 200 μ sine

Radial velocity fixed random error = 1 m/s

Radial velocity bias error = 0.7 m/s

The target parameters are:

Altitude = 10 km

Azimuth from radar = 30°

RCS = 0.1 m²

Approach The components of the radar measurement errors are listed in the first column of Table 12.1. The fixed error sources are specified in the problem. The S/N

Table 12.1 Measurement Error Components for the Example Problem and a Range of 200 km (1- σ Values)

<i>Error Component</i>	<i>Range Error (m)</i>	<i>Azimuth Error (mrad)</i>	<i>Elevation Error (mrad)</i>	<i>Radial- Velocity Error (m/s)</i>
S/N-dependent random	3.89	6.54	5.94	23.6
Fixed random	1.00	0.80	0.80	1.0
Fixed scan-dependent random	N/A	0.58	0.53	N/A
Radar fixed bias	2.00	0.40	0.40	0.7
Radar scan-dependent bias	N/A	0.23	0.21	N/A
Atmospheric refraction bias	1.71	N/A	0.16	N/A
Composite error	4.80	6.63	6.04	23.6

is needed to calculate the S/N-dependent random errors. This may be found using the radar parameters specified, but also requires the off-broadside scan loss and the atmospheric loss factors. The off-broadside scan angles are needed for this, and for determining the scan-dependent random and bias errors. The elevation angle is needed for determining the atmospheric loss, and for finding the atmospheric refraction bias error.

The analysis is performed parametrically with range, using the following steps:

- Find the off-broadside scan angles and target elevation angle from the problem geometry.
- Calculate the radar system losses and the S/N.
- Calculate the S/N-dependent random errors.
- Calculate the scan-dependent angular errors.
- Find the atmospheric bias errors, as corrected.
- Combine the measurement error components to find the composite errors.

Solution The radar elevation angle, ϕ_E , may be found using the law of cosines:

$$\sin \phi_E = -\frac{R^2 + r_E^2 - (r_E + h_T)^2}{2Rr_E} \quad (12.5)$$

At a range of 200 km, $\phi_E = 2.19^\circ$, using a 4/3 Earth radius (see Section 2.1). The two-way atmospheric attenuation at this elevation angle, from [3, pp. 252–258], is 1.64 dB. The lens loss from Table 9.6 or [4, p. 323] is 0.24 dB.

The off-broadside scan loss for the phased array for an azimuth scan of 30° and an elevation scan of 17.8° is found to be 2.09 dB, from (3.21) to (3.23). The total radar losses are then $6.0 + 1.64 + 0.24 + 2.09 = 9.97$ dB. The single-pulse S/N is found to be 1.88 dB, from (5.1). The S/N for radar measurement that results from noncoherent integration of 10 pulses with an integration loss of 1.0 dB is found to be 8.71 dB, from (5.17).

The S/N dependent random error is calculated from (8.6), (8.8), and (8.13), for range, angle, and radial-velocity errors, respectively. For the angle errors, the beamwidths at the off-broadside scan angles are found using (3.20). The azimuth beamwidth is 2.31° , and the elevation beamwidth is 2.10° . The radial-velocity resolution

(see Chapter 4) is 90.9 m/s. The resulting values of S/N-dependent random errors are given in the first row of Table 12.1.

The other error components are also listed in Table 12.1. The fixed components are input directly. The scan-dependent angular errors are found by dividing the error coefficient by the cosine of the scan angle (see Section 8.2). The range and elevation-atmosphere bias errors are taken from [5, pp. 368–369]. The values in the table assume that the errors can be corrected to within 5% of their values. The composite errors are found by taking the rss of the error components in each column. These are 1- σ values; 2- σ and 3- σ values may readily be found.

The radial-velocity measurement assumed here uses target Doppler-frequency shift during the 0.5-ms pulse duration. Depending on the pulse spacing, better accuracy might be provided by noncoherent processing of range measurements, as discussed in Section 8.3, and calculated by (8.15) or (8.16).

Spreadsheet Analysis The worksheet showing the problem parameters and the calculations is given in Figure 12.7, and may also be found in file Example Problems 2nd Ed.xls.

The key radar, target, and error parameters are listed at the top of the worksheet. The problem radar parameters are summarized in column B, rows 4 through 17; the target parameters are given in column E, rows 4 through 7; the range error parameters are given in column H, rows 4 through 6; the azimuth error parameters are given in column K, rows 4 through 7; the elevation error parameters are given in column N, rows 4 through 8; and the radial-velocity error parameters are given in column Q, rows 4 and 5. The azimuth off-broadside scan angle is calculated in column K, row 9, and the signal wavelength and radial-velocity resolution are calculated in column Q, rows 7 and 8.

Radar range is given parametrically from 200 to 100 km in column A, rows 20 through 25. The radar elevation angle is calculated in column B, using (12.5), and the elevation off-broadside scan angle is calculated in column C. The off-broadside scan losses for azimuth and elevation scan are calculated in columns D and E, respectively. The atmospheric loss, including lens loss, is calculated in column F, using Function TropoAtten_dB (see Section 9.6.5). These losses, plus the radar system losses, are totaled in column G.

The single-pulse S/N is calculated with Function SNR_dB (see Section 5.7.1), in column H, using the radar and target parameters with the total losses in column G. The integrated S/N, for 10 pulsed noncoherently integrated for radar measurement with 1.0 dB integration loss is calculated in column I, using function Integrated_SNR_dB (see Section 5.7.3). The atmospheric range error is calculated in column J, using Function TropoR_Err_m (see Section 9.6.7), assuming the error is corrected to 5% of its magnitude. This error is combined in with the radar range bias error in column K, using an rss calculation. The composite range error is calculated in column L, using Function RangeError_m (see Section 8.9.1), with the input parameters on the worksheet.

The composite azimuth error is directly calculated in column M, using Function AngleError_mR (see Section 8.9.2), with the input parameters on the worksheet. The elevation-angle error from atmospheric refraction is calculated in column N, using Function TropoEl_Err_mR (see Section 9.6.6), assuming the error is corrected

	A	B	C	D	E	F	G	H	I	J	K	L	M	N	O	P	Q		
1	Composite Measurement Errors (Section 12.5)																		
2																			
3	Radar Parameters			Target Parameters			Range Error Parameters			Az Error Parameters			El Error Parameters			Rad Vel Error Parameters			
4	Pp, kW	10		4/3Earth,km	8485		Fixed, m	1.0		Fixed, mrad	0.8		Fixed, mrad	0.8		Fixed, m/s	1.0		
5	Gt, dB	39.5		Tgt H, km	10		Bias,m	2.0		Fix Scan,ms	0.5		Fix Scan,ms	0.5		Bias, m/s	0.7		
6	Ar, m2	6		RCS, dBsm	-10		Correct,%	5		Bias, mrad	0.4		Bias, mrad	0.4					
7	Ts, K	500		Tgt Az, deg	30					Bias Scan,ms	0.2		Bias Scan,ms	0.2		lambda,m	0.0909		
8	L, dB	6											Correct,%	5		Resol, m/s	90.91		
9	F, GHz	3.3								AzScan, deg	30								
10	tau, ms	0.5																	
11	R Res, m	15																	
12	Npulses	10																	
13	Int L, dB	1																	
14	Az beam deg	2																	
15	El beam deg	2																	
16	Az, deg	0																	
17	El deg	20																	
18																			
19	Range, km	El, deg	ElScan,deg	Az scan	Radar Losses, dB			S/N, dB			Range Errors, m			Az Er, mrad		Elevation Errors, mrad		R Vel Er, m/s	
					El scan	Atmos	Total		Single p	Integ	Atmos		Tot Bias	Composite	Composite	Atmos	Tot Bias	Composite	Composite
20	200	2.19	17.81	1.56	0.53	1.88	9.97	1.88	8.71			1.71	2.63	4.80	6.62	0.16	0.43	6.04	23.61
21	180	2.58	17.42	1.56	0.51	1.66	9.73	3.95	11.49			1.53	2.52	3.91	4.87	0.14	0.42	4.44	17.18
22	160	3.04	16.96	1.56	0.48	1.41	9.46	6.28	14.36			1.33	2.40	3.30	3.58	0.12	0.42	3.27	12.37
23	140	3.62	16.38	1.56	0.45	1.19	9.20	8.86	17.32			1.12	2.29	2.89	2.66	0.10	0.41	2.43	8.83
24	120	4.38	15.62	1.56	0.41	0.99	8.96	11.77	20.49			0.97	2.22	2.63	2.01	0.09	0.41	1.85	6.20
25	100	5.40	14.60	1.56	0.36	0.83	8.75	15.15	24.02			0.82	2.16	2.47	1.56	0.07	0.41	1.46	4.23

Figure 12.7 Worksheet for Composite Measurement Errors (from Example Problems 2nd Ed.xls, Sheet "Sec 12.5").

to 5% of its magnitude. This error is combined with the radar bias error in column O, using an rss calculation. The composite elevation-angle error is calculated in column P, using Function AngleError_mR (see Section 8.9.2), with the input parameters on the worksheet. The radial velocity error is calculated in column Q, using Function DopVelError_mps (see Section 8.9.3), and the parameters on the worksheet.

The four composite measurement errors are plotted as functions of range in Figure 12.8. The errors decrease with decreasing range due to the R^{-4} term in the range equation (Section 5.1), and due to the reduction in propagation losses as the elevation angle increases. The range and elevation-angle errors are also reduced, due to reduced atmospheric refraction errors at the higher elevation angles. The reduction of all the errors is limited by the fixed error components.

Attenuation from rainfall could be added to this calculation, using either data from Table 9.2, or the methodology in [6]. In the spreadsheet analysis, these may be implemented using function RainLocAtten_dBpkm or RainPathAtten_dB, respectively (see Sections 9.6.2 and 9.6.3).

12.6 Detection in Jamming, Chaff, and Noise

Problem Determine the detection probability versus target range for a target in a chaff cloud and screened by a SOJ. The required false-alarm probability is 10^{-6} .

The radar parameters are as follows:

Peak power = 10 kW

Transmit gain = 50 dB

Receive aperture area = 8 m²

System noise temperature = 450K

System losses = 4 dB (transmit loss = 2 dB, receive loss = 2 dB)

Frequency = 9.5 GHz

Pulse durations = 2, 1, and 0.5 ms

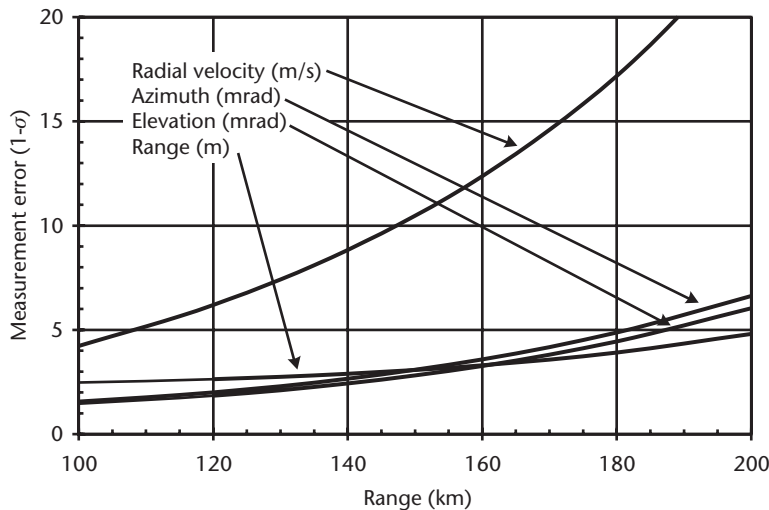


Figure 12.8 Radar measurement errors as functions of range for the parameters in the example problem (from Example Problems 2nd Ed.xls, Sheet "Fig 12.8").

Range resolution = 15 m

Azimuth beamwidth = 1°

Elevation beamwidth = 1°

Sidelobe level = -55 dB

Sidelobe cancellation = 20 dB

Chaff cancellation ratio = 30 dB

The target has an RCS of 0.1 m^2 with Swerling 4 fluctuations. Target range varies from 500 to 100 km. The SOJ has a range of 600 km and an effective radiated power per polarization of 10^8 W . It is a barrage noise jammer that jams the full radar band of 1 GHz. The chaff consists of half-wave dipoles, having a total weight of 1 kg. It is assumed to be uniformly distributed over a sphere with a 3-km radius. The chaff is assumed to have slowed to the atmospheric velocity, much slower than the target velocity, so that the Doppler-velocity resolution provided by the waveform (e.g., a phase-coded pulse) provides the chaff rejection indicated by the chaff CR.

Note that the chaff cloud is unlikely to remain with the target, and to retain the same size and density, as the target travels from 500 to 100 km. This problem, somewhat artificially, assumes that the chaff cloud envelopes the target and has reached the specified size at the time the target is observed at each range.

Approach The jamming, chaff, and noise are assumed to have Gaussian statistics, so their effects may be combined, as shown in (10.27), and the detection probability may then be found, using the value of $S/(J + C + N)$. The problem calls for a parametric analysis with range between 500 and 100 km, assuming the approximate target range is known from cueing. To avoid the minimum-range constraint, the 2-ms pulse is then used only at ranges greater than 300 km, the 1-ms pulse at ranges of 150 to 300 km, and the 0.5-ms pulse at ranges less than 150 km [see (5.26)]. The analysis steps are:

- Calculate the S/N .
- Calculate the S/J .
- Calculate the S/C .
- Combine these to find the $S/(J + C + N)$.
- Find the detection probability.

Solution The S/N is calculated from (5.1). At a range of 500 km, $S/N = 10.2 \text{ dB}$. The 2-ms pulse duration is used, since the range exceeds the minimum range for this pulse. When the range is less than 300 km, the 1-ms pulse is used, and when the range is less than 150 km, the 0.5-ms pulse is used.

The S/J is calculated using (10.11). At 600-km range, $S/J = 12.6 \text{ dB}$, using the 2-ms pulse duration. The pulse duration used for calculating S/J is changed with range, as discussed above. Since the jammer ERP per polarization is specified, no polarization loss is used.

The total RCS of the chaff cloud is calculated using (10.21) as 695 m^2 . The volume of the chaff cloud is 113 km^3 . At a range of 500 km, the entire chaff cloud is in the radar beam. The volume of the chaff in the radar resolution cell is calculated using (10.22), with D_A and D_E each equal to 6 km. The result, with no beamshape

loss, is 0.54 km^3 . The resulting S/C is calculated with (10.25), using a beamshape loss of $\pi/4$, as 15.9 dB. When the range is less than 343 km, the chaff cloud is larger than the radar beam, and $D_A = R\theta_A$ and $D_E = R\theta_E$ are used in (10.22). A beamshape loss of 3.2 dB should be used when the beam is much larger than the chaff cloud. This change in the beamshape loss should be phased in gradually between ranges of about 450 to 250 km.

The combined $S/(J + C + N)$ is calculated using (10.27). The values in dB for the individual signal ratios are first converted to power ratios for use in the equation, and the result is converted back to decibels. For a range of 500 km, the above values are used, giving 7.5 dB. The resulting detection probability may be found, using the methods described in Section 6.3, and data such as from [1, p. 411], as 0.25.

Spreadsheet Analysis The worksheet showing the problem parameters and the calculations is given in Figure 12.9, and may also be found on tab “Sec 12.6” in file Example Problems 2nd Ed.xls.

	A	B	C	D	E	F	G	H	I	J	K
1	Detection in Jamming, Chaff and Noise (Section 12.6)										
2											
3	<u>Radar Parameters</u>			<u>Target Parameters</u>		<u>Jammer Parameters</u>			<u>Chaff Parameters</u>		
4	Pp, kW	10		RCS, dBsm	-10	Rj, km	600		Weight, kg		1
5	Gt, dB	50		Swirling	4	Bj, GHz	1		Radius, km		3
6	Ar, m2	8				ERP/pol, dBW	80				
7	Ts, K	450		Pfa	1.00E-04				lambda		0.0316
8	Lt, dB	2							RCStot, m2		695
9	Lr, dB	2							RCStot, dBsm		28.4
10	F, GHz	9.5							Vol, km3		113
11	tau1, ms	2									
12	tau2, ms	1									
13	tau3, ms	0.5									
14	R Res, m	15									
15	Az beam deg	1	17.5								
16	El beam deg	1	17.5								
17	SL, dB	-55									
18	SLC, dB	20									
19	CR, dB	30									
20											
21											
22	<u>Range, km</u>	<u>S/I+N dB</u>	<u>lbs dB</u>	<u>S/C dB</u>	<u>S/I+C+N dB</u>	<u>Pd</u>	<u>S/N dB</u>	<u>S/I dB</u>			
23	500	8.21	1.05	15.84	7.52	0.2501	10.17	12.62			
24	480	8.92	1.05	15.84	8.12	0.3033	10.88	13.33			
25	460	9.66	1.05	15.84	8.72	0.3614	11.62	14.07			
26	440	10.43	1.05	15.84	9.34	0.4229	12.39	14.84			
27	420	11.24	1.30	16.09	10.01	0.4923	13.20	15.65			
28	400	12.09	1.50	16.29	10.69	0.5608	14.04	16.50			
29	380	12.98	1.90	16.69	11.44	0.6329	14.93	17.39			
30	360	13.92	2.10	16.89	12.15	0.6951	15.87	18.33			
31	344	14.71	2.20	16.99	12.69	0.7388	16.66	19.12			
32	343	14.76	2.30	17.11	12.77	0.7446	16.71	19.17			
33	340	14.91	2.50	17.39	12.97	0.7591	16.87	19.32			
34	320	15.97	2.60	18.01	13.86	0.8178	17.92	20.38			
35	301	17.03	2.90	18.85	14.83	0.8685	18.98	21.44			
36	300	14.08	3.10	19.08	12.88	0.7531	16.03	18.49			
37	280	15.28	3.15	19.72	13.94	0.8226	17.23	19.68			
38	260	16.56	3.20	20.42	15.07	0.8788	18.52	20.97			
39	240	17.95	3.20	21.11	16.24	0.9210	19.91	22.36			
40	220	19.46	3.20	21.87	17.49	0.9511	21.42	23.87			
41	200	21.12	3.20	22.70	18.83	0.9714	23.07	25.53			
42	180	22.95	3.20	23.61	20.26	0.9842	24.90	27.36			
43	160	25.00	3.20	24.64	21.80	0.9918	26.95	29.41			
44	151	26.00	3.20	25.14	22.54	0.9940	27.96	30.41			
45	150	23.11	3.20	25.20	21.02	0.9885	25.06	27.52			
46	140	24.31	3.20	25.80	21.98	0.9924	26.26	28.72			
47	120	26.98	3.20	27.13	24.05	0.9968	28.94	31.39			
48	100	30.15	3.20	28.72	26.37	0.9987	32.11	34.56			

Figure 12.9 Worksheet for Detection in Jamming, Chaff and Noise (from Example Problems 2nd Ed.xls, Sheet “Sec 12.6”).

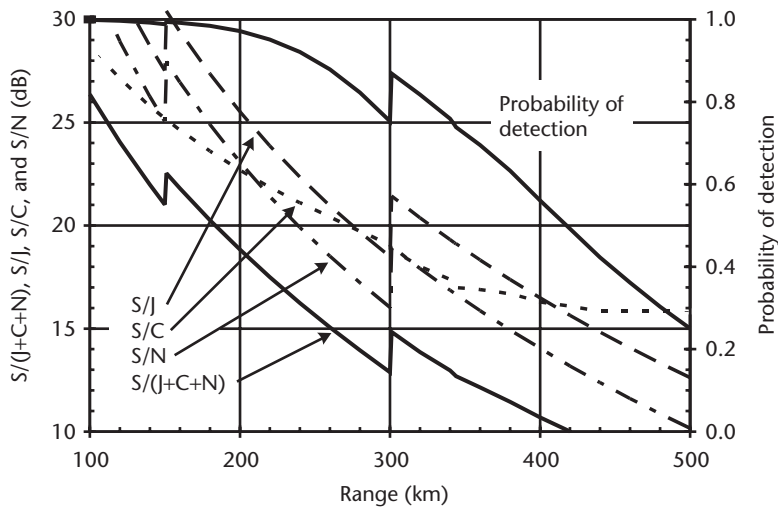


Figure 12.10 Detection probability, $S/(J + C + N)$, and its constituents, as functions of range for the example problem (from Example Problems 2nd Ed.xls, Sheet “Fig 12.10”).

The key radar, target, jammer, and chaff parameters are given at the top of the worksheet. Parametric radar ranges from 500 to 100 km are given in column A, rows 23 through 48. The $S/(J + N)$ is calculated in column B, using Function `SL_SJNR_dB` (see Section 10.7.4).

The total chaff RCS and total chaff volume are calculated below the chaff parameters. The S/C is calculated in column D, using Function `SCR_Chaff_dB` (see Section 10.7.6). The values for beamshape loss are input in column C. A loss of $/4 = 1.05$ dB is used at the longer ranges, when the chaff cloud is well within the beam; a 3.2-dB loss is used for the shorter ranges, when the beam is significantly larger than the chaff cloud; and intermediate values are input for the beamshape loss in the crossover region.

The combined $S/(J + C + N)$ is calculated in column E, as described earlier. The resulting probability of detection is calculated in column F, using Function `Prob-Det_Factor` (see Section 6.7.3). The combined $S/(J + C + N)$ and P_D are plotted as functions of range in Figure 12.10. The detection probability is 0.95 at a range of about 220 km, and 0.99 at a range of about 160 km.

Columns G and H are used to calculate S/N , using Function `SNR_dB` (see Section 5.7.1), and S/J , using Function `SL_SJNR_dB` with T_s is set to zero. These, along with the S/C from column D, are also plotted in Figure 12.10. The dips in S/N and S/J when minimum range requires shorter pulse durations at ranges of 300 and 150 km are evident. The S/C is constant for ranges greater than about 450 km. At ranges shorter than about 350 km, it increases inversely with R^2 . Between these ranges is the region where the beam becomes smaller than the chaff cloud and the beamshape loss phases in. The $S/(J + C + N)$ and detection probability reflect these features.

This methodology could also be used with rain clutter instead of chaff, and with MLJs. Ground and sea clutter usually has nonGaussian statistics, so it may not strictly be combined with noise and noise jammer signals for detection calculations. Nevertheless, it is sometimes instructive to find the combined $S/(J + C + N)$ in such cases to understand the interactions of the various interference sources.

12.7 Problems

The following problems are provided to assist in reviewing this chapter and to ensure a basic understanding of the material. For maximum benefit, the problems should first be solved without using the VBA custom radar functions. Solutions to these problems are given in Appendix E, Section E.12.

1. How would the approach to the example problem in Section 12.2, False-Alarm Probability Optimization, change if the confirmation pulses were required to produce a detection probability of 0.99 at a fixed false-alarm probability of 10^{-4} ? Calculate the resulting value of relative power for a search P_{FA} of 10^{-6} and a Swerling 3 or 4 target.
2. How would the approach to the example problem in Section 12.4, Cued Search Using a Dish Radar, change if the cued search volume was defined by a conical angular sector having a half-angle of 3° ? Is there a minimum search range in this case? If the false-alarm probability is specified at 10^{-6} , what is the range for a detection probability of 0.9?
3. A radar having the parameters given in Table 12.2 tracks an exoatmospheric target at a 10-Hz rate. The target range is 3,000 km, the elevation angle is 10° , and the RCS is 10 m^2 . The radar is being jammed by a sidelobe barrage noise jammer with a range of 4,000 km from the radar, an elevation angle of 5° from the radar, an ERP per polarization of 10,000W, and a bandwidth of 50 MHz. After 20 seconds of tracking, the target position is predicted at 200 seconds after the tracking is completed. Find the $3\text{-}\sigma$ value of the largest error semi-axis of the predicted position.
4. How would the approach to the example problem in Section 12.3, Cumulative Detection Over Long Periods, change if confirmation required target detection on both of the two dwells following the initial detection? Calculate the probability of confirmation for a detection that occurs at time 300 seconds in the problem. What is the probability of detection and confirmation at this time?

Table 12.2 Radar Parameters for Problem 3

<i>Parameter</i>	<i>Value</i>
P_p	200 kW
τ	10 ms
B	5 MHz
PRF	10 Hz
G_T	37 dB
A_R	200 m^2
T_S	450K
L_F	4.5 dB
θ	3.0°
f	425 MHz
SL	-42 dB
σ_{RF}	3.0m
σ_{RB}	20m
σ_{AF}	0.1°
σ_{AB}	0.05°

Table 12.3 Radar Parameters for Problem 6

<i>Parameter</i>	<i>Value</i>
P_p	250 kW
P_A	50 kW
A_R	10 m ²
f	9.5 GHz
θ_A, θ_E	0.64°
T_S	500K
L_F	3.0 dB
El BS Angle	15°

5. How would the approach to the example problem in Section 12.5, Composite Measurement Errors, change if the target is at an altitude of 1,000 km, the elevation angle is 5°, the radar frequency is 425 MHz (UHF), the gain is 40 dB, the receive antenna aperture area is 400 m², the pulse duration is 10 ms, and the target RCS is 10 m²? Solve for the composite measurement errors, assuming normal daytime ionospheric conditions.
6. Consider a FFOV phased-array radar with the parameters given in Table 12.3. The radar is to perform two functions simultaneously:
 - Search the horizon at a 5-degree elevation angle, $\pm 30^\circ$ in azimuth from the array broadside, and detect targets at range 2,000 km with $P_D = 0.99$ and $P_{FA} = 10^{-6}$.
 - Track targets at a 1-Hz rate with $S/N = 15$ dB. The targets may be assumed to be uniformly distributed in range between 1,000 and 2,000 km, in elevation angle between 5 and 30°, and in azimuth between $\pm 30^\circ$ of the array broadside.

The targets have $RCS = 1$ m² with Swerling 4 statistics, and vertical velocity components of 1 km/s. Find the number of targets that may be tracked simultaneously, while maintaining the specified search.

References

- [1] DiFranco, J. V., and W. L. Rubin, *Radar Detection*, Englewood Cliffs, NJ: Prentice Hall, 1968.
- [2] Barton, D. K., and W. M. Hall, "Antenna Pattern Loss Factor for Scanning Radar," *Proc IEEE*, Vol. 53, No. 9, September 1965, pp. 1257–1258.
- [3] Blake, L. V., "Prediction of Radar Range," Chapter 2 in *Radar Handbook*, M. I. Skolnik, (ed.), New York: McGraw-Hill, 1970.
- [4] Morchin, W., *Radar Engineer's Sourcebook*, Norwood, MA: Artech House, 1993.
- [5] Barton, D. K., and H. R. Ward, *Handbook of Radar Measurements*, Dedham, MA: Artech House, 1984.
- [6] Crane, R. K., "Prediction of Attenuation by Rain," *IEEE Trans. on Communications*, Vol. COM-28, No. 9, September 1980, pp. 1717–1733.

Selected Bibliography

Techniques and data for radar systems analysis are given by Barton and by Barton, Hamilton, and Cook. Some sources of data useful for radar analysis are:

- Antenna parameters: Appendix A of Barton and Ward.
- Sky noise: Skolnik, pages 366–368 (1962), and pages 461–464 (1980).
- Detection probability: Chapters 10 and 11 of DiFranco and Rubin.
- Tropospheric loss: Blake (1970), and updated using new data (1986, 1990).
- Lens loss: Chapter 15 of Morchin.
- Tropospheric measurement errors: Appendix D of Barton and Ward.

Software models for solving radar system problems are given by Barton and Barton, and by Leonov and Leonov.

Barton, D. K., *Radar System Analysis*, Englewood Cliffs, NJ: Prentice Hall, 1964.

Barton, D. K., *Modern Radar System Analysis*, Norwood, MA: Artech House, 1988.

Barton, D. K., and W. F. Barton, *Modern Radar System Analysis: Software and User's Manual: Version 2.0*, Norwood, MA: Artech House, 1993.

Barton, D. K., P. Hamilton, and C. E. Cook, (eds.), *Radar Evaluation Handbook*, Norwood, MA: Artech House, 1991.

Barton, D. K. and H. R. Ward, *Handbook of Radar Measurement*, Norwood, MA: Artech House, 1984.

Blake, L. V., "Prediction of Radar Range," Chapter 2 in *Radar Handbook*, M. I. Skolnik, (ed.), New York: McGraw-Hill, 1970.

Blake, L. V., "Prediction of Radar Range," Chapter 2 in *Radar Handbook*, 2nd ed., M. I. Skolnik (ed.), New York: McGraw-Hill, 1990.

Blake, L. V., *Radar Range-Performance Analysis*, Norwood, MA: Artech House, 1986.

DiFranco, J. V., and W. L. Rubin, *Radar Detection*, Englewood Cliffs, NJ: Prentice Hall, 1969.

Leonov, S. A., and A. I. Leonov, *Radar System Simulation Software*, Norwood, MA: Artech House, 2001.

Morchin, W., *Radar Engineer's Sourcebook*, Norwood, MA: Artech House, 1993.

Skolnik, M. I., *Introduction to Radar Systems*, New York: McGraw-Hill, 1962.

Skolnik, M. I., *Introduction to Radar Systems*, 2nd ed., New York: McGraw-Hill, 1980.

Appendix A

List of Symbols

A	Effective antenna aperture area
A_A	Antenna area
A_E	Effective aperture area of a phased-array element in the array; area of corner reflector projected in the direction of radar
A_R	Receive antenna effective aperture area
A_S	Surface area contributing to clutter
A_T	Transmit antenna effective aperture area
$A\varphi$	Array effective aperture area at scan angle
a	Target dimension; clutter scattering-effectiveness parameter; parameter in burnthrough equation
$a(x)$	Antenna current density as a function of distance from the antenna center
a_A	Azimuth acceleration of scanning beam
a_{AM}	Maximum antenna acceleration in azimuth direction
a_{EM}	Maximum antenna acceleration in elevation direction
a_R	Target radial acceleration; rain attenuation in decibels per kilometer
a_T	Maximum target acceleration; tropospheric attenuation in decibels per kilometer
B	Signal bandwidth
B_A	Phased-array bandwidth
B_i	Receiver bandwidth for search train i
B_J	Bandwidth of noise jammer
B_N	Noise bandwidth
B_R	Receiver bandwidth
B_S	Subpulse bandwidth
b	Parameter in burnthrough equation
C	Power at the radar receiver output due to clutter of chaff return signals
CR	Clutter cancellation ration; chaft cancellation ratio (both normally greater than unity)
c	Electromagnetic propagation velocity in a vacuum (3×10^8 m/s)
D	Target cross-range separation; spacing of DPCA antenna phase centers
D_A	Dimension of chaff in resolution cell in the azimuth direction

DC	Transmitter duty cycle
D_E	Dimension of chaff in resolution cell in the elevation direction
d	Element spacing in the array
d_R	Path length in rain
d_T	Path length in the troposphere
E_M	Maximum transmitter pulse energy
ERP	Jammer effective radiated power
E_W	Waveform energy
e	Base of natural logarithms
F	Fraction of active elements in a thinned phased array
F_R	Receiver noise figure
f	Radar frequency
f_B	Beam broadening factor in phased-array search
f_C	Doppler frequency shift of clutter return
f_D	Doppler frequency shift
f_M	Doppler frequency relative to frequency to which receiver filter is matched
f_P	Beam-packing factor
f_R	Frequency resolution
G	Antenna main-beam gain
G_E	Gain of phased-array element in the array
G_H	Maximum gain of antenna having cosecant-squared pattern
G_J	Gain of jammer antenna in the direction of the radar
G_R	Receive antenna gain
G_T	Transmit antenna gain
G_φ	Array gain at scan angle φ
h_R	Height of radar above the smooth Earth
h_T	Height of target above the smooth Earth
I_n	Modified Bessel function of the order n
J	Jammer power at the radar receiver output
J/N	Jammer-to-noise ratio
K	Signal fluctuation parameter in Chi-square distributions; quality factor for discrimination
k	Boltzmann's constant (1.38×10^{-23} J/K)
k_A	Antenna beamwidth coefficient
k_M	Monopulse pattern difference slope
L	Radar system losses
L_A	Antenna ohmic losses
L_{AR}	Receive antenna ohmic losses
L_{AT}	Transmit antenna ohmic losses
L_{BS}	Antenna pattern beamshape loss
L_D	Detection or demodulation loss

L_E	Antenna losses due to aperture efficiency
L_{ER}	Receive antenna losses due to aperture efficiency
L_{ET}	Transmit antenna losses due to aperture efficiency
L_F	Fixed radar losses (excluding L_S , L_{BS} , and L_P)
L_J	Losses in jammer
L_{MR}	Receive microwave losses
L_{MT}	Transmit microwave losses
L_P	Two-way propagation loss
L_{POL}	Jammer polarization loss
L_{PR}	Two-way loss from rain attenuation
L_{PT}	Two-way loss from tropospheric propagation
L_R	Receive losses
L_{RS}	Scanning loss for rotating search radar
L_S	Two-way off-broadside scan loss for phased array
L_{SA}	Average scan loss in phased-array search
L_{SP}	Radar signal-processing losses
L_{SPI}	Signal processing loss from pulse integration
L_{Sx}	Scan loss for off-broadside scan in the x plane
L_{Sy}	Scan loss for off-broadside scan in the y plane
L_T	Transmit losses
L_X	Target polarization loss for same-sense circular polarization
\ln	Natural logarithm
M	Pulses in pulse train for STAP processing
m	Number of threshold crossings required for detection in m -out-of- n detection
N	Noise power at the receiver output; atmospheric refractivity; index of search dwells; elements in linear array for STAP processing
N_S	Atmospheric refractivity at the Earth's surface
n	Number of pulses integrated or processed; number of coherent dwell, sub-pulse number; atmospheric refractive index
n'	False-alarm number ($n' = 0.693/P_{FA}$)
n_B	Number of beams in phased-array search
n_C	Number of chaff dipoles in resolution volume
n_E	number of radiating elements in a phased-array antenna face
n_M	Number of identical phased array modules
n_P	Number of pulses illuminating target for a rotating search radar, pulses per beam position
n_S	Number of subpulses
n_T	Number of dipoles in chaff cloud
P	Instantaneous transmitted power
P_A	Transmitter average RF power; probability of discrimination false acceptance; probability of target acquisition

PC	Pulse-compression ratio
P_{CONF}	Probability of target confirmation
P_{CUM}	Cumulative detection probability for rotating search radar
P_D	Probability of detection
P_{DN}	Probability of detection for dwell N
P_{DO}	Probability of detection for single observation in cumulative detection
P_{FA}	Probability of false alarm
P_{FAi}	False-alarm probability for search train i
P_{FAO}	False-alarm probability for single observation in cumulative detection
P_J	Jammer power
P_L	Probability of discrimination leakage
P_M	Phased-array module transmitted power
P_N	Power of background noise in the radar receiver
P_P	Transmitter peak RF power
P_{PR}	Prime power supplied to the radar
P_{PT}	Prime power supplied to the transmitter
PRF	Pulse repetition frequency
PRF_i	Pulse repetition frequency for search train i
PRI	Pulse repetition interval
p	Probability density function
R	Range from radar to target
R_A	Radar assured acquisition range in search
R_D	Radar detection range in search
R_F	Far-field range
R_H	Target range in horizon search
R_J	Range from jammer to radar
R_M	Minimum monostatic radar range as limited by pulse duration
R_O	Range offset in range-Doppler coupling
R_p	Radar average acquisition range in search
R_R	Range from radar to Earth tangent point
R_{ref}	Radar reference range
R_T	Range from target to Earth tangent point
R_W	Receive range window length
R_{Wi}	Receive range window length for search train i
R_1	Range at measurement time 1; range of scatterer 1
R_2	Range at measurement time 2; range of scatterer 2
\mathcal{R}_p	Single-pulse peak S/N ($\mathcal{R}_p = 2 \text{ S/N}$)
r	Rainfall rate, mm/h
r_E	Effective Earth radius
r_{FA}	False-alarm rate
r_s	Radius of cued search area

S	Signal power at the receiver output
S/C	Signal-to-clutter ratio; signal-to-chaff ratio
S/J	Signal-to-jammer ratio
S/N	Signal-to-noise ratio
$(S/N)_{CI}$	Integrated signal-to-noise ratio using coherent integration
$(S/N)_{NI}$	Integrated signal-to-noise ratio using noncoherent integration
$(S/N)_{ref}$	Reference signal-to-noise ratio
$(S/N)_1$	Signal-to-noise ratio for scatterer 1
$(S/N)_2$	Signal-to-noise ratio for scatterer 2
SL	Antenna sidelobe level, relative to the main-beam gain
SLC	Sidelobe cancellation ratio for jammer
T_R	Receiver noise temperature
T_S	Radar system noise temperature
t	Time
t_{CI}	Coherent integration time
t_{FA}	Average time between false alarms
t_M	Time relative to the time for which the receiver is matched
t_N	Time duration for pulse train or a series of measurements
t_P	Prediction time; processing time in SAR
t_R	Antenna rotation period
t_S	Search frame time
t_{SM}	Search time that maximizes the assured acquisition range
t_1	Measurement time 1
t_2	Measurement time 2
$u(t)$	Complex waveform modulation versus time
V	Sum of signal-plus-noise values for target observations
V_C	Clutter radial velocity relative to radar platform
V_{ML}	Radial-velocity spread of clutter in the main beam of a moving radar
V_P	Velocity of radar platform
V_R	Radial velocity of target
V_{RO}	Radial-velocity offset in range-Doppler coupling
V_S	Clutter or chaff scattering volume
V_T	Threshold power level in V ; total chaff volume
V_V	Vertical component of target velocity (measured normal to the radar LOS)
V_W	Wind velocity
W_C	Total chaff weight
w	Antenna dimension in the plane in which the pattern is measured
w_{RA}	Real-aperture dimension
w_{SA}	Synthetic-aperture dimension
X	Sum of values for target observations
x	Discrimination measurement parameter

Y	RF signal power, normalized to noise level
Y_T	Normalized threshold power level
α	Change in aspect angle to the target; difference in radar LOS to target; position smoothing parameter
β	Bistatic angle, the angle between the transmitting and receiving LOS measured at the target; velocity smoothing parameter
χ	Output of receiver matched filter
ΔCR	Cross-range resolution produced by SAR
Δf	Change in frequency
Δf_D	Doppler-frequency spread
ΔR	Range resolution
ΔV	Radial-velocity resolution
ΔV_R	Radial-velocity spread
Δ_x	Separation of target and decoy measurement distributions
$\Delta_{\phi E}$	Angular separation of multipath lobes
δR	Change in target range; difference in direct and multipath ranges
ϕ_A	Beam azimuth angle; azimuth coverage in horizon search
ϕ_B	Antenna beam azimuth relative to platform velocity
ϕ_{BA}	Array broadside azimuth angle
ϕ_{BE}	Array broadside elevation angle
ϕ_D	Antenna beam depression angle relative to platform velocity
ϕ_E	Beam elevation angle
ϕ_{EM}	Minimum elevation angle at which range with multipath equals free-space range
ϕ_H	Elevation angle coverage in horizon search
γ	Angle between radar LOS and target rotation axis; acceleration smoothing parameter; grazing angle for surface clutter observation
η_M	Ratio of signal power returned via multipath to that in free space
η_R	Overall radar efficiency
η_T	Transmitter efficiency
η_V	Volume reflectivity; RCS per cubic meter
φ	Scan angle off array broadside
φ_A	Azimuth position of scanning radar beam relative to scan center
φ_M	Maximum off-broadside array scan angle
φ_S	Angular radius of circular scan pattern
φ_x	Array off-broadside scan angle in the x plane
φ_{x1}	Search coverage coordinate 1 in the x plane
φ_{x2}	Search coverage coordinate 2 in the x plane
φ_y	Array off-broadside scan angle in the y plane
φ_{y1}	Search coverage coordinate 1 in the y plane
φ_{y2}	Search coverage coordinate 2 in the y plane

λ	Radar wavelength
θ	Antenna half-power (3-dB) beamwidth; elevation angle in cosecant-squared antenna pattern
θ_A	Beamwidth in the azimuth plane
θ_B	Phased-array beamwidth on broadside
θ_{Bx}	Phased-array beamwidth in the x plane on broadside
θ_{By}	Phased-array beamwidth in the y plane on broadside
θ_E	Beamwidth in the elevation plane
θ_{RA}	Real-aperture beamwidth in SAR
θ_{SA}	Synthetic-aperture beamwidth produced by SAR
θ_x	Beamwidth in x plane (normal to the y plane)
θ_y	Beamwidth in y plane (vertical)
θ_φ	Phased-array beamwidth at scan angle φ
$\theta_{\varphi x}$	Phased-array beamwidth in the x plane at scan angle φ_x
$\theta_{\varphi y}$	Phased-array beamwidth in the y plane at scan angle φ_y
θ_1	Maximum elevation angle for full gain in cosecant-squared antenna pattern
θ_2	Maximum elevation angle for coverage in cosecant-squared antenna pattern
σ	Target RCS; standard deviation of measurement error
σ^0	Surface clutter RCS per unit surface area
σ_A	Standard deviation of angular measurement error
σ_{AB}	Angular bias error
σ_{AF}	Angular fixed random error
σ_{AN}	S/N-dependent angle error
σ_{AS}	Smoothed angular measurement error
σ_{av}	Average RCS value
σ_{A1}	Angle error in angular coordinate 1
σ_{A2}	Angle error in angular coordinate 2
σ_C	Cross-range velocity measurement error; clutter RCS; RCS of chaff in resolution volume
σ_D	Cross-range position measurement error; average RCS of chaff dipole at resonant frequency
σ_F	Accuracy of measurement of Doppler-frequency spread
σ_L	Accuracy of target-length measurement
σ_M	Error in predicted target position due to target maneuver
σ_P	Largest semi-axis of predicted target position error ellipsoid
σ_{PC}	Accuracy of predicted cross-range position
σ_{PD}	Maximum in-plane position measurement error
σ_{PR}	Accuracy of predicted range position
σ_R	Standard deviation of range error
σ_{RB}	Range bias error
σ_{ref}	Reference RCS

σ_{RF}	Range fixed random error
σ_{RN}	S/N-dependent range error
σ_{RS}	Smoothed range measurement error
σ_{R1}	Range measurement error for scatterer 1; range measurement error for radar 1
σ_{R2}	Range measurement error for scatterer 2; range measurement error for radar 2
σ_S	Standard deviation of RCS measurement error
σ_{SB}	RCS bias error
σ_{SF}	RCS fixed random error
σ_{SN}	S/N-dependent RCS measurement error
σ_T	Total RCS of chaff cloud
σ_V	Standard deviation of radial-velocity error; rms clutter velocity spread
σ_{VB}	Radial-velocity bias error
σ_{VD}	Maximum in-plane velocity measurement error
σ_{VF}	Radial-velocity fixed random error
σ_{VN}	S/N-radial-velocity error
σ_{VR}	Clutter velocity spread due to antenna rotation
σ_X	Standard deviation of discrimination measurement
τ	Pulse or waveform duration
τ_C	Compressed pulse duration
τ_M	Maximum transmitter pulse duration
τ_n	Duration of subpulse n
τ_P	Subpulse spacing in time
τ_R	Time resolution
τ_{ref}	Reference pulse duration
τ_S	Subpulse duration
ω_A	Azimuth angular velocity of scanning beam; linear scan rate om bow-tie scan
ω_{AM}	Maximum antenna angular velocity in azimuth direction
ω_{EM}	Maximum antenna angular velocity in elevation direction
ω_R	Antenna angular rotation rate
ω_T	Target rotation rate
ψ	Angle from the antenna beam axis
ψ_B	Solid angle of radar beam
ψ_{BA}	Average solid angle of radar beam in phased-array search
ψ_S	Search solid angle

Appendix B

Glossary

AMTI	Airborne moving target indication
APU	Auxiliary power unit
A Scope	A type of radar display that shows signal amplitude vs. time
AWACS	Airborne Warning and Control System
CCM	Counter-countermeasure
CFAR	Constant-false-alarm rate
Chirp	Term for linear FM
CM	Countermeasure
CR	Clutter cancellation ratio; chaff cancellation ratio (both normally greater than unity)
CRT	Cathode-ray tube
CW	Continuous wave
dB	Decibel
dB_i	Decibel relative to isotropic gain
dB_{sm}	Decibel relative to a square meter
dBW	Decibel relative to a watt
Doppler	Frequency shift in the reflected signal due to target radial velocity
DPCA	Displaced phase center array
ECCM	Electronic CCM
ECM	Electronic CM
erf	Error function
ERP	Effective radiated power, usually of a jammer
ESJ	Escort jammer
FFOV	Full-field-of view (phased array)
FFT	Fast Fourier transform
FM	Frequency modulation
FMCW	Frequency-modulated continuous wave
FOV	Field-of-view
GDOP	Geometric dilution of precision
GHz	Gigahertz
GMTI	Ground moving target indication

HF	High frequency
Hz	Hertz
IF	Intermediate frequency
ISAR	Inverse synthetic aperture radar
ITU	International Telecommunication Union
J/N	Jammer-to-noise ratio
JSTARS	Joint Surveillance and Target Attack Radar
kHz	Kilohertz
km	Kilometer
km/s	Kilometers per second
LFOV	Limited-field-of-view (phased array)
ln	Natural logarithm
LOS	Line-of-sight
m	Meter
m/s	Meters per second
MDV	Minimum detectable velocity
MHz	Megahertz
mks	Meter, kilogram, second measurement system (SI)
mR	Milliradian (used in custom radar functions)
MLJ	Mainlobe jammer
mrاد	Milliradian
ms	Millisecond
msine	Millisine
MTI	Moving target indication
OTH	Over-the-horizon
PC	Pulse-compression ratio
PDF	Probability density function
PPI	Plan position indicator display
PRI	Pulse repetition interval
rad	Radian
RCS	Radar cross section
RF	Radio frequency
rms	Root-mean-square
rpm	Revolutions per minute
rps	Revolutions per second
rss	Root-sum-square
S/C	Signal-to-clutter ratio; signal-to-chaff ratio
S/I	Signal-to-interference ratio
S/J	Signal-to-jammer ratio
S/N	Signal-to-noise ratio
S/(C + N)	Signal-to-clutter-plus-noise ratio; signal-to-chaff-plus-noise ratio

S/(J + N)	Signal-to-jammer-plus-noise ratio
S/(J + C + N)	Signal-to-jammer-plus-chaff-plus-noise ratio
SAR	Synthetic-aperture radar
SBR	Space-based radar
SCR	Signal-to-clutter ratio, or signal-to-chaff ratio
SEASAT	Radar satellite for ocean measurement
SI	International system of units
SIR-C	Spaceborne Imaging Radar – C/X Band Synthetic Aperture Radar
SJR	Signal-to-jammer ratio
SJNR	Signal-to-jammer-plus-noise ratio
SL	Antenna sidelobe level, relative to the mainbeam gain
SLB	Sidelobe blanker
SNR	Signal-to-noise ratio
SLC	Sidelobe canceller, cancellation ratio for jammer
SLJ	Sidelobe jammer
SOJ	Stand-off jammer
SPJ	Self-protection jammer
sr	Steradian
SSJ	Self-screening jammer
STAP	Space-time adaptive processing
TWS	Track while scan
TWT	Travelling-wave tube
UHF	Ultra-high frequency
VBA	Visual Basic for Applications
VHF	Very-high frequency
μs	Microsecond
μrad	microradian
μsine	microsine

Appendix C

Custom Radar Software Functions

The VBA custom radar functions and supporting material described in this book are provided on a computer disk supplied with the book. The disk contains three files:

- Radar Functions 2nd Ed.xla. This is an Excel Add-In file [1, pp. 341–351], containing the VBA code that implements the 43 custom radar functions described in this book.
- Function Test 2nd Ed.xls. This is an Excel file that contains an example exercise of each of the custom radar functions. The Function Arguments parameter boxes for these are illustrated in the sections of this book that describe the functions. The function inputs may be changed to see their impact on the function result.
- Example Problems 2nd Ed.xls. This is an Excel file that contains the spreadsheet analysis solutions to the example Problems given in Chapter 12. These worksheets and the plots of results are illustrated in Chapter 12.

The 43 custom radar functions, and the solutions that each calculate, are given in Table C.1, grouped by topic. The section of the book in which each is described, and the VBA Module number in the Add-In file where each function is located, are also given.

The three files on the disk provided should be copied to the hard drive of the computer where they will be used. While they may be placed in any directory on the hard drive, it is suggested that the Add-In file (Radar Functions 2nd Ed.xla), be placed in the directory containing other Excel Add-In files. For many installations, this is C:\Program Files\Microsoft Office\Office\Library. The Excel files (Function Test 2nd Ed.xls and Example Problems 2nd Ed.xls) will normally be copied to the C:\My Documents directory.

To install the Radar Functions 2nd Ed Add-In into Excel, first open Excel, and then select Tools/Add-Ins. The Add-Ins dialog box shown in Figure C.1 will appear. Find and check Radar Functions 2nd Ed. If Radar Functions 2nd Ed does not appear, use the Browse button and find the directory where it is located, and select it. Also, check the Analysis ToolPak–VBA, which will enable the ERF function used in Function DiscProb_Factor. If Analysis ToolPak–VBA does not appear in the Add-Ins dialog box, the add-in should be installed, using the Add/Remove Programs utility found in the Control Panel. Close the Add-Ins dialog box. The custom radar functions are now available for use in all spreadsheets. If they are no longer wanted,

Table C.1 Listing of Custom Radar Functions by Topic

<i>Topic and VBA module</i>	<i>Section</i>	<i>Function Name</i>	<i>Calculates</i>
Radar equation	5.7.1	SNR_dB	S/N for given radar and target parameters
VBA Module 1			
	5.7.2	Range_km	Radar range for given radar and target parameters
	5.7.3	Integrated_SNR_dB	Integrated S/N for pulse integration
	5.7.4	SP_SNR_dB	Single-pulse S/N that gives a specified integrated S/N
Radar detection	6.7.1	Pfa_Factor	P_{FA} for a given false-alarm rate in search
VBA Module 2			
	6.7.2	FARate_per_s	False-alarm rate for given P_{FA} in search
	6.7.3	ProbDet_Factor	P_D for given signal, target, and detection parameters
	6.7.4	SNR_SP_dB	Single-pulse S/N for given detection, target and processing parameters
Radar search modes	7.8.1	SearchR_Rot1_km	Range for rotating search radar, using radar parameters
VBA Module 3			
	7.8.2	SearchR_Rot2_km	Range for rotating search radar, using reference range
	7.8.3	SearchR_Vol1_km	Range for phased array in volume search, using radar parameters
	7.8.4	SearchR_Vol2_km	Range for phased array in volume search, using reference range
	7.8.5	SearchR_Cue1_km	Range for phased array in cued search, using radar parameters
	7.8.6	SearchR_Cue2_km	Range for phased array in cued search, using reference range
	7.8.7	SearchR_Hor1_km	Range for phased array in horizon search, using radar parameters
	7.8.8	SearchR_Hor2_km	Range for phased array in horizon search, using reference range
	7.8.9	Sr_BowTie1_km	Range for dish radar in horizon search, using radar parameters
	7.8.10	Sr_BowTie2_km	Range for dish radar in horizon search, using reference range
Radar measurement	8.9.1	RangeError_m	Range-measurement error ($1-\sigma$)
VBA Module 4			
	8.9.2	AngleError_mR	Angle-measurement error ($1-\sigma$)
	8.9.3	DopVelError_mps	Coherent radial-velocity measurement error ($1-\sigma$)
	8.9.4	RadVelError_mps	Radial velocity measurement error from range measurements ($1-\sigma$)
	8.9.5	CrossVelError_mps	Cross-range measurement error from angle measurements ($1-\sigma$)
	8.9.6	PredictError_km	Predicted-position error ($1-\sigma$)
Environment and mitigation techniques	9.6.1	SCR_Surf_dB	S/C for surface clutter
VBA Module 5			
	9.6.2	RainLocAtten_dBpkm	Local rain attenuation per kilometer (two-way)
	9.6.3	RainPathAtten_dB	Probable path attenuation from rain (two-way)
	9.6.4	SCR_Rain_dB	S/C for volume rain clutter

Table C.1 (Continued)

<i>Topic and VBA module</i>	<i>Section</i>	<i>Function Name</i>	<i>Calculates</i>
Radar countermeasures and counter-countermeasures	9.6.5	TropoAtten_dB	Tropospheric and lens loss for radar at sea level (two-way)
	9.6.6	TropoEl_Err_mR	Elevation-measurement error from tropospheric refraction for radar at sea level
	9.6.7	TropoR_Err_m	Range-measurement error from tropospheric refraction for radar at sea level
	9.6.8	IonoEl_Err_mR	Elevation-measurement error from ionospheric refraction for radar at sea level
	9.6.9	IonoR_Err_m	Range-measurement error from ionospheric refraction for radar at sea level
	10.7.1	DiscProb_Factor	Discrimination leakage or false-acceptance probability
	VBA Module 6		
	10.7.2	ML_SJNR_dB	S/(J + N) for a noise jammer in radar main beam
	10.7.3	ML_BTRange_km	Radar burnthrough range for a noise jammer in the main beam
Airborne and space-based radar	10.7.4	SL_SJNR_dB	S/(J + N) for a noise jammer in radar sidelobes
	10.7.5	SL_BTRange_km	Radar burnthrough range for a noise jammer in radar sidelobes
	10.7.6	SCR_Chaff_dB	S/C for target in uniform volume chaff
	11.8.1	Graz_Ang_deg	Earth grazing angle for a path from an elevated platform
	VBA Module 7		
	11.8.2	Dep_Ang_deg	Depression angle from an elevated platform to the Earth surface
	11.8.3	MB_Clutter_V_mps	Surface clutter radial velocity at beam center or between beam nulls
	11.8.4	SAR_XR_Res_m	Cross-range resolution for a SAR

open the Add-Ins dialog box and uncheck Radar Functions 2nd Ed [1, pp. 349–350].

The custom radar functions may now be used like the other functions in Excel. In a worksheet, select the cell where the function result is desired. Then select Insert/Function, or click on the function icon (f_x). The Insert Function dialog box, shown in Figure C.2, will appear. In the drop-down box after Or select a category, select User Defined. The custom radar functions will then appear in the Select a function window. Selecting a function will bring up the function's description at the bottom of the dialog box. Double click on the selected function, or click OK.

The Function Arguments parameter box for the selected function will appear. The Function Arguments parameter boxes are illustrated in the book sections that describe the functions. Fill in the required parameter values (indicated by bold type), and the desired optional parameter values (indicated by nonbold type). The function result will appear at the bottom of the Function Arguments parameter box. Click OK, and the result will appear in the worksheet cell [1, pp. 337–340].

Figures C.1 and C.2 show the Add-Ins and Insert Functions dialog boxes, respectively, as they appear in recent versions of Excel. In earlier versions of Excel, the appearance of these boxes is slightly different, and the Insert Function dialog

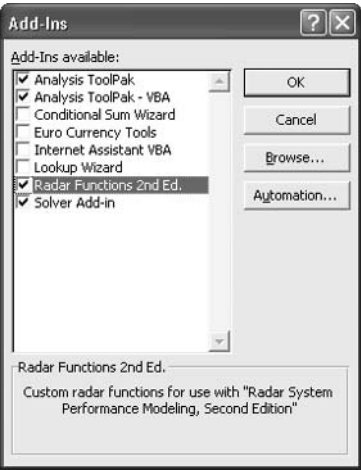


Figure C.1 Add-Ins dialog box with Radar Functions 2nd Ed and Analysis ToolPak–VBA checked (Excel 2002).

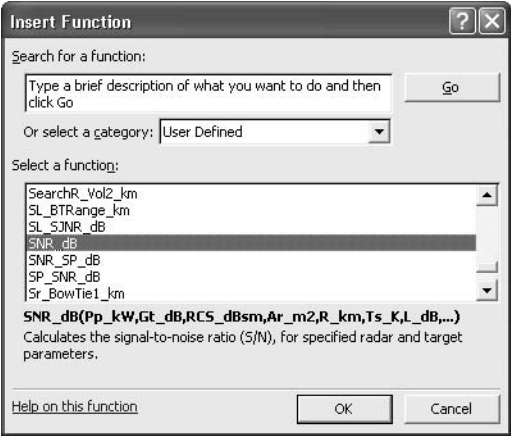


Figure C.2 Insert Function dialog box with User Defined selected, showing custom radar functions (Excel 2002).

box is called the Paste Function dialog box. However, they are functionally the same. These earlier versions are illustrated in Figures C.3 and C.4, respectively. The earlier version of the Function Arguments dialog box is illustrated in Figure 1.3.

The custom radar functions may also be directly entered in worksheet cells. In the cell, type =, the function name, and the input parameters in parentheses, separated by commas. Key Enter. For example, =DiscProb(0.01,3) will produce the output 0.25 (see Section 10.7.1). This input is not case-sensitive.

The radar Functions 2nd Ed.xla file is locked from viewing to prevent accidental modification of the file. It may be viewed, and the functions modified and copied, by unlocking the file. To do this, open Excel, select Tools/Macro/Visual Basic Editor (or key Alt + F11) to view the Visual Basic Editor. In the left-hand window (Project Explorer), double-click on VBAProject (Radar Functions 2nd Ed.xla). Enter the password in the dialog box that appears, and click OK. The password for this file is RADAR. The VBA modules may now be opened [1, pp. 350–351].

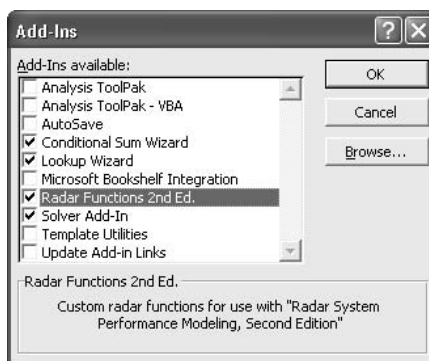


Figure C.3 Add-Ins dialog box with Radar Functions 2nd Ed and Analysis ToolPak–VBA checked (Excel 97).

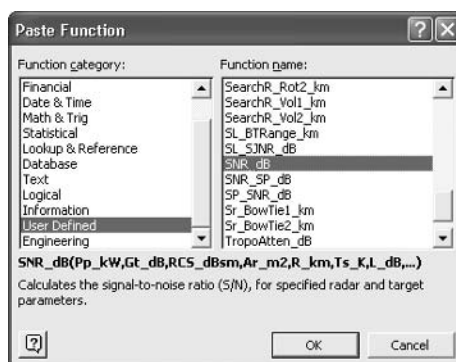


Figure C.4 Paste Function dialog box with User Defined selected, showing custom radar functions (Excel 97).

The radar Functions 2nd Ed.xla file also contains worksheets with data used by the modules. To view and modify these worksheets, first unlock the file, as described above. Then, in the left-hand window of the Visual Basic Editor (Project Explorer), select This Workbook. Click View/Properties Window. In this window, change the property for Is Add In to False, and close the Properties Window. The data worksheets now may be viewed and modified. When finished, go back to the Properties Window, and change the Is Add In property back to True. If any changes are made to Radar Functions 2nd Ed.xla, it is recommended that they be saved with a new file name, so that the original file is preserved.

The two Excel files (Function Test 2nd Ed.xls, and Example Problems 2nd Ed.xls) are protected as read-only. They may be opened by clicking on Read-Only in the dialog box that appears when opening is attempted.

The radar functions described in Chapters 5 through 11 are implemented on the worksheets in Function Test 2nd Ed.xls. The functions are pasted into cells in Row 6, and the input parameters are given in the cells below each function. Changes in the values of these cells will be reflected in the function output. The Function Arguments parameter box may be seen by selecting a cell with a function, and selecting Insert/Function, or by clicking the function icon.

A worksheet in Example Problems 2nd Ed.xls is devoted to each of the five example Problems in Chapter 12. The input parameters are given at the top of the

worksheet, and the calculations are performed below these. Changing the input values will change the results (except for parts of the Problem in Section 12.4, as discussed in that section). The charts used in the figures in Chapter 12 are also included in this file. These plots will change when changes in the Problem inputs produce changes the Problem results.

The parameters in these files may be changed and other modifications may be made. The modified files may be saved with new file names. To modify the original file (not recommended), use the password RADAR when opening the file.

Reference

- [1] Walkenbach, J., *Excel 97 Programming for Windows for Dummies*, Foster City, CA: IDG Books Worldwide, 1997.

Appendix D

Unit Conversion

The models in this book use the metric system [International System of Units (SI)], also known as the mks system (for meter-kilogram-second). This allows for standardization and simplification of the equations. However, many of the examples, problems, and custom radar functions use units that are common to radar usage. For example, power may be specified in kilowatts instead of watts, and radar cross section may be specified in decibels relative to a square meter, rather than square meters. This appendix provides factors that can be used to convert other units to the metric system. It also provides other useful conversion methods and values for constants used in the book.

Factors for converting measurements into the metric system are given in Table D.1. Conversion in the opposite direction can be done by dividing by the factor given.

Unit prefixes, their abbreviations, and their meanings are given in Table D.2.

Constants that are used for radar analysis are given in Table D.3. In this book, common approximations of $c = 3 \times 10^8$ and $k = 1.38 \times 10^{-23}$ are used. This value for c is also commonly used, as it is here, for electrometric propagation velocity in the atmosphere.

Parameters given in decibels can be converted to power a ratio by:

Table D.1 Factors for Converting into the Metric System

<i>To Convert This Unit</i>	<i>To This Unit</i>	<i>Multiply By</i>
Yards	Meters	0.9144
Feet	Meters	0.3048
Inches	Meters	0.02540
Miles	Kilometers	1.609
Nautical miles	Kilometers	1.852
Kilofeet	Kilometers	0.3048
Miles/hour	Meters/second	0.4469
Nautical miles/hour/ (knots)	Meters/second	0.5144
Kilometers/hour	Meters/second	0.2777
Pounds	Kilograms	0.4536
Hours	Seconds	3,600
Minutes	Seconds	60
Degrees	Radians	0.01745 or ($\pi/180$)

Table D.2 Measurement Unit Prefixes and Their Meanings

<i>Prefix</i>	<i>Abbreviation</i>	<i>Meaning</i>
Pico	p	10^{-12}
Nano	n	10^{-9}
Micro	μ	10^{-6}
Milli	m	10^{-3}
Centi	c	10^{-2}
Deci	d	10^{-1}
Deka	da	10^1
Hecto	h	10^2
Kilo	k	10^3
Mega	M	10^6
Giga	G	10^9
Tera	T	10^{12}

$$\text{Power ratio} = 10^{(dB/10)} \quad (D.1)$$

Power ratios can be converted to decibels by:

$$dB = 10 \log(\text{Power ratio}) \quad (D.2)$$

Some radar parameters are specified in decibels relative to the unit. Examples are dBsm for radar cross section relative to a square meter, dBW for power relative to a watt, and dBi for antenna sidelobe level relative to isotropic. These can be converted to their reference units using (D.1).

Radar noise temperatures are usually specified in Kelvin. These can be found from temperatures in degrees Celsius and degrees Fahrenheit by:

$$K = C + 273.15 \quad (D.3)$$

$$K = 273.15 + \frac{5}{9}(F - 32) \quad (D.4)$$

A common room-temperature used in radar noise calculations is 290K, which corresponds to about 62F. This is also the standard temperature defined for use in calculating the noise figure of a receiver [see Section 3.4, (3.33)].

Most of the unit conversions described here, as well as others, can be done using the Excel CONVERT worksheet function [1, pp. 64–65]. Information on using this function can be found in Excel Help, selecting the Index tab, and entering CONVERT.

Table D.3 Constants for Radar Analysis

<i>Constant</i>	<i>Abbreviation</i>	<i>Value</i>
Electromagnetic propagation velocity in a vacuum	c	2.998×10^8 m/s
Boltzmann's constant	k	1.381×10^{-23} J/K
Radius of the Earth	r_E	6,371 km
4/3 Earth radius	$4/3 r_E$	8,485 km

Reference

- [1] *Microsoft Excel Function Reference*, Redmond, WA: Microsoft Corporation, 1962.

Appendix E

Problem Solutions

These problem solutions are calculated using four significant figures, where the input data supports this precision. The answers are rounded to three significant figures, since most practical radar parameters are known only to this or lesser accuracy.

E.1 Chapter 1 Problems

1. $200 \text{ km} = 200 \times 10^3 \text{ m}$. From (1.1), $t = 2 \times 200 \times 10^3 / (3 \times 10^8) = 0.001333 \text{ sec} \approx 1.33 \text{ ms}$. (The propagation velocity $c = 3 \times 10^8$.)
2. The radar frequency, $f = 425 \times 10^6 \text{ Hz}$. The radial velocity from (1.2) is $V_R = 20 \times 3 \times 10^8 / (2 \times 425 \times 10^6) = 7.059 \text{ m/s} \approx 7.06 \text{ m/s}$. Since the Doppler-frequency shift is positive, the target is closing the radar.
3. From (1.4), $10^{(22/10)} = 158.5 \approx 159$.
4. From (1.5), $10 \log(75) = 18.75 \approx 18.8$.
5. From (1.1), $\text{Range} = 3 \times 10^8 \times 0.0035/2 = 525,000 \text{ m} = 525 \text{ km}$.
6. a. Radial velocity $= 700 \times \cos(30^\circ) = 606.2 \text{ m/s} \approx 606 \text{ m/s}$.
b. From (1.2), the Doppler-frequency shift $= 606.2 \times 2 \times 5.5 \times 10^9 / (3 \times 10^8) = 22,230 \text{ Hz} \approx 22.2 \text{ kHz}$.
c. The Doppler-frequency shift is upward for a closing target. The received frequency $= 5,500,000,000 + 22,230 = 5,500,022,2230 \text{ Hz}$.
7. From (1.4), $10^{(15/10)} = 31.62 \approx 31.6$.
8. From (1.5), $10 \log(0.03) = 15.23 \approx -15.2 \text{ dBsm}$.

E.2 Chapter 2 Problems

1. Using (2.1), and the 4/3 Earth approximation, $R_R = (20^2 + 2 \times 8,485 \times 10^3 \times 20)^{1/2} = 18,420 \text{ m} \approx 18.4 \text{ km}$.
2. Using the same equation, $R_R = (2,000^2 + 2 \times 8,485 \times 10^3 \times 2,000)^{1/2} = 184,200 \text{ m} \approx 184 \text{ km}$.
3. Atmospheric and rain attenuation is greater at higher radar frequencies.
4. A dish antenna is well suited for tracking a single target.

5. The range from the radar to the Earth tangent point is found from (2.1), using the 4/3 Earth approximation: $R_r = (25^2 + 2 \times 8,485 \times 10^3 \times 25)^{1/2} = 20,600\text{m} = 20.60\text{ km}$. The range from the Earth tangent to the target is similarly found from (2.2): $R_t = (5,000^2 + 2 \times 8,485 \times 10^3 \times 5,000)^{1/2} = 291,300\text{m} \approx 291\text{ km}$. The total range is the sum of these: $20.60 + 291.3 = 311.9 \approx 312\text{ km}$.
6. Signals in the VHF (30 to 300 MHz) and UHF (300 to 1,000 MHz) bands may be distorted by the ionosphere.
7. Phased-array antennas allow the beam to be rapidly electronically steered.

E.3 Chapter 3 Problems

1. The pulse duration is found using (3.2): $20 \times 10^3 / (2 \times 10^6) = 0.01\text{ sec} = 10\text{ ms}$. With a 10% duty cycle, the transmitter may generate pulses for 0.1 sec or 100 ms each second. The rate at which 10-ms pulses may be generated is $100/10 = 10\text{ Hz}$.
2. The tube peak power of 20 kW is reduced by the internal loss by a power ratio of $10^{(0.7/10)} = 1.175$. The transmitter peak power is then $20\text{ kW}/1.175 = 17.02\text{ kW}$. The average power is found by multiplying by the duty cycle: $17.02\text{ kW} \times 0.2 = 3.404 \approx 3.40\text{ kW}$. The transmitter efficiency is found using (3.3): $3.404\text{ kW}/15\text{ kW} = 0.2269 \approx 22.7\%$. Converting the 1.6-dB ohmic loss to a power ratio gives $10^{(1.6/10)} = 1.445$. The overall radar efficiency is found using (3.4): $3.404\text{ kW}/(28\text{ kW} \times 1.445) = 0.08413 \approx 8.41\%$.
3. The L-band wavelength is $3 \times 10^8 / 1.3 \times 10^9 = 0.2308\text{m}$. The required gain, converted to a power ratio, is $10^{(40/10)} = 10,000$. The effective aperture area is found from (3.8) as $10,000 \times 0.2308^2 / (4\pi) = 42.39\text{ m}^2 \approx 42.4\text{ m}^2$. At X band, the wavelength is $3 \times 10^8 / 9.5 \times 10^9 = 0.03158\text{m}$. The required aperture area is $10,000 \times 0.03158^2 / (4\pi) = 0.7936\text{ m}^2 \approx 0.794\text{ m}^2$.
4. For 40-dB Taylor weighting in one dimension, the aperture efficiency is found in Table 3.1 as 0.76. For weighting in two dimensions, the loss due to aperture efficiency is then $1/0.76^2 = 1.731$. The antenna ohmic loss, converted to a power ratio, is $10^{(0.8/10)} = 1.202$. The physical antenna area from (3.11) is $10 \times 1.731 \times 1.202 = 20.82\text{ m}^2$. The wavelength is found to be $3 \times 10^8 / 3.3 \times 10^9 = 0.09091\text{m}$. The beamwidth coefficient is found from Table 3.1 as 1.25. The elevation beamwidth is found from (3.7): $1.25 \times 0.09091/3 = 0.03788\text{ rad} \approx 37.9\text{ mrad}$ or 2.17° . The azimuth dimension is found to be $20.82\text{ m}^2/3\text{m} = 6.940\text{m} \approx 6.94\text{m}$. The azimuth beamwidth is $1.25 \times 0.0909/6.940 = 0.01637\text{ rad} \approx 16.4\text{ mrad}$ or 0.938° .
5. Each element has an area of $(0.59\lambda)^2$. The total area is $10,000 \times (0.59\lambda)^2$. The gain from (3.9) is $4\pi \times 10,000 \times (0.59\lambda)^2/\lambda^2 = 43,740 = 46.41\text{ dB} \approx 46.4\text{ dB}$. The wavelength is found to be $3 \times 10^8 / 5.5 \times 10^9 = 0.05455\text{m}$. The antenna area is then $10,000 \times (0.59 \times 0.05455)^2 = 10.36\text{ m}^2$, and the linear dimension is $10.36^{1/2} = 3.219\text{m}$. For uniform illumination, the beamwidth coefficient from Table 3.1 is 0.89. The beamwidth is found from (3.7) to be

- $0.89 \times 0.05455/3.219 = 0.01508 \text{ rad} = 15.08 \text{ mrad} \approx 15.1 \text{ mrad}$ or 0.864° .
 For a 30-degree scan, the one-way gain is reduced by $\cos^{-1.25}(30^\circ) = 1.197 = 0.7809 \approx 0.781 \text{ dB}$ (see Figure 3.3). The gain is then $46.41 \text{ dB} - 0.78 \text{ dB} = 45.63 \text{ dB} \approx 45.6 \text{ dB}$. The elevation beamwidth is found from (3.25): $15.08 \text{ mrad}/\cos(30^\circ) = 17.41 \text{ mrad} \approx 17.4 \text{ mrad}$ or 0.998° .
6. The value of Boltzmann's constant from Appendix D is 1.38×10^{-23} . The system noise temperature is found from (3.32): $10^{14}/(1.38 \times 10^{-23} \times 10^6) = 724.6 \text{ K} \approx 725 \text{ K}$.
 7. The radar wavelength is $3 \times 10^8/9.5 \times 10^9 = 0.03158 \text{ m}$. The rotation angle needed to decorrelate the target return is found from (3.34): $0.03158/(2 \times 10) = 0.001579 \text{ rad} = 0.09047^\circ$. The target rotates at $2 \times 360/60 = 12^\circ/\text{s}$, so the time it takes to decorrelate the target RCS is $0.09047/12 = 0.007539 \text{ sec} \approx 7.54 \text{ ms}$. With a PRF of 100 Hz, the radar will observe the target at 10-ms intervals, so the observations will be decorrelated. Decorrelated observations are modeled by Swerling 2 and 4 fluctuations. Since the target has many comparable scatterers, the Raleigh PDF is appropriate, and Swerling 2 fluctuations should be used.
 8. Pulse energy is pulse duration multiplied by peak power: $5 \text{ ms} \times 10 \text{ kW} = 50 \text{ J}$. The number of pulses is $1,000 \text{ J}/50 \text{ J} = 20$.
 9. Duty cycle is ratio of average to peak power = $150,000 \text{ W}/1,000,000 \text{ W} = 0.15 = 15\%$. Average power is peak power times duty cycle = $1,000,000 \text{ W} \times 0.25 = 250,000 \text{ W} = 250 \text{ kW}$.
 10. a. With uniform illumination (no aperture weighting), aperture efficiency is unity, and aperture area equals antenna area: $10 \text{ m} \times 10 \text{ m} = 100 \text{ m}^2$. The radar wavelength = $3 \times 10^8/3.3 \times 10^9 = 0.09091 \text{ m}$. The gain is calculated from (3.9) as $4\pi \times 100/(0.09091^2) = 152,100 = 51.82 \text{ dB} \approx 51.8 \text{ dB}$.
 b. With 30-dB Taylor illumination, the aperture efficiency from Table 3.1 is 0.85, and the effective aperture area is $100 \text{ m}^2 \times 0.85 = 85 \text{ m}^2$. The gain is calculated as above, using 85 m^2 for the aperture area, giving $129,200 = 51.11 \text{ dB} \approx 51.1 \text{ dB}$. The gain may also be found directly by subtracting the aperture efficiency loss [(0.71 dB) from Table 3.1] from the gain in a.
 11. For uniform illumination, the first sidelobe is -13.3 dB relative to the main beam, from Table 3.1. The gain for this case is 51.8 dB , so the isotropic sidelobe level is $51.8 \text{ dB} - 13.3 \text{ dB} = 38.5 \text{ dB}$. For the 30-dB Taylor illumination, the first sidelobe from Table 3.1 is -30.9 dB , the gain is 51.1 dB , and the isotropic sidelobe level is $50.1 \text{ dB} - 30.9 \text{ dB} = 19.2 \text{ dB}$.
 12. a. The azimuth and elevation beamwidths in radians are $1 \times 0.01745 = 0.01745 \text{ rad}$, and $2 \times 0.01745 = 0.03491 \text{ rad}$ [see Table D.1 in Appendix D; multiplying by $(\pi/180)$ also gives this result]. The gain is found using (3.12): $10.735/(0.01745 \times 0.03491) = 17,660 = 42.47 \text{ dB} \approx 42.5 \text{ dB}$.
 b. The beamwidths are found using (3.20): the azimuth beamwidth is $1/\cos(20^\circ) = 1.064^\circ \approx 1.06^\circ$, and the elevation beamwidth is $2/\cos(40^\circ) = 2.611^\circ \approx 2.61^\circ$. Using (3.21), the two-way azimuth scan loss is $\cos^{-2.5}(20^\circ) = 1.168 = 0.6754 \text{ dB}$, and the elevation scan loss is $\cos^{-2.5}(40^\circ) = 1.947 = 2.894 \text{ dB}$. The total loss is the product of those loss power ratios, $2.274 \approx 2.27$, or the

sum of the losses in decibels, $3.569 \text{ dB} \approx 3.57 \text{ dB}$. This loss may also be calculated using (3.22). The total scan angle is $\arccos [\cos (20^\circ) \times \cos (40^\circ)] = 43.96^\circ$. The loss is then $\cos^{-2.5} (43.96) = 2.275 = 3.569 \text{ dB}$. The gain is then $42.47 \text{ dB} - 3.569 \text{ dB} = 38.90 \text{ dB} \approx 38.9 \text{ dB}$.

13. The wavelength is found as $3 \times 10^8 / 9.5 \times 10^9 = 0.03158 \text{ m}$. The area occupied by an FFOV element is then $(0.6 \times 0.03158)^2 = 3.590 \times 10^{-4} \text{ m}^2$. Dividing this into the array area of $5 \times 5 = 25 \text{ m}^2$ gives $25 / (3.590 \times 10^{-4}) = 69,640$ elements. The element spacing for LFOV arrays is found from (3.26): $0.5 \times 0.03158 / [\sin (20^\circ)] = 0.04617 \text{ m}$. The number of elements is then given by $25 / 0.04617^2 = 11,730$ elements $\approx 11,700$ elements.
14. From (3.32) and the value of Boltzmann's constant from Appendix D, the receiver noise power is $1.38 \times 10^{-23} \times 500 \times 10 \times 10^6 = 6.900 \times 10^{-14} \text{ W} \approx 6.90 \times 10^{-14} \text{ W}$.
15. Converting the noise figure from decibels to a power ratio ($10^{(3.5/10)} = 2.239$), and using (3.3), the receiver noise temperature is $290 \times (2.239 - 1) = 359.2 \text{ K} \approx 359 \text{ K}$.
16. a. The wavelength is found to be $3 \times 10^8 / 5.5 \times 10^9 = 0.05455 \text{ m}$. The LOS rotation angle needed to decorrelate the RCS is found from (3.34) as $0.05455 / (2 \times 2) = 0.01364 \text{ rad} = 0.7815^\circ$. At a rotation rate of $10^\circ/\text{s}$, the time for the target to rotate this amount is $0.7815^\circ / 10^\circ/\text{s} = 0.07815 \text{ sec}$. The maximum PRF is the reciprocal of this time: $12.80 \text{ Hz} \approx 12.8 \text{ Hz}$.
b. The frequency change needed is found from (3.35): $3 \times 10^8 / (2 \times 2) = 7.5 \times 10^7 = 75 \text{ MHz}$.

E.4 Chapter 4 Problems

1. The major characteristics are energy content, resolution in range and radial velocity, and rejection of unwanted targets.
2. The time resolution is $1/B = 1/10^7 = 10^{-7}$. The range resolution from (4.4) is $3 \times 10^8 \times 10^{-7} / 2 = 15 \text{ m}$. This may also be found directly from $3 \times 10^8 / (2 \times 10^7) = 15 \text{ m}$ (see Section 4.3). The CW pulse duration is $10^7 \text{ sec} = 0.1 \mu\text{s}$.
3. The frequency resolution is $1/(50 \times 10^{-3}) = 20 \text{ Hz}$. The radar wavelength is $3 \times 10^8 / (3.3 \times 10^9) = 0.09091 \text{ m}$. The radial-velocity resolution from (4.5) is $0.0909 \times 20 / 2 = 0.9091 \text{ m/s} \approx 0.909 \text{ m/s}$. The CW-pulse range resolution is $3 \times 10^8 \times 50 \times 10^{-5} / 2 = 7.5 \times 10^6 \text{ m} = 7,500 \text{ km}$.
4. The range resolution is given by $3 \times 10^8 \times 50 \times 10^{-5} / (2 \times 1,000) = 7.5 \times 10^3 \text{ m} = 7.5 \text{ km}$. This is the CW pulse range resolution from Problem 3 divided by the pulse-compression ratio. The radial-velocity resolution is the same as in Problem 3, 0.909 m/s .
5. The waveform bandwidth is equal to the pulse-compression ratio divided by the pulse duration: $1,000 / (50 \times 10^5) = 2 \times 10^4 \text{ Hz}$. The range offset is found using (4.9): $50 \times 10^{-3} \times 3.3 \times 10^9 \times 300 / (2 \times 10^4) = 2.475 \times 10^6 \text{ m} \approx 2,480 \text{ km}$.
6. The waveform duration is given by the subpulse duration times the number of subpulses: $500 \times 10^{-6} = 5 \times 10^4 = 500 \mu\text{s}$. The range resolution is $3 \times 10^8 \times$

- $10^{-6}/2 = 150\text{m}$ (see Figure 4.7). The signal wavelength is $3 \times 10^8/1.3 \times 10^9 = 0.2308\text{m}$. The radial-velocity resolution is $0.2308/(2 \times 500 \times 10^{-6}) = 230.8\text{ m/s} \approx 231\text{ m/s}$. The peak sidelobe level is approximately equal to the reciprocal of the number of subpulses: $1/500 = 0.002 = -27.0\text{ dB}$.
7. The range-ambiguity spacing is $3 \times 10^8 \times 100 \times 10^{-6}/2 = 1.5 \times 10^4\text{m} = 15\text{ km}$. The range resolution found using the waveform bandwidth: $3 \times 10^8/(2 \times 100 \times 10^6) = 1.5\text{m}$. The signal wavelength is $3 \times 10^8/(9.5 \times 10^9) = 0.03158\text{m}$. The spacing of radial-velocity ambiguities is given by $0.03158/(2 \times 100 \times 10^{-6}) = 157.9\text{ m/s} \approx 158\text{ m/s}$ (see Figure 4.9). The total waveform duration is $200 \times 100 \times 10^{-6} = 2 \times 10^{-2} = 20\text{ ms}$. The resulting radial-velocity resolution is $0.03158/(2 \times 2 \times 10^{-2}) = 0.7895\text{ m/s} \approx 0.790\text{ m/s}$. Note that the ratio of the radial-velocity ambiguity spacing to the radial-velocity resolution is equal to the number of subpulses.
 8. The PRI is the reciprocal of the PRF. The ambiguous range is $3 \times 10^8/(2 \times 200) = 7.5 \times 10^5\text{m} = 750\text{ km}$. For a second-time-around return, the true range is $750 + 300 = 1,050\text{ km}$. For a third-time-around return, the true range is $750 \times 2 + 300 = 1,800\text{ km}$.
 9. From (4.4), the time resolution is $2 \times 10/(3 \times 10^{-8}) = 6.667 \times 10^8\text{ sec} \approx 0.0667\text{ }\mu\text{s}$. The bandwidth is the reciprocal of the time resolution $= 1/(6.667 \times 10^{-8}) = 1.5 \times 10^7\text{ Hz} = 15\text{ MHz}$.
 10. The Doppler-frequency resolution is found from (4.5). Substituting c/f for λ , it is given at X band by $2 \times 100 \times 9.5 \times 10^9/(3 \times 10^8) = 6.333 \times 10^3\text{ Hz} \approx 6.33\text{ kHz}$. For L band it is $2 \times 100 \times 1.3 \times 10^9/(3 \times 10^8) = 8,667\text{ Hz} \approx 8.67\text{ kHz}$. The waveform duration is the reciprocal of the frequency resolution: $1/(6.333 \times 10^3) = 1.579 \times 10^{-4}\text{ sec} \approx 0.158\text{ ms}$ for X band, and $1/8,667 = 1.154 \times 10^{-3}\text{ sec} \approx 1.15\text{ ms}$ for L band.
 11. The volume under the ambiguity-function surface depends only on the waveform energy.
 12. The pulse-compression ratio is equal to the time-bandwidth product [see (4.7)]. For the X-band waveform, $\text{PC} = 1.579 \times 10^{-4} \times 1.5 \times 10^7 = 2,369 \approx 2,370$; and for the L-band waveform, $\text{PC} = 1.154 \times 10^{-3} \times 1.5 \times 10^7 = 17,310 \approx 17,300$.
 13. The pulse duration from (4.7) is $\text{PC}/B = 10^4/(100 \times 10^6) = 10^{-4}\text{ sec} = 100\text{ }\mu\text{s}$. The range resolution $= c/2B = 3 \times 10^8/(2 \times 100 \times 10^6) = 1.5\text{m}$ (see Figure 4.5). The velocity resolution $= \lambda/2\tau = 3 \times 10^8/(2 \times 5.5 \times 10^9 \times 10^{-4}) = 272.7\text{ m/s} \approx 273\text{ m/s}$ (using c/f for λ). The sidelobes extend for a distance corresponding to the plus-or-minus pulse duration $= 3 \times 10^8 \times 10^{-4}/2 = 1.5 \times 10^4 = 15\text{ km}$. The velocity sidelobes extend to plus-or-minus infinity, but the peaks decrease with distance from the time axis.
 14. From (4.9), the range offset is $10^{-4} \times 5.5 \times 10^9 \times 10^3/10^8 = +5.5\text{m}$ for upchirp. For downchirp, it is -5.5m .
 15. The subpulse duration given by $2 \times 15/(3 \times 10^8) = 10^{-7}\text{ sec} = 0.1\text{ }\mu\text{s}$ (see Section 4.2). The wavelength is $3 \times 10^8/(9.5 \times 10^9) = 0.03158\text{m}$. The waveform duration is then $0.03158/(2 \times 1,000) = 1.579 \times 10^{-5}\text{ sec} \approx 15.8\text{ }\mu\text{s}$

- (see Section 4.4). The number of subpulses is $1.579 \times 10^{-5}/10^{-7} = 157.9 \approx 158$. The peak sidelobe level = $1/158 = 0.006329 \approx -22.0$ dB.
16. The range ambiguity spacing specified requires a subpulse spacing of at least $2 \times 10,000/(3 \times 10^8) = 6.667 \times 10^{-5} = 66.67 \mu\text{s}$ (see Figure 4.9). The minimum wavelength is given by $2 \times 6.667 \times 10^{-5} \times 1,000 = 0.1333\text{m}$. The maximum frequency is then $3 \times 10^8/0.1333 = 2.251 \times 10^9 \text{ Hz} \approx 2.25 \text{ GHz}$. The required waveform duration is given by $0.1333/(2 \times 10) = 6.667 \times 10^{-3} \approx 6.67 \text{ ms}$. The number of pulses is then $6.667 \times 10^{-3}/(6.667 \times 10^{-7}) = 100$.
 17. The maximum unambiguous range is $3 \times 10^8/(2 \times 500) = 3 \times 10^5 \text{ m} = 300 \text{ km}$. A target at 700 km range will be viewed after the third pulse is transmitted, and have an apparent range of $700 - (2 \times 300) = 100 \text{ km}$.

E.5 Chapter 5 Problems

1. The receive aperture area is calculated from (3.8), using the gain as a power ratio (3,162), and the calculated radar wavelength (0.09091m), as $3,162 \times 0.09091^2/4\pi = 2.080 \text{ m}^2$. Using (5.5), and converting the engineering parameters in the Problem statement to mks (SI) units, $S/N = 5,000 \times 3,162 \times 3.162 \times 2.080 \times 10^5 / [(4\pi)^2 \times 175,000^4 \times 100 \times 10^6 \times 1.38 \times 10^{-23} \times 450 \times 2.512] = 45.01 \approx 16.5 \text{ dB}$. The pulse duration is found using (4.7) as $10^5/(100 \times 10^6) = 0.001 \text{ sec} = 1 \text{ ms}$. The minimum range for this pulse, from (5.26), is $3 \times 10^8 \times 0.001/2 = 150,000\text{m} = 150 \text{ km}$. Since the target range is larger than this, the minimum-range constraint is not violated.
2. The transmit microwave loss includes loss components from the point where the transmit power is defined, to the transmit antenna terminal. The receive microwave loss includes components from the receive antenna terminal, to the point where the system noise temperature is defined.
3. With uniform illumination, there is no aperture efficiency loss. The transmit gain is given by the element gain (power ratio 3.548) multiplied by the number of elements [see (5.9)], reduced by the antenna transmit ohmic losses (power ratio 1.047): $G_T = 2,000 \times 3.548/1.047 = 6,777 \approx 38.3 \text{ dB}$. This may also be found by adding the number of elements in decibels (33.01 dB) to the element gain, and subtracting the loss: $33.01 + 5.5 - 0.2 \approx 38.3 \text{ dB}$. The receive aperture efficiency loss, $L_{ER} = 0.22 \text{ dB}$ (power ratio 1.052) from Table 3.1. Neglecting losses, the element receive aperture area is found from (3.8), using the calculated wavelength of 0.05455m, as $3.548 \times 0.05455^2/4\pi = 0.0008401 \text{ m}^2$. The effective receive aperture area is given by the element aperture area multiplied by the number of elements [see (5.10)], reduced by the receive antenna ohmic losses and the receive aperture efficiency loss: $A_R = 2,000 \times 0.0008401/(1.047 \times 1.052) = 1.526 \text{ m}^2 \approx 1.53 \text{ m}^2$.
4. The scan loss, L_s , is found from (3.21) as $\cos^{-2.5} (30^\circ) = 1.433 = 1.562 \text{ dB}$. The propagation loss power ratio is 1.202. The reference range is found by rearranging (5.11), converting values specified in decibels to power ratios,

- and taking ratios of parameters in similar units: $R_{ref} = 1,000 \times (1.433 \times 1.202)^{1/4} = 1,146 \text{ km} \approx 1,150 \text{ km}$. The required pulse duration is found from (5.11): $\tau = 5 \times (1/0.1) \times (15.85/31.62) \times (500/1,146)^4 = 0.0009081 \text{ sec} \approx 0.908 \text{ ms}$. The minimum range for this pulse duration from (5.26), is $3 \times 10^8 \times 0.0009082/2 = 136.2 \text{ km}$, so the minimum-range constraint is not violated.
5. For coherent integration, using (5.15), the integrated S/N = $10 \times 5.623 = 56.23 \approx 17.5 \text{ dB}$. Using the same equation rearranged, the single-pulse S/N for 100 pulses integrated is $56.23/100 = 0.5623 \approx -2.50 \text{ dB}$. For noncoherent integration for measurement, using (5.17), the integrated S/N = $10 \times 5.623^2/(1 + 5.623) = 47.74 \approx 16.8 \text{ dB}$. Using (5.18), the single-pulse S/N for 100 pulses integrated is $47.74/200 + [(47.74^2/40,000) + (47.74/100)]^{1/2} = 0.9697 \approx -1.34 \text{ dB}$. For noncoherent integration for detection, using (5.20), the integrated S/N = $10 \times 5.623^2/(2.3 + 5.623) = 39.91 \approx 16.0 \text{ dB}$. Using (5.21), the single-pulse S/N for 100 pulses integrated is $39.91/200 + [(39.91^2/40,000) + (2.3 \times 39.91/100)]^{1/2} = 1.178 \approx 0.712 \text{ dB}$.
 6. The required pulse duration is found from (5.11): $\tau = 5 \times (10^{-3}/0.1) \times (31.62/31.62) \times (750/1,146)^4 = 0.009172 \text{ sec} \approx 9.17 \text{ ms}$. The minimum range for this pulse duration, from (5.26), is $3 \times 10^8 \times 0.009172/2 = 1,376 \text{ km}$, so the minimum-range constraint is violated. The maximum range is found using (5.29): $R = 1,146,000^{4/3} \times [2 \times 0.1 \times 31.62/(3 \times 10^8 \times 0.005 \times 1 \times 31.62)]^{1/3} = 612,700 \text{ m} \approx 613 \text{ km}$. The corresponding pulse duration is $2 \times 612,700/(3 \times 10^8) = 0.004085 \text{ sec} \approx 4.09 \text{ ms}$.
 7. Using (5.1) and converting the engineering parameters in the Problem statement to mks (SI) units, S/N = $20,000 \times 0.001 \times 1,000 \times 1 \times 10/[(4\pi)^2 \times (200,000)^4 \times 1.38 \times 10^{-23} \times 500 \times 3.981] = 28.82 \approx 14.6 \text{ dB}$. The minimum range for a 1-ms pulse from (5.26) is $3 \times 10^8 \times 0.001/2 = 150,000 \text{ m} = 150 \text{ km}$. Since this is less than the target range, the minimum-range constraint is not violated.
 8. Solving (5.5) for R , and converting the problem parameters to mks (SI) units, $R = \{20,000 \times 1,000 \times 1 \times 10 \times 1,000/[(4\pi)^2 \times 63.10 \times 10^7 \times 1.38 \times 10^{-23} \times 500 \times 3.981]\}^{1/4} = 92,460 \text{ m} \approx 92.5 \text{ km}$. Equation (5.12) shows the S/N at 200 km = $63.10 \times (92.46/200)^4 = 2.882 = 4.597 \text{ dB}$. To produce an integrated S/N = 18 dB using coherent integration, from (5.14), $n = 63.10/2.882 = 21.89$. Rounding up, 22 pulses are needed. For noncoherent integration for measurement, from (5.17), $n = 63.10 \times (1 + 2.882)/(2.882)^2 = 29.49$. Rounding up, 30 pulses are needed. For noncoherent integration for detection, from (5.19), $n = 63.10 \times (2.3 + 2.882)/2.882^2 = 39.37$. Rounding up, 40 pulses are needed.
 9. The wavelength at X band is 0.03158m. The element aperture area is found, using (3.8), as $3.162 \times 0.03158^2/4\pi = 0.0002509 \text{ m}^2 \approx 0.000251 \text{ m}^2$. The array gain is $10,000 \times 3.162 = 31,620 = 45.0 \text{ dB}$. This may also be found by converting 10,000 to 40 dB, and adding to the element gain in decibels. The aperture area is $10,000 \times 0.0002509 \approx 2.51 \text{ m}^2$. The system noise temperature is equal to that of each module, 450K. The two-way

microwave ohmic loss is equal to the sum of the losses (in decibels) for each transmit and receive element: $0.1 + 0.1 = 0.2$ dB.

10. Coherent integration. Noncoherent integration.
11. The off-broadside scan loss, from (3.21) and (3.22), is $\cos^{-2.5}(20^\circ) \times \cos^{-2.5}(30^\circ) = 1.674$. Using (5.11), and converting the units specified in decibels to power ratios and taking ratios of parameters in similar units, $R = 500 \times [1 \times 0.1 \times 31.62 / (1 \times 1 \times 15.85 \times 1.674 \times 1.778)]^{1/4} = 254.4$ km ≈ 254 km. For coherent integration, the single-pulse S/N needed to provide 12 dB integrated S/N is found from (5.14), increased by the integration loss (power ratio 1.122): $15.85 \times 1.122/10 = 1.778 \approx 2.50$ dB. This may also be found by subtracting the number of pulses in decibels (10 dB) from the integrated S/N, and adding the integration loss in decibels: $12 + 0.5 - 10 = 2.5$ dB. The range is found using (5.11), as shown above with the power ratio 1.778 replacing 15.85, giving 440 km. A simpler calculation scales from the above result: $R = 254.4 \times (15.85/1.778)^{1/4} = 439.6$ km ≈ 440 km. For noncoherent integration for measurement, the single-pulse S/N is found from (5.18), using the integrated S/N, increased by the integration loss ($15.85 \times 1.122 = 17.78$), as the input: $S/N = 17.78/20 + (17.78^2/400 + 17.78/10)^{1/2} = 2.492 \approx 3.96$ dB. The range, found by scaling from the previous result, is $254.4 \times (15.85/2.492)^{1/4} = 404.0$ km ≈ 404 km. For noncoherent integration for detection, the single-pulse S/N is found from (5.21), using the integrated S/N, increased by the integration loss ($15.85 \times 1.122 = 17.78$), as the input: $S/N = 17.78/20 + (17.78^2/400 + 2.3 \times 17.78/10)^{1/2} = 3.098 \approx 4.91$ dB. The range, found by scaling from the previous result, is $254.4 \times (15.85/3.098)^{1/4} = 382.6$ km ≈ 383 km.
12. Using (5.6) gives $R = \{20,000 \times 0.001 \times 1,000 \times 0.1 \times 10 / [(4\pi)^2 \times 31.62 \times 1.38 \times 10^{-23} \times 500 \times 3.981]\}^{1/4} = 109.9$ km ≈ 110 km. The minimum range from (5.26) is $3 \times 10^8 \times 0.001/2 = 150,000$ m = 150 km. Since this is greater than the range calculated, the minimum-range constraint is violated. The maximum range is calculated from (5.28): $R = \{2 \times 20,000 \times 1,000 \times 0.1 \times 10 / [(4\pi)^2 \times 31.62 \times 3 \times 10^8 \times 1.38 \times 10^{-23} \times 500 \times 3.981]\}^{1/3} = 99.06$ km ≈ 99.1 km. The pulse duration giving this range is found from (5.26) as $2 \times 99,060 / (3 \times 10^8) = 0.0006607$ sec ≈ 0.661 ms. The next shorter pulse available is 0.5 ms. The range using this pulse duration is found from (5.6), or scaling from the above result: $R = 109.9 \times (0.5/1.0)^{1/4} = 92.41$ km ≈ 92.4 km.

E.6 Chapter 6 Problems

1. From (6.3), the normalized threshold level is: $\ln(1/10^{-6}) = 13.82$. Thus, the threshold should be 13.8 times the noise level.
2. From (6.5), the false-alarm rate is $10^{-8} \times 2 \times 10^6 = 0.02$ Hz. The average time between false alarms is the reciprocal of this, or 50 sec. It may also be found using (6.6). Rearranging (6.7), $P_{FA} = 0.02 \times 3 \times 10^8 / (2 \times 10,000 \times 2 \times 10^6 \times 500) = 3 \times 10^{-7}$.

3. Using Figure 6.2, the S/N required for Swerling 1 and 2 targets is 21.2 dB, for Swerling 3 and 4 targets is 17.3 dB, and for Swerling 5 (nonfluctuating) targets is 13.2 dB. Using (5.14), the single-pulse S/N may be found by subtracting the number of pulses coherently integrated, converted to decibels (13.0 dB), from the integrated S/N values found above: for Swerling 1, $S/N = 21.2 - 13.0 = 8.2$ dB; for Swerling 3, $17.3 - 13.0 = 4.3$ dB; for Swerling 5, $13.2 - 13.0 = 0.2$ dB.
4. Reading across from $S/N = 10$ dB on Figure 6.4, and taking the next larger integer, gives: Swerling 1, 35 pulses; Swerling 2, 5 pulses; Swerling 3, 9 pulses; Swerling 4, 4 pulses, and Swerling 5, 2 pulses. Using the same procedure with Figure 6.6 for cumulative detection gives: Swerling 2, 9 pulses; Swerling 4, 10 pulses; Swerling 5, 20 pulses.
5. From Figure 6.2, The integrated S/N needed is 31.8 dB. The single-pulse S/N for coherent integration, from (5.14), is $31.8 - 10.0 = 21.8$ dB. For noncoherent integration, the single-pulse S/N multiplied by the number of pulses integrated is found from Figure 6.5 as 18.4 dB. The single-pulse S/N is then $18.4 - 10.0 = 8.4$ dB. The energy savings by using noncoherent integration is $21.8 - 8.4 = 13.4$ dB. For 1,000 pulses integrated, the single-pulse S/N for noncoherent integration is $31.8 - 30.0 = 1.8$ dB. For noncoherent integration, S/N multiplied by the number of pulses is 23.9 dB, and the single-pulse S/N is $23.9 - 30.0 = -6.1$ dB. The energy savings with noncoherent integration is $1.8 - (-6.1) = 7.9$ dB.
6. From Figure 6.2, the integrated S/N needed is 31.8 dB. The single pulse S/N for coherent integration, from (5.14), is $31.8 - 10.0 = 21.8$ dB. For cumulative detection, the single-pulse S/N multiplied by the number of pulses used is found from Figure 6.7 as 21.8 dB. The single-pulse S/N is then $21.8 - 10.0 = 11.8$ dB. The energy savings by using cumulative detection is $21.8 - 11.8 = 10.0$ dB. For 1,000 pulses integrated, the single-pulse S/N for coherent integration is $31.8 - 30.0 = 1.8$ dB. For cumulative detection, S/N multiplied by the number of pulses is 34.6 dB, and the single-pulse S/N is $34.6 - 30.0 = 4.6$ dB. In this case, the energy is less using coherent integration by $4.6 - 1.8 = 2.8$ dB.
7. The integrated S/N needed for detection is found from Figure 6.2 as 17.3 dB. The single-pulse S/N for coherent integration is $17.3 - 20.0 = -2.7$ dB [from (5.14)]. If noncoherent integration of the 100 Swerling 4 pulses is used, the single-pulse S/N is found from Figure 6.4 as -1.2 dB. If noncoherent integration of 10 Swerling 4 pulse groups is used, the S/N multiplied by the number of groups is 15.8 dB, from Figure 6.5. The S/N of each group is $15.8 - 10.0 = 5.8$ dB. The single-pulse S/N of each of the 10 pulses coherently integrated in a group is $5.8 - 10.0 = -4.2$ dB [from (5.14)].
8. From (6.5), $P_{FA} = 1/(10 \times 10^6) = 10^{-7}$. From (6.7), the average false-alarm rate is $2 \times 250 \times 10^3 \times 200/(3 \times 10^8) = 1/3$ Hz ≈ 0.333 Hz.
9. Using Figure 6.2 and reading across from $S/N = 15$ dB: for Swerling 1 and 2 targets, $P_D = 0.65$; for Swerling 3 and 4 targets, $P_D = 0.78$; and for Swerling 5 (nonfluctuating) targets, $P_D = 0.997$.

10. From Figure 6.3, the coherently integrated S/N required is 17.4 dB for $P_{FA} = 10^{-4}$, and 20.3 dB for $P_{FA} = 10^{-8}$. Using (5.14) and converting the number of pulses (100) to decibels (20.0 dB) and solving in decibels, the single-pulse S/N for $P_{FA} = 10^{-4}$ is $17.4 - 20.0 = 2.6$ dB, and for $P_{FA} = 10^{-8}$ it is $20.3 - 20.0 = 0.3$ dB.
11. The values of single-pulse S/N required for noncoherent integration are found from Figure 6.4, and are given in column 2 of Table E.1 for Swerling 2 targets, and in column 5 of the table for Swerling 4 targets. The values of single-pulse S/N required for coherent integration of stable targets (Swerling 1 and 3) are found by subtracting 10.0 dB from the single-pulse S/N for 10 pulses integrated, and subtracting 20.0 dB for 100 pulses integrated. These are given in column 3 of Table E.1 for Swerling 1 targets, and in column 6 for Swerling 3 targets. The loss for noncoherent integration relative to coherent integration is found by subtracting the S/N values (in decibels) for coherent integration in column 3, and 6 from the S/N values for noncoherent integration in columns 2 and 5. The results are given in columns 4 and 7, respectively. Note that in several cases the loss is a negative value in decibels, which implies a gain or improvement with noncoherent integration, relative to coherent integration.
12. The values of single-pulse S/N required for cumulative detection are found from Figure 6.6, and are given in column 2 of Table E.2 for Swerling 2 targets, and in column 5 of the table for Swerling 4 targets. The values of single-pulse S/N required for coherent integration of stable targets (Swerling 1 and 3) are found by subtracting 10.0 dB from the single-pulse S/N for 10 pulses integrated, and subtracting 20.0 dB for 100 pulses integrated. These are given in column 3 of Table E.2 for Swerling 1 targets, and in column 6 for Swerling 3 targets. The loss for cumulative detection relative to coherent integration is found by subtracting the S/N values (in decibels) for coherent integration in column 3, and 6 from the S/N values for cumulative detection in columns 2 and 5. The results are given in columns 4 and 7, respectively. Note that in one case the loss is a negative value in decibels, which implies a gain or improvement with cumulative detection, relative to coherent integration.
13. From Figure 6.5, the S/N multiplied by the number of pulses needed for noncoherently integrating 10 pulses with $P_D = 0.99$ and a Swerling 4 target is 17.5 dB. The single pulse S/N is then $17.5 - 10.0$ (the number of pulses in decibels) = 7.5 dB. From Figure 6.7, the S/N multiplied by the number of pulses needed for cumulative detection using 10 pulses with $P_D = 0.99$ and Swerling 4 target is 21.5 dB. The single pulse S/N is then $21.5 - 10.0 = 11.5$ dB.

Table E.1 Single-Pulse S/N Values and Losses in Decibels for Chapter 6, Problem 11

Number of Pulses	S/N NCI	S/N CI	Loss	S/N NCI	S/N CI	Loss
	SW 2	SW 1		SW 4	SW 3	
1	21.2	21.2	0	17.3	17.3	0
10	6.3	11.2	-4.9	5.8	7.3	-1.5
100	-1.1	1.2	-2.3	-1.2	-2.7	1.5

Table E.2 Single-Pulse S/N Values and Losses in Decibels for Chapter 6, Problem 12

Number of Pulses	S/N CD	S/N CI	Loss	S/N CD	S/N CI	Loss
	SW 2	SW 1		SW 4	SW 3	
1	21.2	21.2	0	17.3	17.3	0
10	9.6	11.2	-1.6	9.8	7.3	2.5
100	5.9	1.2	4.7	6.9	-2.7	9.6

14. The S/N of 10 pulses, each having S/N = 0 dB, is $0 + 10.0 = 10.0$ dB [from (5.14)]. From Figure 6.4, the number of Swerling 3 observations at 10.0 dB each needed is nine. The decorrelated groups may be treated as Swerling 4. From Figure 6.4, five groups are needed if noncoherent integration is used. From Figure 6.6, 10 groups are needed if cumulative detection is used.

E.7 Chapter 7 Problems

- The radar search performance depends primarily on the product of the radar average transmitted power used for search and the receive antenna effective aperture area, the power-aperture product.
- The optimum detection range may be found using (7.3). The average power used in the search is $100 \text{ kW} \times 0.5 = 50 \text{ kW}$, the total losses are $4.0 + 6.5 = 10.5$ dB, and the search solid angle is $90 \times 45 \times (\pi/180)^2 = 1.234$ sr. Converting from decibels to power ratios, the RCS = 0.03162 m^2 , the S/N = 31.62, and the losses = 11.22. The detection range is $[50,000 \times 20 \times 0.03162 / (16\pi \times 2,000 \times 1.234 \times 31.62 \times 1.38 \times 10^{-23} \times 450 \times 11.22)]^{1/3} = 487,200 \text{ m} \approx 487 \text{ km}$. The search time is found from (7.2) as $487.2 / (4 \times 2) = 60.90 \text{ sec} \approx 60.9 \text{ sec}$ (using kilometers for R_d and kilometers per second for V_R). The assured acquisition range from (7.20) is $487.2 \times 0.75 = 365.4 \text{ km} \approx 365 \text{ km}$, and the average acquisition range from (7.21) is $487.2 \times 0.875 = 426.3 \text{ km} \approx 426 \text{ km}$.
- The rotation period is given by $360/20 = 18 \text{ sec}$ [see notation for t_R under (7.4)]. The PRF is found from (7.4), using degrees rather than radians, as $15 \times 360 / (2 \times 18) = 150 \text{ Hz}$. The single-pulse S/N values are found from Figure 6.4 as 12.3 dB (power ratio 16.98), for Swerling 1 and 4.7 dB (power ratio 2.951), for Swerling 2. The detection range is found using (5.6). The pulse energy, $P_p \tau$, is equal to the average power divided by the PRF: $20,000/150 = 133.3 \text{ J}$. Since more than six pulses illuminate the target, there is no scanning loss. The total losses are found by adding the beamshape loss to the fixed loss: $5.0 + 1.6 = 6.6$ dB (power ratio 4.571). For the Swerling 1 target, the range is $\{133.3 \times 316.2 \times 5 \times 13 / [(4\pi)^2 \times 16.98 \times 1.38 \times 10^{-23} \times 550 \times 4.571]\}^{1/4} = 414,300 \text{ m} \approx 414 \text{ km}$. The range for the Swerling 2 target is found with the same equation, using S/N = 2.951. It may easily be found by scaling from the previous result, as $414,300 \times (16.98/2.951)^{1/4} = 641,600 \text{ m} \approx 642 \text{ km}$.
- The average beam-broadening factor is found using the beamwidth integral values from Figure 7.5. For azimuth, it is $50.5/45 = 1.122$. For elevation, it

is $(10.1 + 37.4)/(10 + 35) = 1.056$. The beam-broadening factor is the product of these: $1.122 \times 1.056 = 1.185$. The average scan loss is similarly found. For azimuth, it is $61.3/45 = 1.36$. For elevation, it is $(10.1 + 41.6)/(10 + 35) = 1.149$. The scan loss is the product of these: $1.362 \times 1.149 = 1.565 = 1.945$ dB. The search solid angle is $90 \times 45 = 4,050^\circ = 4,050 \times (\pi/180)^2 = 1.234$ sr. The detection range is found using (7.17), with the S/N power ratio of 6.310 and total losses as 4.00 (fixed) + 2.50 (beamshape) + 1.945 (scan) = 8.445 dB (power ratio 6.990), as $[100,000 \times 20 \times 0.03162 \times 1.185/(16\pi \times 2,000 \times 1.234 \times 10 \times 6.310 \times 1.38 \times 10^{-23} \times 450 \times 6.990 \times 1.2)]^{1/3} = 568,500\text{m} \approx 569$ km. The search time is found using (7.2) as $570,400/(4 \times 2,000) = 71.07$ sec 77.1 sec. The broadside beam solid angle in degrees [from (7.12)], is $1.3^2 \times \pi/4 = 1.327^\circ$. The number of beams is found using (7.11) and (7.15), and the search solid angle in degrees², as $1.2 \times 4,050/(1.327 \times 1.185) = 3,091 \approx 3,090$. The number of pulses per second is then $3,091 \times 10/71.07 = 434.9$. The pulse duration is found by dividing the radar duty cycle by the number of pulses per second, as $0.2/434.9 = 0.0004599$ sec ≈ 0.460 ms. The minimum range, from (5.26), is 68,980m. This is less than the detection range, so the minimum range constraint is not violated.

5. The number of pulses used in search is the PRF multiplied by the search time: $100 \times 10 = 1,000$. The single-pulse S/N is found from Figure 6.5 by dividing the S/N multiplied by the number of pulses (23.9 dB) by the number of pulses (1,000 converts to 30 dB), as $23.9 - 30 = -6.1$ dB (power ratio 0.2455). Initially assume no beamshape loss, so the losses are 4.5 dB (power ratio 2.818). The detection range is calculated using (7.24), as $\{25,000 \times 10 \times 10^4 \times 10^{-2} \times 2.5/[(4\pi)^2 \times 1,000 \times 0.2455 \times 1.38 \times 10^{-23} \times 500 \times 2.818]\}^{1/4} = 536,600\text{m}$. The approximate radar beamwidth is found from (3.12) as $(10.75/10^4)^{1/2} = 0.03279$ rad ≈ 32.8 mrad $= 1.88^\circ$. The beamshape loss is calculated from (7.26) as $\cos^{-1.3} [2.2 \times 5/(536.6 \times 0.03279)] = 1.313 = 1.184$ dB. Increasing the losses by 1.84 dB in the above calculation reduces the detection range to 501.3 km ≈ 501 km. Further iteration will produce negligible change in the detection range. The width of the beam at the detection range is $501,300 \times 0.03279 = 16,440\text{m} \approx 16.4$ km. This is larger than twice the search radius, so single-beam search is valid.
6. The average beam-broadening factor is found using the beamwidth integral values from Figure 7.5. For azimuth, it is $43.7/40 = 1.093$. For elevation, the beam-broadening from (3.20) is $\cos^{-1}(15^\circ) = 1.035$. The beam-broadening factor is the product of these: $1.093 \times 1.035 = 1.131$. The average scan loss is similarly found. For azimuth, it is $50.6/40 = 1.265$. For elevation, the scan loss from (3.21) is $\cos^{-2.5}(15^\circ) = 1.091$. The scan loss is $1.265 \times 1.091 = 1.380 = 1.399$ dB. The single-pulse S/N needed for detection is found from Figure 6.6 as 11.6 dB (power ratio 14.45). The total losses are 5.0 (fixed) + 2.5 (beamshape) + 1.399 (scan) + 1.5 (propagation) = 10.399 dB (power ratio 10.96). The azimuth search angle is $80^\circ = 80 \times \pi/180 = 1.396$ rad. The detection range is calculated from (7.39), setting $R_H = R_D$, as $[40,000 \times 10 \times$

$1 \times 1.131 / (4\pi \times 1.396 \times 1,500 \times 5 \times 14.45 \times 1.38 \times 10^{-23} \times 400 \times 10.96 \times 1.2)]^{1/3} = 1,485,000\text{m} \approx 1,490\text{ km}$. The elevation beamwidth for search = $32 \times 1.035 = 33.12\text{ mrad}$. The search time is found from (7.37), assuming the search uses a single row of beams, as $1,483 \times 0.03312 / 1.5 = 32.74\text{ sec} \approx 32.7\text{ sec}$. The average azimuth beamwidth is $32 \times 1.093 = 34.98\text{ mrad}$. The number of beam positions searched, using a single row of beams, is found using (7.41) and (7.38) as $1.2 \times 1.396 / 0.03498 = 47.89$, which rounds up to 48. The total number of pulses is $48 \times 5 = 240$, and the number of pulses per second is $240 / 32.74 = 7.330$. The pulse duration is $0.05 / 7.330 = 0.006821\text{ sec}$, and the minimum range from (5.26) is $3 \times 10^8 \times 0.006821 / 2 = 1,023,000\text{m} = 1,023\text{ km}$. This is less than the detection range, so the minimum-range constraint is not violated.

7. Horizon search is a special case of barrier search.
8. The search solid angle is approximately $30^\circ \times 60^\circ = 1,800^\circ$. The value in steradians is found by multiplying this by $(\pi/180)^2$, as 0.5483 sr . To find the average azimuth scan loss, the integrated value for FFOV scan loss is read from Figure 7.5 for 30° as 33.9. The scan loss is then $33.9 / 30 = 1.130$ or 0.5308 dB . The elevation scan, relative to array broadside, is from -10° to $+20^\circ$. The corresponding integral values are read from Figure 7.5 as 10.1 and 21.1, respectively. The elevation scan loss is calculated as $(10.1 + 21.1) / (10 + 20) = 1.040$ or 0.1703 dB . The total scan loss is the sum of these losses (in decibels): 0.7011 dB . The S/N required by the detection parameters is found from Figure 6.2 as 17.3 dB (power ratio 53.70). The total losses are 5.0 (fixed) + 2.0 (propagation) + 2.5 (beamshape) + 0.7011 (scan) = 10.20 dB (power ratio 10.47). The detection range is calculated using (7.1) as $[10,000 \times 9 \times 50 \times 1 / (4\pi \times 0.5483 \times 53.70 \times 1.38 \times 10^{-23} \times 500 \times 10.47)]^{1/4} = 640,600\text{m} \approx 641\text{ km}$. The optimum radial velocity is found using (7.2), as $640,600 / (4 \times 50) = 3,203\text{ m/s} \approx 3.20\text{ km/s}$.
9. The average beam-broadening factor is found using the beamwidth integral values from Figure 7.5. For azimuth, it is $31.5 / 30 = 1.050$. For elevation, it is $(10.1 + 20.4) / (10 + 20) = 1.017$. The beam-broadening factor is the product of these: $1.050 \times 1.017 = 1.068$. The single-pulse S/N is found from Figure 6.4 as 5.8 dB (power ratio 3.802). The detection range is calculated using (7.17) as $[10,000 \times 9 \times 1 \times 1.068 / (16\pi \times 2,000 \times 0.5483 \times 10 \times 3.802 \times 1.38 \times 10^{-23} \times 500 \times 10.47 \times 1.2)]^{1/3} = 808,800\text{m} \approx 809\text{ km}$. The average beam solid angle is given by $1.068 \times 1.25^2 \times \pi / 4 = 1.311^\circ$. The number of beams is found using (7.11) as $1.2 \times 1,800 / 1.311 = 1,648 \approx 1,650$. The search time, from (7.2), is $808,800 / (4 \times 2,000) = 101.1\text{ sec}$. The number of pulses per second is $10 \times 1,648 / 101.1 = 163.0$. The pulse duration is $0.2 / 163.0 = 0.001227\text{ sec} \approx 1.23\text{ ms}$. The minimum range from (5.26) is $3 \times 10^8 \times 0.001227 / 2 = 184,100\text{m} \approx 184\text{ km}$. The assured acquisition range from (7.20) is $0.75 \times 808.8\text{ km} = 606.6\text{ km} \approx 607\text{ km}$. The average acquisition range from (7.21) is $0.875 \times 808.8\text{ km} = 707.7\text{ km} \approx 708\text{ km}$.
10. The number of pulses illuminating the target is found using (7.4) as $1.5 \times 12 \times 250 / 360 = 12.50$. Since more than six pulses illuminate the target, there is

no scanning loss. The S/N needed for a single pulse is found from Figure 6.4 as 17.3 dB. For 12 pulses (converted to 10.79 dB), coherently integrated, the S/N is $17.3 - 10.79 = 6.51$ dB (power ratio 4.477). For noncoherent integration of 12 pulses, the S/N, found from Figure 6.4, is 9.1 dB (power ratio 8.128). The ranges are found using (5.11), with no scan loss or propagation loss, and 1.6 dB (power ratio 1.445) beamshape loss. For coherent integration, the range in kilometers is $100 \times [31.62/(4.477 \times 1.445)]^{1/4} = 148.7 \text{ km} \approx 149 \text{ km}$. For noncoherent integration, the range in kilometers is $100 \times [31.62/(8.128 \times 1.445)]^{1/4} = 128.1 \text{ km} \approx 128 \text{ km}$.

11. The required S/N for a single pulse is found from Figure 6.2 as 17.3 dB. The single-pulse S/N for coherent integration of ten pulses is then $17.3 - 10 = 7.3$ dB (power ratio 5.370). The beam solid angle is $0.01^2 \times \pi/4 = 0.00007854$ sr. Combining (7.30) and (7.31), with no scan or propagation loss, and 2.5 dB (power ratio 1.778) beamshape loss, the detection range (in kilometers) is $[1,000^4 \times 0.2 \times 10 \times 0.1 \times 31.62 \times 0.00007854 / (0.01 \times 1 \times \pi \times 1.2 \times 25^2 \times 10 \times 5.370 \times 1.778)]^{1/2} = 469.9 \text{ km} \approx 470 \text{ km}$. The number of beam positions is found using (7.31) as $\pi \times 1.2 \times 25^2 / (469.9^2 \times 0.00007854) = 135.9 \approx 136$. Rounding up to 136 beam positions, the number of pulses per second is $10 \times 136/10 = 136$. The pulse duration is then $0.2/136 = 0.001471$ sec. The minimum range from (5.26) is $3 \times 10^8 \times 0.001471/2 = 220,700 \text{ m} \approx 221 \text{ km}$.
12. The radar beamwidth in radians is $2.0 \times \pi/180 = 0.03491$ rad. The azimuth acceleration-limited maximum azimuth coverage is found using (7.46) as $0.03491^2 \times 500^2 \times 2 / (8 \times 1.5^2) = 33.85^\circ$. (The units are consistent here since square kilometers is used in the numerator, kilometers per second squared is used in the denominator, and angular acceleration in the numerator is given in degrees per second squared.) The azimuth velocity from (7.47) is $0.03491 \times 500 \times 2 / (4 \times 1.5) = 5.818^\circ/\text{s}$, which is within the antenna capability, so the azimuth coverage calculated above is valid. The azimuth velocity for an azimuth coverage of 25° is calculated using (7.48) as $[0.035 \times 500 \times 2 / (4 \times 1.5)] - \{[0.035^2 \times 500^2 \times 2^2 / (16 \times 1.5^2)] - [25 \times 2/2]\}^{1/2} = 2.828^\circ/\text{s}$. The number of pulses illuminating the target is found from (7.49) as $2 \times 100/2.828 = 70.72$, which rounds up to 71. The single-pulse S/N is found from Figure 6.4 as 8.1 dB.

E.8 Chapter 8 Problems

1. A target need be resolved in only one dimension to allow measurements on it.
2. The standard deviation ($1\text{-}\sigma$), of the S/N-dependent range error is found using (8.6), as $15/(2 \times 63.10)^{1/2} = 1.335 \text{ m}$. The standard deviation of the absolute range error is found using (8.5) as $(1.335^2 + 1^2 + 5^2)^{1/2} = 5.271 \text{ m} \approx 5.27 \text{ m}$. The relative range error is found by omitting the bias term from the calculation as $(1.335^2 + 1^2)^{1/2} = 1.668 \text{ m} \approx 1.67 \text{ m}$. The $3\text{-}\sigma$ values of the absolute and relative errors are $3 \times 5.271 = 15.81 \text{ m} \approx 15.8 \text{ m}$, and 3×1.668

- $= 5.004\text{m} \approx 5.00\text{m}$, respectively. The $3\text{-}\sigma$ range error using smoothing is found using (8.29) as $3 \times (1.335^2/50 + 1^2/50 + 5^2)^{1/2} = 15.02\text{m} \approx 15.0\text{m}$.
3. The S/N-dependent random error on broadside is found using (8.8) as $2.5/[1.6 \times (2 \times 15.85)^{1/2}] = 0.2775^\circ = 4.844 \text{ mrad}$. The broadside angular measurement error is found using (8.7) as $(4.844^2 + 2^2 + 1^2 + 3^2 + 1.5^2)^{1/2} = 6.302 \text{ mrad} \approx 6.30 \text{ mrad}$. At 30-degree scan angle, the beamwidth, from (8.9), is $2.5/\cos(30^\circ) = 2.887^\circ$, and the S/N-dependent random angle error is $2.887/[1.6 \times (2 \times 15.85)^{1/2}] = 0.3205^\circ = 5.593 \text{ mrad}$. The combined fixed random error is the rss of the nonscan-dependent and scan-dependent errors, $\{2^2 + [1/\cos(30^\circ)^2]\}^{1/2} = 2.309 \text{ mrad}$, and the combined angle bias error is $\{3^2 + [1.5/\cos(30^\circ)^2]\}^{1/2} = 3.464 \text{ mrad}$. The angular measurement error from (8.7) is $(5.593^2 + 2.309^2 + 3.464^2)^{1/2} = 6.972 \text{ mrad} \approx 6.97 \text{ mrad}$. The cross-range measurement errors are found using (8.10), as $150,000 \times 0.006302 = 945.3\text{m} \approx 945\text{m}$, and $150,000 \times 0.006972 = 1,046\text{m} \approx 1,050\text{m}$, for broadside and 30-degree scan, respectively.
 4. The wavelength is $3 \times 10^8/(9.5 \times 10^9) = 0.03158\text{m}$. The Doppler-frequency radial-velocity measurement error, from (8.13), is $0.03158/[2 \times 0.001 \times (2 \times 31.62)^{1/2}] = 1.986 \text{ m/s} \approx 1.99 \text{ m/s}$. The compressed pulse duration is $0.001/1,000 = 10^{-6} \text{ sec}$, and the range resolution is $3 \times 10^8 \times 10^{-6}/2 = 150\text{m}$. The range-measurement error (neglecting fixed random and bias components), is found from (8.6) as $150/(2 \times 31.62)^{1/2} = 18.86\text{m}$. The noncoherent radial-velocity measurement error is found using (8.15) as $2^{1/2} \times 18.86/0.02 = 1,334 \text{ m/s} \approx 1,330 \text{ m/s}$.
 5. The S/N-dependent RCS measurement error is found using (8.20) as $2^{1/2} \times 10/(63.10)^{1/2} = 1.780 \text{ m}^2$. Combining with the fixed random error, using (8.19), gives $[1.780^2 + (0.05 \times 10)^2]^{1/2} = 1.849 \text{ m}^2 \approx 1.85 \text{ m}^2$. The rain attenuation will cause an error of $10 \times (10^{(2/10)} - 1) = 5.849 \text{ m}^2 \approx 5.85 \text{ m}^2$. The overall RCS measurement error, from (8.19), is $[1.780^2 + (0.05 \times 10)^2 + 5.849^2]^{1/2} = 6.134 \text{ m}^2 \approx 6.13 \text{ m}^2$. The S/N-dependent error corresponds to $2^{1/2}/(63.10)^{1/2} = 17.80\%$ of the RCS being measured, and the bias error corresponds to $(10^{(2/10)} - 1) = 58.49\%$ of the RCS being measured. Thus, the overall error may be calculated by $10 \text{ m}^2 \times [(17.80^2 + 5^2 + 58.49^2)^{1/2}] \% = 10 \text{ m}^2 \times 61.34\% \approx 6.13 \text{ m}^2$.
 6. The single-pulse range error from (8.6) is $15/(2 \times 15.85)^{1/2} = 2.664\text{m}$. The radial velocity error from (8.16) is $12^{1/2} \times 2.664/(20^{1/2} \times 10) = 0.2064 \text{ m/s} \approx 0.206 \text{ m/s}$. The single-pulse angle error from (8.8) is $1.5/[1.6 (2 \times 15.8)^{1/2}] = 0.1665^\circ = 2.906 \text{ mrad}$. The cross-range velocity error from (8.18) is $12^{1/2} \times 200,000 \times 0.002906/(20^{1/2} \times 10) = 45.02 \text{ m/s} \approx 45.0 \text{ m/s}$. The smoothed range and angle errors, from (8.29) and (8.30) are $2.664/20^{1/2} = 0.5957\text{m} \approx 0.596\text{m}$, and $2.906/20^{1/2} = 0.6498 \text{ mrad} \approx 0.650 \text{ mrad}$, respectively. The error in predicted range position is found from (8.31) as $[0.5957^2 + (0.2064 \times 50)^2]^{1/2} = 10.34\text{m} \approx 10.3\text{m}$. The error in predicted cross-range position is found from (8.32) as $[(200,000 \times 0.0006498)^2 + (45.02 \times 50)^2]^{1/2} = 2,255\text{m} \approx 2.26 \text{ km}$.
 7. The $2\text{-}\sigma$ error bound should be used.

8. a. From (8.6), the $1\text{-}\sigma$ S/N-dependent range error is $3 \times 10^8 / [2 \times 10^7 \times (2 \times 15.85)^{1/2}] = 2.664\text{m}$. Using (8.5), the $1\text{-}\sigma$ absolute range error is $(2.664^2 + 2^2 + 10^2)^{1/2} = 10.54\text{m}$. The $3\text{-}\sigma$ value is then $3 \times 10.54 = 31.62\text{m} \approx 31.6\text{m}$. The $3\text{-}\sigma$ relative range error is found by omitting the bias term when using (8.5) as $3 \times (2.664^2 + 2^2)^{1/2} = 9.994\text{m} \approx 9.99\text{m}$. The $1\text{-}\sigma$ S/N-dependent angle error, from (8.8), is $2/[1.6 \times (2 \times 15.85)^{1/2}] = 0.2220^\circ = 3.875\text{ mrad}$. Using (8.7), the $3\text{-}\sigma$ absolute angle error is $3 \times (3.875^2 + 1^2 + 1.5^2)^{1/2} = 12.82\text{ mrad} \approx 12.8\text{ mrad}$. The $3\text{-}\sigma$ relative angle error is found by omitting the bias term when using (8.8) as $3 \times (3.875^2 + 1^2)^{1/2} = 12.01\text{ mrad} \approx 12.0\text{ mrad}$. The signal wavelength is $3 \times 10^8 / (9.5 \times 10^9) = 0.03158\text{m}$. The $1\text{-}\sigma$ S/N-dependent Doppler frequency radial-velocity error, from (8.13), is $0.03158 / [2 \times 0.01 (2 \times 15.85)^{1/2}] = 0.2804\text{ m/s}$. Using (8.12), the $3\text{-}\sigma$ absolute radial-velocity error is $3 \times (0.2804^2 + 0.2^2 + 0.1^2)^{1/2} = 1.076\text{ m/s} \approx 1.08\text{ m/s}$. The $3\text{-}\sigma$ relative radial-velocity error is found by omitting the bias term when using (8.12) as $3 \times (0.2804^2 + 0.2^2)^{1/2} = 1.033\text{ m/s} \approx 1.03\text{ m/s}$.
- b. The error in cross-range is found by analogy with (8.10). Using the angle-measurement errors calculated above, the absolute error is $500 \times 0.01282 = 6.410\text{ km} \approx 6.41\text{ km}$, and the relative error is $500 \times 0.01201 = 6.005\text{ km} \approx 6.01\text{ km}$.
- c. Using the above result for S/N-dependent range error, and (8.29), the $3\text{-}\sigma$ absolute range error is $3 \times (2.664^2/10 + 2^2/10 + 10^2)^{1/2} = 30.17\text{m} \approx 30.2\text{m}$. The relative range error is found by omitting the bias error term in (8.29) as $3 \times (2.664^2/10 + 2^2/10) = 3.160\text{m} \approx 3.16\text{m}$. Using the above result for S/N-dependent angle error, and (8.30), the $3\text{-}\sigma$ absolute angle error is $3 \times (3.875^2/10 + 1^2/10 + 1.5^2)^{1/2} = 5.888\text{ mrad} \approx 5.89\text{ mrad}$. The relative angle error is found by omitting the bias error term in (8.30) as $3 \times (3.875^2/10 + 1^2/10)^{1/2} = 3.797\text{ mrad} \approx 3.80\text{ mrad}$.
- d. The measurement period is $10\text{ pulses}/5\text{ Hz} = 2\text{ sec}$. The radial velocity error is found using (8.16) and the relative $3\text{-}\sigma$ range error calculated above, as $12^{1/2} \times 9.994 / (10^{1/2} \times 2) = 5.474\text{ m/s} \approx 5.47\text{ m/s}$. The cross-range velocity error is found using (8.18), and the relative $3\text{-}\sigma$ angle error calculated above, as $500,000 \times 12^{1/2} \times 0.01201 / (10^{1/2} \times 2) = 3,289\text{ m/s} \approx 3.29\text{ km/s}$.
9. The beamwidth at a scan angle of 45° is found from (8.9) as $1/\cos(45^\circ) = 1.414^\circ = 24.68\text{ mrad}$. The S/N-dependent random angle error is found from (8.8) as $24.68/[1.6 \times (2 \times 31.62)^{1/2}] = 1.940\text{ mrad}$. The scan-dependent fixed random error is $0.3/\cos(45^\circ) = 0.4243\text{ mrad}$ (see Section 8.2). The fixed random measurement error is the rss of this and the nonscan-dependent error: $(0.4243^2 + 0.2^2)^{1/2} = 0.4690\text{mrad}$. The scan-dependent bias error is $0.2/\cos(45^\circ) = 0.2828\text{ mrad}$. The bias error is the rss of this and the nonscan-dependent bias error: $(0.2828^2 + 0.1^2)^{1/2} = 0.3000\text{mrad}$. The $1\text{-}\sigma$ absolute angle error is found from (8.7) as $(1.940^2 + 0.4691^2 + 0.3000^2)^{1/2} = 2.018\text{ mrad} \approx 2.02\text{ mrad}$.
10. The relative range-measurement error from (8.5) and (8.6) for $\text{S/N} = 20\text{ dB}$ (power ratio 100) is $\{[0.5/(2 \times 100)^{1/2}]^2 + 0.1^2\}^{1/2} = 0.1061\text{m}$. The radial length measurement error may be calculated using (8.22) or (8.23) as $2^{1/2} \times$

$0.1061 = 0.1500\text{m} \approx 0.150\text{m}$. If the S/N is 12 dB, the radial length error is $2^{1/2} \times \{[0.5/(2 \times 15.85)^{1/2}]^2 + 0.1^2\}^{1/2} = 0.1891\text{m} \approx 0.189\text{m}$.

11. For identical radar, the maximum measurement errors will be determined by the radars having the lowest S/N, 12 dB in this case. The range measurement error from (8.5) and (8.6) is $\{[20/(2 \times 15.85)^{1/2}]^2 + 1^2 + 1.5^2\}^{1/2} = 3.984\text{m}$. The $3\text{-}\sigma$ position error is found using (8.27) as $3 \times 3.984/\sin(45^\circ) = 16.90\text{m} \approx 16.9\text{m}$. The radial-velocity measurement error from (8.12) and (8.13) is $\{[10/(2 \times 15.85)^{1/2}]^2 + 0.5^2 + 0.7^2\}^{1/2} = 1.973\text{ m/s}$. The $3\text{-}\sigma$ velocity error is found using (8.28) as $3 \times 1.973/\sin(45^\circ) = 8.371\text{ m/s} \approx 8.37\text{ m/s}$.
12. The largest error semi-axis of the prediction error is determined by the larger angular measurement error, which is produced by the larger beamwidth. This is calculated using (8.8) (neglecting fixed random and bias errors) as $3/[1.6 \times (2 \times 15.85)^{1/2}] = 0.3330^\circ = 5.812\text{ mrad}$. The $3\text{-}\sigma$ prediction error is found using (8.33), with the number of pulses equal to $10 \times 5 = 50$, as $3 \times 12^{1/2} \times 500 \times 0.005812 \times 150/(50^{1/2} \times 10) = 64.06\text{ km} \approx 64.1\text{ km}$.

E.9 Chapter 9 Problems

1. The clutter area limited by radar resolution is found from (9.1) as $50,000 \times 2 \times (\pi/180) \times 150/\cos(15^\circ) = 271,000\text{ m}^2$. The clutter area limited by elevation beamwidth is found from (9.2) as $50,000 \times (2 \times \pi/180)^2/\sin(15^\circ) = 11,770,000\text{ m}^2 \approx 11,800,000\text{ m}^2$. The clutter area is limited by the range resolution so the first result should be used. The clutter RCS is found using (9.3) and a beamshape loss, L_{BS} , of 1.6 dB (power ratio 1.445), as $10^{-3} \times 271,000/1.445 = 187.4\text{ m}^2 \approx 187\text{ m}^2$. The S/C is found, using (9.7), as $10 \times 100/187.4 = 5.336 = 7.272\text{ dB} \approx 5.34$ or 7.27 dB .
2. The radar wavelength is $3 \times 10^8/(3.3 \times 10^9) = 0.09091\text{m}$. The minimum elevation to achieve the free-space return is found, using (9.12), as $0.09091/(12 \times 20) = 0.0003788\text{ rad} \approx 0.379\text{ mrad}$. The separation of the lobes in elevation is found, using (9.11), as $0.09091/(2 \times 20) = 0.002272\text{ rad} \approx 2.27\text{ mrad}$.
3. Precipitation effects are more pronounced at higher radar frequencies. They may usually be ignored at frequencies below about 1 GHz.
4. The rain climate designation for a tropical wet climate is found in Table 9.3 to be region H. The percentage of the year corresponding to 1 hour is $100 \times 1/(24 \times 365) = 0.0001142 \approx 0.0114\%$. The corresponding surface rainfall rate is found from curve H in Figure 9.3 as 140 mm/hr. From curve H in Figure 9.3, the percent of the year that the 16 mm/hr rate is exceeded is 0.45%. This corresponds to $0.45 \times 24 \times 365/100 = 39.42\text{ hr} \approx 39.4\text{ hr}$. The attenuation per kilometer for 5 GHz and 16 mm/hr is found from Table 9.2 as 0.086 dB/km.
5. The rain clutter volume reflectivity is found from (9.15), using the wavelength of $3 \times 10^8/(9.5 \times 10^9) = 0.03158\text{m}$, as $6 \times 10^{-14} \times 10^{1.6}/0.03158^4 = 2.402 \times 10^{-6}\text{ m}^2/\text{m}^3 \approx 2.04 \times 10^{-6}\text{ m}^{-1}$. The range resolution is $3 \times 10^8/(2 \times 10$

- $\times 10^6 = 15\text{m}$ (see Section 4.3). The rain clutter volume is found using (9.14), and converting the beamwidths to radians, as $50,000^2 \times (1 \times \pi/180) \times (3 \times \pi/180) \times 15 = 3.427 \times 10^7 \text{ m}^3$. The rain clutter RCS is found using (9.16), with $L_{BS} = 3.2 \text{ dB}$ (power ratio 2.089), as $2.402 \times 10^{-6} \times 3.427 \times 10^7 / 2.089 = 39.40 \text{ m}^2 \approx 39.4 \text{ m}^2$.
6. At this target range and elevation angle, the target is above the troposphere, so the two-way tropospheric attenuation may be found from Figure 9.4 as 1.3 dB. The two-way lens loss is found from Table 9.6, by interpolation, as $0.31 - (5 - 4) \times (0.31 - 0.10) / (8 - 4) = 0.2575 \text{ dB}$. The total atmospheric loss is the sum of these (in decibels): $1.3 + 0.2575 = 1.558 \text{ dB} \approx 1.56 \text{ dB}$. The elevation angle in milliradians is $1000 \times 5 \times \pi/180 = 87.27 \text{ mrad}$. The elevation and range measurement errors are found from Table 9.7, using interpolation, as $4.0 - (87.27 - 65) \times (4.0 - 2.9) / (100 - 65) = 3.300 \text{ mrad} \approx 3.30 \text{ mrad}$, and $30 - (87.27 - 65) \times (30 - 22) / (100 - 65) = 24.91\text{m} \approx 24.9\text{m}$, respectively.
 7. The daytime ionospheric attenuation is found from Table 9.8 as 1.2 dB. The nighttime attenuation is less than 0.1 dB (see Section 9.4). The normal daytime elevation error is found by scaling with f^2 from the data in Figure 9.5, as $1.3 \times (100/200)^{-2} = 5.200 \text{ mrad} \approx 5.20 \text{ mrad}$. The normal daytime range error is found by scaling with f^2 from the data in Figure 9.6, as $550 \times (100/200)^{-2} = 2,200\text{m} \approx 2.20 \text{ km}$. The nighttime errors are approximately one-third of the daytime values, or 1.73 mrad and 733m (see Section 9.4).
 8. Assuming that the range extent of the clutter is determined by the range resolution, use (9.1) to calculate the clutter area: $100,000 \times 1 \times (\pi/180) \times 15 / \cos(5^\circ) = 26,280 \text{ m}^2 \approx 26,300 \text{ m}^2$. The transition grazing angle is found using the conditions for (9.1) and (9.2): $\tan^{-1}(100,000 \times 1 \times (\pi/180) / 15) = 89.51^\circ \approx 89.5^\circ$. The clutter area is determined by the elevation beamwidth at grazing angles greater than this value. Using (9.3), with $\sigma^0 = -25 \text{ dB}$ (power ratio 0.003162), and $L_{BS} = 1.6 \text{ dB}$ (power ratio 1.445), the clutter RCS is $0.003162 \times 26,280 / 1.445 = 57.51 \text{ m}^2 \approx 57.5 \text{ m}^2$. The S/C is found using (9.7) as $1/57.51 = 0.01739 = -17.60 \text{ dB} \approx 0.0174$ or -17.6 dB . Rearranging (9.7), the clutter cancellation needed is found as $31.62 \times 57.51 / 1 = 1,818 = 32.60 \text{ dB} \approx 1,820$ or 32.6 dB .
 9. The rainfall attenuation coefficient is found in Table 9.2 as 0.13 dB/km. Using (9.2), the two-way loss is calculated as $0.13 \times 20 = 2.60 \text{ dB}$. The exceedance percentage for region D2 is found from Figure 9.3 as 0.6%.
 10. The rain clutter volume is found, using (9.14), as $200,000^2 \times (1.5 \times \pi/180)^2 \times 150 = 4.112 \times 10^9 \text{ m}^3 \approx 4.11 \times 10^9 \text{ m}^3$. The rain clutter reflectivity is found from (9.15), using the wavelength of $3 \times 10^8 / (3.3 \times 10^9) = 0.09091\text{m}$, as $6 \times 10^{-14} \times 4^{1.6} / 0.09091^4 = 8.072 \times 10^{-9} \text{ m}^{-1} \approx 8.07 \times 10^{-9} \text{ m}^{-1}$. The rain clutter RCS is found using (9.16), with $L_{BS} = 3.2 \text{ dB}$ (power ratio 2.089), as $8.072 \times 10^{-9} \times 4.112 \times 10^9 / 2.089 = 15.89 \text{ m}^2 = 12.01 \text{ dBsm} \approx 15.9 \text{ m}^2$ or 12.0 dBsm . The S/C is calculated using (9.17), and adding decibels directly, as $-5 + 30 - (12.01 + 3) = 9.99 \text{ dB}$.

11. The signal path traverses the entire troposphere. The two-way tropospheric loss is found from Figure 9.4 as 1.6 dB. The target slant range is approximately $100/\sin(2^\circ) = 2,865$ km. The lens loss is found from Table 9.6 as approximately 0.8 dB. The total atmospheric loss is the sum of these in decibels: $1.6 + 0.8 = 2.4$ dB. The elevation angle in milliradians is $2 \times 1,000 \times \pi/180 = 34.91$ mrad. The elevation angle error and range error are found by interpolation from the data in Table 9.7, as $6.5 - (34.91 - 30) \times (6.5 - 3.5)/(65 - 30) = 6.079$ mrad ≈ 6.08 mrad, and $52 - (34.91 - 30) \times (52 - 30)/(65 - 30) = 48.39$ m ≈ 48.4 m. The errors corrected to 10% are $6.079 \times 0.1 = 0.6079$ mrad ≈ 0.608 mrad, and $48.39 \times 0.1 = 4.839$ m ≈ 4.84 m.
12. Ionospheric effects are greater at lower frequencies, particularly in the VHF and UHF bands. They may usually be ignored at frequencies greater than 1 GHz.
13. The daytime ionospheric loss is found from Table 9.8 as 0.2 dB. From Table 9.9, the polarization rotation is between $1,800$ and 560° , so it is a problem for linear polarization. The maximum signal bandwidth supported by the ionosphere is found from Table 9.10 as 2.6 MHz. The elevation angle and range errors for a frequency of 200 MHz are found from Figures 9.5 and 9.6, respectively, as 2.3 mrad and 800 m. Scaling inversely with the square of frequency gives $2.3 \times (300/200)^{-2} = 1.022$ mrad ≈ 1.02 mrad, and $800 \times (300/200)^{-2} = 355.5$ m ≈ 356 m. Nighttime errors would be about one-third of these values, and daytime errors for disturbed conditions would be about three times these values.

E.10 Chapter 10 Problems

1. Barrage noise jammers are usually used to mask targets, while pulsed jammers are usually used to create confusion, as discussed in Section 10.1 and shown in Table 10.1.
2. Using Figure 10.6, enter the plot at 0.01 (1%), on the x axis, proceed vertically to the line for $K = 4$, and then horizontally to the y axis. The y -axis value gives the probability of false acceptance as about 0.05 or 5%. The real target will be declared as such 99% of the time, and $80 \times 0.05 = 4$ decoys will be declared to be real targets. Thus, the total number of objects declared to be real targets is $0.99 + 4 = 4.99$, or about 5.
3. The jammer ERP is found using (10.2) as $5,000 \times 100/1.122 = 445,600$ W ≈ 446 kW. If the power radiated on each polarization is one-half the total, the polarization loss is a power ratio of 2, or 3 dB, and the ERP per polarization is 445.6 kW/2 = 222.8 kW ≈ 223 kW.
4. The waveform duration is found using (4.7) as $10^3/10^6 = 0.001$ sec = 1 ms. The value of S/J may be found using either (10.3) or (10.4). Using the latter, jammer bandwidth of 1 MHz, and 3 dB polarization loss, and converting values in decibels to power ratios, it is found as $100,000 \times 15,850 \times 3 \times 10^3 \times 10^6 \times 2/(4\pi \times 350,000^2 \times 10^6 \times 1.513 \times 60) = 0.06805 = -11.67$ dB ≈ 0.0681 or 11.7 dB. If the jammer matches the agile frequency band, its

bandwidth is 300 MHz. The S/J may be found by replacing 10^6 in the numerator above by 300×10^6 , giving a result of $300 \times 0.06805 = 20.42 = 13.10 \text{ dB} \approx 20.4$ or 13.1 dB .

5. For isotropic sidelobes, the sidelobe level is the inverse of the gain (see Section 3.2). The S/(J + N) is found using (10.13), with $\text{SL} = -30 \text{ dB}$, $L_{\text{POL}} = 1$, and $\text{SLC} = 1$, and converting values in decibels to power ratios, as $\{10,000 \times 0.001 \times 10^3 \times 10 \times 2 / [(4\pi)^2 \times 250,000^4 \times 1.413 \times 1.318] \} / \{ [10^5 \times 2 \times 10^{-3} / (4\pi \times 350,000^2 \times 0.5 \times 10^9 \times 1.318)] + 1.38 \times 10^{-23} \times 450 \} = 1.741 \times 10^{-19} / (1.972 \times 10^{-19} + 6.210 \times 10^{-21}) = 0.8559 = -0.6757 \text{ dB} \approx 0.856$ or -0.676 dB . Using the same equation with $\text{SLC} = 20 \text{ dB}$ (power ratio 100) gives $\{10,000 \times 0.001 \times 10^3 \times 10 \times 2 / [(4\pi)^2 \times 250,000^4 \times 1.413 \times 1.318] \} / \{ [10^5 \times 2 \times 10^3 / (4\pi \times 350,000^2 \times 0.5 \times 10^9 \times 1.318 \times 100)] + 1.38 \times 10^{-23} \times 450 \} = 1.741 \times 10^{-19} / (1.972 \times 10^{-21} + 6.210 \times 10^{-21}) = 21.28 = 13.28 \text{ dB} \approx 21.3$ or 13.3 dB . The S/(J + N) without jamming may be found using the same equation with $\text{ERP} = 0$, as $1.714 \times 10^{-19} / 6.210 \times 10^{-21} = 28.03 = 14.48 \text{ dB} \approx 28.0$ or 14.5 dB .
6. The chaff total RCS is found using (10.21). The weight in kilograms is $20 \times 0.4536 = 9.072 \text{ kg}$ (see Table D.1 in Appendix D), and the wavelength is $3 \times 10^8 / 9.5 \times 10^9 = 0.03158 \text{ m}$. The total chaff RCS from (10.21) is $22,000 \times 0.03158 \times 9.072 = 6,303 \text{ m}^2 \approx 6,300 \text{ m}^2$. The total chaff volume is $(4/3) \times \pi \times (5,000/2)^3 = 6.545 \times 10^{10} \text{ m}^3 \approx 6.55 \times 10^{10} \text{ m}^3$. The cross-range dimension of the beam at 500 km range is $2 \times (\pi/180) \times 500,000 = 17,450 \text{ m} = 17.45 \text{ km}$, which is significantly larger than the chaff cloud dimension. The chaff scattering volume is calculated with (10.22), using the chaff cloud dimension for D_A and D_E as $5,000^2 \times 150 = 3.750 \times 10^9 \text{ m}^2$. The S/C is calculated using the second expression in (10.25), as $1 \times (4/\pi) \times 6.545 \times 10^{10} / (6,303 \times 3.750 \times 10^9) = 0.003526 = -24.52 \text{ dB} \approx 0.00353$ or -24.5 dB . If the range resolution is reduced to 1.5m, the chaff volume is reduced by 20 dB to 3.750×10^7 , and the S/C is increased by 20 dB to -4.52 dB . If 20 dB of chaff cancellation is also used, the S/C calculated using (10.25) is as $1 \times 100 \times (4/\pi) \times 6.545 \times 10^{10} / (6,303 \times 3.750 \times 10^7) = 35.26 = 15.47 \text{ dB} \approx 35.3$ or 15.5 dB . This may also be found by adding 20 dB to the previous result: $20 - 4.52 = 15.48 \text{ dB} \approx 15.5 \text{ dB}$.
7. Using Figure 10.6, enter the plot at 0.02 (2%), on the x axis, proceed vertically to the line for $K = 3$, and then horizontally to the y axis. The y -axis value gives the probability of false acceptance as 0.17 or 17%. Rejecting 98% of the decoys corresponds to a probability of false acceptance of 2% or 0.02. Entering the y axis at 0.02 and proceeding horizontally to intersect with the vertical line from 0.02 on the x axis, the value of K may be estimated as 4.1.
8. Since one-half of the total power of 1 kW is used for each of the two polarizations, the power for each is 500W. The ERP per polarization is then found using (10.2), the gain of 5 dB (power ratio 3.162), and jammer loss of 0.2 dB (power ratio 1.047), as $500 \times 3.162 / 1.047 = 1,510 \text{ W} \approx 1.51 \text{ kW}$.
9. A sidelobe blanker should be used with pulsed jammers in the radar sidelobe region, as discussed in Section 10.3.

10. The S/J is found using (10.5) and converting values in decibels to power ratios, as $100,000 \times 0.01 \times 10^5 \times 1 \times 10 \times 10^9 / (4\pi \times 2,000,000^2 \times 1.585 \times 316.2) = 39.70 = 15.99 \text{ dB} \approx 39.7$ or 16.0 dB . (Since ERP per polarization is used, there is no polarization loss.) The burnthrough range is found using (10.6) and converting values in decibels to power ratios, as $\{[316.2 \times 10 / (8\pi \times 10 \times 10^9 \times 1.585 \times 1.38 \times 10^{-23} \times 500)]^2 + 100,000 \times 0.01 \times 10^5 \times 1 \times 10 / [(4\pi)^2 \times 1.585 \times 1.585 \times 31.62 \times 1.38 \times 10^{-23} \times 500]\}^{1/2} - 316.2 \times 10 / (8\pi \times 10 \times 10^9 \times 1.585 \times 1.38 \times 10^{-23} \times 500))^{1/2} = \{[(1.150 \times 10^{12})^2 + 1.155 \times 10^{25}]^{1/2} - 1.150 \times 10^{12}\}^{1/2} = 1,561,000\text{m} \approx 1,560 \text{ km}$. The minimum range for this waveform is found from (5.26) as $3 \times 10^8 \times 0.01/2 = 1,500,000\text{m} = 1,500 \text{ km}$, so the minimum range constraint is not violated (although the margin is small).
11. With isotropic sidelobes, the sidelobe level is equal to the reciprocal of the gain, or -50 dB [see (3.13)]. The $S/(J + N)$ is found using (10.13) and converting values in decibels to power ratios, as $\{100,000 \times 0.01 \times 10^5 \times 1 \times 10 / [(4\pi)^2 \times 2,000,000^4 \times 1.585 \times 1.585]\} / \{[10^{10} \times 10 \times 10^5 / (4\pi \times 2,500,000^2 \times 10 \times 10^9 \times 1.585)] + 1.38 \times 10^{-23} \times 500\} = 1.575 \times 10^{-19} / (8.033 \times 10^{-19} + 6.900 \times 10^{-21}) = 0.1944 = -7.113 \text{ dB} \approx 0.194$ or -7.11 dB . (Since ERP per polarization is used, there is no polarization loss.) Equation (10.13) may be solved for the sidelobe cancellation ratio as follows:

$$SLC = \frac{\frac{S/(J+N)ERP A_R SL}{4\pi R_J^2 B_J L_{POL} L_R}}{\frac{P_p \tau G_T \sigma A_R}{(4\pi)^2 R^4 L_T L_R} - kT_s S/(J+N)} \quad (E.1)$$

The value of SLC is found from (E.1), converting values in decibels to power ratios, as $[10 \times 10^{10} \times 10 \times 10^{-5} / (4\pi \times 2,500,000^2 \times 10 \times 10^9 \times 1.585)] / \{[100,000 \times 0.01 \times 10^5 \times 1 \times 10 / [(4\pi)^2 \times 2,000,000^4 \times 1.585 \times 1.585]] - (10 \times 1.38 \times 10^{-23} \times 500)\} = 8.033 \times 10^{-18} / (1.575 \times 10^{-19} - 6.900 \times 10^{-20}) = 90.77 = 19.58 \text{ dB} \approx 90.8$ or 19.6 dB .

12. The average dipole RCS is found from (10.17), using the wavelength $= 3 \times 10^8 / (5.5 \times 10^9) = 0.05455\text{m}$, as $0.15 \times 0.05455^2 = 0.0004463 \text{ m}^2 \approx 0.000446 \text{ m}^2$. The number of dipoles may be found using (10.18), or directly as $5,000 / 0.0004464 = 1.120 \times 10^7 \approx 1.12 \times 10^7$. The weight of the dipoles is found using (10.21) as $5,000 / (22,000 \times 0.05455) = 4.166 \text{ kg} \approx 4.17 \text{ kg}$. With 100% overhead, the total package weight is twice this value, or 8.33 kg .
13. The cross-range beam dimension is $200,000 \times 1 \times (\pi/180) = 3,491\text{m} \approx 3.49 \text{ km}$. Thus, the cross-range dimensions of the chaff resolution cell, D_A and D_E , are determined by the beam as shown in Figure 10.4(a). The volume of the resolution cell is found using (10.22) as $3,491^2 \times 15 = 182,800,000 \text{ m}^3 \approx 1.83 \times 10^8 \text{ m}^3$. The total chaff volume is $(4/3) \times \pi \times 10,000^3 = 4.189 \times 10^{12} \text{ m}^3$. The RCS of chaff in the resolution cell is found using (10.24) with a 3.2 dB

(power ratio 2.089) beamshape loss, as $10,000 \times 1.828 \times 10^8 / (2.089 \times 4.189 \times 10^{12}) = 0.2089 \text{ m}^2 \approx 0.209 \text{ m}^2$. The S/C from (10.25) is $0.01/0.2089 = 0.04787 = -13.20 \text{ dB} \approx 0.0479$ or -13.2 dB . The required cancellation ratio is found by rearranging (10.25) as $31.62 \times 0.2089/0.01 = 660.5 = 28.20 \text{ dB} \approx 661$ or 28.2 dB .

E.11 Chapter 11 Problems

1. Airborne-radar antenna size and shape must be consistent with the aerodynamic performance of the aircraft, and its weight must be within aircraft capabilities.
2. From (11.2), setting ϕ_A at 0 and 180° , the sidelobe clutter velocity ranges from $350 \times 1 \times \cos(10^\circ) = 344.7 \text{ m/s}$, to $-350 \times -1 \times \cos(10^\circ) = -344.7 \text{ m/s}$. Thus the velocity spread $\approx \pm 345 \text{ m/s}$. The radar wavelength is $3 \times 10^8 / 3.3 \times 10^9 = 0.09091 \text{ m}$. The sidelobe-clutter Doppler-frequency spread is found using (11.5) as $\pm 2 \times 344.7/0.09091 = \pm 7,583 \text{ Hz} \approx \pm 7.58 \text{ kHz}$. The clutter velocity at the center of the mainbeam is also found using (11.2), as $350 \times \cos(60^\circ) \times \cos(25^\circ) = 158.6 \text{ m/s} \approx 159 \text{ m/s}$. The corresponding Doppler-frequency shift is found using (11.5), as $2 \times 158.6/0.09091 = 3,489 \text{ Hz} \approx 3.49 \text{ kHz}$. The mainbeam clutter velocity spread is found using (11.4), as $2 \times 350 \times (1.5 \times \pi/180) \times \sin(60^\circ) \times \cos(25^\circ) = 14.38 \text{ m/s} \approx 14.4 \text{ m/s}$. Using (11.5), the mainbeam clutter frequency spread is $2 \times 14.38/0.09091 = 316.4 \text{ Hz} \approx 316 \text{ Hz}$.
3. High-PRF pulse-Doppler waveforms are used to view targets approaching the front of the aircraft.
4. To avoid range ambiguities, the range ambiguity spacing must be at least 500 km. The pulse-repetition interval then must be at least $2 \times 500,000 / (3 \times 10^8) = 0.003333 \text{ sec}$, and the PRF must be no greater than $1/0.003333 = 300 \text{ Hz}$ (see Section 4.6).
5. Using (11.7), the PRF is $300/2 = 150 \text{ Hz}$.
6. STAP is used to resolve targets that are not resolved in either angle or radial velocity.
7. The radar wavelength is $3 \times 10^8 / (5.5 \times 10^9) = 0.05455 \text{ m}$. For Doppler beam sharpening, the minimum cross-range resolution is found using (11.12) as $0.5 \times (5,000,000 \times 0.05455)^{1/2} = 261.1 \text{ m} \approx 261 \text{ m}$. For side-looking SAR, the cross-range resolution is found from (11.14) as $10/2 = 5.00 \text{ m}$. The processing time for spotlight SAR is found by rearranging (11.6), as $5,000,000 \times 0.05455 / (2 \times 7,000 \times 2) = 9.741 \text{ sec} \approx 9.74 \text{ sec}$. The minimum PRF is found using (11.10) as $4 \times 7,000/10 = 2,800 \text{ Hz}$.
8. From Figure 11.1, the number of satellites required is about nine, and the range to the 1-degree horizon is about 9,000 km.
9. The relative velocity of the target as viewed by the radar is $325 + 350 \times \cos(15^\circ) = 663.1 \text{ m/s}$. To avoid sidelobe clutter, the radar must view this target with unambiguous radial velocity of $633.1 + 325 = 958.1 \text{ m/s}$. The

wavelength is $3 \times 10^8 / 9.5 \times 10^9 = 0.03158\text{m}$. The minimum PRF is $2 \times 958.1 / 0.03158 = 60,680\text{ Hz} \approx 60.7\text{ kHz}$.

10. DPCA is most effective against targets having low radial velocities, such as slowly moving ground vehicles.
11. The matrix dimension is the product of the number of elements and the number of pulses, and equals $700 \times 150 = 105,000$ (see Section 11.5).
12. Side-looking SAR is used to generate strip maps. The cross-range resolution is given by (11.14) as $5/2 = 2.50\text{m}$. The required signal bandwidth is $3 \times 10^8 / (2 \times 2.50) = 6.000 \times 10^7 = 60.0\text{ MHz}$ (see Section 4.3). The minimum PRF is given by (11.10) as $4 \times 1,000/5 = 800\text{ Hz}$. The unambiguous range extent of the strip map is given by $3 \times 10^8 / (2 \times 800) = 187,500\text{m} \approx 188\text{ km}$ (see Section 4.6).

E.12 Chapter 12 Problems

1. The number of search pulses remains the same at 200 per second. The search pulse S/N also remains the same, as was calculated and shown in Figure 12.1, column F (for Swerling 3 and 4 targets). For the sample calculation with search $P_{FA} = 10^{-6}$, this value is 19.12 dB (power ratio 81.66). The number of confirmation pulses also remains the same as that shown in Section 12.2, $666,666 \times P_{FA}$, or $666,666 \times 10^{-6} = 0.6667$ for the sample calculation. However, the S/N for the confirmation pulses is that required for $P_D = 0.99$ and $P_{FA} = 10^{-4}$, is found from Figure 6.3 to be 21.34 dB (power ratio 136.1). The relative power is the sum of the power for search and the power for confirmation, and for the sample case is $200 \times 81.66 + 0.6667 \times 136.1 = 16,420$. This compares with 16,370 for original problem. This analysis assumes that the losses with the search and confirmation pulses are the same. If either waveform uses pulse integration and the losses are different for the two waveforms, the difference in losses should be taken into account in the analysis.
2. The 3-degree search radius is covered using three rings. The analysis in rows 19 through 21 in Figure 12.5 would be carried out, showing that this search angle is feasible, and that 88 pulses illuminate the target. Since the search sector is defined by an angle, rather than by a radius as in the original problem, there is no minimum search range (except that due to minimum range for the search pulse duration, not specified in the problem). The single-pulse S/N to provide $P_D = 0.9$ and $P_{FA} = 10^{-6}$ for a Swerling 4 target with 88 pulses noncoherently integrated may be found from Figure 6.5. The product of the S/N and the number of pulses from this figure is 18.6 dB (power ratio 72.40). The single-pulse $S/N = 72.40/88 = 0.8227 = -0.8474\text{ dB}$. The range to obtain this value of S/N may be found using (5.11), with the 3.2-dB beamshape loss (power ratio 2.089), and using the reference pulse duration and RCS, as $300 \times [2/(0.8227 \times 2.089)]^{1/4} = 311.6\text{ km} \approx 311\text{ km}$.

3. This problem may be solved using the measurement smoothing and prediction techniques discussed in Section 8.6. While these techniques are based on straight, constant-velocity target paths, they may be used with little error for short tracking and prediction times for orbital targets. The steps in solving this problem may be summarized as follows:
 - Calculate the $S/(J + N)$, and the resulting random measurement errors. Combine these with the fixed random errors to find the total random errors.
 - Calculate the prediction errors due to the random measurement errors.
 - Find the bias errors due to tropospheric and ionospheric refraction, and combine with the fixed bias errors to find the total bias errors.
 - Calculate the total prediction errors, and find the largest $3\text{-}\sigma$ value.

Some preliminary parameter calculations are given in Table E.3. The calculation of the duty cycle, wavelength, and range resolution are straightforward. The two-way tropospheric loss (including lens loss) for the target signal is the sum of the atmospheric loss (from Figure 9.4) and the lens loss estimated, using Table 9.6. The one-way jammer loss is found in the same way. The ionospheric loss at this frequency (UHF) may be neglected, as discussed in Section 9.4. The transmit losses and the receive losses for the target signal are each assumed to be one-half of the fixed radar losses (in decibels), from Table 12.1, and one-half of the two-way propagation losses. The receive loss for the jammer is one-half of the fixed radar losses plus the one-way propagation loss for the jammer. The number of pulses in the measurement is the PRF multiplied by the tracking time: $10 \times 20 = 200$.

The S/N and S/J are calculated separately, since the receive losses are different for the target and jamming signals, using (5.1) and (10.11), respectively. The S/N is calculated, using the sum of the transmit and receive losses, 4.84 dB (power ratio 3.048), as $200,000 \times 0.01 \times 5,000 \times 10 \times 200 / [(4\pi)^2 \times 3,000,000^4 \times 1.38 \times 10^{-23} \times 450 \times 3.048] = 82.61 = 19.17$ dB. The S/J is calculated, using the radar transmit loss and increased by 0.21 dB (power ratio 1.050) due to the additional jammer propagation loss, as

Table E.3 Calculated Parameter Values for Chapter 12 Problem 3

<i>Parameter</i>	<i>Value</i>
DC	0.1
λ	0.7059m
ΔR	30m
L_p (tropo, signal)	0.34 dB (two-way)
L_p (tropo, jammer)	0.38 dB (one-way)
L_p (iono)	0 dB
L_T	2.42 dB
L_R (signal)	2.42 dB
L_R (jammer)	2.63 dB
n_p	200

$1,050 \times 200,000 \times 0.01 \times 5,000 \times 10 \times 4,000,000^2 \times 50 \times 10^6 / (4\pi \times 3,000,000^4 \times 1.745 \times 10,000 \times 6.310 \times 10^{-5}) = 74.95 = 18.75 \text{ dB}$. No sidelobe cancellation was assumed in the problem. The $S/(J + N)$ is $1/[1/(S/N) + 1/(S/J)]$, and is found as $1/[(1/82.63) + (1/74.95)] = 39.30 = 15.94 \text{ dB}$.

The random range error from $S/(J + N)$ is calculated using (8.6) as $30/(2 \times 39.30)^{1/2} = 3.384\text{m}$. The random angular error from $S/(J + N)$ is calculated using (8.8) as $3/[1.6 (2 \times 39.30)^{1/2}] = 0.2115^\circ$. These error values are shown in the first row of Table E.4. The fixed random errors given in Table 12.1 are shown in row 2 of Table E.4, and these are combined with the $S/(J + N)$ -dependent errors in an rss fashion in row 3.

The random prediction errors due to these random measurement errors are calculated using (8.34). For range, the quantity R_A is replaced by the range random measurement error, giving $12^{1/2} \times 4.522 \times 200 / (200^{1/2} \times 20) = 11.08\text{m}$. The angular random prediction errors are calculated using the random angular measurement errors in radians ($0.2339 \times \pi/180 = 0.004082 \text{ rad}$), as $12^{1/2} \times 3,000,000 \times 0.004082 \times 200 / (200^{1/2} \times 20) = 30,000\text{m} = 30.00 \text{ km}$. These values are shown in row 4 of the table.

The radar bias errors also affect the accuracy of the predicted target position. The radar bias errors from Table 12.2, the bias errors due to tropospheric refraction from Table 9.7, and the bias errors due to ionospheric refraction from Figures 9.5 and 9.6 (extrapolated) are given in rows 5, 6, and 7 of Table E.4. These are combined in an rss fashion in row 8 of the table, and in row 9, the target position errors resulting from the angular bias errors, calculated by converting degrees to radians and multiplying by the range, are shown. The random prediction errors (row 4), and the position errors due to bias (row 9), are combined in an rss fashion in row 10 of Table E.4, and the $3\text{-}\sigma$ values, rounded to three significant figures, are given in the last row in the table. The largest $3\text{-}\sigma$ error is in 91.2 km , and occurs in the elevation coordinate. The radar measurement errors in this Problem could be reduced by using sidelobe cancellers to increase the S/J (see Section 10.3), or by correcting the tropospheric measurement errors based on the standard atmosphere or measurement of surface refractivity

Table E.4 Tracking and Prediction Errors for Chapter 12, Problem 3

<i>Error Source</i>	<i>Range Errors</i>	<i>Elevation Errors</i>	<i>Azimuth Errors</i>
Jamming and noise	3.384m	0.2115°	0.2115°
Fixed noise	3.0m	0.10°	0.10°
Total random	4.522m	0.2339°	0.2339°
Random predict error	11.08m	30.00 km	30.00 km
Radar bias	20m	0.05°	0.05°
Tropo bias	13.7m	0.11°	N/A
Iono bias	118m	0.02°	N/A
Total bias	120.5m	0.122°	0.05°
Total bias (position)	120.5m	6.440 km	2.618 km
Total predict error	121.0m	30.68 km	30.11 km
3-σ values	363m	92.1 km	90.3 km

(see Section 9.3). Ionospheric propagation errors for normal daytime conditions were used here. Under nighttime conditions, they would be about one-third of these values, and under disturbed ionospheric conditions, they could be as much as three times these values (see Section 9.4).

This analysis assumes that orbital mechanics are used in the target tracking and prediction process. While the approximations in these calculations are reasonable for short tracking and prediction times, they do not consider changes in observation geometry with time, or take into account rotation of the uncertainty volume due to orbital mechanics.

4. The probability of confirmation for two successive detections is given by:

$$P_{CONF} = P_{DN+1} \times P_{DN+2} \quad (E.2)$$

using the notation from (12.4). For a detection at 300 sec, P_{DN+1} (310 sec), may be found from Figure 12.3, column D, as 0.816, and P_{DN+2} (320 sec), may be found as 0.836. The resulting probability of confirmation is $0.816 \times 0.836 = 0.6822 \approx 0.682$. (This compares to 0.970 for the confirmation technique used in the Section 12.3 Problem, where detection with only one of the two following pulses is required.) The detection probability at 300 sec from Figure 12.3 is 0.795. The probability of detection and confirmation is the product of the two probabilities, or $0.795 \times 0.6822 = 0.5423 \approx 0.542$ (compared with 0.771 for the Section 12.3 Problem).

5. The principal changes to the approach to this problem from that described in Section 12.5 are:

- The target geometry calculation requires determination of target range.
- Ionospheric bias errors for range and elevation angle should be included.

The target range may be calculated using the law of sines, as shown in Figure E.1, with the result of 3,194 km. The refraction from the atmosphere (less than 0.2°) is neglected in this calculation.

The radar losses are as follows:

- Azimuth scan loss, from (3.21), is $\cos^{-2.5} (30^\circ) = 1.433$ (1.562 dB).

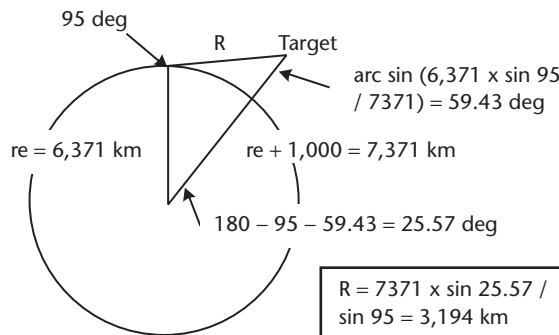


Figure E.1 Target observation geometry for Chapter 12, Problem 5 (1- values).

- Elevation scan loss, from (3.21), is $\cos^{-2.5}(15^\circ) = 1.091$ (0.3764 dB).
- Tropospheric and lens losses, from Figure 9.4 and Table 9.6, is 0.75 dB.
- Fixed radar losses are given as 6 dB.
- Total system losses are the sum of these: 8.688 dB (power ratio 7.393).

The single-pulse S/N is calculated using (5.1) as $10,000 \times 0.01 \times 10,000 \times 10 \times 400 / [(4\pi)^2 \times 3,194,000^4 \times 1.38 \times 10^{-23} \times 500 \times 7.393] = 4.771 = 6.786$ dB. Noncoherently integrating 10 pulses for measurement gives an integrated S/N for measurement, from (5.17), of $10 \times 4.771^2 / (1 + 4.771) = 39.44 = 15.97$ dB.

The S/N-dependent random measurement errors are calculated using the integrated S/N, the resolutions specified, and using Equations (8.6) for range, (8.8) for angle, and (8.13) for radial velocity using Doppler-frequency shift (using the 10-ms waveform duration and the wavelength for the radar frequency given, 0.7059m). The results are given in the first row of Table E.5. The fixed random and radar bias errors are the same as in the Section 12.5 Problem, and are given in rows 2 and 4 of Table E.5, respectively. The fixed random and bias scan-dependent errors for azimuth are the same as in the Section 12.5 Problem. For elevation, the fixed random scan-dependent error is $0.0005 / \cos(15^\circ) = 0.0005176$ rad = 0.5176 mrad, and the bias scan dependent error is $0.0002 / \cos(15^\circ) = 0.000207$ rad = 0.2071 mrad. These values are given in rows 3 and 5 of Table E.5, respectively.

The tropospheric measurement errors may be found using Table 9.7, and by interpolating between the values given and the observation elevation angle of $5^\circ \approx 87$ mrad. The value for elevation error is 3.4 mrad, and the value for range error is 24m. If these are corrected to 5% of their value, as in the Section 12.5 Problem, the errors are 0.17 mrad and 1.2m, respectively. The elevation angle and range measurement errors from normal daytime ionospheric refraction may be found using Figures 9.5 and 9.6, and scaling the errors inversely with frequency squared (see Section 9.4). The elevation error is $1.9 \times (200/425)^2 = 0.4208$ mrad, and the range error is $900 \times$

Table E.5 Radar Measurement Errors for Chapter 12, Problem 5

<i>Error Component</i>	<i>Range Error (m)</i>	<i>Azimuth Error (mrad)</i>	<i>Elevation Error (mrad)</i>	<i>Radial-Velocity Error (m/s)</i>
S/N-dependent random	1.689	2.456	2.456	3.974
Fixed random	1.00	0.80	0.80	1.0
Fixed scan-dependent random	N/A	0.58	0.5176	N/A
Radar fixed bias	2.00	0.40	0.40	0.7
Radar scan-dependent bias	N/A	0.23	0.2071	N/A
Propagation errors	199.3	N/A	0.453	N/A
Composite error	199	2.68	2.71	4.16

$(200/425)^2 = 199.3\text{m}$. These errors are combined in an rss fashion with the tropospheric errors, and the results given in row 6 of Table E.5. The composite error for each measurement is found by combining the error components in an rss fashion. The resulting composite errors are given in the last row of Table E.5, rounded to three significant figures.

6. The steps in solving this problem may be summarized as follows:
 - Calculate the average radar power needed for the specified search function, assuring that the minimum-range constraint is not violated.
 - Calculate the average power needed to track a single target, using parameters averaged over the distribution of target locations.
 - Determine how many such targets may be tracked with the radar average power remaining from search.

Additional parameters that may be calculated or inferred from the problem statement are given in Table E.6. The radar duty cycle and wavelength are straightforward calculations. The transmit gain is calculated using (3.9) as 51.00 dB (1.260×10^5). The elevation off-broadside scan angle is equal to the broadside elevation angle minus the horizon scan elevation. The azimuth scan is specified. A beam-packing factor, f_p , of 1.2 and a beamshape loss, L_{BS} , of 2.5 dB are assumed (see Sections 7.2 and 7.3). The beam-broadening factor, f_B , and average scan loss, L_s , are found using Figure 7.5. The tropospheric propagation loss, L_p , is the sum (in decibels) of the tropospheric loss found using Figure 9.4 and the lens loss found from Table 9.6. The total system loss, $L = 7.7$ dB (power ratio 5.888), is also shown.

The average radar power required to perform the horizon search may be found using (7.39), by setting $R_H = R_D$, and solving for P_A :

$$P_A = \frac{4\pi R_D^3 \phi_a V_v n_p (S/N) k T_s L f_p}{A_R \sigma f_B} \quad (\text{E.3})$$

Table E.6 Calculated and Assumed Parameters For Chapter 12, Problem 6

<i>Parameter</i>	<i>Value</i>
DC	0.2
λ	0.03158m
G_T	51.00 dB
El scan	10°
Az scan	± 30°
f_p	1.2
f_B	1.06
L_s	0.7 dB
L_p	1.5 dB
L_{BS}	2.5 dB
L	7.7 dB

The number of pulses per beam position, n_p , is initially set at seven, near the optimum value (see Section 6.4). The value of $n_p \times S/N$ is found from Figure 6.5 as 17.7 (power ratio 58.88). Substituting this and the other problem parameters into (E.3), gives $P_A = 4\pi \times 2,000,000^3 \times 60 \times (\pi/180) \times 1,000 \times 58.88 \times 1.38 \times 10^{-23} \times 500 \times 5.888 \times 1.2 / (10 \times 1 \times 1.06) = 28,510 \text{ W} = 28.51 \text{ kW}$.

The next step is to determine if the minimum-range constraint is satisfied when seven pulses are used per beam position. The search time is found from (7.37), using the elevation beamwidth for ϕ_H , as $2,000,000 \times 0.64 \times (\pi/180) / 1,000 = 22.34 \text{ sec}$. The average beam solid angle, ψ_{BA} , is found using (7.12) and (7.15), as $1.06 \times (\pi/4) \times 0.64^2 \times (\pi/180)^2 = 1.039 \times 10^{-4} \text{ sr}$. The number of beams used in the horizon scan is found from (7.41) as $1.2 \times 0.64 \times 60 \times (\pi/180)^2 / (1.039 \times 10^{-4}) = 135.1$. The number of pulses per second is then $7 \times 135.1 / 22.34 = 42.33 \text{ Hz}$. Since the average power in search is given by $P_p \times \tau \times \text{PRF}$, the pulse duration, τ , is found as $28,510 / (250,000 \times 42.33) = 0.002694 \text{ sec} = 2.694 \text{ ms}$. This is well within the minimum range constraint, and is likely to be within the radar capability, so using seven pulses per beam position is acceptable. (If the pulse duration were too long for either of these considerations, a larger number of pulses per beam position would have to be used.)

The initial step in analyzing the tracking requirement is to find the average values of the parameters over which the targets are assumed to be uniformly distributed. The effective range is found by averaging R^4 between 1,000 and 2,000 km, giving 1,578 km. The average scan loss is found by averaging the elevation scan loss over -10° to $+15^\circ$, and the azimuth scan loss over $\pm 30^\circ$, using data from Figure 7.5, giving 0.8 dB (power ratio 1.202). The average tropospheric propagation loss is found by averaging over elevation angles from 5° to 30° , using data from Figure 9.4 and Table 9.6, as 0.6 dB (power ratio 1.148). Ionospheric loss is negligible at this X-band frequency. The system losses for track include these and the 3.0-dB fixed loss, and total 4.4 dB (power ratio 2.754).

Using these average values, and the other problem data, the pulse duration required for track may be found using (5.7), as $(4\pi)^2 \times 31.62 \times 1,578,000^4 \times 1.38 \times 10^{-23} \times 500 \times 2.754 / (250,000 \times 1.259 \times 10^5 \times 1 \times 10) = 0.001869 \text{ sec} = 1.869 \text{ ms}$. The average power for tracking a target is then pulse energy multiplied by the tracking rate, or $250,000 \times 0.001869 \times 1 = 467.3 \text{ W}$. The power available for tracking is $50,000 - 28,510 = 21,490 \text{ W}$, and the number of targets that may be simultaneously tracked is $21,490 / 467.3 = 45.99$. Normally, this value would be rounded down to determine the target track capacity, but the value is equal to 46 within the accuracy of the calculation.

Appendix F

Self Test

The following multiple-choice questions will test your comprehension of the material in this book. The answers are given in Section F.2.

F.1 Questions

1. Which of the following is true of detection using a coherent dwell?
 - a. A fluctuating target is required.
 - b. Detection statistics are the same as for a single pulse.
 - c. May require less total energy than using a single pulse.
 - d. Does not require knowledge of target radial velocity.
2. Which of the following factors does *not* affect the tracking rate used by a radar?
 - a. Radar power available for tracking each target with phased-array radar.
 - b. Number of targets in track.
 - c. Expected target maneuver capability.
 - d. Antenna rotation rate for rotating surveillance radar.
3. What is the clutter radial velocity observed from an aircraft having a horizontal velocity of 300 m/s and viewing an azimuth 30° from the aircraft heading and a depression angle of 15° ?
 - a. 39 m/s.
 - b. 251 m/s.
 - c. 290 m/s.
 - d. 300 m/s.
4. A radar has a range resolution of 1.5m, a fixed random range error of 0.3m, and a range bias error of 0.5m. It measures the ranges of two resolved scatterers on a target, with a S/N of 17 dB on each scatterer. What is the $2\text{-}\sigma$ measurement accuracy of the radial distance between these scatterers?
 - a. 0.34m.
 - b. 0.48m.
 - c. 0.95m.
 - d. 1.70m.

5. What is the false-alarm probability for a single observation when the detection threshold is set at 12, relative to the Gaussian background noise level?
 - a. 10^{-12} .
 - b. 6.1×10^{-6} .
 - c. 1.6×10^{-5} .
 - d. 0.18.
6. What is the minimum element spacing in a phased-array antenna having a frequency of 9.5 GHz, that will allow off-broadside scan angles of 20° without generating grating lobes?
 - a. 0.023m.
 - b. 0.046m.
 - c. 1.46m.
 - d. 0.15m.
7. What two factors usually characterize the radar detection process?
 - a. S/N and detection probability.
 - b. Detection probability and false-alarm rate.
 - c. Detection probability and false-alarm probability.
 - d. S/N and false-alarm probability.
8. A phased-array radar has an elevation beamwidth of 2° , fixed random elevation error of 0.7 mrad, scan-dependent random elevation error of 0.3 msine, combined elevation bias from calibration and propagation of 1.2 mrad, and scan-dependent elevation bias of 0.2 msine. If the radar observes a target at an off-broadside angle in elevation of 30° with a S/N of 18 dB, what is the $1\text{-}\sigma$ elevation-angle measurement error?
 - a. 0.89 mrad.
 - b. 2.26 mrad.
 - c. 2.67 mrad.
 - d. 15.26 mrad.
9. A radar having a peak transmit power of 500 kW, pulse duration of 1 ms, transmit gain of 40 dB, and transmit losses of 2.5 dB, is jammed by a mainlobe barrage jammer having an ERP per polarization of 20 dBW, and a noise bandwidth of 500 MHz. What is the S/J for a 5.0 dBsm target and collocated with the jammer at 300-km range?
 - a. 14.5 dB.
 - b. 15.9 dB.
 - c. 22.9 dB.
 - d. 39.2 dB.
10. Which of the following is not a source of radar measurement error?
 - a. Thermal noise.
 - b. Bias from radar calibration error and propagation effects.
 - c. Target radial velocity.
 - d. Clutter, target scintillation, and glint.

11. What is the detection loss from envelope detection of a signal being used for radar detection and having an S/N of 2.5 dB?
 - a. 3.6 dB.
 - b. 2.3 dB.
 - c. 1.9 dB.
 - d. 1.6 dB.
12. A radar has an overall efficiency of 12%, average transmitter power of 25 kW, transmit microwave losses of 0.5 dB, and transmit antenna losses of 1.0 dB. What is the prime power required to operate the radar?
 - a. 147 kW.
 - b. 139 kW.
 - c. 208 kW.
 - d. 294 kW.
13. Which of the following is *not* a characteristic of coherent integration?
 - a. Also called postdetection integration.
 - b. May be limited by signal and target coherence.
 - c. Integration gain equal to the number of pulses integrated.
 - d. Signals added prior to envelope detection in the receiver.
14. For a horizon search mode with a search elevation sector of 1 degree, a target range of 500 km, and a target vertical velocity component of 600 m/s, what search time will assure that the target is observed by the radar?
 - a. 833 sec or greater.
 - b. 833 sec or less.
 - c. 14.5 sec or greater.
 - d. 14.5 sec or less.
15. What is the elevation-angle error due to the normal daytime ionosphere for a ground-based 425-MHz radar viewing a target at an altitude of 1,000 km with an elevation angle of 5°?
 - a. 2.34 mrad.
 - b. 1.85 mrad.
 - c. 0.87 mrad.
 - d. 0.41 mrad.
16. A rotating search radar having a fan beam has a rotation period of 12 seconds, an azimuth beamwidth of 2°, and a PRF of 300 Hz. What is the single-pulse S/N needed to provide a detection probability of 0.9 and a probability of false alarm of 10^{-6} for a Swerling 4 target, using noncoherent integration?
 - a. -6.9 dB.
 - b. 3.5 dB.
 - c. 5.1 dB.
 - d. 16.5 dB.
17. A radar has a PRF of 250 Hz. What is the apparent range of a target having a true range of 1,350 km?

- a. 750 km.
 - b. 150 km.
 - c. 600 km.
 - d. 450 km.
18. What is the maximum total range from a radar having an altitude of 15m to a target having an altitude of 3 km, assuming a smooth Earth?
- a. 196 km.
 - b. 209 km.
 - c. 226 km.
 - d. 242 km.
19. What is the range resolution for a phase-coded waveform having a total duration of 10 ms and 64 subpulses?
- a. 1,500 km.
 - b. 1.5 km.
 - c. 23.4 km.
 - d. 23.4m.
20. A radar has a peak power of 250 kW, duty cycle of 20%, receive aperture area of 25 m^2 , system noise temperature of 500K, and fixed losses of 4.5 dB. Find the range for a volume search $\pm 45^\circ$ in azimuth (x plane), and from 5 to 30° in elevation (y plane), with a search time of 60 sec, a target RCS of -15 dBsm , and a required S/N of 15 dB. Assume the search losses total 6.2 dB.
- a. 857 km.
 - b. 742 km.
 - c. 572 km.
 - d. 76 km.
21. What is the two-way tropospheric attenuation for a 25-km path with normal sea level conditions for a radar operating at 10 GHz?
- a. 0.023 dB.
 - b. 0.43 dB.
 - c. 0.58 dB.
 - d. 1.15 dB.
22. Which of the following is *not* true of cumulative detection?
- a. Range-walk compensation is not needed.
 - b. Special case of m -out-of- n detection.
 - c. May require less total energy than a single pulse.
 - d. Effective against nonfluctuating targets.
23. What is the radial-velocity resolution for a waveform having a duration of 7.5 ms and a frequency of 3.3 GHz?
- a. 6.06 m/s.
 - b. 12.1 m/s.
 - c. 133.3 m/s.
 - d. 606 m/s.

24. Normal radar operation does *not* include which of the following?
- Generation and radiation of RF energy by the target.
 - Generation and radiation of RF energy by the radar transmitter and antenna.
 - Propagation and reflection by the target of electromagnetic radiation.
 - Collection and processing of RF energy by the radar antenna and receiver.
25. If a radar transmitter has a peak power of 2 MW and a duty cycle of 15%, what is the average power of the transmitter?
- 13.3 MW.
 - 300 kW.
 - 0.3 kW.
 - 133 kW.
26. What is the single-pulse S/N required to provide an integrated S/N of 13 dB when 32 pulses are integrated coherently?
- 0.6 dB.
 - 2.1 dB.
 - 19 dB.
 - 2.1 dB.
27. To perform radar measurements on a target, the target must be:
- Resolved from other targets in range and angle.
 - In the center of the radar beam.
 - Free from propagation effects.
 - Resolved from other targets in at least one radar coordinate.
28. Which of the following CM may *not* be used to counter barrage noise jamming threats?
- Frequency agility.
 - Burnthrough.
 - Sidelobe cancellation.
 - Range resolution.
29. A radar having a peak power of 25 kW, pulse duration of 0.5 ms, transmit gain of 30 dB, isotropic sidelobes, and transmit losses of 1.8 dB, is jammed by a sidelobe jammer with an ERP per polarization of 35 dBW, a noise bandwidth of 1.0 GHz, and a range of 250 km. What is the burnthrough range at which a -20 dBsm target is detected with an S/J of 12 dB, assuming 20 dB of sidelobe cancellation?
- 5 km.
 - 30 km.
 - 169 km.
 - 201 km.
30. A radar with a frequency of 5.5 GHz, a 10-ms pulse duration, negligible fixed random errors, and 0.1 m/s bias errors, measures target radial velocity

- using Doppler frequency shift. If the S/N is 20 dB, what is the 3- σ radial velocity measurement error?
- 0.11 m/s.
 - 0.19 m/s.
 - 0.58 m/s.
 - 0.65 m/s.
31. On what factor does the detection performance depend?
- The threshold setting.
 - The S/N.
 - The statistical characteristics of the target and noise.
 - All of the above.
32. What is the noise power in a radar having a system noise temperature of 450K and a bandwidth of 10 MHz?
- $6.2 \times 10^{-11} \text{ W}$.
 - $6.2 \times 10^{-14} \text{ W}$.
 - $6.2 \times 10^{-17} \text{ W}$.
 - $4.5 \times 10^{-8} \text{ W}$.
33. For a monostatic radar, what is the time between transmission and reception of the signal for a target having a range of 250 km?
- 0.833 ms.
 - $1.67 \mu\text{s}$.
 - 1.67 sec.
 - 1.67 ms.
34. A CW pulse has a range resolution of 300m and a radial velocity resolution of 60 km/s. What is the frequency?
- 1,250 GHz.
 - 1,250 MHz.
 - 2.5 GHz.
 - 625 MHz.
35. The product of what two radar parameters is the principal determinant of radar search performance?
- Average transmit power and receive aperture area.
 - Peak transmit power and receive aperture area.
 - Average transmit power and transmit gain.
 - Transmit gain and receive aperture area.
36. What is the two-way lens loss when a ground-based radar observes a target at an elevation angle of 4° and a range of 1,000 km?
- 0.16 dB.
 - 0.31 dB.
 - 0.62 dB.
 - 1.0 dB.

37. Compared with standard daytime ionospheric measurement errors, nighttime ionospheric measurement errors are:
- About one-third as large.
 - About the same.
 - About three times as large.
 - Comparable to tropospheric measurement errors.
38. What type of pulse-Doppler waveform is used to view targets closing the frontal aspect of an airborne radar?
- High PRF.
 - Medium PRF.
 - Low PRF.
 - Any of the above.
39. What is the frequency of a signal having a wavelength of 0.25m?
- 1.2 MHz.
 - 1,200 MHz.
 - 75 GHz.
 - 75 MHz.
40. What is the integrated S/N for radar measurement when 12 pulses, each having S/N of 4.5 dB, are noncoherently integrated?
- 9.2 dB.
 - 14.0 dB.
 - 15.3 dB.
 - 54.0 dB.
41. A radar has a range resolution of 15m, a fixed random range error of 2m, a range bias error from radar calibration of 5m, and a propagation bias error of 3m. What is the resulting $3\text{-}\sigma$ range error when 10 radar measurements, each with a S/N of 12 dB, are smoothed?
- 5.9m.
 - 6.4m.
 - 15.6m.
 - 17.8m.
42. What is the RCS of the clutter for terrain having a clutter reflectivity, σ^0 , of -25 dB, viewed at a range of 15 km and a grazing angle of 10° , by a radar having azimuth and elevation beamwidths of 2.5° , and range resolution of 150m?
- 21.8 dBsm.
 - 23.4 dBsm.
 - 25.0 dBsm.
 - 35.7 dBsm.
43. Which of the following is *not* true for detection using noncoherent integration?
- Integration of a large number of pulses is efficient.

- b. Is usually easier to implement than coherent integration.
 - c. May require less total energy than a single pulse or coherent integration for fluctuating target signals.
 - d. Requires more total energy than coherent integration for coherent target signals.
44. What is the Doppler-frequency shift for a target having a radial velocity of 300 m/s, with a radar having a frequency of 3.3 GHz?
- a. 6.6 kHz.
 - b. 6.6 Hz.
 - c. 3.3 kHz.
 - d. 1,650 Hz.
45. What is the pulse-compression ratio for a waveform having a frequency of 5.5 GHz, range resolution of 15m, and radial-velocity resolution of 25 m/s?
- a. 375.
 - b. 1.5×10^8 .
 - c. 10,900.
 - d. 400,000.
46. Tropospheric refraction is caused by:
- a. Bending of the signal path.
 - b. Anomalous atmospheric conditions.
 - c. Changes in radar frequency.
 - d. Variation in the propagation velocity with altitude.
47. Which of the following search losses is *not* appropriate for phased-array radar?
- a. Propagation loss.
 - b. Scanning loss for rotating search radar.
 - c. Beamshape loss.
 - d. Off-broadside scan loss.
48. What is the S/N for a radar having a peak transmit power of 50 kW, pulse duration of 200 s, transmit gain of 43 dB, receive aperture area of 20 m², system noise temperature of 475K, total losses of 6.5 dB, a target having an RCS of -8 dBsm, and a range of 200 km?
- a. 85.5 dB.
 - b. 19.3 dB.
 - c. 35.3 dB.
 - d. 49.3 dB.
49. A dish radar is usually used for:
- a. Observing and tracking a single target.
 - b. 360° surveillance.
 - c. Tracking multiple targets simultaneously.
 - d. TWS with periodic target revisit.

50. A radar has a reference range of 1,000 km for a pulse duration of 5 ms, a S/N of 15 dB, and a target RCS of 1 m^2 . What is the S/N using the same waveform, for a target having an RCS of -20 dB and a range of 300 km, with two-way propagation losses of 1.6 dB, and no off-broadside scan losses or beamshape losses?
- 26.9 dB.
 - 15.9 dB.
 - 14.3 dB.
 - 16.4 dB.
51. Which of the following is *not* a characteristic of radar CCMs?
- Employed to mitigate countermeasures.
 - May be effective against nonhostile interference.
 - May reflect good radar design practices.
 - Exploit weaknesses in radar design or operation.
52. A dish radar having a 25-mrad beamwidth is used to perform horizon search over 360° azimuth. If the target range is 500 km and has vertical velocity component of 300 m/s, what radar antenna azimuth rate is needed to assure target observation?
- $8.64^\circ/\text{s}$ or greater.
 - $8.64^\circ/\text{s}$ or less.
 - $0.15^\circ/\text{s}$ or greater.
 - $0.15^\circ/\text{s}$ or less.
53. What is the minimum range at which a monostatic radar transmitting a 3-ms pulse may receive a target return?
- 450m.
 - 3 km.
 - 450 km.
 - 45 km.
54. What is the gain of an antenna having a physical area of 8 m^2 , antenna ohmic losses of 0.3 dB, aperture efficiency losses of 0.7 dB, and an operating frequency of 3.3 GHz?
- 9.96 dB.
 - 41.9 dB.
 - 31.4 dB.
 - 39.9 dB.
55. What is the two-way off-broadside scan loss for an FFOV phased-array radar at a scan angle of 25° in the x plane, and a scan angle of 40° in the y plane?
- 1.58 dB.
 - 2.49 dB.
 - 3.96 dB.
 - 7.92 dB.

56. Which of the following techniques may be used when the radar waveform violates the minimum-range constraint, to avoid the minimum-range constraint without reducing the S/N on the target?
- Reduce the pulse duration.
 - Use a discrete pulse duration.
 - Noncoherently integrate several shorter pulses.
 - Coherently integrate several shorter pulses.
57. A dish radar has an average transmit power of 30 kW, transmit gain of 30 dB, receive aperture area of 2.5 m^2 , system noise temperature of 450K, and total losses (including search losses) of 7.5 dB. What is the assured acquisition range when the radar performs single-beam cued search for a 5 m^2 target having a radial velocity of 1.5 km/s, with a search time of 20 sec, a PRF of 100 Hz and a single-pulse S/N of 0 dB?
- 815 km.
 - 878 km.
 - 908 km.
 - 1,585 km.
58. A sidelobe canceller differs from a sidelobe blanker in that:
- No auxiliary antenna is used.
 - The auxiliary antenna signal is adjusted and subtracted from the main antenna signal.
 - The auxiliary antenna signal magnitude is compared with that of the main antenna.
 - It may only be used with pulsed signals.
59. What is the approximate weight of a collection of chaff dipoles at 5.5 GHz that produce a total RCS of 38 dBsm?
- 0.03 kg.
 - 0.05 kg.
 - 5.3 kg.
 - 10.6 kg.
60. Which of the following is *not* a characteristic of rain attenuation?
- Exponential with path length.
 - Increases with increasing radar frequency.
 - Uniform over large areas.
 - Rarely significant at frequencies below 1 GHz.
61. The word radar is derived from an acronym of:
- Radio Direction finding and Ranging.
 - Range, Direction, and Angle Radio.
 - Radio Detection and Ranging.
 - Radiation Detection and Ranging.
62. Which of the following is *not* a characteristic of a linear FM pulse?
- Frequency varies randomly with time.

- b. Time-bandwidth product greater than unity.
 - c. Produces range-Doppler coupling.
 - d. Tolerant to Doppler shift of received signal.
63. Ten pulse returns from a Swerling 2 target are noncoherently integrated. Assuming no signal processing losses from pulse integration, what is the single-pulse S/N required to give a detection probability of 0.99 with a false-alarm probability of 10^{-6} ?
- a. 1.8 dB.
 - b. 6.9 dB.
 - c. 8.4 dB.
 - d. 18.4 dB.
64. When a target above a 30-km altitude is measured by a ground-based radar to have a zero elevation angle, the target's actual elevation angle from the radar is:
- a. 13° above the horizon.
 - b. 13° below the horizon.
 - c. 0.7° above the horizon.
 - d. 0.7° below the horizon.
65. An antenna has an azimuth beamwidth of 2.5° , an elevation beamwidth of 1.5° , and ohmic losses of 0.5 dB. What is the approximate antenna gain?
- a. 39.7 dB.
 - b. 39.2 dB.
 - c. 40.2 dB.
 - d. 4.6 dB.
66. A dish radar with a 1° beamwidth and negligible fixed random and bias errors, observes a target at a range of 250 km with a PRF of 100 and a S/N of 12 dB. What is the $1\text{-}\sigma$ accuracy of the cross-range velocity obtained using the returns from 10 pulses?
- a. 1.7 km/s.
 - b. 5.3 km/s.
 - c. 6.8 km/s.
 - d. 8.5 km/s.
67. A dish radar has transmit and receive microwave losses of 0.2 dB each, transmit and receive antenna ohmic losses of 0.3 dB each, transmit aperture efficiency of 1.0, receive aperture efficiency of 0.85, one-way propagation loss of 2.2 dB, and signal-proceeding losses of 0.6 dB. If the antenna losses are not included in the transmit gain and receive aperture area, what total system losses should be used in the radar equation?
- a. 6.7 dB.
 - b. 6.9 dB.
 - c. 7.7 dB.
 - d. 4.5 dB.

68. Which of the following radar frequencies is in the C band?
- a. 425 MHz.
 - b. 0.55 GHz.
 - c. 5,500 MHz.
 - d. 11 GHz.
69. What is the total energy for a waveform consisting of 30 pulses, each having a 10- μ s duration, if the peak transmitted power is 20 kW?
- a. 0.2J.
 - b. 6J.
 - c. 200J.
 - d. 6 kJ.
70. The function of a CFAR circuit is to:
- a. Maintain the threshold level constant.
 - b. Maintain the detection probability constant.
 - c. Adjust the threshold as the target RCS changes.
 - d. Adjust the threshold as the noise level changes.
71. Which of the following target features may *not* be directly measured by a radar?
- a. Target mass.
 - b. RCS.
 - c. Target radial length.
 - d. Target rotational velocity.
72. Sidelobe jammers often employ much greater ERP than mainlobe jammers , in order to:
- a. Overcome radar sidelobe rejection.
 - b. Overcome stand-off ranges greater than the target range.
 - c. Overcome sidelobe cancellers.
 - d. All of the above.
73. What is the two-way attenuation from rainfall for a radar operating at 5 GHz, for a path of 10 km with a uniform rainfall rate of 4 mm/hr?
- a. 0.015 dB.
 - b. 0.15 dB.
 - c. 0.30 dB.
 - d. 0.75 dB.
74. A radar employs cumulative detection using 10 pulses, with a target having Swerling 4 fluctuations. What is the single-pulse S/N required to give a cumulative detection probability of 0.999 with a false-alarm probability of 10^{-6} ?
- a. 2.3 dB.
 - b. 12.6 dB.
 - c. 18.2 dB.
 - d. 22.6 dB.

75. STAP is often used to:
- Image terrain and ground targets from an airborne or SBR.
 - Detect targets having clutter backgrounds with a ground-based radar.
 - Detect high-velocity aircraft from an airborne radar.
 - Detect slowly-moving ground vehicles in a clutter background from an airborne or SBR.
76. What is the gain in decibels for an antenna having a gain factor of 5,500?
- 3.7 dB.
 - 55 dB.
 - 27.4 dB.
 - 37.4 dB.
77. An antenna has a gain of 35 dB, and employs Taylor 40-dB aperture illumination weighting. What is the first sidelobe level relative to isotropic gain?
- 40 dB.
 - 5 dB.
 - 5.9 dB.
 - 40.9 dB.
78. If the probability of false alarm is 10^{-4} in a radar receiver that is operating continuously, and the signal bandwidth is 2 MHz, what is the average time between false alarms?
- 5 ms.
 - 200 sec.
 - 5 sec.
 - 2 ms.
79. Which of the following is *not* a common characteristic of rotating search radar?
- Track targets with high update rates.
 - Provide search azimuth coverage of 360° .
 - Employ a fan-shaped beam with narrow in azimuth and wide in elevation.
 - Have fixed rotation rates that allow several pulses to illuminate the target.
80. Which of the following is *not* a characteristic of ionospheric effects on radar propagation?
- Affect ground-based radar viewing aircraft targets.
 - Effects vary with various powers of radar wavelength.
 - Affect space-based radar viewing aircraft targets.
 - Effects are rarely significant at frequencies above 1 GHz.
81. A 15-dBsm target is immersed in a uniform chaff cloud that has an RCS density of -80 dBsm per cubic meter. A radar having an azimuth and elevation beamwidths of 1 degree and range resolution of 15m observes the

- target at a range of 150 km. What is the S/C, assuming the chaff cloud is much larger than the beam and no chaff cancellation is employed?
- 14.9 dB.
 - 15.9 dB.
 - 18.1 dB.
 - 42.9 dB.
82. For a volume search radar, if the search time is chosen to maximize the assured target acquisition range, what is that range when the detection range is 1,000 km?
- 1,333 km.
 - 1,000 km.
 - 875 km.
 - 750 km.
83. Which of the following is *not* a characteristic of the ambiguity function for a matched-filter receiver?
- The total volume under its surface depends only on the waveform energy.
 - The value along the time axis is proportional to the squared autocorrelation function of the waveform.
 - The value along the frequency axis is proportional to the spectrum of the waveform.
 - The maximum value occurs at the time and frequency to which the receiver filter is matched.
84. What is the RCS in square meters of a -13 -dBsm target?
- 20 m^2 .
 - 0.05 m^2 .
 - 0.22 m^2 .
 - 0.5 m^2 .
85. Which of the following does *not* contribute to the system noise temperature?
- Sky and ground temperature viewed by the antenna.
 - Noise generated by ohmic losses in the antenna and receive microwave elements.
 - Noise produced in the radar receiver.
 - Mainlobe and sidelobe jamming noise.
86. Twenty pulse returns from a Swerling 3 target are coherently integrated. Assuming 0.5-dB signal processing losses from pulse integration, what is the single-pulse S/N required to give a detection probability of 0.9 with a false-alarm probability of 10^{-6} ?
- 1.4 dB.
 - 3.8 dB.
 - 4.8 dB.
 - 5.8 dB.

87. What is the minimum cross-range resolution at a range of 50 km for a side-looking SAR having a frequency of 9.5 GHz and a horizontal antenna dimension of 3m?
- a. 1.5m.
 - b. 6.0m.
 - c. 15m.
 - d. 19.9m.
88. A radar having a frequency of 9.5 GHz, range resolution of 15m, and a 1.0° pencil beam observes a 5-dBsm target at a range of 100 km, immersed in rain having a rainfall rate of 6 mm/hr. What is the S/C, assuming no clutter cancellation?
- a. -11.9 dB.
 - b. -8.7 dB.
 - c. -6.7 dB.
 - d. -4.9 dB.
89. Which of the following statements is *false*?
- a. The ionosphere may distort radar propagation at UHF.
 - b. Atmospheric and rain losses may be significant at K band.
 - c. S and C bands are often used for multifunction radar.
 - d. L band radar may suffer severe atmospheric losses.
90. A phased-array antenna operating at a frequency of 5.5 GHz has 4,000 elements, each with a gain of 5.1 dB. What is the effective aperture area?
- a. 4.82 m^2 .
 - b. 56.2 m^2 .
 - c. 7.20 m^2 .
 - d. 3.07 m^2 .
91. A pulse-burst waveform has range ambiguities spaced by 2 km. If the frequency is 9.5 GHz, what is the spacing of the radial-velocity ambiguities?
- a. 75 km/s.
 - b. 2,000 m/s.
 - c. 31 m/s.
 - d. 1,185 m/s.
92. On which of the following factors does radar terrain clutter reflectivity, σ^0 , *not* depend?
- a. Radar range resolution.
 - b. Terrain or sea-surface characteristics.
 - c. Radar frequency.
 - d. Grazing angle.
93. Which of the following is *not* a characteristic of volume radar chaff?
- a. Signal return resembles that of the target.
 - b. Many small reflectors around the target.
 - c. Dipoles resonant at the radar frequency are often used.

- d. May have radial velocity different from that of the target.
94. Which of the following characterized GDOP?
- a. Reduction in measurement accuracy from using range and angle measurements.
 - b. Reduction in measurement accuracy when using two radars, one of which has poor range accuracy.
 - c. Reduction in measurement accuracy when the observation angles of two radars differ by nearly 90° .
 - d. Reduction in measurement accuracy when the observation angles of two radars are nearly the same.
95. Features of ground-based radar do *not* include:
- a. Observation of low-altitude targets at long ranges.
 - b. Large weight and prime power capability.
 - c. Fixed or slowly-moving location.
 - d. LOS limited by terrain.
96. What is the two-way ionospheric attenuation for a 150-MHz ground-based radar viewing a target having an altitude of 500 km and an elevation angle of 20° , under normal daytime ionospheric conditions?
- a. 0.5 dB.
 - b. 0.8 dB.
 - c. 1.2 dB.
 - d. 2.7 dB.
97. What target dimension will result in uncorrelated RCS values when the radar frequency changes in steps of 25 MHz?
- a. 6m or greater.
 - b. 12m or greater.
 - c. 6m or less.
 - d. 12m or less.
98. A target complex consists of two real targets and 50 decoys. A discrimination technique having a K factor of 4 provides a probability of target leakage of 1% and a probability of decoy false acceptance of 4.7%. What is the expected number of targets that will be declared to be real targets?
- a. 1.98.
 - b. 2.35.
 - c. 4.33.
 - d. 4.65.
99. Which of the following is a characteristic of bistatic radar?
- a. Transmitting and receiving antennas are separated.
 - b. The same antenna used for transmitting and receiving.
 - c. Corner reflectors produce large signal returns.

d. Common use of radar hardware at a single site.

100. Swerling 3 target RCS fluctuations are produced by:

- a. A target having many comparable scatterers and dwell-to-dwell decorrelation.
- b. A target having many comparable scatterers and pulse-to-pulse decorrelation.
- c. A target having a dominant scatterer and dwell-to-dwell decorrelation.
- d. A target having a dominant scatterer and pulse-to-pulse decorrelation.

F.2 Answers

1. b.	26. d.	51. d.	76. d.
2. b.	27. d.	52. a.	77. c.
3. b.	28. d.	53. c.	78. a.
4. c.	29. c.	54. d.	79. a.
5. b.	30. d.	55. c.	80. a.
6. b.	31. d.	56. d.	81. c.
7. c.	32. b.	57. b.	82. d.
8. c.	33. d.	58. b.	83. c.
9. b.	34. b.	59. c.	84. b.
10. c.	35. a.	60. c.	85. d.
11. a.	36. b.	61. c.	86. c.
12. a.	37. a.	62. a.	87. a.
13. a.	38. a.	63. c.	88. b.
14. d.	39. b.	64. d.	89. d.
15. d.	40. b.	65. b.	90. d.
16. b.	41. d.	66. b.	91. d.
17. b.	42. b.	67. a.	92. a.
18. d.	43. a.	68. c.	93. a.
19. c.	44. a.	69. b.	94. d.
20. c.	45. c.	70. d.	95. a.
21. c.	46. d.	71. a.	96. a.
22. d.	47. b.	72. d.	97. a.
23. a.	48. b.	73. b.	98. c.
24. a.	49. a.	74. b.	99. a.
25. b.	50. c.	75. d.	100. c.

About the Author

G. Richard Curry is a consultant in radar system applications with nearly 50 years of experience in radar system analysis and simulation, radar design and testing, military R&D planning and technology assessment, and research management.

He led analysis of radar system applications in military systems at Science Applications International Corporation (SAIC), and at General Research Corporation (GRC). There, he directed numerous programs, including studies of ballistic missile defense radar systems, air defense architectures, and space-based radar concepts. Prior to that, he analyzed and designed surveillance and tracking radar for the Raytheon Company, performed radar engineering for ballistic missile range testing at Kwajalein, and developed radar signal processing techniques at MIT Lincoln Laboratory. He served in the U.S. Navy as an Electronics Officer, responsible for maintaining and testing shipboard electronic equipment.

Mr. Curry received B.S. degrees in electrical engineering and mathematics from the University of Michigan, and an M.S. in electrical engineering from the Massachusetts Institute of Technology. He is a member of the Radar System Panel of the IEEE Aerospace and Electronic Systems Society.

Index

A

- Accuracy, 167
 - angular measurement, 169–72
 - range measurement, 167–69
 - velocity measurement, 172–74
- Add-Ins dialog box, 326, 327
- Airborne moving target indication (AMTI), 263
- Airborne radar, 263–85
 - advantages, 13
 - clutter characteristics, 266–69
 - clutter features vs. radial velocity, 269
 - configurations, 264–66
 - defined, 263
 - DPCA, 271–73
 - ineffectiveness, 265
 - platform velocities, 270
 - problems, 279–80
 - pulse-Doppler, 77
 - pulse-Doppler processing, 269–71
 - SAR, 274–79
 - STAP, 273–74
 - types, 13
 - uses, 263
 - VBA software functions, 280–85
 - viewing geometry, 266, 267
 - See also* Space-based radar (SBR)
- Airborne Warning and Control System (AWACS), 264
- Ambiguity function, 48–49
 - CW pulse, 50, 54
 - linear FM pulses, 51, 52, 54
 - phase-coded waveforms, 55, 56
 - pulse-burst waveforms, 56, 57
- AngleError_mR function, 186–88
 - Excel parameter box for, 187–88
 - features, 186
 - function output, 187
 - input parameters, 186–87
 - purpose, 186
 - reference equations, 186
- Angular measurement
 - accuracy, 169–72
 - bias errors, 170
 - coordinates, 169
 - error determination, 170–71
 - error examples, 171
 - target uncertainty and, 172
 - See also* Measurements
- Answers, self test, 379
- Antennas, 15–16, 23–30
 - angular measurement sensitivity, 28
 - aperture weighting, 27
 - beamwidth, 24, 25
 - beamwidth coefficient, 24
 - circular, 26–27
 - disk, 15
 - effective aperture area, 25
 - far-field pattern, 23, 24
 - feeds, 28
 - gain, 25, 26
 - gain estimation, 26
 - illumination weighting, 27
 - illustrated, 15
 - losses, 25–26
 - parabolic reflector, 15–16
 - phased-array, 16, 27–28, 30–35
 - polarization, 29
 - range, 23–24
 - rectangular, 26
 - SAR, 279
 - SBR, 265
 - sidelobe levels, 26, 27
 - sidelobes, 27
 - tapering, 27
 - transmit, 27, 68
- Attenuation, 202
 - ionosphere, 209–10
 - rain, examples, 204
 - tropospheric, 206
 - two-way, 206, 210

B

Barrage noise jamming, 233
 Barrier search, 128
 Beam-broadening factor, 126
 Beamshape losses, 65, 113
 Binary detection. *See* Cumulative detection
 Bistatic radar, 19
 Bow-tie horizon search scan, 131

C**Chaff**

cancellation ratios (CR), 243
 clusters, 230
 defined, 230
 detection in, 304–7
 dipole RCS, 241, 242
 resolution volume, 242
 total, RCS, 244
 uniform distribution, 243
 volume, 241–45

Circular scans, 127**Clutter**

Doppler-frequency shift, 268–69
 extent determination, 196
 mainbeam, velocity spread, 268
 plan view, 268
 radial velocity, 266, 267
 range/velocity spread, 266
 reflectivity, 197
 rejection performance, 199
 rejection techniques, 198
 returns, 268
 STAP and, 274
 terrain, 268, 273

Coherent dwells, 100**Coherent integration, 71–72**

conditions, 76
 defined, 71–72
 detection examples, 95
 gain, 72
 knowledge requirement, 92
 limitations, 73
 losses, 72, 92
 performance, 76
 times, 73
See also Pulse integration

Composite measurement errors, 300–304

approach, 300–301
 components, 301
 as function of range, 304
 problem, 300

solution, 301–2
 spreadsheet analysis, 302–4
 worksheet, 303
See also Measurements

Constant-false-alarm rate (CFAR) processing, 91–92**Continuous wave (CW) pulses, 17, 49–51**

ambiguity function, 50
 characteristics, 50
 defined, 49
 limitations, 51
 long, 51
 pulse envelope, 49
 short, 51
See also Waveforms

Counter-countermeasures (CCMs)

defined, 227
 electronic (ECCMs), 227, 243
 list of, 229
 potential, 229
 problems, 248–49
 use of, 227–28

Countermeasures (CMs)

classes, 228, 229
 confusion and deception, 228
 decoy discrimination, 245–48
 defined, 227
 electronic (ECMs), 227
 list of, 229
 mainlobe jamming, 231–37
 problems, 248–49
 sidelobe jamming, 237–41
 summary, 228–31
 VBA software functions, 249–62
 volume chaff, 241–45

Cross-range resolution, 276**CrossVelError_mps function, 190–91****Cued search, 123–27**

approach, 295–96
 defined, 109
 detection range, 125
 with dish radar, 295–300
 geometry, 124
 number of search rings, 299
 parameters, 125
 performance modeling, 295–300
 probability of detection, 299
 problem, 295
 radius, 125, 126
 solution, 296–97
 spreadsheet analysis, 297–300
 worksheet, 298

See also Search

Cumulative detection, 98–101

- approach, 292
- defined, 98
- effective, 101
- examples, 100
- as function of range, 295
- implementation, 98
- for multiple scans, 114
- over long periods, 292–95
- performance modeling, 292–95
- probability, 98
- problem, 292
- pulse S/N requirement, 99
- pulse spacing, 100
- with small numbers of pulses, 100
- solution, 292–93
- spreadsheet analysis, 293–95
- worksheet, 294

See also Radar detection

D

Decoy discrimination, 245–48

- capabilities, 248
- K factor, 246
- measurements for, 245
- probability, 247
- probability examples, 247

Decoys, 230, 231

Dep_Ang_deg function, 281–82

Detection in jamming, chaff, noise, 304–7

- approach, 305
- probability, 307
- problem, 304–5
- solution, 305–6
- spreadsheet, 306–7
- worksheet, 306

Digital signal processing, 271

DiscProb_Factor function, 249–50

Dish antennas, 15

Dish radar

- cued search with, 295–300
- horizon search with, 130–33
- search time, 127
- tracking, 183

Displaced Phase Center Arrays (DPCA), 271–73

- configurations, 272
- defined, 271
- in GMTI, 272
- illustrated, 272
- implementation, 271

- performance limitation, 272–73
- for side-looking radar, 272

Doppler-frequency shift, 177

- of clutter returns, 268–69
- spread, 177
- target rotational geometry and, 177

DopVelError_mps function, 188–89

E

Effective radiated power (ERP)

- defined, 231
- polarization, 236

Electronic counter-countermeasures (ECCMs)

- defined, 227
- pulse-to-pulse frequency agility, 243

Electronic countermeasures (ECMs), 227

Environment

- ionosphere effects, 209–13
- precipitation effects, 201–5
- problems, 213–14
- terrain and sea-surface effects, 195–201
- troposphere effects, 205–9
- VBA software functions, 215–23

Escort jammers (ESJs)

- defined, 231
- range/gain, 232

See also Jammers; Mainlobe jamming

External noise, 65

F

False-alarm probability optimization, 289–92

- approach, 289
- problem, 289
- solution, 289–90
- spreadsheet analysis, 290–92
- worksheet, 291

False alarms, 89–92

- calculations, 90
- CFAR processing, 91–92
- rate, setting, 91
- threshold, 91
- threshold level, 89

See also Radar detection

Fan-shaped beam, 111

FARate_per_s function, 103

Frequency bands, 13–15

- applications, 14
- key characteristics, 13, 14
- list, 14
- types, 13

Frequency modulated continuous-wave (FMCW), 17
 Full-field-of-view (FFOV)-phased arrays, 31–32
 Functional models, 5–6
 defined, 5
 metric system, 6
 Function Arguments dialog box (Excel), 7, 8

G

Geometric dilution of precision (GDOP), 179
 Glint, 170
 Glossary, 319–21
 Graz_Ang_deg function, 280–81
 Ground moving target indication (GMTI), 263, 272

H

High-PRF waveforms, 270
 Horizon search, 128–33
 as barrier search, 128
 bow-tie, 131
 concept, 128
 coverage of targets, 129
 defined, 109
 detection range, 129
 with dish radar, 130–33
 geometry, 128
 observation of target, 130
 parameters, 128
 with phased-array radar, 128–30
 See also Search

I

Insert Function dialog box, 326
 Internal noise, 65
 Inverse SAR (ISAR), 276
 IonoEl_Err_mR function, 222
 IonoR_Err_mR function, 222–23
 Ionosphere
 attenuation, 209–10
 defined, 209
 effects, 209–13
 elevation-angle/range errors, 211–12
 impact on radar propagation, 209
 layers, 209
 measurement errors, 212
 range errors, 213
 refractive index, 211
 signal dispersion, 211
 See also Environment; Troposphere

J

Jammers, 228
 effect on radar performance, 232
 ERP, 231, 232
 escort (ESJs), 231, 232
 Gaussian noise, 234
 mainlobe (MLJs), 229, 231, 236
 pulsed, 229
 self-screening (SSJs), 231
 sidelobe (SLJs), 229, 237
 stand-off (SOJs), 237
 STAP and, 274
 swept spot, 230
 wide frequency band, 229
 Jammer-to-noise ratio (J/N), 236
 Jamming
 barrage noise, 233
 detection in, 304–7
 mainlobe, 231–37
 sidelobe, 237–41
 Joint Surveillance and Target Attack Radar (JSTARS), 264

K

Kalman filters, 181
 Knife-edge shapes, 54

L

Lens loss, 206–7
 Limited-field-of-view (LFOV) phased arrays, 33–34
 Linear FM pulses, 51–54
 ambiguity function, 51, 52
 amplitude, 51
 characteristics, 52
 defined, 51
 examples, 53
 large time-bandwidth products, 53
 range-Doppler coupling, 54
 See also Waveforms
 Low-PRF waveforms, 271

M

Mainlobe jammers (MLJs), 229, 236
 Mainlobe jamming, 231–37
 barrage noise, 233
 examples, 233
 performance, 234
 radar range, 236
 See also Jammers; Jamming
 Maximum angular scan rate, 132

MB_Clutter_V_mps function, 282–83

Measurements

angular, accuracy, 169–72

composite, errors, 300–304

for decoy discrimination, 245

geometry, 166

ionosphere errors, 212

multipath errors, 201

multiradar, 178–80

problems, 183–85

range, accuracy, 167–69

RCS, 174

smoothing, 180–82

target characteristics, 165

target features, 174–78

target radial length, 174

target rotational velocity, 174

VBA software functions, 185–93

velocity, accuracy, 172–74

Medium-PRF waveforms, 270

Microwave loss, 68

Minimum azimuth scan rate, 132

Minimum detectable velocity (MDV), 18, 199, 270

Minimum range constraint, 76–79

example, 77

impact, 78

ML_BTRange_km function, 251–54

Excel parameter box for, 254–55

features, 251

function output, 253

input parameters, 252–53

purpose, 251

reference equations, 251

ML_SJNR_dB function, 250–51

Modular phased-arrays, 68

Monostatic radar, 19

Moving target indication (MTI), 198

airborne (AMTI), 263

ground (GMTI), 263, 272

limitations, 17–18

processing, 17–18

uses, 17

Multipath propagation

geometry, 200

measurement errors, 201

returns, 201

from smooth level surface, 201

Multiple radars, tracking and, 183

Multiple-time-around returns, 59–60

Multiradar measurements, 178–80

advantages, 178

error reduction, 179

target position determination geometry, 178

See also Measurements

N

Noise

calculations, 330

detection in, 304–7

system, temperature, 35–36

temperatures, 330

See also Signal-to-noise ratio (S/N)

Noncoherent integration, 73–74

defined, 73

detection examples, 97

detection with, 95–97

false-alarm probability and, 95

with fluctuating/nonfluctuating targets, 97

gain, 74

implementation, 74–75, 95

See also Pulse integration

O

Organization, this book, 2–3

P

Parabolic reflector antennas, 15–16

Paste Function dialog box, 326, 327

Performance modeling, 287–309

analysis objectives, 288

analysis results, 288

analysis steps, 288

calculations, 288

composite measurement errors, 300–304

cued search with dish radar, 295–300

cumulative detection (long periods), 292–95

detection in jamming, chaff, noise, 304–7

false-alarm probability optimization,
289–92

methodology, 287–89

missing data, 288

problem data review, 288

problems, 308–9

problem solutions, 287–88

Pfa_Factor function, 102

Phase-coded waveforms, 54–56

ambiguity function, 55, 56

binary, 54

characteristics, 55

defined, 54

duration, 56

examples, 56

- Phase-coded waveforms (continued)
 - subpulses, 54
 - See also* Waveforms
- Phased-array antennas, 16, 27–28, 30–35
 - advantages, 30
 - beam broadening, 32
 - beamwidth, 31, 32
 - comparison, 34
 - computer-controlled, 16
 - conformal, 264
 - effective aperture area, 30–31
 - for electronic scan angles, 33
 - element spacing, 33
 - example, 69
 - FFOV, 31–32
 - gain, 30
 - gain reduction, 32
 - ground-based, 16, 34
 - LFOV, 33–34
 - thinned-array beamwidths, 33
 - transmit/receive arrays, 30
 - See also* Antennas
- Phased-array radar
 - beam-packing factor, 117
 - beamwidth, 117
 - grids of circular beams, 117
 - horizon search with, 128–30
 - modular, 68
 - multifunction, 182
 - off-broadside, 119
 - pencil beams, 116
 - scan loss, 117
 - search angular coverage, 118
 - search beams, 116
 - search detection range, 119
 - search sectors, 119
 - tracking, 183
 - volume search with, 116–23
 - X-band, 124
- Polarization, 29
 - circular, 29
 - ERP, 236
 - RCS and, 38
- Power-aperture product, 110
- Precipitation
 - attenuation, 202
 - effects, 201–5
 - rain, 202
- PredictError_km function, 191–93
 - Excel parameter box for, 192
 - features, 191
 - function output, 193
 - input parameters, 191–92
 - purpose, 191
 - reference equation, 191
- ProbDet_Factor function, 103–5
 - Excel parameter box, 105
 - input parameters, 104
 - output, 104
 - purpose, 103
 - reference equations, 104
 - See also* VBA functions
- Problems
 - airborne and SBR issues, 279–80
 - countermeasures and counter-countermeasures, 248–49
 - environment and mitigation techniques, 213–14
 - introduction, 9
 - performance modeling, 308–9
 - radar analysis parameters, 41–42
 - radar configuration, 19–20
 - radar detection, 101–2
 - radar equation, 79–80
 - radar measurement and tracking, 183–85
 - radar search modes, 133–35
 - solutions, 333–61
 - waveforms, 60–62
- Propagation losses, 68, 113
- Pulse-burst waveforms, 56–59
 - ambiguities spacing, 58
 - ambiguity function, 56, 57
 - characteristics, 57
 - defined, 56
 - design variations, 58
 - duration, 59
 - examples, 58
 - See also* Waveforms
- Pulse-Doppler processing, 17, 198, 269–71
 - analog filters and, 271
 - defined, 269
 - high-PRF waveforms, 270
 - low-PRF waveforms, 271
 - medium-PRF waveforms, 270
 - waveforms, 269, 270–71
- Pulsed radar, 16–17
- Pulse integration, 71–76
 - coherent, 71–72
 - example, 76
 - noncoherent, 73–74
 - radar equation and, 75
- Pulse-repetition frequency (PRF), 59
 - fixed, 60
 - jittering, 60

Pulse-repetition interval (PRI), 59
Pulse-to-pulse decorrelation, 39
Pulse-to-pulse frequency agility, 243

Q

Questions, self test, 363–79

R

Radar

- accuracy, 167
- applications, 4–5
- basing, 6, 11–13
- bistatic, 19
- burnthrough, 229
- coverage limitation illustration, 12
- custom functions, 6–9
- CW, 17
- efficiency, 23
- functional models, 5–6
- line-of-sight (LOS), 11
- measurement and tracking, 165–93
- modeling, system-level requirements, 2
- monostatic, 19
- noise temperatures, 330
- operation concept, 3–4
- performance modeling, 287–309
- pulsed, 16–17
- rotating search, 111–16
- SAR, 274–79
- side-looking, 272, 277–78
- See also* Airborne radar; Space-based radar (SBR)

Radar analysis parameters, 21–42

- antennas, 23–30
- phased-array antennas, 30–35
- problems, 41–42
- receiver and signal processor, 35–37
- target RCS, 37–41
- transmitter, 21–23

Radar configurations, 6, 11–20

- antennas, 15–16
- basing, 11–13
- frequency bands, 13–15
- monostatic/bistatic, 19
- problems, 19–20
- signal processing, 17–18
- waveform types, 16–17

Radar cross section (RCS), 37–41

- bias errors, 175
- bistatic, 41
- chaff dipole, 241, 242

- decorrelation, 38, 39
- defined, 37
- LOS effect, 40
- measurement, 174, 175
- radar range as function of, 78
- signal polarization and, 38
- S/N-dependent error, 175
- target rotation/signal frequency and, 38
- target size and, 37

Radar detection, 87–106

- analysis, 88
- calculations, 88
- with coherent dwell, 92–95
- with cumulative detection, 98–102
- defined, 5, 87
- false alarms, 89–92
- with noncoherent integration, 95–97
- performance, 87
- problems, 101–2
- process, 87–89
- process illustration, 88
- range in search, 110
- with single pulse, 92–95
- VBA software functions for, 102–6

Radar equation, 63–85

- basic form, 63
- example, 66
- minimum range constraint, 76–79
- parameter definition, 67–70
- problems, 79–80
- pulse integration, 71–76
- range, 63–67
- reference range, 70–71
- signal bandwidth, 66
- in system performance calculation, 66–67
- VBR software functions for, 80–85

Radar range

- calculating, 76
- equation, 63–67
- fixed random error, 168
- as function of target RCS, 78
- maximum total, 12
- measurement accuracy, 167–69
- minimum constraint, 76–79
- reference, 70–71
- resolution, 165–66

Radar search modes, 109–61

- cued search, 109, 123–27
- design, 111
- horizon search, 109, 128–33
- problems, 133–35
- rotating search, 111–16

- Radar search modes (continued)
 - search equation, 109–11
 - VBA software functions, 135–61
 - volume search, 109, 116–23
- Radial-velocity ambiguities, 60
- Radial-velocity measurement
 - accuracy, 172
 - errors, 173
 - examples, 174
- RadVelError_mps function, 189–90
- Rain, 220
 - attenuation examples, 204
 - climate regions, 203
 - clutter, 205
 - clutter reflectivity, 204
 - rainfall rates, 203
- RainLocAtten_dBpkm function, 215–16
- RainPathAtten_dB function, 216–18
 - Excel parameter box for, 218
 - features, 217
 - function output, 217
 - input parameters, 217
 - purpose, 216
 - reference equations, 217
- Range-Doppler coupling, 54
- RangeError_m function, 185–86
- Range gates, 167
- Range_km function, 81–83
- Range measurement
 - accuracy, 167–69
 - error calculations, 168
 - examples, 169
 - See also* Measurements; Radar range
- Ray tracing, 208
- Receivers, system noise temperature, 35–36, 65
- Reference range, 70–71
 - calculation, 71
 - defined, 70
 - definition of, 71
- Refractivity, 207–8, 209
- RF power, 21
 - average output, 21
 - average transmitted, 22
 - pulse duration, 21
 - radiated by antennas, 22
- Rotating search radars, 111–16
 - azimuth beam, 111
 - azimuth beamwidth, 111, 112
 - beamshape losses, 113
 - elevation coverage, 115
 - example, 115
 - fan-shaped beam, 111
 - maximum altitude detection, 115
 - propagation losses, 113
 - pulse returns, 112
 - scanning loss, 113
 - scattering loss, 113
 - single-pulse S/N calculation, 113
 - stacked elevation beams, 116
- S
- SAR_XR_Res_m function, 283–85
 - Excel parameter box for, 284
 - features, 283
 - function output, 284–85
 - input parameters, 284
 - purpose, 283
 - reference equations, 283
- Scanning loss, 113
- Scan-to-scan decorrelation, 39
- SCR_Chaff_dB function, 259–62
 - Excel parameter box for, 261
 - features, 260
 - function output, 262
 - input parameters, 260–62
 - purpose, 259
 - reference equations, 259
- SCR_Rain_dB function, 218–19
- SCR_Surf_dB function, 215
- Search
 - barrier, 128
 - cued, 109, 123–27, 295–300
 - equations, 109–11
 - horizon, 109, 128–33
 - performance, 111
 - volume, 109, 116–23
- SearchR_Cue1_km function, 145–47
 - Excel parameter box for, 148–49
 - features, 145
 - function output, 147
 - input parameters, 146–47
 - purpose, 145
 - reference equations, 145
- SearchR_Cue2_km function, 147–51
 - Excel parameter box for, 150–51
 - features, 147–48
 - function output, 150
 - input parameters, 148–50
 - purpose, 147
 - reference equations, 147
- SearchR_Hor1_km function, 151–54
 - Excel parameter box for, 153–54
 - features, 151
 - function output, 152–53

- input parameters, 151–52
 - purpose, 151
 - reference equations, 151
- SearchR_Hor2_km function, 154–57
 - Excel parameter box for, 156–57
 - features, 154
 - function output, 155–56
 - input parameters, 154–55
 - purpose, 154
 - reference equations, 154
- SearchR_Rot1_km function, 135–42
 - Excel parameter box for, 137–38
 - features, 135
 - function output, 136–37
 - input parameters, 135–36
 - purpose, 135
 - reference equations, 135
- SearchR_Rot2_km function, 137–39
 - Excel parameter box for, 140–41
 - features, 137
 - function output, 139
 - input parameters, 138–39
 - purpose, 137
 - reference equations, 137
- SearchR_Vol1_km function, 139–42
 - Excel parameter box for, 142–43
 - features, 139–40
 - function output, 142
 - input parameters, 140–42
 - purpose, 139
 - reference equations, 139
- SearchR_Vol2_km function, 142–45
 - Excel parameter box for, 145–46
 - features, 143
 - function output, 144
 - input parameters, 143–44
 - purpose, 142
 - reference equations, 143
- Sea-surface effects, 195–201
- Self-screening jammers (SSJs), 231
- Self-test, 363–79
 - answers, 379
 - questions, 363–79
- Sequential detection, 100
- Sidelobe blanker (SLB) technique, 237, 238
- Sidelobe cancellers (SLCs), 238
- Sidelobe jammers (SLJs), 229, 237
- Sidelobe jamming, 237–41
 - bandwidth, 240
 - examples, 240
 - S/J for, 238
 - S/(J+N) for, 239
 - See also* Jammers; Jamming
- Side-looking radar, 272
- Side-looking SAR, 276, 277–78
 - cross-range resolution, 277–78
 - defined, 277
 - focused processing, 277
 - geometry, 277
 - PRF, 278
 - use of, 278
 - See also* Synthetic-aperture radar (SAR)
- Signal processing
 - digital, 271
 - SAR, 279
 - techniques, 17–18
- Signal processors, 36
- Signal-to-clutter ratio (S/C), 199, 205
- Signal-to-noise ratio (S/N), 5, 63
 - dependent errors, 169
 - integrated, 74
 - of received signal, 63
 - Swerling 5 nonfluctuating targets, 99
- SL_BTRange_km function, 256–59
 - Excel parameter box for, 259–60
 - features, 256
 - function output, 258
 - input parameters, 256–58
 - purpose, 256
 - reference equations, 256
- SL_SJNR_dB function, 254–56
 - Excel parameter box for, 257–58
 - features, 254
 - function output, 256
 - input parameters, 254–56
 - purpose, 254
 - reference equations, 254
- SNR_dB function, 80–81, 82, 83
- SNR_SP_dB function, 105–6
- Solutions, problem, 333–61
- Space-based radar (SBR), 13, 263–85
 - antennas, 265
 - clutter characteristics, 266–69
 - clutter features vs. radial velocity, 269
 - defined, 263
 - DPCA, 271–73
 - ineffectiveness, 265
 - medium-PRF waveforms, 270
 - platform velocities, 270
 - power, 265
 - problems, 279–80
 - pulse-Doppler processing, 269–71
 - radar configurations, 264–66
 - SAR, 274–79

- Space-based radar (continued)
 - STAP, 273–74
 - uses, 263
 - VBA software functions, 280–85
 - viewing geometry, 266, 267
 - waste heat removal, 265
 - weight minimization, 265
 - See also* Airborne radar
 - Spaceborne Imaging Radar-C (SIR-C), 265
 - Space-Time Adaptive Processing (STAP), 273–74
 - application of, 274
 - defined, 273
 - performance-limiting factors, 274
 - processing, 274
 - Spiral scans, 127
 - Spotlight SAR, 18, 276, 278–79
 - defined, 278
 - PRF, 279
 - use of, 278–79
 - See also* Synthetic-aperture radar (SAR)
 - SP_SNR_dB function, 83–85
 - Excel parameter box for, 85
 - features, 84
 - input parameters, 84–85
 - output, 85
 - purpose, 83
 - reference equations, 83
 - See also* VBA functions
 - Sr_BowTie1_km function, 157–59
 - Excel parameter box for, 159
 - features, 157
 - function output, 158
 - input parameters, 157–58
 - purpose, 157
 - reference equations, 157
 - Sr_BowTie2_km function, 159–61
 - Excel parameter box for, 162–63
 - features, 160
 - function output, 161
 - input parameters, 160–61
 - purpose, 159
 - reference equations, 159
 - Stand-off jammers (SOJs), 237
 - Surveillance radar
 - rotating, 41
 - waveform, 45
 - Swept spot jammers, 230
 - Swerling target models, 38, 40
 - characteristics, 89
 - fluctuating, 96
 - Symbols list, 311–18
 - Synthetic-aperture radar (SAR), 274–79
 - antennas, 279
 - beam formation, 275
 - beam pattern, 276
 - defined, 274
 - effect, 275
 - examples, 277
 - Fourier transforms, 18
 - grating lobes and, 276
 - inverse (ISAR), 276
 - processing, 17, 276
 - side-looking, 276, 277–78
 - signal processing, 279
 - spotlight, 18, 276, 278–79
 - techniques, 276
 - time, 18
 - System noise temperature, 35–36
 - definition, 67
 - external noise, 65
 - internal noise, 65
 - minimize, 36
 - specification, 36
- ## T
- Targets
 - azimuth, 112
 - detection range, 123, 127
 - direction, 3
 - Doppler-frequency shift, 177
 - features, measurement of, 174–78
 - fluctuating, 96
 - glint, 170
 - length, 176
 - position measurement, 5
 - radial length, 174
 - radial velocity, 3, 114, 123, 172
 - RCS, 37–41
 - resolution geometry, 166
 - rotational geometry, 177
 - rotational velocity, 175
 - signal returns, 176
 - size, 4
 - unwanted, 47
 - vertical velocity, 130
 - See also* Radar cross section (RCS)
 - Taylor weighting, 70
 - Terrain effects, 195–201
 - blockage, 199
 - clutter, 268, 273
 - Tracking
 - Dish radar, 183
 - filters, 181

- multiple radars and, 183
- phased-array radar, 183
- techniques, 182–83
- Track-while-scan (TWS), 182, 264
- Transmitters, 21–23
 - efficiency, 22, 23
 - power levels, 22
 - pulsed-radar, 22
 - RF power, 21
- TropoAtten_dB function, 220
- TropoEl_Err_mR function, 220–21
- TropoR_Err_mR function, 221–22
- Troposphere
 - attenuation, 206
 - defined, 205
 - effects, 205–9
 - lens loss, 206–7
 - measurement errors, 208
 - See also* Environment; Ionosphere

U

- Unit conversion, 329–30
 - factors, 329
 - prefixes, 330

V

- VBA functions, 323–28
 - airborne and SBR, 280–85
 - AngleError_mR, 186–88
 - countermeasures and counter-
- countermeasures, 249–62
 - CrossVelError_mps, 190–91
 - Dep_Ang_deg, 281–82
 - DiscProb_Factor, 249–50
 - disk, 323
 - DopVelError_mps, 188–89
 - environment and mitigation techniques, 215–23
 - FARate_per_s, 103
 - Graz_Ang_deg, 280–81
 - implementation, 327
 - installing, 323
 - IonoEl_Err_mR, 222
 - IonoR_Err_mR, 222–23
 - list of, 324–25
 - MB_Clutter_V_mps, 282–83
 - ML_BTRange_km, 251–54
 - ML_SJNR_dB, 250–51
 - Pfa_Factor, 102
 - PredictError_km, 191–93
 - ProbDet_Factor, 103–5

- radar measurement and tracking, 185–93
- radar search modes, 135–61
- RadVelError_mps, 189–90
- RainLocAtten_dBpk, 215–16
- RainPathAtten_dB, 216–18
- RangeError_m, 185–86
- Range_km, 81–83
- SAR_XR_Res_m, 283–85
- SCR_Chaff_dB, 259–62
- SCR_Rain_dB, 218–19
- SCR_Surf_dB, 215
- SearchR_Cue1_km, 145–47
- SearchR_Cue2_km, 147–51
- SearchR_Hor1_km, 151–54
- SearchR_Hor2_km, 154–57
- SearchR_Rot1_km, 135–42
- SearchR_Rot2_km, 137–39
- SearchR_Vol1_km, 139–42
- SearchR_Vol2_km, 142–45
- SL_BTRange_km, 256–59
- SL_SJNR_dB, 254–56
- SNR_dB, 80–81, 82, 83
- SNR_SP_dB, 105–6
- SP_SNR_dB, 83–85
- Sr_BowTie1_km, 157–59
- Sr_BowTie2_km, 159–61
- TropoAtten_dB, 220
- TropoEl_Err_mR, 220–21
- TropoR_Err_mR, 221–22
- using, 325

Velocity measurement

- accuracy, 172–74
- angular, 174
- cross-range, 174
- radial, 173–74

Visual Basic for Applications (VBA), 6, 7

Volume chaff, 241–45

Volume search

- defined, 109
- example, 121
- performance, 116, 123
- with phased-array radar, 116–23
- See also* Search

W

- Waveforms, 45–62
 - ambiguity function, 48–49
 - characteristics, 45, 46–49
 - CW pulses, 17, 49–51
 - energy, 46
 - FMCW, 17
 - high-PRF, 270

Waveforms (continued)

linear FM pulses, 51–54

low-PRF, 271

medium-PRF, 270

multiple-time-around returns, 59–60

multipulse, 46

phase-coded, 54–56

problems, 60–62

pulse-burst, 56–59

pulsed, 16–17

radial-velocity ambiguities, 60

resolution, 46–47

surveillance radar, 45

types, 16–17

unwanted targets and, 47

Recent Titles in the Artech House Radar Library

David K. Barton, Series Editor

Advanced Techniques for Digital Receivers, Phillip E. Pace

Airborne Pulsed Doppler Radar, Second Edition, Guy V. Morris and Linda Harkness, editors

Bayesian Multiple Target Tracking, Lawrence D. Stone, Carl A. Barlow, and Thomas L. Corwin

Beyond the Kalman Filter: Particle Filters for Tracking Applications, Branko Ristic, Sanjeev Arulampalam, and Neil Gordon

Computer Simulation of Aerial Target Radar Scattering, Recognition, Detection, and Tracking, Yakov D. Shirman, editor

Design and Analysis of Modern Tracking Systems, Samuel Blackman and Robert Popoli

Detecting and Classifying Low Probability of Intercept Radar, Phillip E. Pace

Digital Techniques for Wideband Receivers, Second Edition, James Tsui

Electronic Intelligence: The Analysis of Radar Signals, Second Edition, Richard G. Wiley

Electronic Warfare in the Information Age, D. Curtis Schleher

EW 101: A First Course in Electronic Warfare, David Adamy

EW 102: A Second Course in Electronic Warfare, David L. Adamy

Fourier Transforms in Radar and Signal Processing, David Brandwood

Fundamentals of Electronic Warfare, Sergei A. Vakin, Lev N. Shustov, and Robert H. Dunwell

Fundamentals of Short-Range FM Radar, Igor V. Komarov and Sergey M. Smolskiy

Handbook of Computer Simulation in Radio Engineering, Communications, and Radar, Sergey A. Leonov and Alexander I. Leonov

High-Resolution Radar, Second Edition, Donald R. Wehner

Introduction to Electronic Defense Systems, Second Edition, Filippo Neri

Introduction to Electronic Warfare, D. Curtis Schleher

Introduction to Electronic Warfare Modeling and Simulation, David L. Adamy

Introduction to RF Equipment and System Design, Pekka Eskelinen

Microwave Radar: Imaging and Advanced Concepts, Roger J. Sullivan

Millimeter-Wave Radar Targets and Clutter, Gennadiy P. Kulemin

Modern Radar System Analysis, David K. Barton

Multitarget-Multisensor Tracking: Applications and Advances Volume III, Yaakov Bar-Shalom and William Dale Blair, editors

Principles of High-Resolution Radar, August W. Rihaczek

Principles of Radar and Sonar Signal Processing, François Le Chevalier

Radar Cross Section, Second Edition, Eugene F. Knott et al.

Radar Evaluation Handbook, David K. Barton et al.

Radar Meteorology, Henri Sauvageot

Radar Reflectivity of Land and Sea, Third Edition, Maurice W. Long

Radar Resolution and Complex-Image Analysis, August W. Rihaczek and Stephen J. Hershkowitz

Radar Signal Processing and Adaptive Systems, Ramon Nitzberg

Radar System Analysis and Modeling, David K. Barton

Radar System Performance Modeling, Second Edition, G. Richard Curry

Radar Technology Encyclopedia, David K. Barton and Sergey A. Leonov, editors

Range-Doppler Radar Imaging and Motion Compensation, Jae Sok Son et al.

Space-Time Adaptive Processing for Radar, J. R. Guerci

Theory and Practice of Radar Target Identification, August W. Rihaczek and Stephen J. Hershkowitz

Time-Frequency Transforms for Radar Imaging and Signal Analysis, Victor C. Chen and Hao Ling

For further information on these and other Artech House titles, including previously considered out-of-print books now available through our In-Print-Forever[®] (IPF[®]) program, contact:

Artech House
 685 Canton Street
 Norwood, MA 02062
 Phone: 781-769-9750
 Fax: 781-769-6334
 e-mail: artech@artechhouse.com

Artech House
 46 Gillingham Street
 London SW1V 1AH UK
 Phone: +44 (0)20 7596-8750
 Fax: +44 (0)20 7630-0166
 e-mail: artech-uk@artechhouse.com

Find us on the World Wide Web at: www.artechhouse.com
